Sedimentology and geochemistry of Upper Jurassic (Iran) and Precambrian (Tasmania) carbonates

By

Mohammad H. Adabi

BSc (Ferdowsi University, Iran)

MSc (George Washington University, USA)

Submitted in fulfilment of the requirements
for the degree of
Doctor of Philosophy

Geology Department
University of Tasmania

January 1997

STATEMENT

This thesis contains the result of research carried out at the Geology Department, University of Tasmania, between 1989-1990, and 1992-1996. Parts of the material presented in Chapters 3, 6, 7 and 11 comprise the following published (or in press) papers:

1- ADABI, M.H. and RAO, C.P., 1991. Petrographic and geochemical evidence for original aragonitic mineralogy of Upper Jurassic carbonates (Mozduran Formation), Sarakhs area, Iran: Sed. Geology, v.72, p. 253-267.

2- RAO, C.P., and ADABI, M.H., 1992. Carbonate minerals, major and minor elements and oxygen and carbon isotopes and their variation with water depth in cool, temperate carbonates, western Tasmania, Australia: Mar. Geology, v. 103, p. 249-272.

3- ADABI, M.H. and AGER, D.V., 1997 (in press). Upper Jurassic brachiopods from North-East of Iran: Paleontology, v. 40, part 1, in press.

4- ADABI, M.H., 1997 (in press). Application of carbon isotope chemostratigraphy to the Renison dolomites (Tasmania, Australia): a Neoproterozoic age: Aust. Jour. Earth Sci., v. 44, No.3, in press.

This thesis contains no material which has been accepted for the award of any other degree or diploma by the University or any other institution, and to the best of the authors knowledge and belief, contains no material previously published or written by another person, except where due reference is made in the text of the thesis.

Date: 31, 1, 1997

Signature: adabi

AUTHORITY OF ACCESS

This thesis may be avialable for loan and copying in accordance with the Copyright Act 1968.

Date: 31, 1, 1997

Signature: 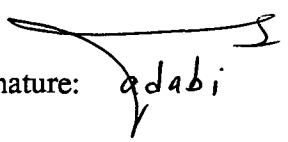

ABSTRACT

This thesis is a study of the origin and diagenetic history of the Upper Jurassic carbonates of the Mozduran Formation (Iran) and the Neoproterozoic carbonates of the Renison Mine (Tasmania, Australia). Therefore, this thesis is structured into two parts:

Part 1:

The Upper Jurassic Mozduran Formation, from north eastern Iran, comprises mainly thick sequences of bedded limestones, dolomitic limestones, dolomites, mudrocks, and locally thick gypsiferous layers. Nine microfacies have been recognized and these were interpreted as representing deposition in environments that include supratidal, intertidal, and shallow to relatively deeper subtidal zones.

The algal-rich biota, diverse skeletal and non-skeletal grains, evaporites and early diagenetic dolomites present in the shallowest part of the basin, are similar to those of modern subtropical shallow marine carbonates. Other petrographic evidence, such as acicular to fibrous isopachous cements, abundant deformed and spalled ooids, and shattered micritic envelopes, suggest an original aragonite mineralogy. Carbonate samples from the relatively deeper part of the basin contain predominantly calcitic skeletons, radial calcite ooids, bladed and radial fibrous marine calcite cements. The most striking features of these carbonates are the absence of bedded evaporites, stromatolites, and gastropods, decreasing detrital quartz content, and abundance of chert and carbonate muds.

Sr/Na covariance plots with respect to Mn, and $\delta^{18}O$ and $\delta^{13}C$ equilibrium lines also support aragonite and a mixture of calcite-aragonite mineralogy in the shallowest and relatively deeper parts of the basin respectively.

Petrographic studies indicate that the Mozduran carbonates were subjected to a complex diagenetic history, including meteoric and burial cementation, early and late dolomitization, micritization, boring, and physical and chemical compaction.

Part 2:

Dolomites and associated clastic sediments of the Neoproterozoic, at Renison in western Tasmania, host significant stratabound replacement tin deposits. Dolomite

samples outside and within the mineralized area were selected for analysis.

The sedimentary textures and elemental and isotopic compositions of dolomites outside of the Renison mine area, clearly indicate dolomicrites probably formed by either direct precipitation or during very early diagenesis, with Mg^{2+} being supplied by seawater. The calculated paleotemperature of seawater during the Neoproterozoic indicates that seawater temperature was around 8 ± 4° C (Irwin equation) or 12 ± 4° C (Land equation). This cool to cold water marine origin is further supported by the presence of diamictites in the Renison sequences and glacial erratics in the lithostratigraphic correlative. Sedimentological features of the Renison dolomites indicate a marine shallow intertidal to supratidal environment.

The carbon isotope chemostratigraphy of the least-altered Renison dolomites, gives an age range of between 570-820 Ma (Cryogenian to Neoproterozoic III).

Petrographic, major and minor elements, together with $\delta^{18}O$ and $\delta^{13}C$ studies, indicate that dolomites, within the mineralized area, have been altered mainly by diagenetic and hydrothermal alteration. The variations in intensity of alteration are mainly dependent on proximity to fractures, faults or mineralization.

Dolomite within the mineralized area is divided into five different types, based on crystal size and mode of origin. Dolomite samples from the mineralized area contain more generations of variable luminescence, reflecting a more complex fluid history in the vicinity of the Renison mine area. Multiple cross-cutting veins, brecciation, crack-seal textures, recrystallization, silicification, deformation and oblitration of original texture, is more pronounced in these dolomites than in the dolomites from the unmineralized area. Less recystallized dolomites, from the mineralized area, generally have more Ca and Mg, less Mn and Fe, and heavier $\delta^{18}O$ and $\delta^{13}C$ values than strongly recrystallized samples. The range of Ca, Mg, Mg/Ca, Sr, Fe, Mn and $\delta^{18}O$ and $\delta^{13}C$ values from the least to most altered dolomites, suggest that magmatic-meteoric hydrothermal fluid infiltration has occurred.

The $\delta^{18}O$ and $\delta^{13}C$ values of the most altered dolomites indicate that temperatures were up to 350° C for magmatically derived hydrothermal fluids. Isotherms on a $\delta^{18}O$ and $\delta^{13}C$ covariance plot illustrate that isotopic variation in the Renison carbonates is a result of changing temperatures and water/rock interactions. Water/rock ratios were predicted to be as high as ~6 (open system), close to the carbonate replacement orebodies, and decreased with declining temperatures away from mineralization.

ACKNOWLEDGEMENTS

There are a number of people that require a special mention - without their advice, assistance and support, my thesis would not have been completed. In particular, I would like to express my sincere gratitude to my supervisor, Dr. Prasada Rao, for his invaluable advice, support, enthusiasm, and expertise, throughout this study. I am very much indebted to the late Professor Derek Ager (from the Swansea University, U.K) for working on brachiopod fossils, and his recent death has meant the loss of a great teacher and researcher. Many thanks must go to Frank Cross of the University College of Swansea, who made the excellent cellulose peels from which the serial transverse sections were drawn. I have benefited greatly from discussions with Dr Max Banks, Dr Clive Burrett, Dr Steve Abbott, and Dr Peter McGoldrick. My gratitude is extended to Dr Paul Kitto, for his guidance and valuble discussion on Renison Mine geology. A special thanks to John Dunster for his friendship, constructive advice, and patient support over the last three years. All software for drafting of the stratigraphic sections, Markov chain analysis, and Fischer plots was provided by him.

The following people reviewed various portions of this thesis and their useful comments and editing is much appreciated: Dr Prasada Rao, Dr Paul Kitto, Dr Clive Calver, and John Dunster. Acknowledgement is also given for the contributions made by reviewers of papers published during the course of this study: Dr J.Veizer, Dr W. Sellwood, Dr K. Kelts (Editorial Board, Sedimentary Geology), Dr P. Doyle (Editorial Board, Paleontology), Dr Gregg Morrison and Dr Clive Calver (reviewers of Australian Journal of Earth Sciences), Professor R. Large, Dr M. Solomon, Dr P. Major, Dr J. Stolz, Dr G. Davidson and Dr D. Cook. Special gratitude is extended to a number of technical staff of the Geology Department and at the Central Science Labratory who assisted me during this study, particularly: Simon Stephens for his skillful work in preparing of hundreds of thin and polished sections, Philip Robinson for technical assistance in XRF and trace element analytical work, Mike Power and Christine Cook for isotope analysis, Wislaw Jablonski for his instruction and assistance in the operation of the Scanning Electron Microscope, Julie Beattie for typing of brachiopod paper, Jeanette Harris, June Pongratz, Marylin Feast, Christine Higgins, and Peter Cornish for their support and assistance on logistical, financial and other

bureaucratic work. I like to thank Debbie Harding for artistic drafting of many of the figures and Fred Koolhof for his superb photographic assistance. The determination of dolomite and insoluble residue compositions which was undertaken by the Tasmania Department of State Development and Resources (formerly the Tasmania Department of Mines) is acknowledged. I am thankful to many research fellows, graduates and PhD students at the University of Tasmania for their humour, assistance as well as friendship including: Dr David Cook, Dr Kin Zaw, Dr Gary Davidson, Dr Aung Pwa, Dr David Selley, John Dunster, Dr Udi Hartono, Dr Rahmat Hermanto, Fernando Della Pasqua, Mark Doyle, Blackwell Singoyi, Bill Wyman, Ingvar Sigurdsson, Jamie Rogers, Peter Winefield, Holger Paulick, David Rawlings, Michael Roach, Russell Fulton, Steve Hunns, Matthew White, Andrew Jones, Bruce Anderson; and Mark Duffett.

Special thanks are offered to my colleagues at the Ferdowsi University of Mashhad (Iran) specifically Dr R. Moussavi-Harami for his helpful discussion in the field. I would like to acknowledge the assistance provided by my former students in various stage of the field work including: Mr Ghadimi, Tarkhani, Amanabadi, Marozi, Zarinkho, Vatanpour, Stilla, Mohammadzadeh, Mashreghi and Safaie. This project was supported financially by the Ministry of Culture and Higher Education of Iran, with additional assistance from the University of Tasmania (Australia) are gratefully acknowledged. Special thanks go to Dr M.Ghezelayagh, representative of Ministry of Culture and Higher Education at Canbera, for tolerating my freguent requests. Thanks is extended to Renison Mine Limited for logistic support and for access to underground workings and drill core material.

Lastly, but by no means least, I am deeply grateful to my wife Zohreh, and my childeren, Mahsa and Golsa for their patience, encouragement, enthusiasm and constant support which they have given me over many years. Zohreh also has actively helped me with sample preparation and trace element analysis, her assistance is greatly appreciated.

CONTENTS

CHAPTER 7: OXYGEN and CARBON ISOTOPES in LIMESTONES

PART II- RENISON CARBONATES

CHAPTER 9: TEMPORAL AND REGIONAL SETTING

CHAPTER 10: EVIDENCE OF COOL WATER ORIGIN FOR DOLOMITE

CHAPTER 11: CARBON ISOTOPE CHEMOSTRATIGRAPHY

CHAPTER 12: HYDROTHERMAL ALTERATION: SOURCE OF THE FLUIDS

LIST OF FIGURES

CHAPTER 4

CHAPTER 5

CHAPTER 6

CHAPTER 7

CHAPTER 8

CHAPTER 9

CHAPTER 10

CHAPTER 11

CHAPTER 12

CHAPTER 13

LIST OF TABLES

LIST OF APPENDICES

PART I

MOZDURAN FORMATION

CHAPTER 1

INTRODUCTION

CHAPTER 1

INTRODUCTION

Carbonate rocks are widespread throughout the world and comprise significant components of the earth's landscapes. Formed throughout geological history, they are host to many economically important deposits. Whilst the economic significance of carbonate rocks are not under question, the precise origin and diagenetic aspects of these carbonates is less clear.

This thesis is a study into the origin and diagenetic history of carbonates, using two very different economically significant areas. As these deposits vary enormously in age and geographic setting, the thesis is structured accordingly: part (1) deals with the Upper Jurassic carbonates from north eastern Iran, which constitute a gas reservoir; and part (2) discusses the Neoproterozoic carbonates of the Renison mine area, Tasmania, Australia, which host ore deposits. In both part (1) and part (2), the same methods are applied to understand the processes involved in the formation and diagenesis of these carbonates.

The Upper Jurassic Mozduran Formation, which is composed mainly of a thick succession of limestone and dolomite, is the main gas reservoir in northeast Iran. The Formation ranges from 120 m to over 1100 m in thickness and is well exposed on the eastern part of the Kopet-Dagh Basin in the Sarakhs area (Fig.1). Due to limited published studies on these carbonate successions, detailed sedimentological, paleontological, petrographic and geochemical analysis have been carried out to interpret the origin, composition and diagenetic history of these rocks. The brachiopod assemblage from the Mozduran Formation was studied for age determination and paleogeographical interpretation. Petrographic, elemental and isotopic evidence are used to reconstruct the original carbonate mineralogy and diagenesis of these rocks. The present study proposes $\delta^{18}O$ and $\delta^{13}C$ criteria that involve the determination of lines of equilibrium for aragonite

and calcite as a function of temperature. Recent and ancient (Jurassic and Ordovician) average $\delta^{18}O$ values of seawater and $\delta^{13}C$ values of atmospheric CO_2 and seawater have been used to differentiate aragonite from calcite. The study of the Mozduran carbonates provides a new insight into the controversy surrounding the occurrence of calcite versus aragonite mineralogy. This variation through Phanerozoic time can be related mainly to the influence of seawater temperature.

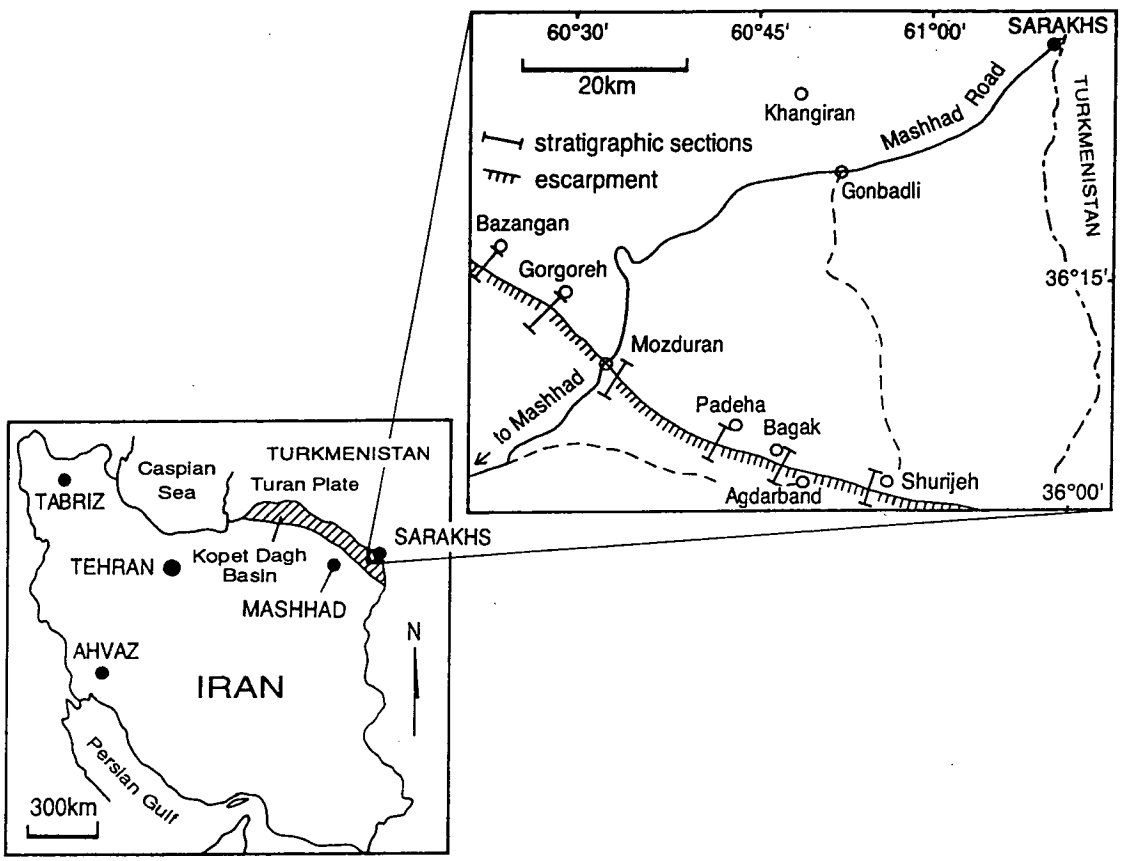

Figure 1.1. Location map of the study area and the sections studied.

The Neoproterozoic Renison dolomites are associated with significant tin ore deposits in western Tasmania. Detailed studies of these carbonate rocks will help in understanding: the origin of dolomites; textural and chemical modifications in the host rocks during the passage of hydrothermal fluids; source and temperature of fluids; timing of dolomitization; and the relationships to mineralization and extent of fluid/rock interaction. An attempt has been made to use carbon isotopes along with oxygen and trace element values of least-altered dolomites to test chemostratigraphy at the Renison mine area and resolve a controversy about the age of these deposits. As some of the least-altered dolomite

samples, which are not affected by hydrothermal fluids, have very heavy oxygen and carbon isotopic values, their documentation makes a significant contribution to the recognition of cold-water dolomite. The results of these investigations are presented in Part II (Chapters 9, 10, 11, 12 and 13).

1.1 Aims and Scope of Mozduran Project

The aims of this study are to:

- determine original carbonate mineralogy
- document the facies variation and inferred depositional environments
- investigate the diagenetic history of the Mozduran carbonates based on petrography and geochemical criteria
- investigate the origin and mechanism of dolomitization.

1.2 Previous work in the Kopet-Dagh Basin

The Kopet-Dagh Basin has received attention from petroleum geologists over the past few decades, as it comprises a thick continuous sedimentary succession of over 10 000 meters from Mesozoic-Tertiary time, which provides favorable conditions for the generation and accumulation of hydrocarbons.

The first study in the eastern Khorasan Provinces was undertaken by Griesback (1887). Reeves, Buie and Wilson (1937) were the first to publish an introductory report on the general stratigraphy of eastern Kopet-Dagh Basin and present a small scale geological map of the Sarakhs area. This was the only map of the Khangiran Anticline until 1962. Preliminary studies of the western Kopet-Dagh Basin were undertaken by Tompson, Hotchkiss and Afshar-Harb (1937). Goldschmid and Fakhrai (1952) from the National Iranian Oil Company visited the Sarakhs area and suggested it contained promising prospects for petroleum exploration.

Pern and Jahanbegloo (1956) presented a detailed stratigraphic section of the Sarakhs sediments in the Abderaz and Qorgoreh localities. The formation name in the Sarakhs area, for Mesozoic and Cenozoic rock units, was introducted for the first time by Ansari and Afshar-Harb (1961). A brief history of geological exploration and geology of the Sarakhs area and the Khangiran gas field was then published by Afshar-Harb (1970). This was the first detailed description of the sediments in the Kopet-Dagh Basin. Kalantari (1969) studied foraminifera from the Middle Jurassic-Cretaceous successions of the Kopet-Dagh region.

Madani (1977) made a detailed study of the sedimentology and stratigraphy of the Lower Jurassic sediments (Kashaf Rud Formation). Huber

(1978) presented a small scale geological map of north-east Iran and discussed the general stratigraphic history of the Kopet-Dagh Basin. Regional investigation of the stratigraphy, tectonics and petroleum geology of the Kopet-Dagh region was carried out by Afshar-Harb (1979). He published a small scale (1:250,000) geological map of the Sarakhs area in 1982. Ruttner (1983) reported the pre-Liassic basement of the Aghdarband area, eastern Kopet-Dagh range, and presented a paper (1988) on coal deposits of Aghdarband in the second Mining Symposium in Iran. Adabi and Harami (1986) studied the geomorphology of the eastern Kopet-Dagh Basin. Kalantari (1987) made a biofacies map of Kopet-Dagh region. Moussavi-Harami (1989) proposed a sedimentary environment for the Upper Jurassic sediments in eastern Kopet-Dagh Basin. Eftekharnezhad and Behrozi (1989) proposed new evidence to consider Kopet-Dagh range as a northern extension of the Afro-Arabian Paleozoic platform.

More recently, numerous studies of various aspects of the Kopet-Dagh sediments have been carried out by some researchers including: Moussavi-Harami and Brenner, 1990, 1992, 1993; Lasemi, 1992, 1996; Mahbobi and Lasemi, 1992; Adabi, 1991, 1992; Adabi and Rao, 1991; Adabi and Rao, 1996; Adabi and Ager (in press).

1.3 Methods of Study

1.3.1 Field methods

Field work for the study of the Mozduran carbonates was carried out during the field seasons of early 1989, 1991, and 1992. Six continuous stratigraphic sections were measured by tape, normal to the strike, in very steep cliffs within a distance of about 65 km.

Samples were collected near significant lithologic changes within the stratigraphic succession of the Shurijeh, Bagak, Padeha, Mozduran, Gorgoreh and Bazangan sections. Lithology, texture, primary and secondary structures and fossils were noted in their corrected vertical position in the field notebooks at a scale of $^{1}/_{500}$. Dolomite rocks were easily recognized in the outcrops due to their yellow to brown colour and lower effervescence after using 10% HCl. The color codes used for hand specimen descriptions are from the Geological Society of America Rock Color Chart (1991) and refer to wet cut faces.

1.3.2 Laboratory methods

1.3.2.1 Petrographic and sedimentological analysis

About 600 uncovered polished thin sections were prepared for the study of Mozduran carbonates. Petrographic analysis was carried out on stained (Alizarin red-s and potassium ferricyanide solutions (Dickson, 1965; Lindholm and Finkleman, 1972), for distinguishing calcite, dolomite and ferroan carbonate. Peels were made to determine the texture of carbonates, using the cellulose acetate sheet method of Stewart and Taylor (1965).

Polished thin sections were examined using a conventional microscope to determine composition, texture and diagenetic features such as cementation, re-crystallization and dolomitization. The petrographic classification for carbonates used throughout this report follows Folk's (1959, 1962) limestone classification, and Folk's (1974 a) and Sibley and Gregg's (1987) classifications of dolomite size and textures respectively. Polished, unstained thin sections were examined under a cold cathode electron gun, using a Nuclide ELM-2B Luminoscope. Operating conditions for cathodoluminescence petrography were around 8KV beam energy and approximately 0.6 milliamps beam current. Selected uncovered etched thin sections were observed by a Phillips 505 Scanning Electron Microscope housed at the Central Science Laboratory, University of Tasmania. An accelerating voltage of 20 KV was used.

All stratigraphic sections were computer drafted using modified AUSLOG software. The Markov chain analysis, was performed on two custom-written BASIC programs, based on those of Powers and Easterling (1982) and Wells (1989). The Fischer plots, based on Sadler et al. (1993), were generated using a custom-written spread sheet.

1.3.2.2 Geochemical analysis

Isotopic and trace element studies are useful for understanding the depositional environment, diagenesis and source of fluids. Bulk-rock samples were powdered by a vibrating ring mill with a tungsten carbide head, and further finely ground by agate mortar, mainly for bulk sediment analysis.Various limestone components and dolomite types were separated for both oxygen and carbon isotope and major and minor element analysis, employing a microscope with a dental drill to extract calcite and dolomite crystals from polished slabs. Thick brachiopod shells were sampled for isotope and trace element analysis using needle and dental drills.

Powders of 131 limestone samples from the Mozduran Formation including: 70 bulk sediments; 29 micrites; 4 fauna; 7 intraclasts; 5 spherical grains (oolite, oncolites); 5 later diagenetic spars (vein calcite); 9 void filling cements and also 109 dolomite powders, including bulk, dolomite types and void filling cements from the Mozduran Formation, were dissolved in 1 Mole HCl for two hours and analyzed by Varian AA6 atomic absorption spectrometer for Ca, Mg, Sr, Na, Mn and Fe, using 0.125g samples. The level of precision in analysis was ±1% for Ca and Mg and ±5 ppm for Sr, Na, Mn and Fe (Robinson, 1980). GFS 401, GFS 402 limestone standards and the GFS 400 and NBS 88b dolomite standards were used to monitor the precision. Minor contamination from clay fractions can be expected for the iron results (Robinson, 1980). Press peels of 25 representative bulk-rock powders from the Mozduran Formation were made for insoluble trace elements in HCl such as Ti, K, Ba, Rb, using a Phillips PW 1410 automated X-ray fluorescence spectrometer at the Geology Department, University of Tasmania.

Insoluble residue powders of the Mozduran carbonates were analyzed by X-ray diffraction at the Tasmania Department of Mines to determine insoluble residue compositions. Representative powders of 23 relatively pure dolomite samples of the Mozduran Formation were also analyzed by the XRD technique, for identification of minerals and determining the mole percent Mg substitution in the dolomite lattice by shift of the d (112) peak as a measure of the dolomite stoichimetry (quartz and fluorite was used as an internal standard), using the curve of Goldsmith, et al. (1961). Cell dimensions of eight dolomite samples of the Mozduran Formation were measured for determination of ordered and disordered dolomites. These samples were run on an automated Philips X-ray diffractometer system: PW 1729 generator; PW 1050 goniometer; and PW 1710 printing recorder and microprocessor, with nickel-filtered copper radiation. Data capture and plotting were accomplished with CSIRO software and XPLOT for windows. These samples were calibrated with the addition of an internal standard of natural quartz. The qualitative mineralogy was determined by manual search-match methods. The eleven strongest peaks of the dolomites were used for cell dimension refinement by least-squares, using the Excel templates of Novak and Colville (1989).

Samples with less than 1% Mg were considered as limestone, and samples with more than 10% insoluble residue were not used in trace element interpretation. Carbonates with less than 10% insoluble residue were corrected to 100%.

For oxygen and carbon isotope analysis, 15mg of the powders of 141 limestone samples of the Mozduran Formation, including: 74 bulk sediments; 28 micrites; 6 fauna; 9 intraclasts; 4 spherical grains; 5 late diagenetic spars (vein calcite); 14 void filling cements; and also 114 dolomite powders including bulk, dolomite types and void filling cements, were allowed to react with anhydrous phosphoric acid (H_3PO_4) in reaction tubes in a vacuum at 25° C for limestone samples and at 50° C for dolomite samples for 24 hours respectively. The CO_2 extracted from each sample was analyzed for $\delta^{18}O$ and $\delta^{13}C$ values, using Micromass 602 D gas mass spectrometry at the Central Science Laboratory, University of Tasmania. These values are expressed in conventional per mil notation relative to PDB standard. The precision of data was established with duplicate analysis for both oxygen and carbon, and is ±0.1‰. $\delta^{18}O$ values in dolomite samples reacted with H_3PO_4 at 50° C are depleted in $\delta^{18}O$ by about 1‰ relative to samples reacted with H_3PO_4 at 25° C (Gao and Land, 1991). Therefore, $\delta^{18}O$ values for dolomite were corrected to 25° C by adding 1‰ from each measured $\delta^{18}O$ value to standardise the value. The data are analyzed for correlation and factor analysis using the Statview programme on a Macintosh computer.

Organic carbon of 20 selected limestone and 16 dolomite samples (~2g) was determined by weight loss on heating to 450° C for 24 hours (Krom and Berner, 1983). In this method, presence of sulfur (e.g., siderite or pyrite) may cause a weight gain in samples because sulfur may be converted to SO_2 and thus not give a true result. In order to determine the accuracy of the ashing technique, the ashed samples and untreated samples were analyzed for percentage of total carbon using the Carlo Erba Elemental Analyzer. The total inorganic carbon results in ashed samples, considering the weight loss percent, calculate back to actual weight percent. The total organic carbon (TOC) content was then determined by subtracting the inorganic carbonate carbon of ashed samples from the total carbonate carbon content of unashed samples. The Carlo Erba Elemental Analyzer gives an accuracy of about 0.15% for carbon, while Krom and Berner (1983) suggest an accuracy within ± 0.1%.

CHAPTER 2

TEMPORAL AND REGIONAL SETTING

CHAPTER 2

TEMPORAL AND REGIONAL SETTING

2.1 Mesozoic Climates

2.1.1 Introduction

Determining the origin of Upper Jurassic carbonates in the Kopet-Dagh Basin, requires an understanding of the global aspects of the Mesozoic, particularly Upper Jurassic climates, such as surface and seawater temperature, atmospheric conditions, sea level fluctuations and so on. Different aspects of Mesozoic climates are briefly discussed below.

Mesozoic paleoclimatology has been studied intensively for the last 25 years. Various models of temperature and sea level fluctuations have been proposed. During the Mesozoic Era, the earth was generally recognised as having a relatively warm, equable (uniform) and arid climate (Frakes, 1979; Hallam, 1985, 1993). However, recent paleoclimate modeling studies have shown that the Mesozoic paleoclimate was not equal because interiors of large continents, such as Pangaea, at high and middle latitudes, experienced cold to subfreezing conditions (Frakes and Francis, 1988; Sloan and Barron, 1990; Crowley and North, 1991). Tropical-subtropical conditions extended into mid-latitudes, and at high latitudes a temperate climate existed (Valdes and Sellwood, 1992). The majority of the data indicate an ice-free land throughout the Mesozoic, but Frakes and Francis (1988) have suggested some glaciation during the Jurassic at high northern latitudes and during the Cretaceous at high northern and southern latitudes. There are no proven glacial deposits of Triassic age.

In recent years the General Circulation Model (GCM) has been used for paleoclimate modelling (e.g., Sloan and Barron, 1990; Moore et al., 1992 a, b; Valdes and Sellwood, 1992; Valdes, 1993; Price et al., 1995; Valdes et al., 1995). The GCM is a mathematical simulation based on a set of complicated interrelated equations to estimate the changes in climate resulting from the changing of one or more parameters. More recently, paleoclimate models using an atmospheric GCM simulation, have been proposed to investigate the climate of the Upper Jurassic

(Moore et al., 1992 a, b; Valdes and Sellwood, 1992; Valdes, 1993; Valdes et al., 1995).

2.1.2 Jurassic climates

The start of the Jurassic period was more humid than the Triassic (lack of evaporite deposits in most areas, Frakes, 1979; Valdes and Sellwood, 1992), but this gradually changed and became more arid during the mid to late Jurassic, notably in southern Eurasia (Anderton et al., 1979; Hallam, 1975, 1985). This notable spread of aridity in southern Eurasia (Fig. 2.1) was related to orographic effects, resulting from the collision of the Cimmerian landmass and disappearance of Paleotethys, rather than due to a southward shift of Eurasia (Sengör et al., 1988; Hallam, 1993). Evaporites are known from: northern Europe (Valdes and Sellwood, 1992); the Arabian peninsula; the Purbeckian gypsum basin of northern France and southern England; the northern United States; and northern and eastern Africa (Frakes, 1979). However, it has been argued that such evaporites can precipitate in a hypersaline shallow epeiric sea without the climate necessarily being arid (Shaw, 1964). This means that evaporite distribution can be a function of the local sedimentary environment, rather than the regional climate.

Some evidence indicates a slight increase of temperature through the course of the Jurassic period (Hallam, 1993). As opposed to this, Frakes et al. (1992) argued that the occurrence of glacial dropstone deposits in northern Siberia marks the beginning of a cooler time from the mid Jurassic onwards. As the Upper Jurassic marked a time of significant geographic spread of carbonates and associated reef deposits, Hallam (1993) doubts the existence of the cool interval proposed by Frakes et al. (1992), from the mid Jurassic onwards.

The gradual increase in carbonate deposition through the Jurassic, such as in Germany, North America (Upper Jurassic Smackover Limestone), northwestern India and the north east of Iran (study area) may be partly due to gradual eustatic sea-level rises. The curve by Hallam (1975, Fig. 2.2) shows a more or less gradual transgression of the sea over the continents as the period progressed, interrupted by a notable regression only in the early Bathonian. It is shown in Fig. 2.2 that the Jurassic sea spread from an area of less than 5% at the beginning of the period, to almost 25% in the late Oxfordian (Hallam, 1975).

Haq et al. (1987) and Hallam (1988) proposed sea level curves for Jurassic time (Fig. 2.3). The curves are broadly similar and both record notable rises during the Sinemurian, Toarcian, Bajocian, Callovian, and Kimmeridgian. Small scale fluctuations were noted in both the Hallam (1988) and Exxon eustatic

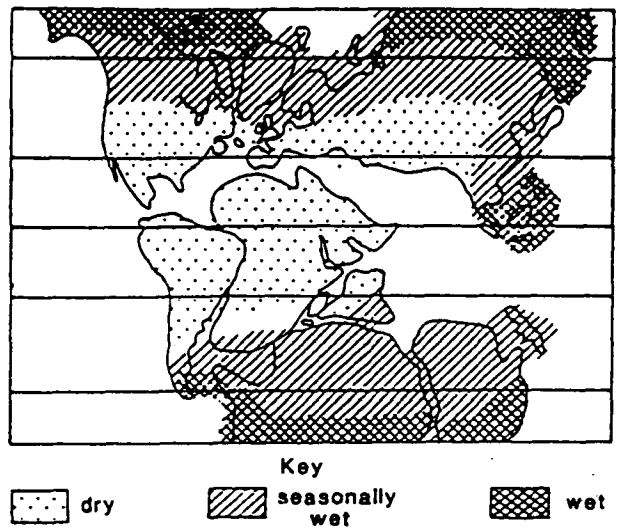

Figure 2.1. Continental humid and arid belts in the Upper Jurassic (from Hallam, 1993).

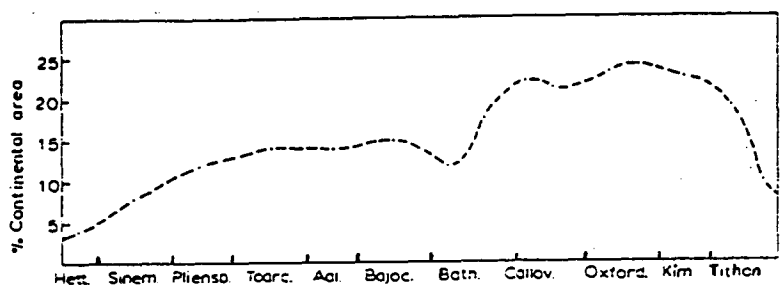

Figure 2.2. Proportion of continental areas covered by the sea through the Jurassic (from Hallam, 1975).

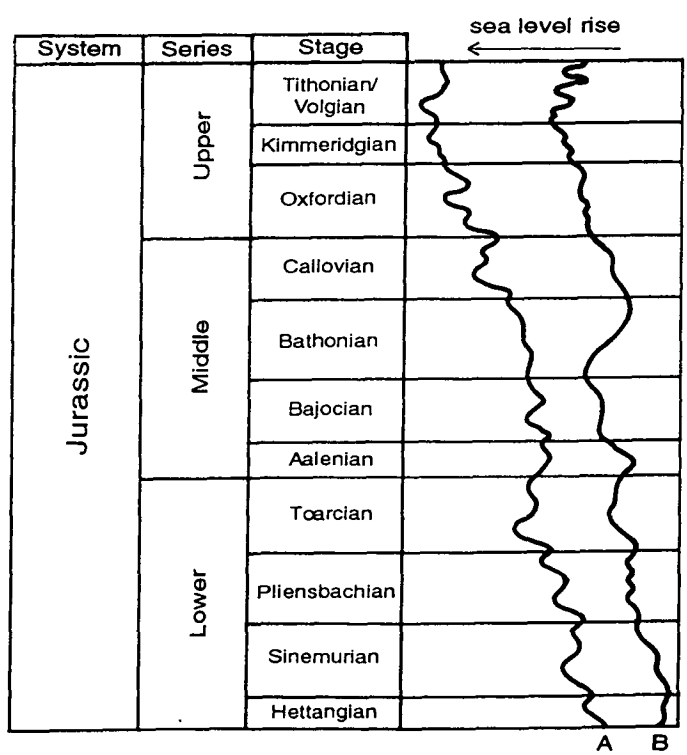

Figure 2.3. Comparison of latest Jurassic eustatic curves (A and B). (A) modified after Hallam (1988); (B) after Haq et al. (1987).

curves (Haq et al., 1987). The unusually noisy Kimmeridgian-Tithonian part of the Exxon curve is probably the result of regional tectonics, rather than rapid sea level oscillations (Hallam, 1988). The rise in sea level at a time when there were no polar ice caps is attributed to large scale sea-floor spreading, which began during the Jurassic, and resulted in a tectono-eustatic rise, due to increases in the volume of mid-ocean ridges (Hallam, 1978; Frakes, 1979).

2.1.2.1 Significance of the Upper Jurassic setting

Introduction

The Upper Jurassic, particularly the Kimmeridgian and Tithonian, were significant stages of the Mesozoic Era for several reasons (Moore et al., 1992 b). Firstly, this time represents an important interval of Pangea's tectonic disintegration (Fig. 2.4). North America completely seperated from Gondwana, and Gondwana was split into a northern and southern continent by the opening of the rift system in the proto-Indian Ocean. By the late Tithonian, the Tethys Sea and the Panthalassa Ocean (paleo-Pacific) were connected (Ross et al., 1992). Secondly, the Triassic-Jurassic high sea level stand occurs within this interval. Thirdly, Upper Jurassic rocks contain world-scale economically important deposits including oil, gas, coal, and evaporites.

The bio- and litho- facies evidence of the Upper Jurassic indicates that the world was warm (Frakes, 1979; Hallam, 1985), with an expanded tropical zone (Hallam, 1985), largely ice-free continents (Frakes, 1979; Christie-Blick, 1982), and arid conditions within the interiors of the continents and in low latitudes (Parrish et al., 1982; Hallam, 1985, 1993). Extensive evaporite deposits have been reported from parts of northern Europe (Valdes and Sellwood, 1992) and as far as about 45° latitude in both hemispheres (Frakes, 1979) during the Upper Jurassic. Thick weathered evaporite deposits have been documented in the eastern Kopet-Dagh Basin by Adabi and Rao, 1991.

Tectonics and paleogeography

Long-term rises and falls in eustatic sea level have been attributed to the large-scale increase and decrease rates of sea-floor spreading (e.g., Pitman, 1978; Hallam, 1978; Frakes, 1979). A progressively rising sea level during the Jurassic period, reached a maximum in the Kimmeridgian throughout the world (Hallam, 1978; Haq et al., 1987). This correlates with widespread calcareous deposits in North Africa, the Middle East, the Americas, and many parts of Europe and is

clearly world-wide. The Exxon eustatic curve (Haq et al., 1987) shows that during the early Oxfordian, sea level corresponds to about 100 m, but during the Kimmeridgian (maximum sea level rise), sea level corresponds to about 175 m. From the late Kimmeridgian through to the late Volgian (late Upper Jurassic), sea level drops to about 25 m. During the Upper Jurassic there were high latitude seas in both hemispheres, a vast Panthalassa Ocean, and the tropical Tethys Sea, with two narrow, westward-trending arms (Moore et al., 1992 a, Fig. 2. 4).

Two rift systems started in the Tethys and moved westward (Rowley, 1992). Another rift system connected the Boreal Sea with the Tethys Sea (Ziegler, 1988). By late Jurrasic time, these three rift systems had fragmented the late Permian-early Mesozoic megacontinent, Pangea. These major plate tectonic events created new oceanic pathways and divided Pangea into three major continental segments: North America; Eur-Asia; and Gondwana (Fig. 2.4). Moore et al. (1992 a) concluded that the late Jurassic represented a late phase of disintegration for the megacontinent, Pangea. The maximum sea level rise during the Kimmeridgian (Haq et al., 1987; Hallam, 1988), is probably due to increased sea-floor spreading and rifting of the Pangean megacontinent. This caused widespread flooding of continental margins and the development of epicontinental seaways (Moore et al., 1992 a), particularly in the Eur-Asian continent (Ziegler et al., 1983; Hallam, 1988). The Kopet-Dagh Basin is an epicontinental sea which was formed due to maximum sea level rise during Upper Jurassic time.

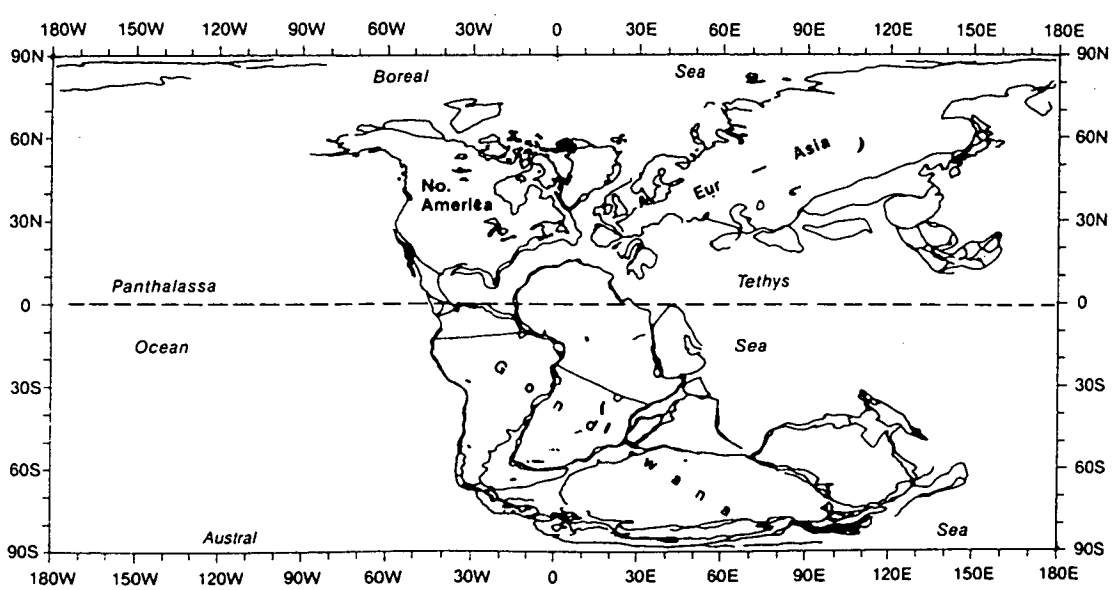

Figure 2.4. Paleogeography during the Kimmeridgian-Tithonian (copied from Moore et al., 1992 a).

Atmosphere

A greenhouse effect may have existed during the Upper Jurassic. Carbon dioxide in the atmosphere is a greenhouse gas (Berner, 1990; Moore et al., 1992 a, b), therefore, changes in CO_2 concentration over time will change global climates. As is well known, an increase in CO_2 during the past century, due mainly to human activities, has caused global warming.

Budyko and Ronov (1979) and Budyko et al., (1985) produced phanerozoic curves of atmospheric CO_2 levels, using compilations of continental volcanism as the source of CO_2 and the formation of carbonates as the CO_2 sink. For the Upper Jurassic the atmospheric CO_2 concentration was 2100 ppm which is about 7.5 times the present level (280 ppm). The 280 ppm CO_2 value equals that of the atmospheric CO_2 during the last interglacial and the Holocene, to the pre-Industrial level (Barnola et al., 1987; Kuo et al., 1990). Berner (1990) calculated the level of atmospheric CO_2 during Phanerozoic time from a weathering feedback function for silicate minerals. He found that during the Upper Jurassic, the CO_2 concentration ranged from about 900 to 1200 ppm, which is about 3 to 4 times that of the present day value. Thus, during the Upper Jurassic, the world possessed an enhanced greenhouse effect. However, the calculated Upper Jurassic atmospheric PCO_2 level, based on the heaviest $\delta^{13}C$ values of micrite in the Mozduran limestons (as discussed later in Chapter 7), gives slightly lower PCO_2 levels (0.5‰) than present day values.

Surface temperature

Vadles and Sellwood (1992) predicted an annual average surface temperature of 20° C for the Kimmeridgian, relative to an assumed annual average present day surface temperature of 14° C. The mean surface temperature from the GCM, around the Kopet-Dagh area, is about 22° C (Vadles and Sellwood, 1992). Predicted surface temperatures close to the Kopet-Dagh Basin, with variable topography range within 15 to about 20° C in winter, and around 30 to 40° C in the summer time (Moore et al., 1992 b). This indicates large surface temperature fluctuations.

Rainfall

Several workers have predicted annual average rainfall during the Upper Jurassic. The following discussion applies their interpretations to the Kopet-Dagh Basin. Valdes and Sellwood (1992) have shown that the large scale rainfall, which dominated over the land, has decreased (Kimmeridgian, 0.30 mm/day;

present day, 0.65 mm/day), but convective rainfall, which dominated over the ocean increased (Kimmeridgian, 2.3 mm/day; present day 1.7 mm/day). This model shows that close to the Kopet-Dagh Basin, average rainfall during the Kimmeridgian was about 1.5 to 2 (mm/day).

Parrish et al. (1982) were the first to qualitatively interpret the annual rainfall over land and compared the results with the distribution of coals and evaporites for the Upper Jurassic (Volgian). In the predicted rainfall distribution map (Parrish et al., 1982) , the Kopet-Dagh Basin falls within the moderately low rainfall zone.

The General Circulation Model (Moore et al., 1992 a) results show low precipitation near the Kopet-Dagh Basin. A total annual precipitation of <500 mm calculated for this area is within the arid zone suggested by Hallam (1985, 1993) and Moore et al. (1992 a). In the GCM evaporite map (Moore et al., 1992 a), the Kopet-Dag Basin falls within the zone of high evaporation rates (~4 mm/day), and in the precipitation-evaporation (P-E) map, the Kopet-Dagh area shows negative values (P-E <0). It was suggested that towards the end of the Jurassic period there was an extensive northward spread of the low-latitude arid zone into a large area of Europe and south Central Asia, marked by abundant evaporites, unlike the early and mid Jurassic, in which coals and ironstones were widespread (Hallam, 1985, 1993, Fig. 2.1). The Kopet-Dagh Basin was located in the subtropical zone during the Upper Jurassic, and evaporite deposits have been reported in this basin (Adabi and Rao, 1991).

2.2 Regional Geology (Kopet-Dagh Basin)

2.2.1 Introduction

The Kopet-Dagh sedimentary basin is located in northeastern Iran (Fig. 1.1) and formed during the early Mesozoic. From mid Jurassic times onwards the basin was covered by a widespread Mesozoic epicontinental sea (Berberian and King, 1981), which marks a period of marine transgression and water deepening over much of the western portion of the Kopet-Dagh Basin. This has been linked with widespread subsidence. The basin acquired a thick sequence (about 10 km) of almost continuous shallow marine to continental sedimentary rocks, ranging from Jurassic to Oligocene in age, with no major sedimentary breaks or volcanic activity, providing a favorable condition for the generation and accumulation of hydrocarbons. Late Miocene uplift brought the Kopet-Dagh rocks along the present day outcrop belt.

2.2.2 Economic significance

A reserve of about 500 billion cubic meters of gas was discovered in late 1960 in the Upper Jurassic and Lower Cretaceous sediments in the Khangiran Anticline (Afshar-Harb, 1970). This structure is located near the Khangiran village in the north-eastern part of Sarakhs area (Fig. 1.1). The Khangiran anticline is about 30 km long, with a maximum width of 15 km. This structure has two different gas horizons. The main reservoir is in the Upper Jurassic Mozduran Formation, which consists mainly of a thick sequence of dolomite, dolomitic limestone, and limestone. The upper smaller gas horizon is in the Lower Cretaceous siliciclastic Shurijeh Formation (Afshar-Harb, 1970). Thick shale intervals, and in some localities gypsum, provide good cap rocks, and the hydrocarbon source rocks in this part of the basin are believed to be the marlstones of the Middle Jurassic Chaman-Bid Formation (Fig. 2.6). According to the paleotemperature analysis of Afshar-Harb (1979), and the fact that gas traps were formed during the late Alpine Orogeny (about 10 Ma), when the basin was uplifted and deformed, these source rocks reached thermal maturity in the late Paleocene (about 50-60 Ma), and gas migration into the present structures took place no earlier than 10 Ma (Moussavi-Harami and Brenner, 1992).

2.2.3 Tectono-sedimentary history

The Kopet-Dagh sedimentary basin (around 600 km long and 200 km wide), formed as an intracontinental basin in northeastern Iran after the Middle Triassic (early Kimmerian) Orogeny, when the Iran and Turan plates had apparently closed (Berberian and King, 1981).

During Liassic time, the Iranian-Kopet Dagh-Turanian landmass was covered unconformably by Liassic coal-bearing fluvial-deltaic to shallow marine deposits (Kashaf-Rud Formation, Madani, 1977). This unconformity between Triassic and Jurassic rocks of the Kashaf-Rud Formation, which is visible in the Aghdarband region (Fig. 1.1) at the base of the eastern Kopet-Dagh Mesozoic sedimentary sequence, occurred in the late Hercynian-early Kimmerian tectonic phase (Huber, 1978). This indicates a united Iranian-Turanian landmass in late Triassic-early Jurassic time. Beznosov et al. (1978) reported that late Jurassic marine carbonates covered the southern part of the Turanian plate. Eftekharnezhad and Behrozi (1989) considered that the Iranian part of the Kopet-Dagh was the northern extension of the Afro-Arabian platform, had an Epi-Baikalian basement, and was not the southern extension of Hercynian Turan plates, as proposed by many authors in the past. Based on Upper Jurassic

brachiopods, Adabi and Ager (in press) concluded that in late Jurassic times, Iran was part of the European plate, as has been previously suggested for Turkey (Ager, 1988), on the basis of similar evidence from Mesozoic brachiopods. They also suggested that brachiopod affinities are all with extra-Alpine Europe and the Russian platform, in particular, the Urals.

The study area which is located in the eastern part of the Kopet-Dagh Basin (Fig. 1.1) contains a sequence of over 4000 m of Jurassic through to Tertiary sediments, deposited in a variety of marine to terrestrial environments, without any major sedimentary breaks or volcanic activity. A simplified geologic map of the eastern part of Kopet-Dagh Basin is given in Fig. 2.5. The thick, relatively continuous sedimentation ranging from the Jurassic to the Eocene, which has been subdivided into 15 different formations (Fig. 2.6), is recorded by the five major transgressive-regressive sequences (Afshar-Harb, 1970, 1979, 1982; Huber, 1978; Kalantari, 1987).

In the Sarakhs area, the first major marine transgression occurred during the Middle Jurassic (from the northwest towards the southeast), when a thick interval of siliciclastic sediments were deposited as deltaic and marine sedimentary complexes (Kashaf-Rud Formation, Fig. 2.6, Madani, 1977). This was continued through Tithonian time, when mainly marine carbonate sediments was deposited (Chaman- Bid and Mozduran Formation).

From near the end of the Jurassic through to the early Cretaceous (Neocomian), the sea withdrew from the eastern Kopet-Dagh Basin toward the northwest, due to an epeirogenic movement related to the late Kimmerian tectonic phase (Huber, 1978). This produced a thick interval of fluvial siliciclastic sediments (Shurijeh Formation) across the eastern part of the basin (Fig. 2.6, Afshar-Harb, 1979; Moussavi-Harami and Brenner, 1990, 1992). During the Upper Jurassic-Lower Cretaceous period, the shoreline of the Mesozoic sea was most probably near the eastern part of the Sarakhs area (Fig. 2.7).

The second transgression took place during the early Cretaceous (Barremian stage), when sea covered the whole area. The thick continuous sedimentation through the late Cretaceous (Tirgan, Sarcheshmeh, Sanganeh, Abderaz and Abtalkh Formation), suggests a stable marine environment during this time, except for a short period during the Turonian (Atamir Formation, Afshar-Harb, 1970, Fig. 2.5). In the eastern Kopet-Dagh Basin, there is a disconformity between Cenomanian and Turonian sediments (Atamir and Abderaz Formation), due to epeirogeny. This disconformity has been confirmed paleontologically (Kalantari, 1969) and is also recorded on the geohistory diagrams as a trending-upward

segment on the tectonic subsidence curve by Moussavi-Harami and Brenner (1992).

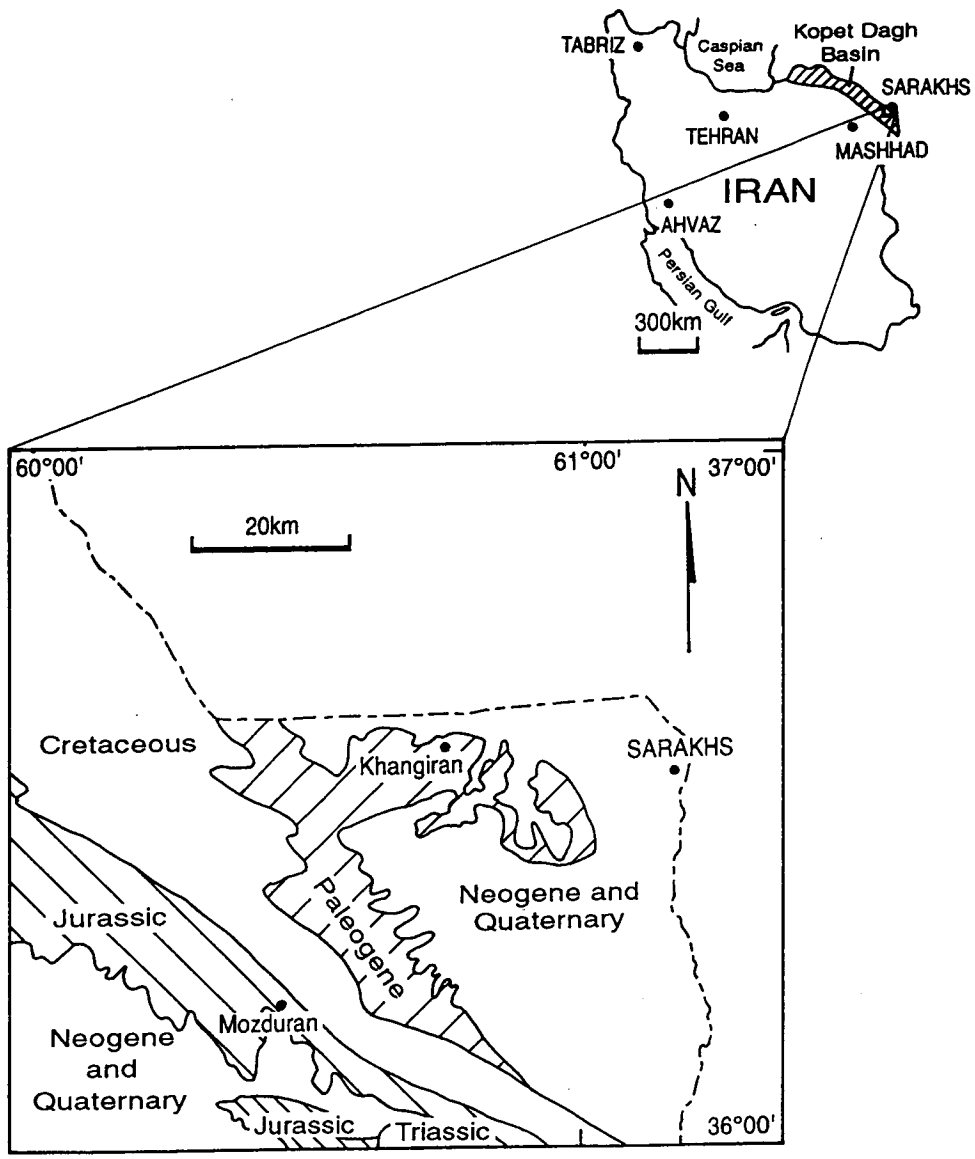

Figure 2.5. Simplified general geologic map of the eastern part of the Kopet-Dagh Basin (modified from Huber, 1978; after Adabi and Moussavi-Harami, 1986).

During the early Maastrichtian through to the Middle Maastrichtian, another regression phase started, due to tectonic uplifting, and the clastic sediments of the Nyzar and Kalat Formations were deposited (Fig. 2.6), suggesting a decrease in the depth of the Cretaceous sea. This phase ends as the Lower Paleocene red beds of the Pestehleigh Formation were deposited disconformably above very shallow marine Upper Cretaceous sediments (Afshar-

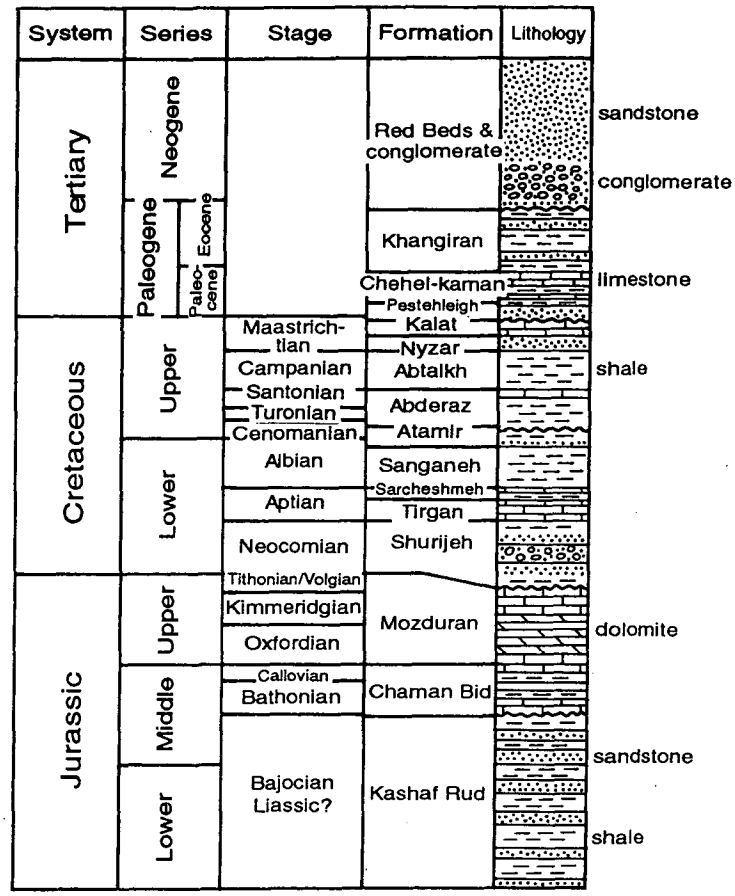

Figure 2.6. Generalized stratigraphic column of the eastern Kopet-Dagh Basin (modified after Afshar-Harb, 1979; Moussavi-Harami and Brenner, 1992).

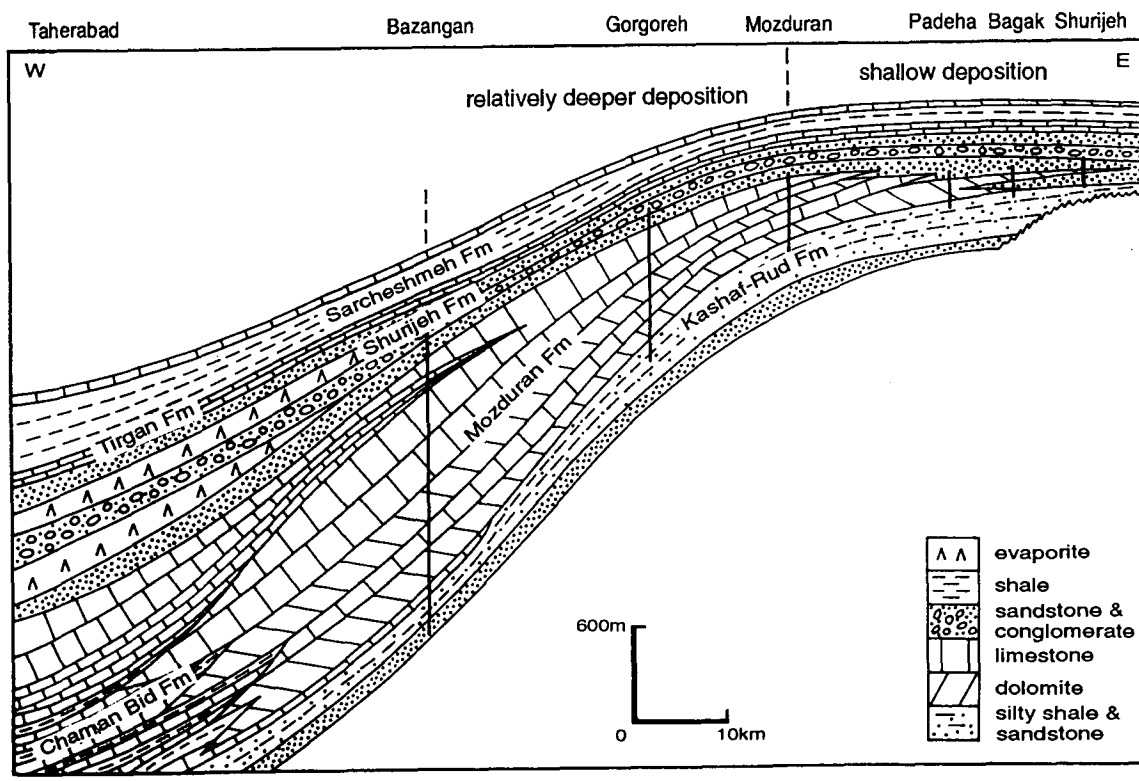

Figure 2.7. Stratigraphic cross section from east to west across the eastern Kopet-Dagh Basin (modified after Afshar-Harb, 1970).

Harb, 1970, Fig. 2.6).

The final marine transgressive phase occurred in the Sarakhs area during Middle Paleocene time, when thick marine sediments of the Chehel-Kaman Formation were deposited (Huber, 1978). From the very late Paleocene to late Eocene, relative sea level dropped, and very shallow-marine to shoreline siliciclastic sediments of the Khangiran Formation were deposited in the last phase of marine sedimentation in the eastern Kopet-Dagh Basin (Fig. 2.6).

The last regression phase of the Tertiary sea occurred during Oligocene (Miocene?) time and non-marine sediments (Red Beds) consisting of conglomerate, sandstone and shale, lie disconformably above the Khangiran Formation in the Sarakhs area, indicating that Kopet-Dagh sedimentation was dominantly non-marine during the Neogene (Fig. 2.6).

The basin started subsiding along major longitudinal faults during Jurassic time (Berberian and King, 1981). Huber (1978) suggested that the Kopet-Dagh fold belt was dissected by numerous active faults. Afshar-Harb (1979) recognized four major basement faults which were active at least since the Jurassic Period. These authors believe that the fault-controlled subsidence in the Kopet-Dagh allowed thick sediments to be deposited. Geohistory diagrams for the eastern part of the basin indicate that during most of post Jurassic time, the major factor contributing to basin subsidence was sediment loading, rather than tectonic subsidence, as highly compressible muds comprise approximately 73% of this part of the stratigraphic section (Moussavi-Harami and Brenner, 1992, Fig. 2.8). They suggested that sediment compaction created additional accommodation space, allowing more sediments to accumulate, thus adding to the sediment loading effect. Moussavi-Harami and Brenner (1992) have also shown that the base of the Upper Jurassic sedimentary strata subsided at a relatively high rate (98.2 m per m.y.), possibly due to tensional tectonic subsidence, which was greatest at the beginning of the Kopet-Dagh Basin formation. This high subsidence rate caused a dominance of carbonate over silisiclastic sediments. Similar rapid subsidence was reported by Afshar-Harb (1979) in the western part of the basin, where four longitudinal faults have been active since the Jurassic.

The total subsidence in the eastern Kopet-Dagh Basin was a result of relatively high rates of tectonic subsidence during the early stages of basin formation, coupled with high sediment supply rates, that continued until around the early Oligocene (Moussavi-Harami and Brenner, 1992). An apparent rise in eustatic sea level, according to curves published by Haq et al. (1987) and Hallam (1988), during some stages of the Upper Jurassic and Upper Cretaceous, also

allowed an increase in accommodation space.

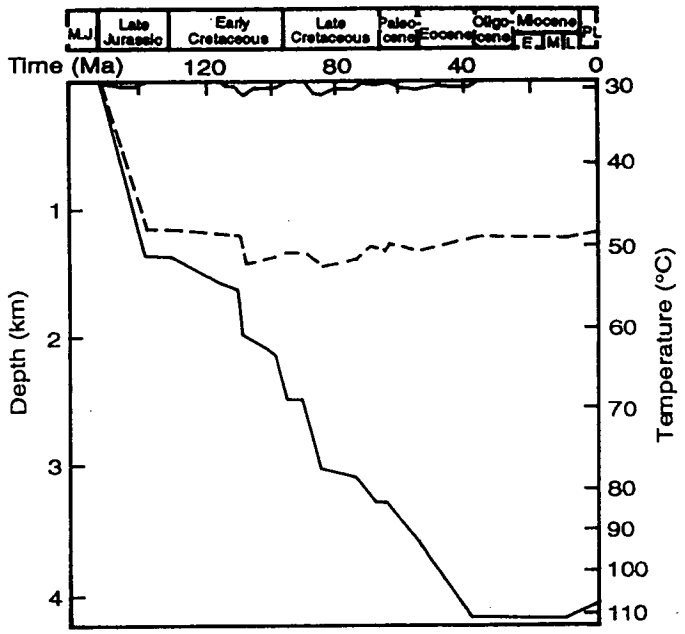

Figure 2.8. Geohistory diagram. Total subsidence (solid line) and tectonic subsidence and uplift (dashed line) for the base of the Upper Jurassic Mozduran Formation (modified after Moussavi-Harami and Brenner, 1992).

The Kopet-Dagh Basin was uplifted and deformed during the late Alpine Orogeny (late Miocene), creating anticline and syncline structures (with a strike SE to NW), such as the Khangiran anticlinal trap gas field.

In the study area, there are poorly sorted, gently folded Pliocene conglomerates, which unconformably overlie the older rocks, suggesting a post Miocene-Pre-Pliocene Orogeny in the area (Huber, 1978).

The northern dip-slopes and foot hills of the Kopet-Dagh were covered by a blanket of loess, brought by winds from the Qara Qum desert in Turkmenistan (former Soviet Union), after the Pleistocene period (Adabi and Moussavi-Harami, 1986).

2.3 Stratigraphy of the Mozduran Formation

2.3.1 Introduction

This study deals with the Upper Jurassic Mozduran Formation, located on the eastern part of Kopet-Dagh Basin in the Sarakhs area (Fig. 1.1), between latitudes ranging from about 36° 00' 00" to 36° 10' 00"N and longitudes ranging from 60° 30' 00" to 61° 00' 00"E.

The Mozduran Formation takes its name from the Mozduran village, where the sequence shows a good vertical development of strata, with sharp and distinctive lower and upper contacts. The type locality of the Mozduran Formation is east of the village of Mozduran, on the Mashhad-Sarakhs road (Fig. 1.1). The formation is well exposed along a steep rocky cliff in the Sarakhs area, and can be traced as continuous outcrops across the Kopet-Dagh Basin in the north east of Iran.

From west to east of the study area, the formation thickness decreases considerably (Fig. 2.7), grading into near-shore, relatively shallow-water, mostly terrigenous facies (Adabi and Rao, 1991). To the west, the Mozduran carbonates become thicker and interfinger laterally into off-shore and relatively deep shallow-marine facies (Chaman-Bid Formation, Figs. 2.6 and 2.7, Afshar-Harb, 1979; Kalantari, 1987). The very thick carbonate sequence in the study area, especially in the Gorgoreh and Bazangan sections, reflects a relatively deep basinal area within widespread epicontinental seas.

Therefore in this thesis, the phrase "the shallowest part of the basin" refers to the east of the study area (Fig. 2.7), which contains abundant mixed carbonate-siliciclastic and terrigenous facies, stromatolites, thick gypsum layers and oolite facies, and is stratigraphically thinner. On the other hand, "the relatively deeper part of the basin", located in the west of the study area, is characterized by a minor amount of terrigenous material, the absence of stromatolites and gypsum beds, the presence of abundant bryozoa, brachiopods, sponge spicules, forams such as Lagenedae and ahermatypic corals, thick marl facies and greater stratigraphic thickness.

The Mozduran Formation, especially in the eastern extremity of the basin, is succeeded conformably by the Shurijeh fluvial siliciclastics (Fig. 2.9 A, Moussavi-Harami and Berenner, 1990), and overly mainly deltaic to shallow marine sediments of the Kashaf-Rud Formation (Fig. 2.9 B, Madani, 1977). A sedimentary gap occurs between the Kashaf-Rud and Mozduran Formation of the Bathonian, and part of the Callovian stages. Callovian Mozduran carbonates overlie the Bajocian Kashaf-Rud Formation (Huber, 1978; Afshar-Harb, 1982).

The Mozduran carbonates, which are the main reservoir rock in the Khangiran structure, are comprised mainly of alternating sequences of thinly to thickly and massively bedded limestone, dolomitic limestones and dolomites, with locally thick layers of gypsum (Adabi and Rao, 1991). A few sandstone beds are present throughout the sequence. Dark greenish grey to red weathering calcareous shale layers are also frequently found interbedded with carbonate

Figure 2.9. View of the Mozduran Formation, which is succeeded by Shurijeh fluvial siliciclastics (red color, A), and overlies the Kashaf-Rud Formation (B).


A
Mozduran Formation
Shurijeh Formation
Mozduran Formation
Shurijeh Formation

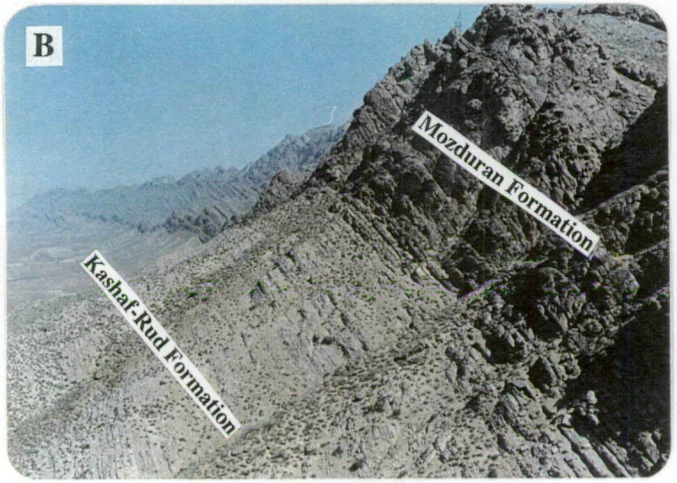
B
Mozduran Formation
Kashaf-Rud Formation

rocks in the succession. Marl interbedded with intramicrite and micritic facies are common mainly in the lower part of the Bazangan section. Dolomites have a distinctive bright yellowish brown colour in the outcrops and form a prominent steep escarpment in the study area. In the type locality, the lower part of the sequence is mainly composed of thick to massive grey dolomites with very rare fossils. The contacts between limestone and dolomite units are often wavy and irregular. The upper units are distinguished by an increasing predominance of fossiliferous limestones and decreasing dolomitization. The Formation is characterized by continuous bedding, laminations, large to small scale cross bedding, cross lamination, occassional moderate branching stromatolites and small stromatolitic domes, and abundant well preserved fossils.

Mozduran carbonates consist of a large diversity of skeletal and non-skeletal grains (mainly ooids, intraclasts and minor pellets), abundant sparry calcite cements, micrite, early and late diagenetic dolomites, and some evaporites (Adabi and Rao, 1991; Adabi, 1992, Adabi and Rao, 1996). During the Upper Jurassic, the Kopet-Dagh Basin was situated at a paleolatitude of about 20° N (Smith et al., 1981), in the subtropical zone. The predominance of shallow-water carbonates and clastics, underlain and overlain by siliciclastic sediments, all indicate a relatively low sea during much of the Upper Jurassic in the northeastern part of the Kopet-Dagh Basin (Adabi and Rao, 1991).

Six stratigraphic sections have been measured in the Shurijeh, Bagak, Padeha, Mozduran, Gorgoreh and Bazangan villages (Fig. 1.1). The type section of the Mozduran Formation is shown in Fig. 2.10. All the measured stratigraphic sections are included in Appendix 1 and briefly discussed below.

Shurijeh section

The Mozduran Formation in the Shurijeh section consists of medium to thick beds of light grey to grey, fine to medium grained quartzarenite, with interbedded, thinly to medium bedded, finely to coarsely crystalline dolomites. Dolomites are unimodal in size and contain a few scattered silt-size quartz grains. Sandstone consists mainly of quartz, some chert, mica, metamorphic rock fragments, weathered feldspar and an appreciable amount of rhombic dolomite. Terrigenous facies are very abundant in this section compared to other measured sections. In the Shurijeh section only a few very thinly to thinly bedded dolomitic limestone and micritic limestones are present. No fossils have been found in this traverse. The contacts with the underlying Kashaf-Rud Formation and the overlying Shurijeh siliciclastic red beds are sharp and distinct. The total thickness

of the Mozduran Formation measured in the Shurijeh section is 120.6 m.

Bagak section

The Mozduran Formation in the Bagak section consists of a sequence of medium to thick beds of dolomite, with minor sandstone and limestone in its lower part; and interbeds of dolomite, dolomitic and oolitic limestones, with minor very fine-to fine grained sandstone in the upper part. Relatively thick weathered gypsiferous layers are present in the middle part of the section. Sandstone is white to grey and medium bedded, with angular to subangular quartz grains. Cross laminations are common sedimentary structures in sandstone beds. Fossils consist of a few scattered small crinoid fragments and ostracods in the lower part, and large crinoid fragments, brachiopods and algae in the upper part of the sequence. The thickness of the Mozduran Formation in the Bagak section is 174.8 m.

Padeha section

The Mozduran Formation in the Padeha section consists dominantly of carbonates, characterized by interbeds of medium to coarsely crystalline dolomite, dolomitic limestone, and limestone facies such as oomicrite, oosparite and intramicrite, with minor intercalated shale and sandstone. The lower part begins with ~2 m of sandy finely crystalline dolomite and ~9 m of thickly bedded, fine grained, light olive gray, dolomitic sublitharenite, before abruptly changing to the thick sequence of carbonates. The limestones are generally grey to dark grey and well-bedded to masive. The limestone layers are characterized by continuous bedding, laminations and small scale cross lamination. The upper part of the sequence, consists of relatively thick weathered gypsiferous layers and oolitic facies. In contrast, dolomites are the principal rock types in the lower part of the Mozduran sequences. Stylolites are very common in both massive limestone and dolomite. The Mozduran Formation contains a moderate abundance of fossils including crinoids, brachiopods and bivalves. Ostracods, forams and calcareous algae are observed in thin section. The total thickness of the Mozduran Formation measured in Padeha is 180.7 m.

Mozduran section (type locality)

The Mozduran Formation takes its name from the Mozduran village in the north-east of the study area. The Mozduran Formation in its type locality (east of the village of Mozduran) consists of a thick alternating sequence of dolomite, limestone and dolomitic limestone, with minor interbedded calcareous shale and

sandstone (Fig. 2.10). The lower part of the sequence consists mainly of ~55 m of thick to massive, unimodal medium crystalline dolomites, which gradually transform to dolomitic limestone and terrigenous facies. The middle and upper part of the sequence consists mainly of limestone facies, which alternate with thinly bedded dolomite and pale to grayish red calcareous shale layers. Carbonate rocks range in color from light olive grey to pale and greyish olive. Gypsiferous layers, common in the Bagak and Padeha sections, are absent in the Mozduran type section, but evidence of calcite pesudomorphs after gypsum are present in a few samples. The limestone is characterized by small scale to medium size cross-bedding (Fig. 2.11 A), and smooth, thin microbial laminations (Fig. 2.11 B), which can be traced laterally into domal stromatolite (Fig. 2.11 C, D), showing spaced laterally linked hemispheroids (LLH-S, Logan et al., 1964). Stylolites, dissolution seams and cross-cutting veins are very common diagenetic features in the Mozduran type section. From the village of Mozduran eastwards, the thickness of the Mozduran formation decreases and changes to clastic facies.

The most abundant faunal assemblages of the Mozduran Formation at the type locality include brachiopods, pelecypods and crinoids. Gastropods, forams and algae are also present throughout the succession. Fossil fragments are rare at the base of Mozduran Formation, but gradually increase towards the top of the sequence. Brachiopod percent increases towards the upper part of the sequence, where it comprises ~80% of the fauna. Algae are also abundant in the upper most part of the succession and comprise ~45% of the biogenic components. The Mozduran Formation conformably overlies the Kashaf-Rud Formation and is conformably overlain by the Shurijeh Formation. The total thickness of the Mozduran formation at the type locality is 506.7 m (Fig. 2.10).

Gorgoreh section

The lower part of the Mozduran Formation begins with about 123 m of thinly to medium bedded, dark to medium grey, continuous cherty limestone facies (mainly biomicrite and intramicrite). Silicification is pervasive in most samples from the basal part of the sequence, and the limestone/silica ratio ranges from 60/20 to 60/40, reaching up to ~ 20/80. The limestone facies abruptly changes to a thick (~133 m) succession of the pale yellowish brown, medium to coarsely crystalline dolomite. Porosity in a few dolomite samples, observed in thin sections, reaches up to ~12%. The dolomite facies occur in the middle part of the formation, followed by alternating sequences of light olive grey, medium bedded dolomitic limestone and medium to coarsely crystalline dolomite. The upper part

Drawn 29-May-95

STRATIGRAPHIC SECTION OF MOZDURAN FORMATION – MOZDURAN TYPE LOCALITY

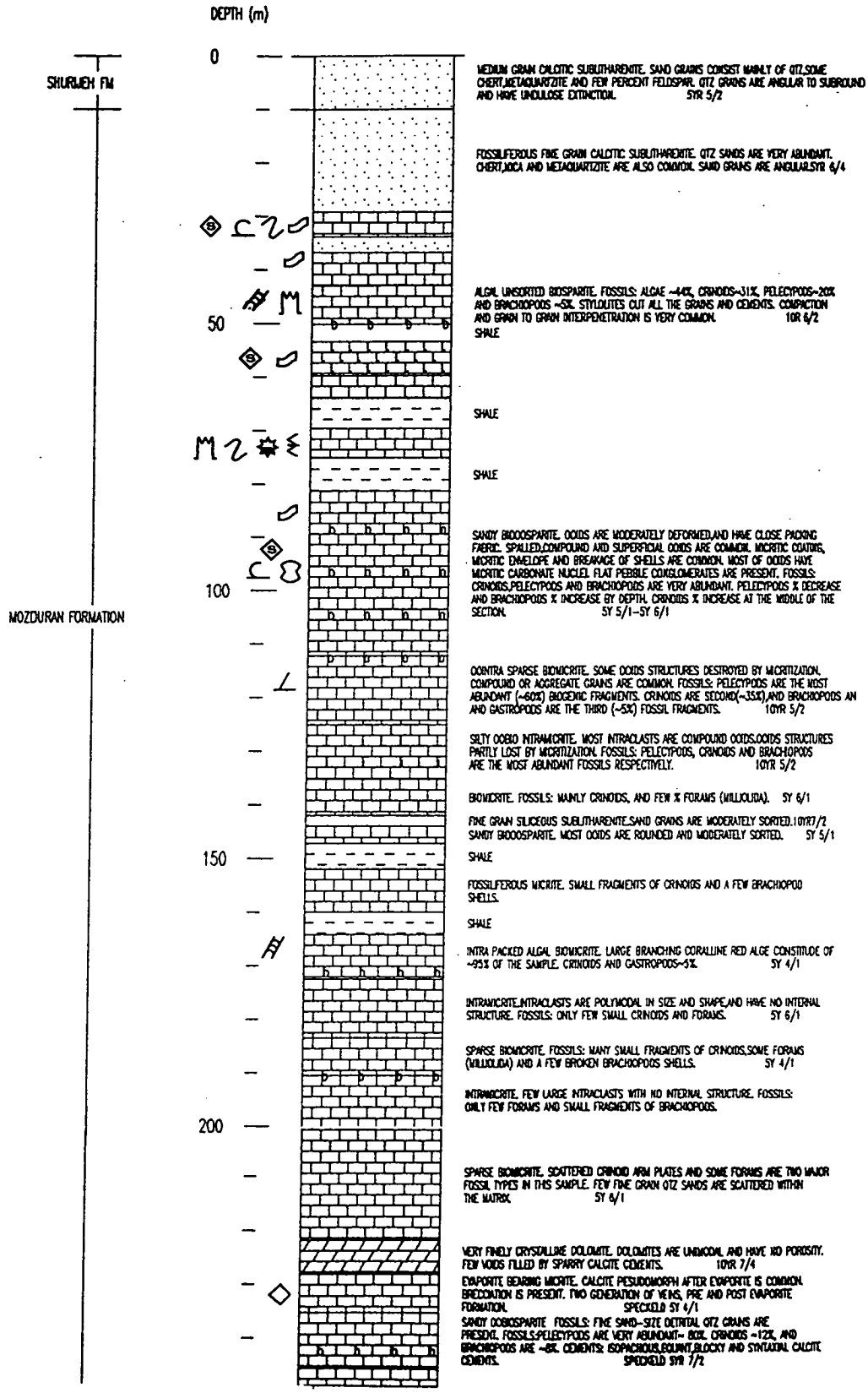

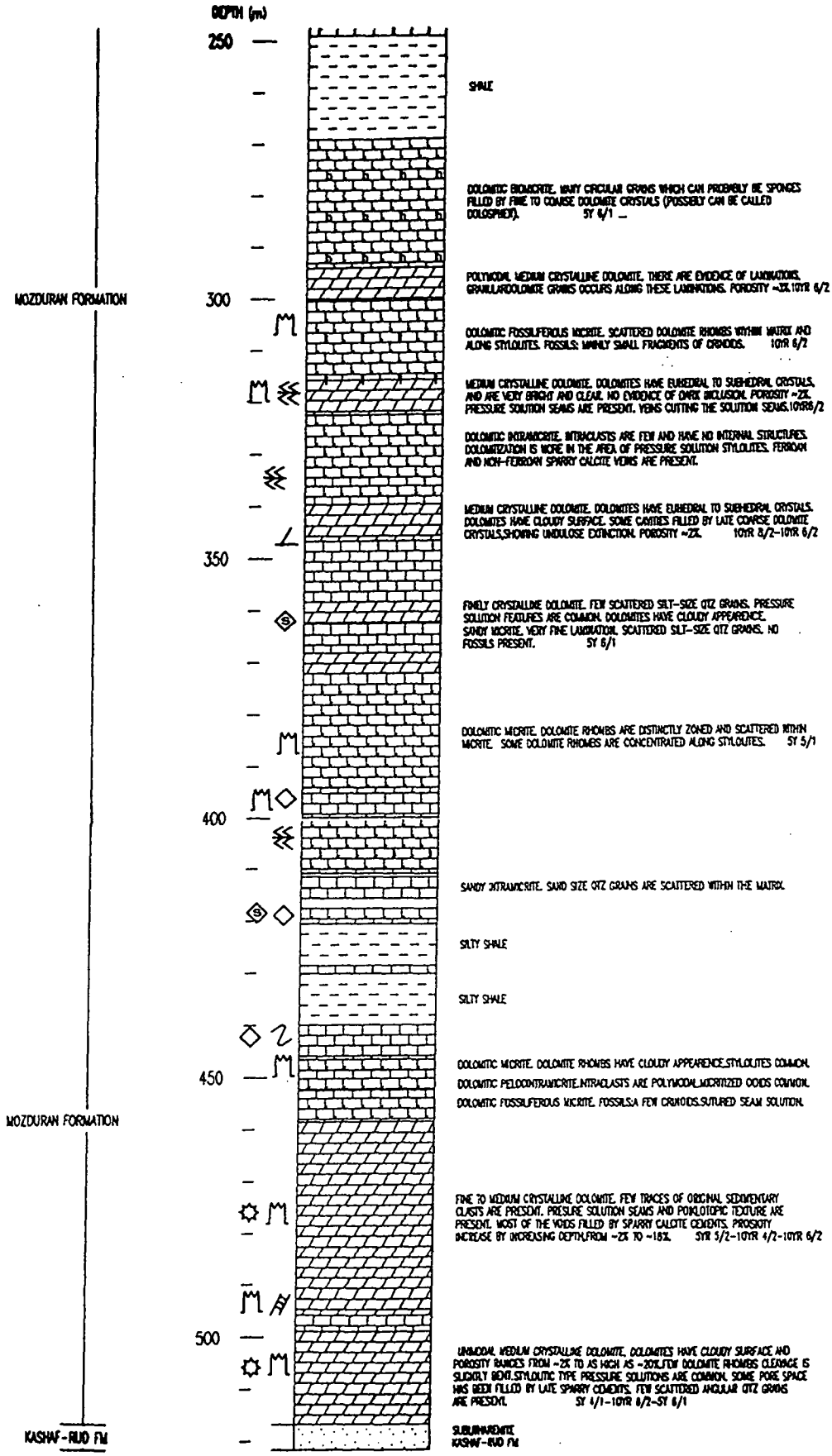

Figure 2.10. The type section of the Mozduran Formation, east of the village of Mozduran.

Figure 2.11. (A) Distinctive low angle cross-bedding (possibly hummocky cross-bedding) structure. (B) Smooth, thin microbially laminated stromatolite. These flat algal mats trace laterally into domal stromatolite. (C) Small scale domal stromatolite showing spaced laterally linked hemispheroids (LLH-S). (D) Close up of stromatolite consisting of spaced domes with some lateral linkage by slightly wavey or crinkly laminations.

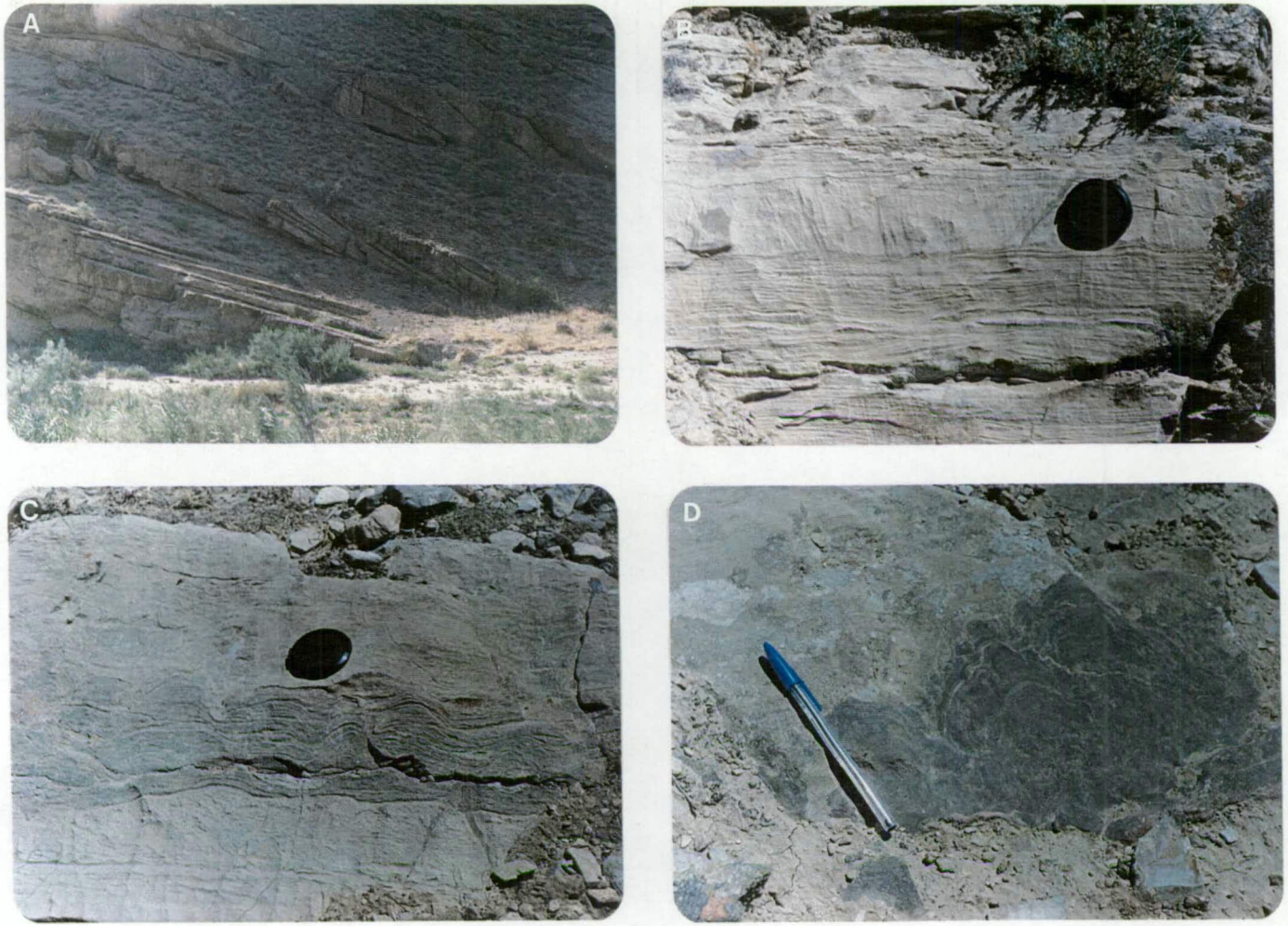
A
B
C
D

of the section consists mainly of ~150 m of medium light grey to pale brown limestone facies (intramicrite, oosparite, biosparite and biomicrite). Fine to relatively coarse lamination, continuous planar and parallel bedding, and cross stratification are characteristic features at this locality.

The Mozduran Formation contains abundant siliceous sponge spicules and crinoids in the lower part of the sequence. Brachiopods, crinoids, pelecypods and particularly bryozoa are the most common fossils in the middle and upper part of the formation. In a few samples, bryozoa comprise up to ~30% of the biogenic components. Small fragments of ostracods, forams (milliolida), solitary corals and algae are also present throughout the section. In the Gorgoreh section, crinoids are the most abundant fauna, followed by pelecypods, brachiopods, and bryozoa respectively. The Mozduran Formation has a gradational contact with the underlying Kashaf-Rud Formation and a sharp and distinctive contact with the overlying Shurijeh Formation. The total thickness of the Mozduran Formation in the Gorgoreh section is 701.8 m.

Bazangan section

The basal part of the Mozduran Formation in the Bazangan section is characterized by an alternating sequence of thinly to medium bedded dark to medium dark grey limestone facies, and thinly bedded argillaceous limestone. Silicification is common, particularly in the lower 47 m of limestone successions. The limestone beds have sharp bases and grade up to medium grey argillaceous layers. These limestones exhibit micritic textures and gradually transform to coarser calcarenite with abundant fossil fragments. The limestone and argillaceous-rich layers are followed by thick, medium crystalline dolomite layers, interbedded with thin to medium beds of light olive grey to light grey limestone facies (mainly intramicrite, pelmicrite and oomicrite). Oncolitic facies are also present in a few massively bedded limestones. The upper part of the Mozduran Formation consists mainly of light grey to greenish grey, medium to thick bedded limestone facies (cheifly oolitic, intraclastic and bioclastic facies), with minor marlstone and sandstone units. In the section studied, the Chaman-Bid Formation, which comprises relatively deep, shallow marine facies, interfingers laterally into the Mozduran carbonates. In a few limestone samples, evidence of gypsum pseudomorphs are present. Flat pebble conglomerate, geopetal structure, small scale cross beds and cross lamination with scoured surfaces, are common sedimentary structures in the Bazangan section. Stylolite, dissolution seams and cross cutting veins are very common diagenetic features.

The limestone beds in the lower part of the formation contain a moderate abundance of fossils, including crinoids and calcareous sponges. Brachiopods, bryozoa and corals are also present in minor amounts. Forams such as milliolida, globegerina and lagenid are observed in thin section. Fossil content decreases in the middle part of the sequence due to increasing dolomitization. In this section, brachiopods, bryozoa and crinoids are the most common fossil fragments. Pelecypods, ostracods and forams are also observed in thin section. The faunal assemblage in the upper part of the formation includes, in order of abundance, crinoids, brachiopods and bryozoa. Algal fragments are also present in a few limestone samples in the upper-most part of the sequence. The lower contact of the Mozduran Formation with the Kashaf-Rud Formation is clearly gradational and conformable. The upper contact with the overlying Shurijeh Formation is sharp and conformable. In the eastern Kopet-Dagh Basin, the thickness of the Mozduran Formation increases to the west of the Mozduran type section, where it reaches 1131 m at the Bazangan section (see Appendix 1).

2.4 Paleontology and Age

The Mozduran Formation contains a moderate abundance of well preserved fossils, including, brachiopods, echinoderms, solitary corals, microbial mats (stromatolite) and gastropods. Bryozoans and solitary corals are more abundant in the west of the study area (Gorgoreh and Bazangan sections), compared to the shallower shelf carobnates in the east. Fossils are generally rare or absent in the lower part of the sequence, and in the Shurijeh section in the east of the study area. A few ammonites are the only fossils present in the few meters above the base of the formation, but are difficult to recover. Brachiopod faunas are well preseved in a few thin limestone beds at the top of the sequence in the Mozduran section (type locality).

Foraminifera studied by Kalantari (1969) indicate that the Mozduran Formation ranges in age from Callovian to Kimmeridgian, but brachiopods studied by Adabi and Ager (in press), clearly indicate an early Tithonian-Volgian age, implying a slightly later age than that given by contemporary foraminifers (Kalantari, 1969). Adabi and Ager (in press) identified five different brachiopod species, namely:

1) *Moeschia subsella*, 2) *Uralella gigantea Makridin*, 3) *Torquirhynchia inconstans*, 4) *Torquirhynchia lehmanni* and 5) *Torquirhynchia speciosa* (Figs. 2.12 and 2.13). Systematic paleontology has been described in Adabi and Ager (in press). The brachiopod assemblage from the Mozduran Formation suggests a

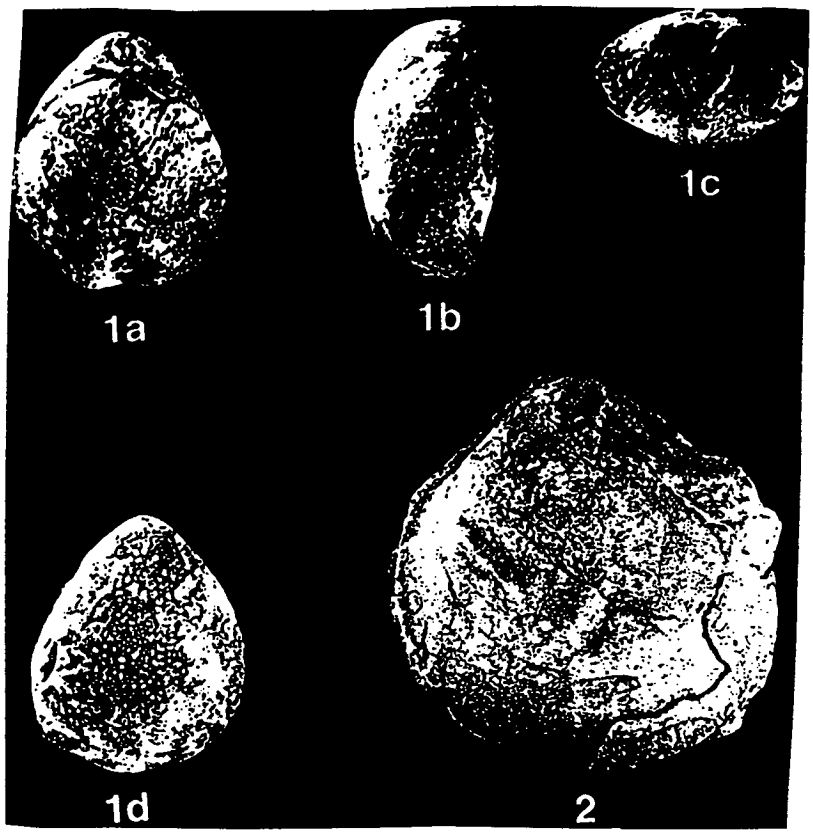

Figure 2.12. (1) a-d. *Mosechia subsella.* Dorsal, lateral, anteior (brachial valve uppermost) and ventral views (X 1 $^{1}/_{2}$). (2). *Uralella gigantea Makridin.* Ventral view of internal cast of pedicle valve (X 1). Photo from Adabi and Ager (in press).

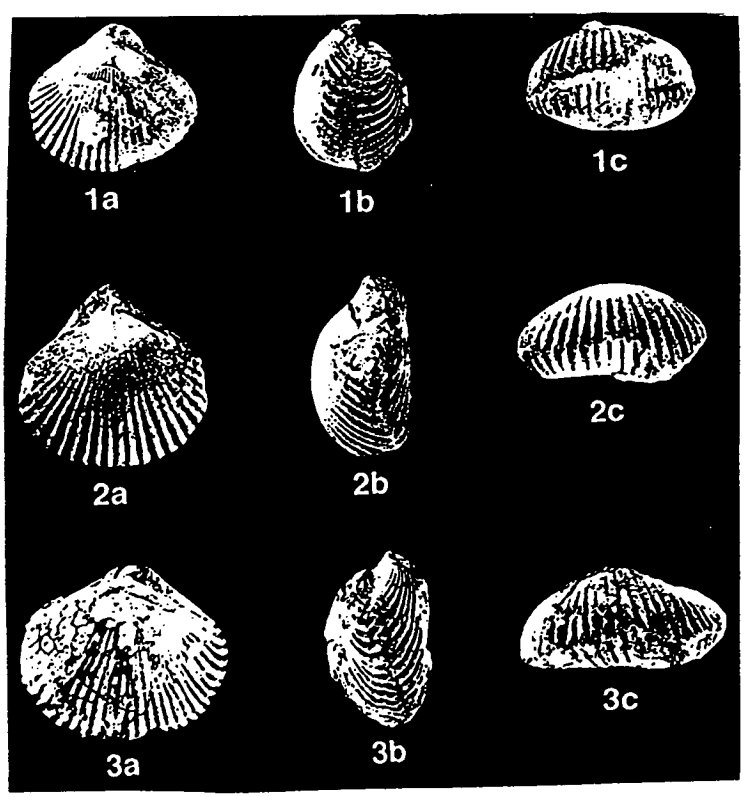

Figure 2.13. (1) a-c. *Torquirhynchia inconstans.* Dorsal, lateral and anterior views (the last with brachial valve uppermost, X 1 $^{1}/_{2}$). (2) a-c. *Torquirhynchia lehmanni.* Dorsal, lateral and anterior views (the last with brachial valve uppermost, X 1 $^{1}/_{2}$). (3) a-c. *Torquirhynchia speciosa.* Dorsal. lateral and anterior views (the last with brachial valve uppermost, X 1). Photo from Adabi and Ager (in press).

shallow water, high energy environment. These brachiopods are particularly interesting from the paleogeographical point of view. The brachiopod fauna shows affinities with European forms, especially those of the Boreal type from Russia, in particular, the Urals. There are no signs of Tethyan forms such as the pygopids, and nothing from the Ethiopian Province, which extended as far north as Sinai and the southern part of the Arabian Peninsula at this time (Adabi and Ager, in press). The traditional interpretation is that the boundary between the Tethyan-Boreal realms roughly follows latitude, therefore, the Boreal realm signifies a cooler climate. However, there are a number of arguments against this (Hallam, 1986; Doyle, 1987). It was suggested that the taxonomic diversity in belemnites not only reduced toward the poles, but appeared to increase northwards from the Boreal Atlantic to the Arctic Province (Doyle, 1987).

Contrary to existing theories, it is concluded that in the late Jurassic, Iran was part of the European plate, as has been previously suggested for Turkey (Ager, 1988), on the basis of similar evidence from Mesozoic brachiopods.

CHAPTER 3

SEDIMENTOLOGY

CHAPTER 3

SEDIMENTOLOGY

3.1 Microfacies Analysis

3.1.1 Introduction

Microfacies types document differences in the kind and significance of sedimentological and biological environmental factors (Flügel, 1982). Sedimentological features observed in the facies studied in the Mozduran Formation will be used in the interperatation of sedimentary environments. Quantitative sedimentological studies have been undertaken to detect and statistically verify cyclicity of the facies in the vertical succession, using Markov chain analysis, and non-random arrangements of bed thickness, using Fischer plots. These results will be discussed in the last part of this Chapter.

In the Mozduran Formation, nine microfacies have been identified: (1) lime mud facies (micrite, dismicrite, dolomitic micrite and fossiliferous micrite); (2) biofacies (biomicrite and biosparite); (3) pelmicrite facies; (4) intraclastic facies (intramicrite and intrasparite); (5) oolite (oomicrite and oosparite) and oncolite facies; (6) sandstone facies; (7) mudrock facies (shale and marl facies); (8) evaporite (weathered gypsiferous) facies; and (9) dolomite facies. Dolomite will be discussed in more detail in Chapter 8.

Microfacies I- Lime mud

This facies consists of micrite, dismicrite, dolomitic micrite and fossiliferous micrite. Rocks containing 99% lime mud and 0-1% bioclasts are classified as micrite. If the fossil content increases from 1-10%, it is regarded as fossiliferous micrite (Folk, 1974 a). Micritic rocks that contain over 10% dolomite of uncertain origin, are termed dolomitic, and if dolomite has a replacement origin, the term dolomitized is used. Disturbed micrite which contains sparry-filled voids of various origins is called dismicrite (Folk, 1974 a).

Dense fine-grained micrites comprise a conspicuous carbonate facies of the Mozduran Formation in all sections studied (Fig. 3.1 A). They form matrix in

many samples, fill cavities, interparticle porosities, and form geopetal structures (Figs. 3.1 B, C). Fenestrate or birds eye texture is present in this microfacies and is filled mainly by sparry calcite cement (Fig. 3.1 D). These structures have irregular shape and are irregularly distributed in the Mozduran carbonate sequences. They are ascribed to gas entrapment in the sediment, and desiccation, and are characteristic of intertidal-supratidal facies (Shinn, 1983). Micrite forms both distinct beds and microbial laminae within the stromatolitic limestone of the Mozduran Formation. Crystal size in fine grained micrites ranges from 5 to 10μm, while in coarser grained micrites range from 10-40μm. Occasionally, micrites due to diagenetic alteration, have been replaced by coarse mosaics of microspar (~10μm) and pesudospar (~40μm), possibly through aggrading neomorphism (Folk, 1974 a). However, Lasemi and Sandberg (1984), suggested that similarities between micrite and microspar crystals indicate their common origin through a one-step neomorphic process of calcitization, based on SEM studies of well lithified Pleistocene micrites from south Florida and the Bahamas. That is, the aragonite mud did not first calcitize to micrite and then alter to microspar by aggrading neomorphism. Early lithification of micrite is indicated by erosion and the formation of abundant micritic intraclasts (Fig. 3.6 D).

Scanning electron microscope studies have shown variation in size and shape of micrite crystals, with intercrystalline boundaries that are irregular, curved and sutured (Figs. 3.1 E-G). In samples from the shallowest part of the basin, SEM studies reveal evidence of aragonite relics in calcitized micrites (Figs. 3.1 E, F). The relics in highly polished (0.05μm alumina), very lightly etched (0.1% formic acid, Lasemi and Sandberg, 1984) samples have a higher brightness, probably in part because of the influence of the incorporated Sr^{+2} on the mean atomic number, and hence on back scattered primary electron emission (Sandberg, 1985). In contrast, the rarity of aragonite relicts and pits in samples studied from the relatively deeper part of the basin suggests a calcite-dominated precursor (Fig. 3.1 G, Lasemi and Sandberg, 1984). Aragonite relic retention, as seen in samples from the Mozduran type section (Fig. 3.1 E, F), is due to the fine scale of the alteration process (Sandberg and Hudson, 1983). It has been suggested that relic retention varies from about 15% to less than 1%. Variation in aragonite relic abundance is likely to be related to such factors as differences in rate of movement of the diagenetic front, saturation state with respect to aragonite, degree of protection by organic coating, and relative abundance of original mineralogies (Lasemi and Sandberg, 1984).

Figure 3.1. Thin section photomicrographs of lime mud facies.

A. Fossiliferous micrite. Micrite containing small coiled foram, sponge and echinoid spine. Thin section no. 23, Bazangan section.

B. Geopetal sediment within a pelecypod shell. Micritic sediment (oomicrite in this example) partially infilled the lower part of the cavity, with the space above finally filled by coarse drusy sparry calcite cement. The contact between micrite and sparry calcite cement indicates the horizontal plane at the time of deposition (white arrow). Geopetal surface indicates that the direction of "up " is to the northwest in the photograph. Thin section no. 27A, Bagak section.

C. Close up of a geopetal infill of a possible brachiopod shell. Thin section no. 66, Mozduran section.

D. Fenestrae or birdseye textures in pelmicritic facies. Fenestrae are filled by sparry calcite cement. Note irregular shape of fenestrae. Thin section no. 56, Bazangan section.

E. Scanning electron micrograph of highly polished micrite with aragonite relics. Thin section no. 26, Mozduran section.

F. Close up of different view of the same sample as photo E. Note the aragonite relic within the micrite (white arrow). This photo is very similar to Figs. 3 C and 5 C of Sandberg (1985).

G. Scanning electron micrograph of micrite, lacking any evidence of aragonite. Thin section no. 83, Bazangan section.

H. Calcitized pseudomorphs after evaporites in micritic facies. Note that a few pseudomorphs have monoclinic shape. Thin section no. 59, Mozduran section.

I. Close up of possible twin pseudomorphs of gypsum. Most evaporites are highly soluble and thus very susceptible to postdepositional removal by leaching. Note fabric selective inclusion-rich dolomite rhombs inside the twin pseudomorphs of gypsum. Thin section no. 31, Mozduran section.

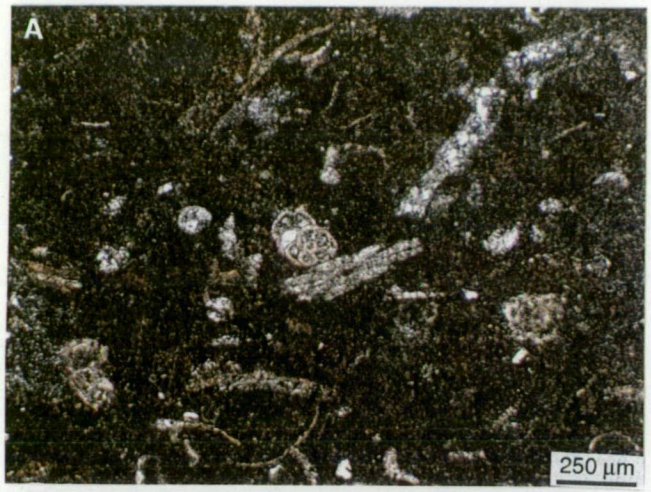
A
250 µm

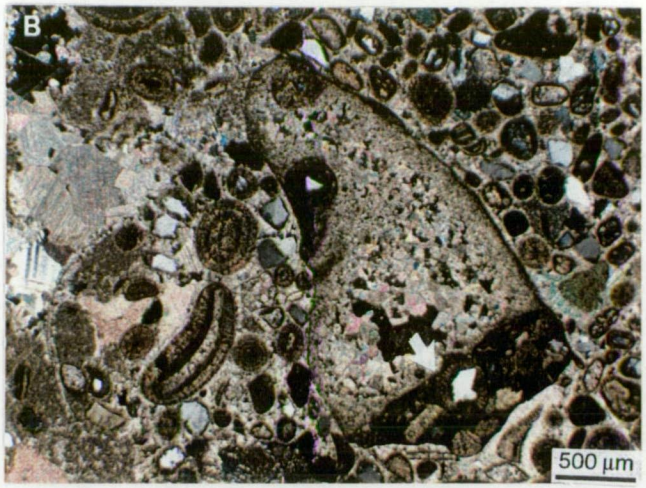
B
500 µm

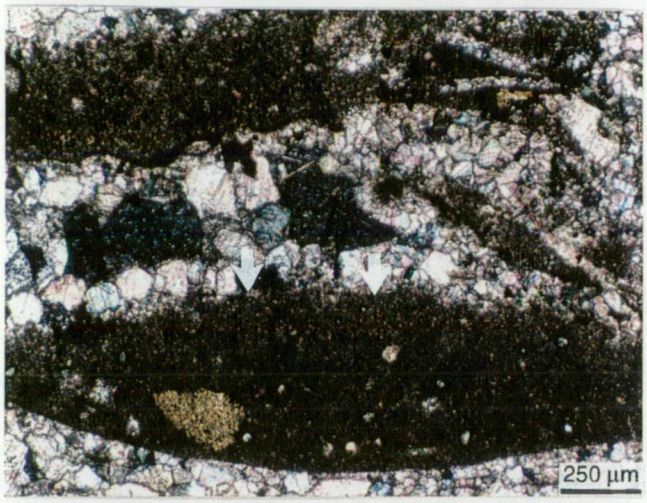
250 µm

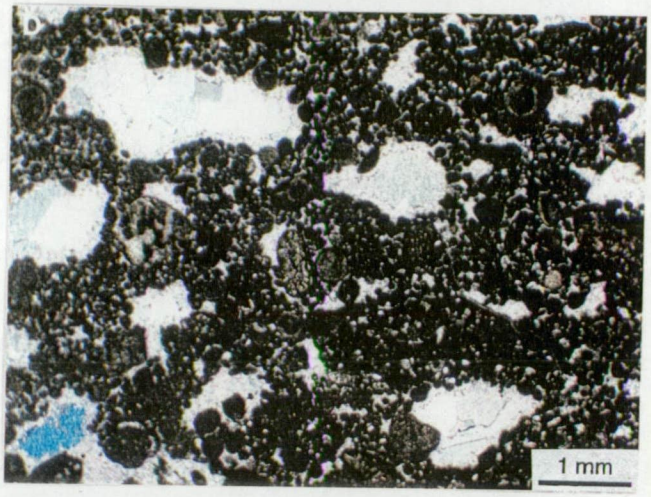
D
1 mm

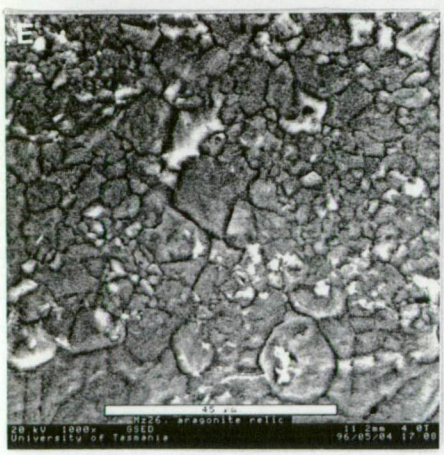
E

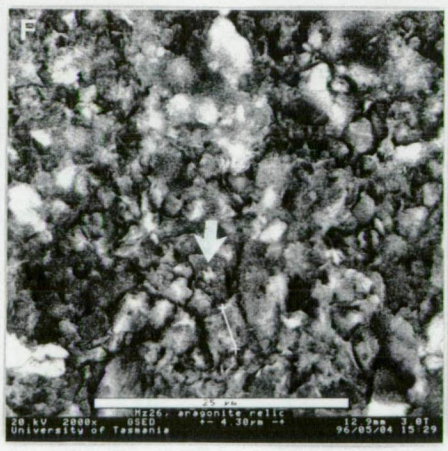
F

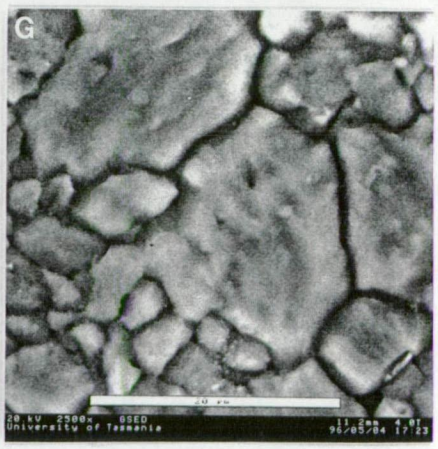
G

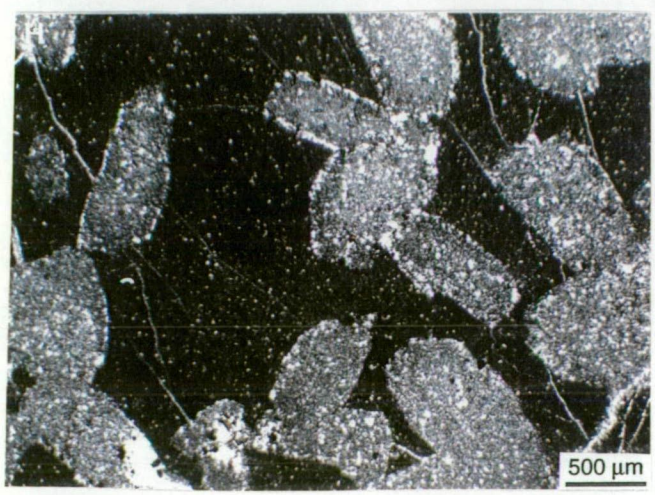
500 µm

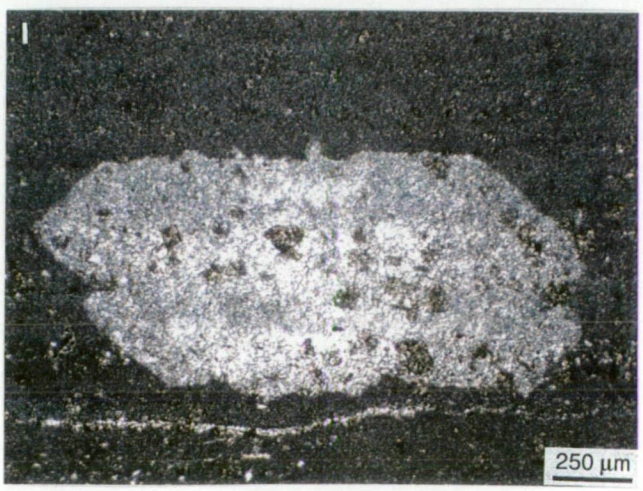
I
250 µm

The possible processes which have been responsible for carbonate mud production in the Mozduran limestones are as follow:

• direct precipitation of calcium carbonate as a result of evaporation of seawater. Such a mechanism has been postulated for much of the aragonitic mud accumulation on the Bahama Bank (Loreau, 1982). The occasional 'whiting' (drifting milky waters due to suspended aragonite needles) has also been suggested as actual inorganic precipitation of aragonitic mud on the Bahama Bank (Shinn et al., 1989). Whitings are known from other places such as the Persian Gulf and Florida Bay. As aragonite is the dominant mineralogy in the shallowest part of the basin and is also present in the relatively deeper part, it is more probable that micrites were the product of inorganic seawater precipitation.

• two other possible sources which have produced lime mud in the Mozduran Formation are the mechanical breakdown of skeletal grains such as molluscan and algal skeletones by waves and currents, and bioerosion of carbonate grains by boring organisms such as sponges (Neumann and Land, 1975, Loreau, 1982). As there are many bivalves, algae and sponges in the samples studied, these organisms could be responsible for carbonate mud production in the Mozduran limestones.

Lime mud microfacies generally consist of either about 90 to 100% lime mud, with 0-10% allochems, or 80% lime mud and up to 20% euhedral dolomites. Scattered silt-size subangular detrital quartz and a few hexagonal authigenic quartz crystals are present in a few samples. The proportion of micrite, bioclasts and dolomites are variable throughout the sequence. Micrites without bioclasts are more pronounced towards the eastern part of the basin where water depth is a minimum. Bioclasts in fossiliferous micrite in the shallowest part of the basin are composed mainly of a few scattered fragments of crinoids, gastropods, ostracods, brachiopod shells and scattered broken pieces of indistinguishable shell fragments. In the relatively deeper part of the basin, bioclasts comprise mainly forams, calcareous sponges and small fragments of crinoids (Fig. 3.1 A).

In dolomitic micrites, dolomite size ranges from 40μm to 0.6 mm, with an average of 0.16 mm. Dolomitization is selective and sometimes pervasive (see dolomite Chapter). Dolomite crystals have a cloudy surface, which may be because of replacement of an early micritic precursor.

Calcite pseudomorphs after evaporites or calcitized gypsum are also very common in this microfacies (Fig. 3.1 H). In some cases, pesudomorphs have a monoclinal or twin shape (Fig. 3.1 I). All the above evidence indicates that this

facies has formed in a quiet low energy environment, ranging from intertidal through supratidal, to relatively deep subtidal environments.

Microfacies II- Biofacies

This facies consists of biomicrite and biosparite. The Mozduran carbonates consist of a large diversity of skeletal grains, such as bivalves (pelecypods), gastropods, brachiopods, crinoids, abundant calcareous algae, bryozoa, siliceous and calcareous sponges, foraminifera, ostracods and corals. Crinoids, brachiopods and pelecypods are the dominant biogenic fragments in both biomicrite and biosparite facies. Bioclasts are commonly poorly sorted and have random orientations. The main skeletal contributors to limestones studied from shallowest and relatively deeper part of the basin are discussed in the following sections.

Mollusca

Bivalves

Bivalves are important contributors to marine carbonate sediments in the Bagak, Padeha and Mozduran sections. Bivalves vary in size from 0.7 mm to 1.6 cm, with an average size of 1.86 mm. In some samples, bivalves comprise only 5% of the total bioclasts, while in others, reach to about 80%. Bivalves with an average of about 30% are the second most abundant bioclast in the Padeha and Mozduran sections. Bivalve fragments in most of the thin sections studied are elongated and curved grains, which are typically disarticulated (Figs. 3.2 A, B). Most bivalve shells possess a micritic envelope, which in several cases has been fractured, and some fragments are non-preferentially oriented as a result of compaction (Figs.3.2 A, B). This feature is called a shattered micritic envelope (Scholle, 1978). The micritic envelope is mostly produced by endolithic cyanobacteria which bore into the skeletal grains (Tucker, 1991). After the death of the cyanobacteria, the borings fill with micrite. In some examples, the margins of bivalve shells have been completely replaced by micrite. Micritic envelopes are relatively resistant to dissolution, but susceptible to dolomitization (Buchbinder and Friedman, 1970). Thus, bivalve fragments are preserved during diagenesis. In bivalves, as the original aragonite mineralogy dissolved, the leaving void is later filled by clear equant to coarse drusy sparry calcite cement (Figs. 3.2 A, B). Thus, due to the dissolution-precipitation mechanism, the original structure of all bivalve grains have not been preserved. Grains are identifiable only on the basis of characteristic shapes outlined by a micritic

envelope. Some bivalve fragments are bored by a boring organism, and the area within the borings has been filled with the micritic sediment, and possibly protected from compaction, thus showing the original fabric (Fig. 3.2 C). In a few examples, pelecypod valves are joined at mid-shell, parallel to hinge lines and are well preserved (Fig. 3.2 D).

In the Gorgoreh and Bazangan sections, bivalves are much less abundant than in the Padeha and Mozduran sections. In the Gorgoreh section, bivalves vary in size from 0.5 to 6.4 mm, with an average size of 1.7 mm. In some samples, bivalves comprise only 5% of the total bioclasts, while in others, range up to about 40%. In the Bazangan section bivalves are rare and only in one thin section (no. 95), range up to about 10%.

Gastropods

Gastropod fragments are common in the Shurijeh, Bagak, Padeha and Mozduran sections. Gastropods comprise <5 to 25% (only in thin section Mz 22) of the total biogenic fragments, with an average of about 5%. Since most gastropods studied have aragonite shells, the internal microstructure of gastropod shells have been obliterated by the dissolution-precipitation processes (Fig.3.2 E). Geopetal fabric is present within the chambers of some gastropods in the Mozduran section (Fig. 3.2 E). Intragranular porosity within chambers are partially infilled by micritic sediment, and the cavity is finally filled with coarse grained sparry calcite cement. In a few samples, ornamented shells of some gastropods have been preserved due to the precipitation of clear calcite cements (Fig. 3.2 F). Gastropods are very rare in biomicrite and biosparite facies from the Gorgoreh and Bazangan sections.

Brachiopods

Brachiopods are the most abundant bioclast in the Bagak, Padeha and Mozduran sections. Brachiopods vary in size from 0.3 mm to 1.6 cm, with an average size of 1.74 mm. Brachiopod fragments are larger in the Mozduran section, with an average size of 2.02 mm, compared to the Bagak and Padeha sections, which have an average size of 1.42 mm. This can be attributed to the better environmental conditions for brachiopods, such as relatively deeper water, less detrital quartz grain input, and normal salinity in the Mozduran section, compared to the Bagak and Padeha sections. In some samples, brachiopods comprise only 5% of the total bioclasts, while in others, range up to about 80%.

Figure 3.2. Thin section photomicrographs of bioclasts (mollusca).

A. Biooosparite. Sections through the large bivalve shell fragments showing micritic envelopes in a sparry calcite cement. This dark micritic envelope is produced by algal boring of original aragonitic bivalve shells. Note the importance of micritic envelopes in preserving bivalve fragments during diagenesis. The original aragonite shell mineralogy has been completely dissolved, and the mould was then filled by thin zones of pink-stained, non-ferroan, and later blue-stained, ferroan drusy sparry calcite cement. This obliterated all relicts of the internal shell structure. The wall of the shell has been fractured and some fragments disoriented. The fractured envelope shows that cementation within the shell void occurred after some compaction. Thin section no. 28 , Padeha section.

B. Close up of shattered micritic envelope in a pelecypod shell. Thin section no. 66, Mozduran section.

C. Biooosparite. Multiple bivalve borings in oosparite facies (black arrow). Note that the area within the borings have been filled with the micritic sediment and possibly protected from compaction, thus preserving the original fabric. Note breakage in bivalve shells in the middle (open arrow) and lower part of the photograph (white arrow). Thin section no. 96 A, Mozduran section.

D. Cross section of pelecypod valves at the mid-shell, perpendicular to hinge line. Note that valve shapes are mirror images of one another. This is generally not true of brachiopods. The fact the pelecypods contain pellets and surrounding rock does not suggest that the valves were infilled prior to incorporation into the sediments. Thin section no. 69, Gorgoreh section.

E. Biomicrite. Longitudinal section, parallel to axis of coiling of a high-spired aragonitic gastropod. Original shell microstructure has been obliterated and the shell is occupied by clear, equant sparry calcite cement, due to the dissolution-precipitation processes. The presence of dirty inclusions of micrite within the sparry calcite cement may indicate very early cementation. Note that the geopetal fabrics in gastropod chambers are in two different orientations (black and white arrows), suggesting some post-depositional movement of shells prior to lithification. Thin section no. 22, Mozduran section.

F. Transverse section through the axis of coiling of a single originally aragonitic gastropod. External projections which are composed of sparry calcite cement show an ornamented shell. Thin section no. 87, Mozduran section.

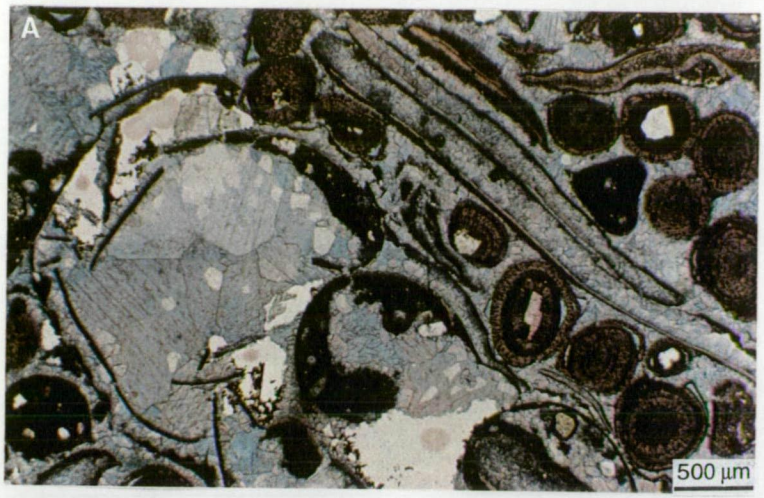
A
500 µm


B
250 µm


C
500 µm


D
1 mm

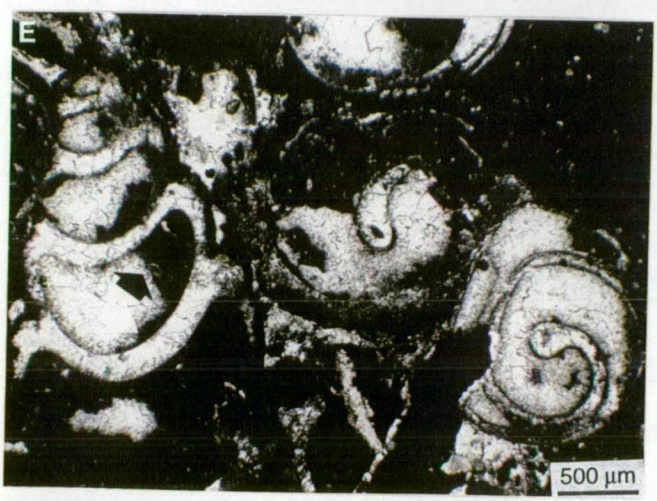
E
500 µm

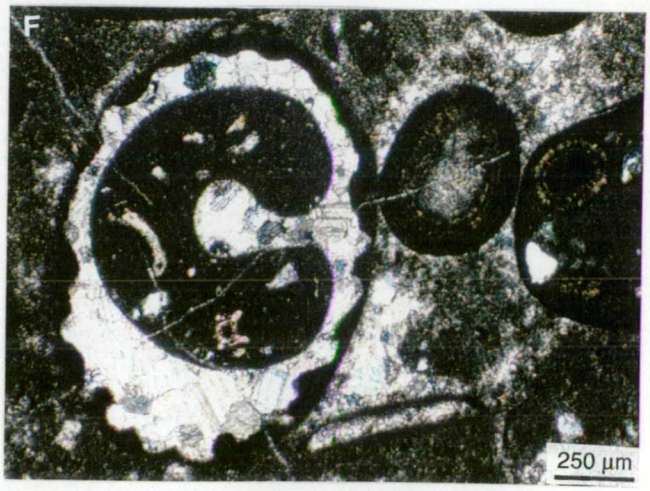
F
250 µm

Brachiopods, with an average of about 35%, are the most abundant bioclasts in the Bagak, Padeha and Mozduran sections.

In the Gorgoreh and Bazangan sections, brachiopods range in size from 0.3 mm to 1.2 cm, with an average of 1.96 mm. They comprise <5 to 70% of the total biogenic fragments, with an average of about 37% in these sections.

Since most articulated brachiopods were composed of low-Mg calcite mineralogy, their shell structures are well preserved. Brachiopod shells in most of the Mozduran sections studied, show good perservation of internal structure, which is obliquely fibrous (impunctate shell, Fig. 3.3 A). Impunctate structure is characteristic of rhynchonellid or spiriferid brachiopods (Adames et al., 1984). In some brachiopod fragments the thin outer prismatic layer has been preserved. Modifications to the shells of certain brachiopods, with punctae and pseudopunctae, can be seen in the Mozduran carbonates. In the punctate brachiopods, such as the terebratulids, fine tubes (endopunctae) are at right angles to the shell wall (Fig. 3.3 B).

Crinoids

Crinoids are wholly marine organisms and have a calcitic mineralogy. Crinoid fragments with single calcite crystals and uniform extinction are major constituents of bioclasts in the Mozduran limestones (Fig. 3.3 C). Some large crinoid fragments show uniform granular microtexture with dusty appearence, as a result of infilling of the fine pores with micrite or sparite (Fig. 3.3 D). In many crinoid- rich sediments in the Mozduran Formation, syntaxial cement overgrowth, which has optical continuity with crinoid grains, often completely destroyed porosity (Fig. 3.2 C). In a few cases, syntaxial rim cements have turbid or dirty inclusions (Fig. 3.3 D), indicating a marine origin,while in many other cases, cements are clear, due to meteoric and burial origin. Most of the crinoidal grains are rounded to elongate in section and in some cases have a central canal, although U-shaped outlines, characteristic of arm plates, are also common (Fig. 3.3 C). In many cases, crinoid fragments with a very fine meshwork are bored. Silicification is more pronounced along the more porous internal parts of many crinoids. It often consists of microquartz (Fig. 3.3 E), and in a few cases, pore-filling chalcedonic quartz (Fig. 3.3 F).

Crinoid fragments in the Padeha and Mozduran sections vary in size from 0.25 mm to 5.2 mm, with an average size of about 0.9 mm. Crinoids are the third most important constituant of bioclasts in these two sections, ranging from 5 to 57%, with an average of about 25%. In sections from the relatively deeper part of

Figure 3.3. Thin section photomicrographs of bioclasts (brachiopods, crinoids and algae).

A. An impunctate brachiopod. Brachiopod shell with parallel fibrous structure running subparallel to the shell edge. Thin section no. 116, Gorgoreh section.

B. A punctate brachiopod. Brachiopod shell has prominent endopunctae (fine tubes) at right angles to the shell wall (white arrow). Note, the punctae filled with micritic sediment. Thin section no. 89, Mozduran section.

C. Crinoid fragments with circular, elongate to platy calcite single crystals, and large syntaxial cement overgrowth in optical continuity. Twin lines of calcite crystals are continuous from grain to cement (see lower right of photograph). Such syntaxial overgrowths are generally early diagenetic. A central canal is present in one of the crinoids in the lower left of the photograph. Thin section no. 100, Bazangan section.

D. Large crinoid fragment with single-crystal structure showing granular microtexture (small pores filled with carbonate mud). Note turbid syntaxial cement overgrowth (white arrow) filled interparticle porosity. Thin section no. 116, Gorgoreh section.

E. Chertification of crinoid fragments. Much of the internal part of crinoids is replaced by chert in the form of microquartz. Thin section no. 27, Padeha section.

F. Porefilling chalcedonic quartz within the internal part of the crinoid fragment (the central part of the photograph). The radiating arrangements identify the chalcedonic quartz. Thin section no. 27, Padeha section.

G. Cellular calcareous coralline algae, probably Lithophyllum (white arrow) at lower right. This example shows differentiation of central hypothallus and the denser, external perithallus. Note the fine cellular structure is well preserved. Cyanophyceae. Type Ortonella or Cayeuxia (black arrow) at upper left. Bifurcated filamentous tubes with acute angles and radial shape. Thin section no. 9, Bazangan section.

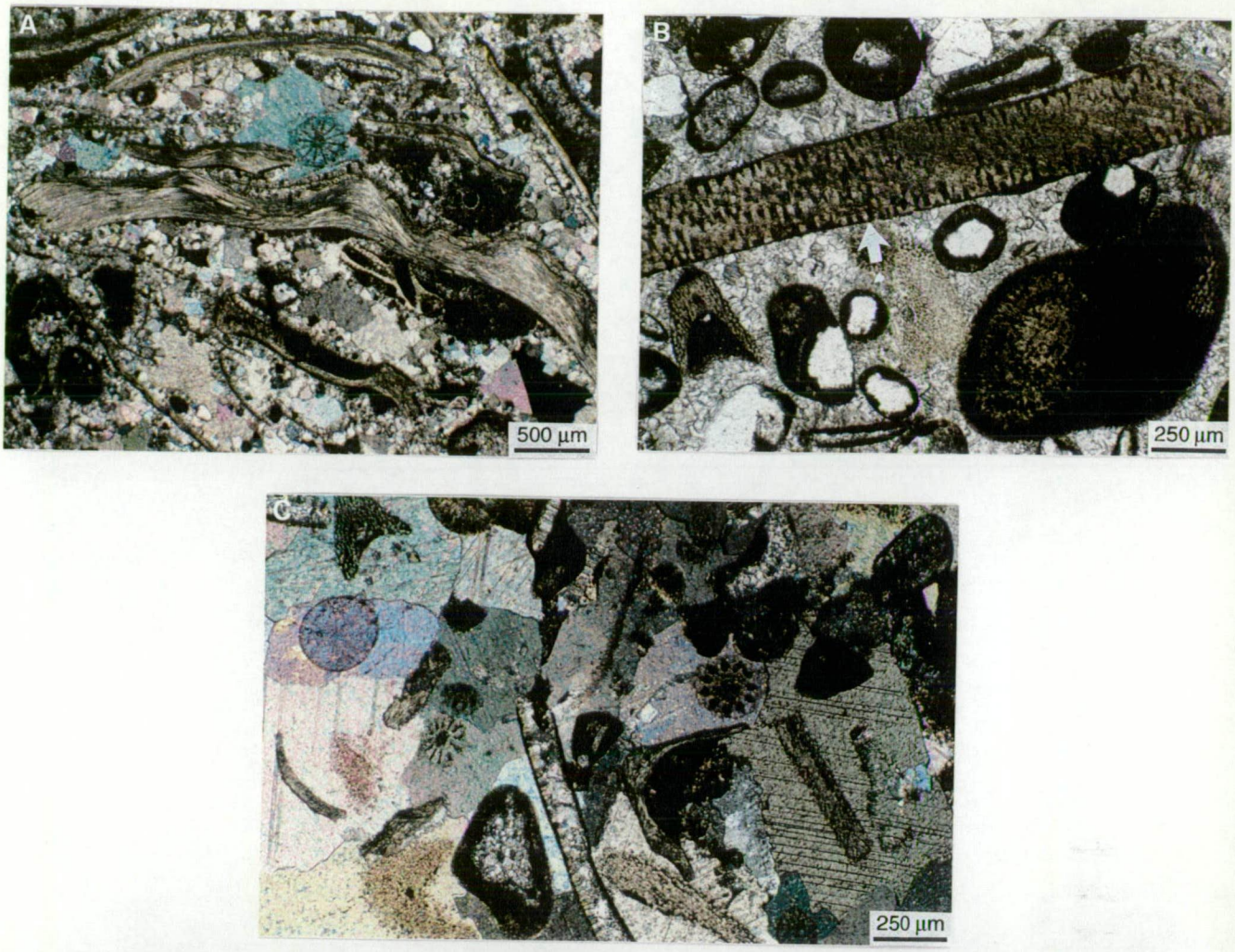
A
500 µm
B
250 µm
C
250 µm
D
250 µm
E
250 µm
F
250 µm
1 mm

the basin (Gorgoreh and Bazangan), crinoid fragments range in size from 0.2 mm to 1.04 cm with an average size of 0.7 mm. Crinoids are the most abundant biogenic fragments in these two sections, ranging from 10 to 95%, with an average of about 51%. In the dolomitized part of the Mozduran sequence, especially in the Gorgoreh and Bazangan sections, many crinoid fragments are mimically replaced by dolomite (see dolomite Chapter).

Algae

Calcareous algae and cyanobacteria (formerly blue-green algae) have made an important contribution to the Mozduran limestones by providing skeletal carbonate particles, forming laminated fabric (stromatolites), and attacking shell fragments through their boring activity. Two groups are important in the Mozduran carbonates: Rhodophyta (red algae) and Cyanophyta (cyanobacteria).

Rhodophyta

Calcareous red algae such as Corallinaceae are common skeletal algae in some samples, especially in the Mozduran and Bazangan sections. The crustose coralline algae (*Lithophyllum sp.*) are the most important type of calcareous red algae in the Mozduran carbonates. The fine calcified cellular structure, with good textural preservation (due to original high-Mg calcite mineralogy), distinguish these coralline algae from other algal types (Fig. 3.3 G, lower right of photograph). Although red-algal grains are converted from original high-Mg calcite to low-Mg calcite during diagenesis, the fine scale cellular structure is normally preserved (Scholle, 1978). In some of these red-algal grains, reproductive organs called conceptacles, are preserved within the cellular tissue. It has been suggested that some of the coralline algae genera such as lithophyllum live in marine warm water, intertidal to subtidal environments, usually in water depths of a few meters to a few tens of meters (Wray, 1977). This was supported by Flügel (1982) who stated that red algae are predominantly found in normal marine tidal or shallow subtidal areas, usually <25 m, except species of encrusting Corallinaceae such as lithothamnium, which has adapted to water of more than 50 m in depth.

Cyanobacteria

Cyanobacteria have a profound effect on the Mozduran carbonate sediments through their boring activity (formation of a micritic envelope around the grains), and in the production of laminated microbial mats and stromatolites

(Figs. 2.11 B-D). Microbial laminated mats show irregularities in thickness and have a small wavy or undulatory structure. Laminae consist mainly of alternating dark microbially-rich layers and sediment-rich layers of micrites, pelmicrites and scattered rhombic dolomites (Fig. 3.4 A). These microbially laminated carbonate sediments indicate environments protected from wave attack, such as broad intertidal flats (Wray, 1977). The microbially laminated mats are traced laterally into domal stromatolite. Domal stromatolites occur on the small scale (90-250 mm wide and 85-180 mm tall, Figs. 2.11 C, D), and the laminae are continuous from one dome to the next. In samples from the Mozduran section, the domal stromatolites grade up to branching or digitate forms (Fig. 3.4 B). Small domes generally occur in less agitated waters in tidal flat environments (Hoffman, 1976). Glumac and Walker (1994), in their study of stromatoloite origin and diagenesis of Upper Cambrian peritidal carbonates of Tennessee (USA) concluded that microbial laminates, laterally linked hemispheroidal stromatolites, stacked hemispheroidal stromatolites, columnar stromatolites, and digitate stromatolites, respectively indicate an increase in water turbulence from supratidal to upper subtidal depositional environments. It has been suggested that algal mat growth on tidal flats is probably seasonal or related to periodic wettings (Park, 1976). Cyanobacteria are also dominant microbial grains, especially from the shallowest part of the basin (such as the Padeha and Mozduran sections, Fig. 3.4 C). Cyanobacteria type Cayeuxia, similar to that described by Flügel (1982, p.326) from the Upper Jurassic of the Southern Franconian Alb, Germany, is present in the Mozduran carbonates (Fig. 3.3 G, upper left of photograph). This algae consists of bifurcated, calcified, filamentous tubes with acute angles and radial shapes. Another type of microbial-sediment structure, with irregular internal concentric lamination, termed nodule balls or oncoids, are also present in the Mozduran carbonates. This will be discussed later in the oolite facies section.

Calcareous algae and cyanobacteria in the Padeha and Mozduran thin sections vary in size from 0.45 to 9.2 mm, with an average size of about 0.9 mm. In a few samples (such as, Mz 79, Mz 105, Mz 106), skeletal and non-skeletal algae are dominant carbonate grains and comprise between around 40 to 95% of the total bioclasts. Algae in the Padeha and Mozduran sections are more abundant towards the upper part of the sequence. In sections from the relatively deeper part of the basin (Gorgoreh and Bazangan), algal fragments are minor and comprise <5% of the total bioclasts. The gradual disappearance of the microbial fabric, coupled with the generally observed basinward decrease of the rate of early cementation, may reflect a decrease in the strength of current action and an

Figure 3.4. Thin section photomicrographs of bioclasts (algae, bryozoa and sponges).

A. Microbially laminated mats consist mainly of alternating dark microbially-rich layers and sediment-rich layers of micrites, pelmicrites and scattered rhombic dolomites. Thin section no. 101, Mozduran section.

B. Very well developed branching or digitate growth form of microbial mats, producing stromatolite.Thin section no. 79 A, Mozduran section.

C. Algal biosparite. This rock is largely made up of segments of cyanobacteria. Thin section no. 7, Mozduran section.

D. Ramose bryozoans in longitudinal section (white arrow). Most of the zooecia have been filled by sparry calcite cement. Wall structure and zooecia are well preserved. Note transverse section through the stick-like bryozoan colony, showing the overall rounded shape of zooecia (black arrow). Thin section no. 32, Bazangan section.

E. Transverse and longitudinal sections of sponge spicules in a micritic matrix. A few cross sections exhibit internal canals (center of the photograph). Note needle to spindle and multirayed (black arrow) character of spicules. Thin section no. 2, Bazangan section.

F. Close up of spindle shape siliceous sponge spicules. Thin section no. 7, Gorgoreh section.

G. Transverse sections of calcareous sponge in a micritic matrix. Thin section no. 11, Gorgoreh section.

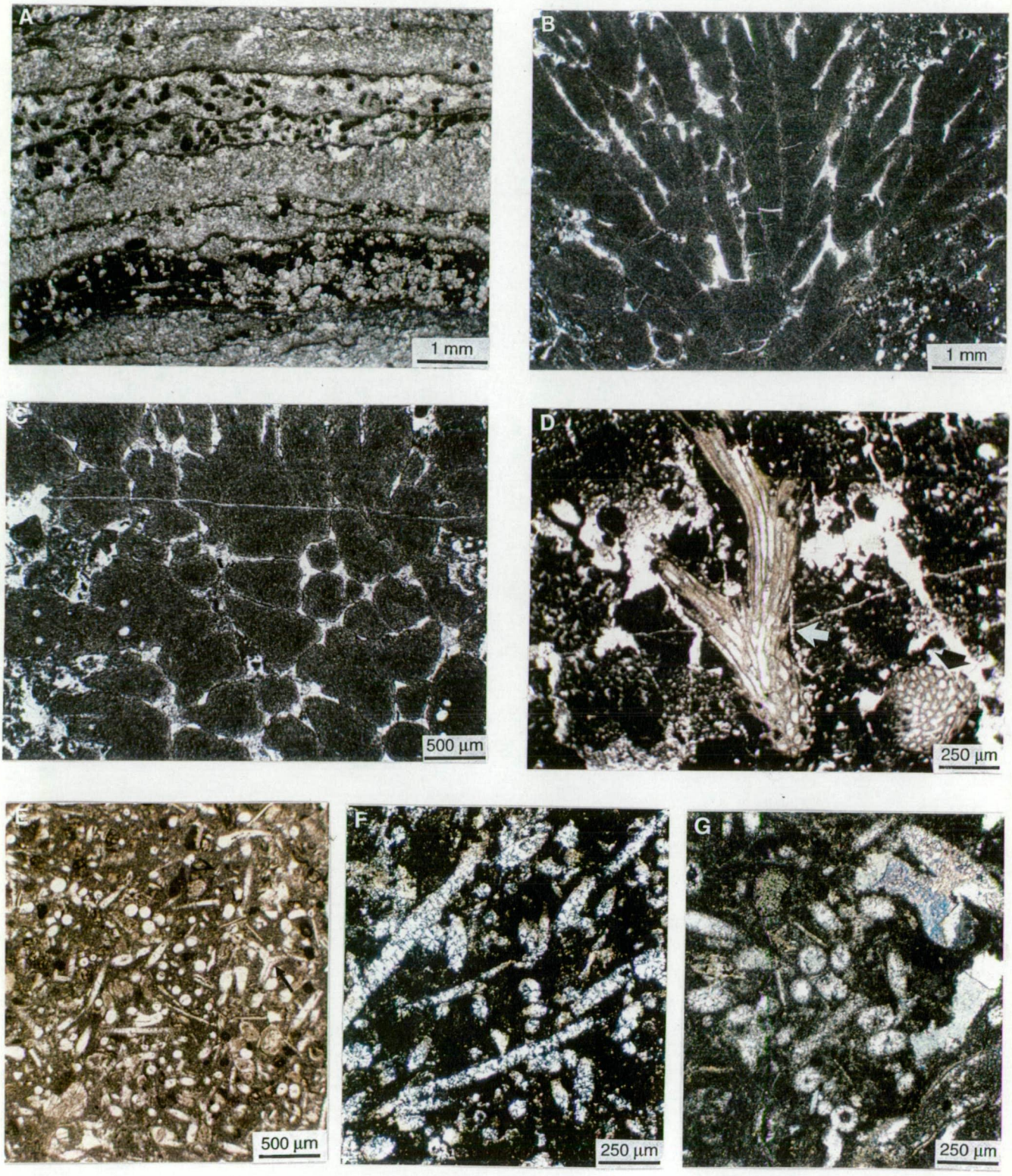
A
1 mm
B
1 mm
C
500 µm
D
250 µm
E
500 µm
F
250 µm
G
250 µm

increase in the sedimentation rate basinward (Bazangan section). In addition, argillaceous lithologies predominating in the Bazangan section may hamper early hardening, as beyond a certain critical threshold of clay content, early cementation is prevented (Massari, 1983).

Bryozoa

Fragments of bryozoans are common in the Gorgoreh and Bazangan sections. These bryozoans are generally associated with calcareous algae, multichamber foraminifera, ostracods and brachiopods. Bryozoa vary in size from 1.2 to 8.4 mm, with an average size of about 1.6 mm. In a few samples (such as, Go 113, Bz 32, 37, 40, 47), bryozoa are common carbonate grains and comprise from 5 to 30% of the total bioclasts. Ramose (having branches) types are the most common bryozoans in the Mozduran carbonates. These show good preservation of wall structure and zooecia, due to calcite mineralogy (Fig. 3.4 D). Zooecia are relatively rounded, and generally less than 100μm. Although most of the zooecia have been filled with sparry calcite cement, some have been infilled with fine sediments (Fig. 3.4 D). Bryozoan skeletons are rare or absent in sections from the shallowest part of the basin, possibly due to strong wave action in very shallow depth, higher salinity, abundant terrigenous input, or fluctuated temperature.

Sponges

Sponge spicules are the most abundant skeletal components of the Mozduran carbonates, occurring in the lower part of the Mozduran sequence in the Gorgoreh and Bazangan sections. Both siliceous (Fig. 3.4 E, F) and calcareous sponges (Fig. 3.4 G) are common in these sections. The size range of sponge skeletons varies from 0.2 to 1.6 mm, with an average of about 0.6 mm, but in transverse sections, spicules often appear circular, with an average size of 80μm. Individual spicules show a variety of shapes, including, tetrahedral, needles to spindle and ray shapes (Fig. 3.4 E, F), with spindles the most common. Some spicules have a central canal or hollow center (Fig. 3.4 E, G). Sponge spicules comprise 5 to more than 80% of the total bioclasts in some samples (e.g., Go, 14-25 and Bz, 2-26). Petrographic features, and the association of sponges with foraminifera, such as globigerina, indicate that sponge spicules flourished in slightly deeper, cooler, and quiet-water environments. Sponge spicules are the most important source of silica in the Mozduran limestones. In the Mozduran carbonates, replacement of calcareous sponge skeletons by silica is also very

common. In the Bagak, Padeha and Mozduran sections, sponge spicules are rare and occur sporadically in some carbonate sediments.

Forams

Foraminifera are common bioclasts in the Mozduran carbonates, particularly in the relatively deeper part of the basin. Multichambered forams are very abundant, and their chambers are arranged serially (biserial type), or are coiled (planispiral type, Figs. 3.5 A, B). *Lagenidae* is present in intraclastic facies in the lower part of the Bazangan section (e.g., thin section no.8). The presence of *lagenidae* indicates a deeper, cooler, water environment (Yassini and Jones, 1995). Quinqueloculine forams with dark micritic walls such as miliolida, are the most common type of forams (Fig. 3.5 B). Miliolida show the variety of shape and arrangement of chambers which resulted from random sectioning through the shells. Miliolid walls, which consist of high-Mg calcite, are largely micritized, and pores are filled partly with micritic mud and sparry calcite cement (Fig. 3.5 B). Most forams are smaller than 0.5 mm in diameter and have porcellaneous microstructures. Although, in a few samples (e.g., Bz 1-8, 32, 47), forams range from 5 to about 25%, they comprise <5% of the total bioclasts.

In the Bagak, Padeha and Mozduran sections, forams occur sporadically in some carbonate sediments.

Ostracods

Ostracods are insignificant in the Mozduran carbonates and only occur in a few carbonate samples in the upper part of the Bazangan section (e.g., Bz 82, 87-88, 97). Ostracods are characterized by small sized (average of 0.2 mm), smooth, thin shells, that are composed of calcite with a finely prismatic or radial-fibrous wall structure. Ostracods occur both as disarticulated thin curved shells and completely articulated (bivalved) shells, with a typical V-shape carapace termination (Fig. 3.5 C). Their association with other organisms, such as crinoids and forams, in the Mozduran samples, indicates that ostracods lived in a shallow marine environment.

Corals

Fossil corals are interpreted as marine animals with calcitic (mostly Paleozoic rugose and tabulate corals) and aragonitic (many post-Paleozoic scleractinian corals) skeletons. In the Mozduran shallow platform carbonates, no hermatypic (reef-building) corals have been observed. Ahermatypic corals, which

Figure 3.5. Thin section photomicrographs of bioclasts (forams, ostracods and corals).

A. Biomicrite. This foraminifer species is planispirally coiled with a keeled shape and relatively thick fibrous-walled texture. Pores are filled mainly with sparry calcite cements. Thin section no. 37, Bazangan section.

B. Biomicrite. This rock is composed mainly of micrite-walled miliolids. In this example, the dark fine grained porcellaneous microstructure of the wall is indistinguishable from the lime mud matrix. Thin section no. 73, Gorgoreh section.

C. Biomicrite. Cross section of articulated and disarticulated ostracods in a lime mud. Note characteristic V-shaped carapace termination and homogeneous prismatic wall structure. Thin section no. 40, Bazangan section.

D. Oblique section through Scleractinia coral showing radial arrangement of septa. The original wall microstructure of this originally aragonitic skeleton has been completely obliterated, by going through a phase of dissolution, and later infilling of the leached void by sparry calcite. Thin section no. 3, Bazangan section.

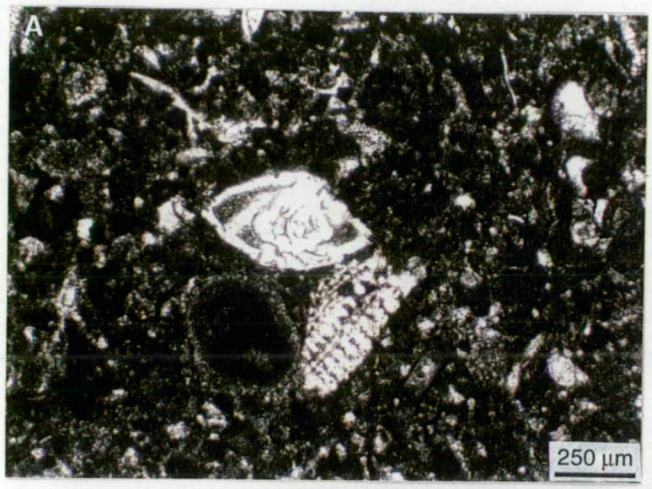
A
250 µm

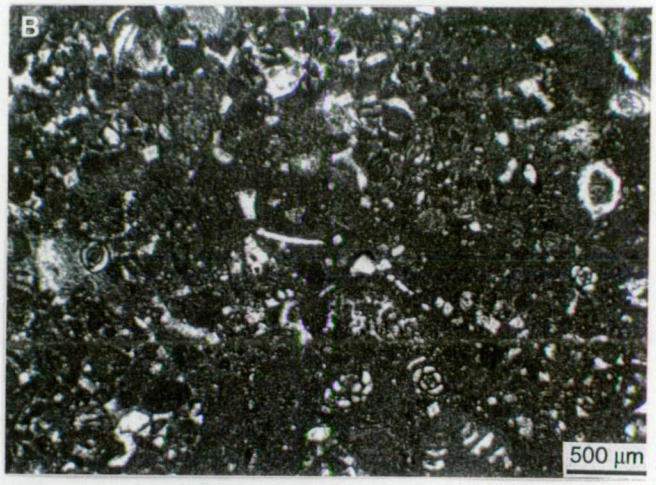
B
500 µm


C
250 µm

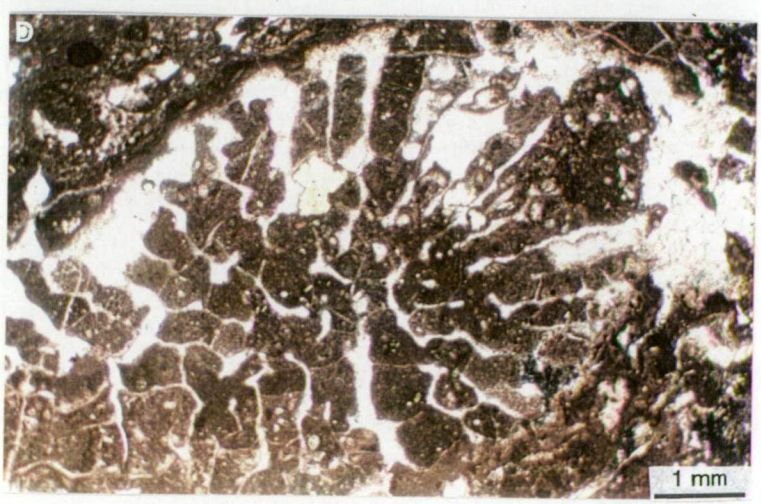
D
1 mm

can occur at greater depth and tolerate colder water (Tucker, 1991), are present locally in the Gorgoreh and Bazangan sections (e.g., Go 113, Bz 3, 4, 46). Solitary corals in the outcrop of the Bazangan sections range up to 10 cm in maximum dimension and are associated with a lime mud matrix. Since Mesozoic scleractinian corals are composed of aragonite, their microstructure is not well-preserved in limestones. Thus, identification is based on the shape of internal chambers and the radial arrangement of septa, perpendicular to the outer wall, in oblique sections (Fig. 3.5 D). The occurrence of ahermatypic solitary corals associated with muddy substrates in the relatively deeper part of the basin (Gorgoreh and Bazangan sections), supports the idea that these corals tend to live in the relatively deeper and cooler water. The oxygen thermometry (see Chapter 7), using micrite and cement values, also indicates cooler water in these sections.

In some biomicrite and biosparite facies, euhedral dolomite rhombs, ranging in size from 60μm to 0.3 mm with an average of 0.15 mm, are scattered within micrite and sparite. Dolomitization is selective and in a few cases, pervasive. Fine sand size detrital quartz grains, with an average size of ~0.2 mm, are present only in a few biomicrite and biosparite samples. Silicification is very intense in biomicrite facies of the lower portion of Gorgoreh and Bazangan sections. Microboring, shattered micritic envelopes, fenestrate structures and stylolitization are present in some biomicrite and biosparite facies. In biosparite facies, syntaxial rim cement, and clear blocky to platy and drusy cements are very common. Primary porosity in biosparite facies in the Gorgoreh and Bazangan sections is completly destroyed by extensive syntaxial overgrowths on crinoid fragments (Fig. 3.3 C).

Microfacies III- Pelmicrite

Pelmicrite facies are found predominantly throughout the Mozduran sequences in the Bazangan section, sporadically in the lower and upper parts of the Gorgoreh and in the lower parts of the Shurijeh and Mozduran sections. These rocks consist of spherical to elliptical, structureless, well sorted grains, composed of microcrystalline carbonates (Fig. 3.6 A). They have a relatively high content of organic matter, which has caused them to appear opaque or dark colored. In the pelmicrite facies of the Bazangan section, pellets comprise up to 35% of the total sediments. Most pellets in the Mozduran carbonates are uniform in size (Fig. 3.6 A), but in a few samples they show considerable irregularity of size. Pellets in all samples studied range in size from 20μm to 0.5 mm, with an average size of 69μm. *Faverina sp.* pellets, with internal patterns of tubules, are present in the

upper part of the Gorgoreh and Bazangan sections (Fig. 3.6 B). They range in size from about 0.4 to 2 mm, with an average size of 0.85 mm. These samples are similar to the fecal pellets described by Horowitz and Potter (1971, p.204), Scholle (1978, p. 111) and Tucker and Wright (1990, p.10). In the Holocene, such fecal pellets are produced by anomuran crustaceans (arthropods). In a few localities, pelmicrite facies hosted scattered euhedral to subhedral dolomite rhombs (Fig. 3.6 C), and coarsely crystalline euhedral outlines of evaporites. Euhedral dolomite crystals range in size from 50μm to 0.19 mm, with an average of 0.1 mm. A few pelmicrite facies (e.g., Mz 36) in the Mozduran section have very fine laminations and contain silt-size quartz grains, which are scattered throughout the sample. Scattered bioclast debris, especially crinoids, are present in a few pelmicrite facies.

Since most pellets of Recent subtidal and shallow intertidal low energy environments such as the Bahama Bank are of fecal origin (Tucker and Wright, 1990), it is assumed that small, even-sized, well sorted, uniform shaped and dark colored pellets in the Mozduran limestones are fecal pellets. This assumption is supported by *Favreina sp.* fecal pellets (Fig. 3.6 B), present in the Gorgoreh and Bazangan sections. However, the origin of some irregular and larger sized pellets, by processes such as micritization of small oolites or rounded skeletal fragments through the boring activities of certain organisms, particularly endolithic algae (Boggs, 1987), can not be ruled out. Flügel (1982) suggested that some pellets which are nonuniform in size and shape may simply be small intraclasts or algal grains.

Microfacies IV- Intraclastic facies

Intraclasts are carbonate fragments (lumps) which are derived by erosion of semiconsolidated or partly cemented carbonate sediments within the basin of deposition. This microfacies is a very abundant calcium carbonate constituent of the Mozduran Formation, especially in the Gorgoreh and Bazangan sections. They are often interbedded or interlaminated with other microfacies within the Mozduran Formation. Intraclasts are generally polymodal in size, ranging from 65μm (very fine sand) to 8.1 mm (gravel), with an average of 0.65 mm (coarse sand). They show some degree of rounding, indicative of transport, but subangular clasts are also common. Most intraclasts are internally homogeneous and consist of micrites (Fig. 3.6 D), while others display internal compositions such as fossils (mainly brachiopods, and pelecypods), oolites, siliciclastic grains and pellets. Adabi and Rao (1991) suggested that large intraclasts containing

bioclasts (Fig. 3.6 E, a, b) may indicate that the subtidal zone was very shallow and that the intraclasts formed by reworking of lithified sediments by strong currents.

In some thin sections (e.g., Ba 27A, Mz 16, Mz 87), intraclasts consist of large aggregate grains (composite ooids), ranging in size from 0.5 to 3.8 mm (Fig. 3.6 E). These carbonate grains are cemented together by micritic materials. The formation of aggregate grains occurs generally in subtidal and intertidal shallow-water environments with restricted circulation (to ~10 m water depth, Flügel, 1982). Intraclasts associated with ooids indicate penecontemporaneous reworking during oolitization in tidal channels, where forces of erosion are prevalent (Adabi and Rao, 1991). It has also been suggested that high energy particles in aggregate grains (ooids) may indicate a change of water turbulence (strong to weak) or a general change in the sedimentary conditions (Winland and Matthews, 1974). In some intramicrites, euhedral to subhedral dolomite rhombs are scattered within the micritic matrix and particularly around intraclasts (Fig. 3.6 F).

Flat pebble conglomerates (Fig. 3.6 G), which are formed by the impingement of tides in lower supratidal environments are present in a few samples. The pebbles range in size from 4.1 mm to 1.28 cm in length, and 1.04 to 2.7 mm in width. The pebbles are often poorly sorted and are largely mud-supported. The matrix consists of scattered silt to fine sand size detrital quartz, a few shell fragments, aggregate grains, and relatively large concentric and radially concentric ooids. These grains have been cemented by micrite.

Intraclastic facies in the Mozduran limestones consist of intramicrite and intrasparite. A carbonate rock that consist of more than 25% intraclasts within a micritic matrix is classified as intramicrite (Folk, 1974 a). Intramicrites are present in the Padeha and the Mozduran sections, but are very abundant in the Gorgoreh and Bazangan sections. In both the Shurijeh and Bagak sections, intramicrites are rare. This facies consists of 35 to 85% moderately sorted and rounded micritic intraclasts. They are polymodal size, ranging from 60μm to 6.4 mm, with an average of 0.64 mm. Intraclast shapes vary from elongate to circular and elliptical. The intraclasts in the intramicrites are composed of dark micritic materials, some angular silt size detrital quartz, and few bioclasts of limited diversity (mainly crinoids and brachiopods). In most cases intramicrites are associated with oolites and biogenic fragments. In a few intramicrites, it is difficult to distinguish between intraclasts and ooids, due to intensive micritization. Bioclasts associated with intramicrite facies are mainly foraminifera (miliolida), brachiopods, bivalves, crinoids and calcareous sponges.

Figure 3.6. Thin section photomicrographs of pelmicrite and intraclastic facies.

A. Small, well sorted, randomly oriented pellets, lacking any recognizable internal structure. Such pellets are generally interpreted as fecal in origin. Large voids are filled by sparry calcite cement. Thin section no. 55, Bazangan section.

B. *Favreina sp.* pellets. Well-sorted loosely packed framework of fecal pellets. Note the internal pattern of tubules, which are formed by elongate projections from the intestinal walls. Tubules are shown in longitudinal and transverse sections. Hollow tubules are now infilled by sparry calcite cements. Thin section no. 88, Bazangan section.

C. Small, even-sized pellets (probably fecal) within the mud matrix. Note their uniformity of shape, good sorting and opaque to dark color. Dolomite rhombs scattered within the matrix. Thin section no. 14 A, Shurijeh section.

D. Intrasparite. Large, rounded, internally homogeneous, polymodal size clasts of micrites. Only traces of silt size quartz grains are present within intraclasts. Note biserial foraminifera in the lower right of photograph (white arrow). Thin section no. 89, Gorgoreh section.

E. Photomicrograph shows large aggregate grains. Some of these grains are similar to the grapestones of modern sedimentary environments. The ooid grains are cemented together by micrite. Note two large grains (a, b) have fragments of brachiopod (a) and pelecypod shells (b). It is therefore likely that these are fragments of locally-reworked sediments, the shells having once been incorporated in a fine-grained sediment which was later eroded to produce intraclasts. Thin section no. 87, Mozduran section.

F. Dolomite rhombs scattered within the matrix and particularly around intraclasts. Thin section no. 56, Gorgoreh section.

G. Long irregular flat-pebble conglomerate, cemented by sparry calcite. Note the mud matrix consists of ooids, one large grain, a few shell fragments and scattered silt to fine sand size quartz grains. Thin section no. 89, Mozduran section.

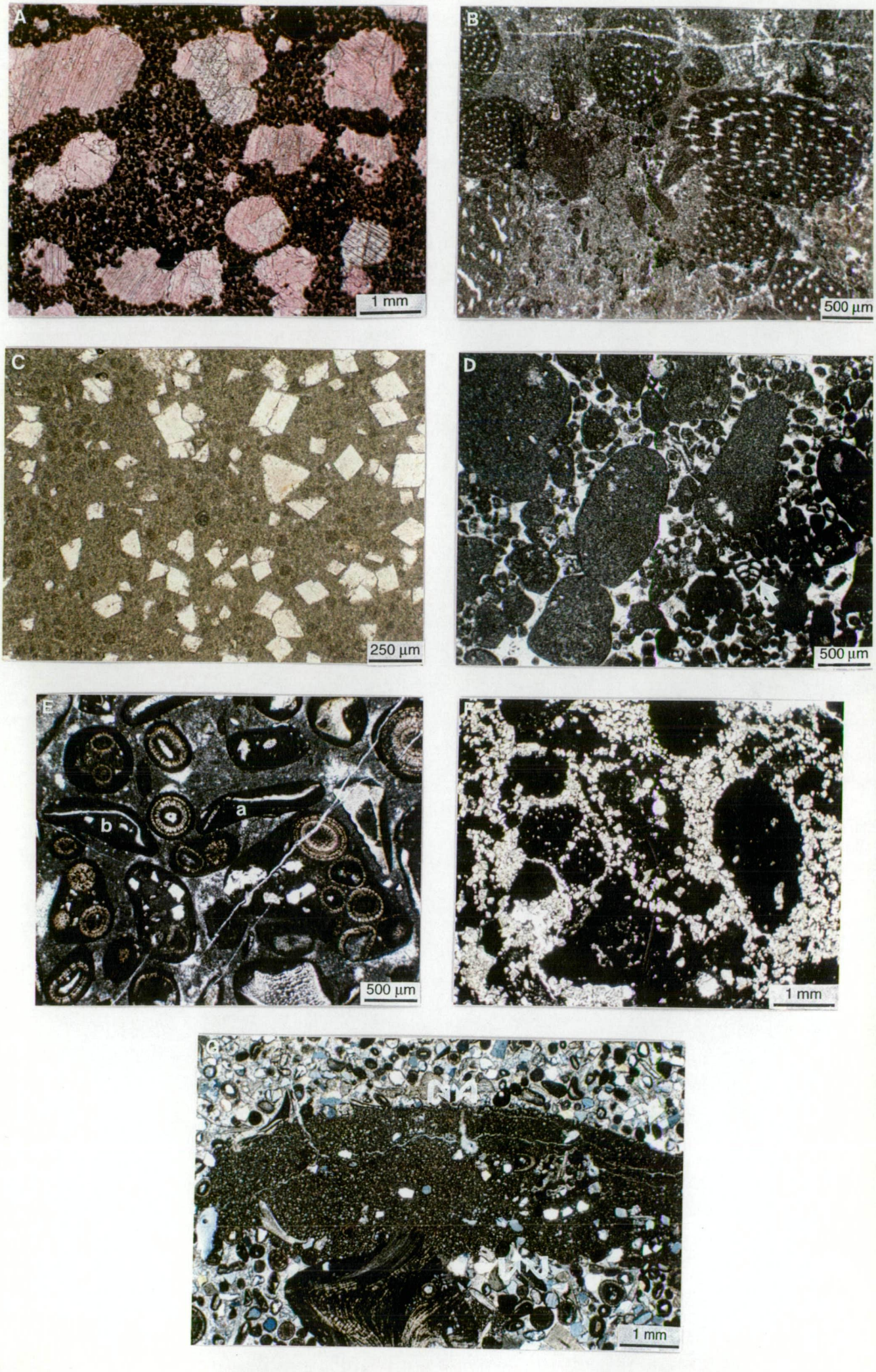
A
1 mm
B
500 µm
C
250 µm
D
500 µm
E
a
b
500 µm
F
1 mm
G
1 mm

become finer towards the upper part of the Gorgoreh and Bazangan sequences, and in many cases contain birdseye (fenestrae) structures and calcitized pseudomorphs after evaporite. In many cases, the intraclast composition is the same as the matrix.

Intrasparite facies are common only in the middle and upper-most part of the Gorgoreh sequence. They often have sharp contacts with underlying dolomite and lime mud facies. This rock consists of 45 to 75% poorly sorted and moderately rounded micritic intraclasts, ranging in size from 80μm to 8.1 mm, with an average of 0.75 mm. Most intraclasts have no internal structure, but a few contain crinoid fossils and 1-2% silt size detrital quartz. The larger intraclasts are usually irregular, but smaller intraclasts are more rounded and sorted than larger ones. Intraclast shape varies considerably in this facies, but they tend to be more spherical to elliptical. Forams (miliolida) and crinoids are the dominant biogenic fragments in this microfacies.

Microfacies V- Oolite facies

Substantial accumulations of ooids are forming today, in tropical and subtropical shallow agitated waters by tidal and storm currents and wave action. These waters are commonly of a slighty higher temperature and salinity than normal open ocean water, with depths usually less than 5 m, but which may reach 10-15 m (Tucker, 1991). Ooids can also form in quieter-marine waters. Almost all modern marine ooids, such as in the Bahamas and Persian Gulf, are composed of aragonite, although bimineralic high-Mg calcite and aragonite ooids have been reported from Baffin Bay, Texas (Land, et al., 1979), and the Pleistocene of Florida (Major et al., 1988).

Oolitic facies in the Mozduran limestones consist of oosparite and oomicrite. The best developed examples of oosparite facies, containing more than 25% ooids within the sparry calcite or dolomite cement, are in the Bagak, Padeha and Mozduran sections. Oolite facies are uncommon in the Gorgoreh section but are present in significant amounts in the Bazangan section (mostly as oomicrite facies). The lack of recognizable ooids in the Gorgoreh section may be due to pervasive dolomitization during diagenesis in these sequences. This microfacies is commonly associated with intraclastic and bioclastic facies and occasionally occurs as a minor component within pelmicrite facies. In some samples, ooids comprise about 55% of the total components, while in others, ranges to about 95% (Fig. 3.7 A).

Most ooids are commonly subspherical to elongate, range in size from 0.12 mm to 1.8 mm, with an average size of 0.4 mm. The nuclei of ooids are commonly carbonate muds and detrital quartz grains, and in some examples the nuclei consist of fossil fragments such as echinoderms, gastropods and brachiopods, particularly in the Bagak, Padeha and Mozduran sections (Fig. 3.7 A). The cortex thickness of ooids is inversely related to the size of the nucleus. In the upper most part of the Mozduran sequences, near the contact with the Shurijeh Formation, ooid nuclei are mainly quartz grains, possibly due to regression phases and a large input of detrital quartz grains by rivers. In most of these ooid samples, due to the regrowth of some quartz in the nucleus, the ooid structures have been replaced to some extent by quartz.

The oolite facies in the Mozduran limestones consist of thick units with an average of 10, 4.2 and 7 m in the Bagak, Padeha and Mozduran sections respectively, and 7.2 m in the Bazangan section. Small scale crossbeds are present in oolite facies of the Mozduran section. Oolitic facies mainly occur in the upper part of the Mozduran sequences, although only a few thin oolitic units are present in the lower part of the Mozduran Formation in the type locality. In many cases, this facies is followed by either sublitharenite or intraclastic facies, indicating shallowing upward sequences. Some oolite beds (e.g., Ba 27 A, Mz 106) consist of small (average 0.14 mm) and large (average 0.7 mm) grain sizes (Fig. 3.7 B). Many of the ooids are poorly preserved due to extensive micritization (Fig. 3.7 C). In some examples, subhedral to almost euhedral dolomite rhombs partially to completely obliterate the ooid structures (see dolomite Chapter). Many samples in the oosparite facies, especially in the Bagak, Padeha and Mozduran sections, show multistage diagenesis involving different generations of calcite and dolomite cements. Some ooids are rimmed with first generation fibrous aragonite cements, followed by equent, drusy or blocky calcite cements (Fig. 3.7 D). In a few cases the cavity is filled with single, coarsely crystalline calcite. Diffuse laminae within many ooid grains provide evidence for aragonite to calcite inversion (Fig. 3.7 D, Adabi and Rao, 1991). The tangential nature of crystals in radially concentric ooids of the Mozduran Formation (Fig. 3.7 E) is similar to that in modern aragonitic ooids in high-energy environments. A few oolite samples are cut by a number of irregular stylolites.

Different types of microstructures are recognized in the Mozduran oolites: (1) tangential, (2) radial, (3) superficial and (4) composite structures. Oolite beds in the Mozduran limestone often consist of a mixture of ooid types (Fig. 3.7 A), although in some samples only one particular type of ooid dominates. The

Figure 3.7. Thin section photomicrographs of oolite facies.

A. Moderately sorted oosparite. Note ooids with well developed radial and concentric structures in a coarse ferroan sparry calcite cement. Ooids have mainly carbonate mud and detrital quartz nuclei. The shape of ooids is mainly related to the size and shape of the nucleus. Two ooid nuclei consist of fossil fragments. Thin section no. 28, Padeha section.

B. Poorly sorted oosparite. Note ooids show bimodal size distribution. Thin section no. 106, Mozduran section.

C. Poorly-washed oosparite. Note most of the ooid textures are partially (a) to completely (b) destroyed, possibly due to micritization by endolithic microbial organisms. Thin section no. 20, Mozduran section.

D. SEM micrograph of etched polished thin sections showing isopachous cements, with uniform crystals and fibrous fabric, forming fringes around ooids. These types of cement are presumed to indicate original aragonite mineralogy. Note diffuse laminae in ooid grains. Thin section no. 96, Mozduran section.

E. SEM micrograph of etched polished thin sections showing tangential nature of crystals in concentric ooids, which is similar to that in modern aragonite ooids in high-energy environments. Thin section no. 83, Mozduran section.

F. Poorly-washed oosparite. Ooids showing strong radial fabrics (white arrow). The radial structure, the irregular shape of ooids, and the occurrence of broken grains, indicate a quiet-water depositional environment. The low-energy coated grains commonly have a strong radial fabric, thus they break easily. The radial fabrics indicate an original calcite mineralogy. Thin section no. 54, Bazangan section.

G. Poorly sorted oosparite, with redeposited quiet-water ooids. Note broken and regenerated ooids (white arrows), compared to normal ooids (black arrow). These coated grains are embedded in a micrite matrix. Thin section no. 59, Bazangan section.

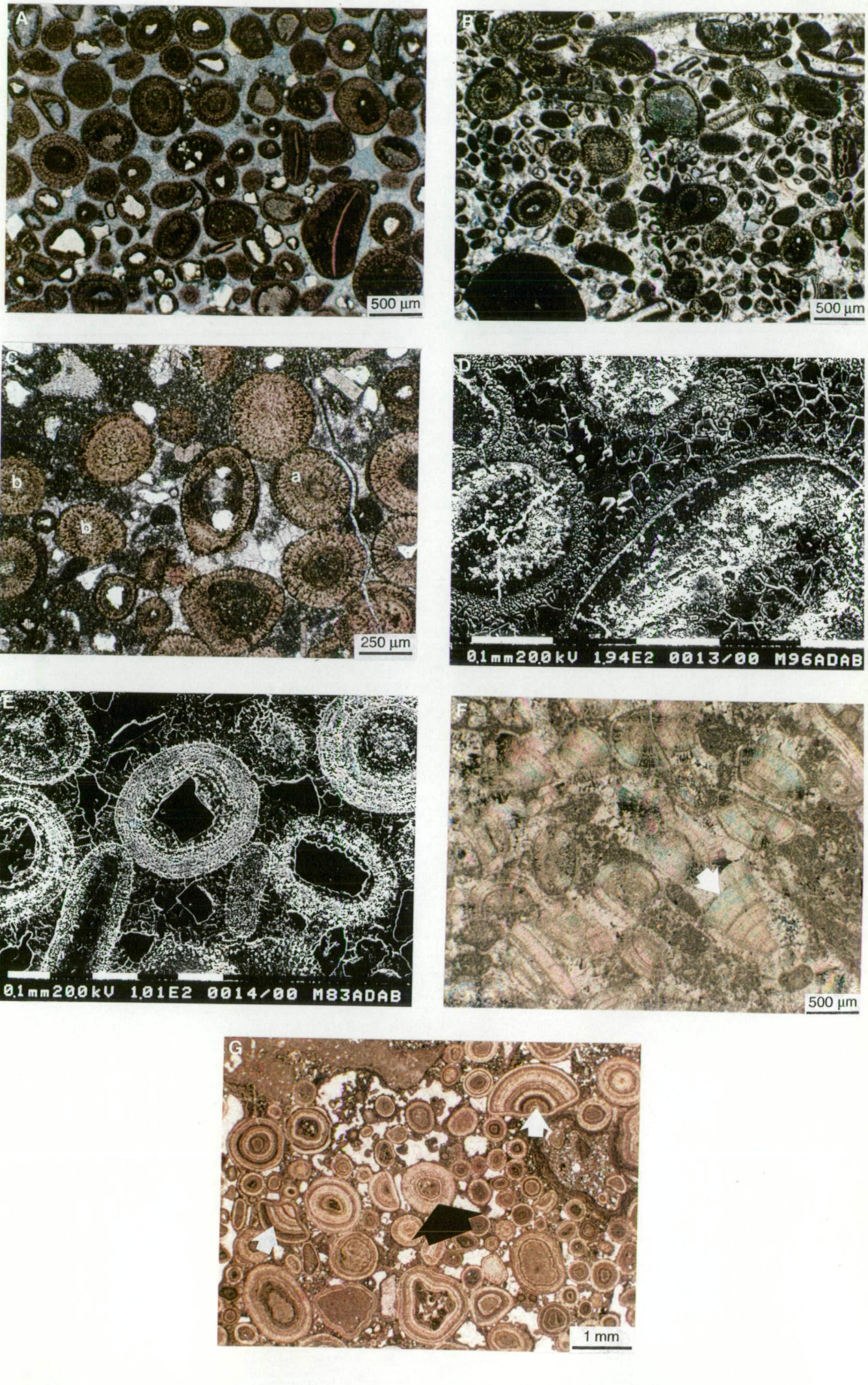
A
500 µm
B
500 µm
C
b
a
b
250 µm
D
0.1mm20.0kV 1.94E2 0013/00 M96ADAB
E
0.1mm20.0kV 1.01E2 0014/00 M83ADAB
F
500 µm
G
1 mm

development of different fabric in ooids is probably determined by environmental factors which will be discussed below.

The tangential (concentric) ooids are the most abundant type in this microfacies. The cortices of this type are composed of light-colored, radially fibrous calcite crystals and darker tangential micritic layers (Fig. 3.7 A). The number of cortex layers are variable but normally do not exceed five. The thickness of micritic tangential layers differ between the slightly irregular ooids and the more regular spherical ooids. In many cases, the cortical layers have been replaced by dolomite rhombs or are partially to completly destroyed by the micritization processes.

Ooids with tangential structures are dominant in modern high energy marine environments, such as platform margin oolitic shoals of the Bahamas and tidal channels of the Persian Gulf (Loreau and Purser, 1973). Thus, this type of ooid is usually interpreted as indicative of high energy conditions. The bioclasts associated with these ooids in many samples support a marine origin.

The radial ooids are the only common ooid type in the Bazangan sections. The radial ooids are characterized by lighter lamellae, typically strong radially oriented fibrous calcite crystals, and thin darker cryptocrystalline layers. They thus break relatively easily (Fig. 3.7 F). Broken and recoated radially structured ooids are common in the Bazangan section, most of which have a micritic nucleus (Fig. 3.7 G). They have few laminae and the laminae thickness is less than the size of the nucleus. Ooids are irregular and sometimes asymmetrical. This type of ooid is absent in the Shurijeh, Padeha, Mozduran and Gorgoreh sections.

Ooids with a radial-fibrous structure are frequently found in modern quiet water environments, such as in lagoons (e.g., Baffin Bay, Texas, Land et al., 1979) and on tidal flats (e.g., the Trucial Coast, Loreau and Purser, 1973), where salinities deviate from normal marine values. These ooids can also originate at greater depth (Flügel, 1982). The irregular shape of ooids, very few laminae, strong radial microstructure and the occurrence of broken and regenerated grains in many of the radially structured ooids in the Bazangan section, reflects a lag of mechanical strength in this type of ooid. They are thus easily broken, even in environments of low turbulence, giving support to the above interpretation (Fig. 3.7 F, G). The occurrence of abraded and recoated grains within the sparry calcite cement indicates a redeposition of these ooid grains within the moderately high-energy environment.

The superficial ooids are present in the Mozduran and Bazangan sections. They usually have large detrital quartz grains, echinoderm fragments or micritic

mud nuclei enclosed by only one or two dark concentric lamella of calcite crystalls (Fig. 3.8 A). Carozzi (1960) restricts the term superficial ooids to those with a single lamina. Ooids with an echinoderm nucleus are important as they isolate the echinoderm grains from pores, preventing cementation by overgrowths. Superficial ooids have been interpreted to occur chiefly in less agitated environments.

Composite (compound) ooids are the least abundant ooid type in the carbonate samples studied. These ooids are usually large irregular aggregate grains with botryoidal external forms, which resemble grapestones in modern environments. They generally consist of three to seven small radial-tangential or micritized ooids forming the nucleus (Fig. 3.8 B), probably due to very high-energy or storm deposition (Adabi and Rao, 1991). As ooids in the micritic matrix are surrounded by sparry calcite cements, these grains are possibly reworked. Composite ooids are present only in the Padeha and Mozduran sections and have been discussed with the intraclastic facies.

In most oolitic facies in the Bagak, Padeha and Mozduran sections, the general absence of micrite, the occurrence of moderately sorted grains, the spherical nature of ooids, association with diverse marine biota, and absence of any feature indicating deposition in a restricted hypersaline or brackish water environment, suggests that ooids formed in high-energy channel to upper subtidal marine environments. On the other hand, the presence of carbonate mud, few laminae, broken and recoated ooid grains with strong radial fabric and irregular shapes, in oolite facies in the Bazangan section, indicate that they formed in a quieter-water marine environment.

Deformed ooids

In the Mozduran Formation, spalled cortices (Fig. 3.8 C) are very common within the oolite facies, particularly in the shallowest near shore marine environments. Such fabrics are referred to as spalled ooids (e.g., Bathurst, 1975; Scholle, 1978; Wilkinson et al., 1984). In such ooids, where outer laminae are detached from inner laminae, due to dissolution of aragonite, the outer laminae are broken and may have undergone collapse (Scholle, 1978; Tucker, 1989; Adabi and Rao, 1991). Wilkinson et al., (1984) suggested that spalled ooids may record the formation of bimineralic aragonite-calcite cortices.

Figure 3.8. Thin section photomicrographs of oolite, oncoid and sandstone facies.

A. Oosparite. Superficial ooids with only one (or two) lamella. Thin section no. 92, Bazangan section.

B. Compound ooid. Note many radial-concentric ooids in the micritic matrix are surrounded by sparry calcite cements. This aggregate grain was possibly reworked in a very high energy environment. Thin section no.95, Bazangan section.

C. Oosparite. Note ooids exhibiting a number of spalled external laminae (black arrows). Such fabrics are produced during diagenetic transformation from aragonite to calcite. Ooids are surrounded by coarse equant to drusy non-ferroan followed by ferroan (blue stained) sparry calcite cements. Thin section no. 28 , Padeha section.

D. Plastically deformed ooids (white arrows). Note compaction of ooids has produced various types of contact. Longitudinal (a) and concavo-convex (b) contacts are formed in response to plastic deformation. The majority are sutured contacts (c) formed during pressure dissolution. Thin section no. 20 , Mozduran section.

E. Micro-oncoids. Microbially laminated grains with a maximum of about 2 mm in diameter. The outer surfaces are not as smooth as most ooids (white arrow) due to algal origin. Note Cyanophyceae (possibly type Cayeuxia, label a) grains with bifurcated filamentous tubes in the lower left of the photograph. The radial fabrics, the asymetrical growth and lack of organisms indicate low energy shallow marine water conditions. Thin section no. 43, Bazangan section.

F. Micro-oncoids. Microbially laminated grain in the middle left of the photograph has grown on the radially textured quiet water ooids. Note the wavy nature of the laminae. The radial fabrics, occurrence of broken grains, micritic matrix and shape of grains, indicate a low energy environment. Thin section no. 71, Bazangan section.

G. Sublitharenite. Note grains are angular to subround and consist mainly of quartz, some chert and metaquartzite. Dolomite occurs as scattered rhombs within intercrystalline porosity. Thin section no. 112, Bazangan section.


A
500 µm


B
500 µm

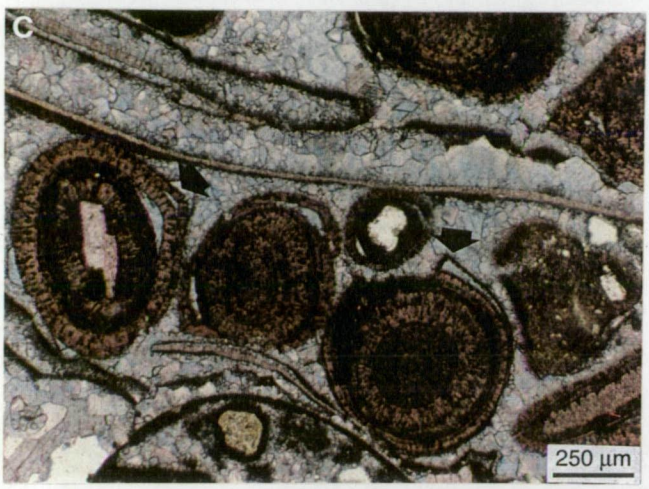
C
250 µm

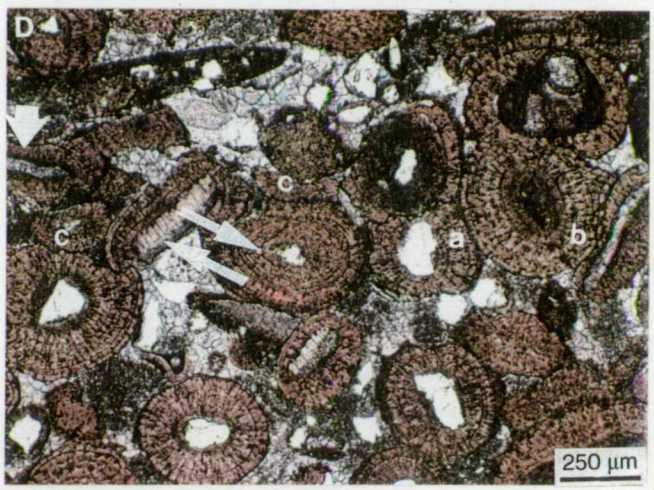
D
c
c
a
b
250 µm

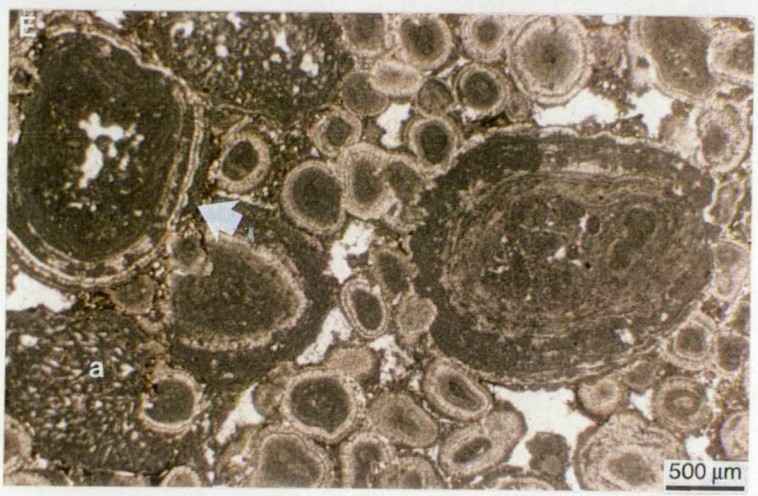
E
a
500 µm


F
500 µm

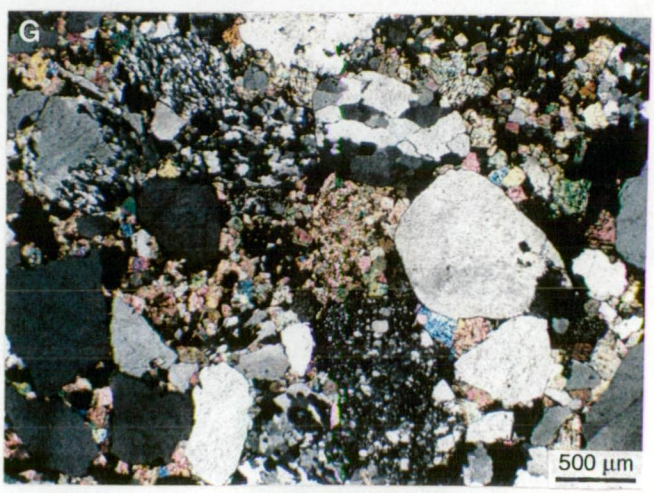
G
500 µm

It has been reported that aragonitic ooids form in near shore high energy settings and calcitic ooids are dominant in low energy settings (Land et al., 1979; Tucker, 1985). Given and Wilkinson (1985) also suggested marine aragonites are generally found where conditions are favorable for the rapid precipitation of a carbonate phase, such as shallow tropical systems where wave agitation and current flow rates are maximized. Moore and Druckman (1981) reported that in the subsurface of Alabama and Louisiana, oolitic units in the Smackover Formation exhibit two basic fabrics that are separated in space. Aragonitic ooids are dominant shoreward, whilst calcitic ooids with well preserved radial fabric occur basinward. In the Mozduran oolitic facies, fibrous, isopachous marine cement of probable aragonite mineralogy around ooids (Fig. 3.7 D), diffused laminae indicating aragonite to calcite inversion (Fig. 3.7 E, Adabi and Rao, 1991), and spalled cortices—evidence of aragonite dissolution (Scholle, 1978; Wilkinson et al., 1985; Tucker, 1989, Adabi and Rao, 1991), are very common in the shallowest, high energy near shore environment. The tangential nature of the crystals in concentric ooids (Fig. 3.7 E) is similar to that in modern aragonitic ooids in high-energy environments. In contrast, radial calcitic ooids are abundant in the relatively deeper, low energy environment, similar to the Holocene ooids described by Loreau and Purser (1973) in the Persian Gulf. These spatial variations have been related to increasing Mg/Ca ratios (Folk 1974 b), atmospheric-hydrospheric CO_2 levels (Mackenzie and Pigott, 1981), or temperature fluctuations of marine water (Adabi and Rao, 1996). However, Wilkinson et al. (1984) concluded that local variations in ooid mineralogy can be controlled by kinetic factors such as rate of crystal growth. Given and Wilkinson (1985) suggested that in a higher energy setting, increased CO_2 degassing gives rise to a higher CO_3^{2-} ion concentration and, hence, to enhanced aragonite precipitation. Local variations in CO_2 degassing, however, do not explain why some ooids are bimineralic. It has also been recorded that variations in ooid mineralogy are related to grain diameter. Smaller ooids are more calcitic, while larger ooids are more aragonitic (Given and Wilkinson, 1985). Since water chemistry is probably invariant during cortex accretion, they concluded that this relationship suggests that some physical factor related to ooid size may determine the mineralogy of precipitated carbonate phases. No relationship between size and original mineralogy of ooids was noted in the Mozduran Formation.

In a temporal context, spalled ooid fabrics resulting from aragonite dissolution are significant, as they are not equally distributed throughout the geologic column (Wilkinson et al., 1984). Aragonite as marine cement and

spalled ooids, which record aragonite dissolution, are restricted to rocks of Cambrian-Lower Ordovician, Pennsylvanian-Triassic, and Quaternary age (see Fig. 7, in Wilkinson et al., 1984). These periods correspond to times of global sea-level low-stands and support the suggestion of Mackenzie and Pigott (1981) and Wilkinson et al. (1985), that aragonite forms during times of general continental emergence. However, the presence of a moderate amount of marine aragonitic isopachous cement around ooids, diffused laminae within the ooids, and the abundance of spalled ooids in the Upper Jurassic Mozduran carbonates, corresponding to times of eustatic high-stands (see Fig. 7, in Wilkinson et al., 1984), does not support the above interpretation. In addition, petrographic evidence, along with geochemical studies (which will be discussed later in Chapter 5 and 6) indicate that during the formation of the Upper Jurassic Mozduran carbonates, aragonite was the dominant mineralogy in the shallowest part of the basin (Adabi and Rao, 1991). This is in contrast to the more calcitic mineralogy from the relatively deeper part of the basin. Tucker (1991) briefly mentioned that some anomalies do occur in the broad eustatic trend, notably in the Upper Jurassic strata, where aragonite ooids are recorded. Controversy about secular trends in ooids, in particular, carbonate mineralogy will be discussed later in Chapter 5.

Many ooids in the Mozduran limestones exhibit variable degrees of postdepositional deformation. In the Mozduran Formation, plastically deformed ooids (Fig. 3.8 D) give rise to longitudinal (Fig. 3.8 D, label a) and concavo-convex (Fig. 3.8 D, label b) contacts. Pressure-solution contacts (sutured contacts) are also very common in many oolite samples (Fig. 3.8 D, label c). These features will be discussed later in Chapter 4.

Oncoid subfacies

Oncoids have been defined as irregularly laminated, non-concentric calcium carbonate grains, which are derived from biogenic accretions by microscopic algae and bacteria (algal-cyanobacterial). They occur more often in Recent hypersaline, low energy marine environments (shallow subtidal, with a maximum depth of ~5 m, Flügel, 1982; Peryt, 1983). However, some oncoids have been described from normal seawater (Catalov, 1983), fresh water phreatic zones, and lacustrine and fluvial environments (Peryt, 1983). As discussed by Wright (1983), their morphology is related to the degree of agitation during oncolite growth. Oncoids which grew in higher energy conditions have sub-spherical and rounded forms, are well laminated and have a dense fabric. Those

which grew in lower energy conditions are more irregular in form, less well laminated, and have a spongy fabric. If these coated grains have a diameter of <2 mm they are called micro-oncoids, while oncoids have larger diameters (Tucker and Wright, 1990). Similar ancient marine oncoids or micro-oncoids are taken to be indicative of near shore low energy shallow marine water. Upper Jurassic oncoids and micro-oncoids have been described from deeper marine environments with very low sedimentation rates by Massari (1983), who concluded that these grains formed by accretion of mud and other sediment grains by a "snow-ball" mechanism. The formation of oncoids under conditions of low rates of sedimentation has been supported by Catalov (1983).

Oncoids and micro-oncoids comprise a minor component of the Mozduran carbonates and only occur in a few carbonate samples in the middle part of the Bazangan section (e.g., Bz 43, 71, 89). In the Bazangan section many of these grains have a diameter of less than or around 2 mm. They occur together with relatively quiet water radial ooids, algae (Cyanophyceae, possibly type Cayeuxia), and aggregate grains, and are characterized by wavey and crinkly layers (Fig. 3.8 E). Oncoid and micro-oncoid shape varies considerably (subspherical, elliptical to irregular) and size ranges up to 2.2 mm. The size of these grains in the Mozduran carbonates are similar to the size of Recent-hypersaline micro-oncoids (1-2 mm), and much smaller than those of Recent-marine and freshwater origin (cm-sized, Flügel, 1982, Table 16). These coated grains are generally embedded in a micrite matrix containing significant amounts of carbonate mud (Fig. 3.8 F). In most cases they possess a distinctly concentric, dark micritic laminae, derived possibly from microbial coating. This is poorly to moderately developed around cores of micrite, older oncoid grains (double oncoids or compound oncoids) and radially structured ooids (Fig. 3.8 F). In a few cases, these grains show partially overlaping laminae. The dark laminae are made up of grains 5-10μm in size. The light laminae are made up of grains 15-20μm in size.

Many of these coated grains are deformed by compaction. Grain interpenetration and grain to grain dissolution and stylolitization are common. Quartz is the only noncarbonate mineral which has been taken up by few micro-oncoids in very small amounts. Encrusting organisms on the envelopes of these micro-oncoids are completely lacking. The matrix of this submicrofacies is mainly micrite with a relict peloidal texture. Micrites are inhomogeneous because of different coloring and grain size. Irregularly distributed fenestral fabrics, indicative of intertidal and supratidal environments, are present in some oncoid and micro-oncoid samples.

On the basis of the different facies criteria and rock texture, such as the presence of micrite, peloids, radial fibrous ooids, relatively continuous micritic laminations, poor to moderate sorting, fenestral fabric and the rare occurrence to absence of organisms (fauna), this submicrofacies is assigned to low to moderate energy, intertidal to shallow subtidal environments. The presence of Cyanophyceae, possibly genus Cayeuxia, associated with micro-oncoids of the Mozduran Formations (Fig. 3.8 E), and their internal microfabric, are convincing evidence of microbial or cyanophyte origin.

Microfacies VI- Sandstone facies

Sandstone facies in the Mozduran Formation consist of sub-litharenite to litharenite beds, ranging in thickness from several centimeters to several meters. This facies is widespread in the Shurijeh section, but decreases towards the western part of the study area. In the Bagak, Padeha and Mozduran sections, sandstone facies are common at the base and upper-most part of the Mozduran sequences, where they lie on sharp, erosional surfaces. However, a few thin sandstone beds occur sporadically throughout the middle part of the carbonate dominated section, only in the Mozduran type section. The sandstones are fine to coarse grained, with grains ranging from 20 μm to ~0.7 mm, with an average size of ~0.2 mm. Grains are angular to subrounded and range from poorly sorted to moderately sorted. Sand grains consist mainly of quartz (>75%), some chert, metaquartzite and phyllite, with some rare large mica and a small percentage of feldspar (mainly microcline and plagioclase, Fig. 3.8 G).

A variety of different cements, including silica, calcite and dolomite, have been recognized in thin sections. Dolomite cements are widespread and have rhombic crystal shapes, with an average size of ~ 50μm (Fig. 3.8 G). However, in a few sandstone samples, dolomite occurs as scattered rhombs within intercrystalline porosity. Evidence of partial replacement of quartz by dolomite is present in many sandstone units. In these cases, the host quartz grains at the contacts, where dolomite crystals penetrated quartz, show embayments. This indicates that fluid chemistries were not strongly undersaturated with respect to quartz. Maliva and Siever (1988; 1990) suggested that once dolomite crystals began to grow, the force of crystallization was adequate to cause dissolution of quartz by pressure solution along dolomite/quartz crystal boundaries.

Small scale, low angle, planar cross-stratification is present in a few sandstone beds. Ripped-up mudstone clasts were observed sporadically in the Mozduran type section, near the base of sandstone beds, which are interpreted as

having formed in channels cutting across a tidal flat environment during a regressive phase of sedimentation. The variation in size and composition of detrial grains in this facies may indicate that the clastic grains were sourced from nearby metamorphic, igneous and sedimentary terrains, that probably constituted a paleotopographic high to the SW.

Microfacies VII- Mudrock facies

Mudrocks are the most abundant sediments, constituting about 50% of the geologic column (Pettijohn, 1975; Tucker, 1991). However, as mudrocks do not have a wide range of textures and structures, they are not easily studied. In addition, because of their fine grained nature and complex composition, their origins are not well understood, compared to other sedimentary rocks. In this study, mudrock facies refers only to shales and marlstones.

Shale facies

In the Mozduran Formation, relatively thick laminated sequences of shale facies, ranging in thickness from 3.2 m to ~20 m, are present in the Bagak, Padeha and Mozduran sections. Individual beds are usually less than 0.5 m thick and generally grade vertically to limestone facies. Shale sequences dominate the basal portion of the Formation and occur sporadically throughout the upper carbonate dominated section. Most shales are finely laminated, and range from clastic to slightly calcareous. Laminations are thus interpreted as being related to variation in grain size or changes in composition. Laminations of shale range from 0.03 to ~1.0 mm in thickness, with most laminations in the range of 0.1 to 0.6 mm. Laminations consist of silt size detrital quartz grains, interbedded with layers of finer detrital grains (possibly clays). Although the laminae generally display gradational contacts, in a few examples, the basal contacts of the laminae are sharp, and the upper contacts are either sharp or gradational. Micaceous materials are also present in a few samples and show a uniform orientation parallel to the bedding. In some calcareous shales, fissility is less pronounced, possibly due to increasing carbonate contents. Calcareous shales have been distinguished in the field, by their less fissile nature and their effervescence in diluted hydrochloric acid. Shales are mostly red to brownish red in the Bagak, Padeha and Mozduran sections. In contrast, in the Bazangan section, shales are grey to greyish black. In a few localities, yellow colored shales are also present.

The red and brownish red colors in shales have been attributed to deposition in an oxidizing environment in the presence of ferric oxide. However,

it has been suggested that the red color is developed after deposition of shales, through the aging process of a hydrated iron oxide precursor (see Pye, 1983 for review). The grey and greyish black colors in shales are possibly due to finely disseminated organic matter (Tucker, 1991). Organic matter tends to reduce the ferric iron to a nonred ferrous state (Pettijohn, 1975). The presence of yellow colored shales may be due to the mixing of green minerals and organic matter (Tucker, 1991). The sedimentary associations of the shales, such as parallel laminae with gradational contacts, represent deposition from suspension under relatively quiescent conditions (Kuehl et al., 1988). However, the presence of sharp basal contacts in a few laminae may suggest conditions of increased bottom shear stress (Kuehl et al., 1988).

Marl facies

Marl proper is a semifriable mixture of clay materials and lime carbonate. It has been defined as a rock with 35 to 65% carbonate and a complementary content of clay (Pettijohn, 1975).

Marls are widespread in the lower 330 m of the Mozduran Formation in the Bazangan section, where they range in thickness from 3.80 to 19.60 m, and are mostly interbedded with intraclastic and mud lime facies. In a few cases, marls grade up to calcareous shales, but are less fissile than these shales. This facies is highly weathered and all outcrops are difficult to sample.

It is assumed that the clastic clay mineral content in the marls, in the Bazangan section, was derived from a source area to the SW and deposited out of suspension below the fairweather wave-base. Due to the lack of fossil fragments in the lower part of the Mozduran sequences in the Bazangan section, it is concluded that calcium carbonate in the marl facies was possibly derived from inorganic precipitation of carbonate. The association of marls with intraclastic facies containing *Lagenidae* (such as thin section no. 8, Bazangan section), suggests a deeper marine water environment for deposition of the Mozduran marl facies. Afshar-Harb (1970, 1979) also suggested that the occurrence of *Lagenidae* in this part of the basin indicates a deeper water environment. Yassini and Jones (1995) found that modern *Lagena* are living in the middle shelf to continental slope environments. Sarntheim and Walger (1973) suggested that many modern marl sediments in the Persian Gulf were deposited in calm marine environments of moderate depth, without intensive ocean current energy. The Upper Jurassic Birmenstorf Beds and the Effing Marls of the Central Swiss Jura, which consist of argillaceous and silty thin-bedded mudstone and wackestones with marly

intercalations, are formed in the deeper-marine environment (Flügel, 1982, p.499).

Microfacies VIII- Evaporite (weathered gypsiferous) facies

Backround

Evaporite minerals and their pseudomorphs are common components of shallow marine carbonates (Pettijohn, 1975). Evaporite has been defined as a rock that was originally precipitated from a saturated surface or near-surface brine in hydrological systems driven by solar evaporation (Warren, 1996). However, some researchers restrict the term evaporite to those rocks precipitated directly from solar evaporation of hypersaline waters at the earth's surface (e.g., Lucia, 1972). Warren (1996) classified such evaporites as primary and suggested that with the exception of a few Neogene examples, there are no completely primary evaporite beds. Evaporites formed as displacive intrasediment crystal growths, as replacive or as cements in preexisting evaporite and non-evaporite beds are called secondary evaporites (Warren and Kendall, 1985; Demicco and Hardie, 1994, Warren, 1996). This secondary mode of precipitation occurs both syndepositionally and later during burial diagenesis (Warren, 1996). Under the classification of Warren (1996), tertiary evaporites are those formed during basin uplift. When gypsum is buried to depths greater than several hundred meters and the temperature rises above 50-60°C, all gypsum dehydrates to anhydrite. Upon uplift, the anhydrite is exposed to the surface and comes into contact with fresh water, where it is normally rehydrated and converted to gypsum.

Evaporite sediments are formed mainly in arid regions of low latitude, especially where temperatures are very high, average annual rainfall is very low and evaporation is very high (e. g., the Trucial Coast of Persian Gulf and Texas). The main site of modern marine sulphate precipitation is in the high intertidal and supratidal zones (Tucker, 1991), where seawater is brought close to the surface by capillary action or from surface flooding (flood recharge). Gypsum is here precipitated displacively within the sediments as discoidal, rosette, or twinned crystals (Kendall and Warren, 1988).

Mozduran Formation

As has been discussed in Chapter 2, during the Upper Jurassic, the study area falls within the zone of high evaporation rates (Moore et al., 1992 a), within the arid belts of Hallam (1993), and within the moderately low rainfall zone of Parrish et al. (1982) and Valdes and Sellwood (1992).

In the Mozduran Formation, relatively thick evaporite facies are present in the Bagak and Padeha sections. These are tertiary evaporites, exposed during basin uplift. The evaporite outcrops are deeply weathered and no bedding features etc could be identified. However, the lithology can be confirmed by powdery samples recovered by digging. Relatively thick sequences of weathered evaporitic facies, ranging in thickness from 9.6 m to ~31.6 m, with a total thickness of ~64 m, occur in the Padeha section. These evaporites are overlain by thin lime mud or dolomitic sublitharenite facies. In the Padeha section, evaporitic facies range from 7.2 m to 11.2 m with a total thickness of 18.4 m.

Identifications of sulphate minerals are made on the basis of general crystal shape and petrographic characteristics. Thin section studies of a few samples from the Padeha section, show that the crystals have low relief and weak birefringence, confirming gypsum mineralogy. Gypsum crystals range from 40μm to ~1 mm, with an average of ~0.2 mm. Calcitized pseudomorphs after gypsum in the form of swallow tail twin crystals (Fig. 3.1 I, Rubin and Friedman, 1977; Spencer and Lowenstein, 1990) and monoclinic forms (Fig. 3.1 H) in a micritic matrix are prsent in many samples (e.g., Mz 31, Mz 59, Bz 7, Bz 15, Bz 105). Calcitized pseudomorphs after gypsum in the form of discoial (lozenge) to lenticular morphology, are present only in a few samples (e.g., thin section no. Mz 24). The pseudomorphs consist of crystals ranging from 75μm to 0.35 mm, with an average of 90μm. Clear molds with euhedral crystal outlines (e.g., thin section no. 14 A) and intraformational collapse breccias (Adabi and Rao, 1991, in Fig. 3B) are also present.

Discoidal or lenticular morphology present in the Mozduran carbonates are characteristic features of displacive intrasediment growth of gypsum crystals in modern evaporitic environments (see Demicco and Hardie, 1994). Intrasediment growth provides unequivocal evidence of post-depositional crystallization in an evaporitic environment (Demicco and Hardie, 1994). Tucker (1991) suggested that discoidal form is typical of high-intertidal facies. The presence of molds with euhedral crystal outlines indicate postdepositional removal of former evaporites by leaching. Intraformational collapse breccias are interpreted to be due to the removal of evaporites by meteoric water.

Although the thin section study of sulphate minerals in the Mozduran Formation supports the gypsum mineralogy, there is no convincing structural evidence, such as chicken wire texture, bottom-nucleated gypsum crystals, lamination etc, to prove whether these evaporites formed in subaerial dominated settings (such as coastal sabkhas) or subaqueous dominated settings (such as

coastal salinas). However, the sedimentary association with calcite pseudomorphs after evaporites, such as the lack of marine organisms (fossils), few scattered dolomite rhombs, presence of birdseye textures, and few scattered fine silt-size quartz grains within the micritic matrix, may suggest that these evaporites formed in high intertidal to supratidal zones in a sabkha type setting.

3.2 Quantitative Stratigraphy and Sedimentology

Studies of variations in the thickness of beds, and determining whether the upward transition of one facies to another is significant, generally require a statistical approach. Statistical analysis, using Fischer plots to verify non-random arrangements of bed thickness, and Markov chain analysis to test for a non-randomness of facies in vertical sequences, have gained popularity in recent years, although this has not been without some controversy.

3.2.1 Markov chain analysis

Terminology and methodology

Markov chain analysis has been employed to investigate the vertical order (or non-random arrangement) of sedimentary successions. If the observed vertical sequence of lithologies is ordered, it is possible to determine in which way this ordering occurs. This technique enables the rejection of random sedimentation, with a stated degree of confidence. Markov chain analysis has been widely used by a number of investigators (Gingerich, 1969; Read, 1969; Selley, 1970; Miall, 1973; Ethier, 1975; Cant and Walker, 1976), to validate the presence of ordered and cyclic successions of facies in sedimentary rocks. However, it has been shown independently by both Carr (1982) and Powers and Easterling (1982) that these early studies were not entirely justifiable statistically and require modification. They proposed a method termed the quasi-independence model (initially developed by Goodman, 1968) to overcome this problem. This model of quasi-independence can be tesed using a chi-square statistic and can also be applied to embedded matrices which allows the preservation of both row and column totals.

Markov chain analysis begins by breaking the sedimentary sequence into a number of units (usually defined as facies) and recording the upward transitions from one to the next. There are two ways of recording the observed upward transitions: Sampling the section at fixed intervals; or recording every lithological change by logging the contacts between facies. The sampling method poses a number of problems, such as determining an appropriate sample interval to use. If

the sample interval is too small, thick beds may be recorded many times, and alternatively, if the sample interval is too large, thin beds may be missed or recorded infrequently. The later technique, known as the logging method, is most widely used, as it has the advantage of not missing any thin beds that may be important in evaluation of the sedimentary successions. However, it does ignore the possibility of two units of the same type overlying one another, which makes it impossible to distinguish between, for example, ABC ABC and ABCA ABCA. The logging method produces a diagonal of embedded structural zeroes in the transition count matrix, which tend to complicate the statistical analysis. The sampling of fixed intervals technique was suggested to avoid these problems, but it is dependent on the choice of an appropriate sample interval, and its statistical treatment is usually complicated by unduly large diagonal elements. Thus, the fixed interval sample method has not been employed in this study.

If transitions are logged over a continuous section, the row and column totals of the transition count matrix must be the same, or differ by a maximum of two. Only two row totals can not equal their corresponding column totals (Powers and Easterling, 1982). If the data fail these preliminary tests, they must have included gaps or faults in the sequence. In all the sections studied in the Mozduran Formation there was no mismatching of row and column totals (only differ by a maximum of two) indicating no gaps or faults in the sequence studied.

In both methods, the results are recorded in a transition count matrix. The transition count matrix shows the number of times a given microfacies type or unit is succedded by another. The transition count matrices are converted to transition probability matrices for both the sampling and logging techniques. These are then compared to the independent trials matrix (Gingerich, 1962; Read, 1969 ; Selley, 1970) or the quasi-independence model (Carr, 1982; Powers and Easterling, 1982), generated by assuming random sedimentation. The independent trials matrix of Gingerich (1969), Read (1969) and Selley (1970) has the advantage of ease of calculation. However, this method works only for row (not column) totals, and so is not entirely justifiable statistically. In contrast, the quasi-independence model (Carr, 1982; Powers and Easterling, 1982) preserves both row and column totals, thus, is more meaningful. Powers and Easterling (1982) propose an iterative procedure for calculating row and column factors, that can be multiplied to give expected cell values.

Subtraction of the expected transition random matrix from the observed transition matrix produces the difference matrix. In the difference matrix, the positive values represent those transitions which have a higher than random

chance of occurring. Thus, the greatest positive elements of the difference matrix are usually used to construct the preferred sequence (the so-called modal cycle). Similarly, using the Gingerich (1969) and Selley (1970) methods, where significant negative differences represent disfavored transitions, are commonly ignored by some recent researchers, such as Okhravi and Lahijani (1994). Their studies utilized the Powers and Easterling (1982) normalised probability differences technique to evaluate both positive and negative departures from expected transition values, and thus identify "extreme" difference cells. Those values above +2 and below -2 (i.e., outside of ~98% of the standard normal distribution) make the greatest contribution to non-randomness.

Markov chain analysis in the Mozduran Formation

Markov chain analysis combined with microfacies techniques was used to understand the sedimentation pattern of the Mozduran Formation in four stratigraphic sections (the Padeha, Mozduran, Gorgoreh and Bazangan sections). This study uses a custom-written computer program in BASIC by Wells (1989), which is based on a slight modification of the Markov analysis used by Powers and Easterling (1982). Wells (1989) has added the binomial probabilities and a test of symmetry (the asymmetry matrix) to Powers and Easterling's (1982) methods of the Markov chain analysis.

A sequence chi-squared matrix is calculated in this program, using the equation [observed - expected]^2/expected. The sum of the chi-square scores and the degrees of freedom is compared to a table of chi-square values: if the sum exceeds a given value, then the overall matrix is non-random. Principal successions for each facies can be determined from binomial probabilities. Binomial probabilities between 0.1 and 0.2 do not allow the determination of these successions (Wells, 1989).

Symmetry tests of whether transitions generally are reversible, allow the determination of whether transitions from, for example, facies A to facies B occur as frequently as transitions from B to A. The higher the chi-square scores, the more unidirectional (nonreversible) the transition (Wells, 1989). Both the methods of Wells (1989) and Powers and Easterling (1982) are used for comparison in the Gorgoreh and Bazangan sections (see Appendix 2).

Markov chain analysis in the Padeha section confirmed non-random sedimentation with more than 90% to less than 95% (90% < x< 95%) confidence levels. The asymmetry chi-square matrix indicates that the Padeha sequence is

randomly asymmetrical, with confidence levels of <90%, and thus has no ordered symmetry.

In the Mozduran type section, the hypothesis that the observed vertical arrangement of lithofacies is random can be confidently rejected. There is more than 95% (95% < x< 97.5%) probability that sedimentation has been non-random and that the vertical arrangement of lithofacies form a Markov chain. However, it is imposible to statistically justify a preferred sequence of facies. The asymmetry chi-square matrix indicates that the Mozduran sequence is randomly asymmetrical, with confidence levels of < 90%.

Markov chain analysis in the Gorgoreh section confirmed non-random sedimentation with 98 to 99% (98% < x< 99%) probability. The asymmetry chi-square matrix indicates that the Gorgoreh sequence is randomly asymmetrical, with confidence levels of < 90%.

In the Bazangan section, the chi-squared test of significance indicates that there is less than 90% chance (<90%) for non-random sedimentation. The asymmetry chi-square matrix indicates that the Bazangan sequence is randomly asymmetrical, with confidence levels of < 90%.

The various matrices and significant preferred transitions, along with binomial probabilities and confidence levels in all sections studied, are included in Appendix 2. The results of Markov chain analysis, including, calculated χ^2 values, degrees of freedom and percent chance for non-randomness and asymmetry in all sections studied, are summarized in Table 3.1. The Markov analysis of the Mozduran Formation in the Mozduran type locality (based on the Wells, 1989 method) is shown in Table 3.2.

The results of Markov chain analysis in all sections studied in the Mozduran Formation are not convincing when compared to other published examples of Markov chain analysis (e.g., with 99.99% confidence level), and it is statistically imposible to justify any preferred sequences. This is probably because it is impossible to distinguish all the primary sedimentary facies after pervasive secondary dolomitization, which has occurred randomly throughout the sequences.

Table 3.1. Results of Markov chain analysis of the Mozduran Formation.

		Sections Analyzed			
		Padeha	Mozduran	Gorgoreh	Bazangan
	Number of facies	9	9	7	10
Randomness	Degrees of freedom	55	55	29	71
	Chi-Square value	69.53	73.5	46.75	77.58
	% Chance non-random	90 < x < 95	95 < x < 97.5	98 < x < 99	x < 90
Asymmetry	Degrees of freedom	13	21	11	21
	Chi-Square value	10.39	17.75	7.12	9.84
	% Chance non-random	x < 90	x < 90	x < 90	x < 90

Table 3.2. Markov analysis of the Mozduran Formation in the Mozduran type section. Based on the Wells (1989) method.

Number of facies: 9
Facies:

1 Micrite-biomicrite (variably fossiliferrous)
2 Biosparite
3 Intramicrite
4 Pelmicrite
5 Oomicrite
6 Oosparite
7 Dolomite
8 Shale
9 Sublitharenite

Raw-data matrix

No	#1	#2	#3	#4	#5	#6	#7	#8	#9	Total
1	0	0	6	1	0	1	4	5	0	17
2	2	0	0	0	0	1	0	1	0	4
3	4	1	0	0	1	0	2	1	1	10
4	0	0	1	0	0	0	0	0	0	1
5	1	0	0	0	0	1	0	0	0	2
6	1	0	0	0	0	0	1	1	3	6
7	6	0	0	0	1	1	0	0	0	8
8	2	3	1	0	0	2	0	0	0	8
9	1	0	2	0	0	1	0	0	0	4
	17	4	10	1	2	7	7	8	4	60

Expected values for quasi-independence

No	1	2	3	4	5	6	7	8	9
1	-	1.5	4.2	0.36	0.73	2.71	2.81	3.21	1.5
2	1.49	-	0.68	0.06	0.12	0.44	0.45	0.52	0.24
3	4.2	0.68	-	0.16	0.33	1.23	1.27	1.46	0.68
4	0.36	0.06	0.16	-	0.03	0.1	0.11	0.12	0.06
5	0.72	0.12	0.33	0.03	-	0.21	0.22	0.25	0.12
6	2.36	0.38	1.07	0.09	0.18	-	0.71	0.82	0.38
7	3.16	0.51	1.43	0.12	0.25	0.93	-	1.1	0.51
8	3.21	0.52	1.46	0.12	0.25	0.94	0.97	-	0.52
9	1.49	0.24	0.68	0.06	0.12	0.44	0.45	0.52	-

Difference matrix

No	1	2	3	4	5	6	7	8	9
1	-	-1.5	1.8	0.64	-0.73	-1.71	1.19	1.79	-1.5
2	0.51	-	-0.68	-0.06	-0.12	0.56	-0.45	0.48	-0.24
3	-0.2	0.32	-	-0.16	0.67	-1.23	0.73	-0.46	0.32
4	-0.36	-0.06	0.84	-	-0.03	-0.1	-0.11	-0.12	-0.06
5	0.28	-0.12	-0.33	-0.03	-	0.79	-0.22	-0.25	-0.12
6	-1.36	-0.38	-1.07	-0.09	-0.18	-	0.29	0.18	2.62
7	2.84	-0.51	-1.43	-0.12	0.75	0.07	-	-1.1	-0.51
8	-1.21	2.48	-0.46	-0.12	-0.25	1.06	-0.97	-	-0.52
9	-0.49	-0.24	1.32	-0.06	-0.12	0.56	-0.45	-0.52	-

Sequence chi-squared matrix

No	1	2	3	4	5	6	7	8	9
1	-	1.5	0.78	1.16	0.73	1.08	0.51	0.99	1.5
2	0.17	-	0.68	0.06	0.12	0.72	0.45	0.45	0.24
3	0.01	0.15	-	0.16	1.37	1.23	0.42	0.14	0.15
4	0.36	0.06	4.33	-	0.03	0.1	0.11	0.12	0.06
5	0.1	0.12	0.33	0.03	-	2.92	0.22	0.25	0.12
6	0.78	0.38	1.07	0.09	0.18	-	0.11	0.04	18

7	2.56	0.51	1.43	0.12	2.29	0.01	-	1.1	0.51
8	0.46	11.85	0.14	0.12	0.25	1.19	0.97	-	0.52
9	0.16	0.24	2.58	0.06	0.12	0.72	0.45	0.52	-

Asymmetry chi-square matrix

No	1	2	3	4	5	6	7	8	9
1	-	-	-	-	-	-	-	-	-
2	2	-	-	-	-	-	-	-	-
3	0.4	1	-	-	-	-	-	-	-
4	1	0	1	-	-	-	-	-	-
5	1	0	1	0	-	-	-	-	-
6	0	1	0	0	1	-	-	-	-
7	0.4	0	2	0	1	0	-	-	-
8	1.29	1	0	0	0	0.33	0	-	-
9	1	0	0.33	0	0	1	0	0	-

Sequence chi-squared sum=73.5573 55 degrees of freedom
Asymmetry chi-squared =17.7523 21 degrees of freedom

Principal succession for facies
Binomial probabilities listed

Micrite-biomicrite (variably fossiliferrou) to Intramicrite	(conf. <0.95;	BP=0.2251)
Biospartie to Oosparite	(conf. <0.95;	BP=0.3712)
Intramicrite to Dolomite	(conf. <0.95;	BP=0.3695)
Pelmicrite to Intramicrite	(conf. 0.95-0.99	BP=0.1620)
Oomicrite to Oosparite	(conf. <0.95;	BP=0.2011)
Oosparite to Sublitharenite	(conf. >0.99;	BP=0.0044)
Dolomite to Micrite-biomicrite (variably fossiliferrous)	(conf. <0.95;	BP=0.0466)
Shale to Biosparite	(conf. >0.99;	BP=0.0120)
Sublitharenite to Intramicrite	(conf. <0.950	BP=0.1359)

Other significant preferrd transitions

(NB: binomial probabilities between 0.1 and 0.2 don't mean much)

Binomial probability for cell 1 , 3 = 0.225092425942421
Binomial probability for cell 1 , 5 = 0.476625919342041
Binomial probability for cell 7 , 1 = 4.655976966023445E-002

3.2.2 Fischer plots

Terminology and methodology

Fischer plots have great application in the study of cyclic shallow-water carbonates and are best suited for peritidal cycles, in which thickness is largely controlled by sea level (Osleger and Read, 1991). Fischer plots illustrate deviations from average cycle thickness throughout a stratigraphic interval, which can be related to the relative changes in accommodation space through time, by using the horizontal axis as a relative time scale (Fischer, 1964; Read and Goldhammer, 1988; Goldhammer et al., 1990). However, Sadler et al. (1993) stressed that Fischer plots are graphic displays, that plot the cumulative departure from a mean unit (or cycle) thickness against unit (or cycle) number (not time or depth), through a vertical sequence of upward-shallowing peritidal carbonates with stacking patterns. The details of the plot construction are given in Sadler et al. (1993). Since the plot is based upon the mean thickness of all its units, it resembles an erratic bridge that begins and ends at the same elevation. As thinner-than-average peritidal cycles are more common, the form of waves in Fischer plots are predominantly asymmetric (rise steeply and fall more gradually). Sadler et al. (1993), suggested a lower limit of 50 units or cycles for peritidal carbonates, because plots of less than 50 cycles will often fail to reveal the non-random stacking pattern that characterises longer sections of peritidal carbonate cycles.

In Fischer plots, each unit may be classed as either thick or thin, relative to the mean thickness of all units in the section. Groups of consecutive occurrence of adjacent units, thicker or thinner than the mean, are then defined as runs. On the Fischer plot, a run of units thicker or thinner than the grand mean have positive or negative slopes respectively. The total number of runs is shown by r, the actual number of units thicker than the mean is n1, and the actual number of units thinner than the mean is n2. The Z score,which is used to test for randomness in the size of runs, can be calculated directly from the following equation (see Sadler et al., 1993):

$$Z = \frac{r - \left\{ \frac{2n_1 n_2}{n_1 + n_2} + 1 \right\}}{\sqrt{\left\{ \frac{2n_1 n_2 \left(2n_1 n_2 - n_1 - n_2\right)}{\left(n_1 + n_2\right)^2 \left(n_1 + n_2 - 1\right)} \right\}}}$$

A Z-score of -2, means an r value of two standard deviations below the expectation for random stacks. Standard tables of area under the normal curve reveal that there is a greater than 97.7% (or less than a 2.3%) chance that random stacking could produce fewer runs (Saddler et al. 1993). They have proposed that Fischer plots have predominantly negative Z-scores, indicating that the data in peritidal carbonates have significantly fewer and, thus, longer runs compared to random stacking. In other words, there is a greater than 97.7% chance that sedimentation in peritidal carbonates is non-random. A completely random stack would have a Z score of 0.00, n_2/n_1 of 1.0 and r/n_1+n_2 of 0.5. Saddler et al. (1993) also suggested that the asymmetry of the wave trains on Fischer plots is strongly influenced by the skewness of the frequency distribution of unit thickness (as there is no limit to maximum unit thickness), and should not routinely be attributed to tectonic or eustatic processes. Since bed-thickness distributions are predominantly positively skewed, the typical wave form is likely to rise steeply and fall gently in plots of any facies succession.

The Fischer plots presented in this study have been generated by a custom-written spreadsheet which plots both a conventional Fischer plot and a histogram of unit thickness. The plots are relative to the mean. The grand mean, rather than zero, has been used as a datum.

Fischer plots from the Mozduran Formation

Fischer plots have been generated for the Mozduran Formation in four stratigraphic sections (see Appendix 3) that cover a lateral distance of about 60 km. The Z score and other statistical parameters are shown in Table 3.3. Although the validity of Fischer plots depends on the number of units (at least 50 units) in peritidal carbonates, Fischer plots were generated in the Padeha section with only 37 units for correlation. As Fischer plots provide a valuable correlation tool, they could prove useful in studying cyclic sequences of widely differing thicknesses, in which biostratigraphic control is typically poor (Read and Goldhammer, 1988). The Z score in the Padeha section indicates that there is 98.84% chance that the observed thickness variations in beds is non-random. The Z score in the Mozduran section indicates that there is 61% chance that such a plot is non-random. The Z score in the Gorgoreh section indicates that there is 94.5% chance that the observed thickness variations in beds is non-random, and that the plot is not being unduely affected by any abnormally large thicknesses. The statistical analysis of the Fischer plot in the Bazangan section indicates that there is 87% chance that such a plot is non-random.

Table 3.3. Statistical analysis of the Fischer plots.

	Sections Analyzed			
	Padeha	Mozduran	Gorgoreh	Bazangan
Number of beds	37	68	72	104
Mean thickness	4.89	7.45	9.75	11.32
Standard Deviation	4.01	6.35	7.07	8.55
Total thichness	180.7	506.7	701.7	1131.9
Maximum bed thickness (m)	20.8	30.8	42.4	54.5
Minimum bed thickness (m)	0.8	0.7	2.2	2.5
Number of thick beds (n_1)	14	21	26	38
Number of thin beds (n_2)	23	47	46	66
n_1/n_2	0.6	0.44	0.56	0.57
Number of runs (r)	12	29	28	44
r/n_1+n_2	0.32	0.42	0.38	0.42
Z score	-2.27	-0.29	-1.6	-1.11
% Chance non-random	98.84	61	94.5	87

Fischer plots have been used to interpret variation in relative sea-level. Fischer (1964) introduced the concept that if cumulative cycle thicknesses of peritidal carbonates were corrected for linear subsidence and plotted aginst time, using an average cycle period, then the plots show departures in relative sea level. On Fischer plots of peritidal cyclic succession, it has been suggested that if there is a long term rise in sea level (or an increase in sudsidence), relatively thick cycles of storm dominated, open marine subtidal carbonate facies, or thick, deep ramp, shale-based cycles will develop (Read and Goldhammer, 1988; Osleger and Read, 1991). Stacks of thick cycles plot as positive slopes and are presumed to have formed under conditions of increased accommodation space provided by a rise in relative sea-level. If there is a long term fall, thin cycles of more restricted shallow subtidal facies will develop. Stacks of thin cycles plot as negative slopes and are presumed to reflect reduced accommodation space during relative sea-level fall. The cycles on the rising part of the plots are interpreted as the transgression system tract, with open marine facies. The maximum positive departure (or peaks on the curve) corresponds to the maximum flooding surface (Vail, 1987), approximating the net eustatic highstand of sea level. Cycles on the falling limb of the plots constitute the highstand systems tract, characterized by carbonate cycles that progressively thin upward in the sequence, and contain the most early dolomite. These reflect a decrease in accommodation potential.

In areas of low subsidence rates (Padeha section), the amplitudes of the plots are lower than those with high subsidence rates (Bazangan section). The area with the lower subsidence rate probably has many cycles omitted on the fall, compared with the area with the higher subsidence (Read and Goldhammer, 1988). The subsidence rate was calculated by thickness/ time, and average cycle period by, duration of formation [m.y.] × thickness of measured cyclic section divided by number of cycles in the measured section × thickness of formation. The subsidence rates for the Padeha, Mozduran, Gorgoreh and Bazangan sections are 10.6, 29.8, 41.3 and 66.6 m per million years respectively, calculated by using 17 m.y. (Cowie and Bassett, 1989) for the Upper Jurassic period. The average cycle periods for the Padeha, Mozduran, Gorgoreh and Bazangan sections are 0.46, 0.25, 0.23 and 0.16 m.y. respectively. In the Padeha section, most cycles which show evidence of subaerial exposure, such as birds eye structure and /or gypsum pseudomorphs and algal structure, are on the falling portions of the Fischer plot. Thick weathered gypsiferous layers are also on the falling portions of the plot.

The Fischer plot and histogram of unit thickness of the Mozduran Formation in the Mozduran type section show stacks of relatively deeper subtidal cycles on the rising segments of the plot (Fig. 3.9). These cycles are characterized by relatively thick shale beds, dark dense muddy carbonate (micrite-fossiliferous micrite), biosparite, oosparite and intramicrite facies. Sand-size detrital quartz grains, gypsum pseudomorph crystals, stromatolite and birds eye structures are rare. The falling portions of the Fischer plot are characterised mainly by thin, sandy intramicrite, dolomite, and a few sublitharenite and oolitic facies. Some oolite facies are intercalated with thin beds of sublitharenite. Most of the sublitharenites become common toward the troughs on the plot. The common lithofacies within these shallow platform cycles are sandy intramicrite, sandy micrite, micritized oomicrite, stromatolites and algae, associated with subaerial exposure textures, evaporite-solution collapse, gypsum pseudomorphs and flat pebble conglomerates, all of which are indicative of shallow, restricted conditions. Cycles on the the rising portions of the Fischer plot are considerably thicker than those on the falling portions. The variation in cycle thickness in the Mozduran Formation can be related to the total amount of accommodation space provided by subsidence and eustatic sea-level changes (Osleger and Read, 1991). Most of the algae are located on the falling portions of the Fischer plot, which may indicate a long-term fall in sea level.

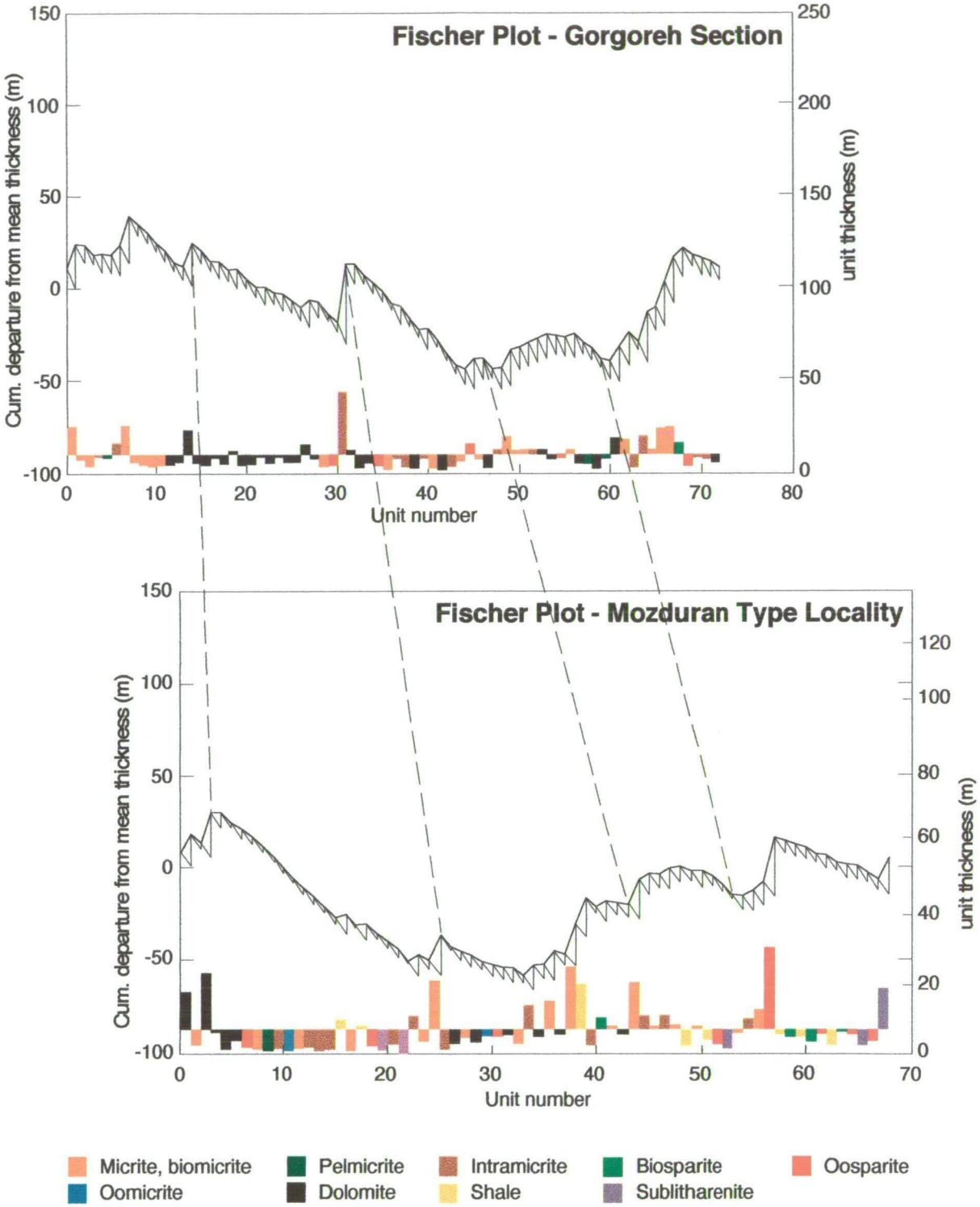

Figure 3.9 Fischer plot and histogram of unit thickness of the Mozduran Formation in the Mozduran and Gorgoreh sections.

The Fischer plot of the Gorgoreh section shows stacks of relatively deeper subtidal cycles on the rising segments of the plot. (Fig. 3.9) These cycles are characterized by mainly sponge biomicrite and some biointramicrite cycles. There is no evidence that indicates shallow, restricted conditions on the rising segments of the plot. In the Gorgoreh section, as dolomite beds are very common and randomly distributed throughout the sequence, the primary texture of rocks has been completely oblitrated. Therefore, facies interpretation is very difficult in this section.

The Bazangan Fischer plots illustrate a significant difference in cycle thickness and lithofacies composition between stacks of cycles on the rising and falling segments of the plot, which can be related to the rising and falling of relative sea level. The subtidal-dominated cycles are considerably thicker than those of the landward peritidal-dominated cycles. The Bazangan facies are dominated by shallowing-upward peritidal sequences. The carbonate cycles consist mainly of alternating sequences of marl, intramicrite, micrite, and a few shale beds, overlain by a few dolomite layers, pelmicrite, oomicrite and intramicrite (subtidal), grading up into fossiliferous and algal biomicrite, peloidal, and oolitic facies (subtidal to lower intertidal origin), which are capped by laminated micrite (intertidal to supratidal facies).

Boss and Rasmussen (1995) tested the use of Fischer plots as sea-level curves on a shallow carbonate platform (Great Bahama Bank), where accommodation was created primarily by sea-level rise (the Holocene postglacial rise) over the platform margin (i.e., subsidence was minimal). Results of this survey demonstrated that Holocene sediment (cycle) thickness and accommodation are not correlated. Consequently, Fischer plots constructed by using Holocene cycle thicknesses are poor representations of the Holocene transgression. The interpretation of Boss and Rasmussen (1995), has been recently contested and the subject remains controversial.

Effect of sedimentation rate on the form of Fischer plots

The Fischer plots of some relatively deeper subtidal successions of cyclic carbonates, show an opposite trend to that expected from the above examples. Within the Bazangan section, a thick succession of shallow restricted cycles of fossiliferous to biomicritic facies with evidence of subareial exposure and many gypsum pseudomorph crystals, which would be expected to be associated with a long-term fall in sea level, plot as a positive slope on the Fischer plot. In contrast, the plot of the thin deeper subtidal facies, which would be expected to form a

long-term rise in sea level, plot as a negative slope. One reason for this result may be that the relative thickness of subtidal cycles is controlled by sedimentation rates, rather than by sea-level-determined accommodation space (Osleger and Read, 1991). Thick biomicritic facies may have accummulated rapidly within the zone of optimal carbonate productivity, rapidly filling to near sea level. In contrast, the thinner, argillaceous, deeper water cycles may simply have accumulated slowly. Thus, the resulting trend on the Fischer plot is an *apparent* long-term rise and fall in sea level.

3.3 Depositional model

During the Upper Jurassic, the Kopet-Dagh Basin was covered by a widespread epicontinental sea, which marked a period of maximum marine transgression. The transgression most probably had a direction from west to the east of the study area, with the west remaining relatively deeper.

The depositional setting of the Mozduran Formation is interpreted to be a carbonate ramp with a very gentle slope, deepening to the west. "Carbonate ramps are a type of carbonate platform where there is no major break of slope from shoreline into deeper water" (Tucker et al., 1993). They are also characterized by gradual facies transitions (Sami and James, 1993). On ramps, a high energy grainstone facies is developed on the landward part of the ramp, in contrast to rimmed shelves, which are located on the basinward edge of the shelf (Wright, 1986). Large reefal structures are generally absent on ramps (Tucker et al., 1993).

The very gentle gradient (Fig. 2.7), the gradual facies transition, the presence of oolite facies in the most landward margin of the basin (such as the Bagak section, see Appendix 1), and the lack of reefal structures, are used as evidence for a ramp carbonate setting in the most eastern part of the Kopet-Dagah Basin. However, Lasemi (1996) suggested that the Mozduran Formation was deposited on a rimmed carbonate platform adjacent to a deeper marine environment, and that oolite facies are restricted to the platform margin.

The Trucial Coast region in the Persian Gulf is regarded as a recent example of a carbonate ramp (Wilson, 1975). Carbonate ramps have been suggested for the Upper Jurassic Smackover Formation, USA (Moore, 1984), the Upper Jurassic carbonates of the Lusitanian Basin, Portugal (Ellis et al., 1990), and the Upper Jurassic carbonates in the Central Iberian Chain, northeast Spain (Aurell and Melendez, 1993).

During deposition of the Upper Jurassic Mozduran carbonates, a combination of differential sediment loading subsidence (Moussavi-Harami and

Brenner, 1992), and eustatic sea level change (Haq et al., 1987; Hallam, 1988, see Fig. 2.3) caused facies and thickness change across the ramp. Thus, the ramp facies is divided into three main zones. These are referred to as the inner, middle and outer ramp zones, corresponding to supratidal-intertidal (tidal flat), shallow and deeper subtidal facies respectively (Fig. 3.10).

Inner ramp zone (supratidal-intertidal zone)

This is the landward portion of the carbonate province which underwent less to moderate subsidence, compared to the higher subsidence rate in the relatively deeper part of the basin. The inner ramp zone is divided into supratidal and intertidal facies (Fig. 3.10). The supratidal facies consists mainly of very finelly crystalline dolomite, sandy micrite, and weathered gypsiferous beds. The presence of scattered detrital sand to silt-sized grains, birdseye textures, calcitized pseudomorphs after gypsum, and the general absence of marine organisms, supports a supratidal origin.

The sandy pelmicrite and intramicrite facies, microbial laminated mats and stromatolites, calcite pseudomorphs after gypsum and fenestral textures are characteristic features of the upper intertidal zone. In contrast, the oolite and biofacies, along with intrasparite facies, were deposited in the high-energy (wave-agitated) lower intertidal to upper shallow subtidal environments. The oolite facies are scattered throughout the stratigraphic sections in the shallowest part of the basin. The lack of mud matrix, the high faunal diversity and density (such as, brachiopods, echinoderms and bivalves), large-scale cross-bedding, and lack of fenestral fabrics support this interpretation.

Mid-ramp zone (shallow subtidal)

In this zone the sequence is thicker and lithologies consist predominantly of thinly to medium bedded, dark to medium grey, intramicrite, biomicrite facies. Fauna consist mainly of sponge spicules, crinoids and forams (milliolida). Although pervasive dolomitization of the limestone sequence in this zone has destroyed most of the sedimentary textures, fine to relatively coarse laminations, continuous planar and parallel bedding and low to medium faunal diversity are characteristic features of this zone. Lithology, faunal distribution and sedimentary structures, suggest medium energy deposition, largely below wave-base.

Outer ramp zone (deeper subtidal)

This is the thickest sequence with the greatest subsidence rate. This sequence, which was probably deposited below the storm wave-base, is characterized mainly by alternating sequences of thinly to medium bedded dark grey lime mud facies and thinly bedded marl and shale facies. The limestone beds contain a moderate abundance of fossils, including sponge spicules, crinoids, benthic forams (milliolida, globegerina and Lagenid), bryozoa and solitary corals. The oolite facies, fenestral fabrics, calcite pseudomorphs after gypsum, and detrital silt-sized quartz grains are absent in the deepest part of the outer ramp. The lithology, sedimentary textures and faunal distribution in this part of the basin are characteristic features of deeper water environments (Afshar-Harb, 1979; Elmi, 1990). In the Bazangan section, the deeper water facies are overlain by a few medium to coarsely crystalline replacement dolomites, pelmicrite, oomicrite, oncolites and intramicrite facies (shallow subtidal or middle ramp facies), grading up into mostly oolitic and biofacies (lower intertidal), which are capped by laminated lime mud (upper intertidal to supratidal) facies. Therefore, the vertical succession reveals a shallowing-upward arrangement of facies. The outer ramp facies is possibly the main source of hydrocarbons in the Mozduran reservoir (Afshar-Harb, 1979).

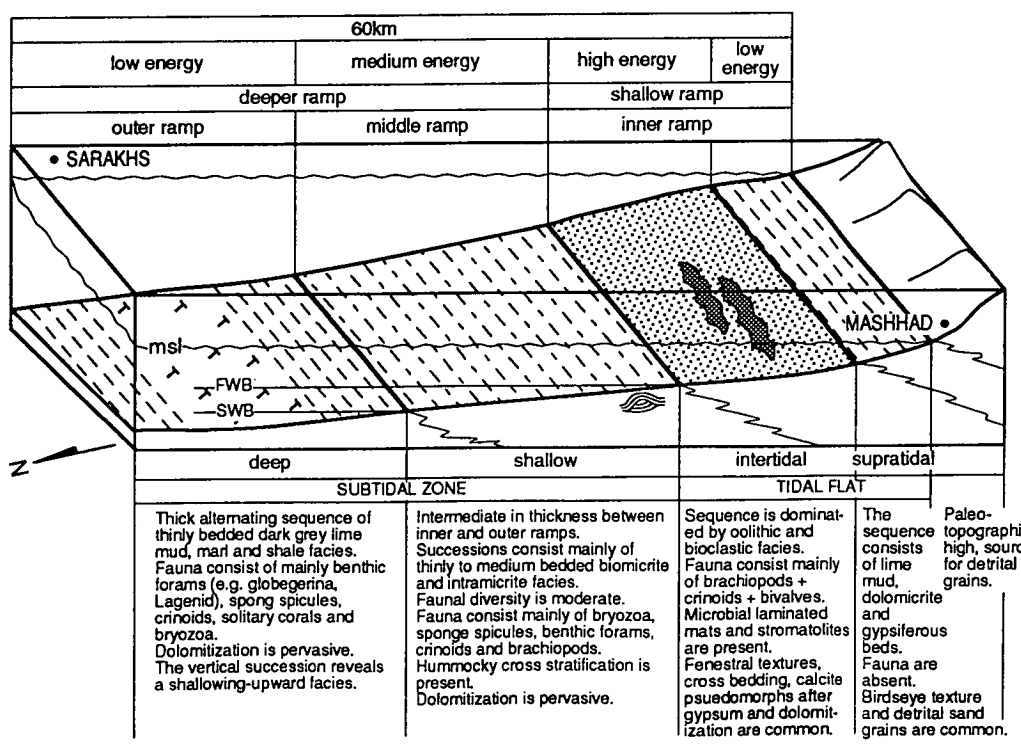

Figure 3.10. Generalized model for deposition of the Upper Jurassic Mozduran Formation in the eastern Kopet-Dagh Basin.

Although deposition of most facies in the Mozduran Formation preferentially occurred during transgression phases, some facies, such as three thin layers of fine to medium-grained sublitharenite-litharenite, measured throughout the stratigraphic sections, occurred during regression phases. This can be related either to eustatic sea level changes (Haq et al., 1987; Hallam, 1988) or to localized tectonic base-level activities, as suggested by Afshar-Haeb (1979) and Berberian and King (1981).

Detrital sand grains and most of the terrigenous facies were being sourced from the exposed pre-existing sedimentary and plutonic rocks (hinterland area) that formed paleotopographic highs in the south. This is reflected by a decreasing abundance of sand size detrital grains towards the north-west part of the study area.

Markov chain analysis in all stratigraphic sections measured confirmed non-random sedimentation (Table 3.1). Fisher plots indicate that observed thickness variations in beds is also non-random (Table 3.3). The variation in bed thickness in the Mozduran Formation is attributed to the total amount of accommodation space provided by subsidence and eustatic sea-level changes. The increasing number of beds from 37 in the Padeha section (east of the study area) to 104 in the Bazangan section (west of the study area) can be related to the significant increase in accommodation space. The sediment accomodation space in the Mozduran carbonate resulted from sediment loading subsidence (Moussavi-Harami and Brenner, 1992), which was concomitant with eustatic sea level rise across the basin. Sedimentation rates were much lower in the outer ramp zone, as reflected by the increase in number of thin beds in the Bazangan section (66), compared to the Padeha section (23). In contrast, sedimentation rates increased relative to the accomodation rate, resulting in the progradation of marginal facies over the deeper ramp facies.

At the end of the Upper Jurassic, there was a regional regression which involved a general withdrawl of the sea basinward (to the west of the study area). This resulted in the deposition of fluvial sediments of the overlaying Shurijeh Formation.

CHAPTER 4

LIMESTONE DIAGENESIS

CHAPTER 4

LIMESTONE DIAGENESIS

4.1 Introduction

The study of the diagenetic history of the Mozduran carbonates is based mainly on conventional and cathodoluminescence microscopy, in conjunction with some elemental and isotopic analysis of carbonate cements. The Mozduran limestones have undergone several diagenetic alterations including: multiple cementation; micritization; physical and chemical compaction; silicification; and dolomitization. The following is an overview of major diagenetic features in the Mozduran limestones which may be used to infer original and diagenetic environments, and timing and geochemical conditions during carbonate cement formation (e.g., Marshall and Ashton, 1980; James and Choquette, 1984; Lohmann, 1988; Machel and Burton, 1991; Heydari and Moore, 1993).

4.2 Cementation

Petrographic investigation of the Mozduran limestone reveals that sparry calcite is the main pore filling cement, which occurs in interparticle, intraparticle, moldic and fenestral porosities and along the fractures. Dolomite cements occur in minor amounts in the Mozduran carbonates and are discussed later in Chapter 8.

Different generations of sparry calcite cement are recognized in the Mozduran limestones, ranging from marine through meteoric to burial cements.

4.2.1 Marine cementation

The main cementation features formed under marine conditions in the Mozduran limestones are 1) acicular to fibrous, 2) radial fibrous, 3) bladed, and 4) equant sparry calcite cements, which occur as intra- and intergranular cements. Turbid syntaxial overgrowths and micritic cements are present as minor

components.

4.2.1.1 Acicular to fibrous isopachous cements

These cements occur as: isopachous (i.e., of equal thickness) fringes around allochems such as ooids (Figs. 4.1 A-E); growing as intergranular cement within red algae components (Fig. 4.1 F); or as isopachous lining in a single small intergranular pore (Figs. 4.2 A-C). The acicular to fibrous crystals range in size from 12 to 64μm, commonly nucleate on grains, and grow outward, normal to the grain surfaces. These cements were possibly composed of aragonite mineralogy, due to the identical morphology to that of Recent warm water shallow marine aragontic cements (Given and Wilkinson, 1985; Adabi and Rao, 1991). Aragonite cements are rarely preserved as aragonite in the limestones as the mineral is metastable. However, the crystal fabrics of acicular cements in the Mozduran limestones appear to be mostly in their original state and have not been significantly affected by dissolution, but rather altered through calcitization processes. The fibrous cements generally have length to width ratios of 6:1 to 12:1 (Folk, 1965).

Cathodoluminescence petrography illustrates that acicular to fibrous cements are dull to non-luminescent (Figs 4.1 B, 4.2 B), possibly indicating a marine origin. Marine cements are typically non-luminescent, since seawater contains negligible amounts of trace elements as activators (such as Mn) and quenchers (such as Fe). Thus, marine cements are characterized by non-luminescence and early generations within a filled pore. However, exceptions may exist. For example, Major et al. (1987) have reported luminescence in modern bladed magnesian calcite marine cements from the Little Bahama Bank.

These acicular to fibrous isopachous cements of the Mozduran limestones are considered to be marine, based on several petrographic evidences, such as: 1) they are first generation cements which predate other cements, 2) they have acicular to fibrous fabrics, 3) they commonly form isopachous fringes around the grains or cavity wall, 4) they are succeeded by bladed, equant, and then followed by later coarsely crystalline sparry calcite cements, and 5) the crystals are nonferroan and non-luminescent (Marshal and Ashton, 1980; James and Choquette, 1983; Tucker, 1991). All the above evidence supports early marine phreatic (below the water table) cementation, where pores were constantly water-filled. Modern aragonite cements with acicular fabrics are forming inorganically in intertidal to shallow marine subtidal environments, supporting the above interpretation. Acicular to fibrous isopachous cements are present only in sections

Figure 4.1. Petrographic features of early marine cement.

A. Oosparite facies with an early isopachous acicular to fibrous (F) intergranular cement. Thin section Mz 58.

B. Same area as in A under cathodoluminescence. Note acicular to fibrous cements are dull luminescent (D, black arrow).

C. Close up of the same thin section under plain polarized light. Note clear acicular to fibrous (F) calcite cements (white arrows).

D. SEM photomicrograph illustrating the first generation of fibrous isopachous cement around the micritized ooids, followed by columnar or bladed cement with rhombic termination (RT). Note porosity was completely occluded by equant to subequant late pore filling calcite cement. Thin section Mz 109.

E. SEM image illustrating an acicular to fibrous isopachous cement in an oolitic facies. Note enlarged view of enclosed area on the right hand side of photo. Thin section Mz 95.

F. Photomicrograph showing fibrous crystals (F), growing as intragranular cement within the red algae components. Thin section Mz 106.


A
F
250 µm

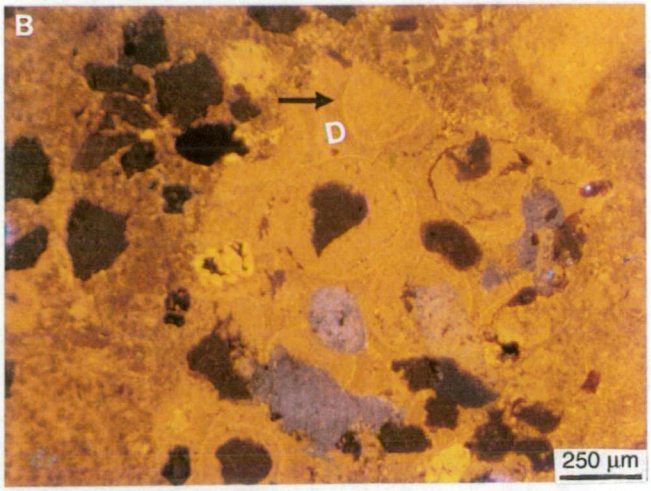
B
D
250 µm

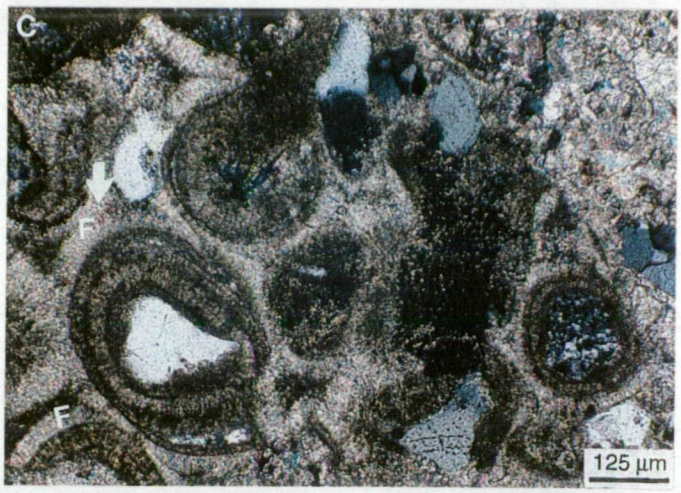
C
F
F
125 µm

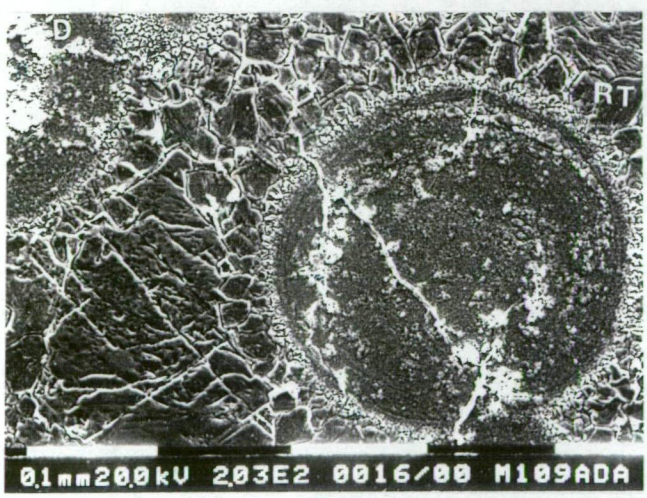
D
RT
0.1mm20.0kV 2.03E2 0016/00 M109ADA

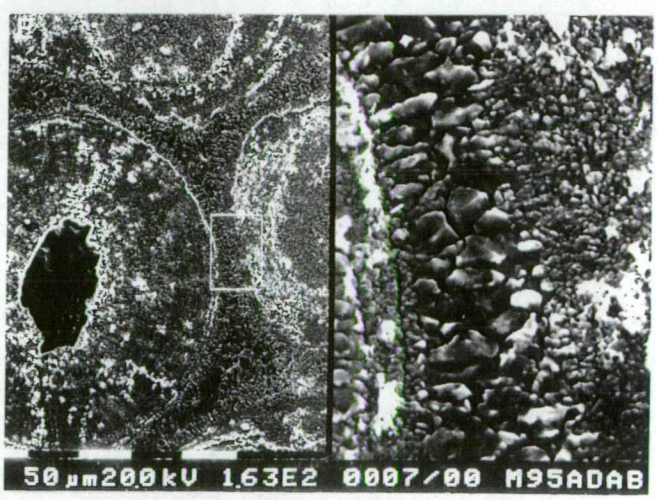
E
50µm20.0kV 1.63E2 0007/00 M95ADAB


F
F
F
250 µm

from the shallowest part of the basin (Fig. 2.7), which was inferred to have an original aragonitic mineralogy (Adabi and Rao., 1991). The significance of Upper Jurassic aragonite mineralogy in relation to seawater temperature, is discussed later in Chapters 5, 6, and 7. Although the acicular to fibrous cements are rarely preserved, they can comprise up to ~6% of the total bulk carbonates. In the Mozduran Formation, the calcite cements are more common than aragonitic cements, and occur particularly in the relatively deeper part of the basin (Fig. 2.7). The calcite cements are discussed in the following sections.

Unfortunately, acicular to fibrous cements were too fine-grained to sample for elemental and isotopic analysis.

4.2.1.2 Bladed isopachous sparry calcite cements

In the Mozduran limestones, bladed calcite cements occur as interparticle spars, particularly on ooids (Figs. 4.2 D, 4.3 E), skeletal fragments (Figs. 4.5 B, F), intraclasts, and within cavities (Fig. 4.2 F). Individual crystals often show bladed crystal morphology with scalenohedral terminations. The bladed crystals are oriented perpendicular to the substrate and grow as an isopachous fringe. The bladed cements in the Mozduran limestones are commonly followed by a later generation of clear equant, drusy mosaic or platy calcite cements (Figs. 4.2 F, 4.3 E, 4.5 A, C). The succession from bladed to coarser calcite cements may record changing pore fluids, starting with normal marine fluids and progressing through more meteoric to burial fluids. Bladed cements generally have length to width ratios of 1.5:1 to 6:1 (Folk, 1965). In the Mozduran limestones, the bladed calcite crystals are 30-80μm long and generally less than 20 μm wide, commonly forming isopachous fringes. The isopachous nature of these cements indicates early cementation (as an open framework is needed for fringes to form around the allochems) and are interpreted as marine cement (James and Choquette, 1983; Hird and Tucker, 1988). The bladed calcite fabrics, forming isopachous fringes around the grains, were interpreted as marine high-Mg calcite cements (Bricker, 1971; Prezbindowski, 1985; Aissaoui, 1988). However, Longman (1980) suggested this type of cement morphology can develop in both meteoric and marine environments. The bladed calcite cements constitute ~3-4 % of the total bulk carbonate compositions.

Cathodoluminescence petrography illustrates that bladed calcite crystals are mostly non-luminescent (Figs. 4.2 G, 4.3 F). However, in a few thin sections, early bladed cements exhibit bright luminescence (Fig. 4.2 E). Two interpretations for such variations in luminescence are plausible. First, it is possible that the

Figure 4.2. Petrographic features of early marine cement.

A. Isopachous lining of thin early acicular to fibrous cement (F) in a single small intergranular pore. Note remainder of pore is filled by late coarsely crystalline clacite cements. Thin section Mz 22.

B. Same area as in A under cathodoluminescence. Note early acicular to fibrous cements are non-luminescent (black arrows).

C. Close up of the same area as in A. Note well defined acicular to fibrous (F) isopachous cements (white arrows). Thin section Mz 22.

D. Ooids rimmed with first generation bladed calcite cement (black arrows). Thin section Mz 109.

E. Same area as in D under cathodoluminescence. Note early luminescent bladed calcite cement, followed by dull (dark-brown) luminescence of late calcite cement.

F. Thin section photomicrograph showing isopachous bladed calcite cement (BC) lining the cavity. Note sharp boundary between the bladed calcite crystals (BC) and the adjacent later coarse calcite crystals filling the rest of the cavity. The bladed calcite crystals illustrate scalenohedral terminations. Note micritic cement (MC) occurs between two generations of bladed calcite cement. Thin section Bz 60.

G. Same area as in F under cathodoluminescence. Due to the non-luminescent character of the bladed calcite crystals, these cements are inferred to be marine rather than meteoric in origin.

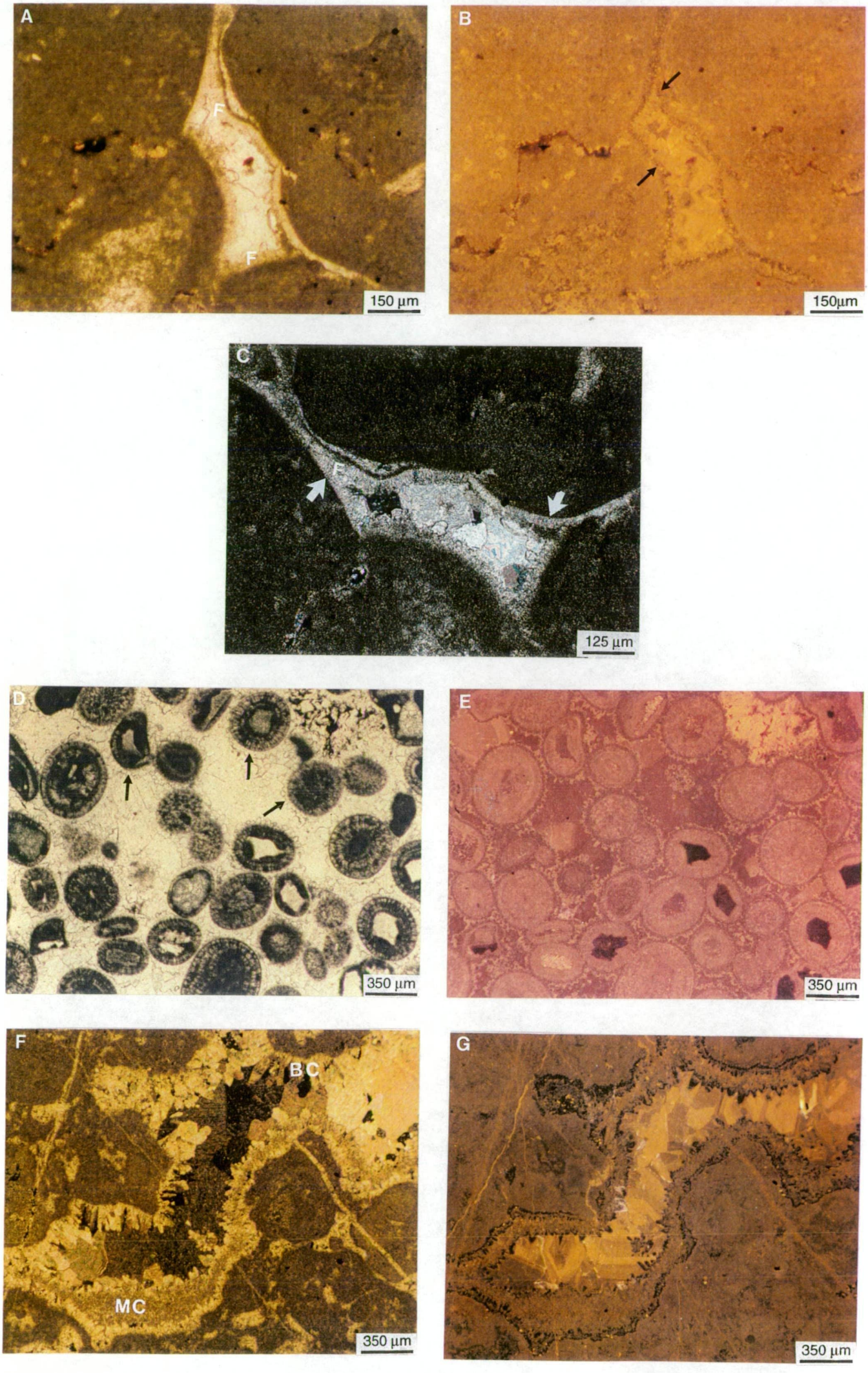
A
F
F
150 µm
B
150µm
C
F
125 µm
D
350 µm
E
350 µm
F
BC
MC
350 µm
G
350 µm

change in luminescence intensity is primary. For example, Adams and Schofield (1983) reported that Holocene marine cements are generally non-luminescent, but when precipitated in locally reducing intergranular micro-environments, may luminesce brightly. It is possible, therefore, that these early cements record variable degrees of communication between pore fluids and overlaying marine water, variable degrees of Mn^{2+} incorporation into the growing calcite cement and variable Eh (Wilkinson et al., 1985).

Alternatively, variation in early cement luminescence may be a late diagenetic attribute. Stabilization of high-Mg calcite cement to low-Mg calcite in manganese enriched pore fluids, particularly in reducing conditions, would result in the formation of luminescent calcite (Wilkinson et al., 1985).

These type of cements are termed bladed spar by James et al. (1976), fibrous Mg-calcite by Shinn (1971), and Palisade cement by Schroeder (1973).

Thin bladed cement rinds were too small to drill for elemental and isotopic analysis.

4.2.1.3 Radial fibrous cements

Radial fibrous calcite cements in the Mozduran limestones occur as elongate crystals oriented perpendicular to the substrate, and often show a cloudy appearence relative to later clear sparry calcite cements. The lack of subcrystals, straight cleavages, and absence of undulatory extinction are characteristic features of radial cements (Fig. 4.3 A). The crystals are non-ferroan, commonly 8-26μm in width and 32-150 μm in length, and often show rhombic terminations. The radial fibrous cements comprise up to ~4% of the total bulk carbontes. The radial fibrous cements can be originally low-or high-Mg calcite. It is difficult to determine original mineralogy, since Mg in high-Mg calcite is lost during diagenesis. However, the presence of rhombic terminations in the calcite crystals, are commonly interpreted as being former Mg-calcites (James and Ginsburg, 1979; Pierson and Shinn, 1985; Scofffin, 1987). Although there has been much discussion about the origin of this cement, it is now interpreted as primary marine precipitation (Kendall, 1985).

4.2.1.4 Equant isopachous sparry calcite cements

In the Mozduran limestones coarse equant isopachous sparry calcite cement is present on oolitic facies (Fig. 4.3 B). This cement constitutes up to ~7% of the total bulk carbonates. The coarse equant sparry calcite cements are mostly of meteoric and burial origin. However, they also occur as first generation

cements in many shallow marine Holocen settings (James and Ginsburg, 1979; Pierson and Shinn, 1985). Even though most Holocene low-Mg calcite is typically equant, coarse equant high-Mg calcite has also been reported from several recent shallow marine settings (Pierson and Shinn, 1985). Since the equant high-Mg calcite has also been reported from the Jurassic hardground cements (Wilkinson et al., 1985), it is therefore possible that coarse equant isopachous sparry calcite cements in the Mozduran limestone were precipitated as marine high-Mg calcite. Wilkinson et al. (1985) suggested that the presence of equant morphology as both low-Mg and high-Mg calcite in Holocene settings may indicate that calcite cement morphology is related to rates of precipitation and other kinetic variables, rather than to ambiant Mg/Ca ratios. A staining technique suggested that the cement contains less than one percent $FeCO_3$ in solid solution (Lindholm and Finkelman, 1972).

Equant isopachous cements were too fine-grained to sample for elemental and isotopic analysis.

4.2.1.5 Turbid syntaxial overgrowth cements

Syntaxial, or epitaxial, overgrowth cements grow as single crystals on echinoderm grains, which are the second most common biogenic fragments in the Mozduran limestones. Two kinds of syntaxial overgrowth cements are recognized in the Mozduran Formation: 1) turbid syntaxial and 2) clear syntaxial overgrowth cements. The clear syntaxial overgrowth cements are discussed later in this Chapter.

Turbid syntaxial overgrowth cements are inclusion rich and show a cloudy appearance (Fig. 4.3 C). These type of cements are present only in sections from the relatively deeper part of the basin. Meyers (1978) interpreted inclusion-rich syntaxial cements as strictly marine cements. Further supporting evidence that syntaxial overgrowth cement can occur in the marine environment is provided by Maliva (1989). In a few samples, the turbid syntaxial cements comprise up to ~5% of the total bulk rocks. Under cathodoluminescence, turbid syntaxial overgrowth cements display blotchy luminescence (Fig. 4.3 D).

A marine origin of the turbid syntaxial overgrowth cements is confirmed by the heavy oxygen ($\delta^{18}O$= –2.4‰ PDB) and carbon ($\delta^{13}C$= 3.6‰ PDB) values, compared with lighter oxygen and carbon values of the meteoric and burial cements (see following sections). Trace element analysis indicates that the Sr concentration is higher (321 ppm) than Mn (85 ppm) and Fe (32 ppm) concentrations. Elemental and isotopic compositions of carbonate cements are

Figure 4.3. Petrographic features of early marine cement.

A. Radial fibrous calcite cements (RC) lining the cavity. Equant calcite completes cavity occlusion. Thin section Bz 54.

B. Non-ferroan isopachous equant calcite (EC) cements around ooids, followed by ferroan coarse sparry calcite cement. Thin section Mz 109.

C. Thin section photomicrograph of turbid syntaxial (TS) overgrowth. Note cements are inclusion rich (white arrow). Thin section Go 116.

D. Same area as in C under cathodoluminescence. Note turbid syntaxial overgrowth illustrated by blotchy luminescence.

E. Thin section photomicrograph of composite oolites showing early micritic cements (white arrows) in contact with ooids and second generation bladed isopachous sparry calcite cement (BC). Micritic cement costitutes an addition of new material on the ooid grain surfaces (white arrows). The micritic cements seem to be older than the bladed cements. Note scalenohedral termination in each individual bladed calcite crystal (black arrows). Intergranular pores are completed by a third generation of coarsely crystalline equant sparry calcite cement. Thin section Bz 59.

F. Same area as in E under cathodoluminescence. Note micritic and bladed cements are non-luminescent. This may suggest micritic cement is coeval or slightly older than bladed cement. The coarsely crystalline cements show an alternating sequence of a moderately bright zone followed by a dark red-brown zone.

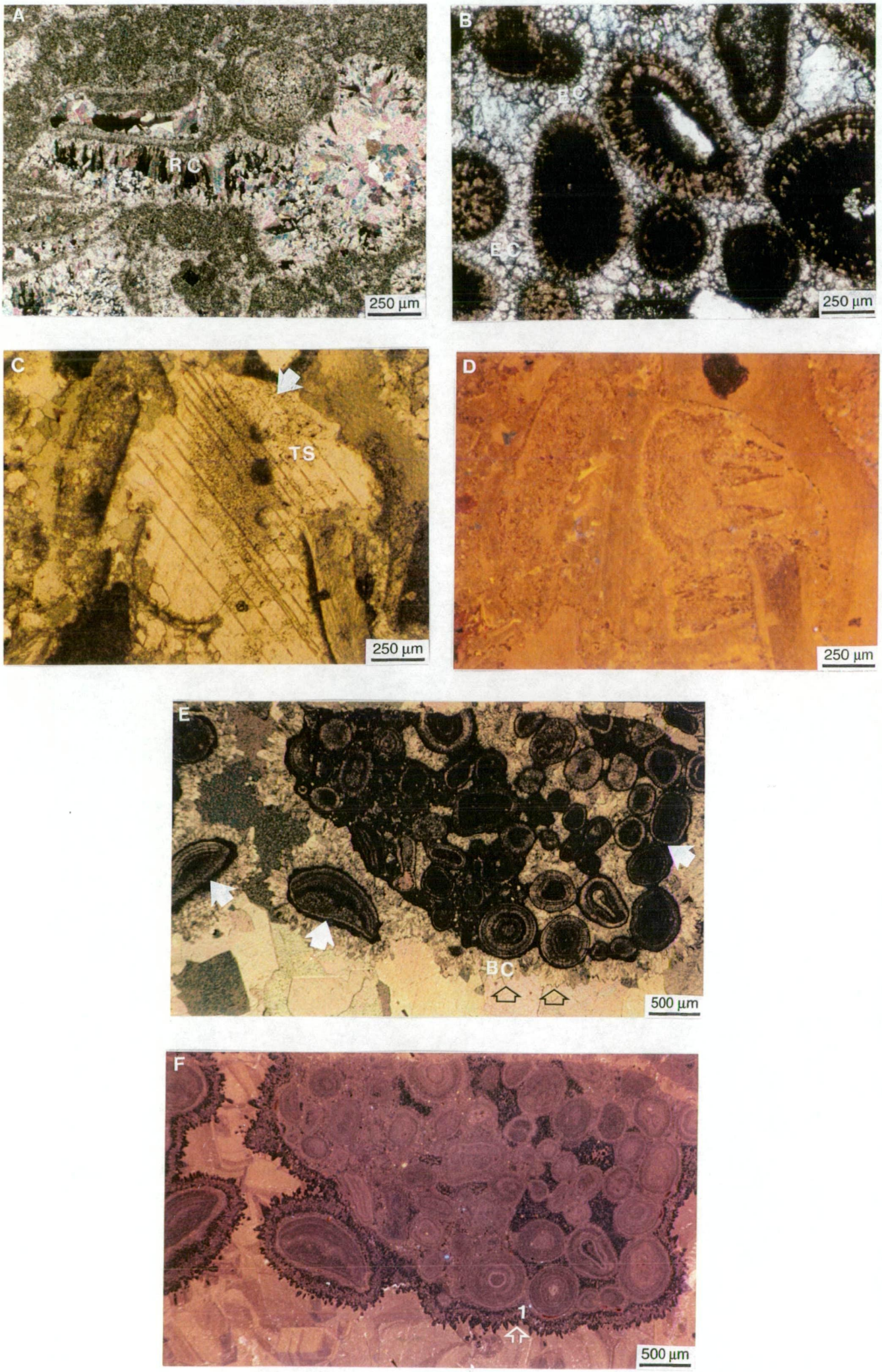
A
RC
250 µm
B
RC
RC
250 µm
C
TS
250 µm
D
250 µm
E
BC
500 µm
F
1
500 µm

discussed later in Chapter 7.

4.2.1.6 Micritic cements

Micritic cements are present as a minor component, particularly in the oolitic facies, where the cement origin is clear. The micritic cement generally constitutes an addition of new material on the grain surface, and forms a regular coating on the outer surface of the grain (Fig. 4.3 E). These features distinguish them from micritic envelopes, which result from alteration of particle surfaces. Although the micritic cements are difficult to distinguish from depositional micrite, the criteria for recognition of micritic cements includes: 1) massive appearance (as opposed to laminated), 2) an absence of fossil material within the micrite, and 3) anti-gravitational fabric (Steinhauff, 1989). The presence of an isopachous fringe of fibrous to bladed calcite (presumably marine) in contact with micritic cements, and the massive appearance and absence of fossil debris within the micrite, may suggest that the micrite is a marine cement (Figs. 4.2 F, 4.3 E). Micritic cement is known to precipitate directly from seawater (Bricker, 1971). Under cathodoluminescence, micrite cements are non-luminescent (Figs. 4.2 G, 4.3 F). This also probably supports a marine origin.

Cement fabric relationship

In the Mozduran limestones the relationships between adjacent areas and differing fabrics provide some evidence for marine diagenesis. Marine fabric relationships included here are 1) marine boring and micritized allochems and 2) geopetal micrite.

Marine boring and micritized allochem

Marine borings in the Mozduran limestones are present in many biofacies samples. The bores (5-10μm in diameter) are particularly common in pelecypod shells and filled by marine micrites (Fig. 3.2 C).

Micritic envelopes on carbonate allochems are nearly ubiquitous in the Mozduran limestones. Their thicknesses are highly variable, ranging from about 5 to more than 100μm (Figs. 4.6 E, 4.7 C). Marine borings and micritic envelopes are inferred to be a product of early marine mechanical destruction by boring micro-organisms such as endolithic cyanobacteria, mostly into the skeletal debris. In a few examples, repeated boring and filling causes a dense micritic envelope, whilst in others, thin micritic envelopes around the bivalve shells underwent various degrees of collapse during compactional and aragonite dissolution events

(Fig. 3.8 C).

Geopetal micrite

In the Mozduran limestones, skeletal interiors of some fauna such as gastropods and space inside of the brachiopod valve, are partially filled with depositional micrites (Figs. 3.1 B, C, 4.4 C). This indicates an approximately horizontal surface at the time of deposition. The depositional micrites are overlain by equant to drusy sparry calcite cements. The non-luminescent nature of these micrites may suggest a marine origin (Fig. 4.4 D).

Control on marine cement mineralogy and morphology

There are a number of views on the controls of marine cement mineralogy and morphology, many of which are presented in Bricker (1971). The controls on the mineralogy and crystal morphology of inorganic carbonate precipitation appears to be related to the Mg/Ca ratio, carbonate supply rate $(CO_3)^{2-}$, PCO_2 levels, and substrate (Folk, 1974 b; Given and Wilkinson, 1985). However, Rao, (1981a) suggested that temperature is also a major control on carbonate mineralogy and morphology. Early marine cements in the Mozduran limestones exhibit variable morphology. If it is assumed that the composition of marine water was uniform across the Upper Jurassic shelf, the occurrence of different crystal forms can not be attributed to variations in the Mg/Ca ratio (Wilkinson et al., 1985). Such variations in the marine cement morphologies, could be due to some undocumented kinetic factor such as different rates of crystal growth (Wilkinson et al., 1985), or fluctuations in seawater temperature. The mineralogy of marine cements also can be controlled by some other factors such as the presence of Mg^{+2} and SO_4^{2-} in seawater, which favors aragonite precipitation, while, aragonite precipitation is inhibited by PO_4^{3-} (Walter, 1986). She suggested that low-Mg and high-Mg calcite are precipitated where PO_4^{3-} is formed from the degradation of organic matter and SO_4^{2-} is depleted by SO_4^{2-} bacterial reduction. In addition, Tucker (1991) suggested that in many permeable limestones, aragonite is precipitated in preference to high-Mg calcite, where fluid-flow rates are higher. Thus, the rate of carbonate supply $(CO_3)^{2-}$ is higher. Acicular and elongate morphologies are also related to higher $(CO_3)^{2-}$ supply rates, rapid fluid flow, and the result of preferential growth along the C-axis (Given and Wilkinson, 1985). On the other hand, equant crystal morphology has been related to lower $(CO_3)^{2-}$ supply and slow fluid flow rates. Therefore, the presence of variable morphology and mineralogy in the Mozduran marine cements may indicate that

factors controlling mineralogy and morphology of the marine cements are very complex.

4.2.2 Meteoric cementation

The meteoric environment is subdivided by the ground water table into vadose (above the water table) and phreatic (beneath the water table) settings. Vadose cements such as meniscus, pendent or gravitational cements, which are an excellent indicator of vadose meteoric water precipitation (Longman, 1980; James and Choquette, 1984), are absent in the Mozduran limestones. This is probably due to a dry climate during the Upper Jurassic period.

4.2.2.1 Phreatic meteoric cementation

Carbonate sediments in shallow warm water marine environments are composed mainly of aragonite and high-Mg calcite. These minerals are metastable with respect to fresh water and alter very rapidly. The mineral transformation takes place by dissolution of one mineral and precipitation of calcite. This new calcite, called diagenetic calcite (dLMC), can be precipitated as: cement in open voids; between or within the grains; or on a microscale inside a particle, replacing the original aragonite or magnesium calcite.

The principal types of meteoric cements found in these limestones include: 1) equant cement, 2) syntaxial (epitaxial) overgrowth cement, and 3) platy cement. These meteoric cements are more abundant in samples from the shallowest part of the basin.

Equant sparry calcite cements

Equant sparry calcite is the typical cement of meteoric and burial environments (James, 1991), but can also be the seafloor cement in some Ordovician and Jurassic hardgrounds (Wilkinson et al., 1985). The precipitation of equant calcite cement is favored by relatively higher PCO_2, and low CO_3^{2-} contents. Thus, the meteoric phreatic zone, with relatively low temperature and slow unagitated fluid flow, is the best setting for this type of cement (Given and Wilkinson, 1985; Steinhauff, 1989). Clear anhedral equant crystals of sparry calcite cement (with a length:width ratio of less than 1.5:1), ranging in size from 60 to 760μm, with an average of 200μm, are very common in the Mozduran limestones (Figs. 4.4 A, C). Equant sparry calcite cement usually occurs as a later void-filling cement, and often post dates precipitation of fibrous or bladed calcite cements (Figs. 4.4 B). Cement crystals also occlude fenestral and moldic

Figure 4.4. Sequence of paired plain light and cathodoluminescence photomicrographs of coarsely crystalline meteoric cement.

A. Thin section photomicrograph of equant calcite cement (EC) filling intergranular voids. Thin section Mz 66.

B. Same area as in A under cathodoluminescence. The equant calcite cements show bright-yellow luminescence (zone 2). Cements between brachiopod shells show dark-brown luminescence (zone 1), possibly indicating marine origin. Brachiopod shells are non-luminescent (white arrows).

C. Geopetal micrite. Note space inside the brachiopod valve partially filled with depositional micrites. Depositional micrites are followed by a coarse crystalline drusy mosaic of equant calcite cement (DC). Thin section Mz 66.

D. Same field of view as in C under cathodoluminescence. Note the early non-luminescent micrite is succeeded by an alternating sequence of bright to dull luminescence, and a final dull to non-luminescent generation of late cement, which filled remaining intergranular porosity.

E. Close up of the same area as in C. Note planar, interlocking boundaries (green arrow) and increase of crystal size towards pore center. Thin section Mz 66.

F. Close up of the same area as in D. Note pronounced multiple generations of calcite zoning. The delicate growth zones possibly result from subtle variations in Mn and Fe contents. The cavity is filled, from oldest to youngest by: dark-red zone 1; bright-yellow zone 2; dull luminescent zone 3; moderately bright-yellow zone 4; dull luminescent zone 5; fine band of moderately bright-yellow zone 6; and dull red zone 7. Note in bright-yellow zone 4, there are a few thin alternating bright, dark subzones. The late cavity fill (dull red zone 7) has no subzones.

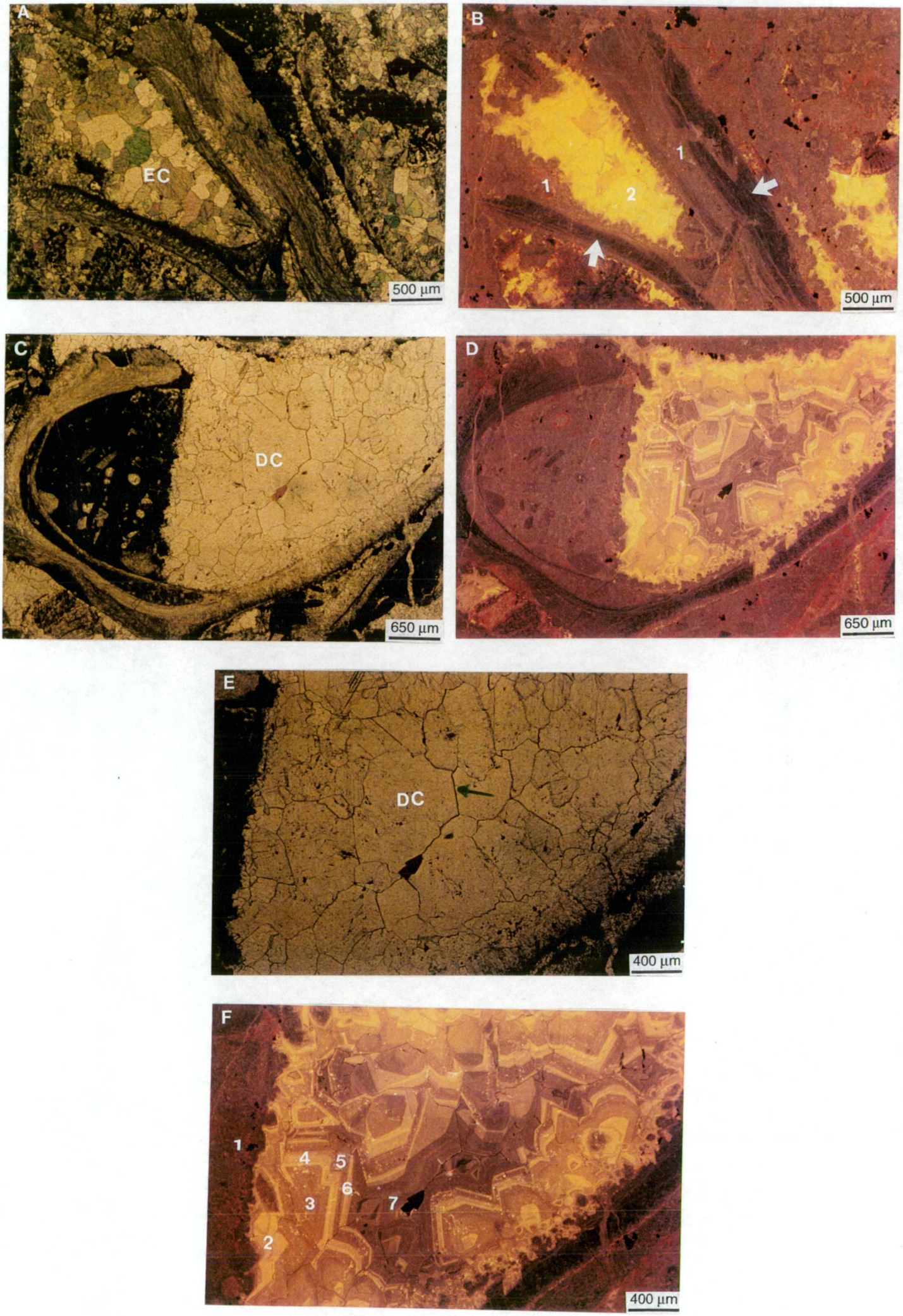
A
EC
500 µm
B
1
2
1
500 µm
C
DC
650 µm
D
650 µm
E
DC
400 µm
F
1
2
3
4
5
6
7
400 µm

porosities. The equant calcite crystals often increase in crystal size from a pore margin towards the center of an open pore as preferentially oriented crystal growth (Bathurst, 1975, Figs. 4.4 C, E). This type of growth pattern is called a drusy mosaic. Drusy cement has typically interlocking planar crystal boundaries (Fig 4.4 E), which are a characteristic feature used to differentiate cement from neomorphic spar. In some samples, the equant sparry calcite cements comprise up to ~10% of the total bulk rocks.

Although distinguishing meteoric phreatic cements from burial cements is difficult, many authors have referred to the cathodoluminescence behaviour of meteoric calcites (Choquette and James, 1987; Mussman et al., 1988; Niemann and Read, 1988). These equant spars illustrate cement zones ranging from very dull to non-luminescent at the pore margins, to dull with a zone of bright luminescence towards the center of the pores (Figs. 4.4 D, F). This may indicate a change in composition of fluid chemistry from oxidizing meteoric water to more reducing pore fluid during burial. In a few examples, an elongate to subequant mosaic of drusy calcite cement (Fig. 4.5 A) shows unzoned bright-yellow luminescence (Fig. 4.5 B). This may indicate a relatively uniform composition of fluid chemistry.

The drusy cement was sampled from the Mozduran section (sample Mz 66) for isotopic analysis. This showed a depletion in oxygen ($\delta^{18}O$= – 6‰ PDB) and carbon ($\delta^{13}C$= 1.1‰ PDB,) relative to least-altered micrites ($\delta^{18}O$= – 1.2‰, $\delta^{13}C$= 4‰ PDB, see Chapter 7). Equant cements from the Bazangan section (sample Bz 26), also show relatively similar oxygen ($\delta^{18}O$= – 6.6‰ PDB) and carbon ($\delta^{13}C$= 0.4‰ PDB) values, compared with the drusy mosaic of equant calcite cement from the Mozduran section (sample Mz 66). Present day coastal rains, from low-latitude settings, have average ^{18}O values of –2‰ SMOW (Dansgaard, 1964). These isotopic values, along with the bright-yellow luminescent nature of these cements and crystal morphology of the calcite crystals, supports the interpretation that these cements were precipitated probably during exposure to meteoric fluids.

Platy sparry calcite cements

Platy cements are common in the oolitic facies and occur mainly within fenestral and interparticle porosities (Fig. 4.5 C). Cement crystals are coarse, clear, non-ferroan, and range in size from 350 to 650μm. The large platy crystals may be due to slow growth or a low nucleation rate (Tucker, 1991). In some cases, preexisting bladed calcite crystals are preserved around the margins of the

platy calcite cement (Fig. 4.5 C). The platy sparry calcite cements can constitute up to ~20% of the total bulk rocks in a few samples.

Under cathodoluminescence, platy cements display bright-yellow luminescence (Fig. 4.5 D), and do not show any compositional zoning, indicating transition from a shallow to deeper burial environment (Meyers, 1974; Grover and Read, 1983).

Isotopic analysis of the platy cement (sample Mz 109) indicates that it is depletd in both oxygen ($\delta^{18}O$= –6‰ PDB) and carbon ($\delta^{13}C$= 0.3‰ PDB), relative to the least-altered micrite ($\delta^{18}O$= –1.2‰ PDB, $\delta^{13}C$= 4‰ PDB, see Chapter 7) and marine turbid syntaxial overgrowth cement ($\delta^{18}O$= –2.4‰ PDB, $\delta^{13}C$= 3.6‰ PDB). Platy sparry calcite cement from sample Mz 31 has similar oxygen ($\delta^{18}O$= –6.2‰ PDB), but lighter carbon ($\delta^{13}C$= –2.8‰ PDB) values, compared with sample Mz 109. The Mn concentrations (average 128 ppm) are about two times higher than Fe concentrations. A meteoric origin of the platy calcite cement is confirmed by the bright-yellow luminescence and very light carbon and oxygen values.

Elemental and isotopic composition of carbonate cements is discussed later in Chapter 7.

Syntaxial (epitaxial) overgrowth cements

Syntaxial overgrowth cements on echinoderm debris consist of clear, inclusion-free, non-ferroan sparry calcite. Syntaxial cements are extensive in the Mozduran limestones and occur mainly within the biosparite and oosparite facies (Fig. 4.5 E). They range in size from 750 to 1650μm and are in optical continuity with their host, underlying echinoderm fragments. Traditionally, syntaxial calcite overgrowths on echinoderm debris have been considered as meteoric (Longman, 1980; Flügel, 1982) or burial (Kaufman et al., 1988) cements, since such cement is exceedingly rare in the modern shallow marine setting (Tucker and Wright, 1990). Syntaxial overgrowth cements comprise up to ~4% of the total bulk rocks.

Under cathodoluminescence, syntaxial rim cements exhibit uniform bright-yellow luminescence (Fig. 4.5 F). No compositional variation is present in these cements.

4.2.3 Burial cementation

It is now clear that most of the carbonate cement in many well lithified limestones occurred during burial diagenesis. Burial diagenetic processes are defined as "any change or collection of changes that take place below the zone of

Figure 4.5. Sequence of paired plain light and cathodoluminescence photomicrographs of coarsely crystalline meteoric cement.

A. Thin section photomicrograph of an elongate to subequant mosaic of drusy calcite cement (DC). Thin section Bz 95.

B. Same area as in A under cathodoluminescence. Note sharply defined boundary between early bladed calcite crystals (white arrow) of dull zone 1 (red-brown), very bright zone 2 (yellow), and finally dull zone 3 (moderately dark red-brown). In this example, there is no delicate banding in the bright-yellow luminescent zone, compared to Figs 4.4 D and F.

C. Thin section photomicrograph of platy calcite (P) cements filling intergranular voids between ooid grains. Thin section Mz 109.

D. Same area as in C under cathodoluminescence. Note early dull luminescent zone 1, followed by bright-yellow luminescent zone 2. There is a sharp boundary between early and late platy (P) calcite cement.

E. Syntaxial overgrowth (S) cement on crinoid grain. Note cements are inclusion free. Thin section Mz 109.

F. Same area as in E under cathodoluminescence. The sequence of calcite cements, oldest to youngest are: dull zone 1 (red-brown) around crinoid, brachiopod and bivalve fragments (black arrows); bright zone 2 (moderately bright-yellow); and dull zone 3 (dark red-brown).

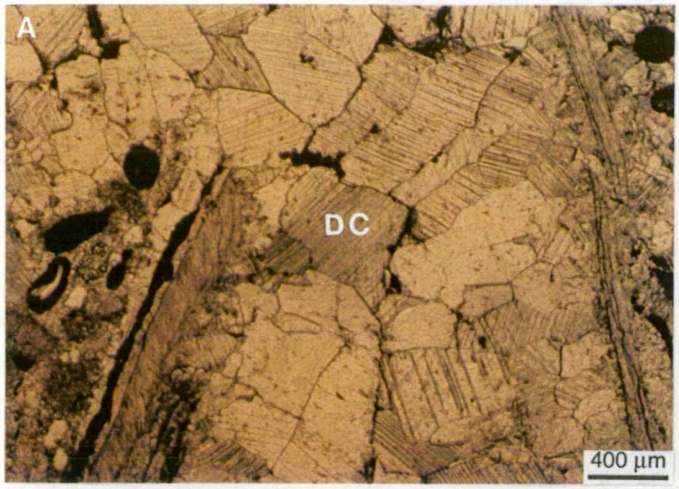
A
DC
400 µm

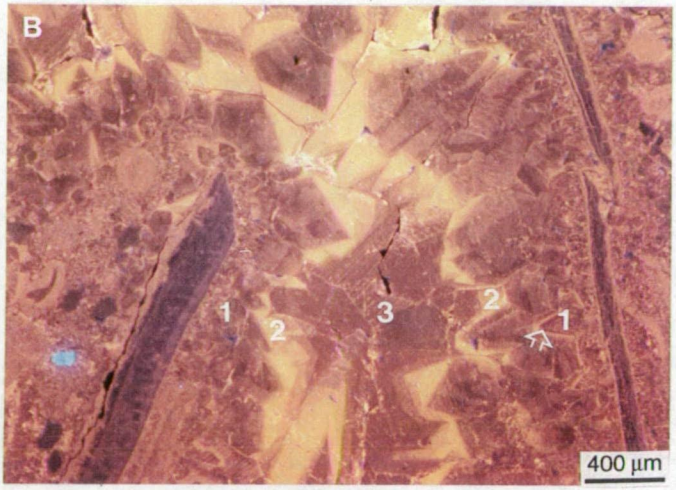
B
1
2
3
2
1
400 µm

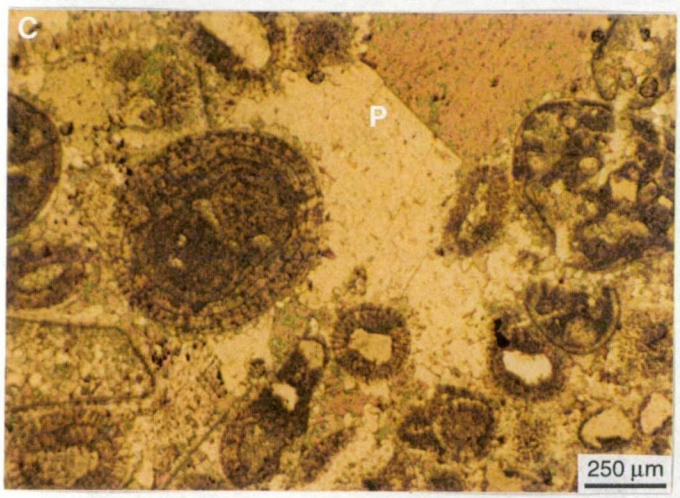
C
P
250 µm

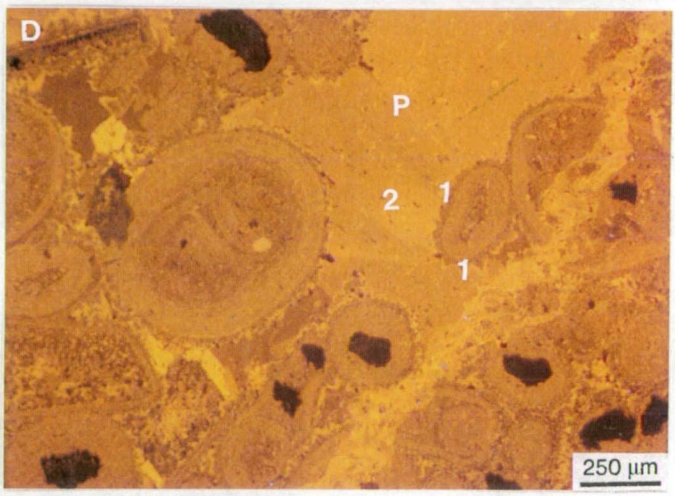
D
P
2
1
1
250 µm

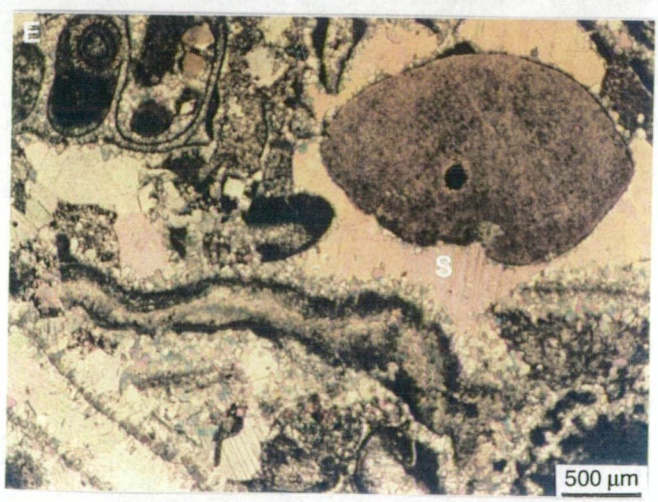
E
S
500 µm

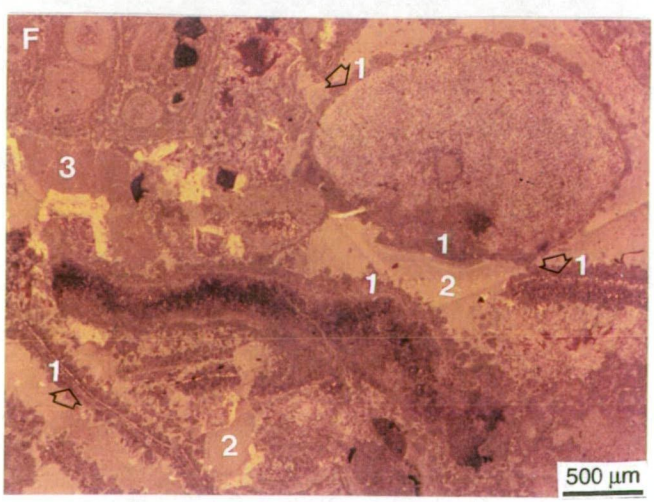
F
1
3
1
1
2
1
1
2
500 µm

near-surface diagenesis and above the realm of low-grade metamorphism" (Choquette and James, 1987). Burial cementation is promoted by increasing temperature. The geohistory diagram indicates that the total subsidence for the base of the Upper Jurassic Mozduran formation was ~ 4 km, and temperature increased up to ~ 110° C (Moussavi-Harami and Brenner, 1992). The determination of a burial origin for sparry calcite cements in the Mozduran limestones is based on several petrographic and textural criteria. These include: large crystal size (Fig. 4.7 A); broken and collapsed micritic envelopes present within sparry calcite (Figs. 3.2 A, B); fractured grains included within spar (Fig. 4.8 A); sutured and concave-convex contacts between grains before spar precipitation (Fig. 4.8 D, C); cement healing of fractured grains or spalled ooid cortices (Fig. 4.6 A); cement occurrence in the center of the pores (Figs. 4.6 B, D, F); dull luminescence (Figs. 4.6 B, D, F and Figs. 4.7 B, D); cement crystals cross cutting stylolites; and cement occurrence in tectonic veins (Fig 4.7 E).

Continued burial cementation in the Mozduran Formation resulted in the occlusion of all remaining porosities. These porosities have resulted from dissolution of original aragonitic depositional grains, probably in the meteoric diagenetic environment. Morphologically, these late cements occur as inter and intraparticle equant sparry calcite crystals (Figs. 3.8 C, 4.6 A-D), as syntaxial overgrowth on echinoderm debris (Fig. 4.6 E), and as poikilotopic sparry calcite (Figs. 4.7 A, C). Burial cements fill most of the secondary porosities, such as moldic (Fig. 4.6 C), fracture (veins, Fig. 4.7 E) and interparticle pore space. Burial cementation is mostly present in samples from the relatively deeper part of the basin.

4.2.3.1 Equant sparry calcite cements

Equant sparry calcite cement, ranging in size from 65 to 520μm, is common in the Mozduran limestones (Figs. 4.6 A-D). This type of cement is also known as coarse equant-mosaic calcspar (Choquette and James, 1987). Although, equant cements are mostly ferroan (Fig. 4.3 B), non-ferroan equant sparry calcite cements are also present. The temporal relationship between compactional feature and ferroan equant mosaic calcspar (such as Fig. 4.3 B), provides good evidence for burial origin. Equant cements occlude inter and intraparticle porosities and usually occur as a last void filling cement. Equant cement heals fracture grains, such as spalled ooid cortices (Fig. 4.6 A), and thus is clearly a post-compaction precipitate. Some late ferroan and non-ferroan equant cements also fill voids developed during the dissolution of molluscan aragonitic shells (Figs. 3.8 C, 4.6

C). The equant soarry calcite cements comprise up to ~4% of the total bulk rocks.

Under cathodoluminescence, equant sparry cements are dull (dark-brown) to non-luminescent (Figs. 4.6 B, D).

The $\delta^{18}O$ and $\delta^{13}C$ composition of the equant sparry calcite cements analyzed (samples, Bz 57, 55, Go 70, 83, 91, 99) ranged from -4.4‰ to -6.5‰, and 3.8‰ to 2.2‰ PDB respectively. The $\delta^{18}O$ values of these cements are depleted significantly relative to the least-altered micrite (see Chapter 7) and marine turbid syntaxial cement. However, the $\delta^{13}C$ values of these cements are close to or slightly depleted relative to the least-altered micrite and marine cement, because $\delta^{13}C$ values are least affected by temperature during burial.

The cement morphology, the dull to non-luminescent nature of these cements, and lighter oxygen values than micrite and marine cement, may support burial origin.

4.2.3.2 Syntaxial overgrowth cements

The syntaxial cements are very extensive in the Mozduran limestones, particularly in echinoderm rich biofacies. Syntaxial overgrowth cement reaches very large sizes and fills entire pores (Fig 4.6 E). The large size of these crystals may indicate more rapid growth than that of equant crystals (Longman, 1980), with which overgrowth often competes. It has been suggested that the syntaxial overgrowths may develop preferentially over drusy mosaics in larger pores (Hird and Tucker, 1988). The formation of syntaxial overgrowth was inhibited around the echinoderm grains (Fig. 4.6 E), due to the presence of a micritic envelope around the grain. Syntaxial overgrowth cements consist of up to ~15% of the bulk rocks.

Under cathodoluminescence, syntaxial overgrowth exhibits multistage overgrowth cements (Fig. 4.6 F). It is clear that they originated in two quite different diagenetic environments. The earliest part of the overgrowths (zone 2) are bright-yellow luminescent, and probably precipitated in the shallow meteoric environment. The latest part (zone 3) shows dull (red-brown) luminescence, and probably originated during deeper burial diagenesis (Choquette and James, 1987). Since the zoned brightly luminescent crystals generally give way to dull luminescent crystals towards pore interiors, the burial dull cements often occupy a more central pore position.

The syntaxial overgrowth cement (sample Mz 109) has a $\delta^{18}O$ value of -6 ‰ and $\delta^{13}C$ value of 2.7‰ PDB.

Figure 4.6. Sequence of paired plain light and cathodoluminescence photomicrographs of coarsely crystalline burial cement.

A. Thin section photomicrograph of spalled cortices (white arrows). Equant cement is post ooid dissolution, as it heals the spalled ooid cortex. Note bivalve shells filled with equant calcite cement. Thin section Pa 28.

B. Same area as in A under cathodoluminescence. Note spalled cortices and most intergranular voids are filled by late dull (dark-brown) luminescent calcite cement (black arrows).

C. Aragonitic shell of gastropod leached and filled with equant sparry calcite cement. Thin section Bz 57.

D. Same area as in C under cathodoluminescence. Note gastropod chambers mainly lined with dark red to non-luminescent cement.

E. Thin section photomicrograph showing syntaxial overgrowth on large crinoid grain. Crinoids are readily recognizable by cloudy appearance. Note micritic envelopes (white arrows) around small echinoderm (SE) have obstructed the formation of syntaxial overgrowth. Thin section Mz 109.

F. Same area as in E under cathodoluminescence. Early diagenetic cement (white arrow) is dull zone 1 (red-brown). Clear syntaxial overgrowth in large echinoderm (LE) grain exhibits moderately bright-yellow zone 2 and bright-red to dark-red zone 3. These variations may represent a change in oxidation and reduction conditions of fluid during marine (zone 1), meteoric (zone 2), and burial (zone 3) diagenesis.


A
350 µm

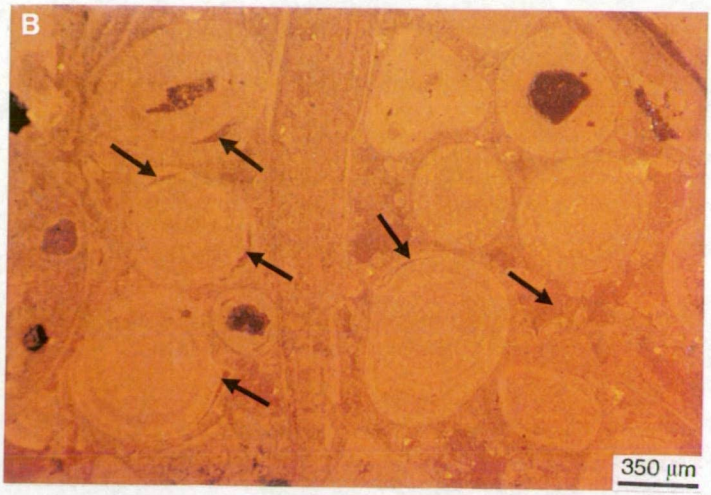
B
350 µm

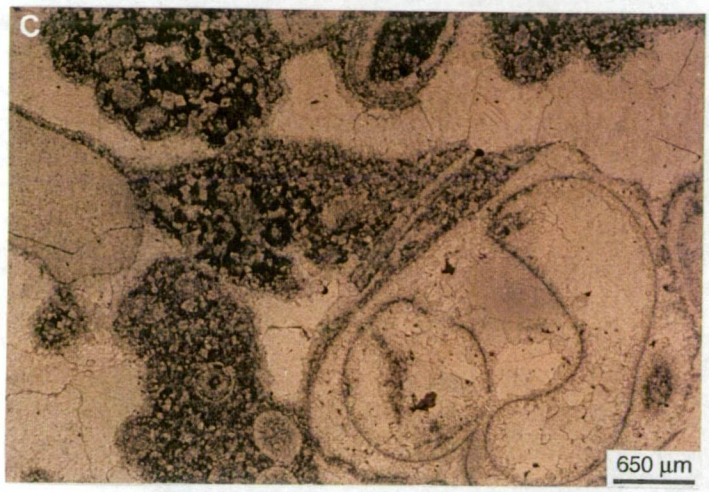
C
650 µm

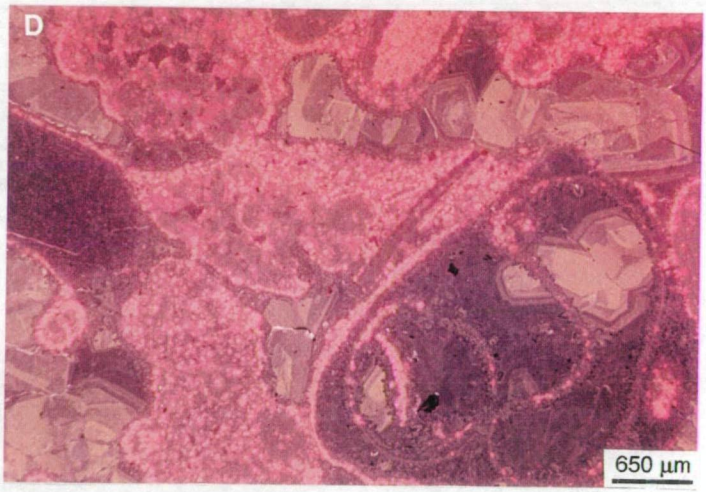
D
650 µm

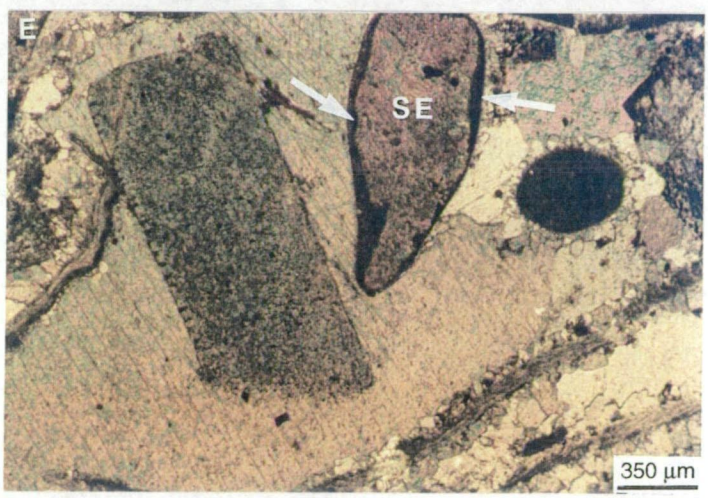
E
SE
350 µm

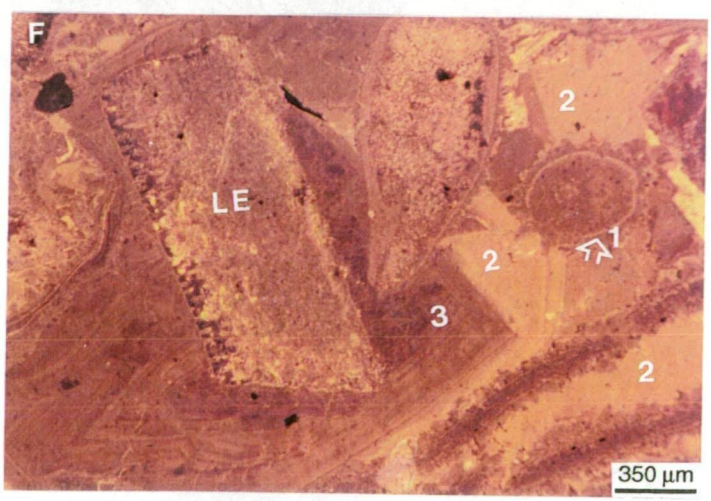
F
LE
1
2
2
3
2
350 µm

4.2.3.3 Poikilitic sparry calcite cements

This type of cement is recognized by its very large crystals, which can reach several millimeters or more in size, with the ability to enclose several grains (Fig. 4.7 A). In some cases, poikilitic calcite crystals completely fill all pore spaces after the early generation of bladed sparry calcite cement (Fig. 4.7 C). They have probably resulted from a very low nucleation rate of calcite crystals and slow growth. They may precipitate from pore-fluids that are only just supersaturated with respect to CaCO (Tucker and Wright, 1990). In a few samples, the Poikilitic calcite cements comprise up to ~20% of the total bulk rocks.

Under cathodoluminescence, these cements typically show dull luminescence. This is illustrated in Fig 4.7 B. In this figure, the earliest cement, with bladed crystal morphology, shows dull luminescence (black arrow). This may reflect precipitation in an oxic marine environment. The late portion of the cement, which shows bright-yellow luminescence, probably originated during shallow meteoric diagenesis (zone 1), whilst, the latest part (zone 2), which shows dull (dark-brown) luminescence, probably precipitated during increased burial depth. It has been suggested that many limestones shows a non-luminescent (to dull)-bright-dull zonation with increasing burial due to the increasing reducing nature of pore-fluids (Grover and Read, 1983; Frykman, 1986). In Fig. 4.7 D, large poikilitic cement shows only dull luminescence.

The $\delta^{18}O$ composition of the poikilotic sparry calcite cements analyzed (samples Pa 12, 28), ranges from -7.2‰ to -7.6‰ PDB. The $\delta^{13}C$ composition of this cement type ranges from 2‰ to 2.4‰ PDB. The $\delta^{18}O$ values of these cements are the most depleted values among the carbonate cements, possibly due to a higher temperature, corresponding to increasing depth of burial.

The cement crystal morphology, the luminescence intensity and isotopic composition of these cements, all support a burial origin.

Vein calcites

Coarse mosaics of equant calcite veins are common in the Mozduran Formation (Fig. 4.7 E). In all cases, the vein calcites are tectonic in origin and cut all the depositional grains, stylolites, and late diagenetic dolomites. Under cathodoluminescence, the coarse sparry calcite veins show mainly dull luminescence (zone 1), with minor multiple zonation of bright-yellow luminescence (zone 2, Fig. 4.7 F).

Isotopic analysis of the several vein calcites indicates that $\delta^{18}O$ values

Figure 4.7. Sequence of paired plain light and cathodoluminescence photomicrographs of coarsely crystalline burial cement.

A. Poikilitic cement (PO) engulfs surrounding grains. Note early bladed calcite cement around large ooid grain. Thin section Pa 12.

B. Same area as in A under cathodoluminescence. The cavity is filled by bright-yellow zone 1, and dull (dark-red) luminescent zone 2 poikilotopic cement. Note early bladed calcite cements are dull luminescent (black arrow).

C. Cavity lined with large poikilitic (PO) calcite cement. Thin section Pa 28.

D. Same area as in C under cathodoluminescence. The cavity is filled with dull (red-brown) luminescent zone 1. Note intra and intergranular voids finally filled with late dull (dark-brown) luminescent equant calcite cements.

E. Thin section photomicrograph illustrating coarsely crystalline sparry calcite vein. Thin section Go 26.

F. Same area as in E under cathodoluminescence. Note compositional zoning in calcite crystals. The vein is filled by dull (red-brown) luminescent zone 1, followed by light-yellow luminescent zone 2 calcite cement.

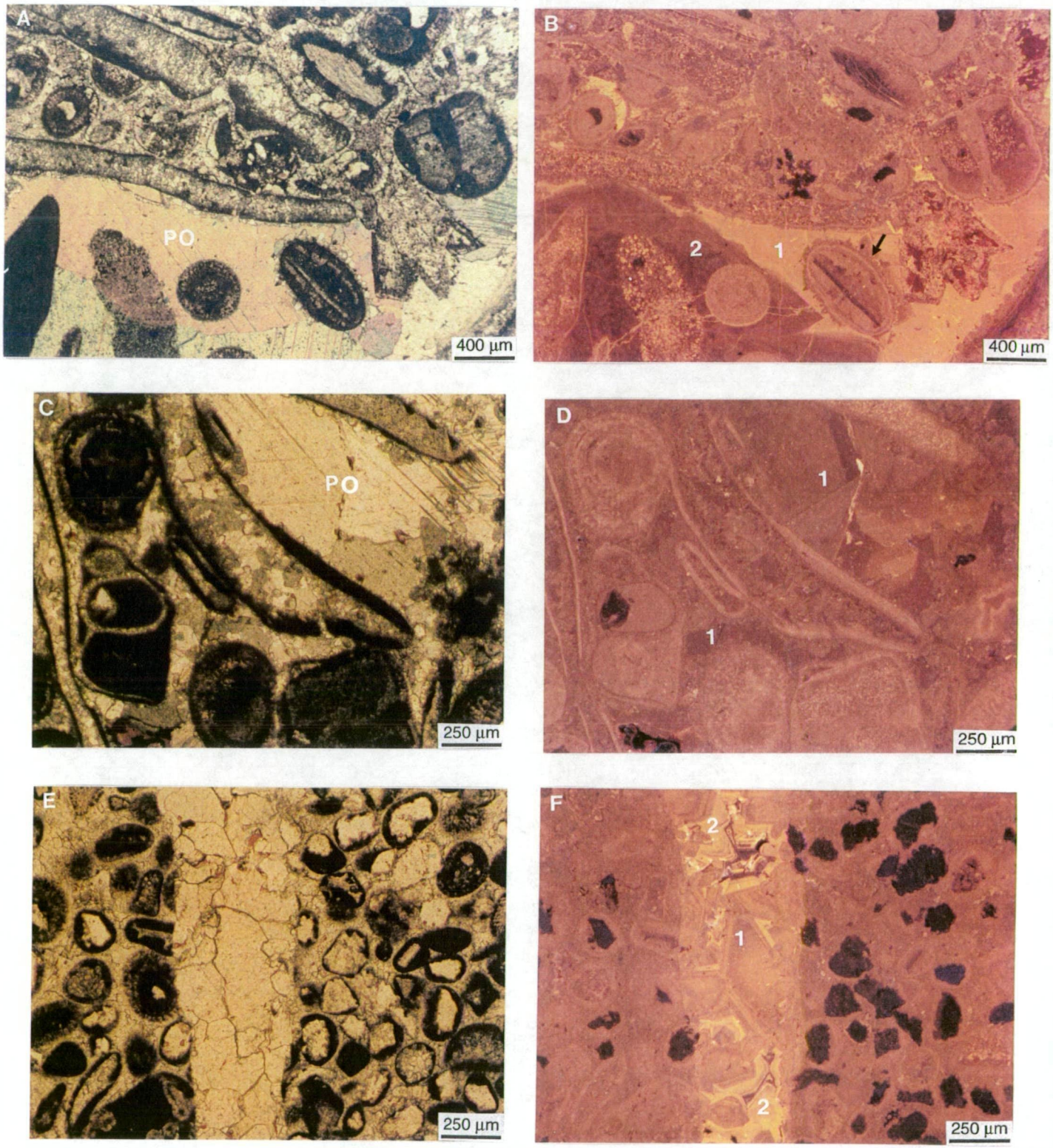
A
PO
400 µm
B
2
1
400 µm
C
PO
250 µm
D
1
1
250 µm
E
250 µm
F
2
1
2
250 µm

ranged from -9.4‰ to -12.4‰ PDB, while $\delta^{13}C$ values ranged from 3.4‰ to -5.2‰ (Fig. 7.22). The very depleted $\delta^{18}O$ values of these vein calcites, compared to the limestone cements, is consistent with their formation under higher temperatures. In a few vein calcites, the very depleted $\delta^{18}O$ values, along with the heavy $\delta^{13}C$ values (Fig. 7.22) and the dull luminescent nature of these calcite veins, supports a burial origin. However, the moderately depleted $\delta^{13}C$ values of some other vein calcites, along with multiple zonation of bright-yellow luminescence, may indicate meteoric origin. The $\delta^{18}O$ and $\delta^{13}C$ variations in vein calcites are discussed later in Chapter 7.

4.2.4 Controls on cathodoluminescence

Cathodoluminescence (CL) features depend on the presence of some elements, called "activators", which are stimulated to emit light when bombarded with energetic electrons, and some elements, called "quenchers", which prevent emission (Walker, 1985). In a number of recent papers, cathodoluminescence in carbonates has mostly been related to variations in trace element chemistry, particularly Mn^{2+} as the main activator, and Fe^{2+} as the main quencher (e.g., Machel, 1985; Hemming, et al., 1989; Meyers, 1989; Machel and Burton, 1991). This is assumed to be due to the presence of Mn^{2+} and Fe^{2+} in sufficent amounts in most sedimentary environments to influence the CL intensity of sedimentary carbonates. It has been suggested that visible luminescence requires at least 10-20 ppm Mn^{2+} activators in calcite when Fe^{2+} content is less than 200 ppm (Ten Have and Heijnen, 1985; Hemming et al., 1989; Mason and Mariano, 1990). However, there is still some debate in the literature about the positions of the limiting values of the activators and the quenchers. Other trace elements such as, Pb^{2+}, Cu^{2+}, Zn^{2+}, Mg^{2+} (?), Ag^{+}, Bi^{+}, and several Rare Earth Elements (particularly Eu^{2+}, Eu^{3+}, Sm^{3+}, Tb^{3+}, Dy^{3+}) are also potential activators, whilst Co^{2+} and Ni^{2+} are potential quenchers of luminescence (Machel, 1985; Marshall, 1988; Machel et al., 1991). It has been also suggested that lattice imperfections and organic compounds may influence cathodoluminescence intensity (Machel, 1985; Machel and Burton, 1991).

Very recently, it has been suggested that the causes of CL intensity are complex due to many activators and quenchers in sedimentary environments, other than Mn^{2+} and Fe^{2+} (Savard et al., 1995). Therefore, the simple Fe-Mn model can not be applied directly to natural calcites, at least at low Fe-Mn concentrations. Savard et al. (1995) have introduced four chemical domains based

on Fe-Mn concentrations. In the main domain, ranging from 20 to 225 ppm Mn and about 20 to 1400 ppm Fe, all types of luminescence have occurred. This undifferentiated domain is also identified from a compilation of data in the literature (see Fig. 1 and 3 in Savard et al., 1995). Since most diagenetic calcite cements have Fe and Mn concentrations that fall within the field of mixed cathodoluminescence, the current interpretation that redox (Eh-pH) conditions in an aquifer control the CL intensity in calcites, needs to be reevaluated (Savard et al., 1995). The types of calcite CL reported in the study of Savard et al. (1995) do not appear to be constrained by the diagenetic environment. The concept of cement stratigraphy, in which the alternating CL zones in carbonate cements have been attributed to changes in the composition of basinal waters, has been criticised (for a review, see Savard et al., 1995).

However, in this study, diagenetic interpretation is based on textural feature and CL intensity, in conjunction with elemental and isotopic characteristics of the Mozduran carbonate cements.

In the Mozduran carbonates, Mn^{2+} is probably the main CL activator and Fe^{2+} is the main CL quencher, measured in sufficient quantities. However, it was not possible to adequately assess the role of the rare earth elements such as Eu, Dy and Sm as activators, and the possibility of Co^{2+} and Ni^{2+} serving as a quencher of CL, as REE analysis from these samples was not undertaken. Therefore, CL intensities of calcite cements in the Mozduran Formation may be a function of those factors that control availability and incorporation of Mn^{2+} and Fe^{2+} into the calcite lattice, such as increases in temperature and the rate of precipitation (see paper by Heydari and Moore, 1993).

4.2.5 Time, temperature, duration and source of calcite cementation

The relationship of calcite cements relative to grain fracturing, grain-to-grain pressure dissolution, stylolites, and late fractures, suggests that most of the diagenetic calcite cements are post compactional (Figs. 4.6 A, 4.8 A, D) and precipitated in a burial environment. However, minor marine and to some extent, meteoric calcite cementation occured in the Mozduran limestones. These relationships suggest that part of the calcite cementation began after grain deformation and grain-to-grain pressure dissolution, and ceased probably at the time of gas migration into the Mozduran carbonate reservoirs. According to burial history curves (Moussavi-Harami and Brenner, 1992), the paleotemperature analysis of Afshar-Harb (1979), and the fact that the formation of the Khangiran gas traps occurred during the late Alpine Orogeny, these Upper Jurassic source

rocks did not reach thermal maturity before the late Paleocene (~50-60 my years ago). Gas migration into the present structures probably occurred at about 3.5 km of burial during late Miocene-early Pliocene time (~10 my years ago). This restricts calcite cementation to a depth range of about 100 m to about 3.5 km, a temperature range of 30 to about 100° C (assuming a geothermal gradient of 25° C/km), and a time span of 130 my. The source of calcium carbonate for calcite cementation in this depth of burial was either from connate pore waters, or derived by pressure dissolution processes along grain contacts and stylolites. Previous studies have illustrated that sufficient carbonate is released by pressure dissolution to account for calcite cementation (e.g., Scholle and Halley, 1985; Moore, 1989; Finkel and Wilkinson, 1990; Heydari and Moore, 1993). The extent of physical and chemical compaction in the Mozduran limestones is discussed in the following sections.

4.3 Compaction

Compaction refers to any process that decreases the bulk volume of rocks (Flügel, 1982). This includes, "mechanical processes" that decrease the bulk volume of single grains (grain deformation) or that cause closer grain packing (re-arrangement), and "chemical processes" which decrease the volumes of grains and cement minerals.

The Mozduran limestones were affected by both physical and chemical compaction during the shallow to deep burial stage, which resulted in the formation of different compactional features and fabrics.

4.3.1 Physical compaction

The Mozduran limestone contains many different varieties of physical (mechanical) compaction features induced by overburden pressure. As a result of minor precipitation of early cement, a rigid framework was not created in the sediment grain interpenetrations and close packing fabric resulted from compaction. Physical compaction can obliterate desiccation cracks and fenestae or birdseyes in peritidal sediments (Choquette and James, 1987). The absence of desiccation cracks and the presence of birdseye textures only in a few samples in these shallow water peritidal carbonates, is attributed to physical compaction. Physical compaction features in the limestone studied, are more pronounced in grain supported sediments. The textures produced by physical compaction in the Mozduran carbonates are: fractured grains of various kinds such as pelecypod grains (Fig. 4.8 A); spalled and broken cortical layers of ooids (Fig. 3.8 C);

fractured and collapsed micritic envelopes (Figs. 3.2 A, B); deformed acicular to fibrous marine cements (Fig. 4.8 B); and overpacking and interpenetration of grains (concavo-convex contacts, Fig. 4.8 C).

4.3.1.1 Grain breakage and plastic deformation

Petrographic observations in grain-supported limestones reveals breakage of grains. Grain breakage is evidenced more in ooids with concentric fabrics (typically aragonite originally, Tucker and Wright, 1990) which break and crack along the lamellae so that cortical layers are spalled off— "spalled ooids" (Fig. 3.8 C). Such textures may indicate that cementation was late relative to deformation. Choquette and James (1987) suggested that cements which heal fractured grains or spalled ooid cortices are good indicators of burial origin. The breakage of bioclastic grains such as pelecypod grains (Fig. 4.8 A) is also common in these limestones.

Shattered micritic envelopes (Figs. 3.2 A, B) illustrate collapse or fracturing by physical compaction, due to ealier dissolution of the host bioclast. These textures indicate compaction or deformation of sediments before major cementation. This is a common feature of originally aragonitic shells subjected to early meteoric dissolution (Tucker and Wright, 1990). Due to the fragile nature of these envelopes, however, little compaction is required to destroy them (Figs. 3.2 A, B).

Plastic deformation (the deformation referred to as "plastic" appeared fractureless in thin sections at the magnification used) of fibrous marine rim calcite cements around ooids (Fig. 4.8 B), suggests that physical compaction occurred shortly after burial. Thus, compaction postdates early marine cementation. Thin rinds of marine cements prevented grain interpenetration and grain-to-grain contacts.

Overpacking and interpenetration of grains, which is a common feature in most oolitic and bioclastic facies in the Mozduran limestones, has produced various types of contacts. The majority of these are sutured (Fig. 4.8 D) and concavo-convex contacts (Fig. 4.8 C), with a number of longitudinal and tangential (point) contacts. Longitudinal and concavo-convex contacts form due to plastic deformation, whereas sutured contacts form due to pressure dissolution. The pressure dissolution contacts are discussed later in the following section. In some oolitic facies, there are many undeformed ooids among the crushed and deformed ooids (Fig. 4.8 D). The co-occurrence of highly deformed and undeformed ooids within the range of a thin section will suggest compaction-

Figure 4.8. Photomicrographs of compactional features and silicification.

A. Breakage of pelecypod grain due to physical compaction. Note cementation postdates grain breakage. Thin section Go10.

B. Deformation of acicular to fibrous marine cements around ooids (white arrow). Physical compaction postdates early marine cementation. Thin section Mz 95.

C. Overpacking and concave-convex contacts between grains (white arrow). Note longitudinal contact between depositional grains (solid white arrow). Cementation postdates physical compaction. Thin section Pa 27.

D. Grain to grain pressure dissolution. Stress is concentrated at the points where the grains meet, thus, part of one or both the grains are dissolved. Most of the contact types are sutured (white arrow), fewer are point contact. Note the presence of undeformed ooids. Thin section Mz 20.

E. Pressure dissolution stylolites. Solution zone, marked by stylolitic insoluble residue, is shown cutting crinoid fragment. Loss of a large volume of limestone is apparent from the truncation of the crinoid. Thin section Mz 66.

F. Pervasive silicification of the lime mud facies. Note silicified limestone composed mainly of a finely crystalline mosaic of quartz crystals with pin-point extinction. Megaquartz and chalcedonic quartz occur as a pore-filling cement. Thin section Go 15.

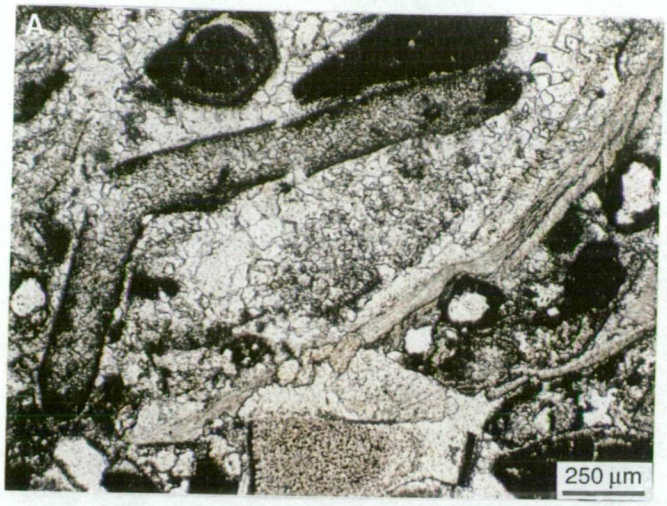
A
250 µm

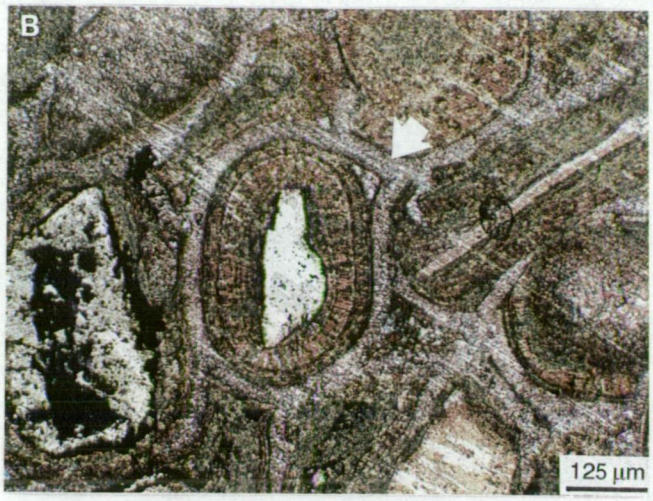
B
125 µm

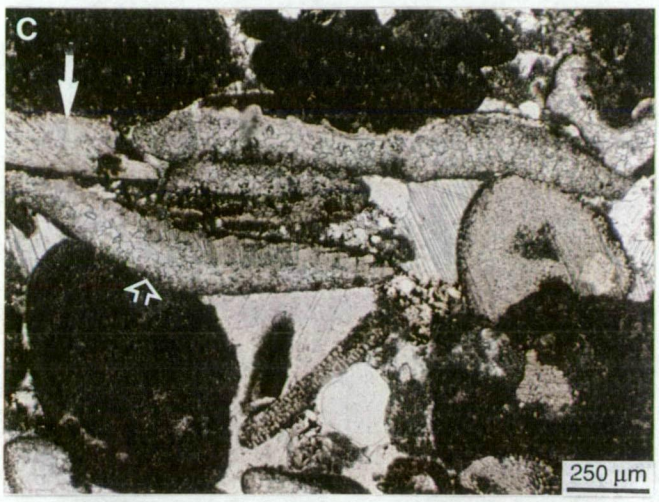
C
250 µm

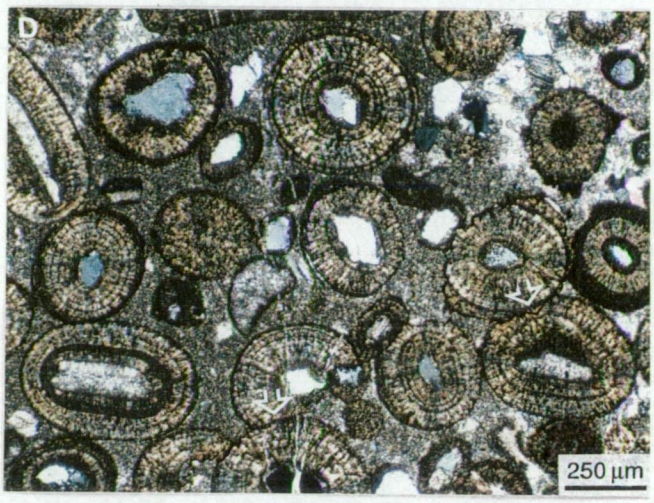
D
250 µm

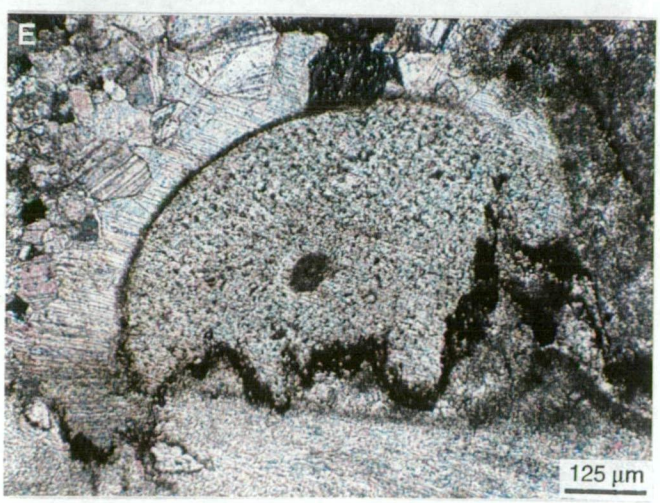
E
125 µm

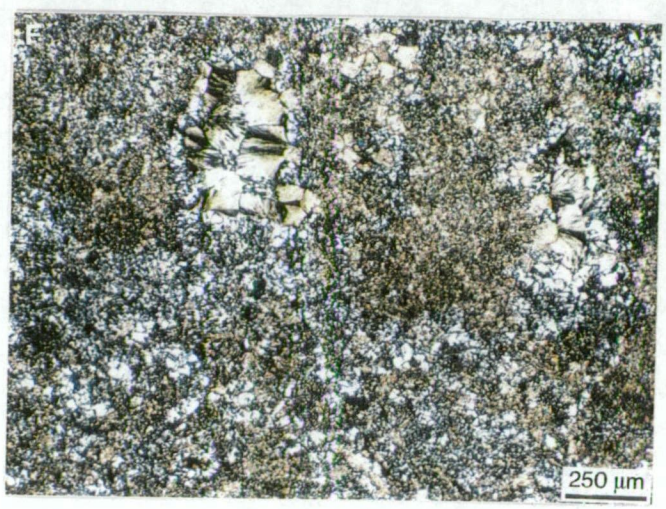
F
250 µm

deformation in an unlithified (unconsolidated) state and the resultant fabric formed is due to heterogeneous transmission of stress from grain to grain (Bhattacharyya and Friedman, 1979; Sarkar et al., 1982). Experimental compaction of ooids under deep burial diagenetic temperature and pressure (equivalent to a burial depth of 3.5 to 6.5 km), produced many fractured grains, as well as pressure dissolution between grains (Bhattacharyya and Friedman, 1984). The results of these experiments seem to correspond well with the interpretation that grain breakage and deformation in the Mozduran limestones occured during shallow to deep burial.

4.3.2 Chemical compaction

Chemical compaction or pressure dissolution is a process which results from the increased solubility of grains and sediment due to overburden or tectonic stress. It is known to be responsible for thickness reduction and is also an important source of $CaCO_3$ for burial cementation (Choquette and James, 1987, Finkel and Wilkinson, 1990). There have been numerous descriptions and classifications of pressure dissolution features (recent examples include Wanless, 1979; Buxton and Sibley, 1981; Bathurst, 1987; Choquette and James, 1987; Railsback, 1993 a). A combination of these classifications has been used here. Three types of pressure dissolution compaction are present in the Mozduran limestones: 1) sutured grain to grain contact, 2) sutured seam stylolite, and 3) non-sutured stylolite (dissolution seam). Fitted fabric has not been observed.

4.3.2.1 Sutured grain to grain contact

Sutured grain to grain contact is the most abundant type of pressure dissolution feature in the Mozduran limestones (Fig. 4.8 D). This involves the pressure dissolution of two grains pressed together at a sutured contact, and creates a thin solution film at the contact without any insoluble residue (Choquette and James, 1987). Pressure dissolution at grain to grain contact is more abundant in oolitic facies (Fig. 4.8 D). This type of dissolution feature in the Mozduran limestone indicates a lack of early cements, thus, grain to grain dissolution has taken place before calcite spar precipitation.

4.3.2.2 Sutured seam stylolites

Stylolites are another common type of pressure dissolution feature of the Mozduran limestones. They are usually irregular to peaked low amplitude (Fig. 4.8 E). The amplitute of peak stylolites reaches up to about 4 mm wide and 2 mm

high. These stylolites transect the rock fabric, cutting across grains, cements, matrix and veins. The style of pressure dissolution is different in various lithologies or rock fabrics (Buxton and Sibley, 1981; Railsback, 1993 a). Stylolites are most abundant in well cemented oosparite and biosparite (Fig. 4.8 E), whereas in mud-supported rocks, stylolites are less common or virtually absent. This observation is in general agreement with the conclusion of Railsback (1993 a), that stylolite development in well cemented rocks results from juxtaposition of grains and cement, whereas, an abundance of pressure-resistant grains in cement-poor grainstones inhibits stylolite development. The cross-cutting relationship between stylolites and rock fabric in the limestone studied indicates that stylolites were formed during late burial diagenesis (Bathurst, 1987). Stylolites in the study area are believed to have occurred due to overburden pressure during continuous subsidence of the Upper Jurassic sediments to a depth of about 4 km, until the late Miocene, when the basin was uplifted and deformed. Stylolite formation due to overburden pressure alone occurs at about 1 km of burial (Scholle and Halley, 1985, Heydari, 1990). Thus, stylolites in the Mozduran Formation carbonates have possibly formed at or above 1 km of burial depth. The thickness of insoluble residue and peak amplitude of stylolites in dolomites are generally lower than those of limestones in the Mozduran Formation. This may be due to the heterogeneity of the limestone fabric and high susceptibility of calcite minerals to pressure dissolution compaction (Railsback, 1993 a).

4.3.2.3 Non-sutured stylolite (dissolution seam)

This type of dissolution feature is minor in the Mozduran limestones, forming smooth, undulose seams of insoluble residue, which lack the distinctive sutures of stylolites. This non-serrate pressure dissolution is more abundant in the Mozduran dolomite than in the limestones. Railsback (1993 a) has suggested that dolomite has a lower susceptibility to pressure dissolution than limestone, thus, dolomitic rocks contain enough pressure-resistant elements to inhibit the interpenetration characteristic of stylolites and therefore only allows the development of dissolution seams.

Pressure dissolution is commonly invoked as the major source of $CaCO_3$, especially in limestones lacking early cements (e.g., Hird and Tucker, 1988). In the Mozduran limestones, grain to grain dissolution is clearly observed to have taken place before early calcite spar precipitation (Fig. 4.8 C). There is no petrographic evidence to indicate that the material derived from pressure solution

in the Mozduran limestone was not locally reprecipitated. The grounds for this contention are the low porosity zones, which occur in close proximity to the pressure dissolution features, suggesting that $CaCO_3$ from dissolution has been reprecipitated close-by (Wong and Oldershaw, 1981).

Pressure dissolution has been documented to occur during shallow burial (Buxton and Sibley, 1981; Finkel and Wilkinson, 1990; Railsback, 1993 a). However, pressure dissolution has been known as a deep burial diagenetic process (Scholle and Halley, 1985; Scoffin, 1987). Since the Mozduran limestones were buried up to ~4 km, the pressure dissolution features in these carbonates can be related to deep burial diagenetic processes.

4.4 Silicification

Silica is a minor diagenetic component of the Mozduran limestones, particularly in the shallowest part of the basin. It occurs mainly in the lower portion of the Gorgoreh and Bazangan sections, which are located in the relatively deeper part of the basin. In some samples, silicification is not complete, whilst, in others, silicification is pervasive and most biomicrite and intramicrite facies are almost completely silicified (e.g., thin section Go, 18, 19 , 20).

Silica occurs in two forms: 1) a finely crystalline mosaic of quartz crystals with pin-point extinction, replacing carbonate sediments, and 2) megaquartz and chalcedonic quartz, precipitated as a pore-filling cement (Fig. 4.8 F). Silicification in the lower part of the Gorgoreh and Bazangan sections is directly related to the abundance of siliceous sponge spicules in the carbonate samples. Therefore, sponge spicules are an important source of silica in the Mozduran limestones. Siliceous skeletons are often composed of metastable, amorphous opaline silica, which has a higher solubility than quartz. This solubility difference increases with increasing depth of burial (Tucker, 1991). Thus, the dissolution of biogenic silica, such as sponge spicules, promoted silicification in the Mozdutran limestones.

4.5 Summary of Paragenetic Sequence

As previously discussed, the Mozduran Formation has undergone a complex diagenetic history. The paragenetic sequence in this study includes 17 distinct processes (Fig. 4.9). The order of sequence is based mainly on crystal morphology, cathodoluminescence mineralogy, cement fabric relationships and isotopic compositions.

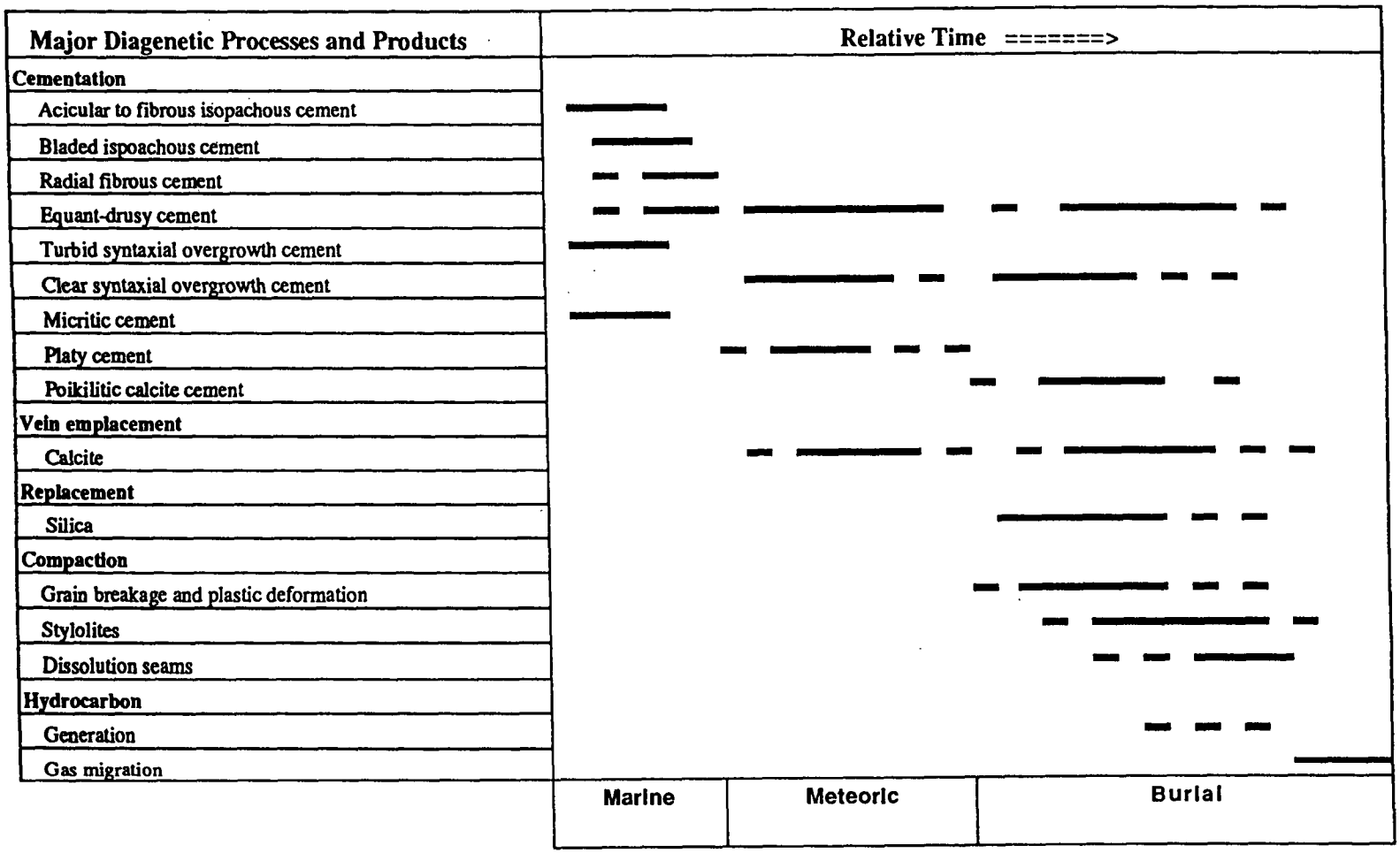

Figure 4.9. Summary diagram illustrating the paragenetic sequence in the Mozduran limestones.

4.6 Discussion and Conclusions

The Mozduran limestones contain a variety of early to late carbonate cements, precipitated in marine, meteoric and burial environments. The early cements in the Mozduran limestones exhibit variable morphology. These include: acicular to fibrous isopachous crystals; bladed, equant isopachous crystals; radial fibrous crystals; micritic cement; and turbid syntaxial rims on echinoderm debris.

Acicular to fibrous cements, which indicate original aragonite mineralogy, are only present in the shallowest part of the basin, whilst calcite cements are dominant in the relatively deeper part of the basin. The variations in cement carbonate mineralogy in the Mozduran limestones can be related mainly to the seawater temperature. Experimental studies confirmed that carbonate mineralogy depends on water temperature. The latitudinal variations in carbonate mineralogy are also related to seawater temperature (see Chapter 5 for discussion). In the Mozduran limestones, the very shallow warm-water sea favored aragonite precipitation, and the relatively cooler and deeper water could account for a more calcitic mineralogy. This interpretation is supported by elemental and isotopic studies (see Chapter 6 and 7). Other petrographic evidence, such as: diffused laminae within ooids (Fig. 3.7 D); the tangential nature of crystals in concentric ooids (Fig. 3.7 E); shattered micritic envelopes (Figs. 3.2 A, B); spalled ooids (Fig.3.8 C); and the presence of aragonite relics within the micrite (Fig. 3.1 E, F), all provide evidence for an original aragonite mineralogy in the shallowest part of the basin.

Almost all early isopachous marine cements are dull to non-luminescent, except for one sample, which shows moderate luminescence. None of the early marine cements exhibit luminescent zoning.

The marine carbonate cements in the Mozduran limestones have an $\delta^{18}O$ value of -2.4‰ PDB. This value is within the range of modern warm water carbonate sediments.

In many carbonate formations, aragonite dissolution has been related to near-surface diagenesis by meteoric water. This statement is based mainly on the extensive occurrence of aragonite dissolution by meteoric water in Pleistocene carbonates, as a result of rapid sea level fluctuations. A meteoric origin of cementation in the Mozduran limestones is supported by: the calcite crystal morphology (mainly drusy mosaic and platy); the occurrence of a few minor regressions during the Upper Jurassic (see Fig. 2.3); very bright-yellow luminescence; and lighter average oxygen ($\delta^{18}O$= -6.2‰ PDB) and carbon ($\delta^{13}C$= -1.6‰ PDB) values, compared to marine calcite cement. The meteoric

calcite cements are mostly abundant in samples from the shallowest part of the basin.

Burial cementation in the Mozduran limestones can be inferred from: the calcite crystal morphology (such as poikilitic cements); paucity of cement, particularly prior to compaction; more positive carbon (up to ~3.8‰ PDB) and very depleted oxygen (~-8‰ PDB) values; and the presence of dull luminescent cement, compared to marine and meteoric diagenetic cements. The relationship of calcite cements with grain fracturing (such as spalled ooids, collapsed micritic envelopes), grain-to-grain pressure dissolution contacts, stylolites, and late fractures, also supports a burial origin of some calcite cements. As cementation is dependent on increasing temperature, the burial depth of ~4 km, for the base of the Upper Jurrasic Mozduran Formation, is sufficient to promote cementation. The burial calcite cements were mostly present in samples from the relatively deeper part of the basin. The CL petrography and isotopic analysis indicate that vein calcites were precipitated in both meteoric and burial environments. Silicification, which is also present only in samples from the relatively deeper part of the basin, is related to burial diagenesis.

CHAPTER 5

ARAGONITE versus CALCITE CONTROVERSY

CHAPTER 5

ARAGONITE versus CALCITE CONTROVERSY

5.1 Background

From the 1950s to mid-1970, there was generally little consideration of the possibility that carbonate mineralogy had changed through the Phanerozoic. Until then, the original mineralogy of all limestones was assumed to be aragonite and high-Mg calcite. Sandberg (1975) was the first to argue, based on the fabric of ooids (Great Salt Lake, Utah and other older limestones), that some ancient ooids were originally composed of calcite, rather than aragonite. It was suggested that if the ooids were originally calcitic (HMC or LMC), change from original HMC/LMC to derived LMC (dLMC) during diagenesis, will preserve the original ooid fabric (radial-fibrous structure), which is characteristic of calcite mineralogy (Sandberg, 1975). On the other hand, originally aragonitic ooids may occur as sparry calcite, or be preserved as oomolds through aragonite dissolution and calcite precipitation. Sandberg (1983) considered that the original mineralogy of moldic ooids can be high-Mg calcite, as calcite with approximately 13% $MgCO_3$, has a solubility equivalent to that of aragonite. Moreover, Walter and Morse (1984), in the reevaluation of magnesian calcite stabilities, suggested that at tropical temperatures of 25-28° C, the solubility of precipitated calcite with about 12 mole% Mg approaches that of aragonite. Therefore, high-Mg calcites can dissolve as readily as aragonite.

However, individuals such as Schroeder (1979) and Budd (1983) differed from these views, on evidence of the limited porosity developed during high-Mg calcite dissolution in subaerially exposed Cenozoic sequences. Wilkinson et al. (1985) also argued that selective dissolution of high-Mg calcite components, resulting in moldic porosity is, however, a process virtually undocumented in natural carbonate sequences. They stated that all magnesian calcite components in carbonate sequences transform to low-magnesium calcite, while retaining the finest details of original fabric. In their opinion, the bulk of natural observations strongly suggested that oomoldic fabric recorded

the former presence of aragonite.

It has been argued that there had been a secular variation in Phanerozoic oolite compositions, with aragonite ooids occurring in the late Precambrian-Cambrian, mid-Carboniferous to Triassic, and Tertiary to Recent, and low-Mg calcite ooids occurring in the early and Middle Paleozoic and Jurassic-Cretaceous, mostly as a result of differences in atmospheric PCO_2 levels (Sandberg, 1975, 1983; Mackenzie and Pigott, 1981). Increasing PCO_2 levels were shown to correlate with times of global high sea-level stands, high spreading rates, and high rates of subduction, metamorphism and volcanism, which favor calcite precipitation (the higher PCO_2 levels coincide with phases of active plate movements). Low PCO_2 levels, are associated with low spreading rates and low sea-level stands, which favor aragonite precipitation.

Müller et al. (1972), Folk (1974 b), and many others have suggested that the relative concentration of Mg^{2+} ions versus Ca^{2+} ions may determine the mineralogy of precipitated carbonates. Mg/Ca ratios of modern seas are about 5, and as Müller et al. (1972) suggested, Mg/Ca threshold ratios for calcite and aragonite are about 5. Sandberg (1975) and Milliken and Pigott (1977) concluded that differences in cortical mineralogies are due to variations in marine Mg/Ca ratios. A molar value (Mg/Ca ratio) above 5 is thought to favor the precipitation of aragonite and high-Mg calcite, and a lower Mg/Ca ratio leads to low-Mg calcite precipitation. It was suggested that an increase in the Mg/Ca ratio of seawater during the Cenozoic, due to the extraction of Ca^{2+} by coccoliths and subsequent deposition of large volumes of $CaCO_3$ in a deep ocean area, can account for the change from calcitic ooid mineralogy in the Jurassic-Cretaceous, to the aragonitic ooids of the Cenozoic (Sandberg, 1975). This seems unlikely, as it would have required large volumes of coccoliths to significantly decrease the Mg/Ca ratio of seawater.

Sandberg (1983, 1985) later noted that increases in the Mg/Ca ratio of seawater, due to the extraction of Ca^{2+} by coccoliths, is not in accord with the earlier abundance of aragonite in the Lower Paleozoic or Upper Paleozoic-Lower Mesozoic, nor the occurrence of calcite in the Upper Mesozoic-Lower Tertiary seas. He thus placed greater emphasis on the PCO_2 levels of the atmosphere-hydrosphere system, as proposed by Mackenzie and Pigott (1981). Although experimental studies (Burton and Walter, 1991) do indicate that the Mg content in calcite is related to PCO_2 levels, these changes are more pronounced at low temperatures.

Wilkinson et al. (1985) found that there is a better correlation between mean ooid cortical mineralogy and areas of continents flooded or exposed, than

there is between mineralogy and positions of global sea level. Thus, they suggested that calcite seas correspond to periods of relatively high sea level, with continents in submergent mode, whilst aragonite seas correspond to periods of relatively low sea level and an emergent mode. They mentioned that as changes in PCO_2 and ambient Mg/Ca ratios are related to rates of spreading and global eustasy, both should change in a simultaneous and complementary fashion, to influence cortical mineralogies. They, therefore, concluded that calcite seas correspond to periods of relatively high sea level, high rates of sea floor spreading and subduction, high PCO_2 levels and low Mg/Ca ratios, with continents in submergent mode, whilst aragonite seas correspond to periods of relative low sea level, low rates of spreading, low PCO_2 levels, high Mg/Ca ratios and an emergent mode. The Mg/Ca ratios in the ocean are largely controlled by hydrothermal weathering of basalts at mid-ocean ridges. Mg is extracted from seawater to form clay minerals such as chlorite and epidote. Lower Mg/Ca ratios can thus be expected during periods of high rates of seafloor spreading, which correspond to periods of high sea level stand (Wilkinson et al., 1985).

5.2 Water Temperature as a Control on Carbonate Mineralogy

Modern carbonates are now forming extensively in many regions, in both the southern and northern hemispheres (Lees, 1975; Nelson, 1988), at sea water temperatures ranging from about -2 to 40° C. These carbonates can be subdivided into those produced in: tropical environments (latitudes from 0 to 30° S or N, and summer temperatures >25° C); temperate environments (30 to 50° S or N, and summer temperatures between >10 to 25°C); and polar settings (>50° S or N, and summer temperatures <10° C).

Recent tropical and subtropical carbonates, which occur extensively in regions with a low terrigenous influx have been well studied. In temperate settings, modern shelf carbonates are also forming extensively in many areas (Lees, 1975; Nelson, 1988; Rao and Adabi, 1992; Rao and Jayawardane, 1994), particularly along the southern margin of Australia (Connolly and Von der Borch, 1967; Wass et al., 1970; Collins, 1988; Gostin et al., 1988; Bone and James, 1993; James et al., 1992, 1994). These carbonates differ from tropical carbonates in terms of the: type of skeletal grains (Lees, 1975); mineralogy and diagenesis (Rao, 1981 a; Reeckman, 1988); the range of major and minor elements (Rao, 1986; Rao and Adabi, 1992); and the oxygen and carbon isotope composition (Rao and Green, 1983; Rao and Nelson, 1992). Domack (1988) has reported that polar carbonate sediments are now forming in the Antarctic

glaciomarine environment.

The $CaCO_3$ mineralogy of Recent shallow marine carbonates varies with seawater temperature (Nelson, 1988; Rao, 1981 a; Rao and Adabi, 1992 and references therein). This has also been shown to be the case in experimental studies (Kinsman and Holland, 1969; Burton and Walter, 1987). In Recent tropical warm shallow marine carbonates (temperatures >25° C), meta-stable aragonite is the predominant mineral, with variable amounts of high-Mg calcite (Milliman, 1974). Seawater generally contains three times more Mg (1290 ppm) than Ca (411 ppm). In warm seas, the Mg ions inhibit the growth of low-Mg calcite and force $CaCO_3$ to crystallize as aragonite and high-Mg calcite. This inhibition is either ineffective or neutralized in cold waters, as evidenced by the precipitation of predominantly low-Mg calcite (Rao and Adabi, 1992).

It has been stated that the amount of Mg in marine calcite varies with water temperatures, PCO_2 levels and sulphate concentrations in seawater (Füchtbauer and Hardie, 1976; Burton and Walter, 1987, 1991; Mucci, 1987; Nelson, 1988). Increasing water temperature and/or decreasing PCO_2 levels, increase the Mg content in marine calcite. Calcite precipitating alone from seawater at 25° C contains about 2% Mg in high-Mg calcite. Mg values decrease with decreasing temperature, with 0 to 0.5 Mg% at ~0° C, due to the change from high-Mg calcite to low-Mg calcite. Regardless of temperature, Mg ion concentrations increase linearly with decreasing PCO_2 levels (Burton and Walter, 1991). Therefore, variations in Mg content, other than those attributable to a given temperature, are possibly due to changes in PCO_2 levels. PCO_2 levels generally decrease with decreasing water depth, due to increasing water temperatures. Thus, the Mg concentrations in marine calcite increase with decreasing water depth. Opdyke and Wilkinson (1990) suggested that marine carbonate systems have responded to changes in both temperature and CO_2 concentrations in global oceans.

Experimental studies by Kinsman and Holland (1969) indicate that at 30° C and above, mainly aragonite forms as needles and spherulites. Between 15 and 17° C mixtures of high-Mg calcite and aragonite form as needles and grains, and at 3° C, low-Mg calcite forms as rhombs (50μ) and large plates (100μ). Thus, primary morphology and the type of carbonate minerals can be used to infer the temperatures of formation of marine carbonates (Rao, 1981 a).

Aragonite to calcite ratios in Recent carbonates decrease from tropical to temperate and polar regions (Lees, 1975; Nelson, 1978, 1988; Rao and Adabi, 1992). Similar latitudinal variations in aragonite to calcite ratios also occur in ancient carbonates (Nelson, 1978; Rao, 1981 a, 1988 a; Brookfield, 1988; James

and Bone, 1989; 1992). In Recent warm temperate carbonates (surface temperature <25° C), high-Mg calcite predominates, with some aragonite (Collins, 1988), whereas mixtures of high-to low-Mg calcite, with minor amounts of aragonite, occur in Recent cool temperate marine waters at an average surface temperature of <13° C (Rao and Huston, 1995). In subpolar cold waters of about <5° C, and in cold water deep sea, low-Mg calcite dominates over high-Mg calcite, or pure low-Mg calcite forms (Schlager and James, 1978; Rao, 1988 a). Experimental studies (Kinsman and Holland, 1969; Burton and Walter, 1987) indicate that low-Mg calcite forms alone in water temperatures of <5° C from normal seawater. This result also confirms that carbonate mineralogy depends on water temperature, similar to observations in natural carbonates. Therefore, in ancient carbonates, recognition of original carbonate mineralogy can be used to differentiate tropical, temperate and subpolar carbonates (Nelson, 1978; Rao, 1981b , 1991).

5.3 Discussion

There are important unresolved issues in the literature regarding the roles of aragonite and calcite through time. Wilkinson et al. (1985) reviewed the literature and provide the most comprehensive interpretations. However, there are internal inconsistencies in Wilkinson et al. (1985), in that their data does not fully support their interpretations. For example, they concluded that ooids formed during lowstands record the dominance of aragonite, whereas primary calcite mineralogy dominates during highstands (Fig. 5.1, Wilkinson et al., 1985). However, they have shown that during the Cambrian and Ordovician periods, aragonite cortices are abundant, while there was a period of continental submergence or sea level highstand. Therefore, this interpretation would not explain the occurrence of aragonite during these periods.

Fig. 5.1 (Wilkinson et al., 1985) also shows that during the Upper Jurassic, calcite was the only ooid cortical mineralogy. However, in Fig. 5.2 (Wilkinson et al., 1985) they have shown that during the Upper Jurassic, moldic oolites (due to aragonite dissolution) were dominant. In their Fig. 9 they suggested that there is a general trend relating increasing amounts of cortical aragonite to increasing continental emergence, but during the Upper Cambrian, Lower Ordovician and Lower Silurian, inspite of maximum sea level highstands, the percentages of aragonite fabrics are much higher than in the Carboniferous, Jurassic and Cretaceous periods. Even during the Upper Jurassic, with relatively higher sea level, aragonite fabrics are more abundant than during the mid Jurassic, with relatively lower sea level.

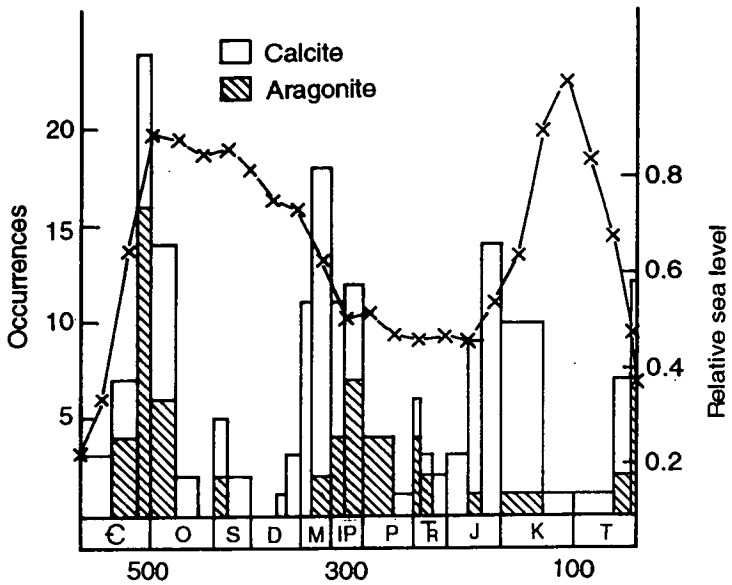

Figure 5.1. Distribution of occurrences of originally calcite and aragonite ooid cortices (redrawn from Wilkinson et al., 1985).

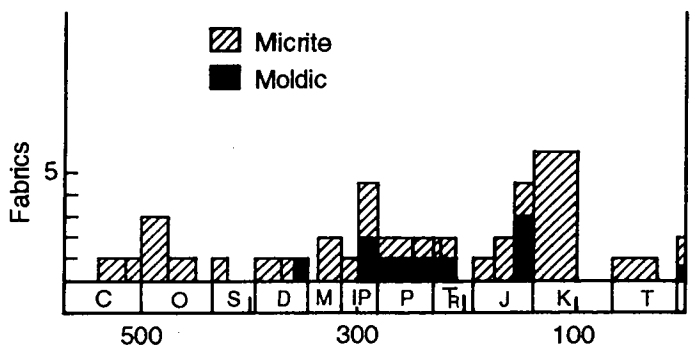

Figure 5.2. Secular variation in the abundance of micritic and moldic oolites (redrawn from Wilkinson et al., 1985).

Based on the above arguments, Wilkinson et al. (1985) concluded that aragonite is the dominant ooid cortical mineralogy in present day environments, due to very slow spreading rates, periods of low PCO_2, and relatively low sea level. This interpretation is not conclusive, as at the present time, the rate of seafloor spreading is moderately high and thus the PCO_2 level, which coincides with the rate of seafloor spreading, should be relatively high. Given and Wilkinson (1985) also placed emphasized on the CO_3^{2-} supply rate, with higher rates favoring aragonite and lower rates favoring high-Mg calcite. However, this asumption has also been questioned (Morse, 1985).

Calcite is the dominant mineral in Recent marine temperate and polar environments at seawater temperatures of about <25° C (Collins, 1988; Gostin et al., 1988; Nelson, 1988; Domack, 1988; James et al., 1992, 1994; Rao and Adabi, 1992; Bone and James, 1993; Rao and Jayawardane, 1994). Aragonite is the dominant carbonate mineral in Recent shallow marine tropical environments at seawater temperatures of about >25° C (Lees, 1975). Therefore, the wide variation in carbonate mineralogy in modern settings does not fully correspond to the PCO_2 levels, position of global sea level, or with the percentage of continental flooding.

As previously discussed in the background, most of the above researchers related the secular variation in carbonate mineralogies to seafloor spreading and plate tectonic processes, which ultimately control seawater chemistry. However, as indicated by several other workers, precipitation of aragonite from seawater is favored over calcite at higher Mg^{2+} and SO_4^{2-} levels, lower PO_4^{3-} levels, and increasing temperature (Mucci and Morse, 1983; Walter, 1986; Burton and Walter, 1987; Railsback and Anderson, 1987). It has been suggested that with increasing seawater temperature, there is a strong increase in $MgCO_3$ incorporation in calcites (Burton and Waler, 1987; Burton, 1988; Mucci, 1987; Oomori et al., 1987). Experimental studies (Burton and Walter, 1987) indicate that calcite precipitated from seawater (at similar atmospheric CO_2) at 5° C contains 6 mol% $MgCO_3$, at 25° C, 8 mol% $MgCO_3$, and at 3° C about 11 mol% $MgCO_3$. Nelson (1978) and Rao (1981a, 1988 a, 1991) studied ancient non-tropical carbonates, suggesting that carbonate mineralogy varies with water temperature and that calcite predominates in ancient cold, shallow-marine limestones. Nelson (1988) proposed that the assumption of change of original mineralogy needs to be re-evaluated with the concept of mineralogical change with water temperature.

Evaluation of Ordovician carbonates of Tasmania, based on petrographic and geochemical criteria (Rao, 1990 b), indicated that aragonite (not calcite) was the predominant mineral in warm tropical Ordovician carbonates. Petrographic and geochemical evidence also suggested that aragonite was the predominant primary mineral in Upper Jurassic shallow marine carbonates, deposited in the N.E of Iran (Adabi and Rao, 1991). These interpretations (Rao, 1990 b; Adabi and Rao, 1991) are not in agreement with the proposed calcitic mineralogy as a dominant carbonate mineral during the Ordovician and the Upper Jurassic periods (Sandberg, 1975; Mackenzie and Pigott, 1981, and Wilkinson et al., 1985).

High PCO_2 levels are postulated by some workers during the Upper

Jurassic (e.g., Moore et al., 1992 a) and consequently a 'Greenhouse Mode' (Hallam, 1993). If we consider this Greenhouse mode, the calcite mineralogy should predominate (e.g., Wilkinson et al., 1985), the temperature should have been higher than that of the present day latitude (Valdes and Sellwood, 1992), and the $\delta^{13}C$ values should be lower, due to higher $\delta^{12}C$ values in the atmosphere. The Mozduran carbonate data, as explained later, do not support this inference because of: the aragonite mineralogy in the shallowest (Adabi and Rao, 1991) and mixture of aragonite and calcite in the relatively deeper part of the basin (Adabi and Rao, 1996); the relatively lower regional temperatures (~16° C in the former Soviet Union, Stevens, 1971 and average of ~20° C in this study); and the relatively higher $\delta^{13}C$ values (+4.3‰). These aspects are discussed later in Chapter 6 and 7. The low PCO_2 level, similar to that of the present day value is in agreement with Valdes and Sellwood's (1992) paleoclimate model for the Upper Jurassic. The low PCO_2 level and high Mg/Ca ratio (supported by abundant evaporite and dolomite in the shallowest part of the basin) correspond to the aragonite sea model of Wilkinson et al. (1985). However, they are not in agreement with the emergent mode (because of continental transgression during the Upper Jurassic), and with the secular variation of carbonate mineralogy proposed by Wilkinson et al. (1985).

There are many examples from different localities which indicate the occurrence of both aragonite and calcite mineralogies. These examples are presented briefly below :

- Ooid mineralogies vary from dominantly aragonite to increasingly calcitic in modern carbonates along a mere 10 km of shore zone in Baffin Bay, Texas (Land et al., 1979).
- Biminerallic ooids (aragonite and high-Mg calcite) have been described from the Pleistocene of the Florida continental shelf (Major et al., 1988).
- The Upper Jurassic Smackover oolite of the Gulf Coast region (southern Arkansas and northern Louisiana) has both formerly aragonitic ooids in a near shore belt, and calcitic ooids in an offshore belt (Swirydczuk, 1988).
- The Upper Jurassic ooids in the Purbeck limestones of Swiss and French Jura also have both aragonite and calcite mineralogies (Strasser, 1986).
- Calcite and aragonite ooids occur in the Upper Pennsylvanian carbonates of southeastern Kansas (Wilkinson et al., 1984).
- Calcite, aragonite and mixed calcitic-aragonitic ooids have been reported from the mid Proterozoic Belt supergroup in Montana (Tucker, 1984).
- The present study also confirms that during the Upper Jurassic, with a similar

atmospheric PCO_2 level and tectonic setting, aragonite is the dominant carbonate mineral in the shallowest (Adabi and Rao, 1991), and mixture of aragonite and calcite in the relatively deeper part of the basin respectively (see Chapter 6 and 7). In this continuous sedimentary basin (ranging from Jurassic to Oligocene), there are no major sedimentary breaks, nor evidence of volcanic activity. Therefore, the mineralogical changes (occurrence of both aragonite and calcite) in the Upper Jurassic Mozduran limestones are attributed mainly to variations in water depth and seawater temperatures.

5.4 Conclusions

As aragonite and calcite mineralogies have been shown to both occur at the same time in several relatively large basins, with similar PCO_2 levels and tectonic settings, such as in Baffin Bay Texas, the Pleistocene of the Florida Shelf, the Upper Jurassic carbonates of Gulf Coast region of the USA, the Upper Jurassic Purebeck limestones of the Swiss and French Jura (in Europe), the Upper Pennsylvanian in southeastern Kansas, and mid Proterozoic Belt supergroup in Montana, the assumption of change of original carbonate mineralogy through time needs to be re-evaluated in the light of mineralogical change with water temperature (Nelson, 1988; Rao, 1991; Adabi and Rao, 1991; Adabi and Rao, 1996). Whilst, the role of Mg/Ca ratios, and SO_4^{2-} concentrations can not be ruled out, due to the presence of evaporite and dolomite beds in the Mozduran sequences, the variation of carbonate mineralogy in the shallow shelf (mainly aragonite) and relatively deeper shelf (mixed calcite and aragonite) in the Mozduran limestones, can be related mainly to changes in seawater temperature.

CHAPTER 6

TRACE ELEMENTS in LIMESTONES

CHAPTER 6

TRACE ELEMENTS IN LIMESTONES

6.1 Introduction

As disscused in Chapter 5, some workers have assumed that the mineralogy of ancient carbonates may have been different from that of modern sediments (Sandberg, 1975, 1983; Mackenzie and Pigott, 1981; Wilkinson, 1982; Tucker, 1984), with calcite being considered the dominant mineral during the early and middle Palaeozoic and Jurassic. It was suggested that the assumption of change of original carbonate mineralogy through time needs to be re-evaluated in the light of mineralogical change with water temperature (Nelson, 1988). Evaluation of Ordovician carbonates of Tasmania (Australia), based on petrographic and geochemical criteria (Rao, 1990 b), indicated that aragonite was the predominant mineral in warm water subtropical Ordovician carbonates. Adabi and Rao (1991) suggested that the relative proportions of trace elements are preserved in ancient carbonates, despite prolonged meteoric diagenesis, and the retention of the relative concentrations of elements exists mainly because of systematic loss and gain of elements during diagenesis.

This study uses major and trace element data to understand the original mineralogy of Upper Jurassic Mozduran limestones from the shallowest (Shurijeh, Bagak, Padeha and Mozduran sections) and relatively deeper (Gorgoreh and Bazangan sections) part of the basin (see Fig. 2.7). The major (Ca, Mg) and trace elements (such as, Sr, Na, Mn, Fe) are related to carbonate mineralogy and those such as, Ba, Ti, Rb and K_2O, are related to bulk sediments characteristics. The trace element (Sr, Na, Mn, Fe) data are compared with Recent tropical and temperate carbonates, originally aragonitic Ordovician subtropical carbonates and originally calcitic Permian subpolar cold water carbonates of Tasmania.

The field for Recent temperate carbonates has been calculated, based on 86 (from a total of 120) bulk carbonate samples with <10% insoluble residue,

from temperate shelf carbonates of western Tasmania (Rao and Adabi, 1992), from the eastern temperate shelf of Tasmania (Rao and Jayawardane, 1994), and from King Island, north of Tasmania (Rao and Amini, 1995). The mean and 80 percentile of these carbonate samples are also presented in this field. The 80 percentile of these samples corresponds to <6.5% insoluble residue. The relevant data are included in Appendix 4 (samples with more than 10% insoluble residue are not shown in Appendix 4).

From the shallowest part of the basin, 102 carbonate samples were analyzed for major and minor elements. Only those samples with less than 1% Mg and less than 10% insoluble residue (34 samples) were used, in order to reduce possible effects of contamination. Trace element variations in carbonates from the shallowest (mainly aragonitic) part of the basin are discussed below, followed by those from the relatively deeper (mainly calcitic) part of the basin. The minimum, maximum, mean and standard deviation values of aragonitic and mixed calcitic-aragonitic limestones in the Mozduran Formation are shown in Tables 6.1 and 6.2 respectively. The elemental and isotopic composition of those carbonates with less than 1% Mg and less than 10% insoluble residue are listed in Tables A5.1 and A5.2 (Appendix 5). All major and minor element analyses of carbonate samples from Shurijeh, Bagak, Padeha and Mozduran sections, regardless of insoluble residue, are shown in Tables A5.3, A5.4, A5.5, A5.6 (Appendix 5).

6.2 Aragonite Mineralogy

In ancient carbonates, the differentiation between originally aragonitic and originally calcitic mineralogy is difficult. As most ancient carbonates affected by meteoric/burial diagenesis are now altered to low-Mg calcites, X-ray diffractograms and Mg contents of ancient limestones are of little use in distinguishing original aragonite from calcite. Low-Mg calcite mainly remains stable, and undergoes only minor chemical changes in open system diagenesis. Calcitic limestones are considered better models for meteoric diagenesis than aragonitic carbonates (James and Bone, 1989). Thus, distinguishing aragonite from calcite is necessary to understand temperatures of deposition, diagenesis and geochemistry of carbonates.

Trace element variations between Recent warm water and cold water carbonate sediments provide a means of differentiating ancient counterparts. This is due to different trace element concentrations in warm and cold water carbonates, resulting from variations in carbonate mineralogy. The Sr and Na

concentrations in ancient limestones decrease appreciably during meteoric and/or burial diagenesis (e.g., Brand and Morrison, 1987; Marshall, 1992; Winefield et al., 1996). Nevertheless, the ratios of Sr/Na in ancient limestones do indicate originally aragonitic limestones from calcitic counterparts (Rao 1991; Adabi and Rao, 1991).

Table 6.1. Minimum, maximum, mean and standard deviation values of aragonitic samples in the Mozduran limestones.

Variables	Minimum	Maximum	Mean	Standard deviation
Ca%	39	39.9	39.5	0.197
Mg%	0.15	0.74	0.35	0.113
Mn ppm	53	529	243	127.67
Fe ppm	328	3745	1191	849.7
Sr ppm	114	408	264	77
Na ppm	79	280	144	47.2
Sr/Na ratio	0.85	3.31	1.94	0.59
I.R%	0	10	4.86	2.74

Table 6.2. Minimum, maximum, mean and standard deviation values of calcitic-aragonitic samples in the Mozduran limestones.

Variables	Minimum	Maximum	Mean	Standard deviation
Ca%	38.45	40.08	39.53	0.322
Mg%	0.08	0.9	0.32	0.174
Mn ppm	17	328	80	56.19
Fe ppm	63	3552	557	645.78
Sr ppm	61	424	168	103.92
Na ppm	44	525	144	92.55
Sr/Na ratio	0.71	3.36	1.29	0.49
I.R%	0	10	3.42	2.6

6.2.1 Strontium

Sr concentrations in Recent tropical bulk limestones range from 8000 to 10000 ppm (Milliman, 1974), whereas in Recent temperate bulk carbonates, the range is lower, from 1642 to 5007 ppm, with a mean of ~3270 ppm (Fig. 6.1, Rao and Adabi, 1992; Rao and Jayawardane, 1994; Rao and Amini, 1995). The Sr content varies due to carbonate mineralogy. Sr increases with increasing aragonite content (Rao and Adabi, 1992) and decreases with increasing calcite content. The Sr concentrations have also been directly related to increasing water temperatures (Morse and Mackenzie, 1990).

As metastable $CaCO_3$ minerals change to calcite during meteoric-burial

diagenesis, the concentration of Sr in diagenetic calcite depends mostly on its partition coefficient and concentration in diagenetic solutions. As Sr has a partition coefficient of <1, and a low concentration in meteoric waters, the diagenetic imprint will show a low concentration of Sr.

Sr concentrations in the limestone samples studied, range from 114 to 408 ppm, with a mean of 264 ppm (Fig. 6.1). Sr values of these samples are much lower than those of their modern counterparts, due to progressive loss of Sr during meteoric diagenesis (Adabi and Rao, 1991). In the upper part of the Mozduran sequence at the type locality (the Mozduran section), the high Sr concentration is possibly due to the abundance of high Sr-bearing fauna such as brachiopods and crinoids (mean of 411 ppm).

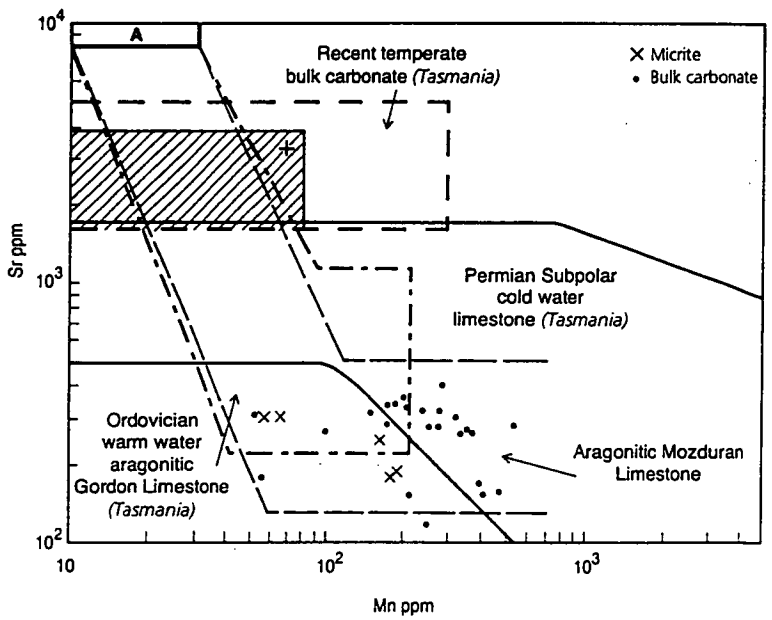

Figure 6.1. Comparison of Sr and Mn field of the Mozduran limestones from the shallowest part of the basin (Adabi and Rao, 1991), with those of subtropical warm-water Ordovician Gordon Limestone (Rao, 1990 b), subpolar cold-water Permian limestone (Rao, 1991), Recent tropical aragonite (A; Milliman, 1974) and Recent temperate bulk carbonate from Tasmania (Rao and Adabi, 1992; Rao and Jayawardane, 1994; Rao and Amini, 1995). Cross symbols indicate the mean value of Sr-Mn in Recent temperate bulk carbonates and the shaded box shows values of about 80% of the total samples. Note the Mozduran pattern is similar to the tropical Ordovician Gordon Limestone.

6.2.2 Sodium

The Na concentrations differ significantly between Recent warm water tropical carbonates, Recent temperate carbonates, and tropical Ordovician and subpolar cold water Permian limestones (Fig. 6.2). Na concentrations in Recent tropical inorganic (abiotic) aragonitic limsetones range from 1500 to 2700 ppm, with a mean of about 2500 ppm, whereas inorganic low-Mg calcites in temperate

regions contain concentrations of around 270 ppm Na (Land and Hoops, 1973; Milliman, 1974; Veizer, 1983; Rao and Adabi, 1992). Na content in high-Mg and low-Mg calcite bryozoa, the dominant fauna in temperate carbonates, is much higher (average ~4500 ppm) than that of inorganic aragonite and low-Mg calcite (Rao and Amini, 1995). This difference is largely due to biochemical fractionation (Land and Hoops, 1973; Rao, 1990 b). Na concentrations in carbonate sediments are related to salinity, biological fractionation, kinetics, mineralogy and water depth (Land and Hoops, 1973; Morrison and Brand, 1986; Rao and Adabi, 1992). Na values increase with increasing salinity, water depth and aragonitic contents.

Na concentrations in the limestones studied from the shallowest part of the basin range from 79 to 280 ppm, with a mean of 144 ppm (Fig. 6.2). Na values of these samples are much lower than those of their modern counterparts, because Na is increasingly lost, with an increase in the influence of meteoric waters (Adabi and Rao, 1991). Na has a partition coefficient of <1, and there is a low concentration in meteoric waters, therefore its diagenetic imprint will also show a low concentration of Na.

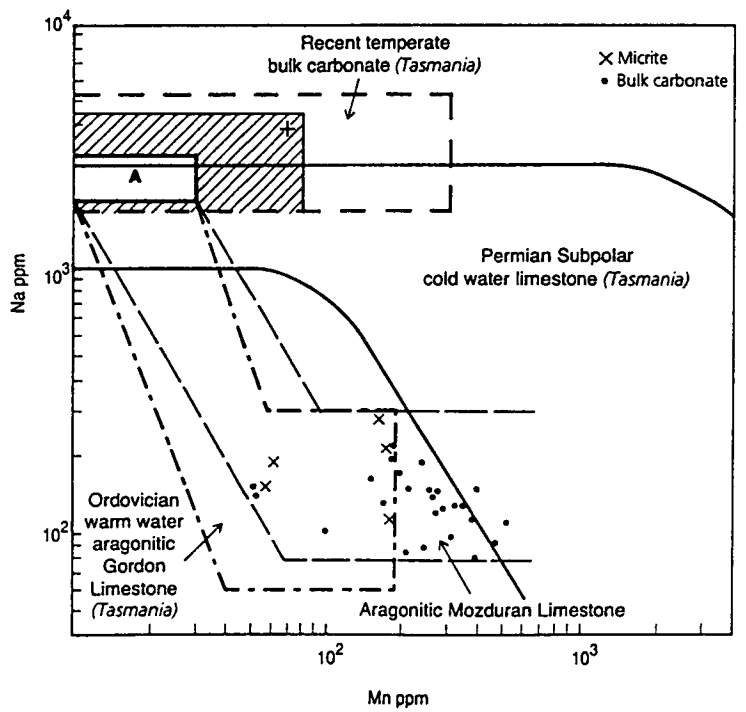

Figure 6.2. Comparison of Na and Mn field of the Mozduran limestones from the shallowest part of the basin (Adabi and Rao, 1991), with those of subtropical warm-water Ordovician Gordon Limestone (Rao, 1990 b), subpolar cold-water Permian limestone (Rao, 1991), Recent tropical aragonite (A; Milliman, 1974) and Recent temperate bulk carbonate from Tasmania (Rao and Adabi, 1992; Rao and Jayawardane, 1994; Rao and Amini, 1995). Cross symbols indicate the mean value of Na-Mn in Recent temperate bulk carbonates and the shaded box shows values of about 80% of the total samples. Note the Mozduran pattern is similar to the tropical Ordovician Gordon Limestone.

The plot of Sr-Na (Fig. 6.3) values shows that most of the limestone samples studied fall within the subtropical warm water aragonitic Ordovician Gordon Limestone field. Winefield et al. (1996) suggested that a Sr-Na plot is particularly useful for facies discrimination (e.g., tropical versus non-tropical settings).

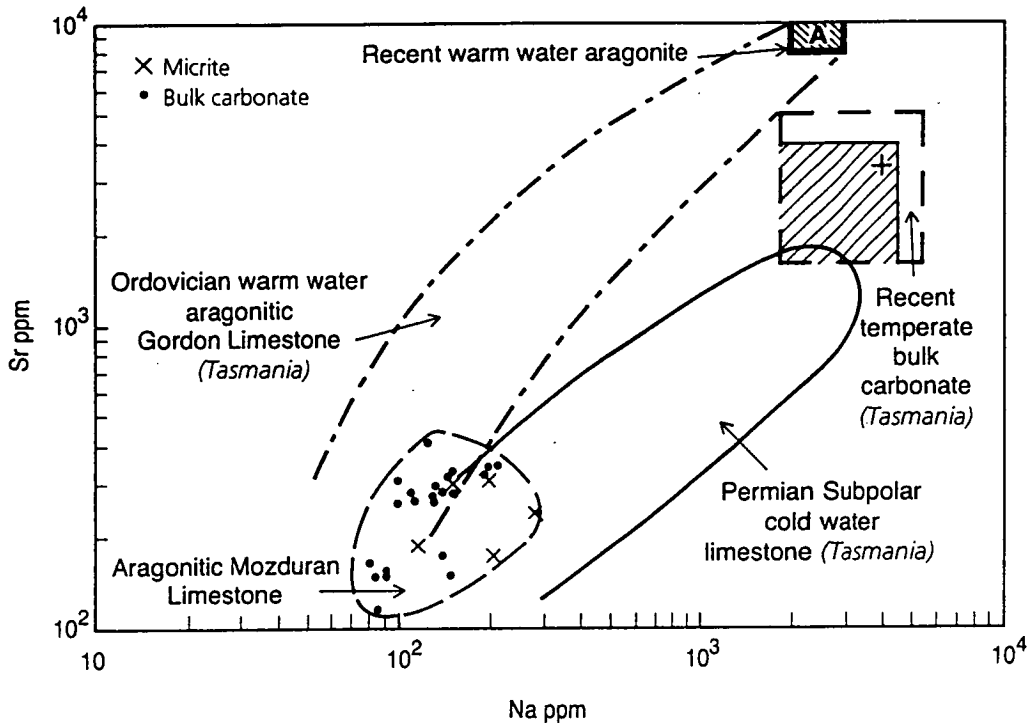

Figure 6.3. Sr and Na variations in the Mozduran limestones from the shallowest part of the basin, compared with fields of subpolar cold water Permian limestones, subtropical warm water Ordovician aragonite (Rao, 1990 b; 1991), Recent tropical shallow marine aragonite (A; Milliman, 1974) and Recent temperate bulk carbonate (Rao and Adabi,1992; Rao and Jayawardane, 1994; Rao and Amini, 1995). Cross symbols indicate the mean value of Sr-Na in Recent temperate bulk carbonates and the dashed box shows values of 80% of the total samples. Note that most of the data falls within the subtropical aragonitic Gordon Limestone field.

6.2.3 Manganese

Mn concentration in limestone samples studied from shallowest part of the basin range from 53 to 529 ppm, with a mean of 243 ppm (Figs. 6.1, 6.2). Recent aragonitic warm shallow marine carbonates have low Mn concentrations (<20 ppm, Milliman, 1974), in contrast to high Mn concentrations in Recent temperate bulk sediments (up to 300 ppm, Rao and Adabi, 1992). Mn contents in most samples studied exceed 20 ppm, unlike aragonitic warm water tropical carbonates, which contain <20 ppm Mn. Mn concentrations increase with an increasing influence of meteoric diagenesis (Brand and Veizer, 1980; Rao, 1990 a), as the partition coefficient of Mn is ~15 and it occurs in high concentrations in

meteoric waters (Pingitore, 1978). Thus, high Mn concentrations in these samples can be attributed to meteoric diagenesis. The concentration of Mn in calcite decreases with increasing rates of precipitation (Pingitore et al., 1988; Mucci, 1988).

Initial concentrations of Mn in these limestones were also low because of the original aragonite mineralogy and relatively high rates of sedimentation (about 30 m/m.y). This was calculated by assuming that the 500 m thickness of the Mozduran Formation measured in the type locality was deposited during the 17 million years assigned to the Upper Jurassic by Cowie and Bassett (1989). This is the minimal rate, however, original rates of deposition of the Mozduran carbonates were higher, due to common stylolitization in these carbonates. Oxidizing conditions common in peritidal environments, largely inhibit the incorporation of Mn in $CaCO_3$, whereas under reducing conditions calcite can take up to a few percent of Mn (Pingitore, 1978; Shanmugam and Benedict, 1983). In the samples studied, Mn is interpreted to reflect an original mineralogy of predominantly aragonite, with oxidizing conditions during deposition, and an increasing influence of meteoric diagenesis (Adabi and Rao, 1991).

Variations in Sr and Na with Mn concentrations (Figs. 6.1, 6.2) indicate two stages of diagenetic stabilization (Adabi and Rao, 1991). The first stage coincides with a significant decrease of Sr and Na and no appreciable increase of Mn. This stage is largely due to the inversion of aragonite to low-Mg calcite which controls Sr and Na repartitioning. The second stage involves an appreciable increase in Mn, with no significant change in Sr and Na concentrations, attributed mainly to meteoric diagenesis involving recrystallisation of low-Mg calcite, and the later addition of sparry calcite cementation which controls Mn repartitioning. These two trends are similar to those observed in warm shallow marine ancient limestones affected by meteoric diagenesis (Brand and Veizer, 1980; Al-Aasm and Veizer, 1986; Rao, 1989).

The plot of Sr-Mn and Na-Mn variations (Figs. 6.1, 6.2) in the limestone samples studied, compared with the subtropical aragonitic warm-water Ordovician Gordon limestone field, shows that the Mozduran limestone pattern is similar to that of the subtropical warm-water aragonitic Ordovician Gordon Limestone (Adabi and Rao, 1991). This evidence indicates that aragonite was the predominant carbonate mineral in this part of the basin.

6.2.4 Iron

The Fe concentrations range from 328 to 3745 ppm, with a mean of 1191

ppm. Little data exist on Fe concentrations in Recent warm water aragonitic shallow marine carbonates. In the limestones studied, Fe contents slighty increase with increasing of Mn concentration (Fig. 6.4), which indicates that Fe concentrations increase with the increasing influence of meteoric diagenesis. The mean Fe concentration is an order of magnitude higher than the mean Mn concentration. Fe concentrations generally increase with increasing insoluble residue (Fig. 6.5), probably because of some leaching of Fe from terrigenous fractions in acid dissolution.

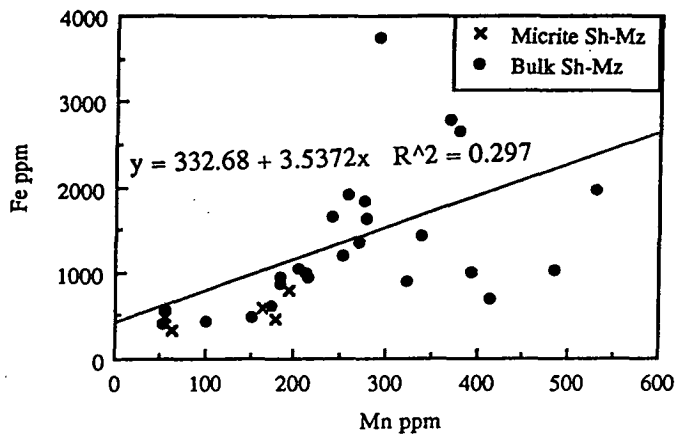

Figure 6.4. Fe and Mn variations, along with regression line, in the Mozduran limestones from the shallowest part of the basin (Adabi and Rao, 1991). Note the concentrations of Fe are a magnitude higher than those of Mn, and Fe contents slighty increase with increasing of Mn concentration.

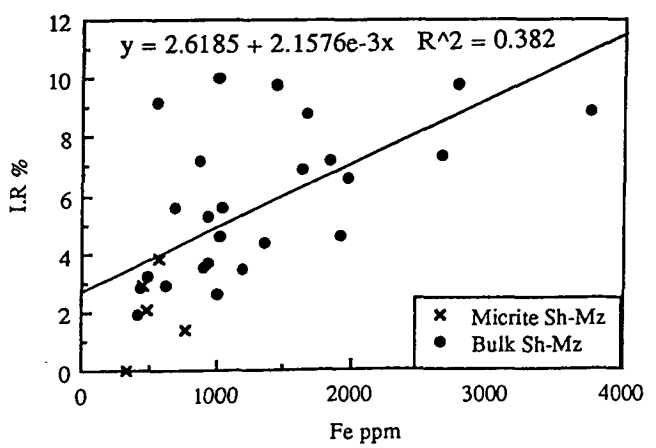

Figure 6.5. Fe and I.R. (insoluble residue) variations, along with regression line, in the Mozduran limestones from the shallowest part of the basin.

6.2.5 Sr/Mn ratio

Bathurst (1975) suggested that limestone diagenesis is mainly a wet dissolution and reprecipitation process. During dissolution and conversion of

metastable aragonite and hig-Mg calcite to stable low-Mg calcite, Sr concentrations decrease and Mn concentrations increase. This process is greatly facilitated by subaerial exposure and fresh water influx (Budd, 1992), resulting in low Sr/Mn ratios. Therefore, covarience of Sr/Mn with Mn provides a useful measure of the degree of dissolution in limestone (Rao, 1991). The Plot of Sr/Mn-Mn variation (Fig. 6.6) shows that some of the limestone data fall within, and some below, the aragonitic Ordovician Gordon Limestone field, which is due to the low Sr value relative to Mn in the Mozduran limestone samples. In this plot, the field of Recent marine temperate bulk carbonate lies above the Ordovician Gordon Limestone field and the Mozduran limestone data, because Recent carbonates have more Sr relative to Mn, which can be expected in a marine diagenetic environment. The Sr/Mn-Mn covariance field of the Mozduran limestone data shows large variations in both Sr/Mn and Mn content, relative to the Gordon Limestone field, indicating a semiclosed to open diagenetic system and dissolution and reprecipitation of stable low-Mg calcite.

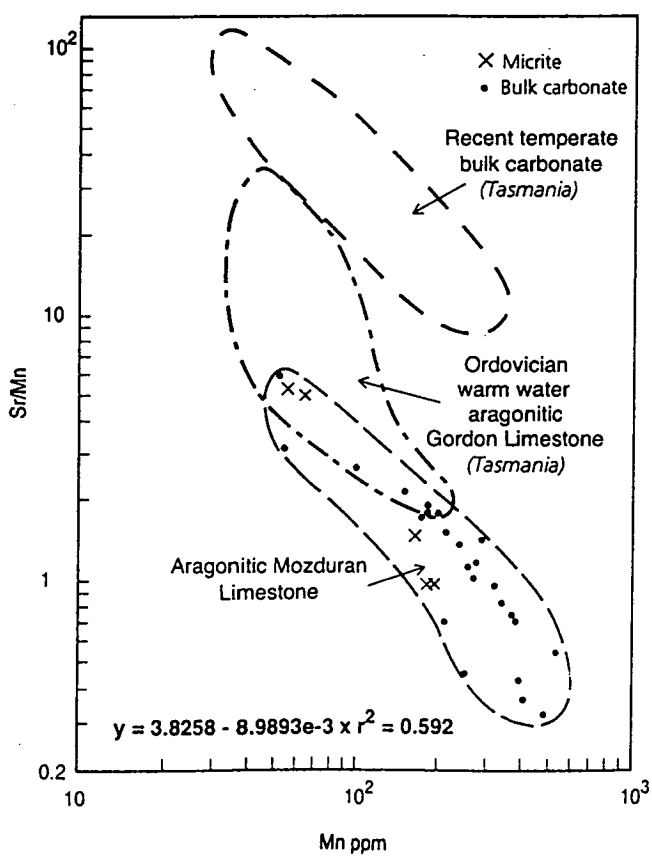

Figure 6.6. Sr/Mn and Mn variations in the Mozduran limestones from the shallowest part of the basin, compared with fields of Recent temperate bulk carbonate and subtropical Ordovician Gordon limestone (Rao, 1991). Note that the Mozduran data fall within and below the aragonitic Gordon limestone field and are far from the calcitic Recent temperate bulk carbonate field.

6.2.6 Sr/Na ratio

Recent and ancient tropical carbonates are differentiated from their non-tropical counterparts by their Sr/Na ratio and Mn content (Rao, 1981 c, 1991; Adabi and Rao, 1991). Recent tropical aragonitic limestones have low Mn content and high Sr/Na ratios, from 3 to 5, in contrast to Recent temperate calcitic limestones, which have high Mn and low Sr/Na ratios of ~1 (Fig. 6.7). The Ordovician subtropical aragonitic Gordon Limestones are characterized by high Sr/Na (up to 10.7) and moderate Mn (Rao, 1990 b). The subpolar calcitic Permian cold-water fauna have very low Sr/Na ratios of ~0.5, and low Mn contents, whereas the bulk Permian subpolar carbonates of Tasmania have Sr/Na ratios of ~1 and high Mn concentrations. The samples from the Mozduran limestones have high Sr/Na ratios (up to 3.3, with a mean of about 2) and moderate to high Mn (Fig. 6.7), similar to the originally aragonitic warm-water Ordovician Gordon Limestone of Tasmania. The high Sr/Na ratios of these limestones are also similar to that for Recent warm water aragonitic sediments. The plot of Sr/Na variation versus Mn (Fig. 6.7) shows that most of the limestone samples fall within the subtropical warm water Ordovician Gordon Limestone field, although a few samples fall within the Recent temperate bulk carbonate field, possibly due to the calcitic mineralogy. The similarity of the trace element data between Recent and ancient aragonitic carbonates, support the interpretation that the Mozduran limestones were originally aragonitic warm-water carbonates.

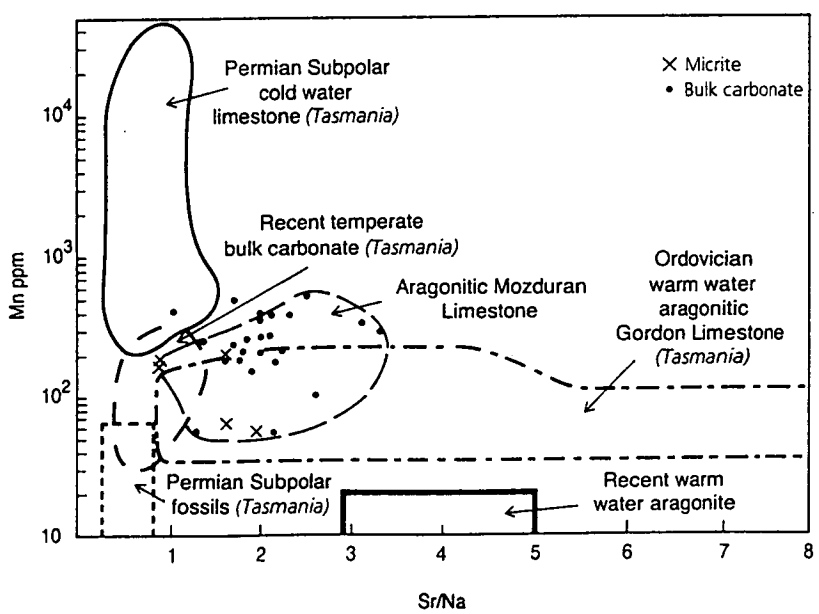

Figure 6.7. Mn and Sr/Na variations in the Mozduran limestones from the shallowest part of the basin (Adabi and Rao, 1991), in comparison with subtropical Ordovician Gordon Limestone and Permian subpolar limestones (Rao, 1991), Recent tropical aragonite (Milliman, 1974) and Recent temperate bulk carbonate from Tasmania (Rao, 1990 a). Note that most of the limestone samples fall within the field defined by the originally aragonitic Gordon limestone.

6.2.7 Barium

Ba and Mn concentrations were used by Friedman (1969) to differentiate shallow marine (Ba <60 ppm; Mn <25 ppm), brackish (Ba <60 ppm; Mn >25 ppm) and fresh water (Ba >60 ppm; Mn >25 ppm) limestones. He suggested that these trace elements can be used as possible enviromental indicators in carbonate sediments. In this study, Ba concentrations range from 7 to 310 ppm (Table 6.3), with a mean of 61 ppm, but most of the samples have values of <60 ppm Ba, indicating a marine origin of limestones. Ba is positively correlated with K_2O, suggesting a concentration of Ba in chlorite/kaolinite, which is the only clay mineral detected in XRD analysis of some insoluble residue of limestone samples (Fig. 6.8).

Table 6.3. Acid insoluble trace element composition of aragonitic Mozduran limestones.

Sample No	Ba ppm	Ti ppm	Rb ppm	K2O%
Sh-33	70	84	5	0.1
Ba-11	97	192	7	0.2
Ba-16	7	129	7	0.1
Pa-10	9	152	9	0.2
Pa-12	15	187	10	0.2
Pa-19	18	175	8	0.2
Pa-28	48	180	8	0.2
Pa-36	19	163	6	0.2
Mz-22	232	202	11	0.2
Mz-24	14	115	7	0.1
Mz-26	25	318	14	0.3
Mz-36	152	386	11	0.3
Mz-41	20	115	8	0.2
Mz-71	8	60	5	0.1
Mz-90	56	147	8	0.2
Mz-95	310	225	11	0.3
Mz-102	10	41	4	0.1
Mz-105	26	72	6	0.1
Mz-107	30	87	7	0.1

6.2.8 Titanium

Ti concentrations range from 41 to 386 ppm, with a mean of 159 ppm (Table 6.3). Ti is positively correlated with K_2O (Fig. 6.8), indicating that much of the Ti is in the clay mineral chlorite/kaolinite. Veizer and Demovic (1973) considered that the relative concentration of Ti and Mn serves as a paleoclimatic indicator. The concentrations of Mn and Ti in the limestones studied are similar to the humid carbonates of Veizer and Demovic (1973).

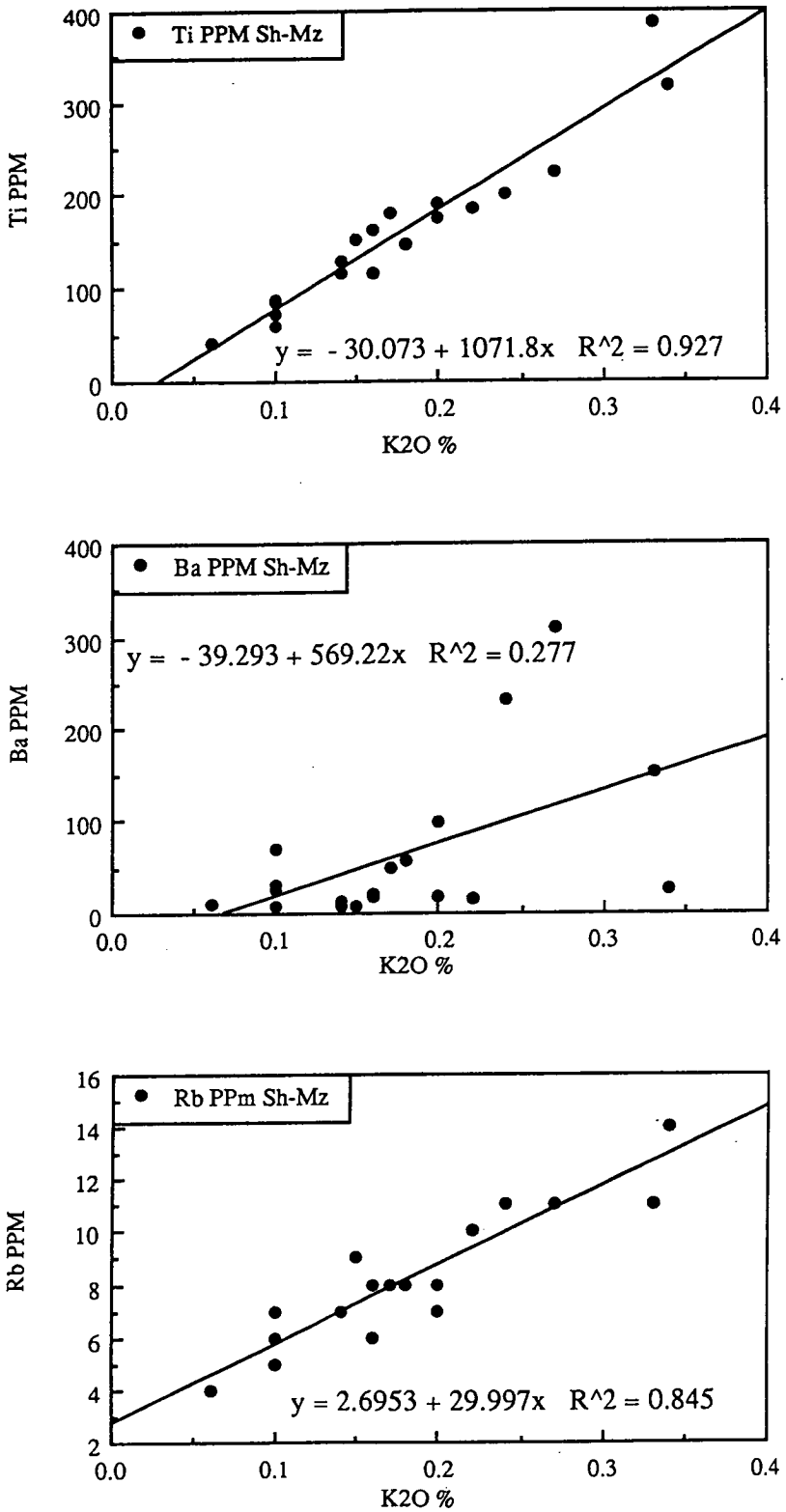

Figure 6.8. Variations of Ti, Ba, and Rb against K_2O, along with regression line, in the aragonitic Mozduran limestone samples.

6.2.9 Rubidium

Rb concentrations range from 4 to 14 ppm, with a mean of 8 ppm (Table 6.3). Reimer (1972) suggested that Rb concentration varies with clay mineralogy. Rb occurs in maximum amounts in illite (468 ppm), moderate amounts in kaolinite (78 ppm), and minimum amounts (44 ppm) in montmorillonite. XRD studies of the insoluble residue of the Mozduran limestones have identified that chlorite/kaolinite is the only clay mineral present in these limestones. Positive correlation between Rb and K_2O (Fig. 6.8) confirms that Rb is substituting for K, probably in chlorite/kaolinite clay minerals. Therefore, the Rb concentrations support the marine origin of clay within the limestones.

6.3 Insoluble Residue

In this study, samples with less than 10% insoluble residue were used. Those with more than 10% insoluble residue are listed in Appendix 5. The insoluble residue ranges from 0 to 9.8%. X-ray analysis of some limestone samples from the Mozduran section indicates that the main non-carbonate minerals are quartz (ranges from 40 to 85%), mica (ranges from 5 to 4.5%) and chlorite/kaolinite (ranges from 5 to 15%, Table 6.4).

Table 6.4. XRD analysis of insoluble residue of aragonitic Mozduran limestones

	Sample No					
	Mz 22	Mz 26	Mz 36	Mz 87	Mz 90	Mz 109
I.R %	3.8	5.6	9.2	8.9	5.5	6.5
Quartz %	50	40	75	80	75	85
Mica %	45	45	10	10	10	5
Feldspar %			5	5	5	5
Chlorite/Kaolinite %		15	5	5	5	5
Pyroxine %	5	5	5		5	
Geothite %					5	

6.4 Calcite-Aragonite Mixed Mineralogy

As was discussed in Chapter 5, in Recent warm temperate carbonates, high-Mg calcite predominates, with some aragonite (Collins, 1988), whereas a mixture of high-to low-Mg calcite, with minor amounts of aragonite occurs in Recent cool temperate marine waters (Nelson, 1988; Morse and Mackenzie, 1990; Rao and Adabi, 1992). This result, along with experimental studies, indicates that carbonate mineralogy mainly depends on water temperature. Therefore, in ancient carbonates, recognition of original carbonate mineralogy,

along with geochemical characteristics, can be used to differentiate tropical, temperate and subpolar carbonates (Nelson, 1978; Rao, 1981 a, 1988 a, b, 1991).

From the relatively deeper parts of the basin (Gorgoreh and Bazangan sections), 185 carbonate samples consisting of bulk rocks, micrites, intraclasts, ooids and cements, were analyzed for major and trace elements. Of these 81 limestone samples with less than 1% Mg and 10% insoluble residue were used. Most of the limestone samples studied in these two sections have trace element values that are more characteristic of a calcite-aragonite mixture, compared to the limestone samples from the shallowest part of the basin, in which aragonite was the predominant carbonate mineral. This might be due to water temperature, as evidenced by the precipitation of predominant calcitic minerals in relatively cooler water (Rao and Adabi, 1992).

Diagenesis of originally calcitic carbonates can be better understood by comparing them with Recent temperate calcitic bulk carbonates, rather than with Recent tropical aragonitic carbonates (James and Bone, 1989). Therefore, limestone data from the relatively deeper part of the basin was compared with Recent temperate calcitic carbonates to recognize the original mineralogy.

6.4.1 Strontium

Sr concentrations in Recent temperate bulk carbonates range from 1642 to 5007 ppm, with a mean of about 3270 ppm (Rao and Adabi, 1992; Rao and Jayawardane, 1994; Rao and Amini, 1995). Carbonate samples studied by Rao and Jayawardane (1994) from eastern Tasmania, indicate that Sr in pure calcite without aragonite, ranges from 700 to 2700 ppm, due to the mixed mineralogy of low- to high-Mg calcites. Therefore, the decrease of Sr from 2700 to 700 ppm is due to increasing amounts of low-Mg calcite, as abiotic low-Mg calcite contains low concentrations of Sr, from 1200 to 1400 ppm (Kinsman, 1969; Rao, 1981b; Rao and Adabi, 1992). The highest Sr value of 2700 ppm corresponds to the Sr value of 3000 ppm observed in modern high-Mg calcite bryozoa (Milliman, 1974). It has been shown that Sr contents decrease with increasing calcite content, but increase with increasing aragonite content (Rao and Adabi, 1992). They have also shown that there is a general trend of decreasing Sr with increasing water depth in western Tasmanian shelf carbonates, due to a decreasing aragonite content with water depth.

Sr concentrations in limestone samples from the Gorgoreh and Bazangan sections range from from 61 to 424 ppm, with a mean of 168 ppm (Fig. 6.9). Sr

values of the limestone samples studied are much lower than their modern counterparts, possibly due to a progressive loss of Sr during non-marine diagenesis. Sr concentrations in diagenetic calcite depend on the partition coefficient and concentration in diagenitic solutions. Most of the samples studied have lower Sr values, compared to their aragonitic counterparts in the shallowest part of the basin (mean, 264 ppm). Sr concentrations are dependent on carbonate mineralogy, and decrease with decreasing aragonite contents and increasing water depth (Rao and Adabi, 1992). Therefore, low Sr concentrations in these limestone samples are due to an increasing water depth and increasing amounts of mixed mineralogy of low- to high-Mg calcite, compared to the mainly aragonitic mineralogy in the shallowest part of the basin (Adabi and Rao, 1996).

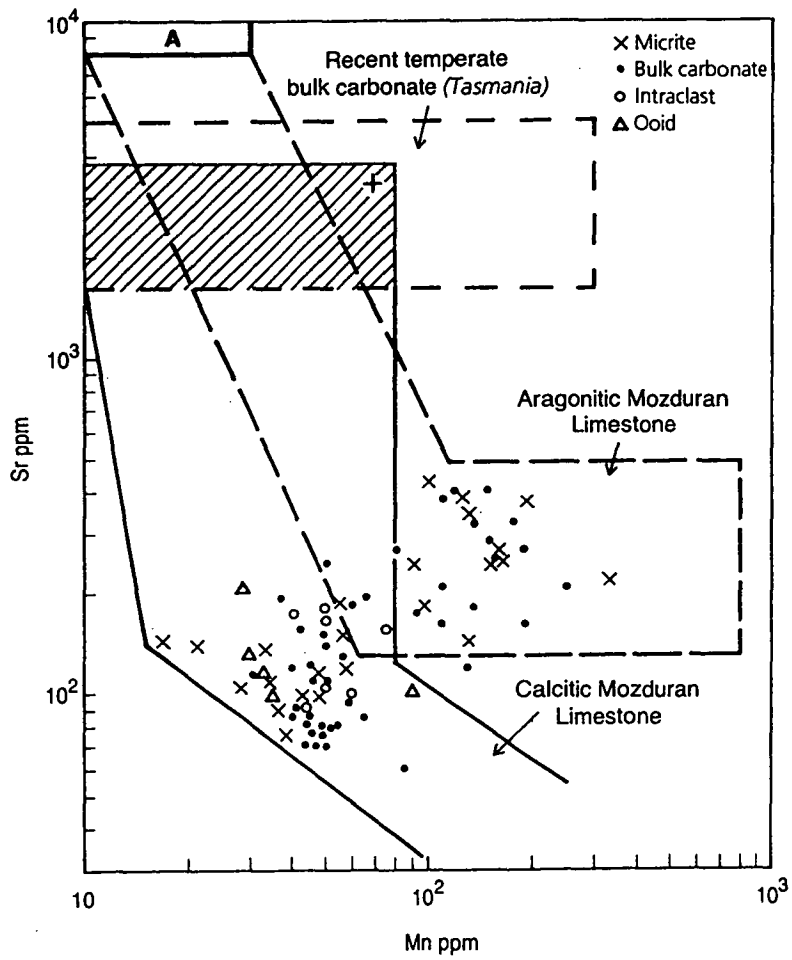

Figure 6.9. Sr and Mn variations in the Mozduran limestones from the relatively deeper part of the basin (Gorgoreh and Bazangan sections), compared with fields of Mozduran aragonitic limestones (Adabi and Rao, 1991), Recent temperate bulk carbonates (Rao and Adabi,1992; Rao and Jayawardane,1994; Rao and Amini, 1995) and Recent tropical aragonite (A; Milliman,1974). Note that most of the limestone samples fall below, and some within the aragonitic Mozduran limestone field, possibly due to the mixed mineralogy of aragonite and calcite. Cross symbol shows the mean value of Sr-Mn concentrations and the shaded box indicates values of about 80% of the total samples in Recent temperate bulk carbonates.

6.4.2 Sodium

Na concentrations in limestone samples from the Gorgoreh and Bazangan sections range from 44 to 525 ppm, with a mean of 144 ppm (Fig. 6.10). Limestone samples studied from this part of the basin have a maximum of 525 ppm Na, compared to maximum values of 280 ppm Na in the shallowest part of the basin, although the mean values of Na are similar in the shallowest and relatively deeper part of the basin. Thus, Na concentrations are interpreted to reflect salinity variations in the depositional environments of the Mozduran limestone.

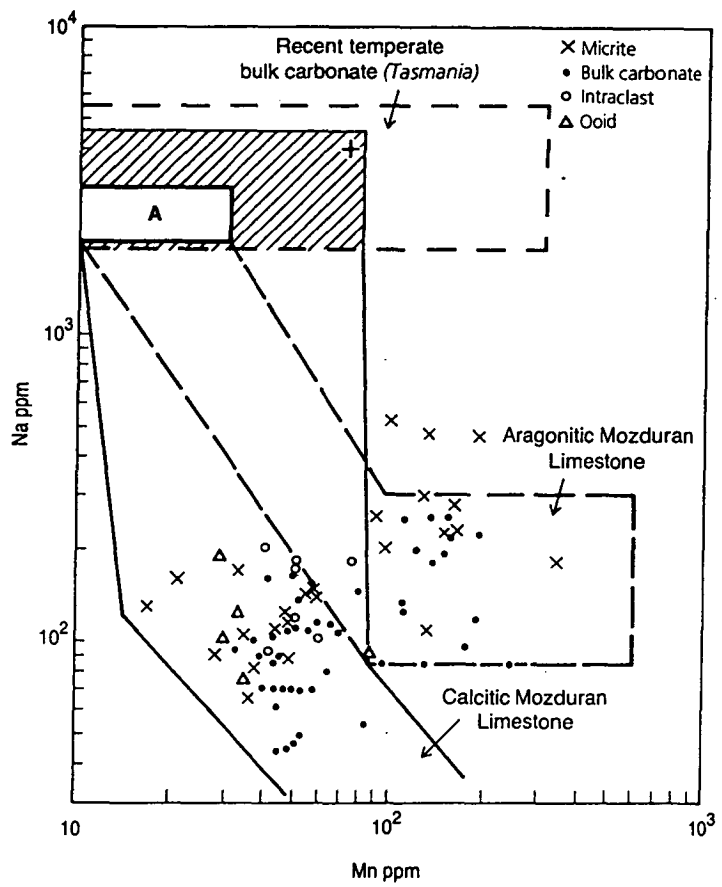

Figure 6.10. Na and Mn variations in the Mozduran limestones from Gorgoreh and Bazangan sections, compared with fields of Mozduran aragonitic limestones (Adabi and Rao, 1991), Recent temperate bulk carbonates (Rao and Adabi, 1992; Rao and Jayawardane,1994; Rao and Amini, 1995) and Recent tropical aragonite (A; Milliman,1974). Note that most of the samples fall below the Mozduran limestone field, possibly due to calcitic mineralogy. Cross symbol shows mean value of Na-Mn concentrations and the shaded box indicates values of about 80% of the total samples in Recent temperate bulk carbonates.

The plot of Na-Sr (Fig. 6.11) variation in these limestone samples shows that there is a systematic loss of both Sr and Na, possibly due to an increasing influence of non-marine diagenesis. The covariance of Na and Sr also shows that Na and Sr are positively correlated, probably due to similar partitioning of these elements in carbonate minerals. This plot also shows that most of the data fall

within the subpolar cold water Permian limestone field (unlike their Mozduran aragonitic counterparts), and some within the aragonitic Mozduran limestone field, because of the mixed calcite and aragonite mineralogy (Adabi and Rao, 1996). In this plot, there is a clear separation of tropical, temperate and subpolar carbonates, due to varible Na contents and higher Sr contents in Recent tropical carbonates, relative to Recent temperate ones.

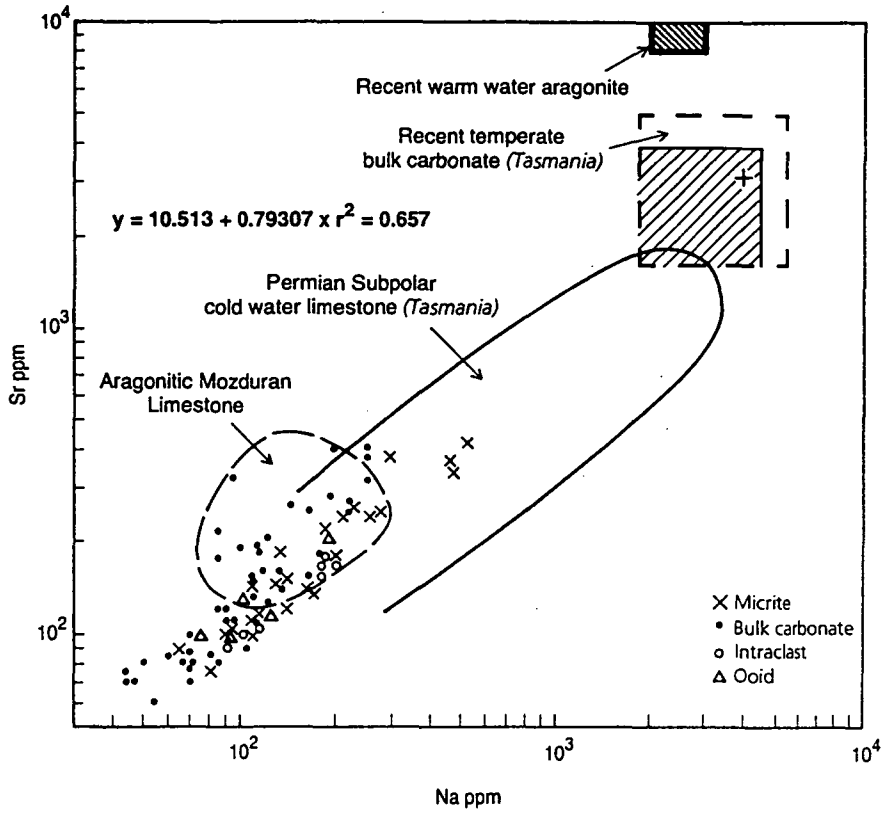

Figure 6.11. Sr and Na variations, along with regression number, in the Mozduran limestones from Gorgoreh and Bazangan sections, compared with fields of subpolar cold water Permian limestone (Rao, 1991), aragonitic Mozduran limestone, Recent tropical aragonite (Milliman, 1974) and Recent temperate bulk carbonate (Rao and Adabi, 1992; Rao and Jayawardane, 1994; Rao and Amini, 1995). Cross symbol shows mean value of Sr-Na in Recent temperate bulk carbonates and the shaded box shows values of about 80% of the total samples. Note that a linear trend exists between Sr and Na concentrations of Recent temperate bulk carbonates, subpolar Permian carbonates and the Mozduran limestone data.

6.4.3 Manganese

Mn concentrations in Recent temperate bulk carbonates range from 1 to 311 ppm, with a mean values of about 69 ppm (Rao and Adabi, 1992; Rao and Jayawardane, 1994; Rao and Amini, 1995). The Mn concentrations in the limestone samples studied from the Gorgoreh and Bazangan sections range from 17 to 328 ppm, with a mean of 80 ppm (Figs. 6.9, 6.10).

Mn concentrations decrease with increasing aragonite percent (Rao and

Adabi, 1992), and increase with increasing influence of meteoric waters (Brand and Veizer, 1980; Rao, 1990 b). Mn concentrations decrease with increasing rates of precipitation (Pingitore et al., 1988; Mucci, 1988). The thickness of carbonates in the Mozduran Formation varies from about 120 m in the Shurijeh section, which is located in the shallowest part of the basin, to about 1130 m in the Bazangan section, which is located in the relatively deeper part of the basin. Therefore, low concentrations of Mn in limestone samples from these two sections is possibly due to calcitic mineralogy and relatively increasing rates of sedimentation. Mn concentrations also decrease with increasing water depth or increasing distance from the shore. Thus, low Mn contents in the Gorgoreh and Bazangan sections, compared with limestone samples from shallowest part of the basin (mean 243 ppm), can be attributed to progressive reduction in terrigenous content, which is consistent with petrography.

The Sr and Mn variations in these limestone samples (Fig. 6.9), compared with fields of the Mozduran aragonitic limestones (Adabi and Rao, 1991), Recent temperate bulk carbonates (Rao and Adabi, 1992; Rao and Jayawardane, 1994; Rao and Amini, 1995), and Recent tropical aragonite (Milliman, 1974), show that most of the samples fall below, and some within the aragonitic Mozduran limestone field, possibly due to the mixed mineralogy of predominantly calcite over aragonite (Adabi and Rao, 1996). The covariance of Na and Mn (Fig. 6.10) also shows that some of the data falls within, and some below, the aragonitic Mozduran limestone field, which indicates mixed mineralogy of aragonite and calcite. In limestone samples which fall below the aragonitic Mozduran field, Sr and Na decrease with increasing Mn concentrations.

6.4.4 Iron

The Fe concentration in the Gorgoreh and Bazangan sections ranges from 63 to 3552 ppm, with a mean of 557 ppm (Fig. 6.12). The mean value of Fe in these two sections is much lower than the mean value of limestone samples from the shallowest part of the basin (mean= 1191 ppm). As Fe concentration decreases with increasing water depth (Rao and Adabi, 1992) and decreasing insoluble residue (Fig. 6.12), the low Fe concentration in these samples can be attributed to increasing water depth and low terrigenous input. In the limestone samples studied, Fe contents increase with increasing Mn concentrations (Fig. 6.13), which indicates an increasing influence of non-marine diagenesis. The Fe concentrations in these samples are a few orders of magnitude higher than the Mn concentration.

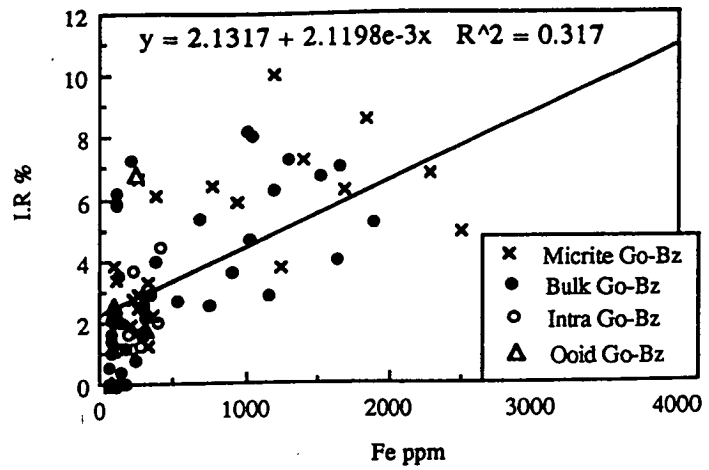

Figure 6.12. Variations of Fe versus I.R. (insoluble residue), along with regression line, in the Mozduran limestone samples from Gorgoreh and Bazangan sections.

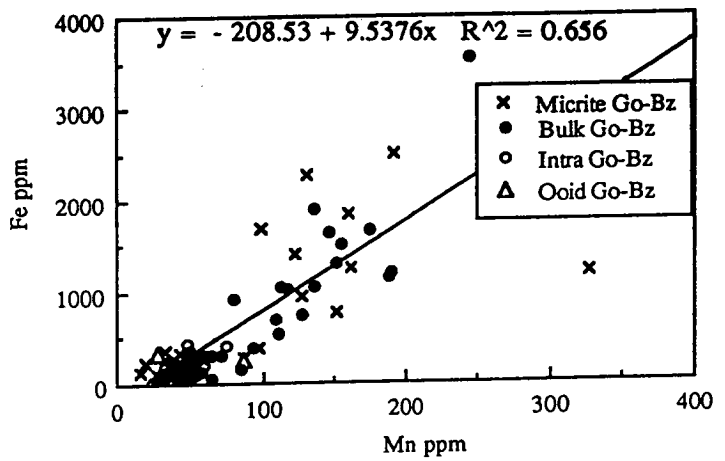

Figure 6.13. Variations of Fe versus Mn, along with regression line, in the Mozduran limestone samples from Gorgoreh and Bazangan sections.

6.4.5 Sr/Mn ratio

During dissolution of aragonite and precipitation of calcite, Sr concentrations decrease and Mn concentrations increase, resulting in a low Sr/Mn ratio. In these limestones the Sr/Mn ratio is higher, with a mean value of 2.53, compared to the aragonitic Mozduran limestone, with a mean value of 1.65. This may indicate less dissolution and precipitation, due to calcitic mineralogy and less aragonite content. Therefore, Sr/Mn and Mn variations provide a useful measure of the degree of dissolution in limestones (Rao, 1991).

The plot of Sr/Mn-Mn variations (Fig. 6.14) shows that most of the limestone data fall outside, and some within, the aragonitic Mozduran limestone field. This may indicate that calcite is the dominant mineral over aragonite. In this plot, limestone data show a similar trend to that of Recent marine temperate

bulk carbonates, possibly because of similar mineralogy.

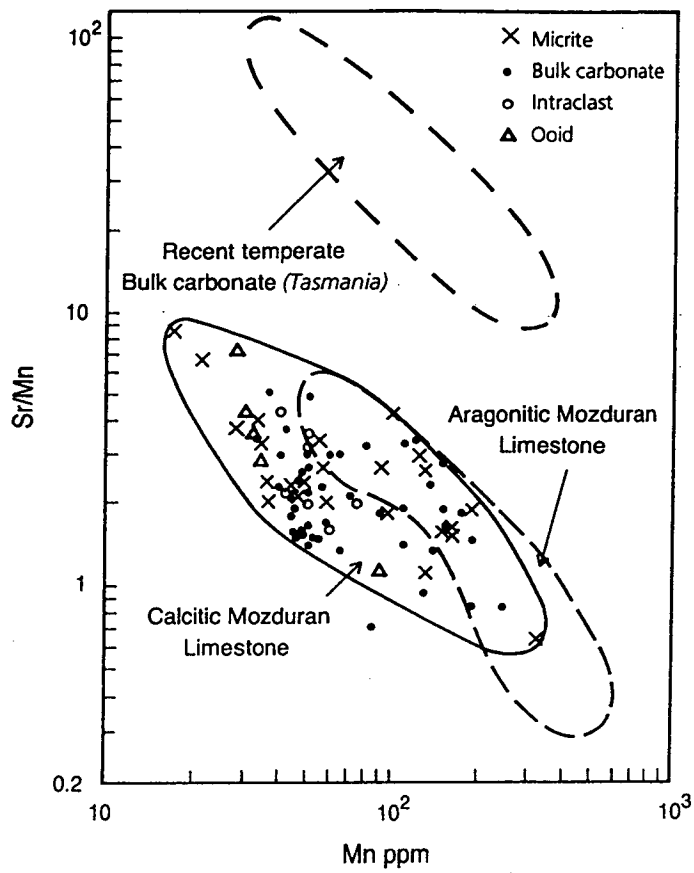

Figure 6.14. Sr/Mn and Mn variations in the Mozduran limestones from Gorgoreh and Bazangan sections, compared with fields of Recent temperate bulk carbonate (Rao, 1991) and aragonitic Mozduran limestone. Note that most of the data fall outside, and some within, the aragonitic Mozduran field, due to mixed mineralogy of predominantly calcite with some aragonite. In this plot, the Mozduran limestone trend is similar and parallel to that of Recent marine temperate bulk carbonates, possibly due to similar mineralogy.

6.4.6 Sr/Na ratio

The Sr/Na ratio in Recent temperate calcitic carbonates is low (ranges from about 0.4 to 1.3, with a mean of ~1), whereas in Recent tropical aragonitic carbonates, the ratio is high (ranges from about 2.9 to 5, with a mean of ~4). The subpolar calcitic Permian fossils have a very low Sr/Na ratio of ~0.5 (Rao, 1991, Fig. 6.15). The mean Sr/Na ratios in aragonitic Mozduran limestone from the shallowest part of the basin are higher (mean values of ~2) than the Sr/Na ratio in limestone samples from the relatively deeper part of the basin (mean of ~1.2). The low Sr/Na ratio in these limestones is similar to that for Recent temperate calcitic carbonates.

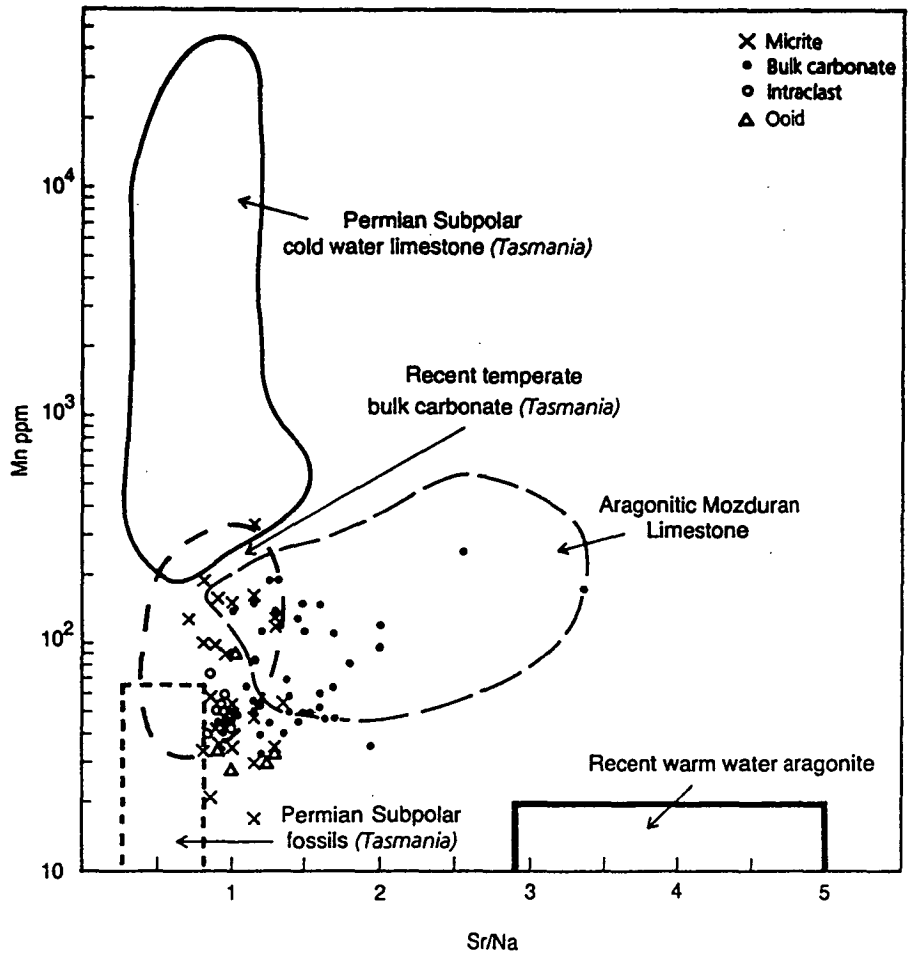

Figure 6.15. Mn and Sr/Na variations in the Mozduran limestones from Gorgoreh and Bazangan sections, compared with subpolar Permian limestones (Rao, 1991), along with fields of Recent tropical aragonite (Milliman, 1974) and temperate bulk carbonate from Tasmania (Rao, 1990 a). Note that most of the data fall within the Recent temperate carbonates, due to calcitic mineralogy. Some of the limestone samples fall within the aragonoitic Mozduran limestone field (Adabi and Rao, 1991) due to aragonite mineralogy.

The plot of covariance of Sr/Na with Mn (Fig. 6.15) shows that most of the limestone data (especially non-skeletal components and micrite) fall within the Recent calcitic temperate bulk carbonate field, and some wihin the aragonitic Mozduran limestone field. This indicates that most of these limestones were composed of predominantly calcite, with variable amounts of aragonite (Adabi and Rao, 1996).

6.5 Comparison with Recent and Ancient Carbonates

Major and trace element variations between Recent warm water, temperate water, and ancient tropical carbonate sediments provide a means of differentiating between modern tropical, temperate and ancient datasets. This is due to the different major (Mg) and trace element (Sr, Na, Mn, Fe) concentrations in warm and temperate water carbonates. Two spidergrams were created for

comparison between the Mozduran data (one with aragonite, Fig. 6.16, and another with mixed aragonite and calcite mineralogy, Fig. 6.17) and tropical and temperate carbonates. In each spidergram, the modern tropical carbonate values (represented by Bahama examples, Milliman, 1974; Veizer, 1983) were used as a normalizing influence, and all elemental values were compared with their modern tropical counterparts. In these graphs, average elemental values were used for comparison between ancient tropical carbonates (Rao, 1990 b, 1991), Recent temperate carbonates of Tasmania (Rao, 1990 a; Rao and Adabi, 1992, Rao and Jayawardane, 1994; Rao and Amini, 1995) and the Mozduran data. Each graph displays some degree of differentiation between modern and ancient tropical data sets and Recent temperate carbonates of Tasmania. The differentiation between modern tropical and temperate carbonates is possibly due to different mineralogy (Mg), temperature (which influences Mg, Sr, and possibly Na), and variation in terrigenous input (Fe, Mn). The difference between ancient and modern tropical carbonates is caused mainly by diagenetic alteration, showing either loss or gain of some elemental values. These spidergrams, with additional elemental data, can be used as a basis of a geochemical model for future carbonate geochemical studies.

6.6 Use of Elemental Geochemistry to Infer Diagenetic Processes

The application of minor and trace element geochemistry to understand the depositional and diagenetic environments of carbonates has been well documented by several researchers (e.g., Milliman, 1974; Brand and Veizer, 1980; Veizer, 1983; Al-Aasm and Veizer, 1986; Morrison and Brand, 1986; Brand and Morrison, 1987; and Morse and Mackenzie, 1990). Recently, Winefield et al. (1996), used a compilation of published examples to identify element-element trends that were either directly or inversely related (i.e., positive or negative slopes on linear regressions) and then infer marine, meteoric, and burial diagenesis for selected limestones in a general sense (Fig. 6.18).

Based on summary matrices for idealized meteoric and burial diagenetic trends, the Mozduran limestone samples from the shallowest part of the basin (Shurijeh, Bagak, Padeha and Mozduran sections) fall in the meteoric (Fig. 6.19 A), and limestone samples from the relatively deeper part of the basin (Gorgoreh and Bazangan sections), indicate burial diagenesis (Fig. 6. 19 B). The matrix for the samples from the shallowest part of the basin, has five out of six regressions in agreement with those for meteoric diagenesis (i.e., regressions have the same sign), one that disagree, giving an overal agreement of 83% (Fig. 6.19 A). The

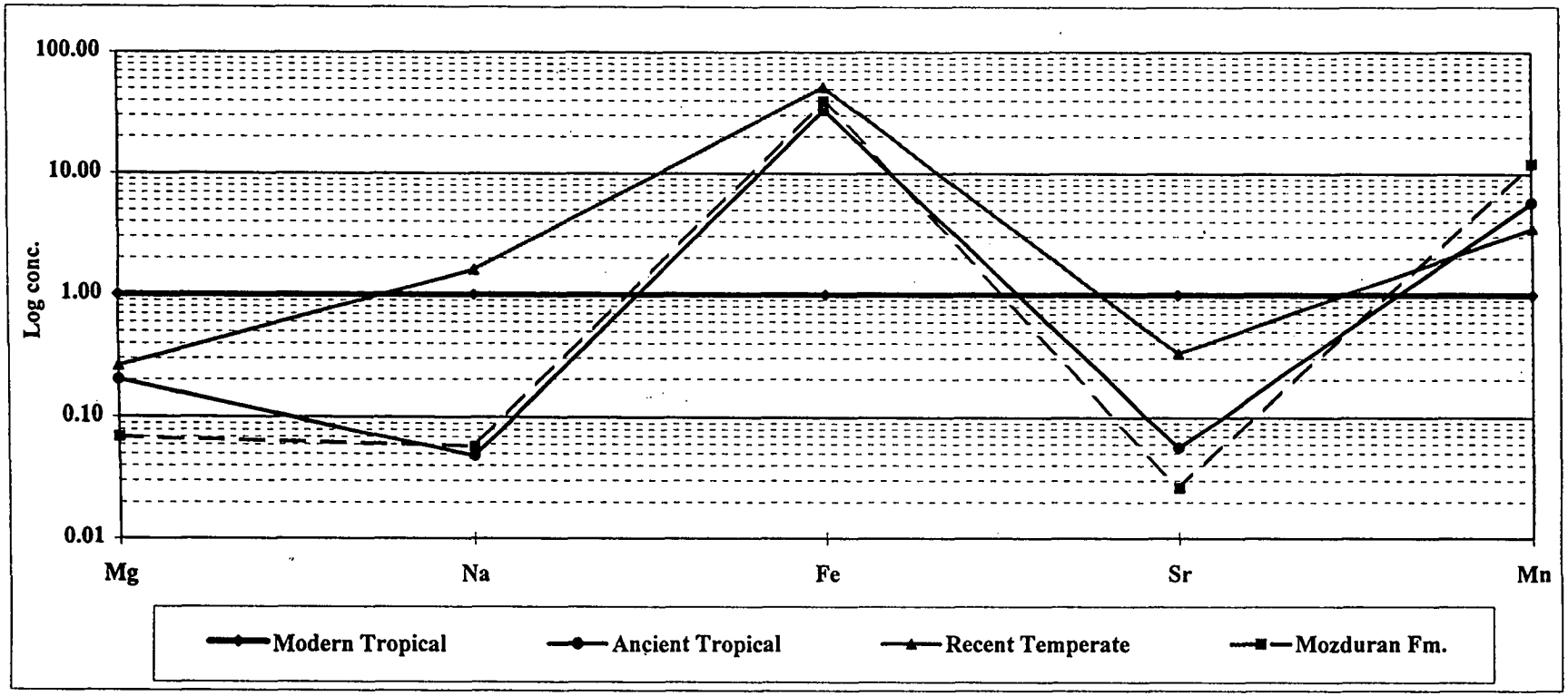

Aragonite samples

	Mg	Na	Fe	Sr	Mn
Modern Tropical	50000	2500	30	10000	20
Ancient Tropical	10000	120	1000	561	115
Recent Temperate	13000	4000	1550	3300	70
Mozduran Fm.	3500	144	1191	264	243
	Mg	Na	Fe	Sr	Mn
Modern Tropical	1.00	1.00	1.00	1.00	1.00
Ancient Tropical	0.20	0.05	33.33	0.06	5.75
Recent Temperate	0.26	1.60	51.67	0.33	3.50
Mozduran Fm.	0.07	0.06	39.70	0.03	12.15

Figure 6.16. Spidergram comparing the elemental compositions of the Mozduran aragonitic carbonates and modern tropical carbonates (Milliman, 1974; Veizer, 1983), ancient subtropical carbonates (Rao, 1990 a, 1991), and Recent temperate carbonates (Rao and Adabi, 1992; Rao and Jayawardane, 1994; Rao and Amini, 1995). The average concentration of elements are normalized relative to modern tropical carbonates (=1.00).

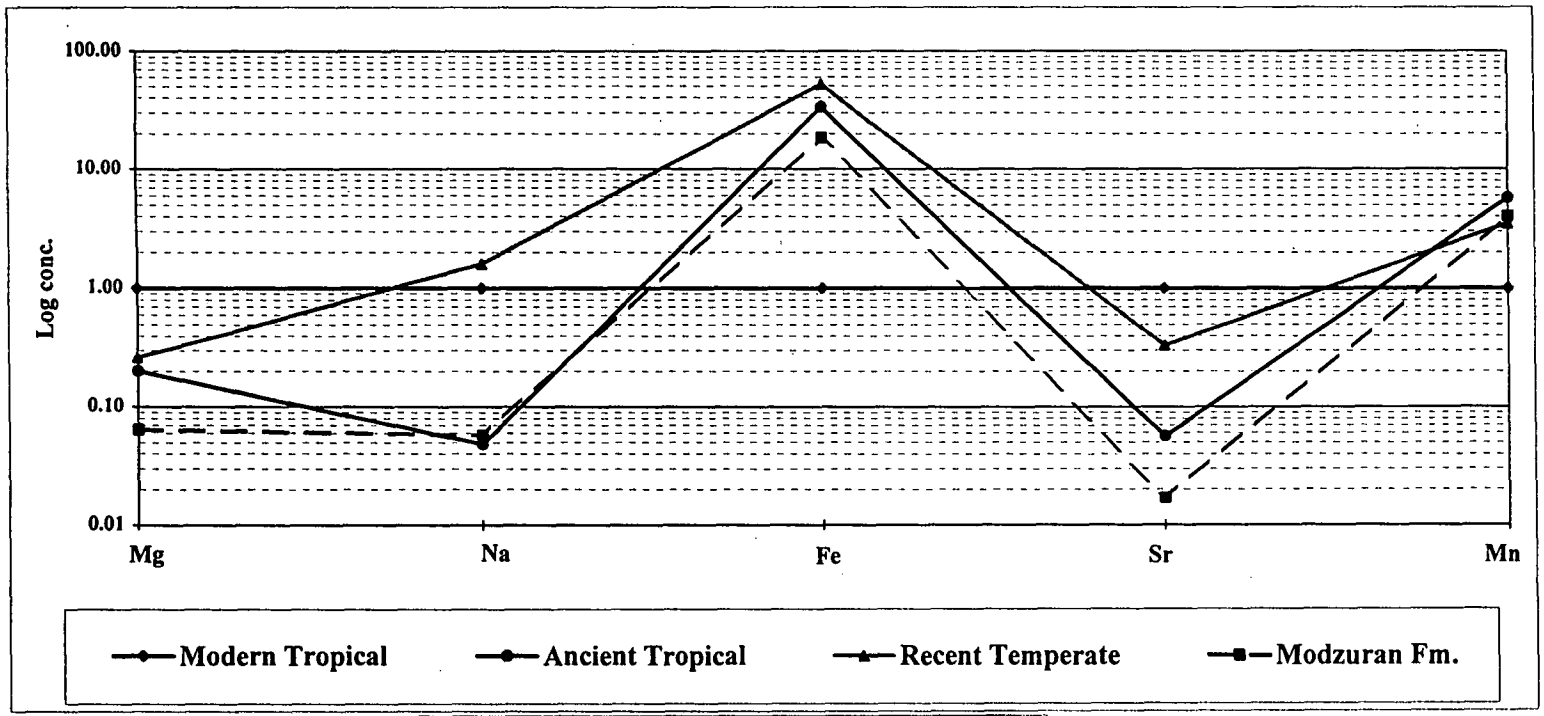

Calcite-aragonite samples

	Mg	Na	Fe	Sr	Mn
Modern Tropical	50000	2500	30	10000	20
Ancient Tropical	10000	120	1000	561	115
Recent Temperate	13000	4000	1550	3300	70
Mozduran Fm.	3200	144	557	168	80
	Mg	Na	Fe	Sr	Mn
Modern Tropical	1.00	1.00	1.00	1.00	1.00
Ancient Tropical	0.20	0.05	33.33	0.06	5.75
Recent Temperate	0.26	1.60	51.67	0.33	3.50
Mozduran Fm.	0.06	0.06	18.57	0.02	4.00

Figure 6.17. Spidergram comparing the elemental compositions of the Mozduran mixed calcite-aragonite carbonates and modern tropical carbonates (Milliman, 1974; Veizer, 1983), ancient subtropical carbonates (Rao, 1990 a, 1991), and Recent temperate carbonates (Rao and Adabi, 1992; Rao and Jayawardane, 1994; Rao and Amini, 1995). The average concentration of elements are normalized relative to modern tropical carbonates (=1.00).

meteoric diagenesis for the shallowest part of the basin was proposed by Adabi and Rao (1991). The matrix for the limestone samples from the relatively deeper part of the basin has six out of six regressions in agreement (100%), with those for burial diagenesis (Fig. 6.19 B).

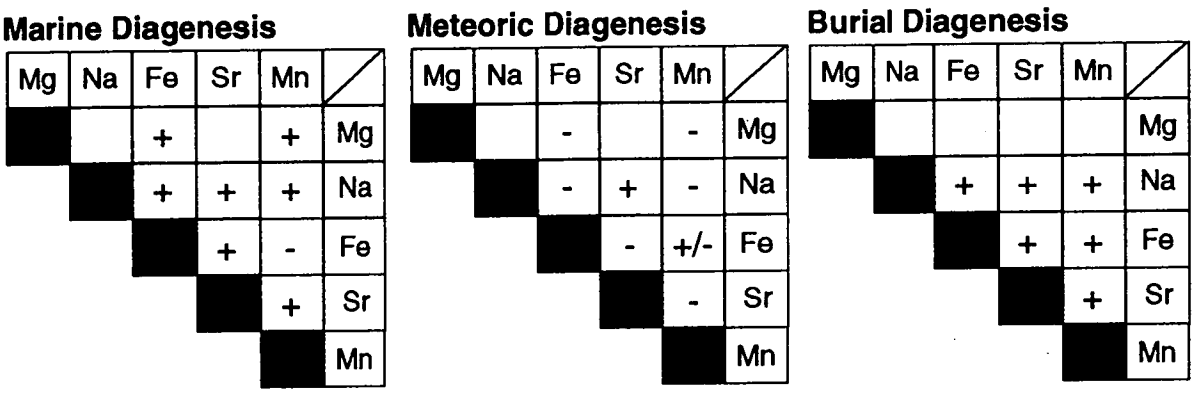

Figure 6.18. Summary matrices for idealized marine, meteoric, and burial diagenetic trends. Positive and negative symbols indicate the sign of the slope of linear regression lines (redrawn from Winefield et al., 1996).

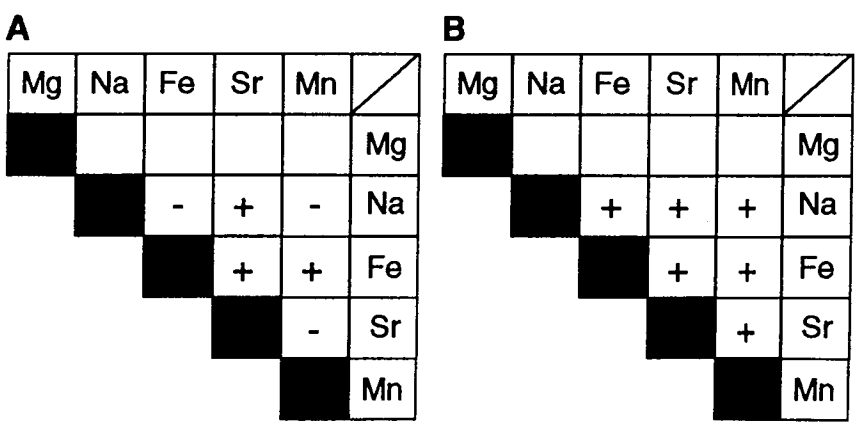

Figure 6.19. Summary elemental matrices for limestone samples from the shallowest (A) and relatively deeper parts of the basin (B). Figure 6.19 A, indicates mainly meteoric and Figures 6.19 B, illustrates mainly burial diagenesis.

6.7 Conclusions

In this study, trace element characteristics are used for recognition of original carbonate mineralogy and diagenetic processes of the Upper Jurassic Mozduran limestone. As carbonate mineralogy in Recent shallow marine carbonates, and in experimental studies, varies with seawater temperature, and aragonite is the predominant mineral in Recent warm shallow marine carbonates and calcite the dominant mineral in Recent temperate marine carbonates, the Mozduran limestone data from the shallowest part of the basin (Shurijeh, Bagak, Padeha, and Mozduran sections) has values characteristic of aragonite. In contrast, the majority of data in the relatively deeper part of the basin (Gorgoreh and Bazangan sections) has values more characteristic of calcite than aragonite. The criteria include the following:

A) Sections studied from the shallowest part of the basin

- The Mozduran limestone in the shallowest part of the basin (Shurijeh, Bagak, Padeha and Mozduran sections) is characterized by moderate Na (mean of 144 ppm), and high Sr (mean of 264 ppm) concentrations. The relative proportion of these elements is similar to that in Recent aragonitic carbonates, but absolute values of these elements suggest appreciable loss of Sr and Na.

- Sr and Na covariance with Mn supports evidence of inversion of aragonite to calcite, with subsequent open phreatic diagenesis. The inversion of aragonite to calcite involves an appreciable loss in Sr and Na concentrations, and a gain of Mn and Fe during diagenesis. The trends of two stages of diagenetic stabilization in these limestones are similar to those observed in warm shallow marine ancient limestones affected by meteoric diagenesis (Brand and Veizer, 1980; Al-Aasm and Veizer, 1986; Rao, 1989).

- Comparison of the Sr, Na and Mn fields of these limestones, with those of the subtropical aragonitic Ordovician Gordon Limestone, shows that the Mozduran limestone pattern is similar to that of the subtropical Ordovician Gordon Limestone.

- A positive correlation exists between Fe and Mn, which suggests the influence of meteoric diagenesis. Fe concentrations are a magnitude higher than Mn, probably due to a reducing phreatic environment and higher partition coefficients for Fe than Mn.

• Sr/Na and Mn variations, compared with the field of aragonitic Ordovician Gordon Limestone, shows that the Mozduran data fall within, or close to, the aragonitic Ordovician Gordon Limestone field, and is far from the calcitic Recent temperate bulk carbonate field.

• High Sr/Na ratios (up to 3.3, with a mean of ~2) in these limestones, which are similar to the Recent tropical aragonitic limestones and the originally aragonitic warm-water Ordovician Gordon Limestone of Tasmania, support original aragonite mineralogy. I still view these data as consistent with a tropical origin, as Sr and Na values in these limestones are similar to the warm water Ordovician Gordon Limestones, and are much lower than those of the calcitic subpolar cold water Permian limestones of Tasmania.

B) Sections studied from the relatively deeper part of the basin

• Sr and Na variations with Mn in these limestone samples, compared with the Mozduran aragonitic limestone field from shallowest part of the basin, shows that most of the data fall outside the Mozduran aragonitic limestone field, possibly due to calcitic mineralogy.

• Sr and Na variations in these limestones, compared with the field of subpolar cold water Permian limestone, shows that most of the data fall within the cold water Permian limestone field, unlike their Mozduran aragonitic counterparts.

• Sr/Mn and Mn variations, compared with the field of aragonitic Mozduran limestone, shows that most of the data fall outside of the aragonitic Mozduran limestone field. These limestone data have a trend similar to that of Recent marine temperate bulk carbonates, possibly because of similar mineralogy.

• The low Sr/Na ratio (mean of ~1.2) in these limestone samples are similar to that for Recent temperate calcitic carbonates (mean of ~1), thus suggesting similar mineralogy. The plot of covariance of Sr/Na with Mn also shows that the most of the data fall mainly within the Recent calcitic temperate carbonate field, due to similar mineralogy.

The reason for differences in trace element concentrations between aragonite and mixed calcite-aragonite mineralogy in the Mozduran limestones, can be attributed to loss of Sr and Na during diagenesis. Aragonite to calcite transformation results in an appreciable loss of Sr and Na, and a gain of Mn and

Fe. Marine calcites have Sr and Na concentrations much higher than those in aragonite, whereas, Mn and Fe concentrations in marine calcites are much higher than those in aragonite. Therefore, calcite to calcite (dLMC) transformation is characterised by low Sr and low Na. Mn and Fe are related to redox potential in the diagenetic environment. Mn and Fe are increased during meteoric diagenesis, because of higher concentrations of Mn and Fe in meteoric water relative to seawater.

The results of trace element variations strongly indicate that, inspite of the assumption by some workers that calcite was considered to have been dominant in the past (particularly during the Jurassic, due to differences in atmosphric CO_2 levels), in the Upper Jurassic Mozduran limestone (with similar CO_2 levels), the variation in carbonate mineralogy is attributed to seawater temperature. This is evidenced by aragonite forming in the shallowest part of the basin (with relatively warmer water), and mainly calcite with some aragonite forming in the relatively deeper water.

Consistent with the interpretation of diagenetic history from petrographic evidences, the geochemical results suggest that meteoric and burial processes dominate in the shallowest and relatively deeper parts of the basin respectively.

CHAPTER 7

OXYGEN and CARBON ISOTOPES in LIMESTONES

CHAPTER 7

OXYGEN and CARBON ISOTOPES in LIMESTONES

7.1 Introduction

Over the last 20 years the study of stable oxygen and carbon isotope compositions of carbonate rocks has been one of the active areas of research in carbonate geochemistry. These studies have particular application in understanding temperatures of deposition, carbonate diagenesis and geochemistry of carbonate rocks.

The $\delta^{18}O$ and $\delta^{13}C$ variations in carbonates are influenced by several factors, including: (1) ambient water temperatures, (2) mineralogy, (3) salinity, (4) biochemical fractionation, (5) $\delta^{13}C$ variations in surface to deep water, (6) present, icehouse, and greenhouse modes, (7) stabilization of carbonate minerals and isotopes and (9) carbonate diagenesis and isotopes. All of these aspects will be discussed later in this Chapter.

The present study evaluates $\delta^{18}O$ and $\delta^{13}C$ criteria, presented by Rao (1993 b, 1996), to differentiate aragonite from calcite in both Recent (tropical, temperate and polar) and Ordovician carbonates to Jurassic carbonates (Adabi and Rao, 1996). This $\delta^{18}O$ and $\delta^{13}C$ technique involves the determination of lines of equilibrium for aragonite and calcite, as a function of temperatures, by considering Recent and ancient average $\delta^{18}O$ values of seawater and $\delta^{13}C$ values of atmospheric CO_2 and seawater. Distinguishing aragonite from calcite will also aid in the recognition of depositional environment, diagenesis and geochemistry of carbonates.

$\delta^{18}O$ and $\delta^{13}C$ compositions of Recent tropical, temperate and polar carbonates are distinct, due to their aragonite and calcite contents, water temperatures and variations of $\delta^{13}C$ in the atmosphere and seawater (Rao and Green, 1983; Rao and Nelson, 1992). Aragonite to calcite ratios in Recent carbonates decrease from tropical, through to temperate and polar regions

(Nelson, 1978, 1988; Rao, 1981 a, b; Rao and Adabi, 1992). Similar latitudinal variations in aragonite to calcite ratios also occur in ancient carbonates (Nelson, 1978; Rao, 1981 a, 1988 a, b; Brookfield, 1988; James and Bone, 1989, 1992).

In carbonate X-ray diffractograms of Recent carbonate sediments, major and minor element concentrations, $\delta^{18}O$ and $\delta^{13}C$ values and petrographic features provide a means of differentiating aragonite from calcite (e.g., Rao and Adabi, 1992) and mole% $MgCO_3$ (Scholle, 1978). The amount of Mg and trace elements, such as Sr and Na, help to differentiate aragonite from calcite, and low-Mg calcite from high-Mg calcite. The $\delta^{18}O$ values of aragonite are 0.6‰ higher than low-Mg calcite, whereas high-Mg calcite $\delta^{18}O$ values increase relative to low-Mg calcite by 0.06‰ per mole% $MgCO_3$ (Tarutani et al., 1969). The $\delta^{13}C$ values of aragonite are ~1.7‰ higher than low-Mg calcite (Rubinson and Clayton, 1969; Gonzalez and Lohmann, 1985; Romanek et al., 1992).

Distinguishing originally aragonitic from originally calcitic mineralogies in ancient carbonates is difficult, due to pervasive alteration to low-Mg calcite, which contains lower concentrations of Mg. X-ray diffractograms and Mg contents of ancient limestones are of little use in distinguishing original aragonite from calcite. The Sr and Na concentrations in ancient limestones decrease appreciably during meteoric and/or burial diagenesis. Nevertheless, the ratios of Sr/Na in ancient limestones do distinguish originally aragonitic limestones from their calcitic counterparts (Adabi and Rao, 1991; Rao, 1991). Petrographic criteria for distinguishing aragonite from calcite is based mainly on comparison of sparry calcite cement and ooid morphology, with that of modern counterparts (eg., Sandberg, 1975; Wilkinson et al., 1985; Strasser, 1986; Swirydczuk, 1988; Adabi and Rao 1991). However, many ancient limestones contain abundant micrite, whose original mineralogy is difficult to determine by conventional or scanning electron microscopy. The $\delta^{18}O$ and $\delta^{13}C$ values of ancient limestones range from original values at the time of deposition or early diagenesis, to altered values during subsequent meteoric and/or burial diagenesis.

This isotopic study provides consistently valid results for $\delta^{18}O$ and $\delta^{13}C$ values, from unaltered and altered bulk carbonates, skeletal and non-skeletal grains, sparry calcite and micrite, and indicates the occurrence of nontropical carbonates and large temperature fluctuations in some shallow marine environments. To extend these isotopic criteria to other geologic ages requires available $\delta^{18}O$ composition of seawater and $\delta^{13}C$ composition of very shallow marine (<30m) carbonates, in equilibrium with the amospheric CO_2 of the period.

In this study, geochemical data, is firstly presented, followed by the

factors which influenced the $\delta^{18}O$ and $\delta^{13}C$ variations in carbonates, covariation of isotopes and trace elements, and water temperatures.

7.2 Geochemical Data

Minimum, maximum and mean values of isotope and trace element compositions of bulk carbonates, components, cements and veins, in aragonitic and mixed aragonitic-calcitic samples from the shallowest and relatively deeper parts of the basin are shown in Table 7.1 A and 7.1 B respectively.

Isotope data are plotted on Fig. 7.1 to 7.6, corresponding to limestone samples from the shallowest to relatively deeper parts of the basin. The isotopic criteria proposed in this study involve the determination of equilibrium lines for aragonite and calcite, and of mixtures of aragonite and calcite, with variable temperatures. This study assumed a present day average value of $\delta^{18}O$ of seawater (0‰ SMOW), $\delta^{13}C$ of atmospheric CO_2 (-7.2‰), and $\delta^{13}C$ value of seawater and corresponding deep shelf seawater from temperate (0‰) and polar regions (-2‰). The $\delta^{18}O$ and $\delta^{13}C$ data of bulk carbonates, skeletal and non-skeletal grains and cements, were then assessed, using comparative data from known aragonite, calcite and mixtures of calcite and aragonite of Recent tropical, temperate and polar carbonates, and from inferred mineralogies of Jurassic and Ordovician carbonates. Temperature equilibrium lines of aragonite, an aragonite-calcite mixture and calcite are also shown on these figures .

The temperature equilibrium $CaCO_3$ line (Fig. 7.1) can be calculated from the temperature equations of $\delta^{18}O$ (Friedman and O'Neil, 1977) and $\delta^{13}C$ (Fontes and Pouchan, 1975), taking $\delta^{18}O$ of water as 0‰ and $\delta^{13}C$ of atmospheric CO_2 as -7.2‰ (Rao, 1993 b). This line passes through the center of the tropical bulk sediment isotopic field (Fig. 7.1), and corresponds to a mixture of aragonite and calcite (Rao and Green, 1983). Recent experimental studies on $\delta^{13}C$ isotopic fractionation in calcite and aragonite (Romanek et al., 1992) indicate that both calcite-CO_2 (gas) and aragonite-CO_2 (gas) enrichment factors are temperature sensitive and are described by the equation:

$$\Sigma \text{ calcite-}CO_2 = 11.98\ (\pm 0.13) - 0.12\ .\ T\ (^{\circ}C)$$

$$\Sigma \text{ aragonite-}CO_2 = 13.88\ (\pm 0.16) - 0.13\ (\pm 0.01)\ .\ T\ (^{\circ}C)$$

Utilizing a $\delta^{13}C$ value for CO_2 gas of -7.2‰, and a $\delta^{18}O$ value for seawater of 0‰, the equilibrium calcite and aragonite lines were drawn at various

Table 7.1. Minimum, maximum and mean values of isotope and trace element compositions of bulk carbonates and components in aragonitic samples (A), and in mixed aragonitic-calcitic samples (B) of the Mozduran Formation, corresponding to the shallowest and relatively deeper part of the basin respectively.

A

		$\delta^{18}O$ ‰ PDB			$\delta^{13}C$ ‰ PDB		
Variable	Number	Minimum	Maximum	Mean	Minimum	Maximum	Mean
Bulk carbonate	22	-4.1	-7.9	-6.6	3.9	-0.3	1.7
Micrite	5	-1.2	-5.6	-3.1	4.3	3.3	4
Brachiopod	5	-6	-6	-6	1.1	1.1	1.1
Void filling cement	6	-6	-7.6	-6.5	2.4	-2.8	0.85

		Mn ppm			Fe ppm			Sr ppm			Na ppm		
Variable	Number	Minimum	Maximum	Mean	Minimum	Maximum	Mean	Minimum	Maximum	Mean	Minimum	Maximum	Mean
Bulk carbonate	25	53	529	265	420	3745	1323	114	408	268	79	209	135
Micrite	5	56	193	131	328	781	527	175	313	243	116	280	190
Brachiopod	3	113	121	116	535	721	645	368	497	437	159	181	170

B

		$\delta^{18}O$ ‰ PDB			$\delta^{13}C$ ‰ PDB		
Variable	Number	Minimum	Maximum	Mean	Minimum	Maximum	Mean
Bulk carbonate	52	-3.5	-7	-5.4	4.1	0.9	2.5
Micrite	23	-1.7	-4.9	-3.6	4.5	2.5	3.4
Intraclast	9	-2.4	-4.4	-3.4	4	2.9	3.2
Ooid	4	-2.1	-5.8	-3.9	2.9	2.1	2.6
Void filling cement	8	-2.4	-6.6	-5.3	3.8	0.4	2.85
Vein	5	-9.4	-12.6	-11	3.4	-5.2	-1

		Mn ppm			Fe ppm			Sr ppm			Na ppm		
Variable	Number	Minimum	Maximum	Mean	Minimum	Maximum	Mean	Minimum	Maximum	Mean	Minimum	Maximum	Mean
Bulk carbonate	46	33	245	83	63	3552	551	61	409	165	44	252	117
Micrite	22	17	328	86	103	2498	652	74	424	181	67	525	194
Intraclast	7	40	76	53	156	424	277	92	179	138	93	206	153
Ooid	5	28	88	43	84	327	174	98	204	129	75	188	117
Void filling cement	5	40	98	74	32	180	80	55	321	117	69	107	87
Vein	5	29	170	104	49	147	91	80	211	122	11	207	88

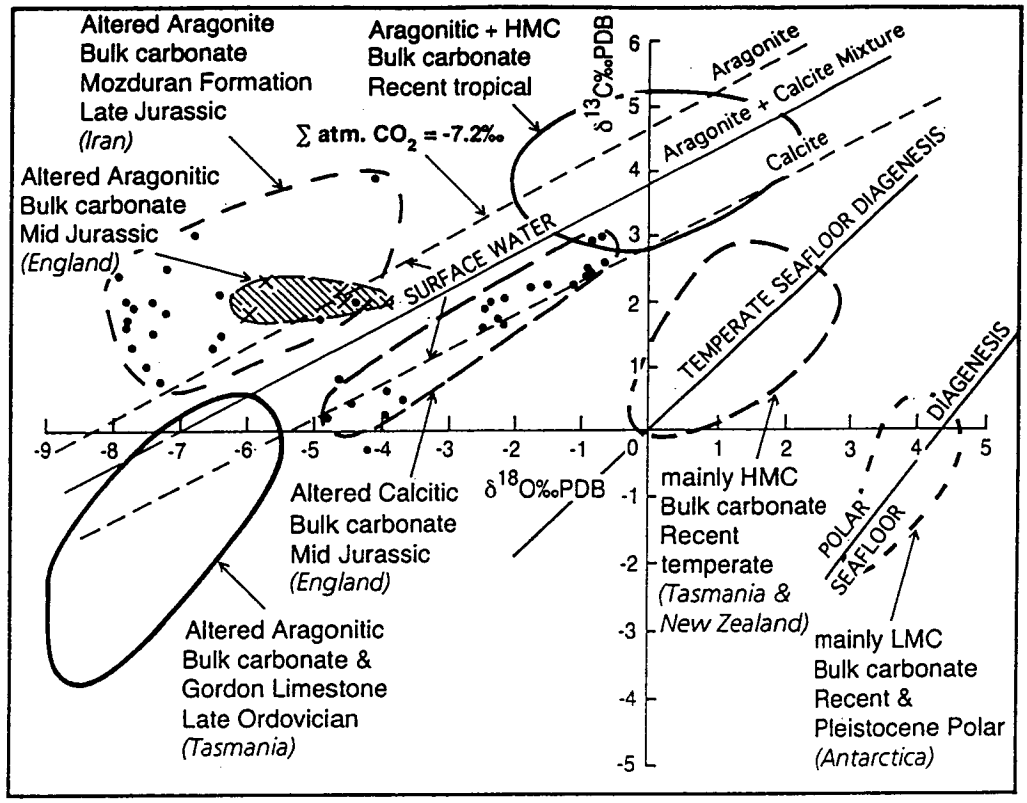

Figure 7.1. $\delta^{18}O$ and $\delta^{13}C$ variations of Recent unaltered bulk carbonates from the tropics (Milliman and Müller, 1977), temperate region of Tasmania and New Zealand (Rao and Nelson, 1992) and polar region of Antarctica (Rao, unpublished data), mid Jurassic of England (Marshall and Ashton, 1980), Upper Jurassic Mozduran Formation (Adabi and Rao, 1991), and late Ordovician of Tasmania (Rao and Wang, 1990). Equilibrium lines for aragonite and calcite and mixtures of aragonite and calcite with variable temperatures were drawn by considering present average values of $\delta^{18}O$ of seawater (0‰ SMOW) and $\delta^{13}C$ of atmospheric CO_2 (-7.2‰). The trend line passing through the temperate isotope field is referred to as temperate seafloor diagenesis (Rao and Nelson, 1992) and the one passing through polar carbonates is referred to as polar seafloor diagenesis. Note the $\delta^{18}O$ and $\delta^{13}C$ isotope fields of Upper Jurassic and mid Jurassic altered aragonitic bulk carbonates fall on the aragonite equilibrium line. The late Ordovician altered aragonitic carbonate falls on the aragonite-calcite mixture line, and mid Jurassic altered calcitic carbonates lie on the calcite equilibrium line.

temperatures (Fig. 7.1). Recent temperate and polar carbonates are mainly calcites and these are in equilibrium with $\delta^{18}O$ and $\delta^{13}C$ values of seawater. The trend line passing through temperate isotope fields is referred to as the temperate seafloor diagenesis trend line, and has a slope of 1 (Rao and Nelson, 1992). The trend line passing through the polar carbonate isotope field is referred to as the polar seafloor diagenesis trend line (Fig. 7.1).

7.2.1 Upper Jurassic Mozduran Formation

The $\delta^{18}O$ values in the Mozduran limestones from the shallowest part of the basin range from -1.2 to -7.9‰ PDB, with a mean of -6‰, whereas $\delta^{13}C$ values range from -0.3 to +4.3‰ PDB, with a mean of +2.2‰ (Figs. 7.1 and 7.2). All $\delta^{13}C$ values are positive (except one sample) and most of the least-altered micrite values fall within the range of Recent tropical shallow marine bulk carbonates, and are far removed from the Recent temperate calcitic bulk carbonate isotope field of Tasmania and New Zealand. Most of the $\delta^{18}O$ values in these limestones are lighter than Recent tropical shallow marine bulk carbonates, due to equilibration with non-marine waters (Adabi and Rao, 1991). Tropical and subtropical coastal meteoric waters are 2 to 3‰ (SMOW) lighter than marine waters in $\delta^{18}O$ (Anderson and Arthur, 1983). The calcites of the Mozduran limestones, in the shallowest part of the basin, which range up to -7.9‰ PDB in $\delta^{18}O$, are thus interpreted to be profoundly affected by non-marine diagenesis (Adabi and Rao, 1991). The Mozduran limestones in the Shurijeh section, consisting of thin limestones and thick terrigenous clastics, show a depletion of $\delta^{13}C$ (-0.3‰, Fig. 7.1). The depletion of $\delta^{13}C$ is possibly characteristic of vadose diagenesis, where soil CO_2 enrichment in $\delta^{12}C$ occurs, due to the decomposition of organic matter. The $\delta^{13}C$ levels in phreatic meteoric calcites approach marine calcite levels, due to increasing amounts of water-rock interaction (Meyers and Lohmann, 1985; Lohmann, 1988). As $\delta^{13}C$ values of the Mozduran samples, from the shallowest part of the basin, are near marine calcite brachiopod values, they are interpreted as undergoing phreatic meteoric diagenesis after deposition.

The $\delta^{18}O$ and $\delta^{13}C$ values of the Mozduran bulk carbonates from the shallowest part of the basin are plotted on Fig. 7.1, along with the isotopic field of Recent tropical warm water bulk carbonates (Milliman and Müller, 1977), the isotopic field of Recent temperate bulk carbonates (Rao and Green, 1983; Rao and Nelson, 1992) and the isotopic field of Recent polar bulk carbonates (Rao, unpublished data). The temperate and polar bulk carbonate isotopic fields are distinctly different from the shallow marine tropical bulk carbonate field (Figs. 7.1 and 7.4), in that they have heavier $\delta^{18}O$ values and a wider range of $\delta^{13}C$ values. Tropical carbonates are in equilibrium with atmospheric CO_2, and thus their isotopic field is cut by aragonite, an aragonite-calcite mixture and calcite lines (Rao, 1993 a, b). Temperate and polar carbonate isotopes do not fall on tropical aragonite, aragonite-calcite mixture or calcite lines, as they are not in equilibrium with atmospheric CO_2. In temperate bulk carbonates, $\delta^{18}O$ and $\delta^{13}C$ values are positively correlated, and the isotopic field is bisected by the seafloor

diagenesis trend line, with a slope of about 1, as these carbonates are in equilibrium with relatively deeper seawater (Rao, 1994). The seafloor diagenesis trend line passes through the middle of the field or 0‰, since under equilibrium conditions both $\delta^{18}O$ and $\delta^{13}C$ values in carbonates vary with water temperature (Rao and Nelson, 1992).

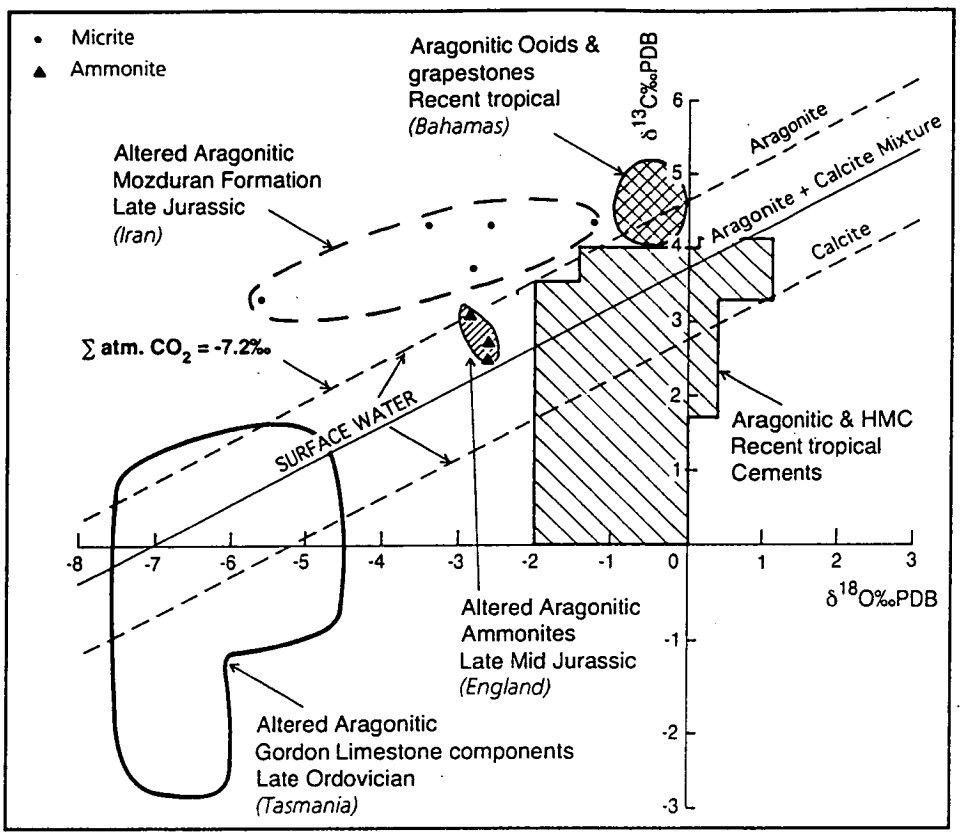

Figure 7.2. $\delta^{18}O$ and $\delta^{13}C$ variations of Recent unaltered aragonitic ooids and grapestones (Milliman and Müller, 1977), aragonite-calcite mixture cements (Al-Aasm and Veizer, 1986), altered aragonitic late mid Jurassic ammonites (Tan et al., 1970), Upper Jurassic aragonitic Mozduran limestone (micrite) and late Ordovician altered aragonitic components (Rao and Wang, 1990). Note that the Upper Jurassic Mozduran micrites do not fall on the aragonite equilibrium line, indicating that these carbonates are not in equilibrium with present atmospheric CO_2 (-7.2‰).

The altered aragonitic micrite and most of the bulk carbonate isotopic fields of the Mozduran limestones fall above the equilibrium aragonite line (Figs. 7.1 and 7.2), indicating that these carbonates are not in equilibrium with atmospheric CO_2 (-7.2‰). It has been suggested that the PCO_2 level during the Upper Jurassic was higher than today (e.g., Budyko, et al., 1985; Berner, 1990; Moore et al., 1992 a), and the calculated Upper Jurassic PCO_2 level, using the

equation of Fontes and Pouchan (1975), gives an atmospheric $\delta^{13}C$ value of -6.7‰ (which is about 0.5‰ lower than present day values, Adabi and Rao, 1996). Thus, by considering an atmospheric $\delta^{13}C$ value of -6.7‰ for the Upper Jurassic period and shifting the temperature equilibrium aragonite and calcite lines by about 0.5‰, the aragonite equilibrium line passes through the micrite and bulk carbonate isotopic fields of the Mozduran Formation (Fig. 7.3). The calculation of PCO_2 levels during the Upper Jurassic is discussed later in this Chapter.

In contrast, the calcite equilibrium line passes through the heavy calcitic brachiopod values of the Mozduran Formation. Other brachiopod values which fall on the aragonite and calcite mixture line have possibly been affected by diagenetic alteration (Fig. 7.3).

The $\delta^{18}O$ values of bulk carbonates, micrite, and non-skeletal grains in the Mozduran limestones from the relatively deeper part of the basin, range from -1.7 to -7‰ PDB, with a mean of -4.7‰, whereas $\delta^{13}C$ values range from +0.9 to +4.5‰ PDB, with a mean of +2.8‰ (Table 7.1 B). All the $\delta^{13}C$ values are positive and most of the non-skeletal grains and bulk carbonates fall within the range of Recent tropical shallow marine bulk carbonates. Most of the $\delta^{18}O$ values in these limestones are lighter than those of Recent tropical shallow marine bulk carbonates, due to diagenetic alterations.

The $\delta^{18}O$ and $\delta^{13}C$ values of the Mozduran bulk carbonates from the relatively deeper part of the basin are plotted on Fig. 7.4. Included are the isotopic field of Recent tropical warm water bulk carbonates (Milliman and Müller, 1977), the isotopic field of Recent temperate bulk carbonates (Rao and Green, 1983; Rao and Nelson, 1992), and the isotopic field of Recent and Pleistocene polar bulk carbonates (Rao, unpublished data). The $\delta^{18}O$ and $\delta^{13}C$ values of the Mozduran non-skeletal grains are plotted on Fig. 7.5. Most of the non-skeletal grains and bulk carbonate isotopic fields fall above the aragonite equilibrium line. This indicates that these carbonates are not in equilibrium with atmospheric CO_2 (-7.2‰). By considering an atmospheric $\delta^{13}C$ value of -6.7‰ (which is about 0.5‰ lower than present day values) for the Upper Jurassic period (Adabi and Rao, 1996), and shifting the temperature equilibrium aragonite, aragonite and calcite mixture and calcite lines by about 0.5‰, both the aragonite and aragonite and calcite mixture equilibrium lines pass through the non-skeletal and bulk carbonate isotopic fields of the Mozduran Formation (Fig. 7.6). This indicates a mixture of both aragonite and calcite mineralogy in these carbonates, unlike the predominantly aragonitic mineralogy in limestone samples from the shallowest

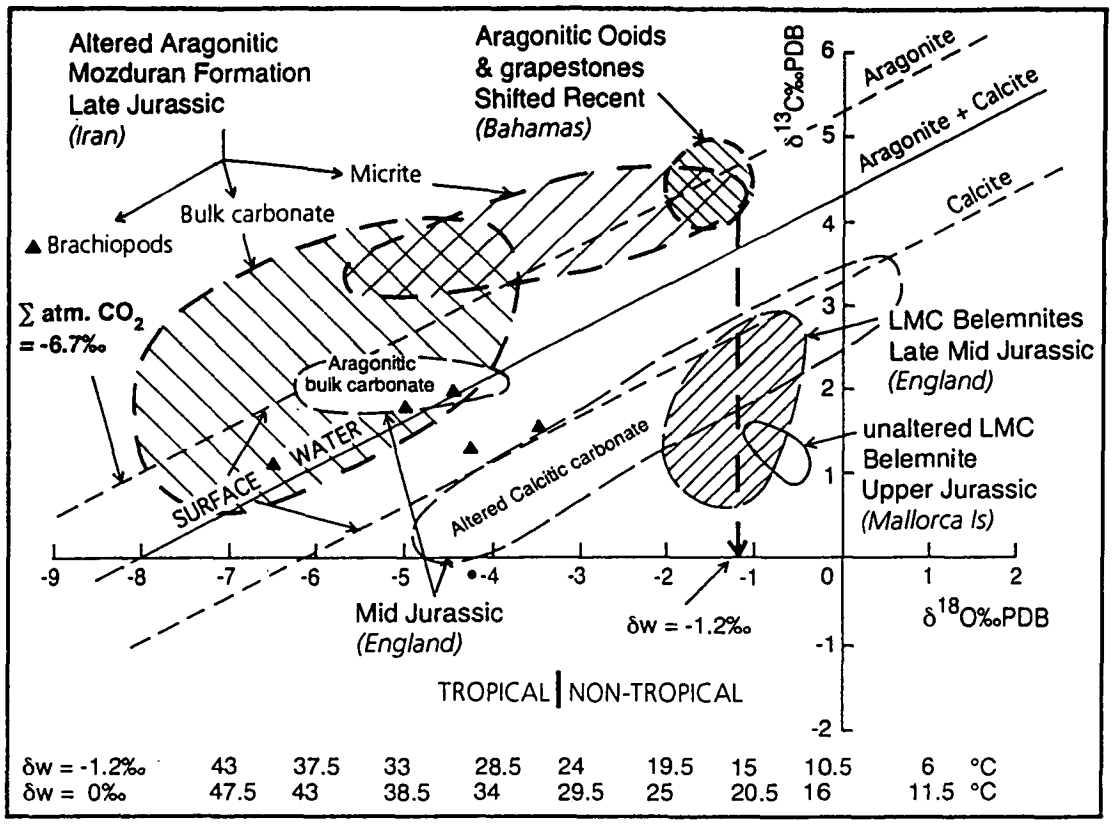

Figure 7.3. $\delta^{18}O$ and $\delta^{13}C$ variations of altered aragonitic Upper Jurassic bulk carbonate, micrite and brachiopods of the Mozduran limestone, altered aragonitic and calcitic bulk carbonate of the mid Jurassic of England (Marshall and Ashton, 1980), late mid Jurassic low-Mg calcite belemnites of Scotland (Tan et al ., 1970), and Upper Jurassic belemnites of Mallorca Island, Spain (Price and Sellwood, 1994). Note aragonite and calcite and aragonite-calcite equilibrium lines are drawn considering atmospheric CO_2 of -6.7‰, and that this aragonite equilibrium line passes through the middle of the Upper Jurassic Mozduran carbonates. The calcite equilibrium line passes through the heaviest Upper Jurassic brachiopod values of Iran. Note that the shifted Recent aragonitic ooids and grapestone isotopic field of the Bahamas, corresponding to a Jurassic seawater $\delta^{18}O$ value of -1.2‰, falls at the edge of the Jurassic isotopic field. The late mid Jurassic of Scotland and mid Jurassic of England isotopic fields do not fall on the calcite equilibrium line, because they are not in equilibrium with atmospheric CO_2 of -6.7‰, but with the value of -7.2‰ (Adabi and Rao, 1996, Figs. 7.1 and 7.4). Upper Jurassic belemnites of Mallorca Island also do not fall on the calcite equilibrium line, as they probably formed in cooler and deeper water. Thus, they are not affected by shallow surface water atmospheric CO_2. Note Jurassic temperatures varied from about 30 to 8°C with subtropical carbonates in Iran and temperate carbonates in England. Ambient water temperature calcite from $\delta^{18}O$ values with $\delta^{18}O$ values of normal seawater (0‰) and Upper Jurassic seawater (-1.2 ‰) are illustrated at the bottom of figure.

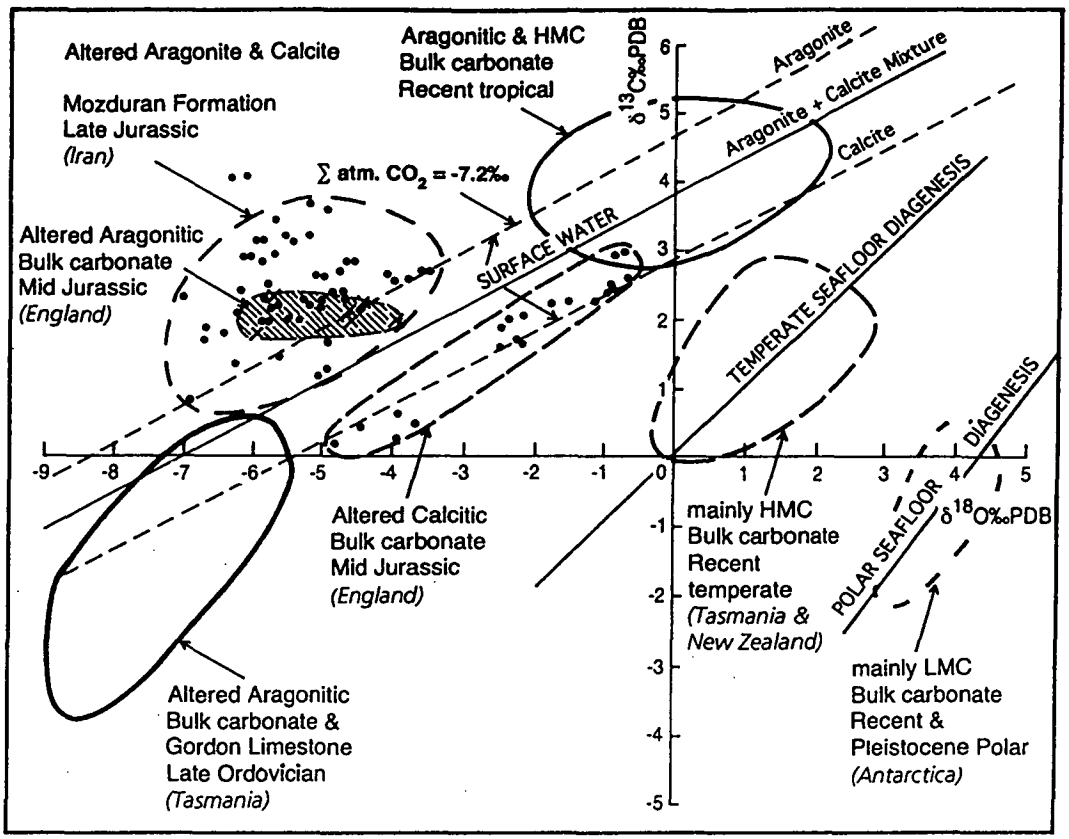

Figure 7.4. $\delta^{18}O$ and $\delta^{13}C$ variations of Recent unaltered bulk carbonates from the tropics (Milliman and Müller, 1977), temperate of Tasmania and New Zealand (Rao and Nelson, 1992), polar Antarctica (Rao, unpublished data), mid Jurassic of England (Marshall and Ashton, 1980), Upper Jurassic Mozduran limestone (Adabi and Rao, 1991), and late Ordovician of Tasmania (Rao and Wang, 1990). Equilibrium lines for aragonite and calcite and mixtures of aragonite and calcite, with variable temperatures, were drawn by considering present average values of $\delta^{18}O$ of seawater (0‰ SMOW) and $\delta^{13}C$ of atmospheric CO_2 (-7.2‰). Note that the $\delta^{18}O$ and $\delta^{13}C$ isotope fields of altered bulk carbonates of the Upper Jurassic Mozduran Formation and mid Jurassic altered aragonitic carbonates fall on the aragonite equilibrium line, late Ordovician altered aragonitic carbonates fall on the aragonite-calcite mixture line, and mid Jurassic altered calcitic carbonates lie on the calcite equilibrium line. Most of the bulk carbonate isotopic fields of the Upper Jurassic Mozduran carbonates fall above the aragonitic eguilibrium line, thus indicating that these carbonates are not in equilibrium with atmospheric CO_2 (-7.2‰, Adabi and Rao, 1996).

part of the basin (Fig. 7.3). The late mid Jurassic LMC belemnites of Scotland and mid Jurassic altered calcitic carbonates of the England isotopic fields, fall at the edge of the calcitic equilibrium line, as these are not in equilibrium with atmospheric CO_2 values of -6.7‰, but with the value of -7.2‰ (Adabi and Rao,

1996, Figs. 7.3 and 7.6). The isotopic field of the Upper Jurassic belemnites of Mallorca Island also do not fall on the calcite equilibrium line, because these belemnites may have lived in cooler sub-surface waters or greater water depth. Thus, these belemnites are not in equilibrium with surface atmospheric CO_2.

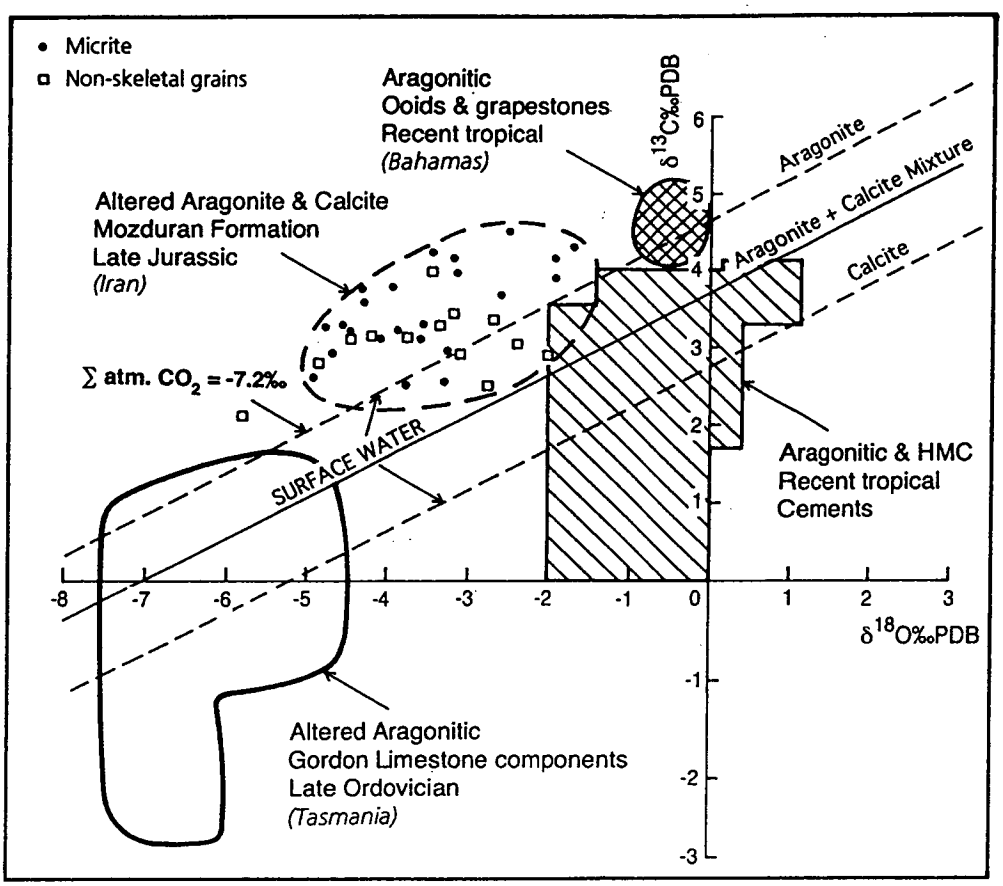

Figure 7.5. $\delta^{18}O$ and $\delta^{13}C$ variations of Recent unaltered aragonitic ooids and grapestones (Milliman and Müller, 1977), aragonite-calcite mixture cements (Al-Aasm and Veizer, 1986), altered aragonitic late mid Jurassic ammonites (Tan et al., 1970), Upper Jurassic altered non-skeletal components, micrites of the Mozduran limestone, and late Ordovician altered aragonitic components (Rao and Wang, 1990). Note that most of the micrite and non-skeletal carbonate isotopic fields of the Upper Jurassic Mozduran limestones fall above the aragonitic equilibrium line, indicating that these carbonates are not in equilibrium with atmospheric CO_2 (-7.2‰, Adabi and Rao, 1996).

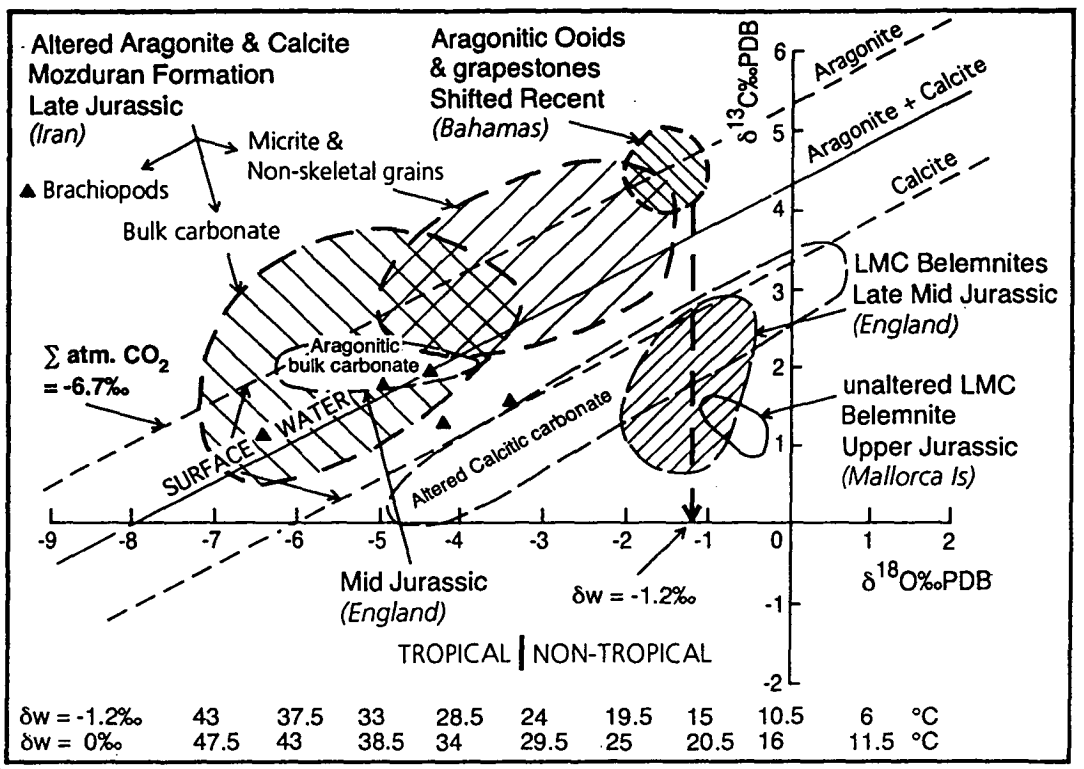

Figure 7.6. $\delta^{18}O$ and $\delta^{13}C$ variations of altered aragonitic Upper Jurassic bulk carbonates, non-skeletal components, micrite and brachiopods of the Mozduran limestone, altered aragonitic and calcitic bulk carbonates of the mid Jurassic of England (Marshall and Ashton, 1980), late mid Jurassic low-Mg calcite belemnites of Scotland (Tan et al., 1970), and Upper Jurassic belemnites of Mallorca Island, Spain (Price and Sellwood, 1994). Aragonite and calcite and aragonite-calcite equilibrium lines are drawn considering atmospheric CO_2 of -6.7‰. Note the aragonite and aragonite-calcite equilibrium lines both pass through the Upper Jurassic Mozduran limestones (from relatively deeper part of the basin), due to mixed carbonate mineralogy (Adabi and Rao, 1996). The calcite equilibrium line passes through the heaviest Upper Jurassic brachiopod values of Iran. The late mid Jurassic of Scotland and mid Jurassic of England isotopic fields fall at the edge of the calcite equilibrium line, as they are not in equilibrium with atmospheric CO_2 of -6.7‰, but with the value of -7.2‰ (Adabi and Rao, 1996, Figs. 7.1 and 7.4). Upper Jurassic belemnites of Mallorca Island also do not fall on the calcite equilibrium line, as they probably formed in cooler and deeper water. Thus they are not affected by shallow surface water atmospheric CO_2. Ambient water temperature calcite from $\delta^{18}O$ values with $\delta^{18}O$ values of normal seawater (0‰) and Upper Jurassic seawater (-1.2‰) are illustrated at the bottom of figure.

7.3 Discussion

7.3.1 Mineralogy

The $\delta^{18}O$ values of carbonates vary with the relative proportions of low-Mg calcite, high-Mg calcite, aragonite and vaterite. The enrichment of $\delta^{18}O$ is high (>0.3‰) in tropical carbonates, due to their higher content of abiotic aragonite and larger amount of Mg in abiotic high-Mg calcite (Tarutani et al., 1969; Gonzalez and Lohmann, 1985). As the volumetrically dominant minerals in temperate carbonates are low- to high-Mg calcites, some aragonite, and possibly vaterite, the enrichment of $\delta^{18}O$ is <0.3‰ (Rao and Adabi 1992). Polar carbonates are characterized by low-Mg calcites and minor amounts of aragonite, so the enrichment of $\delta^{18}O$ will be much smaller than that of temperate carbonates. The $\delta^{18}O$ values of aragonitic molluscs and foraminifera are approximately 0.7‰ heavier than calcite over the temperature range of 3° to 19° C (Grossman and Ku, 1981). The $\delta^{13}C$ values of aragonite are ~1.7‰ heavier than low-Mg calcite (Rubinson and Clayton, 1969; Romanek, et al., 1992).

As mineralogical changes are reflected by bulk carbonates and components, the Mozduran limestone data are compared with sedimentological and isotopic characteristics of Recent tropical, temperate and polar carbonates, and tropical late Ordovician carbonates of Tasmania and the Mid Jurassic of England. Major features of these carbonates are briefly discussed below.

7.3.1.1 Sedimentological characteristics of Recent and ancient examples

Recent carbonates

Major features of Recent tropical, temperate and polar carbonates and their temperatures of formation are summarized in Table 7.2. These carbonates differ from each other in the type of biota, diversity of biota, non-skeletal grains, cements, mineralogy, occurrence of evaporites and early diagenetic dolomites, and concentrations of trace elements and $\delta^{18}O$ and $\delta^{13}C$ values.

Late Ordovician carbonates of Tasmania

These carbonates contain tropical elements, including, biota, diverse non-skeletal grains, abundant stromatolites, early diagenetic dolomites and originally aragonitic and high-Mg calcite mineralogy, similar to modern tropical carbonates (Rao, 1990 b). Plots of Sr and Na versus Mn indicate that these carbonates stabilized from originally aragonitc mineralogy, and are affected by semi-closed meteoric diagenesis (Rao, 1990 b). The heaviest $\delta^{18}O$ values of micrite and non-

luminescent brachiopods confirm tropical depositional temperatures of 23 to 28° C (Rao and Wang, 1990). However, brachiopods can have significantly altered isotope compositions, even if they are not luminescent (Rush and Chafetz, 1990).

Table 7.2. Major characteristics of Recent tropical, temperate and polar carbonates (after Foster 1974; Lees 1975; Domack 1988; Nelson 1988; Rao and Adabi 1992; Rao and Nelson 1992).

Parameter	Tropical (>25°C) eg. Bahama Bank and Persian Gulf	Temperate (19 to 5°C) Tasmania	Polar (-2 to -15°C) Antarctica
Biota	Blue-green algae, corals, molluscs, foraminifera, bryozoans and echinoderms	Bryozoans, foraminifera molluscs, calcareous red algae and barnacles	Brachiopods,bryozoans molluscs and echinoderms
Biota diversity	High	Moderate	Low
Non-skeletal grain	Ooids, pellets, intraclasts and grapestones	Minor intraclast	Rare
Cements	Abundant	Common	—
Mineralogy	Aragonite and high-Mg calcite	High-Mg calcite, low-Mg calcite and aragonite	Low-Mg calcite and aragonite
Evaporites	Abundant	Absent	Absent
Dolomite, early diagenetic	Abundant	Absent	Absent
Trace elements	High Sr, moderate Na and low Mn	Low Sr, high Na and Mn	—
Isotopes: $\delta^{18}O$‰ PDB	Low negative up to -4‰	Moderately positive up to 2.8‰	Highly positive up to 5‰
$\delta^{13}C$‰ PDB	High positive up to 5.2‰	Moderately positive up to 2‰	Low negative up to -2‰

Middle Jurassic of England

These carbonates were originally calcitic, with minor amounts of aragonite and no dolomite and evaporites, and were deposited at a paleolatitude of 35° N (Marshall and Ashton, 1980). These features indicate a temperate climate during the mid Jurassic of England. The heaviest $\delta^{18}O$ values in these carbonates (from the Cowthick hardgrounds) give cold seawater temperatures of 8° C (Adabi and Rao, 1996). Similar water temperatures, of approximately 11° C, existed at

about 29° N latitude in Russia, in the mid Jurassic, and were considered to be cool temperate (Stevens, 1971). Although there is no evidence of glaciation during the Jurassic, mid Jurassic seawater temperatures were cooler than those at present (Frakes, 1979).

7.3.1.2 Recognition of aragonite from calcite

Unaltered and altered isotopic composition of bulk carbonates

Recent tropical, temperate, and polar bulk carbonate $\delta^{18}O$ and $\delta^{13}C$ values plot in distinct fields (shown on Figs. 7.1 and 7.4). $\delta^{18}O$ values from tropical carbonates are the lightest (approximately -2‰), temperate carbonates are moderately heavy (-0.2 to 2.8‰), and polar carbonates are the heaviest (3 to 4.4‰), corresponding to water temperatures of about 25° C, 17 to 4° C and 3 to -3° C, respectively. These temperatures obtained from $\delta^{18}O$ thermometry are similar to average measured seawater temperatures in tropical, temperate and polar regions. The heaviest $\delta^{18}O$ values, up to 2‰ in tropical carbonates, are due to higher salinities and aragonitic, and high-Mg calcite mineralogies of abiotic precipitates (Milliman and Müller, 1977; Gonzalez and Lohmann, 1985). In contrast to $\delta^{18}O$ variation, $\delta^{13}C$ values from Recent bulk carbonates are heaviest in tropical carbonates (2.8 to 5.2‰), moderately heavy in temperate carbonates (0 to 2.7‰ bulk carbonates) and lightest in polar carbonates (0.4 to -2‰). This marked variation in $\delta^{13}C$ values is mainly due to changes in $\delta^{13}C$ values of seawater and the carbonate mineralogy of samples (Gonzalez and Lohmann, 1985; Rao and Nelson, 1992).

The Recent tropical bulk carbonate isotope field lies between equilibrium for calcite and aragonite lines, as these minerals are in equilibrium with atmospheric CO_2 in surface waters (Figs. 7.1 and 7.4). In contrast, temperate and polar bulk carbonates are calcitic and are in equilibrium with $\delta^{13}C$ in seawater, rather than atmospheric CO_2. These non-tropical carbonates range from 30 to >200 m in water depth and thus are deeper shelf carbonates, whereas isotope data from tropical carbonates are mainly <10 m in water depth. The mid and late Jurassic altered aragonitic bulk carbonates from England and Iran fall on the equilibrium aragonite line (Adabi and Rao, 1996), whereas the late Ordovician altered aragonitic bulk carbonates fall partially on the aragonite-calcite mixture equilibrium line and extend to lighter values (Figs. 7.1 and 7.4), due to extensive meteoric diagenesis (Rao, 1990 b). The mid Jurassic altered calcitic bulk carbonates from England fall on the calcite equilibrium line (Adabi and Rao,

1996, Figs. 7.1 and 7.4). Therefore, the examples of Jurassic and Ordovician carbonates studied here, were originally in equilibrium with atmospheric CO_2.

Unaltered and altered isotopic composition of aragonite

$\delta^{18}O$ and $\delta^{13}C$ values of Recent aragonitic ooids and grapestones from the Bahamas are closely clustered and fall on the aragonite equilibrium line (Figs. 7.2 and 7.5). The recent aragonitic and high-Mg calcite cement field for $\delta^{18}O$ and $\delta^{13}C$ (Al-Aasm and Veizer, 1986) extends from the aragonite equilibrium line to ~0‰ $\delta^{13}C$, possibly due to a decrease of $\delta^{13}C$ values with increasing water depth. The altered aragonitic micrite and bulk carbonates from the shallowest part of the basin, and micrite, bulk carbonates and non-skeletal grains, such as intraclasts and ooids from the relatively deeper part of the basin, from Upper Jurassic Mozduran carbonates, have $\delta^{18}O$ and $\delta^{13}C$ values that fall slightly above the aragonite equilibrium line (Figs. 7.1, 7.2, 7.4 and 7.5). The altered aragonitic micrite, sparry calcite cement (mainly isopachous and void filling) and non-skeletal grains, such as ooids, pellets and intraclasts, from late Ordovician limestones of Tasmania, have $\delta^{18}O$ and $\delta^{13}C$ values that fall on the aragonite equilibrium line and extend to lighter values, revealing an 'inverted J-trend' characteristic of meteoric diagenesis (Lohmann, 1988). The altered aragonitic late mid Jurassic ammonites of Scotland (Tan et al., 1970) have $\delta^{18}O$ and $\delta^{13}C$ values that fall on the aragonite equilibrium line (Fig. 7.2). Therefore, the Mozduran Formation, the Gordon Limestone of Tasmania and ammonites from Scotland, formed mainly in shallow waters, as their $\delta^{18}O$ and $\delta^{13}C$ values are in equilibrium with atmospheric CO_2.

Unaltered and altered isotopic composition of low-Mg calcite

$\delta^{18}O$ and $\delta^{13}C$ values of Recent shallow marine unaltered low-Mg calcite brachiopods from the tropical environment of Jamaica, lie on the equilibrium calcite line, whereas those from shallow (32 to 399 m) temperate to subpolar regions (Rao, 1993 b) fall on a temperate seafloor diagenesis trend line (Fig. 7.7). These brachiopod $\delta^{18}O$ values are in close equilibrium with respect to measured water temperatures in tropical (~23° C) and temperate to subpolar (18 to 3° C) regions. Both the worldwide Ordovician brachiopod $\delta^{18}O$ and $\delta^{13}C$ values (Wadleigh and Veizer 1992) and those of Ordovician brachiopods of Tasmania, plot on the calcite equilibrium line. Upper Jurassic brachiopods of the Mozduran Formation plot on the aragonite and aragonite-calcite mixture trend lines, due to a relatively lower atmospheric CO_2 content (-6.7‰) during the Upper Jurassic.

Therefore, Mozduran brachiopods do not fall on the temperature equilibrium calcite line, as they are not in equilibrium with present CO_2 (-7.2‰), although it has been suggested that these brachiopods have been diagenetically altered (Rush and Chafetz, 1990). Late mid Jurassic of Scotland low-Mg calcite belemnite $\delta^{18}O$ and $\delta^{13}C$ values (Tan et al., 1970) fall on the Recent calcite equilibrium trend line (Adabi and Rao, 1996, Fig. 7.7).

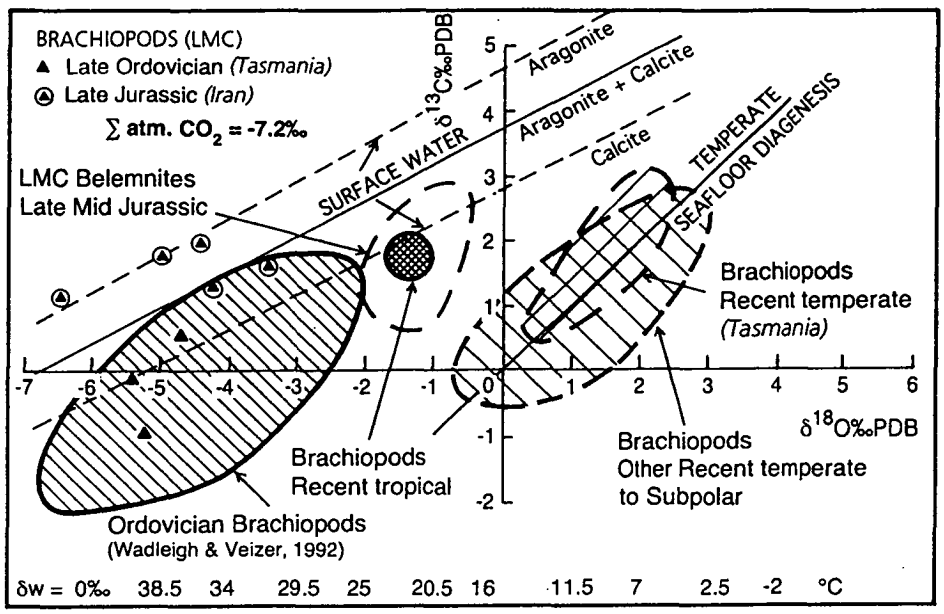

Figure 7.7. $\delta^{18}O$ and $\delta^{13}C$ of Recent unaltered low-Mg calcite brachiopods from the tropics, temperate and polar regions, altered low-Mg calcite brachiopods from the Ordovician (Wadleigh and Veizer, 1992) and late mid Jurassic low-Mg calcite belemnites (Tan et al., 1970). These all fall on the temperature equilibrium calcite line, as they are in equilibrium with atmospheric CO_2. Temperate to subpolar brachiopods fall on the seafloor diagenesis trend line. The Upper Jurassic brachiopods of the Mozduran, do not fall on the temperature equilibrium calcite line, as they are not in equilibrium with present atmospheric CO_2 (-7.2 ‰).

7.3.2 Stabilization of carbonate minerals and isotopes

Stabilization of aragonite, high-Mg calcite (HMC) and low-Mg calcite (LMC) to diagenetic low-Mg calcite (dLMC), mainly takes place in meteoric and/or burial environments involving dissolution and reprecipitation. The change from aragonite to LMC is a one step process (Sandberg and Hudson, 1983; Martin et al., 1986) that involves a change of $\delta^{18}O$ and $\delta^{13}C$ values and is influenced by the chemistry of the reacting fluid and water-rock interaction. The change from HMC to LMC is a multistage dissolution and reprecipitation process that occurs at the microscale (Land, 1967; Sandberg, 1975; Brand and Veizer,

1980; Turner et al., 1986; Budd and Hiatt, 1993). Each dissolution and reprecipitation event produces calcite with slightly lower Mg and $\delta^{18}O$ and $\delta^{13}C$ values than its predecessor. The change from LMC to dLMC is minor and very slow. Thus, original LMC preserves original or near original $\delta^{18}O$ and $\delta^{13}C$ compositions (Wadleigh and Veizer, 1992). Subaerial exposure and early meteoric diagenesis changes original $\delta^{18}O$ and $\delta^{13}C$ values of LMC (Rush and Chafetz, 1990). The change from LMC (original or diagenetic) to another dLMC involves a very minor change in $\delta^{18}O$ composition, whereas $\delta^{13}C$ values may vary due to reaction with CO_2 released from organic matter. This relationship between minerals and their corresponding $\delta^{18}O$ and $\delta^{13}C$ values is recognized in Mozduran bulk carbonates (Figs. 7.1 and 7.4), aragonitic components and cements (Figs. 7.2 and 7.5), and LMC biota (Fig. 7.7). These are thus valuable in the recognition of original aragonite from calcite.

7.3.3 Salinity

The $\delta^{18}O$ values of Recent aragonitic, and high-Mg calcite of warm shallow marine carbonates, are heavier than equilibrium values of approximately 25° C, partly due to higher salinities (Figs. 7.1 and 7.4) than those of temperate and polar shallow seas. In classical tropical shallow marine carbonates, the salinity ranges from 36 to more than 100‰, such as those from the Persian Gulf (37 to >100‰), the Great Bahama Bank (36-46‰) and Shark Bay (55 to 300‰). For temperate carbonates, the salinity is between 34.3 and 35.5‰ and thus, $\delta^{18}O$ values are normal seawater values (Rao and Nelson, 1992). The polar Antarctic Recent carbonates (Rao, unpublished data, Figs. 7.1 and 7.4) are strongly affected by upwelling water, with the effect of melt-water being minor, due to a lack of appreciable melting of ice sheets (Taviani et al., 1993). The most enriched $\delta^{18}O$ values of the Mozduran limestones indicate that salinity was near normal at the time of limestone deposition, as there is no appreciable change to heavier $\delta^{18}O$ values compared to micrite in these limestones. This interpretation is consistent with trace element analysis, showing relatively moderate Na concentrations in these limestones. However, the occurrence of evaporites within the Mozduran sequences, suggests that there were local occurrences of higher salinity.

7.3.4 Biochemical fractionation

The $\delta^{18}O$ and $\delta^{13}C$ values higher or lower than those expected from known salinities and temperatures are due to biochemical fractionation, the rate of skeletal precipitation, kinetic fractionation, and photosynthesis of blue-green

algae. As temperature lines of equilibrium aragonite, calcite, and equal mixtures of aragonite and calcite, pass through much of the bulk carbonate isotopic field of Recent tropical carbonates (Figs. 7.1 and 7.4), the effect of biochemical fractionation is small. The biochemical fractionation in tropical skeletons is higher than in inorganically precipitated marine cements (Gonzalez and Lohmann, 1985; McConnaughey, 1989). In temperate and polar bulk carbonates and skeletons, biochemical fractionation is minimal, because both $\delta^{18}O$ and $\delta^{13}C$ isotope values are in equilibrium with seawater, ambient water temperatures (Rao and Nelson, 1992; Taviani et al., 1993) and the rate of formation (Rao, 1994). In the Mozduran limestones, only brachiopods are analyzed, and the heavy $\delta^{18}O$ values of these brachiopods correspond to reasonable temperatures during the deposition of these limestones. $\delta^{18}O$ values of Recent tropical brachiopods studied by Anderson (written communication, 1993) fall on the temperature equilibrium calcite line (Fig. 7.7) and are in close equilibrium with respect to measured seawater temperatures in the tropical region (23° C). Lines of temperatures of equilibrium aragonite and aragonite-calcite mixtures pass through much of the bulk carbonate and components isotopic field of the Mozduran carbonates. This indicates that most of the Mozduran limestones were inorganically precipitated. Therefore, the effect of biochemical fractionation might be negligible. This interpretation is also valid with respect to heavy $\delta^{18}O$ brachiopod values.

7.3.5 $\delta^{13}C$ variation in surface to deep water

The atmospheric CO_2 content determines the $\delta^{13}C$ value in surface waters. The temperature equilibrium line between aragonite and calcite and the line of equal proportions of aragonite and calcite (drawn assuming a present average $\delta^{13}C$ value of -7.2‰), passes through Recent bulk tropical carbonates, but not through Recent temperate and polar carbonates (Figs. 7.1 and 7.4). This is due to shallow marine tropical carbonates formed at water depths of mostly <10 m, where they are in equilibrium with atmospheric CO_2. In shallow marine temperate carbonates, $\delta^{13}C$ values vary with water depth (Rao and Nelson, 1992). Upwelling, cold deep waters have depleted $\delta^{13}C$ values, due to the oxidation of organic matter at depth. As this upwelling water mixes with deep basin water, the concentration of dissolved $\delta^{13}C$ increases. The Tasmanian (32 to 399 m) and New Zealand (6 to 920 m) shelf temperate carbonates are mainly deeper shelf carbonates, and thus their $\delta^{13}C$ values are in equilibrium with bottom seawater, rather than surface water (<6 m). Antarctic polar carbonates

formed in deeper shelves (>10 to 250 m), are strongly influenced by upwelling waters (Domack, 1988; Taviani et al., 1993). The Mozduran limestone data fall on the aragonite and aragonite-calcite mixture temperature equilibrium lines of surface water, due to shallow marine water origin. Therefore, most of the Upper Jurassic Mozduran limestone data are in equilibrium with surface water $\delta^{13}C$ values of atmospheric CO_2 (-6.7‰, Adabi and Rao, 1996).

7.3.6 Present, icehouse, and greenhouse modes

The atmospheric CO_2 levels largely control climatic variations, with warmer conditions experienced during periods of high CO_2 levels (Greenhouse mode), and cooler conditions prevailing during periods of low CO_2 levels (Icehouse mode; James and Choquette, 1983). Present climate and seawater temperatures are controlled by the occurrence of icesheets and the circulation of polar water. The coincidence of $\delta^{18}O$ and $\delta^{13}C$ values of Ordovician aragonitic bulk carbonates, cements and non-skeletal grains, with the Recent aragonite temperature equilibrium line, and the coincidence of brachiopod values with the Recent low-Mg calcite equilibrium temperature line, shows a correspondence to present day average $\delta^{13}C$ values of -7.2‰ in the atmosphere. This indicates that similar conditions to the present day prevailed during the Ordovician. Conditions similar to today also existed during the mid Jurassic, as indicated by $\delta^{18}O$ and $\delta^{13}C$ values of calcite, that coincide with the calcite temperature equilibrium line constructed using the present day average $\delta^{13}C$ value of -7.2‰ in the atmosphere. The Upper Jurassic $\delta^{18}O$ and $\delta^{13}C$ fields of altered aragonitic bulk carbonates and micrite (Fig. 7.3), and non-skeletal grains and bulk carbonates (Fig. 7.6) of the Mozduran Formation are transected by the aragonite, and aragonite and calcite mixture equilibrium lines respectively, coinciding with a $\delta^{13}C$ value of -6.7‰ in the atmosphere. This slightly lower CO_2 content during the Upper Jurassic of Iran is probably tending towards an icehouse mode.

7.3.7 Carbonate diagenesis and isotopes

Three major isotope models related to carbonate diagenesis depict variations of $\delta^{18}O$ and $\delta^{13}C$ values from unaltered to altered carbonates. The first model considers depletion of $\delta^{18}O$ and near constant $\delta^{13}C$ (a horizontal shift) with increasing temperature. This is a widely observed trend in non-organic deep burial carbonates (Al-Aasm and Veizer, 1986; Choquette and James, 1987; Hurley and Lohmann, 1989). However, this model is not applicable to data presented in this study, because $\delta^{13}C$ values vary with $\delta^{18}O$ values. The second

model is an 'inverted J-trend' (Meyers and Lohmann, 1985; Lohmann, 1988), with a shift in both $\delta^{18}O$ and $\delta^{13}C$ from original values. The shift in $\delta^{18}O$ values increases due to variation in $\delta^{18}O$ fractionation in meteoric water, with increasing latitude (Dansgaard, 1964). This model is applicable to the Ordovician Gordon Limestone of Tasmania. In the Mozduran limestones, although the inverted J-trend is not present, the petrographic and trace element analysis in the shallowest part of the basin, indicates the presence of meteoric diagenesis. In the third model, depletion of $\delta^{13}C$ with increasingly lighter $\delta^{18}O$, which can occur in burial environments due to diagenesis of organic matter with increasing temperature, is common in some ancient limestones (Al-Aasm and Veizer, 1986). This trend is present in the Mozduran limestones, probably due to organic diagenesis (as evidenced by abundant gas reservoirs in these carbonates) during shallow to deep burial.

The observed $\delta^{18}O$ and $\delta^{13}C$ trend in the Mozduran limestones probably results from burial overprinting of earlier meteoric diagenesis, as supported by trace elements and petrographic studies. As the meteoric diagenesis is expected to largely lower $\delta^{13}C$ values, the absence of the very light $\delta^{13}C$ values in the Mozduran limestone samples can be due to the arid climate and lack of soil development.

7.4 Covariation of Isotopes and Trace Elements in the Mozduran Limestone

Carbonate diagenesis and mineralogical composition of carbonate rocks can be better understood by combining oxygen and carbon isotopes with trace elements. The trace element and isotopic composition of carbonate samples studied from the shallowest part of the basin have been compared with fields of Recent temperate bulk carbonates of Tasmania (Australia), Ordovician aragonite, subtropical warm water Ordovician aragonite (Gordon Limestone, Rao, 1991), and Upper Jurassic aragonite. In contrast, the trace element and isotopic composition of carbonate samples from the relatively deeper part of the basin have been compared with fields of Recent temperate bulk carbonates of Tasmania, Upper Jurassic Mozduran brachiopods and Upper Jurassic aragonite-calcite mixture.

The isotopic and elemental composition of the Upper Jurassic aragonite, and aragonite-calcite fields have been derived as follows:

In calculating the oxygen values during the Upper Jurassic period, it has been assumed that the Jurassic seawater was free from icecaps (Ager, 1975; Frakes, 1979; Hambrey and Harland, 1981; Valdes and Sellwood, 1992), and would have been isotopically lighter than at present. Therefore a $\delta^{18}O$ value of -1.2‰ SMOW is used (Shackleton and Kennett, 1975; Marshall and Ashton, 1980; Anderson and Arthur, 1983; Price and Sellwood, 1994). As abiotic aragonite is presently forming in seawater temperatures between about 16 and 40° C, the $\delta^{18}O$ values in aragonite during the Upper Jurassic, at these temperatures, were about -0.6‰ to -2.6‰ PDB. As such, the $\delta^{18}O$ values of abiotic calcites are depleted by 0.6‰ relative to aragonite.

In calculating the $\delta^{13}C$ values in Upper Jurassic aragonite, the $\delta^{13}C$ values of the heaviest micrites from the Mozduran limestones, that approximately overlap on shifted Recent tropical aragonitic ooids and grapestones of the Bahamas (Fig. 7.3), have been used. These $\delta^{13}C$ values range from +3.7 to +4.3‰ PDB. Trace element compositions of Recent tropical aragonitic carbonates (Milliman, 1974) have been used for determining the Upper Jurassic aragonite field (Mn ~20 ppm, Na ~ 2700 ppm, Sr ~10 000 ppm).

In calculating the $\delta^{18}O$ values in aragonite-calcite mixture mineralogy during Upper Jurassic time, it was assumed that Recent temperate carbonates (which are the mixture of aragonite and calcite), are forming in seawater temperatures between about 10 to 20° C. Thus, $\delta^{18}O$ values at these temperatures were about +0.3‰ to -2.2‰ PDB, determined by considering Jurassic seawater $\delta^{18}O$ values of -1.2‰ SMOW. In calculating the $\delta^{13}C$ values in the Upper

Jurassic aragonite-calcite mixture, the $\delta^{13}C$ values of the heaviest micrites from the Mozduran limestones, that approximately overlap on Recent tropical aragonitic and high-Mg calcite cements (Fig. 7.5), have been used. These $\delta^{13}C$ values are in the range of +3.8 to +4.2‰ PDB.

In the trace element calculation of the Upper Jurassic calcite-aragonite mixture, the proportion of 30 to 40% aragonite and 60 to 70% calcite was assumed. This assumption is based on the trace element concentrations of the mixed calcitic-aragonitic Mozduran limestone data, compared with those of the aragonitic Mozduran limeston data and calcitic Recent temperate bulk carbonates of Tasmania (see Figs. 6.7 and 6.15). The Sr values of Recent tropical aragonitic carbonates are about 10 000 ppm, whereas in abiotic calcites, they are 1200 ppm (Veizer, 1983). Therefore, the calculated Sr values in the calcite-aragonite mixture during Upper Jurassic time, will be in the range of approximately 3840 to 4720 ppm. The Mn values of Recent tropical aragonitic carbonates are about 20 ppm, while mean Mn values in Recent temperate bulk carbonates is about 70 ppm. Since Mn is not controlled by abiotic or biotic calcite, the mean Mn values of Recent temperate bulk carbonates have been used.

Based on the above assumption of a mixture of 30 to 40% aragonite and 60 to 70% calcite, the Mn values in the calcite-aragonite mixture during Upper Jurassic time, will be approximately in the range of 50 to 55 ppm. The Na values of Recent tropical aragonitic carbonates are about 2700 ppm, whereas abiotic calcite contains concentrations of around 270 ppm Na (Veizer, 1983). Therefore, the calculated Na values in the calcite-aragonite mixture, during the Upper Jurassic, will be approximately in the range of 1000 to 1242 ppm. The Upper Jurassic brachiopod field (used in carbonate samples from the relatively deeper part of the basin) is based on the ranges of elemental and isotopic compositions of brachiopod samples from the study area shown in Table A5.1 (Appendix 5).

7.4.1 Oxygen versus trace elements in aragonitic limestone samples

7.4.1.1 Oxygen versus strontium

The $\delta^{18}O$ values of Recent temperate bulk carbonates of Tasmania are heavier, and Sr concentrations higher, than those of the subtropical Ordovician Gordon Limestone and Upper Jurassic Mozduran limestones (Fig. 7.8). The trend of Sr variation with $\delta^{18}O$ shows that Sr values are relatively constant throughout the range of $\delta^{18}O$ values. The Sr values of these carbonate samples are much

lower than their modern counterparts, because of progressive loss of Sr during diagenesis. The plot of $\delta^{18}O$-Sr values (Fig. 7.8) also shows that most of the Mozduran aragonitic bulk samples fall within the subtropical Gordon Limestone field, possibly due to similar mineralogy.

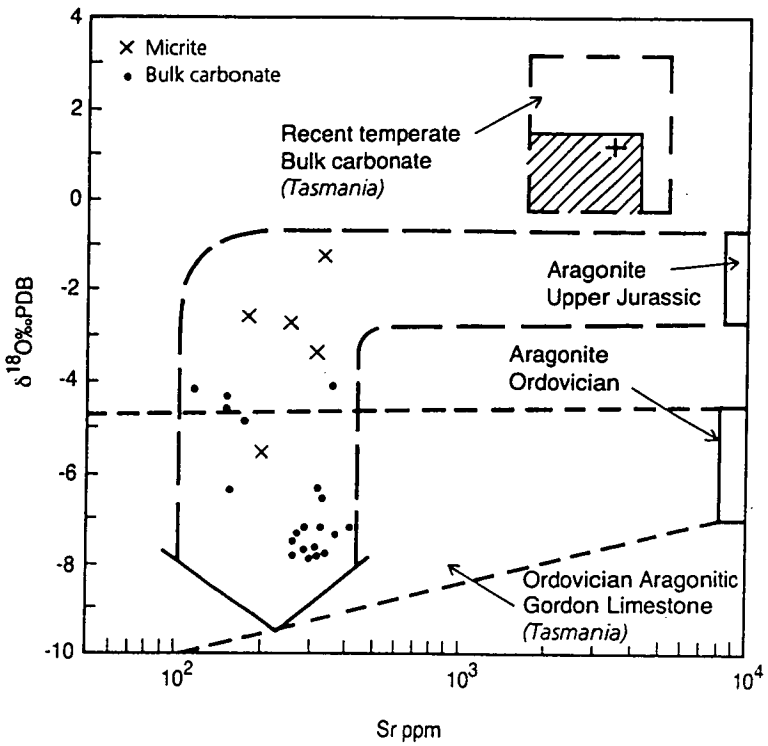

Figure 7.8. Sr-$\delta^{18}O$ variations in aragonitic Mozduran limestone, along with the fields of Recent temperate bulk carbonates from Tasmania, subtropical Gordon Limestone (Rao, 1991) and Upper Jurassic aragonite. Note Sr values are relatively constant throughout the range of $\delta^{18}O$ values.

7.4.1.2 Oxygen versus sodium

The Tasmanian temperate carbonate $\delta^{18}O$ values are heavier, and the Na concentrations higher, than those of the subtropical Ordovician Gordon Limestone and aragonitic Mozduran limestone, as these modern temperate carbonates are not affected by meteoric/burial diagenesis (Fig. 7.9). There is a marked decrease of Na in the subtropical Gordon Limestone (Rao, 1991) and aragonitic Mozduran limestone (Adabi and Rao, 1991), due to meteoric diagenesis. The $\delta^{18}O$ values in most micritic samples are within the range of $\delta^{18}O$ values of the Upper Jurassic aragonite, indicating that these micrites were probably affected by marine diagenesis. In contrast, the Na values in bulk carbonates decrease with decreasing lighter $\delta^{18}O$ values, indicating that these samples were most affected by meteoric waters during diagenesis.

The plot of $\delta^{18}O$-Na values also shows that most of the Mozduran bulk

samples fall within the subtropical Gordon Limestone field, possibly due to similar mineralogy (Fig. 7.9). The $\delta^{18}O$ values of the Mozduran aragonitic bulk samples are appreciably depleted, compared with the Gordon Limestone samples. The shift in Ordovician Gordon Limestone $\delta^{18}O$ values from marine aragonite to calcite is small (~-4.5 to ~-9.5‰ PDB), of about 5‰ PDB (Fig. 7.9). In contrast, in the Mozduran aragonitic limestones the shift in $\delta^{18}O$ values from marine aragonite to dLMC is large (~-1.2 to ~-8‰ PDB). This shift in $\delta^{18}O$ values can be due to a combination of both meteoric and burial diagenesis.

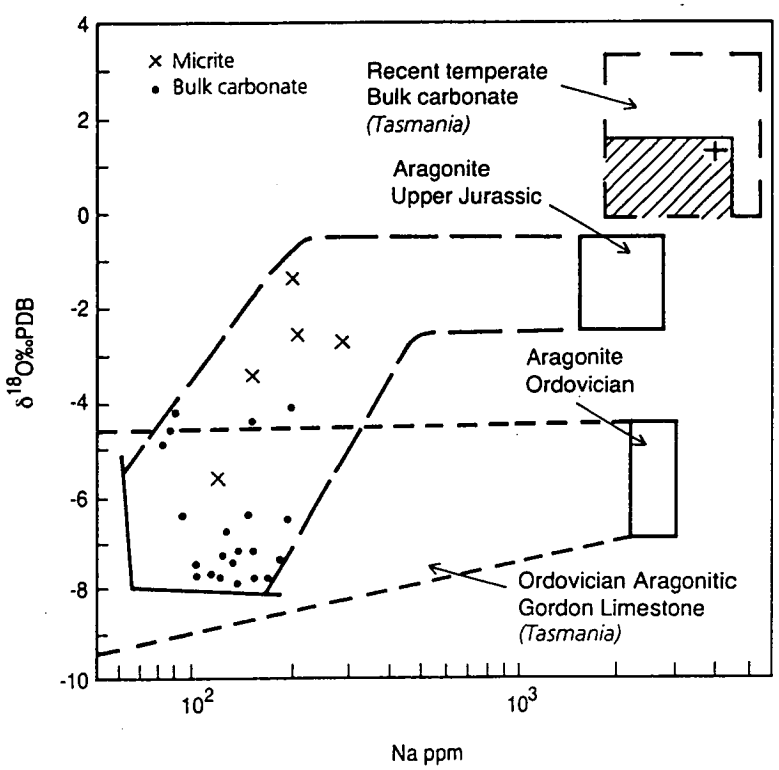

Figure 7.9. Na-$\delta^{18}O$ variations in aragonitic Mozduran limestone, along with the fields of Recent temperate bulk carbonates from Tasmania, subtropical Gordon Limestone (Rao, 1991) and Upper Jurassic aragonite. Note Na content increases with increasing heavier $\delta^{18}O$ values.

7.4.1.3 Oxygen versus manganese and iron

The Recent temperate bulk carbonate $\delta^{18}O$ values are uniform throughout the range of Mn concentrations, due to the marine origin of Mn (Rao, 1991). The heaviest $\delta^{18}O$ value of micrite in aragonitic Mozduran limestone corresponds to the lowest concentrations of Mn, as -1.2‰ $\delta^{18}O$ represents Upper Jurassic marine calcite values. There is an inverse relationship between $\delta^{18}O$ and Mn values (Fig. 7.10) in the aragonitic Mozduran limestone. This is due to the increase of Mn with increasingly lighter $\delta^{18}O$ values, through dissolution of aragonite by meteoric

waters and reprecipitation of calcite (Adabi and Rao, 1991). Mn values are dependent on oxidizing and reducing conditions. In oxidizing (aerobic) conditions, only small amounts of Mn can enter into carbonate lattices, whereas, in semi-reducing to reducing (dysaerobic to anerobic) conditions, large amounts of Mn enters into the carbonate lattices. Thus, low Mn content corresponds to oxidizing conditions, and high Mn concentrations correspond to reducing conditions (Fig. 7.10). As Mn contents in most of the Mozduran data are > 200 ppm, this indicates dysaerobic or semi-reducing conditions. Fe values do not correlate with $\delta^{18}O$ values ($r^2 = 0.2$).

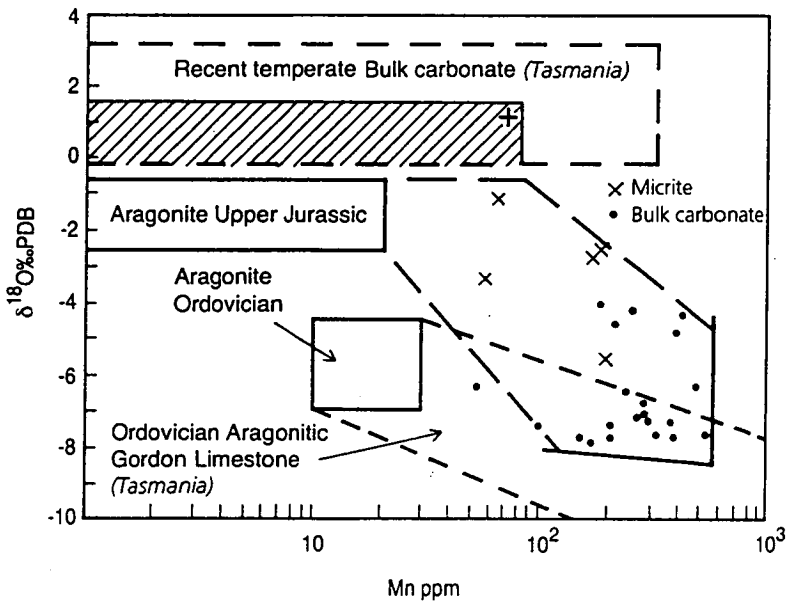

Figure 7.10. Mn-$\delta^{18}O$ variations in aragonitic Mozduran limestone, along with the fields of Recent temperate bulk carbonates from Tasmania, subtropical Gordon Limestone (Rao, 1991) and Upper Jurassic aragonite. Note Mn content increases with increasing lighter $\delta^{18}O$ values.

7.4.2 Carbon versus trace elements

7.4.2.1 Carbon versus strontium

The $\delta^{13}C$ values are uniform throughout the range of Sr values in the Recent temperate bulk carbonates (Fig. 7.11). In the originally aragonitic Mozduran limestone, the higher Sr values in micrite correspond to the heaviest $\delta^{13}C$ values of + 4.3‰ PDB, which represent most probably marine $\delta^{13}C$ values for the Upper Jurassic aragonitic Mozduran limestone. The Sr values are relatively constant throughout the range of $\delta^{13}C$ values, although the lower Sr values in bulk carbonates correspond to the lightest $\delta^{13}C$ values of -0.3‰ PDB. In the aragonitic Mozduran limestone, because the heavier $\delta^{13}C$ values are in micrite

and the lighter values are in bulk carbonates, it is interpreted that bulk carbonates were profoundly affected by non-marine diagenesis. The range from marine to meteoric calcite $\delta^{13}C$ values is about 4‰ in the Mozduran limestone, whereas this difference between marine and meteoric calcite in the Gordon Limestone is 6‰ (Rao, 1991). This indicates greater dissolution of the Gordon Limestones than the aragonitic Mozduran limestone.

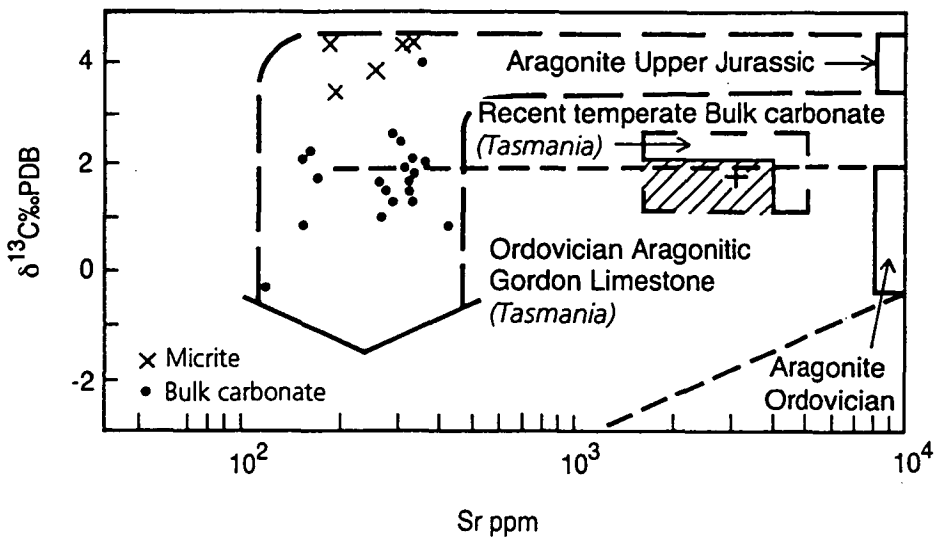

Figure 7.11. Sr-$\delta^{13}C$ variations in aragonitic Mozduran limestone, along with the fields of Recent temperate bulk carbonates from Tasmania, subtropical Gordon Limestone (Rao, 1991) and Upper Jurassic aragonite.

7.4.2.2 Carbon versus sodium

The $\delta^{13}C$ variation is uniform throughout the range of Na in Recent temperate bulk carbonates, due to their marine origin (Fig. 7.12). In the aragonitic Mozduran limestone, Na values decrease with increasingly lighter $\delta^{13}C$ values, due to meteoric diagenesis (Adabi and Rao, 1991). As $\delta^{13}C$ values are very low in freshwater, the $\delta^{13}C$ values will be low when fresh water dissolution is initiated, but will later increase to approach marine calcite levels, due to increasing water-rock interaction (Meyers and Lohmann, 1985; Lohmann, 1988). The heaviest $\delta^{13}C$ values and the highest Na concentrations are in micrite, indicating that micrites were less affected by meteoric diagenesis. The $\delta^{13}C$ values in micrites are within the range of $\delta^{13}C$ values of Upper Jurassic aragonite. The plot of $\delta^{13}C$-Na values shows that over half of the Mozduran aragonitic bulk samples fall within the subtropical Gordon Limestone field (Fig. 7.12), possibly because of similar mineralogy.

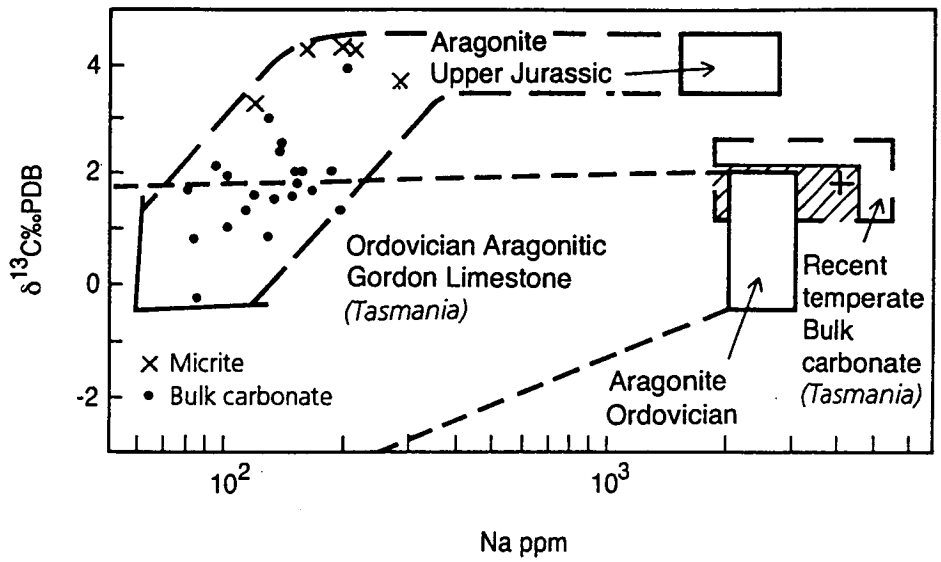

Figure 7.12. Na-$\delta^{13}C$ variations in aragonitic Mozduran limestone, along with the fields of Recent temperate bulk carbonate from Tasmania, subtropical Gordon Limestone (Rao, 1991) and Upper Jurassic aragonite. Note Na content increases with increasing heavier $\delta^{13}C$ values.

7.4.2.3 Carbon versus manganese and iron

The $\delta^{13}C$ values are uniform throughout the range of Mn values in the Recent temperate carbonates due to their marine origin (Fig. 7.13). The lowest Mn values in the less altered micritic samples in the aragonitic Mozduran limestones, correspond to the heaviest $\delta^{13}C$ values of +4.3‰ PDB (the Upper Jurassic marine value). The $\delta^{13}C$ values decrease with increasing Mn values, due to meteoric diagenesis (Adabi and Rao, 1991). The Fe values do not correlate with $\delta^{13}C$ values ($r^2 = 0.19$).

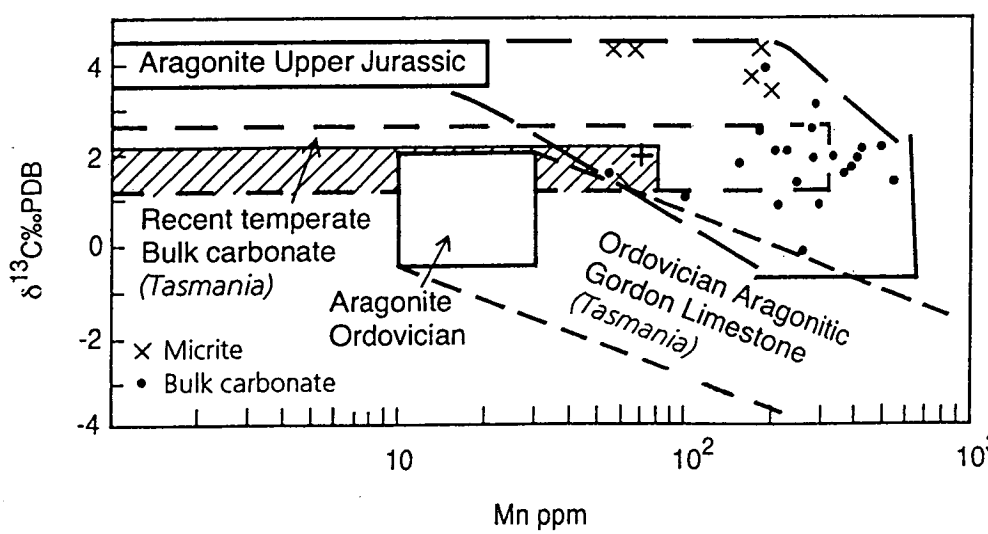

Figure 7.13. Mn-$\delta^{13}C$ variations in aragonitic Mozduran limestone, along with the fields of Recent temperate bulk carbonates from Tasmania, subtropical Gordon Limestone (Rao, 1991) and Upper Jurassic aragonite. Note Mn content increases with increasing lighter $\delta^{13}C$ values.

7.4.3 Correlation and factor analysis in original aragonitic limestones

7.4.3.1 Correlation matrix

The correlation matrix of variables studied (Table 7.3 A) indicates that Mg% (-0.59) is negatively correlated with Ca%, possibly due to incorporation of Mg in the calcite lattice, whereas Mn values are positively correlated with Fe (0.52) and I.R% (0.61). Fe and Mn values are positively correlated because both are related to each other. The positive correlation between Mn and Fe contents is possibly due to terrigenous inputs, which were later incorporated into the diagenetic dLMC calcite lattice, in a reducing marine environment. Fe content shows a strong positive correlation with I.R% (0.72), as Fe is derived from non-carbonate fractions. Fe concentrations are higher in carbonate fractions contaminated with terrigenous clastics, than in pure carbonate fractions. Sr values are positively correlated with the Sr/Na ratio (0.57), whereas the Sr/Na ratio is inversely correlated with $\delta^{18}O$ values (-0.68). The Na values are positively correlated with $\delta^{13}C$ values (0.63), but are inversely related with the Sr/Na ratio (-0.51). The positive correlation between $\delta^{18}O$ and $\delta^{13}C$ values may indicate that these values vary with mineralogy, water temperatures and water depth. No significant relationship exists between values of Na and Mg, and other variables.

7.4.3.2 Factor analysis

Factor analysis establishes relationships between variables and four factors that account for 75% of total variance.

Unrotated factor matrix

The unrotated factor matrix (Table 7.3 B) indicates that:

Factor 1 is positively related with Mn (0.67), Fe (0.78), the Sr/Na ratio (0.72) and I.R% (0.70), and inversely related to Na (-0.61), $\delta^{13}C$ (-0.72) and $\delta^{18}O$ (-0.80) values. The positive relationships between Mn, Fe and I.R% in factor 1 reflect a terrigenous source and incorporation of Fe and Mn in carbonates in a reducing marine environment. The negative values of Na, $\delta^{13}C$ and $\delta^{18}O$ may be related to salinity or seawater temperatures.

Factor 2 is positively correlated with Mg (0.70) and Sr (0.61), and inversely related to Ca (-0.67) and Mn (-0.51). The positive relationships between Mg and Sr may indicate that the Mg and Sr contents are in the calcite lattice. The inverse relationships between Mg and Mn can be attributed to meteoric diagenesis.

Table 7.3. Correlation matrix (A) and unrotated factor matrix (B) of elemental, insoluble residue and isotopic data of aragonitic limestone samples, Mozduran Formation.

A

	Ca%	Mg%	Mn ppm	Fe ppm	Sr ppm	Na ppm	Sr/Na ratio	I.R%	∂13C PDB	∂18O PDB
Ca %	1									
Mg %	**-0.596**	1								
Mn ppm	0.137	-0.391	1							
Fe ppm	-0.284	-0.042	**0.529**	1						
Sr ppm	-0.032	-0.004	-0.303	0.286	1					
Na ppm	0.019	0.019	-0.442	-0.251	0.345	1				
Sr/Na ratio	-0.022	-0.103	0.153	0.487	**0.572**	**-0.512**	1			
I.R %	-0.02	-0.344	**0.619**	**0.727**	0.185	-0.105	0.266	1		
∂13C PDB	0.008	-0.175	-0.392	-0.46	0.105	**0.634**	-0.428	-0.369	1	
∂18O PDB	-0.224	0.229	-0.349	-0.447	-0.386	0.425	**-0.687**	-0.37	**0.586**	1

B

	Factor 1	Factor 2	Factor 3	Factor 4
Ca %	0.055	**-0.671**	0.462	-0.419
Mg %	-0.262	**0.701**	**-0.542**	-0.033
Mn ppm	**0.672**	**-0.516**	-0.214	0.316
Fe ppm	**0.777**	0.245	-0.015	0.473
Sr ppm	0.214	**0.611**	**0.744**	-0.006
Na ppm	**-0.61**	0.124	**0.538**	0.439
Sr/Na ratio	**0.728**	0.391	0.241	-0.358
I.R %	**0.706**	-0.125	0.148	**0.586**
∂13C PDB	**-0.724**	-0.08	0.432	0.235
∂18O PDB	**-0.798**	-0.085	-0.238	0.35

Table 7.4. Correlation matrix (A) and unrotated factor matrix (B) of elemental, insoluble residue and isotopic data of calcitic-aragonitic limestone samples, Mozduran Formation.

A

	Ca%	Mg%	Mn ppm	Fe ppm	Sr ppm	Na ppm	Sr/Na ratio	I.R%	∂13C PDB	∂18O PDB
Ca %	1									
Mg %	**-0.652**	1								
Mn ppm	-0.373	0.185	1							
Fe ppm	-0.414	0.257	**0.803**	1						
Sr ppm	-0.399	0.394	**0.573**	**0.659**	1					
Na ppm	**-0.505**	0.419	0.443	**0.625**	**0.723**	1				
Sr/Na ratio	0.142	-0.069	0.283	0.247	0.431	-0.241	1			
I.R %	-0.328	0.196	**0.608**	0.484	**0.66**	0.446	0.288	1		
∂13C PDB	-0.137	-0.03	-0.018	0.141	-0.102	0.244	-0.272	-0.131	1	
∂18O PDB	-0.182	0.094	-0.252	-0.126	-0.049	0.314	**-0.5**	-0.084	**0.554**	1

B

	Factor 1	Factor 2	Factor 3	Factor 4
Ca %	**-0.645**	-0.391	-0.416	0.248
Mg %	**0.526**	0.293	**0.681**	-0.106
Mn ppm	**0.794**	-0.252	-0.238	-0.3
Fe ppm	**0.842**	-0.076	-0.288	-0.3
Sr ppm	**0.875**	-0.148	-0.022	0.33
Na ppm	**0.776**	0.436	-0.087	0.203
Sr/Na ratio	0.238	**-0.768**	-0.118	0.041
I.R %	**0.733**	-0.22	-0.095	0.37
∂13C PDB	0.032	**0.663**	**-0.548**	-0.265
∂18O PDB	-0.034	**0.837**	-0.188	0.333

Factor 3 is positively correlated with Sr (0.74) and Na (0.54) and inversely related to Mg (-0.54). These relationships may be due to carbonate mineralogies. The positive correlation between Sr and Na is probably due to similar partitioning of these elements in carbonate minerals.

Factor 4 is positively correlated with I.R% (0.59). This reflects a terrigenous source.

In the plot of unrotated factor matrix values for factor 1 and 2 (Fig. 7.14), the horizontal plane is defined at the most positive end by Fe, I.R and Mn, and at the most negative end by Na, $\delta^{18}O$ and $\delta^{13}C$ values. Fe is an important variable in factor 1 (0.78), along with Mn (0.67) and I.R (0.70). Thus, Fe, Mn and Fe and I.R contents are positively related, with r^2 values of 0.30 and 0.38 respectively (Figs. 6.4, 6.5). $\delta^{13}C$ is positively correlated with Na and $\delta^{18}O$ contents, with r^2 values of 0.38 and 0.32 respectively. The positive relationships between $\delta^{13}C$, $\delta^{18}O$ and Na values in this factor analysis may indicate that these values vary with water temperature and water composition. The most positive end of the vertical plane is represented by Mg, and the most negative end by Ca. Ca is an important variable in factor 2 (-0.67), along with Mg (0.70). Thus, Ca and Mg are inversely related, with an r^2 value of 0.31. This may be due to the incorporation of Mg in the calcite lattice.

In the plot of factor matrix values for factor 1 and factor 3 (Fig. 7.14), the vertical plane is defined at the most positive end by Sr and Ca, and at the most negative end by Mg. In this plot, the horizontal plane is defined at the most positive end by Fe, Mn and I.R, and at the most negative end by $\delta^{18}O$, $\delta^{13}C$ and Na.

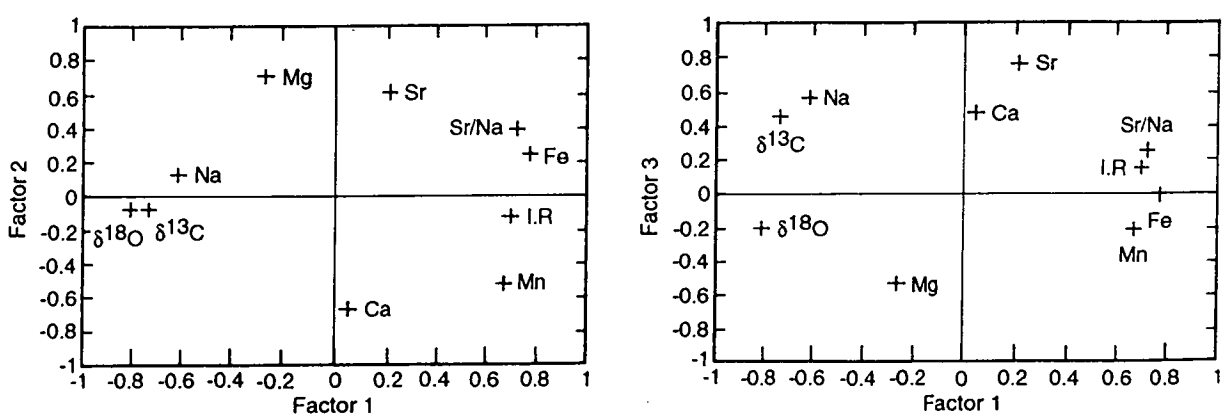

Figure 7.14. Standard unrotated factorial plots indicating the relationship of variables in aragonitic Mozduran limestone samples.

7.4.4 Oxygen versus trace elements in mixed calcitic-aragonitic limestones

7.4.4.1 Oxygen versus strontium

The variation of $\delta^{18}O$ with Sr values in micrites, intraclasts, ooids and bulk carbonates are shown in Fig. 7.15. The Sr values are relatively constant throughout the range of $\delta^{18}O$ values. The lower Sr concentrations and heavier $\delta^{18}O$ values in some micrites can be attributed to the inorganic calcitic mineralogy, whereas, the higher Sr values corresponding to the heavier $\delta^{18}O$ values in a few other micritic samples can be due to aragonite mineralogy, as Sr concentrations are higher in aragonite than calcite (Rao and Adabi, 1992; Rao and Jayawardane, 1994). The very low Sr concentration in most Mozduran limestone samples is possibly due to an inorganic origin of these carbonates. Although a few samples fall within the brachiopod field, the Upper Jurassic brachiopod field falls at the edge of the Mozduran limestone field, indicating that most of the limestone samples are abiotic precipitated calcium carbonates (Fig. 7.15).

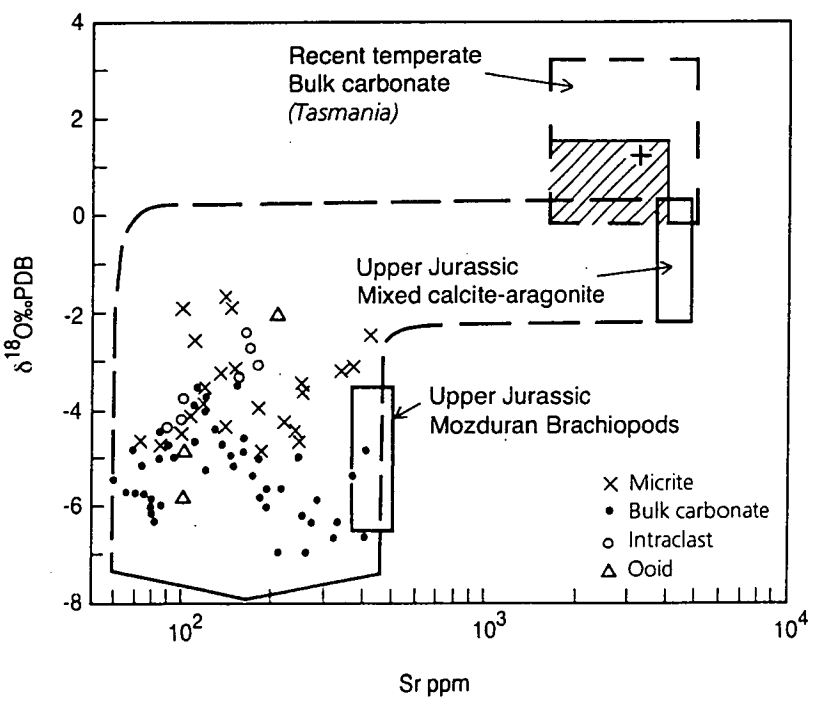

Figure 7.15. Variation of Sr versus $\delta^{18}O$ values in micrites, components and bulk carbonates from the Mozduran limestone (in the relatively deeper part of the basin), along with the fields of Recent temperate bulk carbonates from Tasmania, Upper Jurassic mixed calcite-aragonite and Upper Jurassic Mozduran brachiopods. Note Sr values are relatively constant throughout the range of $\delta^{18}O$ values.

7.4.4.2 Oxygen versus sodium

The Na values show a slight decrease with increasingly lighter $\delta^{18}O$ values (Fig. 7.16). The high Na concentrations (>400 ppm) and heavy $\delta^{18}O$ values (~-2.5 to -3.5‰ PDB) in some micrites can be attributed to the aragonite mineralogy. In contrast, the very low Na concentrations (<200 ppm) and the heavy $\delta^{18}O$ values (~-1.5 to -3.5‰ PDB) in some other micrites, intraclasts and ooids, possibly indicates calcite mineralogy. The very low Na and very light $\delta^{18}O$ values suggest that some of the limestone samples are heavily altered, due to non-marine diagenesis.

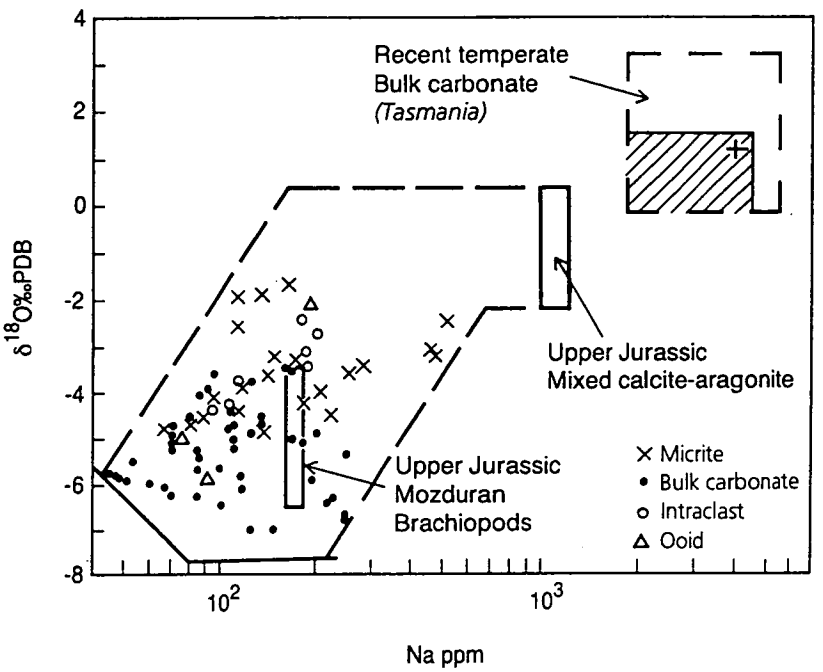

Figure 7.16. Variation of Na versus $\delta^{18}O$ values in micrites, components and bulk carbonates from the Mozduran limestone (in the relatively deeper part of the basin), along with the fields of Recent temperate bulk carbonates from Tasmania, Upper Jurassic mixed calcite-aragonite and Upper Jurassic Mozduran brachiopods. Note Na content slightly increases with increasing heavier $\delta^{18}O$ values.

7.4.4.3 Oxygen versus manganese and iron

The Mn values show a slight increase with increasingly lighter $\delta^{18}O$ values (Fig. 7.17). This trend indicates that most of the samples were affected by non-marine water during diagenesis in semi-reducing (dysaerobic) to reducing conditions. The very heavy $\delta^{18}O$ values and very low Mn concentrations of a few micrite samples may indicate less altered original aragonite mineralogy. As

micrites are assumed to be least affected by non-marine waters, because of low permeability, the relatively heavy $\delta^{18}O$ values and high Mn concentrations in some other micrites, compared to most of the bulk samples, may suggest calcite mineralogy. In Recent temperate bulk carbonates, the Mn concentrations range up to 300 ppm. The Fe values do not correlate with $\delta^{18}O$ values, as indicated by the regression line value of 0.019.

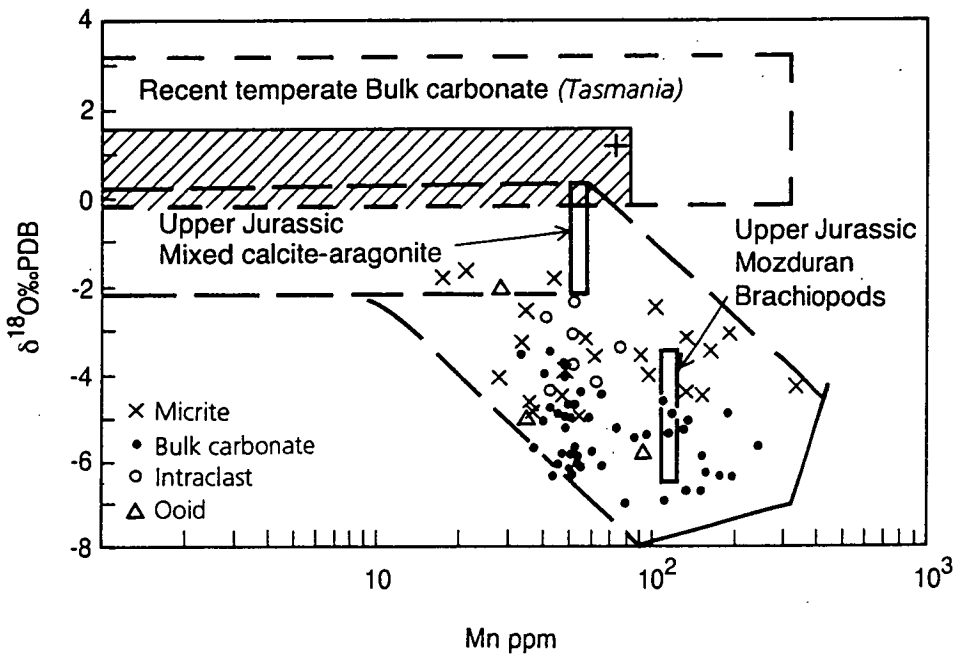

Figure 7.17. Variation of Mn versus $\delta^{18}O$ values in micrites, components and bulk carbonates from the Mozduran limestone (in the relatively deeper part of the basin), along with the fields of Recent temperate bulk carbonates from Tasmania, Upper Jurassic mixed calcite-aragonite and Upper Jurassic Mozduran brachiopods.

7.4.5 Carbon versus trace elements

7.4.5.1 Carbon versus strontium

The variations of $\delta^{13}C$ with Sr values are illustrated in Fig. 7.18. The Sr values slightly decrease with increasingly lighter $\delta^{13}C$ values. Experimental studies (Rubinston and Clayton, 1969; Romanek et al., 1992) have indicated that the $\delta^{13}C$ values are enriched in aragonite, relative to calcite, by 1.7‰. In a few micritic samples, Sr values increase with heavier $\delta^{13}C$ values, possibly indicating aragonite mineralogy. However, the heavy $\delta^{13}C$ values of some micrites and intraclasts, which correspond to low Sr concentrations, can be due to calcitic mineralogy. Thus, the pattern of $\delta^{13}C$-Sr values indicate mixed carbonate

mineralogy. The heaviest $\delta^{13}C$ values of +4.5‰ PDB, which correspond to the highest Sr values, probably represent marine $\delta^{13}C$ values for these limestones. The heaviest $\delta^{13}C$ values and the highest Sr concentrations are in micrites, indicating that micrites are less affected by diagenesis, as the permeability of micrites is low.

The Upper Jurassic brachiopod field falls at the edge of the Mozduran limestone field, with a few samples falling within the brachiopod field. Most of the samples fall within the range of +2 to + 4‰ PDB $\delta^{13}C$ and 70 to 300 ppm Sr values (Fig. 7.18). As $\delta^{13}C$ values are very low in freshwater, the relatively heavy $\delta^{13}C$ values in most of the samples studied, suggest that these limestones were least affected by vadose meteoric diagenesis. The very low Sr values in these limestones can be due to the inorganic origin (abiotic calcite) of these carbonates, which were subsequently affected mostly by burial waters during diagenesis.

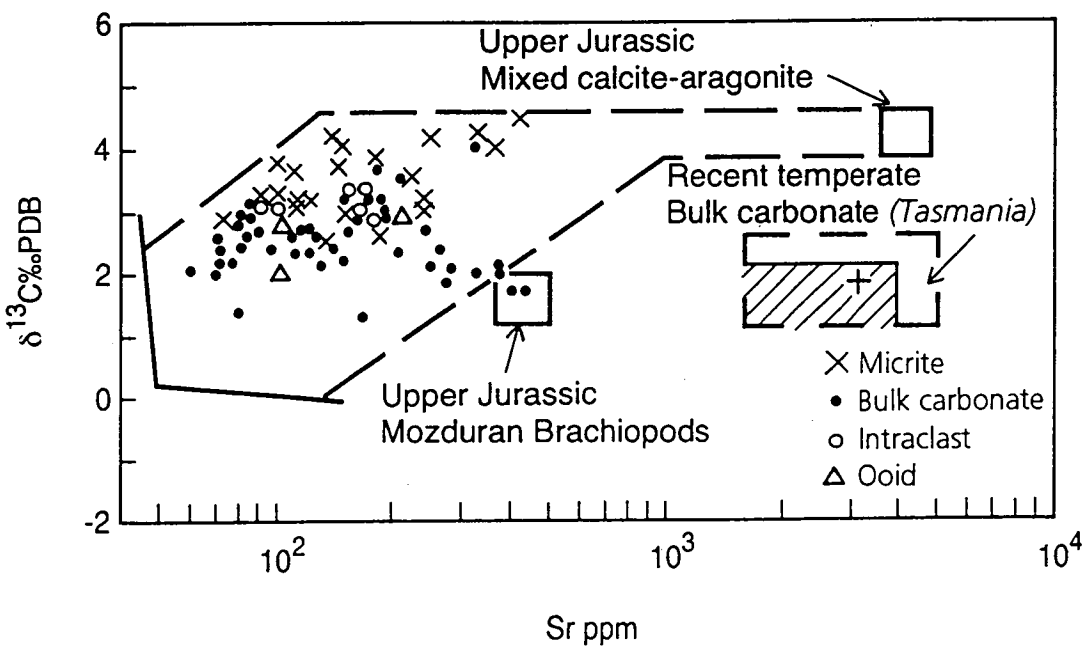

Figure 7.18. Variation of Sr versus $\delta^{13}C$ values in micrites, components and bulk carbonates from the Mozduran limestone (in the relatively deeper part of the basin), along with the fields of Recent temperate bulk carbonates from Tasmania, Upper Jurassic mixed calcite-aragonite and Upper Jurassic Mozduran brachiopods. Note Sr values increase with increasing heavier $\delta^{13}C$ values.

7.4.5.2 Carbon versus sodium

The Na values show a slight positive relationship with $\delta^{13}C$ (Fig. 7.19). The high Na concentrations (~300 to >500 ppm) and heavy $\delta^{13}C$ values (>+4‰ PDB) in some micrites can be attributed to the aragonite mineralogy. In

contrast, the low Na concentrations (<200 ppm) and the heavy $\delta^{13}C$ values (with a range of ~+3 to > + 4‰ PDB) in some other micrites and intraclasts, may indicate calcite mineralogy. The very low Na and relatively light $\delta^{13}C$ values in some bulk carbonates, suggest that these samples are altered due to low-Mg calcite precipitation during diagenesis. The Upper Jurassic brachiopod field falls at the edge of the Mozduran limestone field.

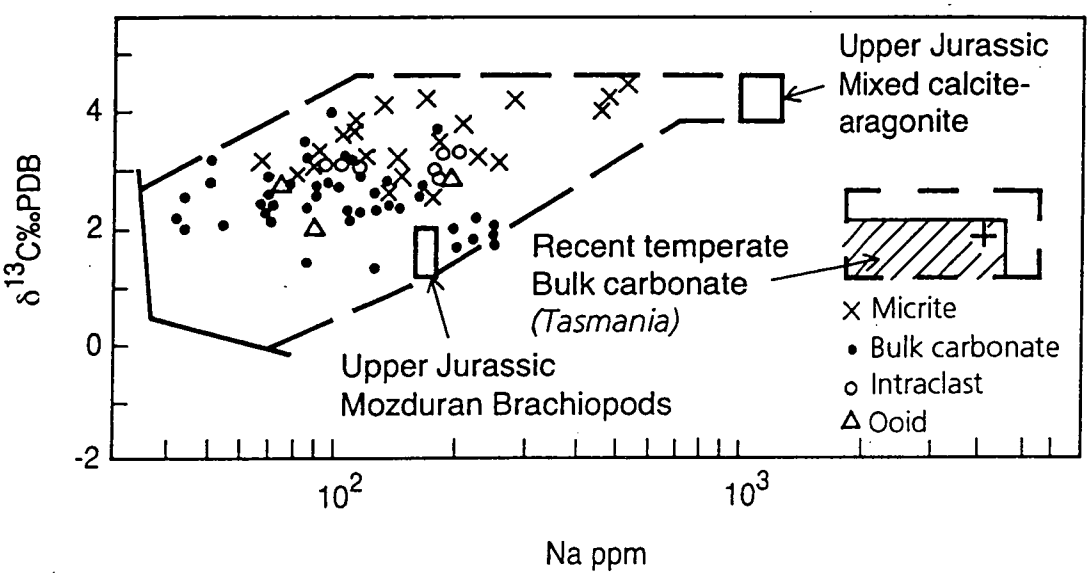

Figure 7.19. Variation of Na versus $\delta^{13}C$ values in micrites, components and bulk carbonates from the Mozduran limestone (in the relatively deeper part of the basin), along with the fields of Recent temperate bulk carbonates from Tasmania, Upper Jurassic mixed calcite-aragonite and Upper Jurassic Mozduran brachiopods. Note Na content slightly increases with increasingly heavier $\delta^{13}C$ values.

7.4.5.3 Carbon versus manganese and iron

The plot of $\delta^{13}C$-Mn values (Fig. 7.20) shows that most of the samples fall within, or at the edge of the Recent temperate bulk carbonate field. The Upper Jurassic brachiopod field also falls within the field of Recent temperate bulk carbonates, due to their marine origin. The lowest Mn values (17 ppm) in these limestones corresponds to +4.1‰ PDB $\delta^{13}C$, which is the Upper Jurassic marine carbonate value. The heavy $\delta^{13}C$ values (>+3‰ PDB) and the very low Mn concentrations (<40 ppm) in some micrites, suggesting the least diagenetic change, possibly indicates an original aragonite mineralogy. Mn content is <20 ppm in Recent aragonitic sediments. In contrast, the heavy $\delta^{13}C$ values (>+3‰ PDB) and relatively higher Mn concentrations (range from ~100 to >300 ppm) in

some other micrites, can be due to calcitic mineralogy. Thus, the pattern of $\delta^{13}C$-Mn values suggests mixed carbonate mineralogy.

The Fe values do not show any correlation with $\delta^{13}C$ values ($r^2 = 0.034$). Except for a few samples that contain unusually high Fe, the majority of Fe values are generally uniform throughout the range of $\delta^{13}C$ values. Meteoric diagenesis results in an increase of both Mn and Fe concentrations, with increasingly lighter $\delta^{13}C$, which is not the case in the samples studied.

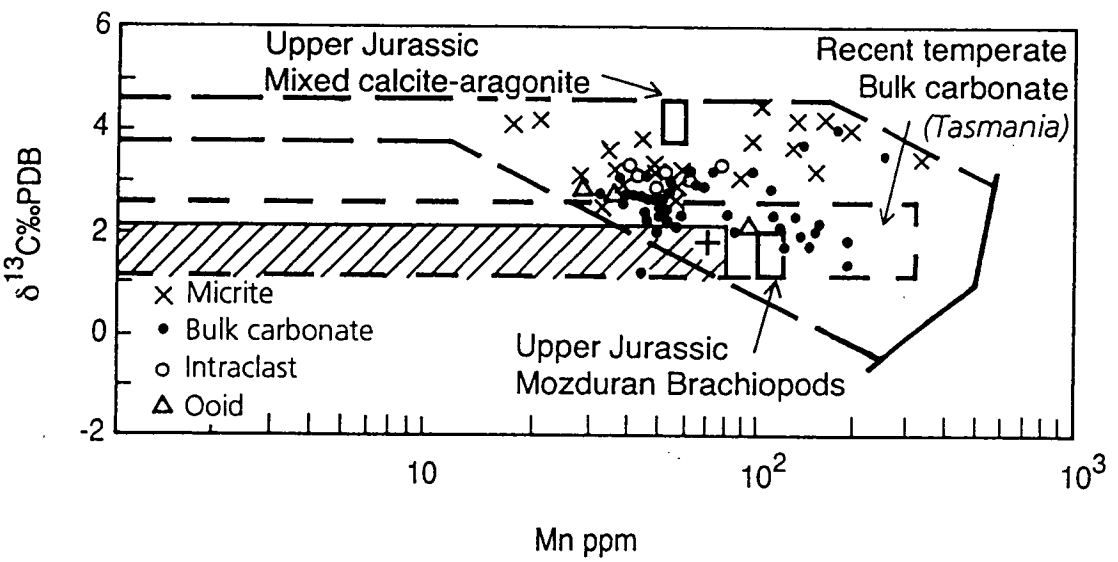

Figure 7.20. Variation of Mn versus $\delta^{13}C$ values in micrites, components and bulk carbonates from the Mozduran limestone (in the relatively deeper part of the basin), along with the fields of Recent temperate bulk carbonates from Tasmania, Upper Jurassic mixed calcite-aragonite and Upper Jurassic Mozduran brachiopods.

7.4.6 Correlation and factor analysis in mixed calcitic-aragonitic limestones

7.4.6.1 Correlation matrix

The correlation matrix of variables studied (Table 7.4 A) indicates that Ca is inversely related to Mg (-0.65) and Na (-0.50), due to the incorporation of Mg and Na in the calcite lattice. Incorporation of Mg in calcite in a marine environment is demonstrated by the common occurrence of high-Mg calcites in tropical to temperate shallow marine limestones. Substitution of Na in the calcite lattice takes place in the marine environment. Mn values are positively correlated with Fe (0.8), I.R (0.61) and Sr (0.57). The positive relationships between Mn and Fe, with a r^2 value of 0.65 (Fig. 6.13), Mn and I.R%, with a r^2 value of 0.41, and between Fe and I.R%, with a r^2 value of 0.32 (Fig. 6.12),

possibly indicate a terrigenous source. Fe and Mn contents increase with increasing insoluble residue%, and with the incorporation of Fe and Mn in carbonates in a reducing marine environment.

Slightly positive relationships between Mn and Sr, with a r^2 value of 0.35, may indicate that Sr is derived to some extent from non-carbonate fractions (clay minerals). Fe content is positively correlated with Sr (0.66) and Na (0.62). This may be due to the incorporation of these elements in carbonates in a dysaeraobic marine environment. The weak relationship between Fe and I.R (0.48), and good relationships between Mn, Fe and I.R in the correlation matrix, may indicate that Fe contents are partly derived from I.R and partly from marine seawater. Sr content is positively correlated with Na (0.72), and I.R (0.66). This positive relationship between Sr and Na is probably due to similar partitioning of these elements in carbonate minerals. The positive relationship between Sr and I.R is possibly due to the derivation of Sr from non-carbonate clay minerals (contamination). The Sr/Na ratio is inversely related to $\delta^{18}O$ (-0.5), whereas $\delta^{13}C$ is positively correlated with $\delta^{18}O$ values (0.55). The positive loadings between $\delta^{13}C$ and $\delta^{18}O$ values indicate that $\delta^{13}C$ and $\delta^{18}O$ values vary with water temperature and water depth.

7.4.6.2 Factor analysis

Factor analysis of data comprising major and minor elements, oxygen and carbon isotopes in bulk carbonates, micrites, intraclasts and ooids, along with insoluble residue, indicates that four factors account for 75% of total variance.

Unrotated factor matrix

The unrotated factor matrix (Table 7.4 B) indicates:

Factor 1 is positively correlated with Mg (0.52), Mn (0.79), Fe (0.84), Sr (0.87), Na (0.78) and I.R (0.73), and negatively correlated with Ca (-0.64). The positive correlation between Mg and Fe, and Mn and Sr contents, may be due to marine diagenesis and seawater composition.

Factor 2 is positively correlated with $\delta^{13}C$ (0.66) and $\delta^{18}O$ (0.84) values, and inversely related to the Sr/Na (-0.77) ratio.

Factor 3 is inversely related to $\delta^{13}C$ (-0.55) and positively with Mg (0.68).

Factor 4. No significant relationship exists between variables.

The plot of unrotated factor matrix values of factor 1 and 2 (Fig. 7.21)

illustrates that the factor 1 plane is defined by opposition between Fe, Mn, Sr, Mg, Na, I.R. and Ca contents, whereas the factor 2 plane is defined by the Sr/Na ratio and $\delta^{18}O$ and $\delta^{13}C$ contents. The plot of unrotated factor loadings of 1 and 3 (Fig. 7.21) indicates that the factor 3 plane is inversely related to $\delta^{13}C$ values and positively related to Mg concentration, whereas the factor 1 plane is inversely related to Ca and positively related to Mg, Mn, Fe, Sr, Na and I.R contents.

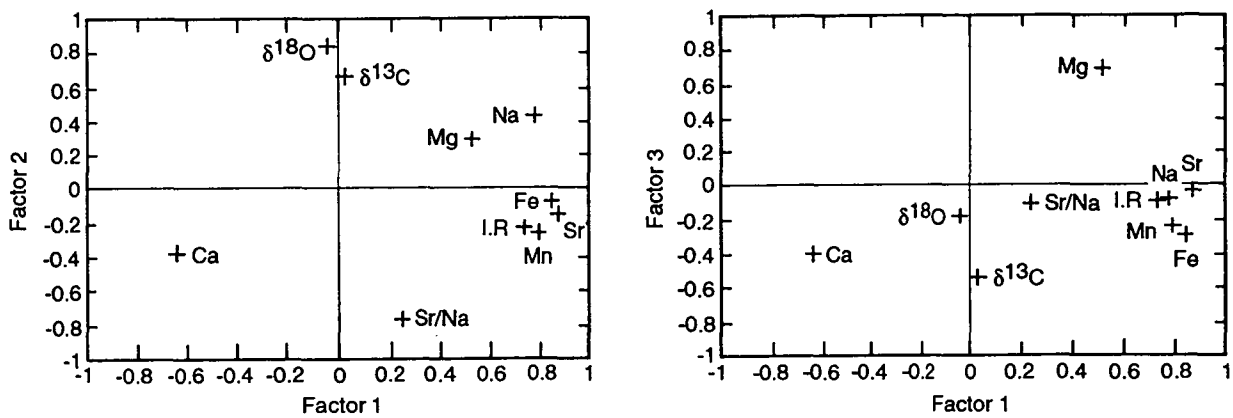

Figure 7.21. Standard unrotated factorial plots indicating the relationship of variables in the mixed calcitic-aragonitic Mozduran limestone samples.

7.5 Limestone Cements

Trace element and stable carbon and oxygen isotope analysis, in conjunction with cathodoluminescence petrography, have been used to gain an understanding of calcite cement generations in different settings (Marshall and Ashton, 1980; James and Choquette, 1984; Meyers and Lohmann, 1985; Lohmann, 1988; Nelson and Smith, 1996). One of the most important aspects arising from these studies is that the calcite cements may reflect a wide variation in composition, indicating marine to meteoric and /or burial environments.

In the present study, the void-filling sparry calcite cements (such as, equant, syntaxial, platy, and poikilitic) and calcite veins were drilled from the Mozduran limestone samples for trace element and isotopic analysis. Elemental and isotopic compositions of these carbonate cements, along with the calcite veins are listed in Table A5. 8 in Appendix 5.

7.5.1 Oxygen and carbon isotopes

Oxygen and carbon isotopic values of the Mozduran pore-filling sparry calcite cements in marine, meteoric, and burial settings are shown in Fig. 7.22. The marine origin of the calcite (turbid syntaxial overgrowth) cement is consistent with isotopic, trace element, and cathodoluminescence evidence (Table A5.8, and

Fig. 4.3 D). The relatively elevated Sr (321 ppm) and Na (107 ppm) contents, corresponding to heavy $\delta^{18}O$ (-2.4‰ PDB) and $\delta^{13}C$ (+3.6‰ PDB) values, along with blotchy luminescence (Fig. 4.3 D), compared to other calcite cements, may indicate marine origin. The field of Upper Jurrasic marine calcite isotopic values, which is very close to the value of the turbid syntaxial overgrowth cement, is further evidence for marine origin (Fig. 7.22). The very low Fe (32 ppm) and Mn (85 ppm) concentrations of the turbid syntaxial overgrowth cement may also support precipitation from marine waters (Table A5.8).

The geochemical data, along with cathodoluminescence petrography and calcite crystal morphology from other calcite cements, show no evidence of marine signature. Therefore, precipitation of the sparry calcite cements from meteoric and burial fluids is more likely.

Isotopic and trace element compositions, along with cathodoluminescence petrography of four equant (drusy) and platy sparry calcite cements in the Mozduran limestones support meteoric origin. The $\delta^{18}O$ values of these cements range from -6‰ to -6.6‰ PDB, with a mean average $\delta^{18}O$ value of -6.2‰ PDB, whereas, the $\delta^{13}C$ values range from +1.1‰ to -2.8‰ PDB, with an average value of -1.6‰ PDB. The shift in $\delta^{13}C$ to lighter values is the most diagnostic feature of these sparry calcite cements. The $\delta^{18}O$ and $\delta^{13}C$ values of these cements fall within the meteoric diagenetic trends of Lohmann (1988). This can be due to the presence of isotopically light soil-gas carbon dioxide (Allan and Matthews, 1982). The $\delta^{13}C$ composition of precipitated carbonates in the zone of soil weathering processes is near to -10‰ (Nelson and Smith, 1996). The relatively narrow range of $\delta^{13}C$ compositions present in these calcite cements is consistent with the decreased development of soil due to an arid climate during the Upper Jurassic. The positive to negative range of $\delta^{13}C$ values, indicate that meteoric waters were buffered from dissolution of the host marine limestone and its components, with the least rock-water interaction at the more depleted end of the $\delta^{13}C$ range. Therefore, the range of $\delta^{18}O$ and $\delta^{13}C$ values, along with the very low concentration of Sr (average 26 ppm) and Na (average 30 ppm), and bright-luminescent nature of these cements (Figs. 4.4 B, D, 4.5 B, D, F), compared with marine calcite cement, possibly indicates meteoric origin. The Mn and Fe contents of these cements are higher than marine calcite cement (Table A5.8). These cements are particularly well developed in samples from the shallowest part of the basin, which were under an increasing influence of fresh water recharge during periods of basin shallowing, due to either uplifing of the hinterland or eustatic lowering of sea level.

The isotopic and trace element compositions of nine other sparry calcite cements (such as poikilitic, equant and syntaxial), along with CL petrography, support burial diagenesis. The $\delta^{18}O$ values of these cements range from -4.4‰ to -7.6‰ PDB, with an average value of -6‰ PDB (Fig. 7.22). The $\delta^{13}C$ values range from +2‰ to +3.8‰ PDB, with an average value of +2.9‰ PDB. The relatively wide variation in $\delta^{18}O$ and narrower variation in $\delta^{13}C$ values of these cements are similar to the burial isotopic model suggested by Al-Aasm and Veizer (1986) and Nelson and Smith (1996). The carbon isotopic signature of burial spar cement is usually similar to a marine value or little depleted, because most of the carbon is derived from host limestones. There is also less fractionation of $^{13}C/^{12}C$ with increasing temperature, compared with $O^{18/16}O$. The CL petrography (dull to non-luminesecnt, Figs. 4.6 B, D, F, and 4.7 B, D), calcite crystal morphologies (Figs. 4.7 A-D), and trace element compositions (low Sr and Na and relatively higher Fe and Mn) are also in favor of burial origin. These cements are more abundant in samples from the relatively deeper part of the basin. The $\delta^{18}O$-$\delta^{13}C$ plots of the Mozduran limestone cements are in close correspondence with those of Nelson and Smith (1996).

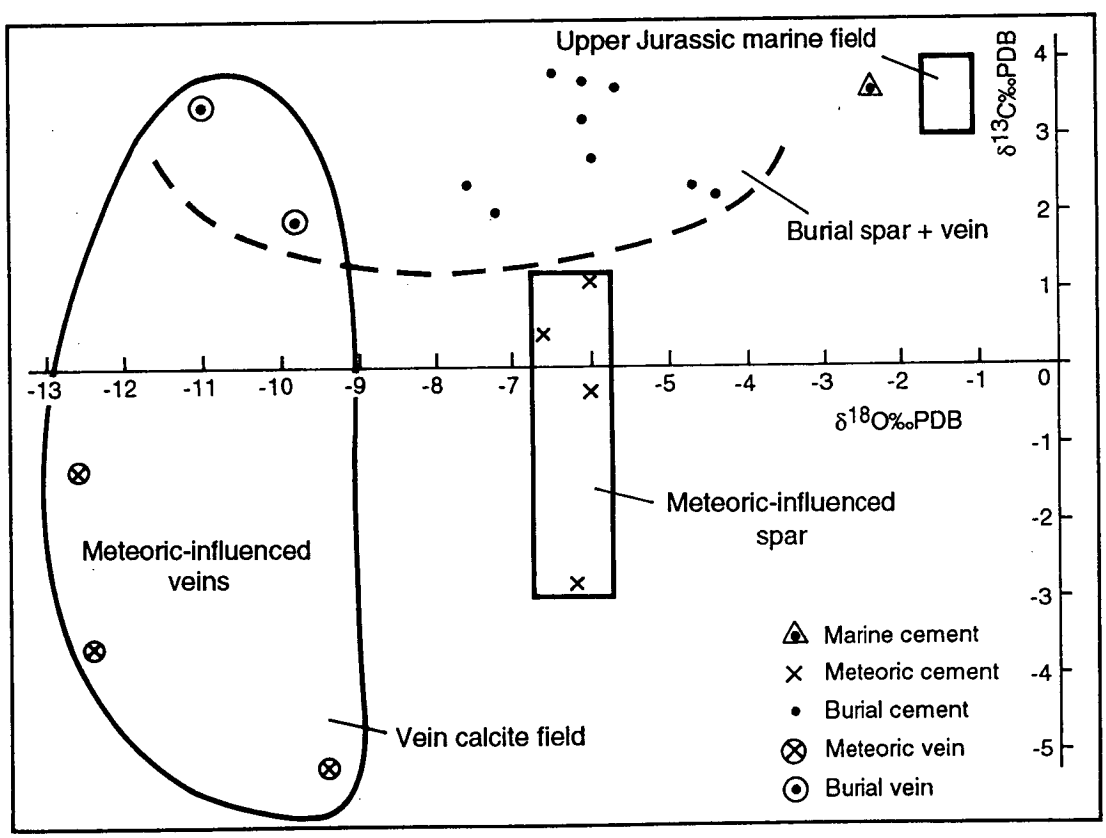

Figure 7.22. $\delta^{18}O$-$\delta^{13}C$ plots for some Upper Jurassic limestone cements and calcite veins. Note multiple generation of calcite cements in marine, meteoric and burial settings.

7.5.2 Covariation of isotopes and trace elements

7.5.2.1 Oxygen versus trace elements

The trend of Sr and Na variations with $\delta^{18}O$ show that Sr and Na contents increase with increasing heavier $\delta^{18}O$ values (Fig. 7.23). This may be due to increasing amounts of rock/water interaction. There is no trend between Mn and Fe variations with $\delta^{18}O$ values.

7.5.2.2 Carbon versus trace elements

The trend of Sr variation with $\delta^{13}C$ shows that Sr content slightly increases with increasingly heavier $\delta^{13}C$ values (r^2= 0.2). The plot of Na-$\delta^{13}C$ values shows that Na and $\delta^{13}C$ are positively related, with a r^2 value of 0.64 (Fig. 7.24). $\delta^{13}C$ and Mn are inversely related, with a r^2 value of 0.66 (Fig. 7.24). The plot of Fe-$\delta^{13}C$ values shows that Fe content slightly increases with increasingly lighter $\delta^{13}C$ values (r^2= 0.3). The inverse relationship between Mn and Fe with $\delta^{13}C$ values is due to non-marine diagenesis.

7.6 Vein Calcites

7.6.1 Oxygen and carbon isotopes

The oxygen and carbon isotope compositions of some vein calcites are plotted on Fig. 7.22. The $\delta^{18}O$ values of vein calcites range from -9.4 to -12.6‰ PDB with a mean value of -11‰ PDB, whereas the $\delta^{13}C$ values range from 3.4 to -5.2‰ PDB with a mean value of -1.1‰ PDB. The very depleted $\delta^{18}O$ values of all vein calcites, compared to limestone cements, indicates that they have formed under higher temperatures. The very depleted $\delta^{18}O$ values of a few vein calcites, corresponding to the heavy $\delta^{13}C$ values (ranging from +1.9‰ to +3.4‰ PDB), along with the dull luminescence, may suggest formation under higher temperatures during post-litification basin subsidence in a burial depth possibly greater than 2 km. However, the moderately depleted $\delta^{13}C$ values of other vein calcites, ranging from -1.3‰ to -5.2‰ PDB (Fig. 7.22), may be due to precipitation under the influence of hot circulating meteoric waters, during uplift of the Mozduran Formation to the surface in the late Miocene. The multiple zonation of bright-yellow luminescence present in these vein calcites (Fig. 4.7 F) also supports this interpretation. The lightest $\delta^{18}O$ value in vein calcites, corresponding to -12.6‰ PDB, assuming a δ_W= -1.2 SMOW for the Upper

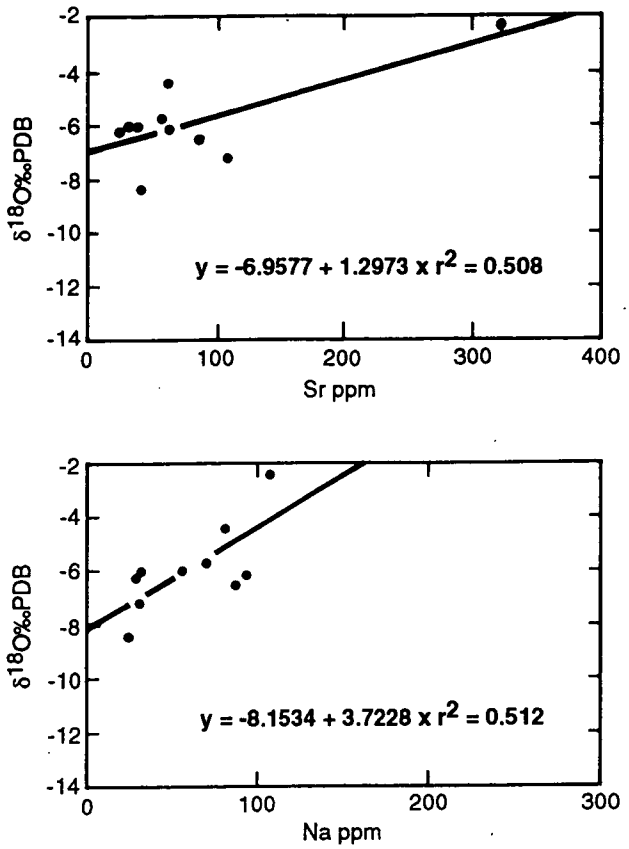

Figure 7.23. Variation of $\delta^{18}O$ values against Sr and Na, along with regression lines.

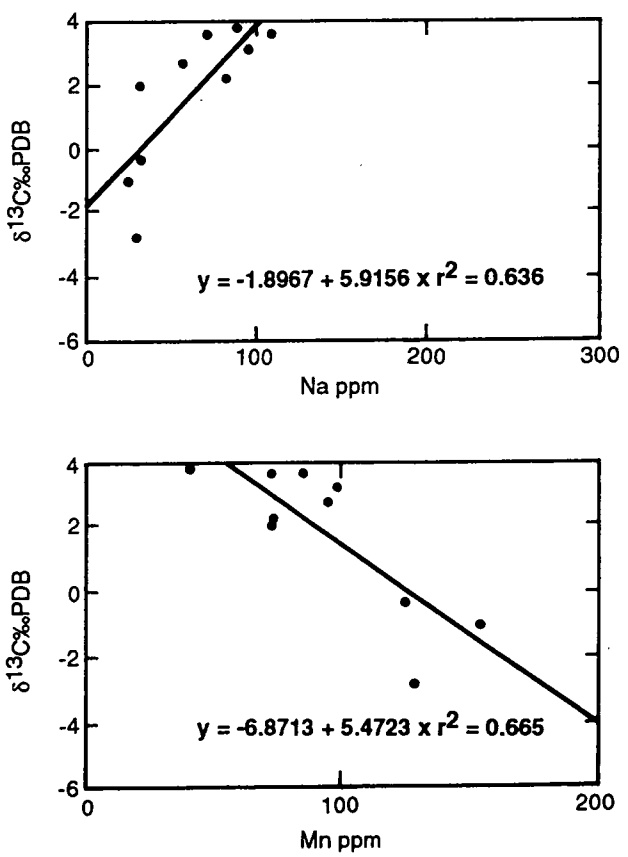

Figure 7.24. Variation of $\delta^{13}C$ values against Na and Mn, along with regression lines.

Jurassic, gives a diagenetic temperature of ~80° C. However, by assuming a δ_W=0 SMOW (present value), the lightest $\delta^{18}O$ value gives a diagenetic temperature of ~90° C. These diagenetic temperatures indicate the influence of hot fluid during vein calcite formation. The principles of oxygen isotope paleothermometry and temperature equations are presented below.

7.7 Water Temperature

7.7.1 Principles of oxygen isotope paleothermometry

Paleotemperature determination in the marine carbonate realm using oxygen isotopic ratios in skeletal materials pioneered by Urey (1947) and his colleagues (Epstein et al. 1953; Emiliani, 1954), are now well established (e.g., Hudson and Anderson, 1989; Marshall, 1992) and widely used. This method is based on the observation that the difference between the $^{18}O/^{16}O$ ratio of calcium carbonate, and the water from which it precipitates, is temperature dependent (Spicer and Corfield, 1992). Thus, for the known $^{18}O/^{16}O$ ratio of water, the $^{18}O/^{16}O$ ratios of the mineral, are dependent only on the temperature at similar salinity values. In the warmer water, oxygen isotope values are lighter, while in cooler waters, they are heavier. However, the primary environmental isotopic signals may be obscured in rocks which are affected by post-depositional diagenetic alteration. It has been suggested that the best record of paleotemperature comes from the analysis of pristine, unaltered or least-altered material, with a stable mineralogy or low initial diagenetic potential, such as fossils and abiogenic cements (Gonzalez and Lohmann, 1985; Marshall, 1992).

The carbon and oxygen isotope analysis in carbonates are expressed in conventional 'δ' notation as parts per thousand (per mil‰) difference between an isotopic ratio ($^{18}O/^{16}O$, $^{13}C/^{12}C$) in a sample, compared to the same ratio from that in a standard. For oxygen isotopes this is written as:

$$\delta^{18}O_{sample} = \frac{[\,(\,^{18}O/^{16}O_{sample} - {}^{18}O/^{16}O_{standard}\,)\,]\,1000}{(\,^{18}O/^{16}O_{standard}\,)}$$

A similar equation applies to carbon.

Two standards have been widely used in reporting $\delta^{18}O$ values: the PDB and SMOW standard. The PDB standard is based on the oxygen isotope ratio of a late Cretaceous belemnite from the Pee Dee Formation in South Carolina, USA. Many isotope carbonate sedimentalogists use oxygen relative to the PDB standard. For water and minerals other than carbonates the standard is SMOW-

Standard Mean Ocean Water (see Anderson and Arthur, 1983). The two standards are related by a simple equation (Friedman and O'Neil, 1977):

$$\delta^{18}O_{calcite}\ (vs.\ SMOW) = 1.03086\ \delta^{18}O_{calcite}\ (vs.\ PDB) + 30.86$$

$\delta^{13}C$ values are reported relative to the PDB calcium carbonate standard.

7.7.2 Temperature equations

One of the most important uses of oxygen isotopes in carbonates is as geothermometers (Morse and Mackenzie, 1990). As different carbonate minerals have slight differences in fractionation, paleotemperature equations are different for each mineral. Isotope fractionation is pressure independent, giving it an advantage over other geothermometers, which are generally both temperature and pressure dependent (Morse and Mackenzie, 1990). Ambient water temperatures at which calcite precipitates were calculated using the equation of Epstein et al. (1953) and Craig (1965), and that modified by Anderson and Arthur (1983).

$$T\ (^{\circ}C) = 16.0 - 4.14\ (\delta_C - \delta_W) + 0.13\ (\delta_C - \delta_W)^2 \qquad (1)$$

where T is temperature, δ_C is the oxygen isotope ratio in calcite at 25° C relative to the PDB international standard and δ_W is the oxygen isotope ratio of the water from which the calcite was precipitated relative to the SMOW standard, assuming present-day seawater values of 0 (SMOW).

This equation is derived from measurments of the isotopic composition of the shells of calcareous organisms (molluscs) grown under different conditions, and was used in preference to the equation of O'Neil et al. (1969), which was derived from the experimental inorganic precipitation of calcite over the temperature range 0-500° C. The temperature equation indicates that $\delta^{18}O_{calcite}$ decreases by approximately 1‰ for every 4° C increase in temperature.

It has been suggested that $\delta^{18}O$ values of ancient low Mg-calcite can change during diagenesis, but the heavy $\delta^{13}C$ values tend to be near marine values, despite prolonged meteoric diagenesis (Veizer et al., 1986; Popp et al., 1986; Lohmann, 1988; Wadleigh and Veizer, 1992). Therefore, the temperatures of calcite formation in the Mozduran limestones were also calculated from marine $\delta^{13}C$ values of calcite using the equation of Fontes and Pouchan (1975):

$$T°C = 147.7 - 14.8\ (\delta c - \delta gas) + 0.266\ (\delta c - \delta gas)^2 \qquad (2)$$

Where δc is the $\delta^{13}C$ composition of CO_2 produced from carbonates at 25° C and

δgas is the $\delta^{13}C$ composition of CO_2 in equilibrium with the atmosphere.

Only sea surface waters are in equilibrium with $\delta^{13}C$ in the atmosphere. Therefore, the above temperature equation can only be applied to shallow marine carbonates which are in equilibrium with sea surface water.

7.7.3 Upper Jurassic marine paleotemperatures

In calculating the water temperatures, it has been assumed that the Jurassic seawater was free from icecaps (Ager, 1975; Frakes, 1979; Valdes and Sellwood, 1992) and, therefore, a δ_W of -1.2‰ PDB (equivalent to 16° C) was used (Shackleton and Kennett, 1975; Marshall and Ashton, 1980; Anderson and Arthur, 1983; Lohmann and Walker, 1989; Price and Sellwood, 1994).

The least-altered marine micrite $\delta^{18}O$ values of -1.2‰ PDB from the shallowest part of the basin, corresponding to the lowest Mn and Fe values and very high Sr and Na values, have been used to calculate ambient water temperature. This calculation gives an ambient temperature of 16° C, and is in general agreement with the calculated paleotemperature obtained from belemnite fossils from the Upper Jurassic of Mallorca, Spain, which range from 13.4 to 16° C, with an average of 14.7° C (Price and Sellwood, 1994). Determination of paleotemperature based on Kimmeridgian-Tithonian belemnites from New Zealand (Stevens and Clayton, 1971) and the former Soviet Union (Stevens, 1971), gives a paleotemperature of about 14° C at about 75° S latitude (this is at least 7° C warmer than present-day temperatures), and about 16° C at about 29-40° N latitude.

However, the paleoecology of belemnites is relatively unclear and the range of their paleodepth is still controversial (Doyle, 1992). The δ_W value of 0 (SMOW) used in the paleotemperature equation which corresponds to the present-day seawater value with large icecaps, gives an ambient water temperature of 21° C, which is about 5° C higher than previously predicted. The average heaviest $\delta^{18}O$ values of -2.2‰ PDB in micrites, corresponding to the lowest Mn and Fe values and very high Sr and Na values, gives a temperature of about 20° C. Brachiopods are considered to have a high potential to record original isotopic signatures, due to their low-Mg calcite mineralogy, which is relatively insoluble and resistant to diagenesis (Popp et al., 1986; Veizer et al., 1986; Hudson and Anderson, 1989; Marshall, 1992). Forthermore, Recent examples appear to secrete their shells in isotopic equilibrium (Lepzelter et al., 1983; Morrison and Brand, 1986; Brand and Morrison, 1987). Detailed studies (using cathodoluminescence) have, however, shown that brachiopods can undergo

diagenetic alteration, showing high to low levels of luminescence (Rush and Chafetz, 1990). In contrast, recent work using hot-cathode cathodoluminescence by Barbin et al. (1991) has revealed weak luminescence in the calcareous shells of living organisms, regardless of mineralogical composition. It was concluded that luminescence is not a reliable indicator of diagenetic alteration.

Two of the brachiopod samples studied from the Mozduran limestones fall close to the temperature equilibrium line of calcite, which indicates that these brachiopods are in equilibrium with shallow seawater of tropical temperatures and an atmospheric CO_2 value of -6.7‰ (Figs. 7.3 and 7.6). The lighter $\delta^{18}O$ values in other brachiopods, that fall on the aragonite-calcite equilibrium line, might have undergone diagenetic alteration and thus yield higher temperature estimates than the original depositional temperatures. These brachiopod values were not used in this study. The heaviest brachiopod $\delta^{18}O$ value of -3.5‰ PDB, corresponding to the highest Sr and Na values, gives an ambient temperature of 26° C. This calculated paleotemperature obtained from the Mozduran brachiopods is similar to the temperature calculated from the Recent low-Mg calcite brachiopods (23° C) in the tropical region (data from T. F. Anderson, Fig. 7.7). However, the average heaviest brachiopod $\delta^{18}O$ value of about -4‰ PDB, gives an ambient temperature of 29° C. Therefore, the Mozduran limestones from the shallowest part of the basin were deposited at a temperature range of 16° to 26° or 29° C, indicating relatively large temperature fluctuations.

From the relatively deeper part of the basin, the least-altered marine micrite $\delta^{18}O$ value of -1.7‰ PDB, gives a seawater temperature of 18° C, using the equation of calcite isotope thermometry. The heaviest isotopic values of marine calcite cements are believed to record original isotopic signatures (Gonzalez and Lohmann, 1985; Given and Lohmann, 1986; Lohmann and Walker, 1989; Marshall, 1992). It has also been suggested that inorganically precipitated marine cements are more reliable indicators of the physio-chemical conditions of precipitation than co-ocurring skeletal carbonates (Gonzalez and Lohmann, 1985). Therefore, the heaviest $\delta^{18}O$ values of -2.4‰ PDB of marine calcite cements were used to calculate paleotemperature. The marine cement gives an ambient seawater temperature of 21° C. These calculations thus indicate that the depositional temperature was about 20° C in the relatively deeper part of the basin.

The seawater temperatures predicted in this study also fall within the range of Upper Jurassic seawater temperatures calculated from macrofossil data of mid and northern Europe (Hudson and Anderson, 1989; in their Fig. 3).

The equation of Fontes and Pouchan (1975) was used to calculate seawater temperature from $\delta^{13}C$ values of calcite. Using the heaviest $\delta^{13}C$ value in micrite (4.3‰ PDB), corresponding to $\delta^{18}O$ values of -1.2‰ PDB, and a present day atmospheric $\delta^{13}C$ value of - 7.2‰, gives a calculated temperature of about 12° C, which is 4° C cooler than values predicted by $\delta^{18}O$. Assuming that the paleotemperatures calculated by $\delta^{18}O$ are correct, it is possible to back calculate the Upper Jurassic PCO_2 level using the $\delta^{13}C$ value. This produced an atmospheric $\delta^{13}C$ value of -6.7‰ (which is about 0.5‰ lower than present day values) for the Upper Jurassic (Adabi and Rao, 1996). This gives a similar temperature to that predicted by $\delta^{18}O$ for the shallowest part of the basin. As different genera of brachiopods show different levels of biochemical fractionation of $\delta^{13}C$ (Veizer et al., 1986), the paleotemperatures have not been calculated from $\delta^{13}C$ values of these brachiopods. The heaviest $\delta^{13}C$ value in micrite and cement from the relatively deeper part of the basin, using an atmospheric $\delta^{13}C$ value of -6.7‰, gives a similar temperature to that predicted by $\delta^{18}O$ values.

7.7.4 Mid Jurassic marine paleotemperatures

The heaviest $\delta^{18}O$ values of marine calcite cement for mid Jurassic carbonates from England (0.4‰; Marshall and Ashton 1980) and Upper Jurassic micrite from Mozduran limestone (Iran), give a cold seawater temperature of 8° C and a cool surface seawater temperature of 16° C, assuming a $\delta^{18}O$ value of -1.2‰ for Jurassic seawater (Adabi and Rao, 1996, Fig. 7.3). However, the heaviest $\delta^{18}O$ values from the Upper Jurassic brachiopods of Iran (~-3.5‰), mid Jurassic oysters from England (-2.8‰; Marshall and Ashton, 1980) and belemnites of the late mid Jurassic from Scotland (-0.5‰; Tan et al., 1970), indicate warmer temperatures of 26° C (to 29° C) for Iran, 23° C for England, and a relatively cool to cold temperature of 13° C for Scotland (Adabi and Rao, 1996, Fig. 7.3). This marked difference in Jurassic water temperatures interpreted from $\delta^{18}O$ values of fauna, micrite and bulk rocks, might be due to original abiotic carbonate mineralogies, extreme climatic variations and/or higher salinities. Large temperature ranges occur in some modern carbonate depositional environments. For example, extreme temperature variations occur in present Persian Gulf shallow seawaters, from 40° C in summer to 15° C in winter (Purser and Seibold, 1973). The surface seawater temperature of 13° C, calculated from the heaviest belemnite $\delta^{18}O$ value of the late mid Jurassic from Scotland, at a paleolatitude of 45° N, is similar to modern cool temperate surface seawater temperatures around Tasmania, Australia, at a latitude of about 44° S (Edwards,

1979). The surface seawater temperature of 23° C, calculated from the heaviest oyster $\delta^{18}O$ value of the mid Jurassic from England, at a paleolatitude of about 35° N, corresponds to modern warm temperate seawater temperatures at latitudes around 36° S in southern Australia (Edwards, 1979).

7.8 Conclusions

This study used $\delta^{18}O$ and $\delta^{13}C$ temperature equilibrium lines to differentiate aragonite from calcite in both Recent and ancient carbonates. The Mozduran carbonates formed mainly in shallow waters, as their $\delta^{18}O$ and $\delta^{13}C$ values are in equilibrium with atmospheric PCO_2. The Mozduran limestone data fall mostly above the $\delta^{18}O$ and $\delta^{13}C$ equilibrium lines with respect to present day atmospheric PCO_2 levels of -7.2‰. The calculated Upper Jurassic PCO_2 level, gives an atmospheric $\delta^{13}C$ value of -6.7‰. Using an atmospheric PCO_2 level of -6.7‰, the $\delta^{18}O$ and $\delta^{13}C$ temperature equilibrium lines of aragonite and aragonite-calcite mixture, bisect the Mozduran limestone data, indicating the former presence of these minerals during the Upper Jurassic. The heavy $\delta^{18}O$ brachiopod values fall on the shifted temperature equilibrium calcite line, as they are in equilibrium with an atmospheric PCO_2 level of -6.7‰, but not with the present atmospheric PCO_2 level of -7.2‰. In contrast, the late mid Jurassic low-Mg calcite belemnites of Scotland and the mid Jurassic calcitic bulk carbonate of England, fall on the calcite equilibrium line, corresponding to atmospheric PCO_2 levels of -7.2‰, but not with the value of -6.7‰.

The covariation of isotope and trace element plots, also support aragonite and mixed aragonite-calcite mineralogy from the shallowest and relatively deeper parts of the basin respectively. The observed $\delta^{18}O$ and $\delta^{13}C$ isotopic trend in the Mozduran limestones results from burial overprinting of earlier meteoric diagenesis. This is supported by trace elements and petrographic studies.

The $\delta^{18}O$-$\delta^{13}C$ plot separates the carbonate cements into marine, meteoric and burial diagenetic environments. The marine cement is enriched in $\delta^{18}O$ (-2.4‰ PDB) and $\delta^{13}C$ (+3.6‰ PDB) values, compared with meteoric and burial calcite cements. The meteoric calcite cements are characterized by moderately depleted $\delta^{13}C$ values from about +1.1‰ to -2.8‰ PDB. The burial cements mostly retain calcite marine $\delta^{13}C$ values, ranging from +2‰ to +3.8‰ PDB. The marine, meteoric and burial calcite cementations are supported with trace elements and cathodoluminescence studies. The $\delta^{18}O$ and $\delta^{13}C$ values of vein calcites indicate that a few vein calcites were precipitated in burial environments, whilst, those with moderately depleted $\delta^{13}C$ values, were precipitated under the influence

of hot circulating meteoric water. The lightest $\delta^{18}O$ values in vein calcites, by assuming a δ_W =0 SMOW, give a temperatures of ~90° C.

The heaviest $\delta^{18}O$ value of the mid Jurassic carbonates of England gives a cold seawater temperature of ~8° C, while the heaviest $\delta^{18}O$ value of LMC belemnite from the late mid Jurassic of Scotland gives a temperature of ~13° C, similar to modern cool temperate surface seawater temperatures around Tasmania, Australia at a similar latitude. The heaviest $\delta^{18}O$ value of the Upper Jurassic marine micrite from the Mozduran Formation gives a seawater temperature of 16° C, whereas the heaviest and least-altered value of brachiopods corresponds to a warm seawater temperature of ~29° C. The temperature fluctuations in the Iranian shallow sea are similar to those in the present subtropical Persian Gulf, where temperatures fluctuate in the coastal areas from 40° C in summer to 15° C in winter.

CHAPTER 8

MOZDURAN DOLOMITE

CHAPTER 8

MOZDURAN DOLOMITE

8.1 Introduction

Dolomite is a major component of many sedimentary rocks and has received considerable attention by carbonate petrologists over the past 200 years, mainly because large quantities of oil, gas and important base-metal ores (such as lead, tin and zinc) are hosted by dolomite rocks. A major problem in the study of ancient dolomites is to explain the origin of extensive thick massive dolomite in the stratigraphic record. Recent published reviews on dolomites and dolomitization are numerous and reflect a wide variety of ideas regarding the origin of dolomite, its geochemistry, source of magnesium and the mechanism of dolomitization (e.g., Friedman and Sanders, 1967; Land, 1980, 1985; Zenger et al., 1980; Machel and Mountjoy, 1986; Hardie, 1987; Shukla and Baker, 1988; Mazzullo, 1992). As there are a variety of dolomite types in nature, it is clear that a single process of dolomitization does not exist (Amthor and Friedman, 1992).

Recent studies have repeatedly stressed the complex diagenetic origins of aerially widespread thick ancient dolomites, involving both early- and late-diagenetic dolomitization and alteration (e.g., Mattes and Mountjoy, 1980; Gregg and Sibley, 1984; Gregg and Shelton, 1990; Gao and Land, 1991; Kupecz and Land, 1991). These studies confirmed that an entire spectrum of dolomitization can occur, given adequate time, heat and fluid sources.

Platform carbonates of the Upper Jurassic Mozduran Formation consist of aerially widespread limestone and thick dolomite. The thickness of the dolomite beds is commonly in the order of 40 cm. However, some dolomitized beds are thicker, with a thickness of >3 m. The dolomite beds are laterally persistent over several kilometers along the outcrop lengths, although the dolomite types may vary laterally. Massive dolomite beds are mostly confined to

the basal part of the Mozduran sequence. Dolomite beds are also common through the middle part of the sequence, but disappear towards the upper part , in which thick limestone beds are widespread. Within the dolomitized part of the sequence, there are some undolomitized intervals that consists mainly of limestone beds. In an eastward (landward) direction the increase in dolomite proportion, particularly very fine to finely crystalline dolomites, relative to limestone (e.g., Shurijeh, Bagak and Padeha sections) is attributed to very shallow marine conditions, which were accompanied locally by evaporite deposists (Adabi and Rao, 1991). Limestones are more abundant in the westward direction where more open marine conditions prevailed during the deposition of Mozduran Formation carbonates.

The above features indicate a paleogeographic control on the distribution of the Mozduran dolomites. Mozduran dolomites comprise the main gas reservoir of the Kopet-Dagh Basin. However, inspite of their scientific and economic significance, the diagenetic origins of these rocks have been very little studied. This study indicates that the Mozduran dolomites were subjected to a complex diagenetic history, ranging from a wide spectrum of early-to-late diagenetic dolomitization. Five different types of dolomite and fabrics were recognized. Variations in dolomite types may reflect differences in formation time, formation mode, or the composition of the precursor limestone.

Detailed petrographic studies combined with elemental (109) and isotopic (114) analyses were used to describe the origin and the possible mechanism of dolomitization in the Upper Jurassic Mozduran Formation. The elemental and isotopic compositions of these dolomites, along with insoluble residue percent are listed in Table A5.9 (Appendix 5). XRD results of dolomite samples are listed in Table A5.10 (Appendix 5). The organic carbon results are summarized in Table A5.11 (Appendix 5).

8.2 Petrographic Study

Five different varieties of dolomite and fabrics are identified according to crystal size distribution (unimodal or polymodal) and crystal boundary shape (planar or nonplanar), using the classification of dolomite-rock textures proposed by Sibley and Gregg(1987), which is based largely on the fundamental classification of Friedman (1965). Although this classification scheme is principally descriptive, it carries genetic implications, as size distribution is controlled by both nucleation and growth kinetics, and crystal boundary shape is controlled by growth kinetics (Sibley and Gregg, 1987). It is suggested that

unimodal size distributions in dolomites result from a single nucleation event on homogeneously distributed nucleation sites, combined with uniform growth rates, whilst polymodal size distributions may develop from a heterogeneous distribution of nucleation sites, multiple periods of nucleation, or variations in the local growth rate (Sibley and Gregg, 1987). At low supersaturation and/or low temperatures, planar dolomite crystals will develop. At high supersaturation, referred to as the critical saturation, or above a given temperature, referred to as the critical roughening temperature, nonplanar dolomite crystals may form (Sibley and Gregg, 1987). The critical roughening temperature for dolomite has been estimated to lie between 50 and 100° C (Gregg and Sibley, 1984).

In this study, the classification of dolomites is based on detailed petrographic and cathodoluminescence studies. Crystal size of dolomites were measured by looking at the maximum crystal diameters, which were then subdivided using Folk's (1974 a) dolomite grain size scale.

The five kinds of dolomite are characterized as follows:

Type 1 Very fine to finely crystalline dolomite

Unimodal mosaics, planar-s (subhedral), very fine to fine-crystals comprise this type of dolomite (Fig. 8.1 A). Crystal sizes range from about 10 to 60μm, with an average size of approximately 40μm. These dolomites are dense and dark in color, non-porous, unfossiliferous, preserve traces of depositional textures, such as laminations and intraclasts, and are commonly associated with scattered detrital quartz grains (Fig. 8.1 C, D). Patches of fine-crystalline clear dolomite intercalated with very fine-crystalline dark dolomite mosaics are present in this type of dolomite. Based on abundances estimated from all the stratigraphic sections studied, type 1 dolomite accounts for about 12% of the total dolomite by volume.

The luminescence pattern is characterized by a homogeneous dull to dirty-orange color (Fig. 8.1 B). Type 1 dolomites are similar to the dolomite-rock texture type 1 of Amthor and Friedman (1992).

Interpretation

The crystal size of dolomite can be used to distinguish between early and late diagenetic dolomite (e.g., Gregg, 1985; Lee and Friedman, 1987; Amthor and Friedman, 1992; Ye and Mazzullo, 1993). On the basis of very small crystal size and fabric, the presence of scattered detrital quartz silt, preservation of original depositional textures, absence of fossils and uniform luminescence (dull

to dirty orange), type 1 dolomite is considered to have been formed under near-surface, low-temperature conditions (Sibley and Gregg, 1987; Gregg and Shelton, 1990). They possibly resulted from penecontemporaneous or early replacement of a carbonate precursor soon after deposition, in a supratidal to upper intertidal setting. Seawater (e.g., Saller, 1984; Land, 1985; Mitchell et al., 1987) or interstitial solutions enriched in Mg might be responsible for dolomitization. Studies of Holocene dolomites from intertidal-flat settings in the Bahamas support direct dolomite precipitation, as a void-filling cement (Lasemi et al., 1989). Recently, dolomite has been synthesized at 60° C by Usdowski (1989), who suggested that although the reaction rates are slow, dolomite formation can occur at the earth surface in peritidal systems. As ground temperatures in some tropical settings are as high as 50° C (e.g., Persion Gulf), such hot temperature conditions would facilitate the formation of dolomite.

It has been suggested that crystal size is controlled by an interplay between nucleation and rate of growth (Spry, 1969). Both nucleation and growth rates increase with temperature. Sibley and Gregg (1987) recognized the importance of crystal growth mechanisms to the understanding of dolomite rock textures. They suggested that fine particles have a very large surface area compared to their volume, and thus a rapid nucleation rate, as the large surface area provides numerous active sites for nucleation. If nucleation rates increase faster than crystal growth rates, relatively finer dolomite crystals are developed, even at high temperatures. Experimental study (Sibley et al., 1987) also shows that the induction stage (time until nucleation and growth of dolomite to detectable amounts) of dolomite formation increased with increasing crystal size of the reactant (decreasing surface area). This may explain the early dolomitization of fine carbonate lime muds in supratidal to upper intertidal settings in the Mozduran Formation.

Type 2 Fine to medium crystalline dolomite

This type forms fine to medium-crystalline euhedral dolomite rhombs mainly floating within the lime mud matrix (idiotopic fabric of Friedman, 1965; idiotopic-P (porphyrotopic) of Gregg and Sibley, 1984; and planar-P dolomite of Mazzullo, 1992, Fig. 8.1 E). In many other examples, dolomite crystals are supported with intercrystalline areas filled by sparry calcite cement (idiotopic-E of Gregg and Sibley, 1984; and planar-e dolomite of Sibley and Gregg, 1987, Fig. 8.1 G). In some planar-e dolomite textures, dolomite rhombs are floating within the sparry calcite cement, forming poikilotopic texture (Friedman, 1965,

Figure 8.1. Plain and cathodoluminescence photomicrographs in dolomite types 1 and 2.

A. Very fine to finely crystalline, unimodal, planar-s (subhedral) dolomite. Thin section Sh 38.

B. Same view as in A under cathodoluminescence. The finely crystalline dolomite is characterized by uniform dull to dirty orange luminescence.

C. Intraclastic dolomicrite. Note large, semi-rounded, internally homogeneous clasts of dolomicrites are associated with detrital sand to silt-sized quartz grains. These clasts are possibly formed by the impingement of tides in the upper intertidal environments. Thin section Sh 3.

D. Close up of dolomite clast. Note intraclastic dolomicrite is internally homogeneous. Thin section Ba 2.

E. Fine to medium crystalline euhedral dolomite rhombs floating in a limestone matrix. The dolomite crystals are mud-supported rather than crystal-supported. Note dolomite rhombs show a cloudy core and a clear rim (white arrow). Thin section Go 96.

F. Same view as in E under cathodoluminescence. Note the luminescence is orange-red, with thin dark-orange rims (white arrow).

G. Fine to medium crystalline planar-e dolomite. Note dolomite crystals are mostly euhedral rhombs and crystals-supported with intercrystalline area, filled by sparry calcite cements, unlike Fig. 8.1 E. Thin section Go 52.

H. Same view as in G under cathodoluminescence. Dolomites are mostly pink-red luminescent. Note calcite cements with yellow-brown luminescence.

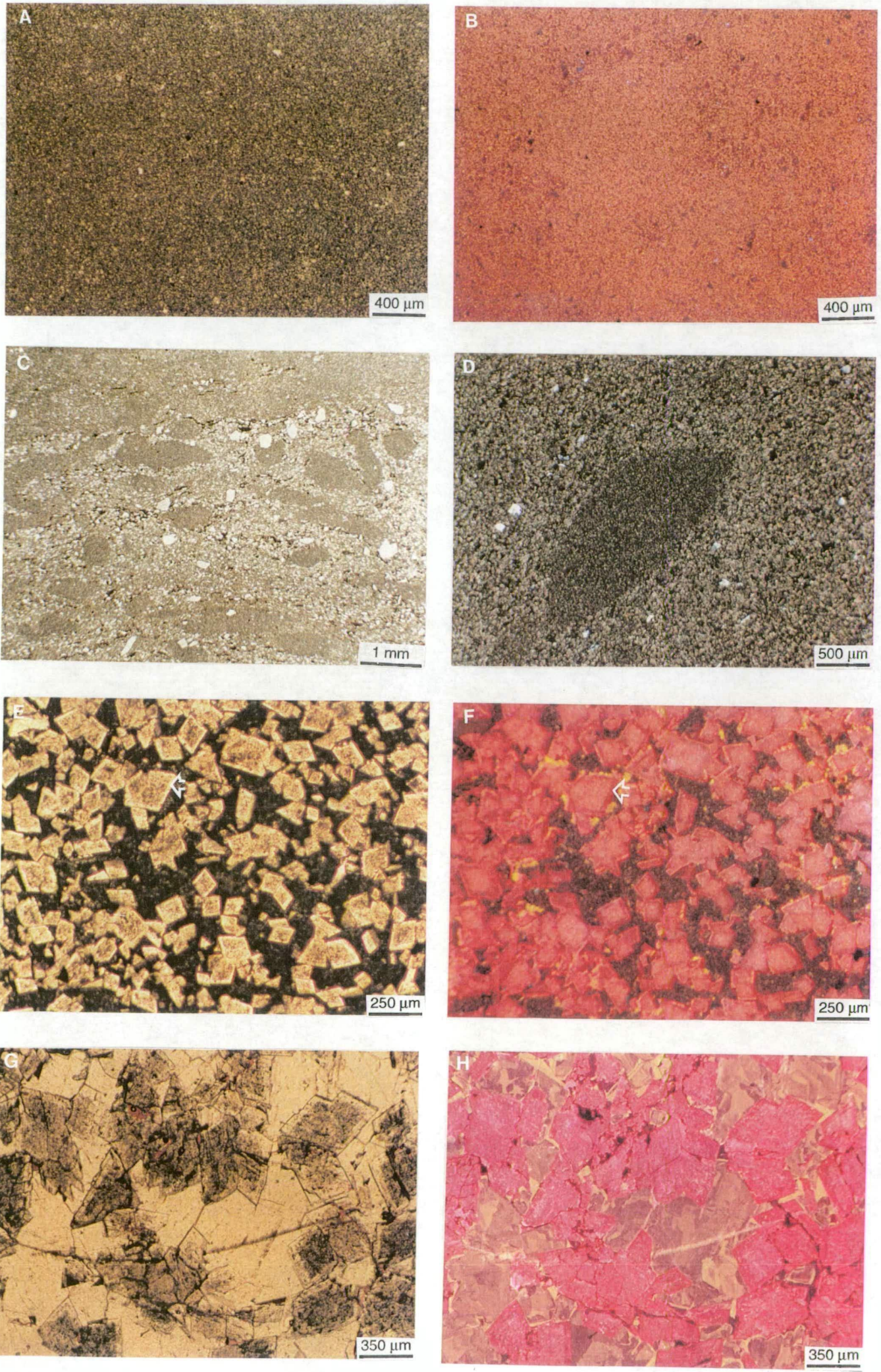
A
400 µm
B
400 µm
C
1 mm
D
500 µm
E
250 µm
F
250 µm
G
350 µm
H
350 µm

Fig. 8.2 A). Isolated rhombs are polymodal in size, ranging from 10 to 220μm, with an average size of approximately 140μm. Dolomite rhombs comprise up to ~ 40% of the total components in a few samples. Most of the dolomite rhombs have a cloudy surface and contain inclusions of micrite (Fig. 8.1 E, G). Many cloudy rhombs are overgrown with a single clear euhedral rim (Fig. 8.1 E, G). In some cases, zoning may be defined by the presence of iron oxide inclusions which cause a brownish appearance. Dolomite rhombs rarely replace fossil fragments, though isolated euhedral rhombs replace other allochems, such as intraclasts and ooids (Fig. 8.2 B). According to Randazzo and Zachos (1984), this type of dolomite-rock texture indicates heterogenous dolomitization. They have noted that during late stage diagenesis, these fabrics often grade into mosaic fabrics (sutured mosaic), which appear to represent the completion stage of dolomitization. Friedman (1965) suggested that this type of fabric may be converted into hypidiotopic or xenotopic dolomite by continuing growth of the dolomite crystals which causes a reduction in the porosity.

Type 2 dolomite shows petrographic features analogous with the type 2 dolomite of Mattes and Mountjoy (1980), type 1 dolomite (where only limestone groundmass is dolomitized) of Shukla and Friedman (1983), as well as the floating dolomite type of Qing and Mountjoy (1989). Scattered dolomite rhombs account for ~10% of the total dolomite by volume in the Mozduran Formation.

Under cathodoluminescence, type 2 dolomites are mostly orange-red to pink-red (Figs. 8.1 F, H). The core of some dolomite crystals are often dull to orange red, while the rim is usually dark orange luminescent (Fig. 8.1 F).

Interpretation

Scattered dolomite rhombs are the main type of dolomite in partially dolomitized Mozduran limestone. They are widspread throughout Mozduran limestones and occur mainly in lime mud lithofacies, but also occur in other lithofacies. Fossil fragments are least affected by this type of dolomitization, suggesting that dolomitization began preferentially in the finer-grained matrix. This interpretation corresponds to that by Qing and Mountjoy (1989). On the other hand, Sibley and Gregg (1987) suggested that if the dolomitizing solution is somewhat less supersaturated with respect to dolomite, the matrix may be dolomitized, but the fossils may remain undolomitized, as at the lower saturation state, very few dolomite nuclei form on the coarser calcite. The other scenario for the evolution of this type of texture is that if the original lime matrix was aragonite and the fossils calcite, dolomite might nucleate selectively in the

aragonitic matrix (Sibley and Gregg, 1987). The latter statement is consistent with observations in most modern settings (e.g., sabkhas), where dolomite selectively replaces aragonite (McKenzie, 1981). However, there are exceptions to this, for example, the magnesian calcite-rich muds in the Coorong Lakes (Von der Borch and Lock, 1979) and the Mg-calcite deposits of Ambergris Cay, Belize, Central America (Mazzullo et al., 1987). Experimental studies also indicate that aragonite is more readily dolomitized than calcite (Gaines, 1980; Sibley et al., 1987). Since aragonite is the dominant carbonate mineralogy in the shallowest part of the basin (e.g., Shurijeh, Bagak, Padeha), and dolomitization is very pervasive in this area, it can be concluded that aragonite promoted dolomitization.

Zenger and Dunham (1988) reported that selective dolomitization of fine mud matrix and peloids vs. skeletal fragments more likely occurs in early diagenesis. It was also suggested that the bulk of the dolomite disseminated in deep-marine sediments formed during early diagenesis (Lumsden, 1988). However, more recently, the partial dolomitization of lime mud has been attributed to dissolution of high-Mg calcite under shallow burial conditions (Mukhopadhyay, 1996). In the Mozduran Formation, dolomite rhombs were observed locally to have precipitated along stylolite seams (Fig. 8.2 C), suggesting that stylolites acted as conduits for the dolomitizing fluids in shallow burial. In some thin sections, floating dolomite rhombs are cross cut by stylolites, suggesting that dolomitization occurred prior to stylolization. However, some dolomite rhombs postdate stylolization, as stylolites are partially replaced by dolomite rhombs (Fig. 8.2 D).

Dolomite rhombs with the appearance of cloudy cores and clear rims have been explained by Sibley (1980), who suggested that cloudy centers and clear rims formed when the dolomitizing fluid changed from near saturation with respect to calcite (cloudy centers) to undersaturation with respect to calcite (inclusion free rims). However, according to Coniglio et al. (1988), dolomite crystals with leached or cloudy cores indicate that the earliest dolomite was the least stable, probably a rapidly precipitated calcian phase, which indiscriminantly incorporated inclusions as well as trace elements.

Type 3 Medium crystalline dolomite

Type 3 dolomite is composed mainly of dense unimodal mosaics of subhedral to anhedral planar-s crystals (Fig. 8.3 A). In many of the dolomite crystals, straight compromise boundaries are well developed and some crystals

Figure 8.2. Diagenetic texture in dolomite type 2.

A. Thin section photomicrograph showing large calcite crystal engulfing dolomite rhombs, forming poikilotopic texture (black arrows). Thin section Go 52.

B. Fabric destructive replacement dolomitization. Depositional components are partially to completely replaced by dolomite rhombs. Note dolomitization is mostly concentrated within fine-grained ooid nuclei. Non-ferroan calcite cements are not affected by dolomitization. Dolomitization possibly occurred during early diagenesis. Thin section Bz 57.

C. Fine to medium crystalline euhedral dolomite rhombs mostly concentrated along pressure-dissolution zones. Note some dolomite rhombs are distinctly zoned. Thin section Mz 31.

D. Stylolite partially replaced by a few dolomite rhombs, suggesting dolomite rhombs postdate stylolitization (white arrows). Thin section Bz 69.

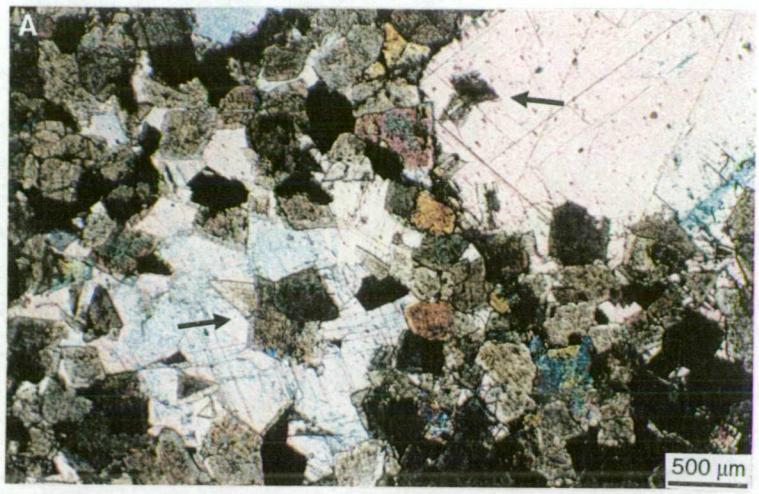
A
500 µm


B
500 µm

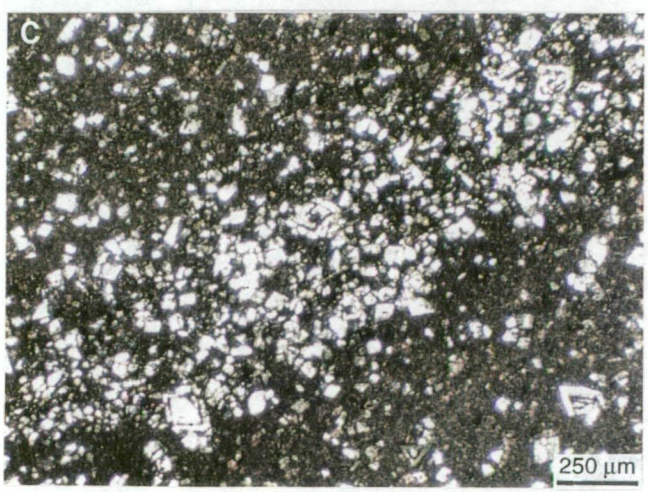
C
250 µm

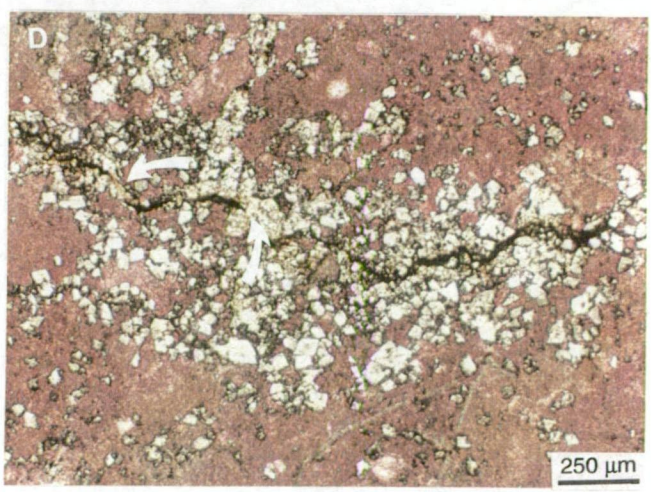
D
250 µm

have preserved crystal-face junctions (Fig. 8.3 C). In type 3 dolomite, intercrystalline porosity is generally low. Examination by reflected light indicates that some of the intercrystalline porosities are probably filled by amorphous iron hydroxide. This type of dolomite is referred to as hypidiotopic by Friedman (1965), idiotopic-S by Gregg and Sibley (1984) and as planar-s texture by Sibley and Gregg (1987) and Mazzullo (1992). The crystal sizes range from 70 to 260μm, with an average of about 220μm. Dolomite type 3 is texturally destructive and largely modifies or obliterates ealier diagenetic features. Therefore, original sedimentary textures have not been recognized. Although the dolomite crystals are mostly clear, in some samples, dolomite shows cloudy inclusion-rich cores (Fig. 8.3 D). Type 3 dolomites are the most common and widespread dolomite texture within the dolomitized portions of the Mozduran Formation. Type 3 dolomite shows petrographic features similar to type 3 dolomite of Shukla and Friedman (1983) and matrix dolomite of Qing and Mountjoy (1989). The medium crystalline dolomite is the second most abundant dolomite type in the study area, forming about 20% of the total dolomite by volume.

Under luminoscope, dolomite crystals commonly are dark orange-red luminescent (Fig. 8.3 B).

Interpretation

In dolomite type 3, most dolomite crystals are subhedral to anhedral with relatively straight, compromise boundaries and some crystal-face junctions. According to Jackson's (1958) crystal growth model, at low temperatures, crystals grow by the addition of atoms layer by layer onto a crystal face, resulting in the development of faceted crystal faces and euhedral and subhedral crystal mosaics. Morrow (1982) suggested that planar-s texture can be the result of slow grain growth from initial state, where fine crystalline dolomite rhombs are scattered throughout the limestones. According to Sibley and Gregg (1987), plannar-s fabric suggests slow grain growth under a continuous flux of dolomitizing fluid at low temperature. Therefore, dolomite texture type 3 is considered to represent a diagenetic replacement of preexisting limestone and/or recrystallization of early formed dolomite (Fig. 3.8 E), or replacement of other facies such as sandstones (Fig. 8.3 F), possibly below critical roughening temperature (<60° C suggested by Gregg and Shelton, 1990 and Mazzullo, 1992).

Figure 8.3. Diagenetic texture in dolomite type 3.

A. Thin section photomicrograph of unimodal, tightly interlocking, subhedral to anhedral dolomite crystals. Note depositional textures have been completely obliterated by medium to coarsely crystalline dolomite crystals. Thin section Sh 42.

B. Same view as in A under cathodoluminescence. Dolomites mostly show dark orange-red luminescence. However, a few dolomite crystals exhibit bright-yellow to dark-red subzone luminescence.

C. Unimodal, planar-S dolomite with well developed crystal-face junction (white arrow). Note dark inclusion-rich zone within some dolomite crystals, may indicate replacement of precursor muddy carbonates. Thin section Sh 36.

D. Unimodal, dense, euhedral to subhedral dolomite crystals with little intercrystalline porosities. Note most dolomite crystals exhibit cloudy centers and clear rims (white arrow). Thin section Pa 8.

E. Thin section photomicrograph of polymodal, subhedral, planar-s dolomite. Note original or early diagenetic finely crystalline textures are partly preserved. Thin section Go. 47.

F. Thin section photomicrograph of unimodal, dense, interlocking mosaic of anhedral dolomite crystals. Note detrital quartz grains floating in the dolomite crystals show corroded margin. Presence of undigested quartz grains within the dolomite crystals may indicate replacement of quartz by dolomite. Thin section Ba 8.

G. Unimodal, planar-s dolomite with mimically replaced crinoid. Thin section Go 66.

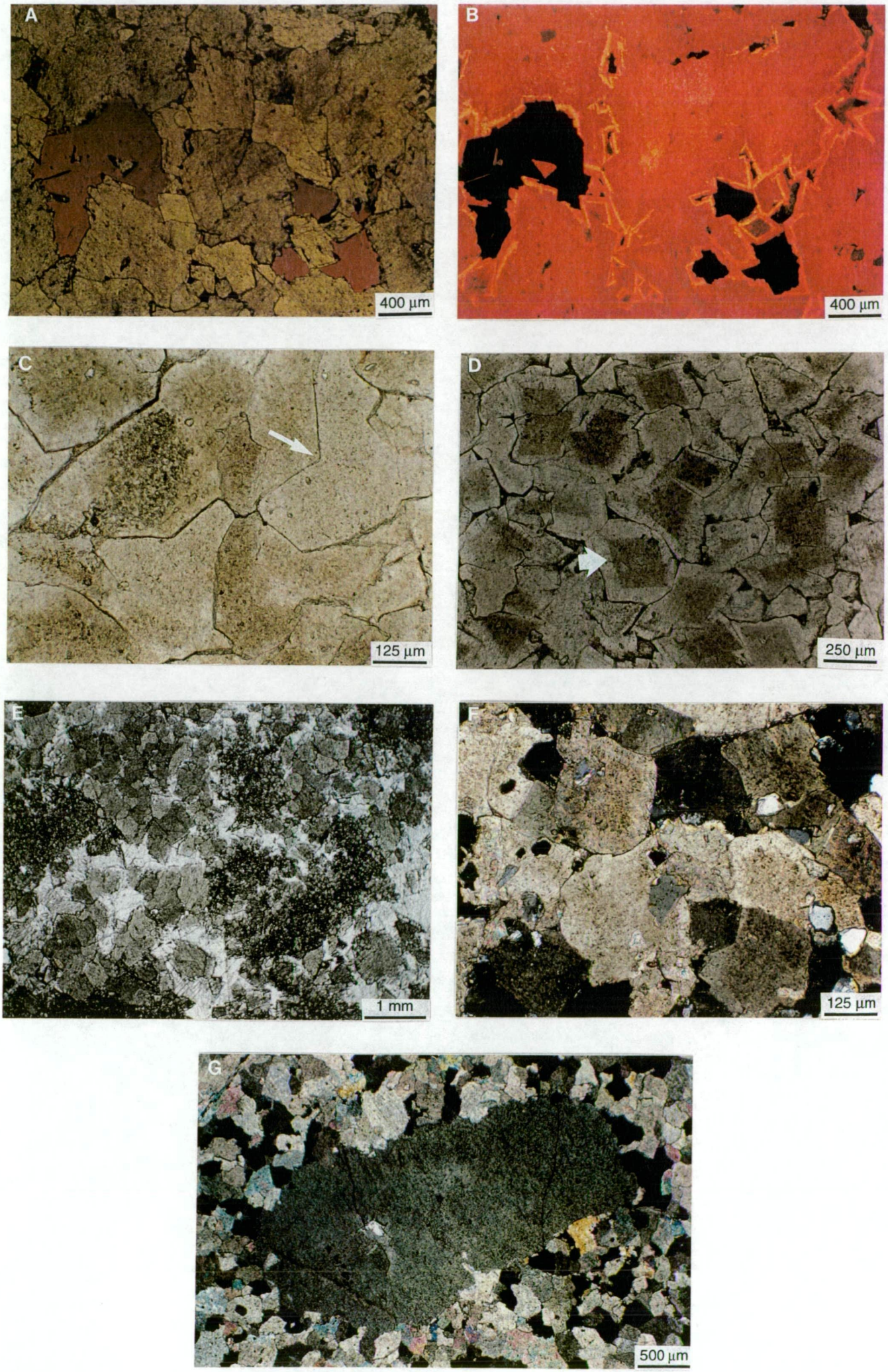
A
400 µm
B
400 µm
C
125 µm
D
250 µm
E
1 mm
F
125 µm
G
500 µm

Type 4 Medium-coarsely crystalline dolomite

Dolomite type 4 consists of unimodal, dense, closely packed mosaics of coarse (240-1100μm, with an average of ~500μm), nonplanar-A (anhedral) crystals, often characterized by nonmimically replaced allochems (such as, ooids, Fig. 8.4 A, C). Nonmimic replacement refers to preservation of the form, but not the structure of an allochem, and requires only a few dolomite crystals or nuclei to replace the allochem (Sibley and Gregg, 1987). The dolomite crystals have irregular intercrystalline boundaries, commonly with undulatory extinction and rarely preserved crystal-face junctions (Fig. 8.4 A, C). This dolomite-rock texture corresponds to the xenotopic texture of Friedman (1965), xenotopic-A texture of Gregg and Sibley (1984), nonplanar texture of Sibley and Gregg (1987) and nonplanar-A texture of Mazzullo (1992). In some dolomite samples, medium-coarsely crystalline dolomite shows planar-s texture. Therefore, the distinction between dolomite type 3 and dolomite type 4 is often difficult. The differentiation between these two dolomite types was made qualitatively and in some samples quantitatively, based on higher numbers of preserved crystal-face junctions (>30%, Mazzullo, 1992) in type 3 dolomite and common undulatory extinction present in type 4 dolomite. In this type of dolomite, clear-rim, cloudy zoning is absent. Type 4 dolomite is texturally similar with type 3 of Shukla and Friedman (1983), type 3 of Lee and Friedman (1987), type 6 dolomite of Amthor and Friedman (1991), as well as with zone 2A dolomite of Barnaby and Read (1992). Medium-coarsely crystalline dolomite is the most abundant dolomite type in the Mozduran Formation, forming about 55% of the total dolomite by volume.

Under cathodoluminescence, this type of dolomite has relatively homogeneous dark-red luminescence and shows no zonation (Fig. 8.4 B).

Interpretation

As has been discussed above, it is assumed that the carbonate texture is controlled by the temperature at which the crystals grow. Jackson (1958), Jackson and Gilmer (1976) and others, noted that above a given temperature, referred to as the critical roughening temperature (CRT), atoms are added randomly to the crystal surface, faceted crystal faces do not form, and the resulting texture is an interlocking mosaic of anhedral crystals. Based on experimental data (Jackson and Gilmer, 1976; Gregg and Sibley, 1984) and studies of different types of naturally occurring dolomites (such as in Persion Gulf sabkha), Gregg and Sibley (1984) and Sibley and Gregg (1987) estimated

Figure 8.4. Diagenetic texture in dolomite types 4 and 5.

A. Unimodal, tightly packed, nonplanar, medium-coarsely crystalline dolomite, with nonmimically replaced allochem (ghosts of ooids). Dolomitization obliterated the original depositional fabric. Only in rare samples are precursor allochems (in this example-ooids) preserved as relict ghosts. Short white arrows point to circular ooid ghost. Note irregular intercrystalline boundaries and lack of porosity. Thin section Sh 42.

B. Same view as in A under cathodoluminescence. Dolomite crystals show homogeneous dark-red luminescence. Porosities are shown by black colors.

C. Close up of a portion of photograph A. Note nonmimically replaced ooid has quartz nucleus (black arrow). Dolomite crystals at the center of the photograph showing sweeping (undulatory) extinction in crossed polarized light.

D. Medium to coarsely crystalline planar-C (cement) dolomite, filling large pore space. These cements represent the final phase of dolomitization and postdate all other types of dolomite. Thin section Go 67.

E. Same view as in D under cathodoluminescence. Euhedral planar-C dolomite crystals exhibiting dark-red luminescence. The finely crystalline dolomites show orange-red luminescence.

F. Clear, euhedral, planar-C dolomite crystals, lining void space, cut by pressure dissolution seam. Note that dolomite crystals grew from the wall of the void space. Thin section Go 39.


A
400 µm

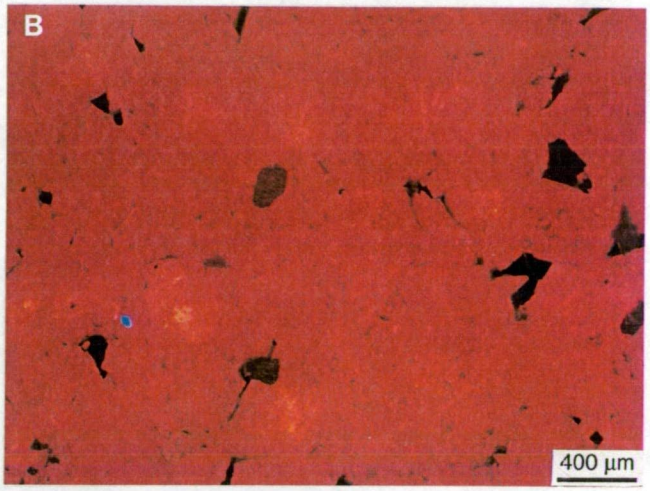
B
400 µm


C
250 µm

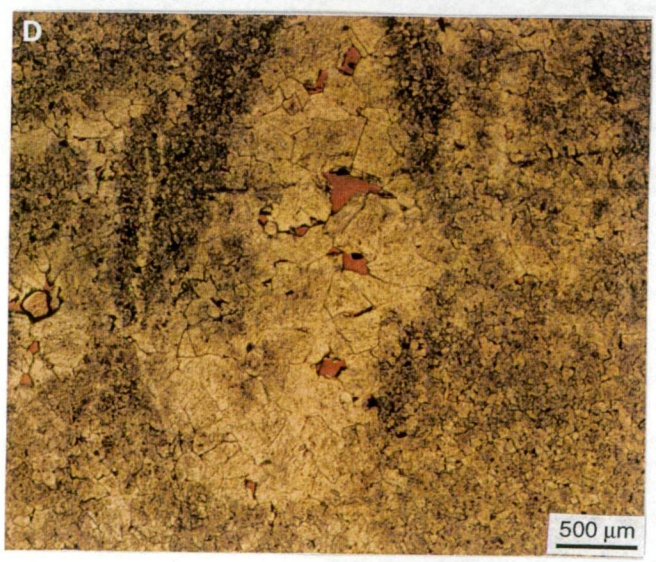
D
500 µm

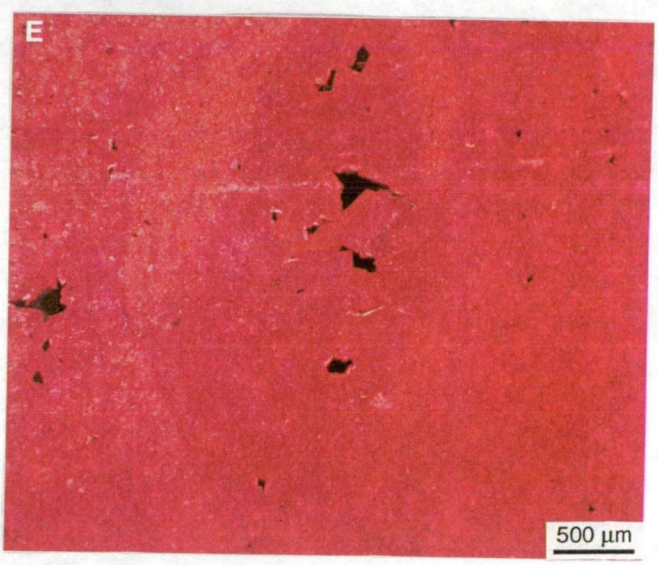
E
500 µm


F
500 µm

that the CRT for dolomite lies between 50 and 100° C. The lower temperature limit of 50° C is based on similar temperatures a few inches below the surface in the Persion Gulf sabkha, and the upper limit of 100° C is based on an approximate estimate of temperature for fracture-ralated dolomites. However, Gregg and Shelton (1990) suggested that the nonplanar dolomite textures would be developed above 60° C.

According to Gregg and Sibley (1984), Sibley and Gregg (1987), Gregg (1988) and Gregg and Shelton (1990), neomorphic dolomites and dolomites that replaced limestones at elevated temperatures show coarsely crystalline nonplanar textures. There is other evidence which supports the formation of nonplanar dolomite at higher temperatures. These include: 1) absence of nonplanar texture in Pliocene and Recent dolomites, which were subjected only to near-surface temperature (<50° C); 2) presence of nonplanar texture in dolomite from the Galena Group (Ordovician, Wisconsin and Iowa), formed by neomorphism of planar dolomite at temperatures above 80° C (Gregg and Sibley, 1984); 3) presence of nonplanar texure in dolomites synthesized in the labratory bombs at 250 and 300° C (Gregg and Sibley, 1984); and 4) occurrence of nonplanar dolomite in the Huecs Limestone at Marble Canyon, Texas, which resulted from progressive recrystallization of preexisting dolomites near an igneous intrusion at a temperature ≥ 250° C (Gregg and Sibley, 1984).

Although the distinction between recrystallization and/or neomorphic origin and replacement origin in coarsely crystalline dolomites is difficult, Gregg and Sibley (1984) and Lee and Friedman (1987) suggested that the presence of allochem ghosts (such as ooid ghosts) in a dolomite, supports direct replacement of limestone, rather than neomorphism of preexisting dolomite. It is also believed that allochem ghosts indicate relatively slow replacement of a precursor limestone, where the saturation state with respect to dolomite is low, but the residence time of the rock in the dolomitizing solution is quite long, leading to a low porosity dolomite (Sibley and Gregg, 1987). Kaldi and Gidman (1982) also stated that the replacement of precursor carbonates by dolomite is slow (volume-for-volume replacement) and involves dissolution and reprecipitation.

All the above evidence, along with temperature calculated from oxygen isotope data (see isotope section), supports the conclusion that type 4 dolomite in the study area, with coarse, nonplanar anhedral textures, possibly formed by replacement of precursor limestones (e.g., oolithic facies), above 60° C temperature, after shallow burial and during gradual sudsidence of the Kopet-

Dag Basin, as suggested by Moussavi-Harami and Brenner (1992). Temperature calculation based on $\delta^{18}O$ data supports formation of dolomite type 4 at an elevated temperature (see isotope section).

Type 5 Coarsely crystalline planar-C (cement) dolomite

This type consists of clear, coarsely crystalline, planar-C (cement), often euhedral dolomite crystals, lining voids, vugs and fractures, and occurs as major void-filling dolomite (Fig. 8.4 D, F). However, in a few examples, dolomite cement shows planar-s texture. Planar-C dolomites are partly responsible for occlusion of open spaces and fractures, and considered to be relative late-stage diagenetic products. They consist of polymodal dolomite, with crystal sizes ranging from 220 to over 500μm. The crystal size is normally related to the size of the open space, with crystal size increasing from the wall towards the center (Fig. 8.4 D, F). No replacement features were observed in this dolomite type. Dolomite cements are characterized by their distinctive milky-white color (Fig. 8.5 F), unit extinction under crossed polars, general lack of inclusion, and presence of rhombic terminations where they occur adjacent to pore spaces (Fig. 8.5 F). Thus, planar-C dolomite is the principal textural type associated with void and fracture-related dolomite. Type 5 dolomite is texturally similar with type 5 dolomite of Amthor and Friedman (1991). Dolomite cements are the least abundant dolomite types, and have an abundance of about <3%.

In many dolomite samples, voids and cavities have been filled by very late diagenetic coarsely crystalline sparry calcite cements (Figs. 8.5 A, C, E). These pore-filling calcite cements, which are very common in dolomite facies, can easily be mistaken for dolomite cements. However, the staining technique, geochemical analysis and CL characteristics distinguish these as calcite rather than dolomite cements.

The luminescence pattern in euhedral dolomite cement is characterized by homogeneous orange-red luminescence. In contrast, the pore-filling late sparry calcite cements have either bright-yellow luminescence (Fig. 8.5 B, D), possibly indicating meteoric origin, or exhibit dull to dark-brown luminescence (Fig. 8.5 F), which may indicating burial origin.

Interpretation

Paragenetic relationships indicate that euhedral and planar-s dolomite cements are the last major dolomite generation, as they postdate all other dolomite types. Dolomite cement does not show saddle morphology or

nonplanar texture, indicating formation at elevated temperature (over 100° C, Radke and Mathis, 1980; or > 60° C, Greeg and Shelton, 1990). Whilst this is the case, it has been suggested that dolomite formed above the CRT, may locally develop mosaics of euhedral crystals and planar textures, as a result of precipitation in pores (Mozzullo, 1992). This applies to the Mozduran dolomite cements, as they are a product of late stage diagenesis in a deeper burial environment. Paleotemperature calculation from oxygen isotope values of dolomite cements also supports formation at an elevated temperature (see isotope section). In some samples, this type of dolomite is cross-cut by dissolution seams (Fig. 8.5 F), indicating that the dolomite cements predate the dissolution seams.

The paragenetic sequence of the observed diagenetic features of the Mozduran dolomites is summarized in Figure 8.6.

Figure 8.5. Sequence of paired plain light and cathodoluminescence photomicrographs of late pore-filling calcite cements in dolomites.

A. Pore-filling single crystal sparry calcite cements in dolomite facies, forming poikilotopic texture. Note sparry calcite cement postdates dolomitization. Thin section Mz 4.

B. Same view as in A under cathodoluminescence. Note late sparry calcite cement exhibits bright-yellow luminescence (possibly meteoric in origin), in contrast to dark-red luminescence in medium crystalline dolomite.

C. Late pore-filling drusy sparry calcite cement in medium to coarsely crystalline dolomite facies. Thin section Mz 14.

D. Same view as in C. Late pore-filling sparry calcite cement displays bright-yellow luminescence.

E. Mosaic of equant sparry calcite cements filling the cavity in medium crystalline dolomite. Thin section Go 101.

F. Same view as in E. Pore-filling sparry calcite cement exhibits dull to dark-brown luminescence (possibly burial in origin), unlike CL photomicrographs in B and D.

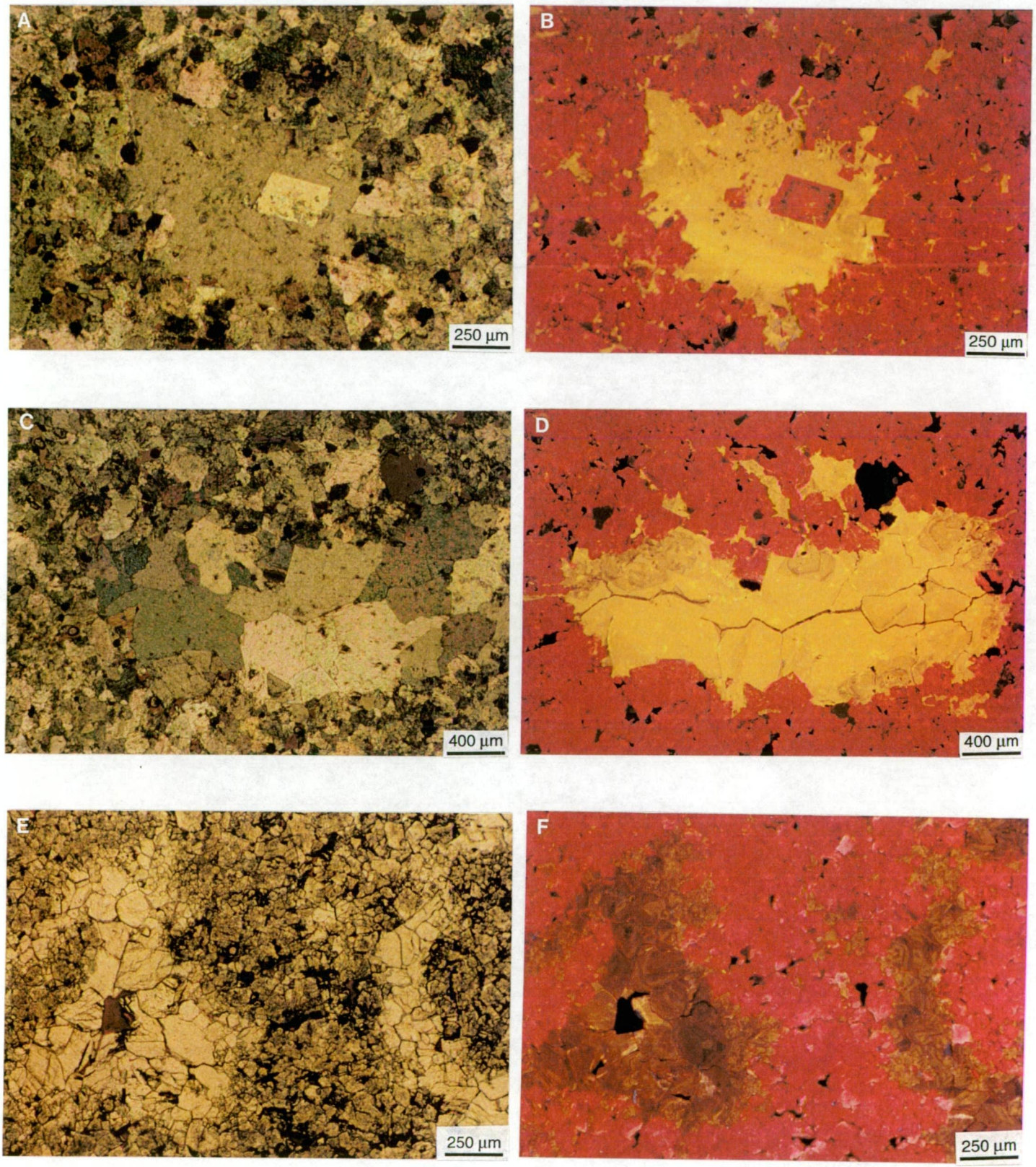
A
250 µm
B
250 µm
C
400 µm
D
400 µm
E
250 µm
F
250 µm

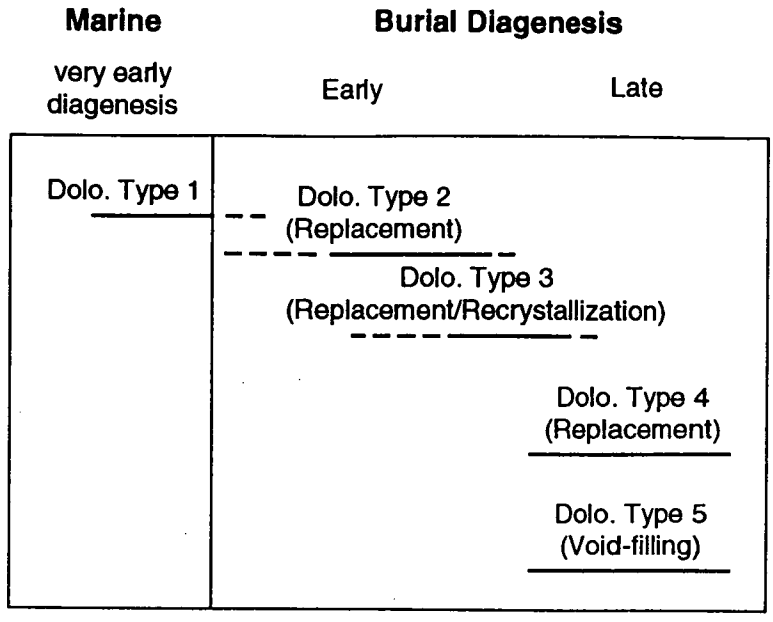

Figure 8.6. Paragenetic sequence in the Mozduran dolomites. The bars indicate relative timing and dashed lines indicate uncertainty in timing.

8.3 Dolomite Geochemistry

8.3.1 Dolomite stoichiometry and ordering

XRD analysis of different dolomite types, regardless of crystal size, (using the peak-search computer mode in the 28 to 32 degree 2Øs range, revealing average d_{104} values of 2.8876) indicate that most dolomites are very nearly stoichiometric, ranging from 47.5 to 51, with an average of 49.2 mole% $MgCO_3$ (Table A5.10, in Appendix 5). Average lattice constants are "aO"= 4.8077 and "cO"=16.0232, clearly indicating that the dolomites are very close to being ideal and structurally well ordered (Fig. 8.7), in accordance with Land (1985). It has been suggested that because of very low free energy, ideal dolomites are thermodynamically the most stable and least soluble form of mixed Ca-Mg carbonates (Mazzullo, 1992). Many studies have assumed that an increase in ordering and stoichiometery indicates that dolomite has undergone alteration in either the form of recrystallization or neomorphism (Land, 1983; Gregg and Sibley, 1984; Usdowski, 1989; Gregg and Shelton, 1990). Most Holocene and Cenozoic peritidal dolomites are typically poorly ordered and less stoichiometric, as determined by their unit cell measurements (Land, 1985; Mazzullo, 1992). Therefore, an increase in ordering and stoichiometry in the Mozduran dolomites, may imply alteration during transformation or stabilization from poorly ordered and less stoichiometric to better ordered and more stoichiometric.

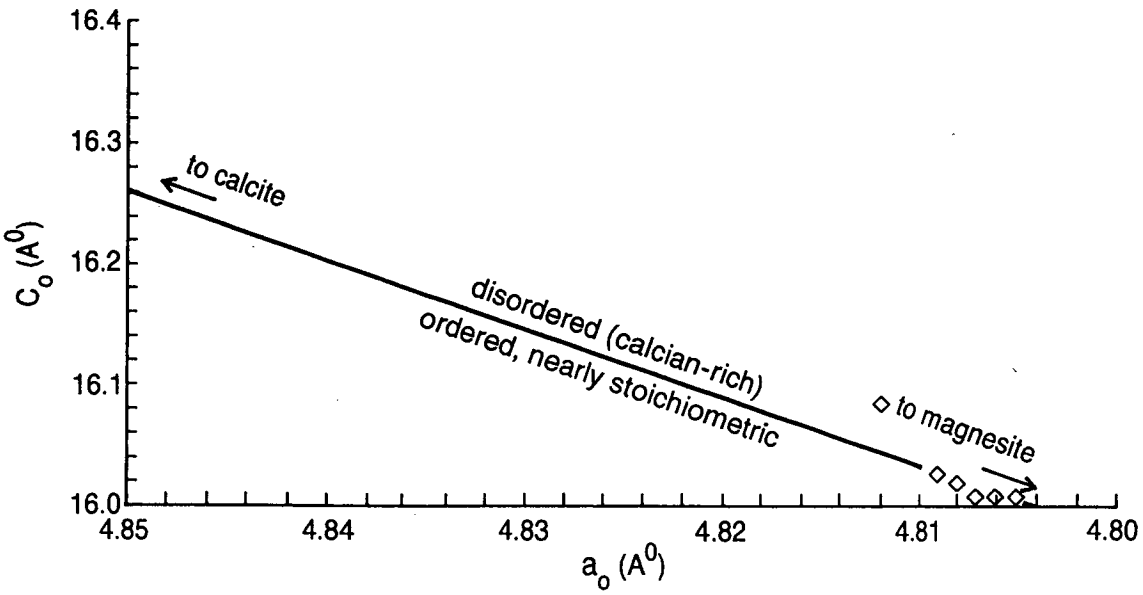

Figure 8.7. Unit cell measurment of the Mozduran dolomites (adapted from Land, 1985). The Mozduran dolomite samples fall within the ideal phases shown in Land (1985). However, truly ideal dolomite is apparently very rare in sedimentary rocks.

8.3.2 Organic carbon

Organic carbon in the Mozduran dolomites ranges from 0.64 to 5.5%, with an average of 2.2%, based on percent weight loss of ashed samples (Table A5.11, in Appendix 5). However, the difference between the inorganic carbon percent of ashed samples and total carbon percent of unashed samples, determined by Carlo Erba, shows a lower range of organic carbon. The total organic carbon measured by Carlo Erba ranges from 0.15 to 1.6%, with an average of 0.7% (Table A5.11, in Appendix 5). This is high compared with average Mozduran limestones total organic carbon value of about 0.35%, based on percent weight loss of ashed samples, and 0.13% measured by Carlo Erba (Table A5.7, in Appendix 5). The "average" organic carbon in limestone worldwide is about 0.3% (Pettijohn, 1975, Tucker, 1991). The relatively high organic carbon values are consistent with the dolomite's grey to dark brown color and fetid smell when being crushed. Organic carbon contents are higher in the Gorgoreh and Bazangan sections, with an average of 0.91%, than in the Shurijeh, Bagak and Mozduran sections, with an average of 0.33%, based on Carlo Erba determination. However, based on weight loss calculation, the average total organic carbon values in the Gorgoreh and Bazangan sections are even higher (2.8%), in contrast to ~1.2% for the Shurijeh, Bagak and Mozduran sections. The higher organic content of the Gorgoreh and Bazangan sections

(~three times) is explained by their greater depth of deposition. The very high organic content in Mozduran dolomites, compared to limestones, may indicate that dolomitization is favored in limestones that originally contained higher organic matter concentrations.

The preservation of a large amount of organic matter, which corresponds to relatively high $\delta^{13}C$ values in Mozduran dolomites, may be due to high rates of burial or dysaerobic (oxygen-deficient) conditions. Positive $\delta^{13}C$ values, which correlate with oceanic anoxic events and a high burial rate of organic matter, due to increased rates of organic productivity through eustatic sea-level rise, have been reported in Jurassic limestones (Jenkyns and Clayton, 1986). The transgressive events produce widespread shallow seas, which in turn increase rates of organic matter production (Jenkyns, 1980; Tucker, 1986 a). As the marine transgression from the northwest, during the Callovian, resulted in the deposition of the Mozduran carbonates in the study area, such a scenario can explain the high organic matter contents of limestones which have been replaced by dolomite. Irrespective of the degree of anoxia, the major control on organic matter accumulation does appear to be the primary production (Pedersen and Calvert, 1990). Although organic matter can be largely derived from phytoplanktons which live in the upper water level, much of the organic matter in the Mozduran carbonates is assumed to be of algal origin. This interpretation is based mainly on the presence of abundant algal fragments, oncolites and microbial-sediment structures in the Mozduran Formation. Organic rich dolomite similar in age to the Mozduran Formation is known to occur in the Kimmeridgian Clay of Dorset, England (Irwin, 1980).

8.3.3 Trace elements

Trace element analyses of different dolomite types are summarized in Table 8.1 and plotted in Figure 8.8.

8.3.3.1 Strontium

The Sr concentration in the Mozduran dolomites ranges from 19 to 219 ppm, with an average value of 60 ppm (Table A5.9, in Appendix 5). Sr values in dolomites are much lower than in limestones (average value of 194 ppm). The lower Sr concentration in dolomite relative to limestone is mainly due to the smaller Sr partitioning coefficient in dolomite (Land, 1980; Veizer, 1983). Sr generally substitutes for Ca, and as Ca concentration in dolomite is half that in calcite, the Sr values are less in dolomite than calcite. Sr concentrations in

dolomite types 1 and 2 are relatively higher than those in dolomite types 3, 4, and 5 (Table 8.1). The plot of Sr against Mg indicates that Sr concentration decreases with increasing Mg% (Fig. 8.8). This may be due to the more stoichiometric nature of pure dolomite samples. Vahrenkamp and Swart (1990) have shown that the Sr values in Tertiary marine dolomite decrease with increasing dolomite stoichiometry. The Sr value in stoichiometric dolomite is about 50 ppm. This value increases to about 253 ppm at 40 mol% $MgCO_3$ (Vahrenkamp and Swart, 1990). Unit cell measurments of five out of six representative Mozduran dolomite samples show that dolomites are stoichiometric (Fig. 8.7).

Table 8.1. Geochemical characteristics of different types of dolomites

Dolomite Type	Relative Abundance	Trace Element (ppm)					Isotopes (PDB)		
		n	Sr	Na	Mn	Fe	n	$\delta^{18}O‰$	$\delta^{13}C‰$
very fine - finely crystalline dolomite	12%	8	79	273	374	4238	14	-3.6	+2.08
fine - medium crystalline dolomite	10%	14	114	183	199	1890	13	-5.7	+2.81
medium crystalline dolomite	20%	18	53.5	241	256	1684	18	-6	+2.87
medium - coarsely crystalline dolomite	55%	63	49	313	296	1195	61	-7.4	+2.86
pore-filling coarsely crystalline dolomite cement	<3%	6	42	227	202	259	8	-7.9	+2.2

8.3.3.2 Sodium

The Na concentration in the Mozduran dolomites ranges from 116 to 522 ppm, with an average value of 276 ppm (Table A5.9, in Appendix 5). The average Na concentrations of different dolomite types are similar, ranging from 183 to 313 ppm (Table 8.1). These average values are much higher than those of dolomite formed in a normal marine environment, which typically has 110 to 160 ppm Na (Veizer, 1983). The plot of Na versus Mg% shows that Na concentration increases with increasing Mg% (Fig. 8.8). Although the more stoichiometric dolomite has low Na values, the higher concentration of Na in pure and more stoichiometric dolomite in the Mozduran Formation may be due to a higher salinity of dolomitizing fluids. Na has been used in many instances as an indicator of paleosalinity (Veizer, 1983; Land , 1985; Sass and Bein, 1988).

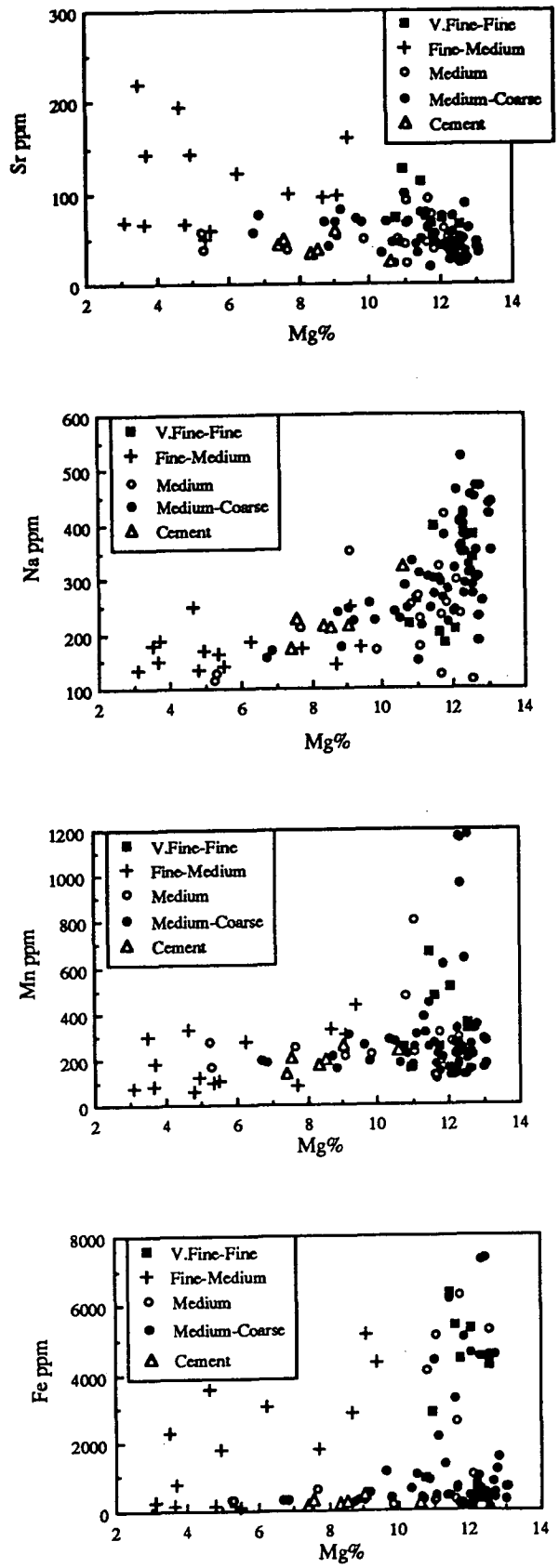

Figure 8.8. Variation of Sr, Na, Mn, and Fe versus Mg% in different dolomite types.

8.3.3.3 Manganese and Iron

The Mn and Fe concentrations in the Mozduran dolomites range from 64 to 1179 ppm (average 278 ppm), and from 113 to 7332 ppm (average 1619 ppm, Table A5.9, in Appendix 5). The average Mn and Fe values of different dolomite types (Table 8.1) are much higher than those of the Mozduran limestones, which have average Mn and Fe values of 124 and 728 ppm respectively. Mn and Fe in dolomite generally substitutes for Mg. Therefore, appreciable Mn and Fe concentrations in dolomite are due to a higher concentration of Mg in dolomite than in limestone. As the distribution coefficients of Mn and Fe in both calcite and dolomite are greater than unity (Pingitore, 1978; Veizer, 1983), the higher concentrations of these elements in the Mozduran dolomites may indicate reducing conditions (Land, 1986). Reducing conditions increase with increasing burial depth. As most dolomites in the Mozduran Formation formed at shallow to relatively deeper burial depth, high Mn and Fe values are expected. It is intresting to note that dolomite samples from the Gorgoıeh and Bazangan sections have relatively less Fe concentration than dolomite samples from the shallowest part of the basin (Table A5.9, in Appendix 5). This enrichment in Fe is attributed to the availability of appreciable amounts of terrigenous sediment in these sections and the presence of higher amounts of insoluble residue in these dolomites. The plot of Mn and Fe concentrations versus Mg% are shown in Fig. 8.8.

8.3.4 Oxygen and carbon isotopes

The oxygen and carbon isotope compositions of different dolomite types are plotted in Fig. 8.9, and average isotope values are summarized in Table 8.1. The $\delta^{18}O$ values in the Mozduran dolomites have a wide range, from -1.1‰ to -9.3‰ PDB, with an average of -6.5‰ PDB (Fig. 8.9). The $\delta^{18}O$ values in the Mozduran dolomites are relatively lighter than those in limestones. In limestones, the $\delta^{18}O$ values range from -1.2‰ to -7.9‰ PDB, with an average of -5‰ PDB. Isotopic compositions of dolomites in all sections studied fall into three distinct fields that correlate with grain size (Fig. 8.9). The decreasing $\delta^{18}O$ values from dolomite type 1 through dolomite type 5 probably resulted from an increasing temperature of the dolomitizing fluids, associated with increasing burial depths (see section 8.4 and 8.5).

The $\delta^{13}C$ values in all dolomite samples are positive (except two samples), and range from -1.3‰ to +5‰ PDB. The range of $\delta^{13}C$ values in dolomite and limestone (-0.3‰ to + 4.5‰ PDB) are similar and both have

average $\delta^{13}C$ values of +2.7‰. The average $\delta^{13}C$ values in all dolomite types are also very narrow, ranging from +2.08 to 2.87‰ PDB (Table 8.1). The similar range and average $\delta^{13}C$ values in dolomite and limestone in the Mozduran Formation, indicate that $\delta^{13}C$ values in dolomite are inherited from the limestone precursor during replacive dolomitization, and thus have a more normal marine value. The narrow range of $\delta^{13}C$ values in almost all dolomite samples, also suggests that the influence of meteoric water was negligible. Therefore, it is unlikely that the Mozduran dolomites formed in a mixing-zone environment. The absence of widely variant $\delta^{13}C$ values (positive to very negative values) may suggest that the sulphate reduction zone was very shallow and dolomitization occurred later in relatively deeper depth after sulphate reduction was completed. This interpretation is supported by the estimated depth of dolomitization in the Mozduran Formation (see section 8.5).

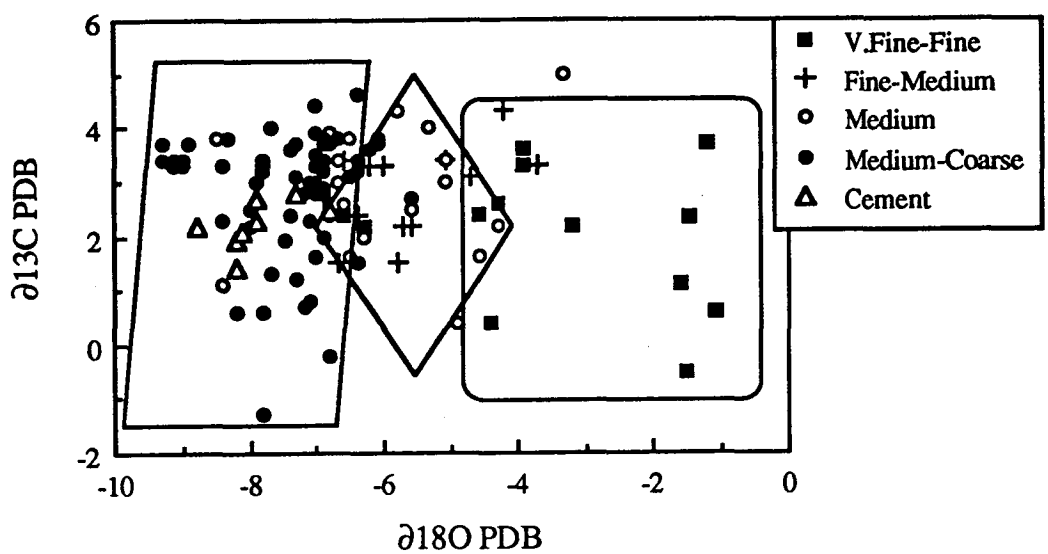

Figure 8.9. Plot of $\delta^{18}O$ versus $\delta^{13}C$ values of different dolomite types. Note isotopic compositions of dolomites fall into three distinct fields that correlate with grain size.

The $\delta^{18}O$ values in very fine to finely crystalline dolomite (dolomite type 1) range from -1.1‰ to -6.9‰ PDB (Table A5.9, in Appendix 5), with an average of -3.6‰ PDB. The $\delta^{18}O$ values in dolomite type 1 are significantly heavier than those of other dolomite types (Fig. 8.9). The $\delta^{13}C$ values in dolomite type 1 range from -0.5‰ to +3.7‰ PDB, with an average of +2.08‰ PDB. Dolomite type 1 is interpreted as the earliest formed dolomite in the Mozduran Formation. However, geochemical evidence, such as high Fe and

depleted $\delta^{18}O$ values (-6.9‰ PDB) indicates that the some of the very fine to finely crystalline dolomite has undergone further alteration, possibly under elevated temperature, later in the diagenetic history.

The $\delta^{18}O$ values in fine to medium crystalline dolomite (dolomite type 2) range from -3.7‰ to -6.9‰ PDB (Table A5.9, in Appendix 5), with an average of -5.7‰ PDB. These $\delta^{18}O$ values are lighter than those in dolomite type 1, but are heavier than most of the $\delta^{18}O$ values in dolomite types 3, 4, and 5 (Fig. 8.9). The $\delta^{13}C$ values in dolomite type 2 range from +1.5‰ to +4.3‰ PDB, with an average of +2.81‰ PDB.

The $\delta^{18}O$ values in the medium crystalline dolomite (dolomite type 3) show a wide range, from -3.3‰ to -8.5‰ PDB, with an average of -6‰ PDB. $\delta^{18}O$ values in type 3 dolomite are lighter than dolomite type 1, but heavier than most of the dolomite types 4 and 5. Some of the oxygen values in dolomite type 3 partially overlap with oxygen values in dolomite type 2 (Fig. 8.9). The $\delta^{13}C$ values in dolomite type 3, range from +0.4‰ to +5‰ PDB, with an average value of +2.87‰ PDB.

The $\delta^{18}O$ values in medium-coarsely crystalline dolomite (dolomite type 4) range from -5.6‰ to -9.3‰ PDB, with an average of -7.4‰ PDB. Dolomite type 4 has the lightest $\delta^{18}O$ values compared to other dolomite types, possibly indicating formation at elevated temperature. The $\delta^{13}C$ values in dolomite type 4 range from -1.3‰ to +4.6‰ PDB, with an average of +2.86‰ PDB.

The pore-filling dolomite cements (dolomite type 5), have a narrow range of $\delta^{18}O$ values, from -6.8‰ to -8.8‰ PDB, with an average of -7.9‰ PDB. The coarsely crystalline dolomite cement has the lowest average $\delta^{18}O$ value, compared to other dolomite types (Table 8.1). The range of $\delta^{18}O$ values in dolomite type 4 and 5 are very similar. The $\delta^{13}C$ values in dolomite type 5 range from +1.4‰ to +2.8‰ PDB, with an average of +2.2‰ PDB. The dolomite cements have a typical marine $\delta^{13}C$ signature (average +2‰ PDB). The light $\delta^{18}O$ values in these cements, by considering their marine $\delta^{13}C$ signature, may indicate precipitation from marine pore fluids at more elevated temperature during deep burial diagenesis. The calculated paleotemperature supports precipitation of dolomite cement at an elevated temperature (see section 8.4).

8.3.5 Covariation of isotopes and trace elements

8.3.5.1 Oxygen versus trace elements

The trace element and $\delta^{18}O$ values of different dolomite types are plotted on Figure 8.10.

The plot of $\delta^{18}O$-Sr values shows that Sr concentration is higher in dolomite samples which contain more positive $\delta^{18}O$ values. The higher Sr concentration in some fine-grained dolomites, with most enriched $\delta^{18}O$ values, may indicate that they have been least effected by diagenetic processes. In contrast, lower Sr concentration in coarse-grained dolomites, with more depleted $\delta^{18}O$ values, may be due to the more stoichiometric nature of coarse-grained dolomites.

The plot of $\delta^{18}O$-Na values shows that Na concentration is similar within the entire range of $\delta^{18}O$ values (except in a few coarsely crystalline dolomites). The similar range of Na in different dolomite types, with a wide range of $\delta^{18}O$ values, may suggest a similar salinity of dolomitizing fluids.

The plot of Mn and Fe versus $\delta^{18}O$ values shows that Mn and Fe concentrations are relatively similar throughout the range of $\delta^{18}O$ values, possibly due to formation under reducing conditions.

8.3.5.2 Carbon versus trace elements

The plot of $\delta^{13}C$-Sr values (Fig. 8.11) shows that Sr concentrations are similar throughout the range of $\delta^{13}C$ values, except in a few fine-grained dolomite samples.

The plot of $\delta^{13}C$-Na (Fig. 8. 11) shows that Na concentration in most of the dolomite samples increases with increasing $\delta^{13}C$ values. This may suggest higher water/rock interaction.

The plot of $\delta^{13}C$ versus Mn and Fe (Fig. 8.11) does not show any correlation.

8.4 Temperature of Formation

The calculated temperature from the heaviest $\delta^{18}O$ values of very fine to finely crystalline dolomite yield a temperature of 34° C. This temperature is similar to the temperature of modern supratidal settings, such as the Persian Gulf sabkha, in which dolomite is forming today. Type 4 dolomite yields temperatures within the range of 84 to 113° C. Type 5 dolomite cements give

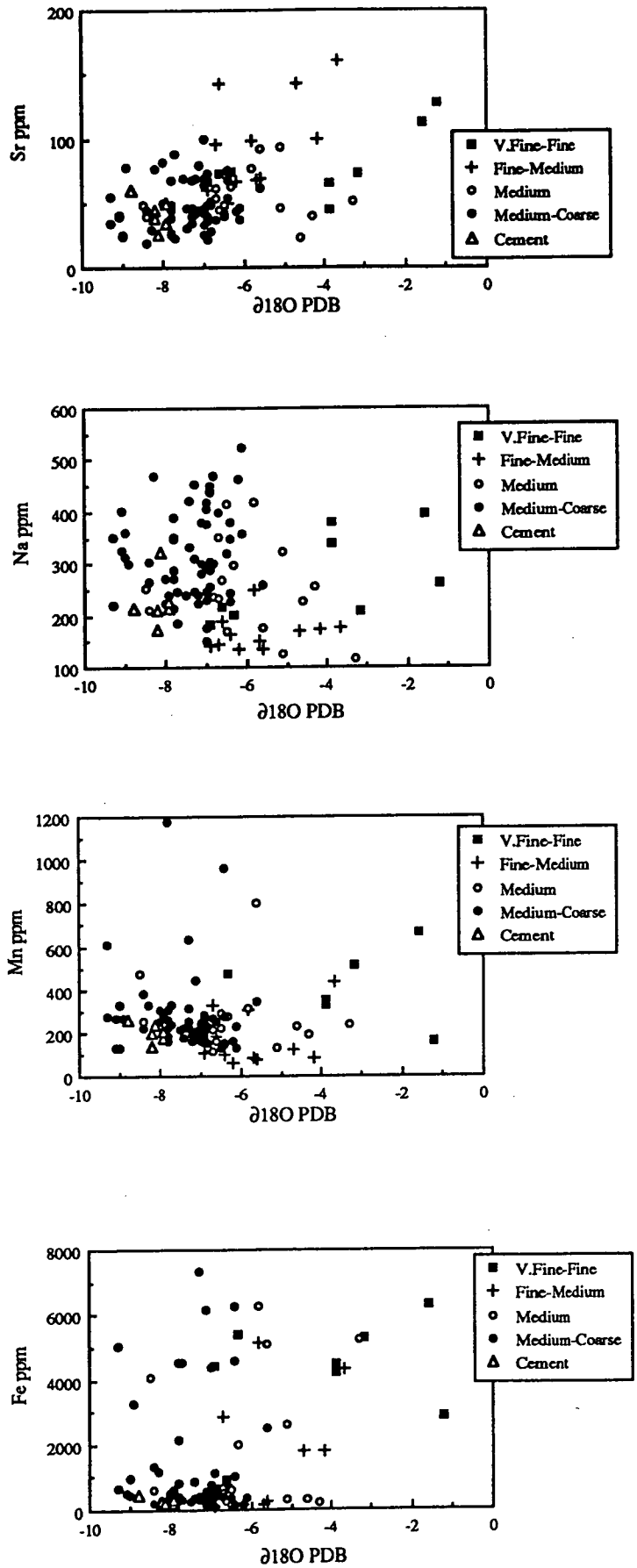

Figure 8.10. Variation of Sr, Na, Mn, and Fe versus $\delta\ ^{18}O$ values.

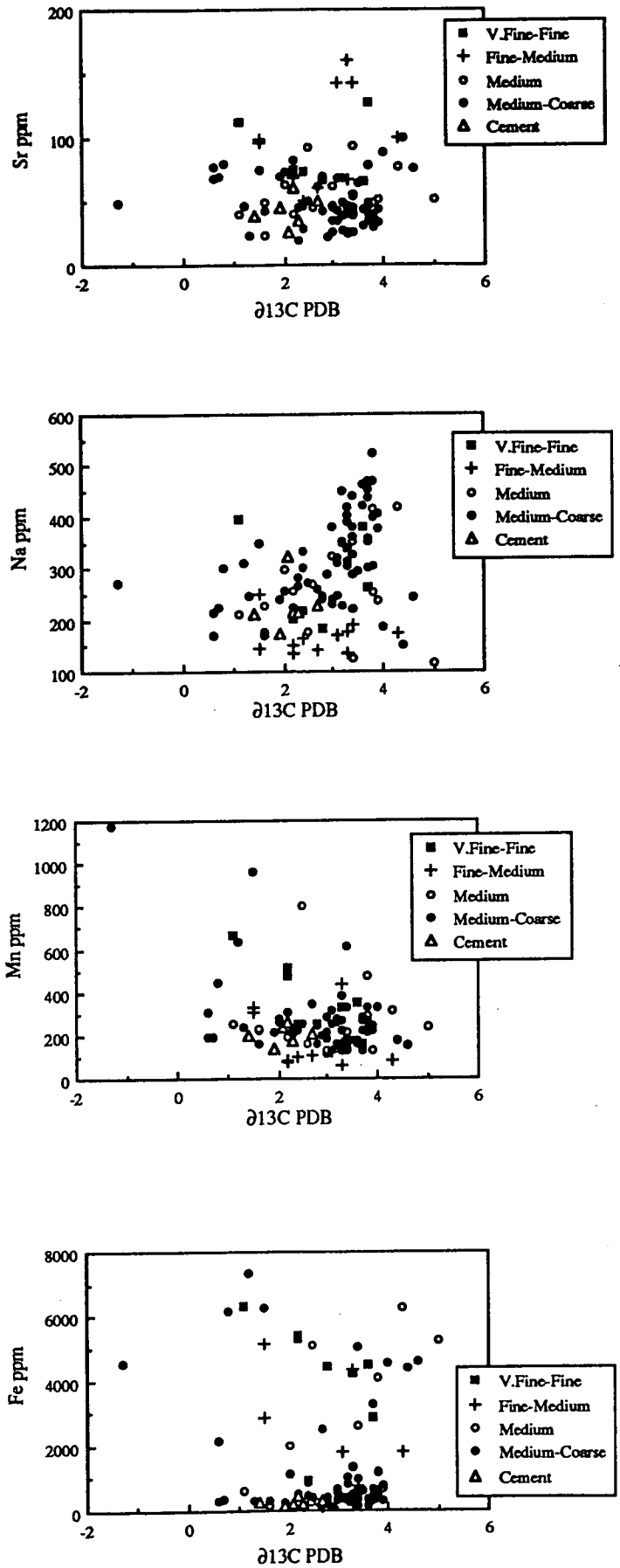

Figure 8.11. Variation of Sr, Na, Mn, and Fe versus $\delta^{13}C$ values.

temperatures in a range of 94 to ~110° C.

The temperature calculations are based on Land's (1985) equation:

$$T\ (^{\circ}C) = 16.4 - 4.3\ ([\ \delta^{18}O_{dol.} - 3.8] - \delta_{water}) + 0.14\ ([\ \delta^{18}O_{dol.} - 3.8] - \delta_{water})^2$$

For temperature calculation of dolomite type 1 (the earliest formed dolomite), the δ_W value of -1.2‰ (SMOW) was used for the Upper Jurassic seawater (Price and Sellwood, 1994). However, for temperature calculations of dolomite type 4 and 5, the δ_W of +2‰ (SMOW), as basinal fluid value, was assumed. The estimated range of $\delta^{18}O$ values for basinal fluids is +2‰ to +8‰ SMOW (Srinivasan et al., 1994). The $\delta^{18}O$ value of +2‰ SMOW, gives reasonable temperatures for dolomite types 4 and 5, which is consistent with the geohistory diagram constructed for the basin (Moussavi-Harami and Brenner, 1992).

8.5 Burial History

The estimated maximum burial depth of the Upper Jurassic Mozduran Formation in the eastern Kopet-Dagh Basin is about 4 km (Moussavi-Harami and Brenner, 1992, Fig. 8.12). Calculated temperatures from stable oxygen isotope compositions of medium-coarsely crystalline dolomite and pore-filling dolomite cement (ranging from 84 to 113° C, and 94 to ~110°C respectively), suggest that these dolomites formed between burial depths of ~3.5 and ~4.5 km. If we assume that temperature was the main control, dolomite types 2 and 3 probably formed at a shallower depth (between ~ 1 to ~<3.5 km) than dolomite types 4 and 5, as their average $\delta^{18}O$ values are about 1.5 to 2‰ heavier (Table 8.1).

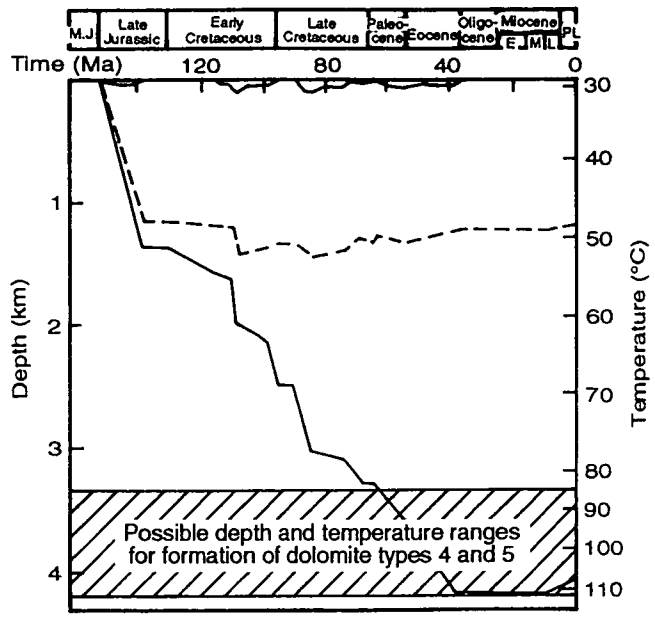

Figure 8.12. Possible burial depths for formation of dolomite types 4 and 5 on the burial history diagram (modified after Moussavi-Harami and Brenner, 1992). Note medium to coarsely crystalline dolomite and pore-filling dolomite cements probably formed at depths of ~3.5 to ~4.5 km, based on oxygen isotope data.

8.6 Timing of Dolomitization

It is believed that various types of dolomite in the Mozduran formation formed in different diagenetic environments at different times, producing distinctive petrographic and geochemical characteristics. On the basis of petrographic and geochemical features of different dolomite types, there appears to be three main times of dolomitization:

1) The very fine to finely crystalline dolomites formed under near surface, low temperature conditions, in a supratidal to upper intertidal setting, by normal marine water, probably during the Upper Jurassic. This interpretation is borne out by many lines of evidence such as: a) crystal size and fabric, b) preserved traces of depositional textures, c) the most enriched $\delta^{18}O$ value (-1.1‰ PDB), which is similar to the Upper Jurassic δ_W of -1.2‰ (SMOW), and d) the inferred low temperature of formation (~34° C).

2) Dolomite type 2 probably formed in shallow burial. The following petrographic and geochemical relationships such as: a) crystal size and fabric, b) dolomite formation in pre- and post-stylolitization, and c) relatively heavier $\delta^{18}O$ values compared to dolomite types 3, 4, and 5, support this interpretation.

Dolomite type 3 is interpreted as having formed in shallow to intermediate burial. The proposed shallow to intermediate burial origin is based

on: a) planar crystal boundaries, b) the relatively lower range and average $\delta^{18}O$ values, compared to dolomite types 4 and 5, and c) the inferred intermediate temperature of formation. Dolomitization in dolomite types 2 and 3 probably occurred during the early to late Cretaceous.

3) Dolomite type 4 is recognized as a product of late (deeper) burial diagenesis, on the basis of petrographic and geochemical characteristics, such as: a) crystal size and fabric (nonplanar texture), b) very depleted $\delta^{18}O$ values, and c) the inferred elevated temperature (ranging from 84 to 113° C).

The petrographic and geochemical relationships of dolomite type 5, such as: a) occurrence as void-filling cement in late stage fractures and vugs, b) association with dissolution seams, c) cross-cutting of other dolomite types, d) very depleted $\delta^{18}O$ values, and e) the inferred elevated temperature (ranging from 94 to ~110° C), support a late (deeper) burial diagenetic origin. If these estimated temperatures are resonable, dolomitization in dolomite type 4 and cement precipitation in dolomite type 5 probably had been taking place from the Paleocene through the Eocene. This interpretation is based on the burial history of the area (Fig. 8.12).

Dolomitiztion in dolomite type 4 and cement precipitation in dolomite type 5 probably resulted from sedimentary and tectonic loading, and tilting and uplift of the basin. Three episodes of regional tectonic uplift occurred in the basin during the late Cretaceous (99-95 Ma), Paleocene (74-70 Ma), and Eocene (63-54 Ma, Fig. 8.12, Moussavi-Harami and Brenner, 1992).

8.7 Magnesium Source

It has been suggested that for early or penecontemporaneous dolomitization, the only source of magnesium may be marine seawater (Land, 1985, Given and Wilkinson, 1987). This source of Mg^{2+} only applies to the finely crystalline dolomite (dolomite type 1) which is the earliest generation of dolomite formed under near-surface, low temperature conditions in a tidal flat environment, possibly through tidal pumping of seawater. The presence of floating dolomite rhombs (dolomite type 2) within the lime mud matrix more likely occurs during early shallow burial diagenesis. There is abundant evidence that some scattered dolomite rhombs and irregular patches in some carbonate sequences, particularly in mudstone and wackestone facies, occurred during early mechanical compaction (e.g., Kendall, 1977; Qing and Mountjoy, 1989). Therefore, one of the most probable sources for magnesium in dolomite type 2 may be pore water enriched in Mg^{2+}, due to dissolution of high-Mg calcite

during early shallow burial, as suggested by Cander et al. (1988), and Mukhopadhyay (1996).

Although the burial dolomitization model might be criticized because of an inadequate Mg^{2+} source and delivery mechanism in the deep subsurface (Morrow, 1982; Land, 1985), recent published papers indicate that dolomitization at burial depth is significant (e.g., Lee and Friedman, 1987; Machel and Anderson, 1989; Barnaby and Read, 1992). This supports the burial dolomitization model proposed by others (e.g., Mattes and Mountjoy, 1980; Zenger and Dunham, 1980; Zenger, 1983; Gregg, 1985). The magnesium for the medium to coarsely crystalline (types 3, 4, 5) dolomites is likely to be derived from, 1) compaction of underlying shales, and/or 2) basinal brines.

Kahle (1965), Mattes and Mountjoy (1980), McHargue and Price (1982) and Sternbach and Friedman (1984) have suggested that sufficient magnesium ions for dolomitization can be generated from the transformation of smectite (Mg^{2+} lost) to illite during shale diagenesis at burial depth. Such conversion releases magnesium to the pore fluids, which migrate upwards, to dolomitize the overlying carbonates. Magara (1976) has demonstrated that in thick, compacting shale sequences within basins, the net direction of water movement is vertically upwards. As some massive dolomites occur in the lower-most portion of the Mozduran Formation, and are directly underlain by thick (>1000 m) alternating sequences of shale and sandstone, the compacting clays can be a possible magnesium source for dolomitization of the lower part of sequence. It is worthwhile to note that normal shale compaction curves show a reduction of original shale porosity to about 35 percent at burial depths of 600 meters, dropping to below 25 percent at about 1100-1200 meters (Mattes and Mountjoy, 1980). However, Land (1985) discussed that magnesium released by this conversion is consumed by the formation of authigenic chlorite and not by the precipitation of dolomite. In the Mozduran carbonates authigenic chlorite is absent.

Basinal brines have been suggested to be an important magnesium source for dolomitization at burial depth (Gregg, 1985; Lee and Friedman, 1987; Qing and Mountjoy, 1989; Gao and Land, 1991; Srinivasan et al., 1994). For relatively thick medium to coarsely crystalline dolomite beds, which are present throughout the middle and upper part the Mozduran sequence, basinal brines may be an important source for magnesium. The fluid was possibly expelled from the basin and moved eastward along porous and permeable conduit systems, due to gradual and progressive sedimentary and tectonic loading and

tilting of the west side of the basin by thick Cretaceous and early Tertiary sequences. Lasemi (1996) suggested that dolomitization in the Mozduran Formation possibly occurred by Kohout convection during the transgressive and highstand phases of sea level.

Pressure dissolution of limestone as another source of magnesium for dolomitization has been suggested by some workers (e.g., Wanless, 1979; McHargue and Price, 1982). Pressure dissolution is not an important source for magnesium because minor amounts of stylolite-concentrated dolomite have been observed in the Mozduran dolomites.

Recently, Barnaby and Read (1992) suggested that magnesium required for burial dolomitization can be derived from the dissolution of dolomitic units located elsewhere. As there are no dolomitic units adjacent to the basin, the possibility of dissolution of external dolomitic rocks as a major magnesium source for dolomitization in the study area is ruled out.

8.8 Conclusions

Petrographic and geochemical studies reveal that five different dolomite-rock textures have resulted from multistage dolomitization. Dolomite type 1 consists of very fine to finely crystalline dolomite, forming penecontemporaneously or by early replacement of carbonate mud, soon after deposition, with Mg possibly derived from seawater. Dolomite type 1 has the most enriched $\delta^{18}O$ values compared to other dolomite types. On the basis of crystal size, fabric, and absence of fossils, dolomite type 1 is considered to have been formed in a supratidal to upper intertidal setting, under near surface, low temperature (~34° C) conditions. Dolomite type 2 consists mainly of euhedral rhombs either floating in a limestone matrix, or within intercrystalline areas filled by sparry calcite cement. This dolomite type resulted from replacement of precursor calcium carbonate, mainly during early shallow burial, and Mg was probably derived from dissolution of high-Mg calcite. Dolomite type 3 is considered to represent a diagenetic replacement of preexisting limestone and/or recrystallization of an early formed dolomite, possibly after some burial. Dolomite type 4 has medium to coarse nonplanar crystals, often characterized by nonmimically replaced allochems, possibly developed during deep burial (~3.5 to ~4 km), in temperatures ranging from 84 to 113° C.

The last dolomitizing events are represented by dolomite type 5, which consists of coarsely crystalline planar-C (cement) dolomite, lining voids, vugs and fractures. This dolomite type has been interpreted as having formed at the

latest diagenetic stage, at elevated temperature, ranging from 94 to ~110° C. Dolomite types 4 and 5, with the highest temperatures of formation, compared to other dolomite types, possibly formed during the period of maximum burial, between Paleocene and Eocene time. Dolomite crystals are commonly dark orange-red luminescent and are stoichiometric in composition.

Compaction of shales and clay diagenesis, combined with basinal brines, could produce enough magnesium for shallow to deep burial dolomitization (dolomite types 3 and 4), and dolomite cementation (dolomite type 5). Basinal brines possibly conducted updip along porous and permeable conduit systems, from west to east of the study area, as a result of tilting and sedimentary and tectonic loading, particularly in the western side of the basin.

As a result of strong dolomitization and recrystallization, and/or neomorhism, original textures of the precursor sediments have been obliterated, except in a few samples, in which the only traces of original depositional textures have been preserved. The dolomite crystals are generally non-ferroan in composition, although ferroan dolomites are also present in some samples. Some dolomite crystals underwent pressure dissolution, as indicated by the presence of crystal-cutting stylolites and dissolution seams. The presence of higher concentrations of organic matter in dolomites than limestones (2 to 5 times higher), may indicate that dolomitization occurred preferentially in limestones that originally had higher concentrations of organic matter.

PART II

RENISON CARBONATES

CHAPTER 9

TEMPORAL AND REGIONAL SETTING

CHAPTER 9

TEMPORAL AND REGIONAL SETTING

9.1 Aim and Scope of Study

This study focuses on four aspects of the Renison Proterozoic carbonates:

- determining primary vs secondary dolomitization, environment of deposition and paleoclimate (see Chapter 10).
- application of chemostratigraphy to determine the age of the Renison carbonates (see Chapter 11).
- study of the sources of hydrothermal fluids responsible for carbonate alteration, the temperature range for carbonate replacement mineralization, and the extent of fluid/rock interaction (see Chapter 12).
- interpretation of diagenetic history of the Renison carbonates (see Chapter 13).

9.2 The Significance of the Proterozoic Setting

9.2.1 Atmosphere

The aspects of the Proterozoic atmosphere, based mainly on geological evidence such as studies of banded iron-formations (BIFs), paleosols, and the distribution of red beds, have been discussed recently by many researches (e.g., Klein, 1992; Holland, 1992; Lowe, 1992; Kasting, 1992). All of this evidence indicates an increasing O_2/CO_2 ratio through most of Proterozoic time.

Banded iron-formations are the most abundant chemical sediments throughout much of Proterozoic time and their chemistry and temporal distribution provide important clues about the evolution of the Proterozoic ocean and atmosphere. All iron-formations older than about 1.9 Ga represent very similar chemical systems. Iron-formations formed between 0.8 and 0.6 Ga are distinctly different and more highly oxidized. Thus after about 1.85 Ga, the atmosphere and oceans became highly oxygen enriched and the ocean as a whole became depleted in iron (Klein, 1992).

Studies of Proterozoic paleosols indicate that there was a significant increase in the atmospheric O_2/CO_2 ratio during the age range between 2.2 to 1.8 Ga. The distribution of red beds supplies additional evidence for a rise in the oxygen content of the atmosphere during Proterozoic time.

A three-stage model for the rise of O_2 during the Proterozoic period has been proposed by Kasting et al., (1992). During Stage I, termed "reducing", the entire atmosphere/ocean system was essentially devoid of free oxygen (prior to 2.4 Ga). Atmospheric O_2 levels predicted during this stage are in the order of 10^{-14} PAL (times the present atmospheric level) or lower (Schopf, 1992). During Stage II (from 2.4 to ~1.85 Ga), surface environments were oxidized and the deep ocean was reduced. Atmospheric O_2 levels were ~0.03 PAL during Stage II. In Stage III, beginning ~1.85 Ga, the deep ocean became oxic and therefore depleted in iron (Klein, 1992).

Proterozoic CO_2 levels from Climate Model calculations (Kasting, 1992) indicate that atmospheric CO_2 levels declined during the Proterozoic. Atmospheric PCO_2 levels during the early Proterozoic were probably about 60 times greater than the present level. In the late Proterozoic, during global glaciation, PCO_2 levels were probably three times greater than the present value. Thus, CO_2 (greenhouse gas) was probably one of the most important constituents of the Proterozoic atmosphere. The process by which CO_2 is lost from the atmosphere/ocean system over long time periods involves weathering of silicate minerals on the land, followed by deposition of carbonate minerals on the sea floor (Kasting, 1992). The inferred ranges of atmospheric CO_2 and O_2 during Archean and Proterozoic times are shown in Fig. 9.1.

9.2.2 Ocean chemistry

Although the salinity and chemistry of Proterozoic seawater is still poorly constrained, Holland (1992) suggested that salinity and chemistry of Proterozoic seawater did not differ greatly from that of modern seawater. Since several Proterozoic normal marine sequences of carbonates, gypsum ± anhydrite, followed by halite have been documented, the proposed "soda ocean " by Kempe and Degens (1985) is not appropriate at least before 1.4 Ga.

Siderite studies show a ^{13}C depletion of about 4‰ with respect to modern marine carbonates. This ^{13}C depletion of siderites during early Proterozoic time indicates that the ocean system was stratified with respect to the isotopic composition of carbon, unlike present-day oceans in which the $\delta^{13}C$ gradient is small (Klein, 1992). Secular variation in $\delta^{18}O$, $\delta^{13}C$, $\delta^{34}S$ and Sr isotopes has

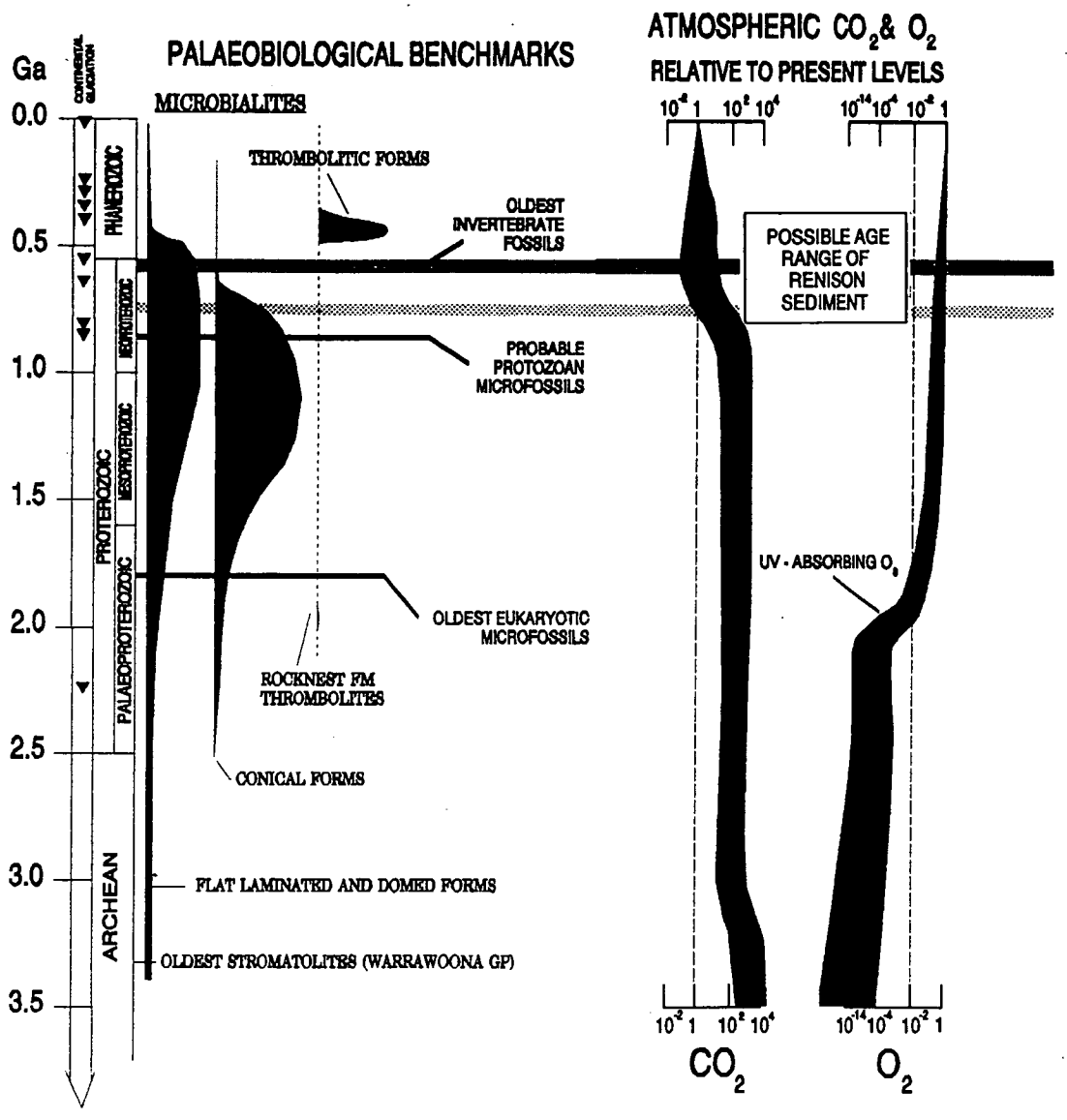

Figure 9.1. Inferred ranges of atmospheric CO_2 and O_2, and paleobiological benchmarks (after Schopf, 1992; with additional material from Plumb, 1991 and Walter et al., 1992).

been reported from Neoproterozoic sequences (Veizer and Hoefs, 1976; Veizer, 1989; Kaufman and Knoll, 1995).

9.2.3 Climate

Climate has been postulated to be a major control on carbonate mineralogy and sedimentation. Little is known about the Proterozoic climate other than the existence of a series of glacial events. The Proterozoic period was marked by five well-documented glacial periods (Harland, 1983). The first one was at ~2.3 Ga (Huronian glacial), and the next four occurred during the late Proterozoic as a series of glacial and interglacial intervals. During the late Proterozoic, from the four glacial periods, only two major phases of glaciation have been widespread and well documented worldwide (Harland, 1983; Derry et al., 1992; Kaufman and Knoll, 1995). These aspects are discussed in more detail in Chapter 10.

9.2.4 Life

The Archean and Proterozoic temporal distributions of major biological groups, paleobiological benchmarks, and the temporal distribution of paleoenvironmental indicators are summarised by Schopf (1992). Prokaryotes and Eukaryotes (in the form of single-celled algae, multicelled algae and protozoans) were present during the late Proterozoic when Renison deposits were formed. Stromatolites with wavy type and rhombic shape microbial laminae (Walter et al., 1992) are present only in small amounts in the Renison mine area. Grotzinger (1990) proposed that the decline of stromatolites in the late Proterozoic, was due to the decrease in carbonate saturation of seawater. The non-elongate, low domal type stromatolite (present in Renison mine) has been reported from less agitated waters and protected tidal flats (Hoffman, 1976). The finely laminated nature of some dolomite beds and the good preservation of microbial mats in the Renison deposits indicates the absence of any burrowing or boring activities by organisms. Additionally, Walter et al. (1992) supported the idea that the fine lamination of Proterozoic stromatolites can be cited as evidence of possible precipitation, in contrast to Phanerozoic "trapping and binding" stromatolites which often show poor lamination. The paleobiological benchmarks during Archean and Proterozoic times are shown in Fig. 9.1.

9.3 Regional Geology

Extensive Proterozoic carbonates occur in western Tasmania (Calver, 1989). These carbonate sequences occur within the central part of the Dundas Trough, a north-south trending eugeosyncline, consisting of Proterozoic to early Paleozoic sedimentary rocks. This trough is bounded to the east by the Proterozoic Tyennan Massif, composed of deformed and metamorphosed siltstone, quartzites, and possibly mafic volcanics, and to the west by a less deformed and metamorphosed late Proterozoic quartzite-quartz wack-slate sequence of the Rocky Cape Massif (Solomon, 1981; Corbett, 1981; 1992; Corbett and Turner, 1989, Fig. 9.2). Dalziel (1992) suggested that these quartz-rich metasediments were deposited as turbiditic sequences into a continental setting between western USA and Australia.

The oldest sediments in the Dundas Trough are the shallow shelf carbonates and siliciclastics of the Success Creek Group (~1000 m; late Proterozoic, Patterson et al., 1981; Morrison, 1982; Brown, 1986, 1989) which unconformably overly the Oonah Formation. The Success Creek Group is conformably followed by a thick succession of relatively shallow marine carbonates, siliciclastics and volcaniclastics of the Crimson Creek Formation, in the Mt Lindsay-Parsons Hood area (~5000 m; Vendian, Brown 1989) for which some workers have assumed an early Cambrian age (Patterson et al., 1981; Morrison, 1982; Moreland, 1988, see Chapter 11). The Crimson Creek Formation is interbedded and intruded by tholeiite sills and dikes. The Crimson Creek Formation is overlain with presumed conformity (Williams, 1976) by a fossiliferous flysch-type sequence of siliciclastics called the Dundas Group (~3800 m; middle to late Cambrian, Corbett, 1981; Crawford et al., 1992, Fig. 9.3). This unit forms the major infill of the Dundas Trough. Boundaries with the underlying Crimson Creek Formation are commonly faulted (Brown, 1986). Deposition of the Dundas Group sediments, in the central Dundas Trough, was accompanied by the development of the Mount Read Volcanic Belt, along the eastern margin of the trough (Fig. 9.2). The Mount Read Volcanic Belt has a thickness of at least 2800 m and consists mainly of dacitic and rhyolitic flow, breccias, ash-fall and ash-flow tuffs with minor sedimentary intercalations.

The Dundas Group is in turn overlain by late Cambrian to early Ordovician coarse siliciclastic sediments (100-1200 m), known as the Owen Conglomerate (Banks, 1962; Campana and King, 1963), which were largely derived from the Tyennan nucleus in the east. This unit was followed unconformably by regionally transgressive shallow marine peritidal carbonates in

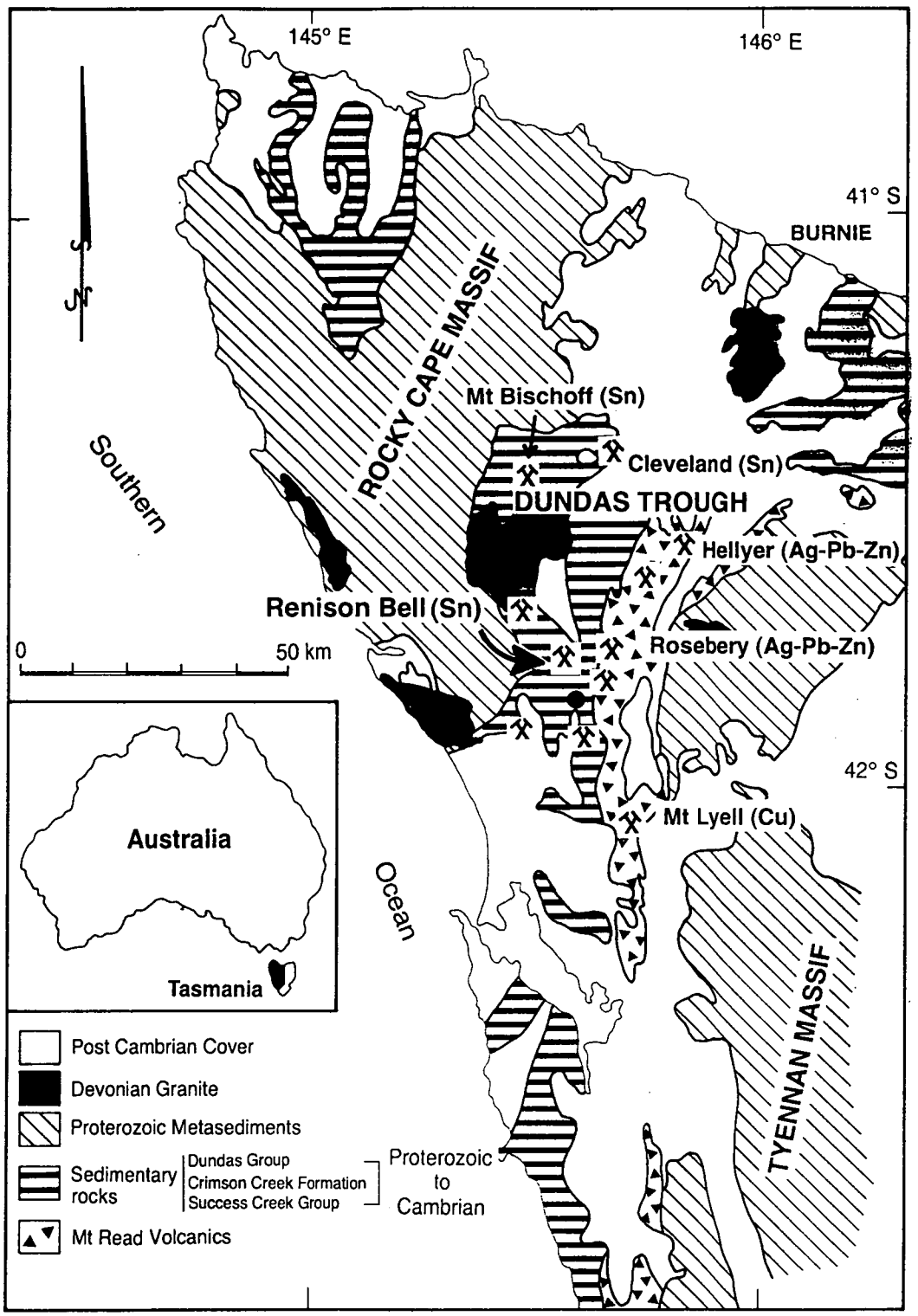

Figure 9.2. Regional geology of western Tasmania and the location of the Renison tin mine within the Paleozoic Dundas Trough (modified after Moreland, 1988).

the early Ordovician (Gordon Group) and Silurian to early Devonian shallow marine clastic shelf sediments of the Eldon Group (Fig. 9.3). These are unconformably overlain by Pleistocene sediments.

Sedimentation in western Tasmania was interrupted in the Middle Devonian by a period of intense deformation, due to major orogenic episodes correlated with the Tabberabberan Orogeny (Solomon, 1981; Corbett, 1981; Crawford et al., 1992). This Orogeny produced regional north-northwest trending open folds with steep reverse faults and later wrench reactivations (Berry, 1989). During the late Devonian to early Carboniferous, widespread granitoid plutons (340 to 375 Ma; Solomon, 1981) were emplaced into the Dundas Trough. Mineralization in parts of western Tasmania are believed to be genetically associated with the emplacement of these granitoids.

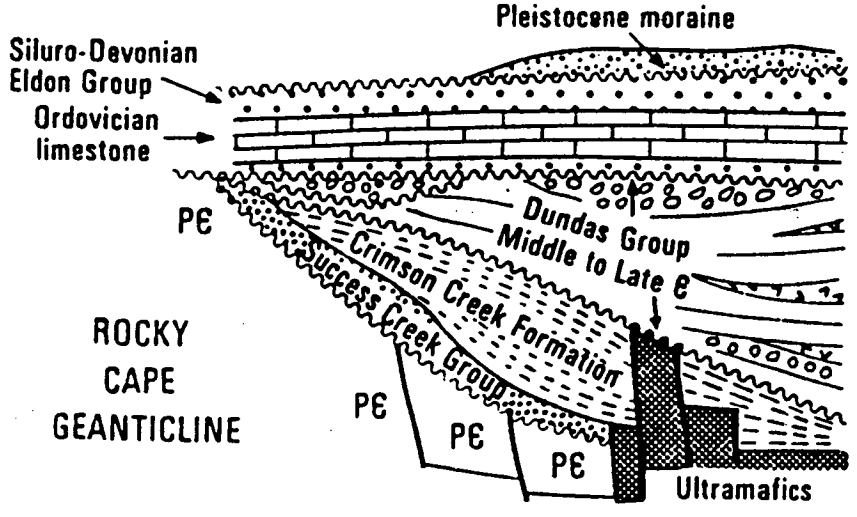

Figure 9.3. Diagrammatic section across the Dundas Trough (Corbett, 1981).

9.4 Renison Mine Geology

9.4.1 Previous study

Preliminary descriptions of the Renison mine deposits have been undertaken since 1900, when mining operations began in this area (e.g., Waller, 1902; Ward, 1909; Herman, 1914; Condor, 1918; Stillwell and Edwards, 1943; Blissett, 1962). More detailed and comprehensive geological studies of the Renison mine area have been undertaken by many authors, for example:

- Groves (1968) briefly described the ore mineralogy at the Renison and more

extensively Pine Hill Granitoids

- Collins (1972) studied the geology and mineralogy of the South Renison Bell area
- Patterson (1979) and Patterson et al. (1981) researched the geological setting and mineralization at Renison Bell area
- Ward (1981) examined the mineralogy of the Pine Hill Granite
- Morrison (1982, 1993) described the stratigraphy and sedimentology of the Renison Mine Sequence
- Davis (1985) studied the nature and the mechanisms of the stratabound mineralization at Renison Mine
- Jones and Evans (1985) reported the trace element and stable isotope variations in rocks of the Renison Mine Sequence
- Holyland (1987) discussed the structure and hydrodynamics of the Renison Tin Mine
- Leaman (1990) described the form of the Pine Hill Granite based on a gravity survey
- Lea (1991) proposed a refined model for orebody formation in the Renison Mine Lease exploration report
- Haines (1991) studied the stratigraphy and sedimentology of the Lower Crimson Creek Formation and related mafic igneous rocks in Renison Bell Mine
- Kitto (1992, 1994) dissussed structural and geochemical controls on mineralization at Renison

Since the geology of the Renison mine area has been discussed by the above researchers, only a summary of the Renison mine geology is presented below.

9.4.2 General geology of the Renison district

Renison, the largest primary tin producer in Australia, is situated at Renison Bell on the west coast region of Tasmania, south-east of the Proterozoic Rocky Cape Massif, at latitude 41° 47' S, and longitude 145° 26' E (Fig. 9.2). Renison also is the largest stratabound, carbonate replacement tin deposit in western Tasmania. The other major stratabound deposits in western Tasmania occur at Mt Bischoff (Groves et al., 1972; Halley, 1987) and Cleveland (Collins, 1981).

The Success Creek Group, which are host sediments to tin mineralization, outcrop mainly in the central and western region of the mine area (Fig. 9.4) and unconformably overly a Proterozoic basement (Brown, 1986). The Crimson

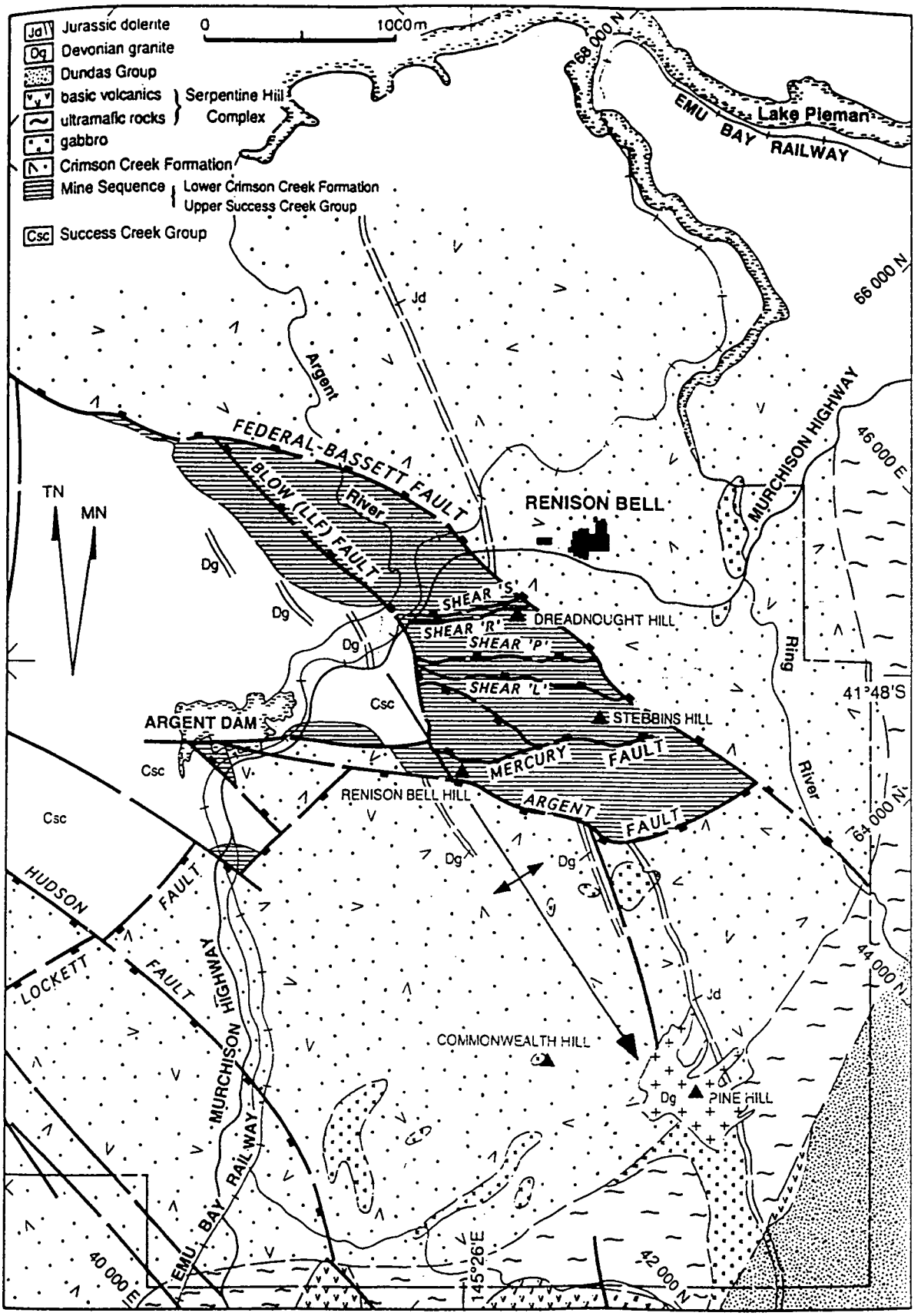

Figure 9.4. Geological Map of the Renison district (Kitto, 1994).

Creek Formation, which conformably overlies the Success Creek Group occurs over most areas of the mine lease (Fig. 9.4).

The Serpentine Hill Ultramafic Complex is located to the east and southeast (with an arcuate shape near Pine Hill granite) of the mine area. Berry and Crawford (1988) described this unit as part of an early middle Cambrian allochthonous thrust sheet.

The Dundas Group outcrops in the far southeast corner of the mine lease, adjacent to the Serpentine Hill Complex (Fig. 9.4). The Dundas Group sequences overly the Crimson Creek Formation.

The Pine Hill Granite is exposed in the southeast part of the mine lease and forms a north-west plunging ridge beneath the mine area (Kitto, 1994, Fig. 9.4). It is suggested that the Pine Hill Granite supplied the source of hydrothermal fluids responsible for carbonate replacement and vein styles of cassiterite mineralization (Leaman, 1990; Lea, 1991; Kitto, 1992, 1994; Adabi et al., 1996 b).

9.4.3 Stratigraphy

The Neoproterozoic sedimentary rocks at Renison occur within the central part of the longitudinal Paleozoic Dundas Trough, bounded by the Proterozoic Tyennan and Rocky Cape Massif (Soloman, 1981). In the Renison mine area, the Success Creek Group, Crimson Creek Formation, Dundas Group, Serpentine Hill Complex and Pine Hill Granite are present. The stratigraphy of the Renison mine area has been described by many authors (e.g., Collins, 1972; Patterson, 1979; Patterson et al., 1981; Moreland, 1988; Haines, 1991; Kitto, 1992), with the most comprehensive studies by Morrison (1982, 1993). The detailed stratigraphic units at Renison are summarised in Figure 9.5.

The Renison deposit at the mine area occupies the upper part of the Success Creek Group and the lower part of the Crimson Creek Formation. This portion is called the Mine Sequence by mine geologists (Fig. 9.5). The Mine Sequence generally consists of alternating sequences of dolomites and siliciclastics. Dolomites occur in three main units, which in ascending order, are known as the No.3, No.2 and No.1 dolomites.

9.4.3.1 Success Creek Group

The Neoproterozoic Success Creek Group, a 1000^{+} m thick shallow shelf sequence of siliciclastic facies hosting the No.2 and No.3 dolomites of the Renison Mine Sequence, are the oldest rocks in the mine area. The Success Creek

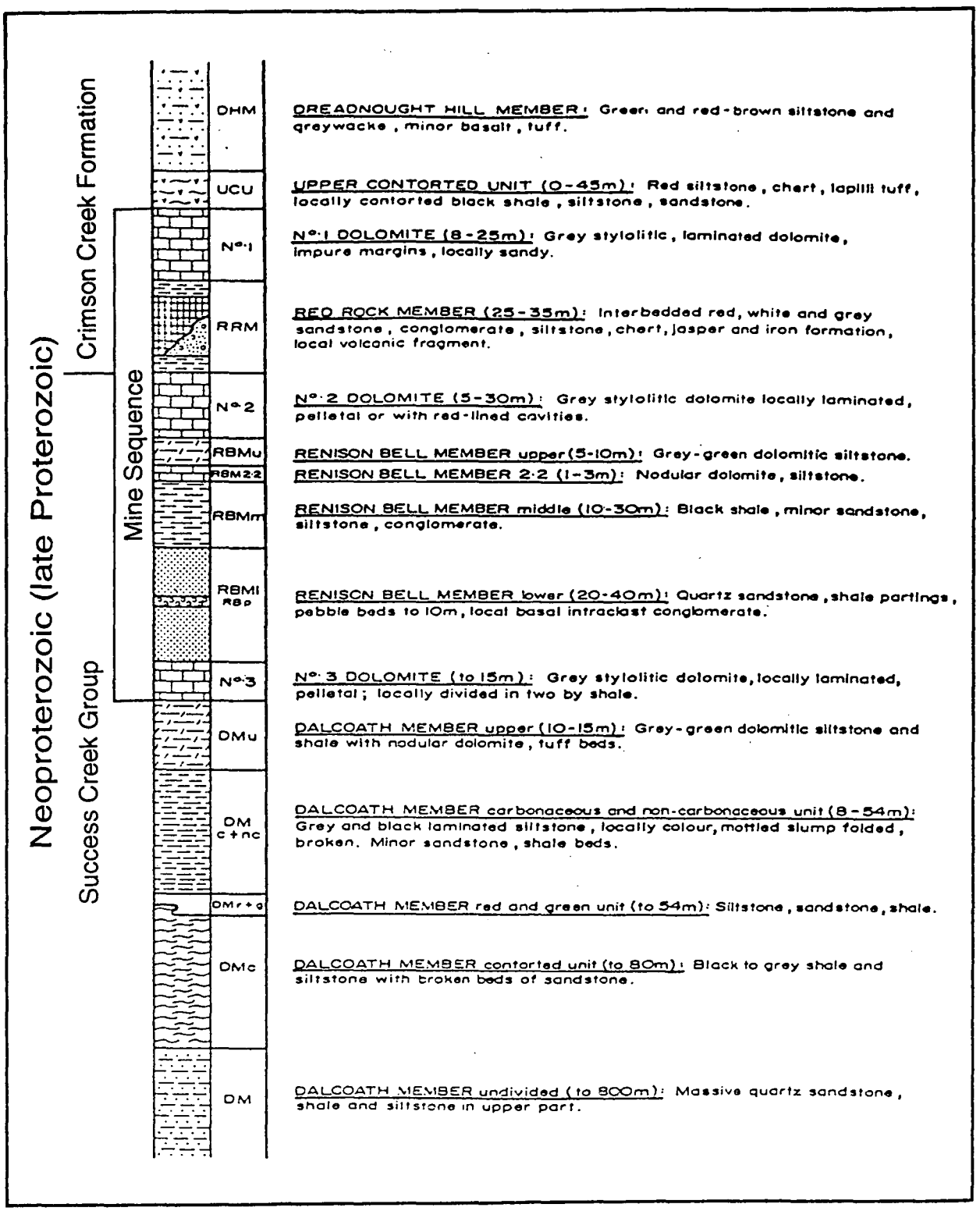

Figure 9.5. Stratigraphy of the Renison mine sequence (modified after Morrison, 1982).

Group formed locally in rift basins along a thinned continental margin (Morrison, 1982; Brown, 1986, 1989).

The Success Creek Group, which hosts the Renison deposits is correlated on stratigraphic grounds with the dolomite bearing sequences at Smithton, Savage River, Birthday Bay, Jane River and the Weld River Group (William, 1978; Morrison, 1982). It is intresting to note that almost all dolomite bearing sequences are within or marginal to the Proterozoic massifs, rather than restricted to the Dundas Trough (Fig. 9.6). Their stratigraphy and sedimentology is comparable to late Proterozoic (Adelaidean) sequences elsewhere in Australia (Morrison, 1982). The K-Ar dating of detrital muscovite from the Oonah Formation below the Success Creek Group, gives an age of 708 ± 6 Ma (Turner, 1993).

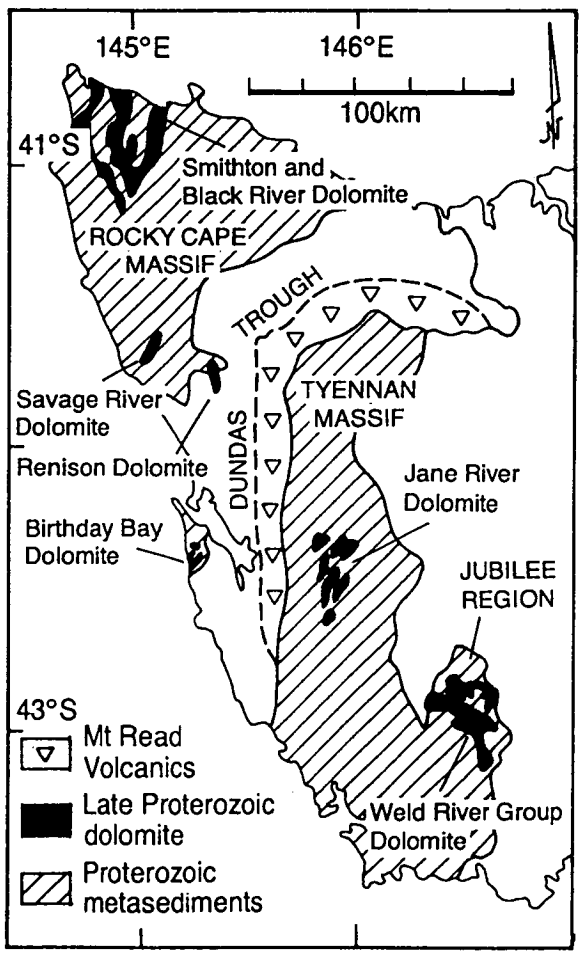

Figure 9.6. Simplified geological map of western Tasmania showing the distribution of Neoproterozoic dolomite-bearing sequences (black). Note association of dolomites with Proterozoic rather than Cambrian sequences (modified after Morrison, 1982; Corbett and Turner, 1989).

The Dalcoath Member, the basal unit of the Renison mine sequence, within the Success Creek Group, consists of at least 800 meters of massive, well sorted quartz sandstone, with interbedded micaceous sandstone, siltstone and shale (Patterson et al., 1981, Figs. 9.5, 9.7 A). Diamictite has also been reported from this basal unit (Morrison, 1982; Brown, 1986). In the upper part, this unit is overlain by the "Dalcoath Contorted" (up to 80m thick) and consists of intensely contorted, laminated, black to grey shale and siltstone with broken beds of sandstone. Soft-sediment deformation with later tectonic overprinting is the nature of the contortion (Brown, 1986). A lithologically equivalent, relatively undisturbed carbonaceous and non-carbonaceous laminated siltstone and shale, with variable thickness (8-54 m) overlies this sub-unit. Wavy, lenticular, cross bedded and locally slump structures are present. The final sub unit is the "Dalcoath Upper" (10-15 m), which consists of laminated shale and siltstone units with weakly folded and nodular dolomite beds.

The Dalcoath Member is overlain by the No.3 dolomite (up to 15 m, Figs. 9.5, 9.7 B), which hosts the known stratabound mineralization. This unit, within the mine area, consists of dolomicrosparite and dolomicrite with abundant vein and saddle dolomite. Dolomite has minor but variable amounts of quartz, chlorite, talc and muscovite (Adabi et al., 1996 b). The dolomite consists of massive to finely laminated light to dark grey beds.

The Renison Bell Member (RBM) conformably overlies the No.3 dolomite, and consists of the three subunits (Figs. 9.5, 9.7 C). The Lower Member comprises 20-40 m of massive fine grained quartz sandstone, shale partings and pebble beds with local basal conglomerate. The Middle unit (10-30 m) consists of laminated micaceous black shale, with minor thin sandstone, siltstone and conglomerate. The Upper RBM consists of a dolomite unit (1-3 m, called the 2.2 dolomite, Figs. 10.5, 10.7 C) which is overlain by grey-green dolomitic siltstone (5-10 m).

The Upper RBM passes with apparent conformity into the No.2 dolomite (5-30 m) of massive to thinly laminated dolomite with shaley partings and occasional dolomitic shale interbeds. Petrographically, the No.2 dolomite unit within the mine area consists mainly of dolomicrite (sometimes associated with clasts) and dolosparite, and to some extent dolomite veins (Adabi et al., 1996 b).

9.4.3.2 Crimson Creek Formation

The Crimson Creek Formation includes the No.1 dolomite horizon and a thick (~1000 m) sequence of siliciclastic and carbonate rocks (Morrison, 1982).

Figure 9.7. Samples from Renison mine sequence (modified after Kitto, 1994).

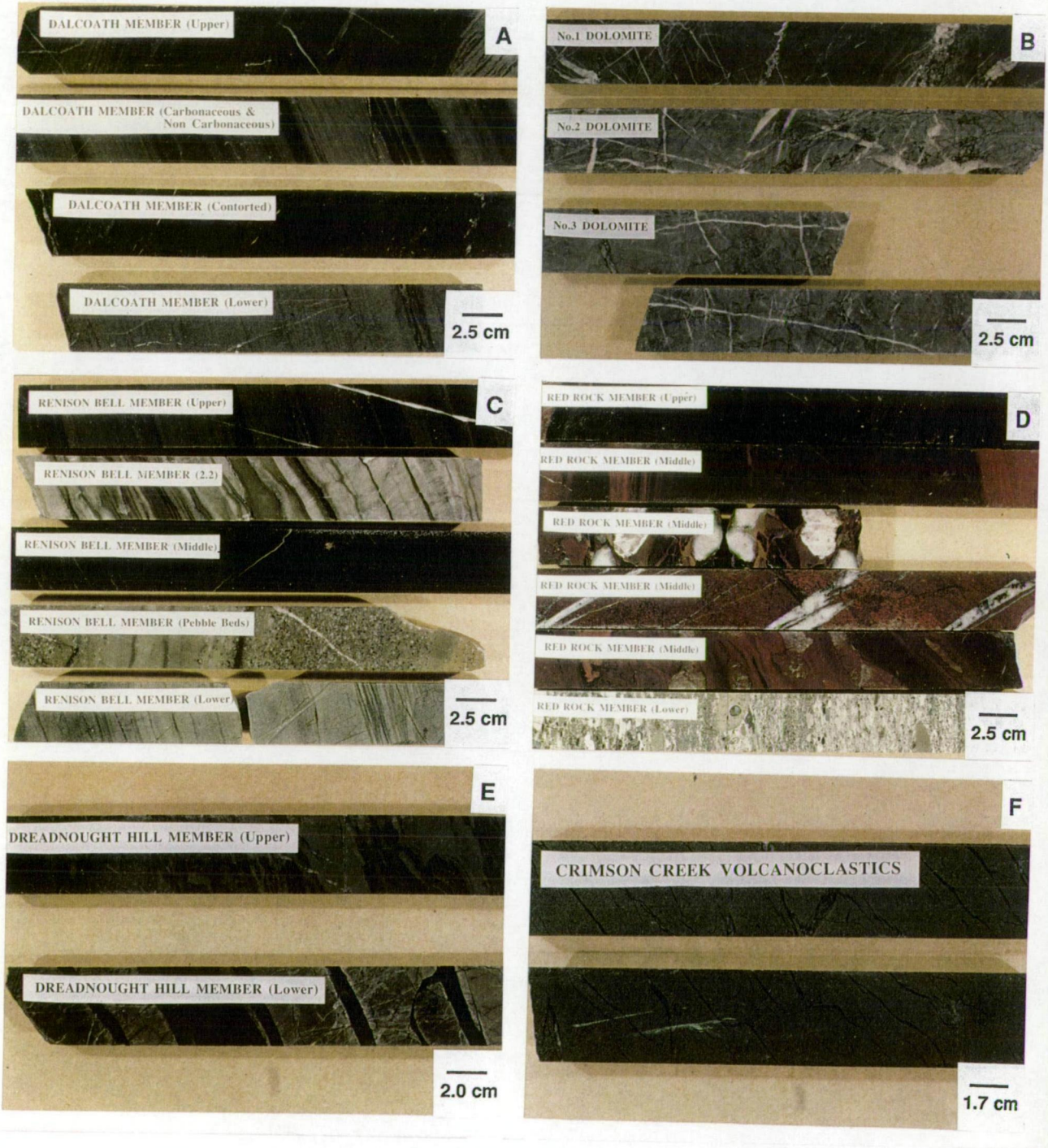
DALCOATH MEMBER (Upper)
A
DALCOATH MEMBER (Carbonaceous & Non Carbonaceous)
DALCOATH MEMBER (Contorted)
DALCOATH MEMBER (Lower)
2.5 cm
No.1 DOLOMITE
B
No.2 DOLOMITE
No.3 DOLOMITE
2.5 cm
RENISON BELL MEMBER (Upper)
C
RENISON BELL MEMBER (2.2)
RENISON BELL MEMBER (Middle)
RENISON BELL MEMBER (Pebble Beds)
RENISON BELL MEMBER (Lower
2.5 cm
RED ROCK MEMBER (Upper)
D
RED ROCK MEMBER (Middle)
RED ROCK MEMBER (Middle)
RED ROCK MEMBER (Middle)
RED ROCK MEMBER (Middle)
RED ROCK MEMBER (Lower)
2.5 cm
E
DREADNOUGHT HILL MEMBER (Upper)
DREADNOUGHT HILL MEMBER (Lower)
2.0 cm
F
CRIMSON CREEK VOLCANOCLASTICS
1.7 cm

The Red Rock Member (25-35 m, Fig. 9.7 D), which forms a very distinctive marker horizon, unconformably (especially near Argent Dam) overlies the No.2 dolomite and is defined as the base of the Crimson Creek Formation (Djakic, 1981; Morrison, 1982, Fig. 9.5). This member shows a highly variable thickness and lithology characteristic of a fluvial environment, and has been divided into three units; a basal siltstone-fragmental tuffaceous group, a middle conglomerate-grit-sandstone-carbonates group; and an upper chert-iron formation and carbonate group (Morrison, 1982).

The final No.1 dolomite horizon (8-25 m, Figs. 9.5, 9.7 B) within the Crimson Creek Formation, conformably overlies the underlying Red Rock Member and marks the temination of Mine Sequence type deposition. The No.1 dolomite horizon within the mine area consists of dolomicrite, dolomicrosparite and dolosparite. Vein and saddle dolomites are present. Chert and detrital quartz are also common as impurities (Adabi et al., 1996 b).

The No.1 dolomite horizon is succeeded by the Dreadnought Hill Member (Fig. 9.7 E), which represents the basal sequence of an overlying rock of massive to thinly bedded siltstone, shale, sandstone and sandy limestone of the Crimson Creek Formation. It is at least 1000 m thick in the Renison mine area (Patterson et al., 1981; Morrison, 1982). In a preliminary version of stratigraphy of the Crimson Creek Formation, Morrison (1993) subdivides the lower 900 m of the Crimson Creek Formation into four main units based on different lithologies and sedimentary cycles. Three different diamictite horizons in ~300, 600 and 800 meters of the Crimson Creek Formation in the Renison mine area have also been recognized by Morrison (1993). Basaltic sills and dikes are relatively common in the Crimson Creek Formation in the mine area (Taylor, 1954; Patterson et al., 1981, Brown, 1986, Fig. 9.7 F).

The Success Creek Group and the Crimson Creek Formation are generally considered older than early-middle Cambrian, but younger than the Penguin Orogeney (720 Ma, Solomon and Griffiths, 1974). A Neoproterozoic age has been suggested for the Success Creek Group and Crimson Creek Formation based on acritarch (acid resistant, organic walled algal cysts) studies (G. Vidal, unpublished, quoted in Morrison, 1982).

Pre-Devonian rocks in the Renison mine area are intruded by Pine Hill Granite, south-east of Renison Bell (Fig. 9.10). East and north of Renison Bell, the older sediments are unconformably overlain by discontinuous patches of Quaternary deposits.

9.4.3.3 Correlation with Smithton Basin (northwest Tasmania)

Successions similar to the Renison sequence formed within the Smithton Basin in the northwest of Tasmania (Fig. 9.8). Brown (1986) suggested a Neoproterozoic age for the Success Creek Group and the Crimson Creek Formation based on radiometric age dating and lithological and chemical correlation with the sequence in the Smithton Basin. The Success Creek Group and Black River Dolomite (in the Smithton Basin) are correlated on broad lithostratigraphic grounds and stromatolite-bearing units (Fig. 9.8). The stromatolite fragments in the Success Creek Group in the Mt Lindsay area (west of Renison mine, Brown, 1986) belong to *Baicalia cf. B. burra* and are similar to those obtained from stromatolitic breccias in the Black River Dolomite in the Smithton Basin (Griffin and Preiss, 1976). The Crimson Creek Formation has been correlated with the formation overlying the Black River Dolomite in the Smithton Basin (Fig. 9.8) on the basis of lithological similarities and the presence of tholeiitic basalt flows with a similar lithology and chemistry to those in the Crimson Creek Formation (Brown, 1989). The K-Ar whole-rock ages of 588 ± 8 and 600 ± 8 Ma (Brown, 1986) obtained from two dolorite dikes intruding the Rocky Cape Group near the Smithton Basin are lithologically and chemically similar to the tholeiitic of the Kanunnah Subgroup (Fig. 9.8), which are in turn geochemically, stratigraphically and petrographically correlated with the Crimson Creek Formation. Petrographic variations between basalt samples from different areas within the Crimson Creek Formation and the Smithton Basin are fairly small. The range and characteristic patterns of rare earth and trace element values for basaltic rocks from the Crimson Creek Formation and the Kanunnah Subgroup of the Smithton Basin are very similar (Brown 1989).

Carbon isotope chemostratigraphy, using global compilation carbon isotope curves, supports the Neoproterozoic age of about 570-820 Ma for the Crimson Creek Formation and Success Creek Group respectively (Adabi, in press). Carbon isotope chemostratigraphy will be discussed in Chapter 11. The stratigraphic and facies variation between all diamond drill holes studied in the Renison mine area is shown in Fig. 9.9.

9.4.4 Geologic structure of the Renison mine

The structural geology of the Renison mine area has been studied by Patterson et al., 1981; Davies, 1985; Holyland, 1987; Lea, 1991; and Kitto, 1992, 1994, so only a brief summary of the geologic structure will be provided here.

The Renison Bell area is located on the north-eastern flank of a regional

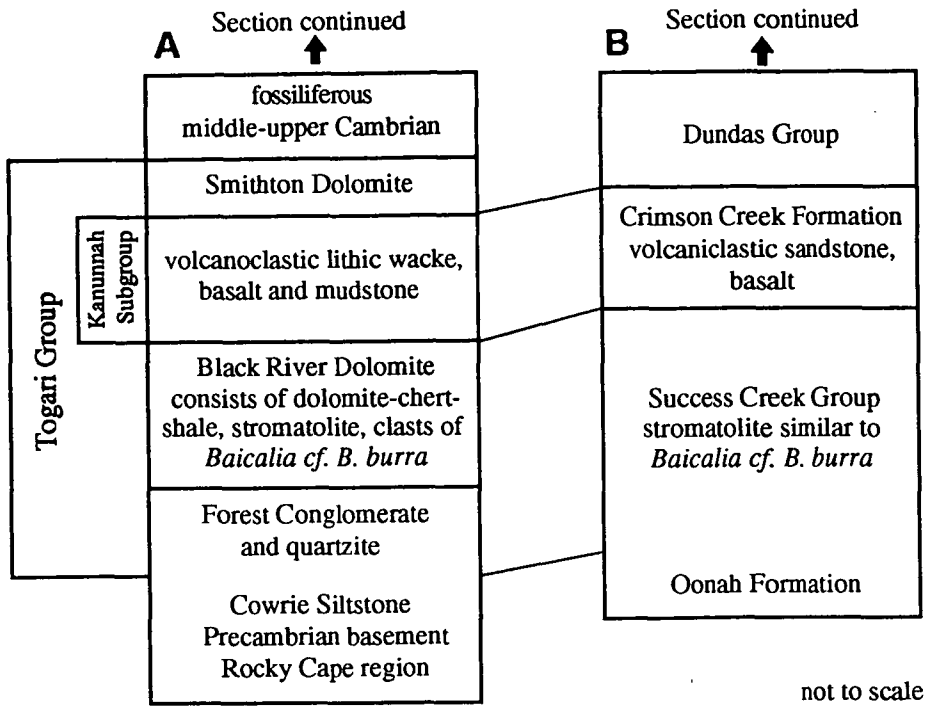

Figure 9.8. Stratigraphic sequence in Smithton Basin (A), correlated with Success Creek Group and Crimson Creek Formation in Dundas Trough (B), modified after Brown (1989).

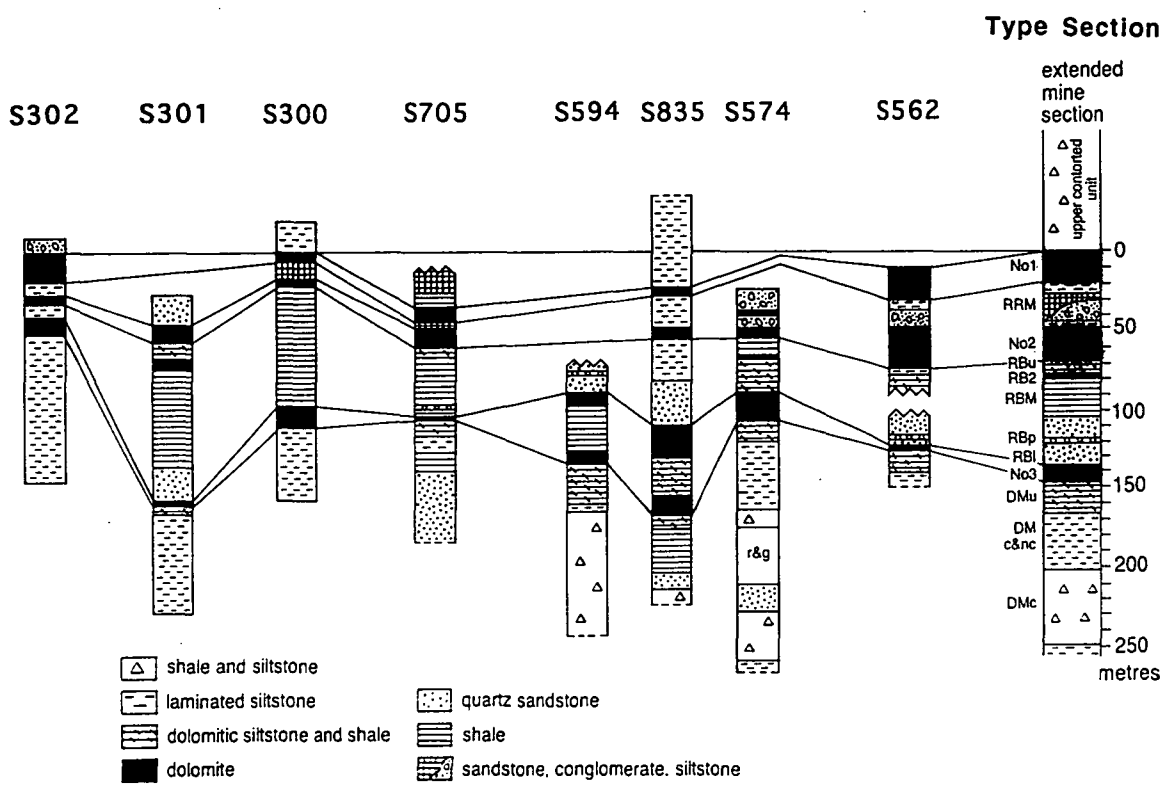

Figure 9.9. Comparison and tentative correlation of stratigraphic sections studied with the Type Section of Renison mine. Note stratigraphic and facies variations in the mine area (modified after Morrison, 1982).

anticline structure, which strikes approximately north-west and plunges shallowly south (Fig. 9.10, Blissett, 1962; Patterson et al., 1981).

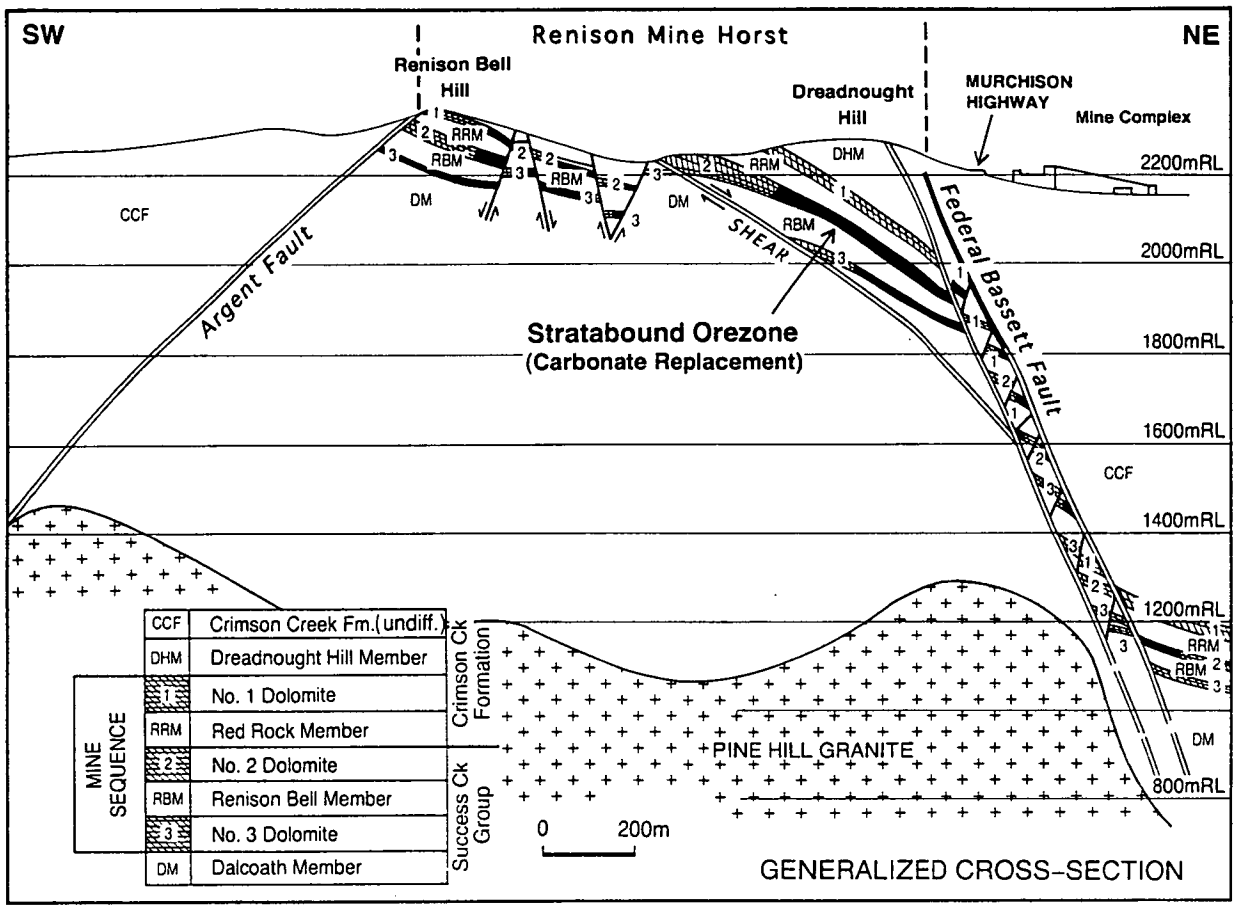

Figure 9.10. Schematic cross section of the Renison deposit showing the location of the Renison mine horst and the distribution of stratabound carbonate-replacement tin deposits (modified after Cannard, 1991).

The regional fault structures at Renison are attributed to a tensional regime associated with emplacement of the Devonian Pine Hill Granite (Fig. 9.10, Lea, 1991; Kitto, 1992, 1994). Major faults are exclusively normal, with dips generally in the range of 55-80° (Patterson, 1979). The Mine Sequence is disrupted by at least three major groups of mineralised faults formed during the forceful emplacement of the Pine Hill Granite (Kitto, 1992, 1994), known as:

- The Federal-Bassett Fault (FBF) and Blow Fault Complex (BFC)
- The Transverse Faults which are also called the Shear Fault
- A series of north-south striking faults which form minor horst and graben structures

The Federal-Bassett Fault (FBF), which is a major fault in the mine area, has an inferred strike length of several tens of kilometres and dips to the northeast at approximately 70°, along the north-eastern margin of the Pine Hill Granite (Lea, 1991; Kitto, 1992). The FBF has a vertical component of movement of at least 1000 meters near Renison mine (Patterson, 1979). The FBF is inferred to project steeply upward from the northeast margin of the granite ridge into the overlying Success Creek Group and Crimson Creek sediments (Kitto, 1994). The Renison mine area is bounded to the northeast by the Federal-Bassett Fault and to the southwest by the less steep, westerly dipping Argent Fault. The Argent Fault together with the FBF, which are the major boundary faults of the central uplifted block, defines the Renison mine horst (Fig. 9.10).

The Blow Fault Complex (BFC) is subparallel to the FBF and forms the western boundary to economic tin mineralization at Renison. The BFC in the south of the study area is terminated by the Argent Fault (Fig. 9.10) and in the north is interpreted to either terminate against the FBF or change strike and run parallel to the FBF (Marjoribanks, 1990). The BFC strikes north-south and dips steeply east. The BFC and FBF are boundary faults to the interconnecting Transverse Faults.

The Transverse Faults, which have been termed at Renison the Transverse Shear (Fig. 9.10), are a series of east-west trending faults that interconnect with the FBF and BFC structures. These shallow faults which dip to the northeast, dissect the mine horst.

Within the mine area, there are also a series of north- south oriented minor host and grabens which developed above the Transverse Faults east of the BFC. The BFC bounds a major horst block west of the study area. Kitto (1992) has shown that extensive brittle deformation occurred due to these fault structures.

Numerous researchers believe that at Renison, the fault structures developed due to forceful asymmetrical emplacement of the Upper Devonian Pine Hill Granite beneath the mine area, which is related to the Tabberabberan Orogeny (Patterson et al., 1981; Davis, 1985; Holyland, 1987; Lea, 1991).

The age of the major longitudinal faulting in the area was considered to be pre-ore (Hall and Solomon, 1962; Gilfillan, 1965) and the age of Transverse faults were regarded as post-ore because they displaced ore bodies (Hall and Solomon, 1962; Groves, 1968).

CHAPTER 10

EVIDENCE OF COOL WATER ORIGIN FOR DOLOMITE

CHAPTER 10

EVIDENCE OF COOL WATER ORIGIN FOR DOLOMITE

10.1 Introduction

Proterozoic carbonates are abundant in many parts of the world. These have been recently studied to understand: secular variation in seawater isotopic composition (e.g., Veizer and Hoefs, 1976; Zempolich et al., 1988; Burdett et al., 1990; Kaufman et al., 1993; Kaufman and Knoll, 1995); original carbonate mineralogy (Grotzinger and Read, 1983; Tucker, 1986 a; Zempolich et al., 1988); and various diagenetic aspects (e.g., Tucker, 1983; Zempolich et al., 1988). Proterozoic carbonates are widespread in western Tasmania, Australia (see Fig. 9.2). No previous geochemical and cathodoluminesece studies have been undertaken of the least-altered dolomites away from hydrothermal alteration at the Renison mine.

10.2 Aim and Scope of Study

In this chapter, petrographic, elemental and isotopic compositions of Renison dolomite away from the mineralized area are investigated to recognize:

- Dolomite types
- Origin of dolomite (primary vs secondary dolomitization)
- Isotopic composition and temperature of Neoproterozoic seawater
- Environmental significance of the least-altered dolomite

10.3 Methods of Study

Dolomite samples from three diamond drill holes (S594, S705 and S835), which are located within a few km of the mine area, were selected to study the least-altered dolomites (Fig. 10.1). Ninety six uncovered polished thin sections were stained (Dickson, 1965) to differentiate carbonate types. Polished thin sections have been examined using conventional and cathodoluminescence microscopy to determine composition, texture and diagenetic features. Twenty

four representative powdered samples of relatively pure dolomite were analyzed by XRD to identify dolomite mineralogy and determine the mole % Mg substitution in the dolomite lattice, as a measure of the dolomite stoichiometry. The samples were calibrated with the addition of an internal standard of natural quartz. The mol.% Mg in dolomite was determined by the Goldsmith et al. (1961) method. Cell dimension was measured for determination of ordered and disordered dolomites (Land, 1985). Organic carbon of 20 selected samples (~2 g) was determined by the ashing technique over 24 hours (Krom and Berner, 1983). The total carbon of 10 ashed and untreated samples was determined by the Carlo Erba Elemental Analyser (for a detail description, see Chapter 1). In the ashing method, sulfur may be converted to SO_2 during ashing, causing a weight gain in samples. The absence of siderite or pyrite in samples analyzed suggests that this did not occur. Powders of 50 and 89 different dolomite types were selected for elemental and isotopic analysis respectively. For stable isotopes analysis, dolomite powders were allowed to react with phosphoric acid in reaction tubes under vacuum conditions at 50° C for 24 hours. Details of the geochemical techniques used are described in Chapter 1.

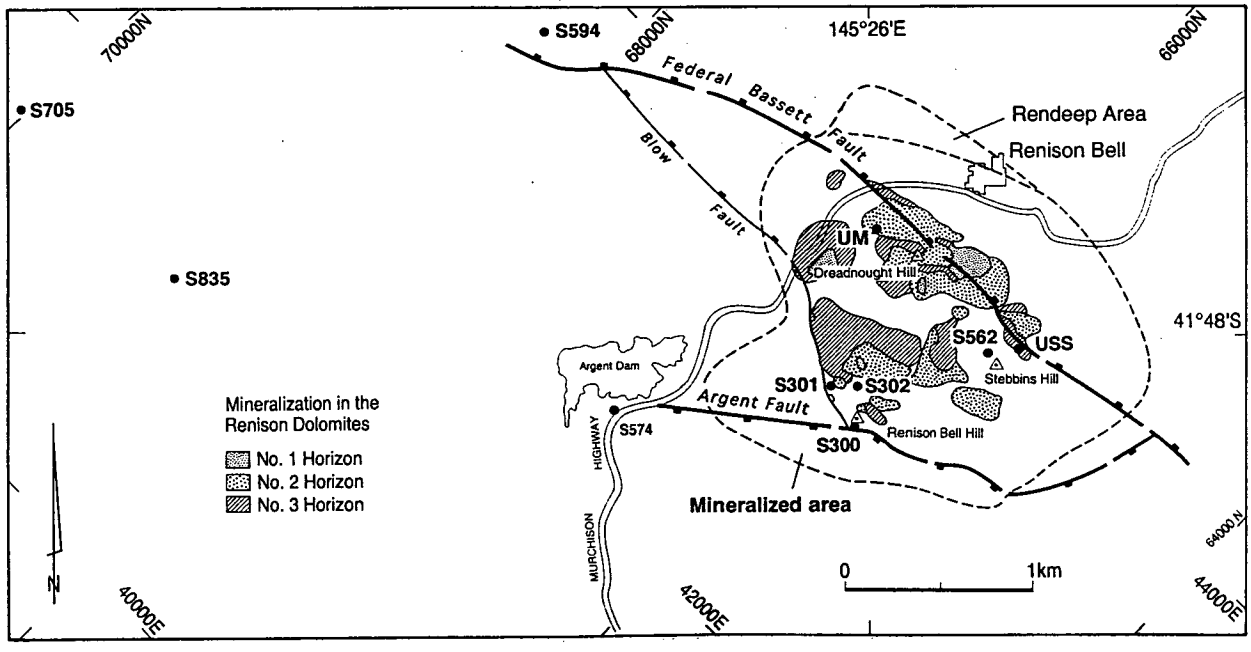

Figure 10.1. Diamond drill hole (DDH) locations and underground sample sites at Renison. The mine area is bounded by three major faults, which include the Federal Bassett Fault, the Argent Fault and the Blow Fault. Note drill holes S705, S835 and S594 are far from the mine area, and thus, are least affected by hydrothermal alterations. UM = Murchison Orebody, underground sample. USS = South Stebbins Orebody, underground sample.

10.4 Analytical Results

The XRD results of dolomite samples are listed in Table A6.1 (Appendix 6). The organic carbon results are summarised in Table A6.2 (Appendix 6). The data on major and minor elements and oxygen and carbon isotope values of dolomite samples from three diamond drill holes (S594, S705 and S835) are listed in Table A6.3 (Appendix 6).

10.5 Cool to Cold Water Conditions in the Neoproterozoic

The Neoproterozoic Era was a time of repeated continental glaciation, including one of the Earth's most severe "refrigerations" (Kaufman et al., 1993). Four glacial periods have been recognized during the Neoproterozoic. Of these, only two major phases of glaciation were widespread and are well documented worldwide (Harland, 1983; Derry et al., 1992; Kaufman and Knoll, 1995). The first of these was ~730 Ma (Sturtian glacial, Kaufman and Knoll, 1995), and the second, ~600 Ma (Varanger glacial, Derry et al, 1992, see Fig. 11.1). These glacial periods have been recognized in most countries, including, Australia, China, USA, Greenland, Newfoundland, the former USSR, South Africa, Norway, Sweden, Scotland, Namibia and Canada (Harland, 1983). The Neoproterozoic period was a time of intensely cold climate, with extensive low-latitude ice sheets (Frakes, 1979; Harland, 1983; Williams, 1979, 1993; Embletone and Williams, 1986; Kasting, 1992) and glacio-marine deposits (Yeo, 1986). Evidence of ice is found in almost all continents, except Antarctica. In most of the examples cited above, the low to equatorial paleolatitudes have been obtained (Harland, 1983). The term "snowball Earth" has been proposed for the Neoproterozoic low-latitude global glaciation by Kirschivink (1992 a). According to Gough (1981) the sun's output was about 18% less than today during the early Proterozoic (2.5 Ga) and 6.5% less during the Neoproterozoic (0.8 Ga). Luminosity of the sun was less than today during the Proterozoic, and its brightness has increased linearly with time (Gough, 1981). Based on the grounded ice sheets, Embleton and Williams (1986) suggested that the mean annual air temperature was below 0° C at or near sea level in low latitudes during the Neoproterozoic.

The low latitude glaciations have been attributed to earth obliquity, which was considerably increased (>54°) during Neoproterozoic glaciations (William, 1975, 1993). As the obliquity of the earth increased, the tropics received less radiation from the sun annually, than the pole, and hence were preferentially glaciated (Williams, 1975; Embleton and Williams, 1986; Williams, 1993). Due

to the high obliquity, seasonality was much stronger than today, thus, deposition of varves was very widespread, extending into very low paleolatitudes (Embleton and Williams, 1986). However, Kirschivink (1992 a) argued against the high obliquity of the earth during the Neoproterozoic, suggesting that as most of the solar energy absorbed by the earth today is trapped in the tropical oceans (in contrast to the continents which are relatively good reflectors), a slight drop in sea level would convert large areas of energy-absorbing oceanic surface to highly reflective land surface, thus, enhancing the glacial tendency. The evidence of equatorial glaciation is also supported by the orientation of the Earth's magnetic field from the lithified rocks. The flat magnetic vectors from Proterozoic glacial sediments indicate glaciation around the equator (Hambrey, 1992). Thus, the Neoproterozoic world had the most extensive glaciation in the earth's history and a truly icehouse climate (Hambrey, 1992).

The presence of diamictites (matrix-supported conglomerates) in most Neoproterozoic sediments are characteristic features of these sequences. The close association of diamictites with carbonates in Neoproterozoic sequences, have been attributed to extremely rapid changes in climate (from cold to warm), or strong seasonal variations with a warm summer (Williams, 1979; Preiss, 1987). This interpretation is based mainly on the inference that carbonates are formed mainly in warm water. The presence of stromatolites, common in glacial sequences, were taken as further evidence that carbonates were deposited in warm water (Hambrey, 1992). However, recent studies indicate that limestone can form in cool to cold water (Nelson, 1988; James and Bone, 1992; Rao and Adabi, 1992; Rao and Amini, 1995), as can stromatolites in saline lakes, such as in the Dry Valley, an area of Antarctica free of ice (Hambrey, 1992). Cold water marine dolomites have also been reported recently from different localities (Saller, 1984; Mullins et al., 1988; Flood and Chivas, 1995). Schermerhorn (1983) postulated that the late Proterozoic diamictites were the product of glaciation. Carbonates interbedded with diamictites in the late Proterozoic of South Australia have been interpreted as cold water precipitates, similar to the Antarctic Lakes deposits (Walter and Bauld, 1983). The late Proterozoic Virgin Spring and Sour Dough limestones of the Death Valley region, eastern California, are closely associated with glacial-marine diamictites (Tucker, 1986 b). The presence of diamictites in late Proterozoic sediments of glacial origin have been questioned by some researchers. For example, Tucker (1986 b) raised questions with regard to how a glaciation can occur in equatorial regions at low altitude, and how a late Proterozoic sequence of glacial origin, contains warm-water sediments, such as

limestone and dolomite. Fortunately, these questions have already been discussed and appear clearly answered. Renison sediments occurred between two major global glaciations (i.e., Sturtian and Varanger glacials) and diamictites have been reported in these sequences (Morrison, 1982; 1993).

10.5.1 Glacial deposits in Australia

Extensive glaciogenic deposits of Neoproterozoic age occur in a belt of sedimentary basins (e.g., Kimberley, Amadeus and Adelaide basins) running northwest-southeast across central Australia (Fig. 10.2, Williams, 1979, Brookfield, 1994). From four distinct glacial periods in Neoproterozoic time, only two glacial periods (i.e., Sturtian and Marinoan, with at least two phases of glaciation) have been well documented in the above basins (Williams, 1979; Harland, 1983; Powell et al., 1994). The association of dolomite with tillites, and particularly the presence of glacial erratics in these sediments, indicates cold water conditions throughout most of Neoproterozoic time. Such conditions have also been documented from other parts of the world (summarized in Harland, 1981, 1983).

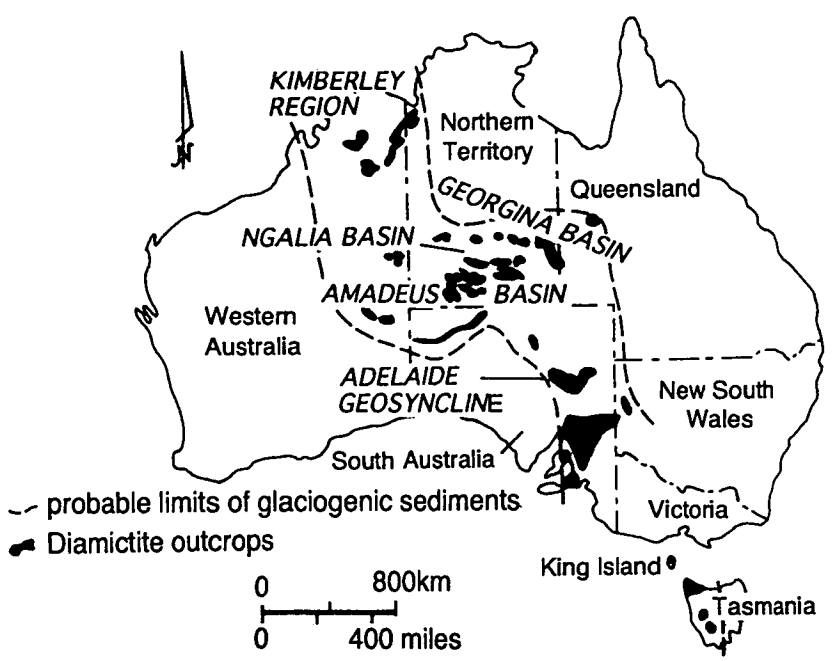

Figure 10.2. Distribution of Neoproterozoic glaciogenic rocks in Australia (modified after Williams, 1979; Brookfield, 1994).

The paleolatitudes of Australia, including Tasmania, was about 30 to 50° N at ~720 Ma and ~10 to 30° N at ~ 580 Ma-close to the equator (Powell et al.,

1994). The Vendian glacial reconstruction of Neoproterozoic continents by Kirschvink (1992 b), places Australia within a few degrees north of equator. Paleomagnetic studies also agree that most glaciogenic sequences of Neoproterozoic age accumulated in low paleolatitudes (Embleton and Williams, 1986).

In Tasmania, there are three areas in which Neoproterozoic sediments of possible glaciogenic origin are known: King Island; Trowutta area (southern part of the Smithton Basin); and the Wedge River Beds (near the south eastern margin of the Tyennan Massif (Jago, 1981). Jago (1981) found possible dropstones within fine-graded sandstone and siltstone layers in King Island. He also interpreted that the isolated clasts in meta-sandstone of the Wedge River Beds are possibly ice-transported dropstones. Corbett (personal communication, 1995) also believes that there is positive evidence of glaciogenic origin in the Wedge River Beds. Moreover, in the Weld River Group (Jubilee Region), thick diamictite (mixtite) units interbeded with dolomites have been recognized by Calver (1989). These diamictite units are composed of 5-30% angular to sub-rounded clasts (pebble to cobble sized), in a black, carbonaceous, dolomitic sandy mudstone matrix. He pointed out that there is some variation in composition, maximum clast size and clast-matrix proportion within and between diamictite units. The presence of dropstones in laminated dolosiltite in the Weld River Group has been recently reported by Calver (1995).

In the close proximity to the Renison tin mine, diamictites have been reported from the basal unit of the Success Creek Group (Morrison, 1982; Brown, 1986). In a preliminary version of the stratigraphy of the Crimson Creek Formation, Morrison (1993) recognized three different diamictite horizons in ~300, 600 and 800 meters of the Crimson Creek Formation in the Renison mine area. Diamictites in the Renison mine area are poorly sorted with a fine grained matrix, the majority of clasts being subangular to subrounded, with varying size and composition (Fig. 10.3). Diamictites have been interpreted as density or debris flow deposits by some researchers. However, they could have formed as glacial deposits or from icebergs floating on the overlying sea, releasing debris into the underlying sediment. All the above evidence, especially the presence of dropstones, raises the possibility of Neoproterozoic glaciation in Tasmania. Tasmania was at a paleolatitiude of ~20° N at ~720 Ma and near the equator at ~580 Ma (Powell et al., 1994), corresponding to the Sturtian and Marinoan glacials respectively.

Figure 10.3. Polished slabs of diamictite from Crimson Creek Formation, Renison mine. Note subangular to subrounded clast with varying size and composition. Drill hole No. S1026 (329m and 388.5m).

10.6 Dolomite Stoichiometry and Ordering

XRD analysis of 24 Renison dolomites away from the mineralized area (using the peak-search computer mode in the 28 to 32 degree 2θs range, reveal average d_{104} values of 2.889), indicating that some dolomites are nearly stoichiometric and some dolomites are calcian-rich (Fig. 10.4), ranging from about 46 to 49.4 with an average of 47.85 mole% Mg CO_3. Average lattice constants are "aO"= 4.813 and "cO"= 16.02, clearly indicating that, following Land (1985), the dolomites are close to being ideal and structurally well ordered (Fig. 10.4). The nonstoichiometeric composition of some dolomite samples suggests a syndepositional to early diagenetic, non-evaporitic, marine pore water origin (Lumsden and Chimahusky, 1980) and less water/rock ratio (Sperber et al., 1984). The calcium-rich nature of some of these dolomites is probably a result of their initial formation as protodolomites and incomplete recrystallization to stoichiometric dolomites. This is also supported by petrographic evidence (see petrographic section).

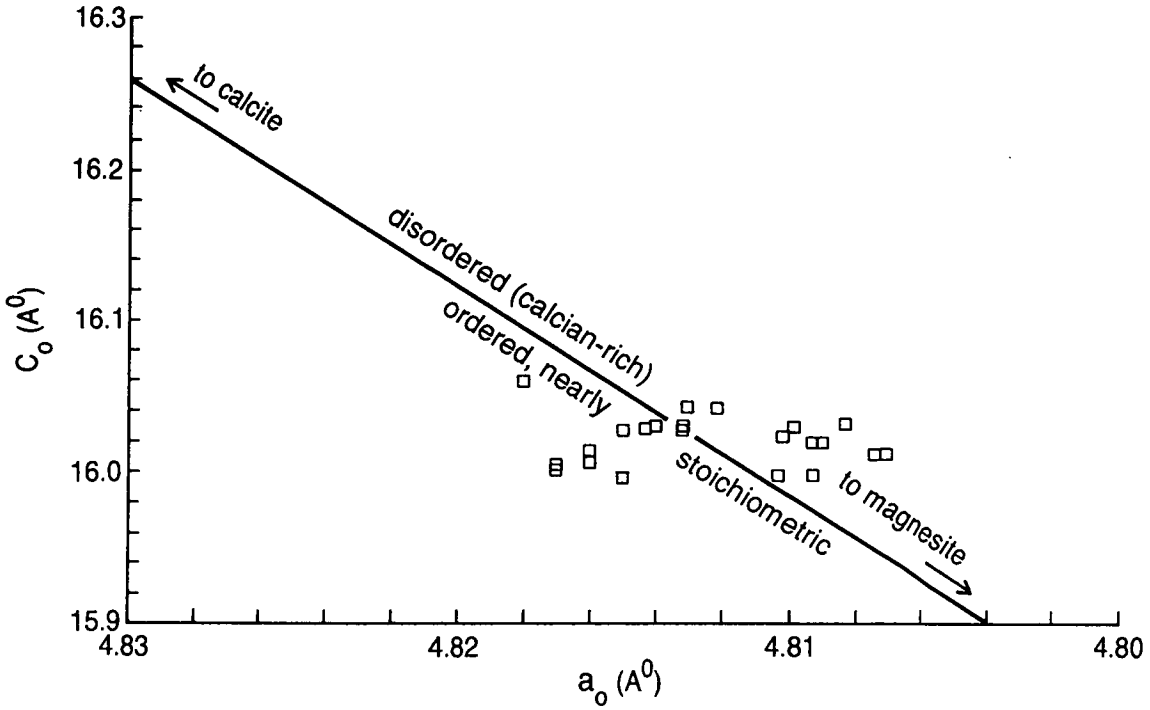

Figure 10.4. Unit cell measurment of some representative Renison least-altered dolomites (adapted from Land, 1985). The data ranges from ordered (nearly stoichiometric) to disordered (calcian-rich).

10.7 Organic Carbon

Organic carbon in the Renison dolomites reaches ~1% with an average of 0.45%, determined by the Carlo Erba Analyser (Table A6.2 in Appendix 6). The amount of organic carbon is relatively higher in dolomicrite than other coarsely crystalline dolomites. The organic matter is probably finely disseminated throughout the dolomite as submicroscopic particles. The brown to black color of some dolomite samples is attributed to this organic carbon. In most aqueous sedimentary environments, organic matter can not be preserved due to sufficient oxygen for aerobic microbial decomposition of the organic matter. The preservation of a moderate amount of organic matter in the Renison dolomicrites could be due to an increase in preservational potential of the organic carbon, probably in the presence of oxygen-deficient water. A prolonged period of marine anoxic condition in the Neoproterozoic has been suggested by Derry et al., 1992 and Kaufman et al., 1993. However, Pedersen and Calvert (1990) suggested that high primary production of organic matter controls the formation of organic-carbon rich sediments. The widespread microbially laminated mats along with large algal fragments indicate that organic matter in the Renison dolomite may be largely derived from algae.

10.8 Petrograhic Study

10.8.1 Normal petrographic microscopy

The following section presents a summary of the petrographic observations of dolomite samples from the unmineralized area. The interpretation of these textures and paragenetic sequences is given in Chapter 13.

The dolomites studied typically have an aphanetic to coarse grained texture, and in some cases the dolomites display laminae 1-3 mm thick. The principal lithifacies are micrite, intraclasts, cryptalgal fragments and occasionally stromatolites. Oolite is present in only one sample. In some dolomite samples impurities include distinct shale and siltstone laminae which range up to several millimeters in thickness. Some minor impurities, such as chlorite, muscovite and quartz, are also present in the dolomite studied. Angular clasts of very finely crystalline dolomites are very common in some dolomite beds. Silica veins and fenestral fabric are present in a few dolomite samples. The only evidence of evaporite is pseudomorphs in two samples.

Fabrics identified by normal petrographic microscope have been classified according to crystal size.

- very finely crystalline dolomite (dolomicrite, < 5μm to ~ 16μm)
- finely crystalline dolomite (dolomicrosparite, ~16μm to ~ 62μm)
- medium crystalline dolomite (dolosparite, ~16μm to ~ 250μm)
- coarse to very coarsely crystalline dolomite (vein dolomite, >250μm)

Dolomicrites are the most abundant and vein dolomites the least abundant dolomite types in this study. Staining of thin sections showed that dolomites are mostly nonferroan, although in few case are slightly ferroan. The dolomite types are characterized as follows:

Type 1 Very finely crystalline dolomite (dolomicrite)

Dolomicrites are the most abundant dolomite types away from the Renison mine area. The crystal size ranges from < 5μm to ~ 16μm, with an average size of about 10μm. These dolomites are dense, nonporous and generally dark-grey to dark-brown in thin sections (Fig. 10.5 A). In dolomicrites, original depositional texture such as intraclasts, microbial fabric and laminations are well preserved. Intraclasts are polymodal in size and shape and have no internal structure, except a few scattered detrital quartz grains (Fig. 10.5 B). Microbially laminated dolomite (stromatolite) consists of dark (organic rich) layers alternating with light, sediment-rich laminae (Fig. 10.5 C). Laminae are usually less than a few millimeters thick, but some may reach to a few centimeters. The alternating

Figure 10.5. Sedimentary and diagenetic texture in dolomicrite.

A. Photomicrograph of very finely crystalline dolomite (dolomicrite). Thin section S705, 169 m.

B. Photomicrograph shows larger, less regular intraclast with scattered detrital quartz grains within dolomicrite matrix. Thin section S705, 187.4m.

C. Irregular microbially laminated dolomite (stromatolite). Note darker (organic rich) layer alternating with white coarser dolomite grains. Thin section S705, 183 m.

D. Thin section photomicrograph showing presence of algal fragments in dolomicrite. Thin section S705, 186.5 m.

E. Well preserved original sedimentary structure consisting of alternation of fine to very fine grained dolomites. Thin section S705, 246.8 m.

F. Photomicrograph showing fenestral fabric. Irregular fenestrae are filled by coarser grained dolomite. Thin section S835, 198.4 m.

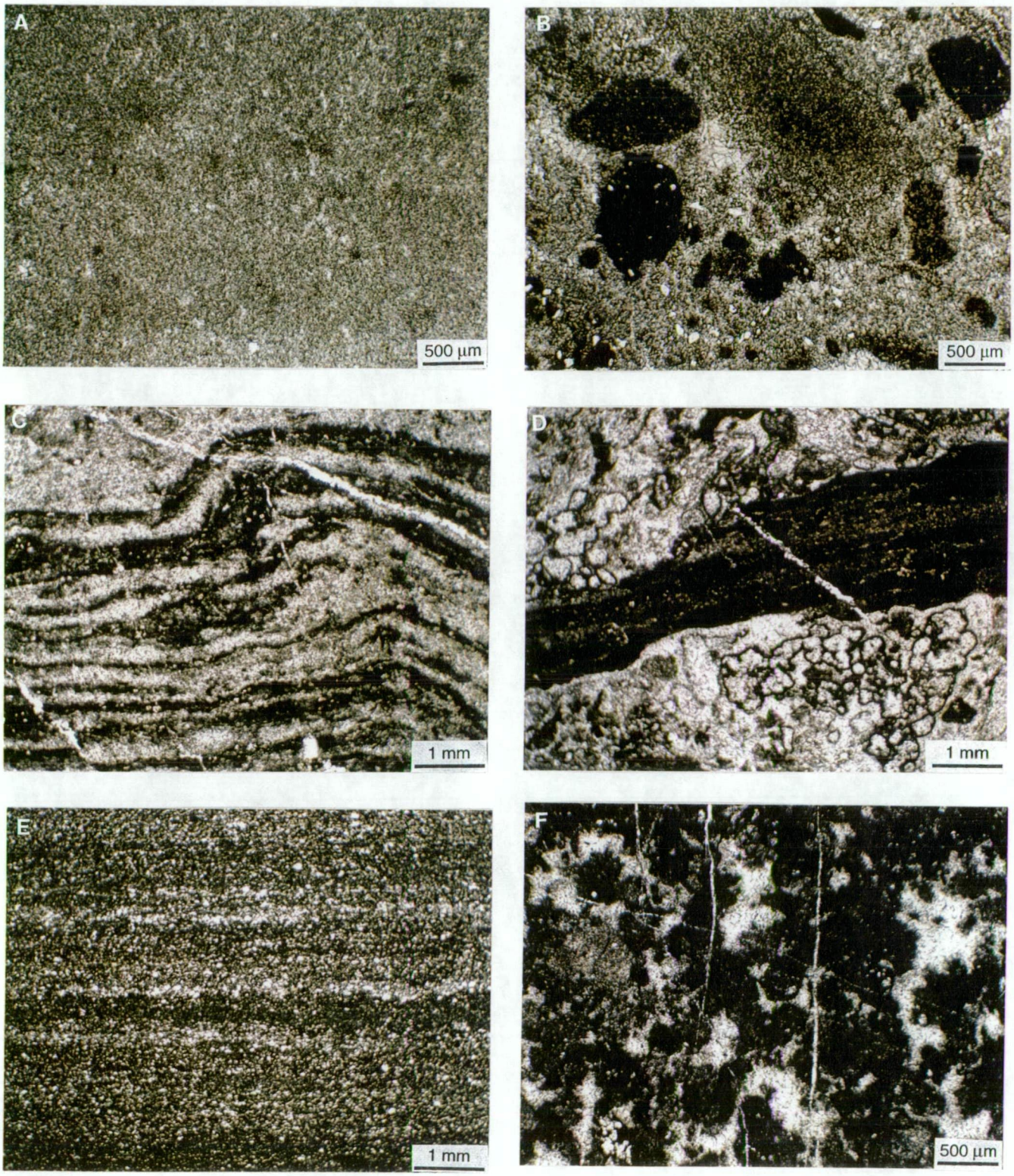
A
500 µm
B
500 µm
C
1 mm
D
1 mm
E
1 mm
F
500 µm

laminae show the growth of a microbial mat (dark organic rich layer), followed by sedimentation. Microbially laminated dolomites show some irregularities in thickness, which can distinguished them from laminae deposited by physical processes. Algal fragments and relic filament structures are also present in many dolomicrite samples (Fig. 10.5 D). In some thin sections, the finely laminated dolomites commonly consist of alternations of fine (light) to very fine grained (dark color) dolomites (Fig. 10.5 E), with some scattered detrital quartz silt also present. The laminae are less than five millimeters thick. Fenestral fabric is present in a few dolomicrite samples (Fig. 10.5 F). In dolomicrite facies there is no evidence to indicate dolomite is not an original precipitate and therefore, considered as a cement. Dolomicrites are referred to as original dolomite in this study.

Dolomite rock texture (using Sibley and Gregg, 1987) includes unimodal very fine subhedral to anhedral planar-s type boundaries.

Type 2 Finely crystalline dolomite (dolomicrosparite)

Dolomicrosparites are the second most abundant dolomite type in this study. They range in size from ~16μm to ~ 62μm (Fig. 10.6 A) and are generally light grey to mid-grey in hand specimen. In thin section, they comprise a mosaic of white dolomite crystals with massive or patchy texture. Dolomicrosparites are formed through dolomicrite recrystallization (Adabi, et al., 1996 b). In some samples dolomicrites are partly recrystallized, while in others, recrystallization is complete (Fig. 10.6 B). In partly recrystallized samples, remnants of original texture of very finely crystalline dolomicrites are preserved (Fig. 10.6 A). Dolomicrosparites can be distinguished from cements by their irregular grain boundaries (Fig. 10.6 B). Recrystallized dolomite is more pronounced in samples having wispy stylolitic texture (Fig. 10.6 C). In one example, dolomicrosparites sharply overly dolomicrites with stylolites at the contact (Fig. 10.6 D).

In terms of dolomite rock texture, dolomicrosparites are mostly unimodal and crystals are subhedral to anhedral with planar-s type boundaries.

Type 3 Medium crystalline dolomite (dolosparites)

Dolosparites are the third most abundant dolomite type in this study. They occur mostly in voids, cavities and vugs (Figs. 10.7 A, B) with crystal size ranging from 16μm to about 250μm. Dolosparites are generally white to light grey in hand specimen and white in thin sections. The dolomicrites (original dolomite) and dolomicrosparites (early diagenetic dolomite) are cut by dolosparite that has been

Figure 10.6. Sedimentary and diagenetic texture in dolomicrosparite.

A. Photomicrograph illustrating finely crystalline dolomite (dolomicrosparite). Note remnants of original dolomicrite and irregular margins of dolomite crystals in dolomicrosparite. Thin section S705, 186 m.

B. Recrystalization of dolomicrites eventually results in total recrystallization to dolomicrosparite. Note evidence of a few inclusions of dolomicrite crystals in the recrystallized dolomicrosparite, and the irregular margins to dolomite crystals. Thin section S705, 202.9 m.

C. Photomicrograph showing wispy stylolitic texture in recrystallized dolomicrosparite. Thin section S705, 201.8 m.

D. Sharp stylolite boundary between dolomicrite and dolomicrosparite. Thin section S705, 179.1 m.

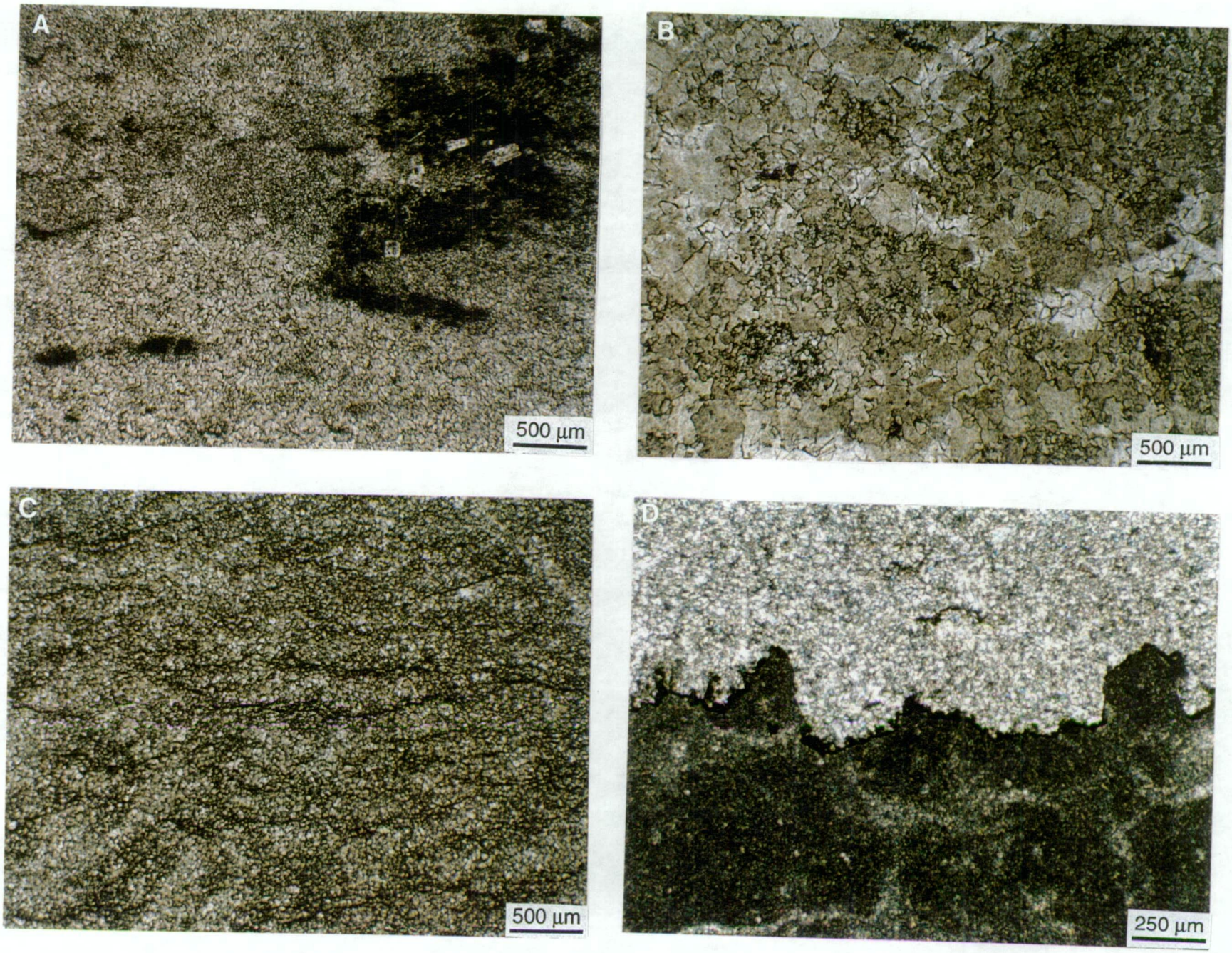
A
500 µm
B
500 µm
C
500 µm
D
250 µm

assigned as a late diagenetic cement. Cavities are generally patchy with irregular shape, filled with a mosaic of medium to coarsely crystalline dolomite. However, cavities with a rim of delicately bladed early diagenetic dolomite cement, followed by coarser grained dolosparite are present in some samples (Fig. 10.7 B). In some cavities the dolospar cement is followed by silica cements, infilling the rest of the cavities. The association of dolosparite cements with stylolites has been recognized in a few dolomite samples (Fig. 10.7 C).

In terms of dolomite rock texture, dolosparites consist of polymodal, dense, closely packed mosaics of coarse subhedral to anhedral nonplanar crystals, with predominantly curved, serrated or irregular intercrystalline boundaries (Sibley and Gregg, 1987). This type of dolomite is referred to as xenotopic by Friedman (1965).

Type 4 Coarse to very coarsely crystalline dolomite (vein dolomite)

Dolomite veins with crystal sizes larger than 250μm are very rare in the dolomites studied. Vein dolomite is in sharp contact with the host wall rock and generally cuts original, early and late diagenetic dolomites. Vein dolomites are more common in No.1 and No.3 than No.2 dolomites and are often cut or replaced by silica veins (Fig. 10.7 D). The vein dolomite displays undulose extinction, similar to the saddle dolomites of Radke and Mathis (1980), in only a few samples.

10.8.2 Cathodoluminescence microscopy

Cathodoluminescence microscopy has been used to document growth zones of dolomite crystals and to understand dolomite sequences. In this study, 96 polished thin sections were examined under cathodoluminescence, but most of the samples were dull to non-luminescent. The cathodoluminescence characteristics of different dolomite types are discussed below.

Type 1 Very finely crystalline dolomite (dolomicrite)

Very finely crystalline dolomites show dark red-brown (dull) luminescence (Fig. 10.8 B, see plain light photomicrographs, Fig. 10.8 A for comparison).Where this occurs, the dolomicrite pre-dates all other dolomite types. These massive dolomicrites do not exhibit any CL zonation.

Figure 10.7. Sedimentary and diagenetic texture in dolosparite and vein dolomite.

A. Void filling dolosparite cement within intraclastic dolomicrites. Note fibrous early diagenetic cement around dolomicrite clasts (white arrow), followed by coarse clear dolosparite cements. Thin section S835, 201.6 m.

B. A cement-filled cavity within dolomicrite. The cavity is filled by bladed early diagenetic dolomite (black arrows), followed by a mosaic of coarse grained dolosparite. Thin section S835, 198.4 m.

C. A cement-filled cavity of clear median and coarsely crystalline dolosparite. Thin section S835, 222.3 m.

D. Photomicrograph showing vein dolomite cut and replaced by late diagenetic silica. Thin section S835, 203.4 m.

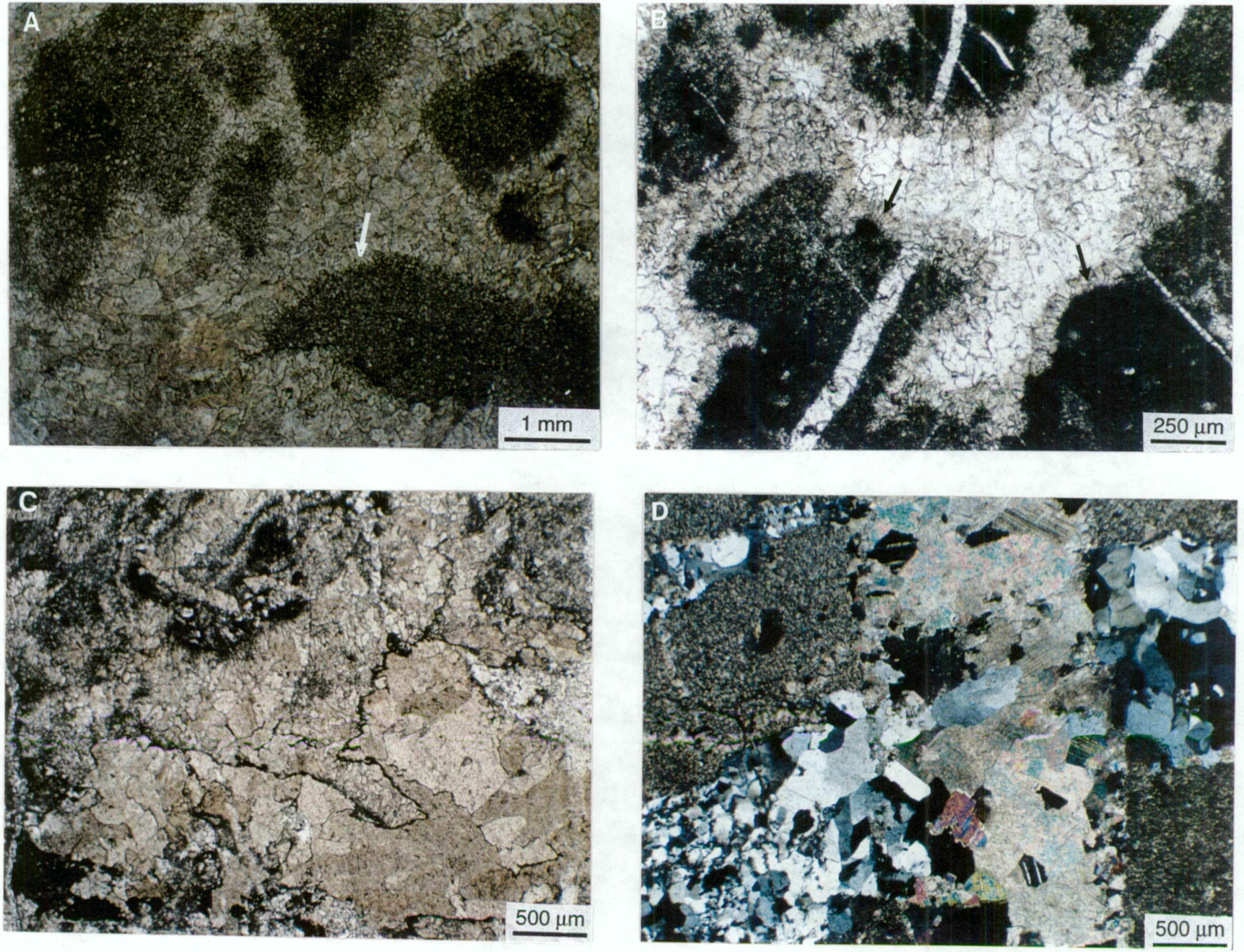
A
1 mm
B
250 µm
C
500 µm
D
500 µm

Type 2 Finely crystalline dolomite (dolomicrosparite)

Dolomicrosparite generally shows bright yellow luminescence (Fig. 10.8 D) and post-dates dolomicrite formation. Plain light photomicrographs (Fig. 10.8 C) are also provided for comparison.

Type 3 Medium crystalline dolomite (dolosparites)

Cavities filled by medium crystalline dolosparite cement exhibit different intensities of luminescence. For example, in Fig. 10.9 B cavities display dull luminescence in zone 1, followed by very bright-yellow luminescence in zone 2 dolomite cements. In a few examples the cavities show fold zonation of a delicate band of moderately bright-yellow zone 1, dark brown zone 2, greenish-gray zone 3, bright-yellow lnminescent zone 4 and non-luminescent zone 5 dolomite cements (Fig. 10.9 D). At the rim of some cavities (e.g., Fig. 10.9 F), the fibrous dolomite cements exhibit finely banded dull luminescence, which is followed by a delicate banding of bright-yellow luminescence, and finally dull to non-luminescent coarsely crystalline dolomite cements. The dull to non-luminescent cements generally occupy a large proportion of the porosity and are the final void fill in most cavities. Plain light photomicrographs for each CL photo are shown in Figs. 10.9 A, C and E.

Type 4 Coarse to very coarsely crystalline dolomite (vein dolomite)

CL zonation patterns are present in very coarsely crystalline vein dolomites (Fig. 10.9 H). The sequence of luminescent zones, from oldest to youngest is: moderately bright zone 1 (orange); dull zone 2 (dark brown); very bright zone 3 (yellow); and dull zone 4 (dark red-brown). In very bright zone 3, there are several thin subzones. A plain light photomicrohgraph is shown in Fig. 10.9 G. In many other examples, vein dolomites are non-luminescent and cut all dolomite types (Fig. 10.9 B).

Figure 10.8. Sequence of paired plain light and cathodoluminescence photomicrographs in dolomite types 1 and 2.

A. Massive very finely crystalline dolomicrites (plain light). Thin section S594, 281.2 m.

B. Same area as in A under cathodoluminescence. The dolomicrites show dark red-brown (dull) luminescence.

C. Thin section photomicrograph illustrating finely crystalline dolomite (dolomicrosparite). Note the presence of a few clasts of original dolomicrites within dolomicrosparite (plain light). Thin section S705, 180.4 m.

D. Same area as in C under cathodoluminescence. Dolomicrosparite shows dark to modertely bright-yellow luminescence.

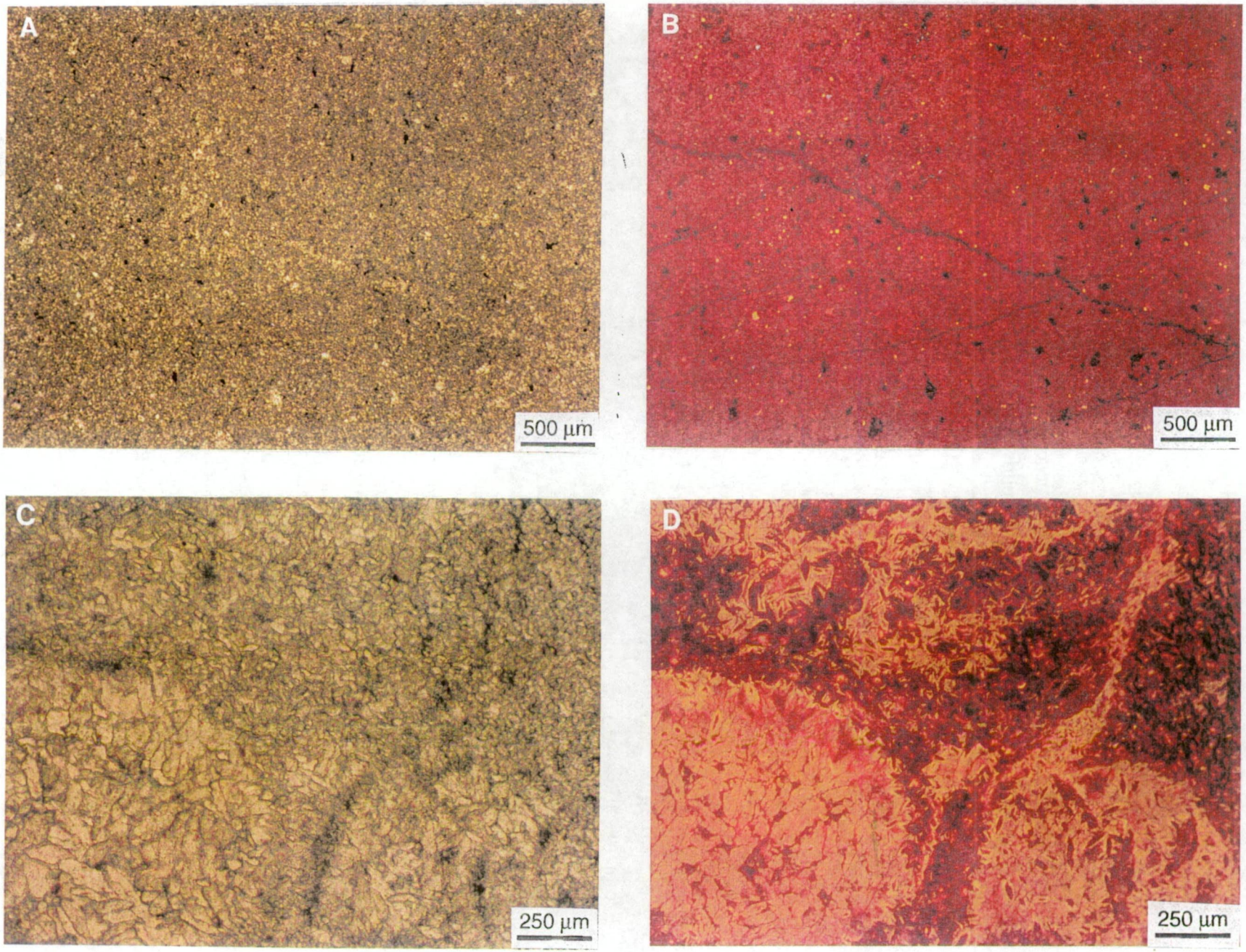
A
500 µm
B
500 µm
C
250 µm
D
250 µm

Figure 10.9. Sequence of paired plain light and cathodoluminescence photomicrographs in dolomite types 3 and 4.

A. Cavity filled by coarsely crystalline dolomite cements (plain light). Note cross cutting veins through dolosparite cements. Thin section S594, 281.2 m

B. Same area as in A under cathodoluminescence. Cavity filled by dull luminescent zone 1, followed by very bright-yellow luminescent zone 2 dolomite cements. Note that non-luminescent veins cross cut all dolomite types.

C. Large cavity filled by coarsely crystalline dolomite cements (plain light). Note increasing crystal size of dolomite towards the centre of the cavity. Thin section S705, 203.4 m.

D. Same area as in C under cathodoluminescence. The dolomite cements consist of multiple generations of zoning. The cavity is filled, from oldest to youngest by: a delicate band of moderately bright-yellow zone 1; dark brown zone 2; greenish-gray zone 3; bright-yellow luminescent zone 4; and non-luminescent zone 5 dolomite cements. Note very late stage dolomite vein cut through dolomicrosparite cavity.

E. Cavity filled by fibous (F) and clear coarsely crystalline dolomite (C) cements (plain light). Thin section S705, 213.4 m.

F. Same area as in E under cathodoluminescence. The sequence of luminescence zones, oldest to youngest is: fine bands of moderately bright-yellow zone 1; dull luminescent zone 2 at the rim of the cavity (fibrous dolomite); delicate banding of moderately bright-yellow zone 3; and dull to non-luminescent zone 4.

G. Vein filled by coarsely crystalline dolomite (plain light). Note sharp contact with the host wall rock. Thin section S835, 200.8 m.

H. Same area as in G under cathodoluminescence. The vein is filled, from oldest to youngest by: moderately bright zone 1 (orange); very bright-yellow zone 2; dull zone 3 (dark brown); very bright zone 4 (yellow); and dull zone 5 (dark red-brown). Note in very bright zone 4, there are few thin alternating dark, bright subzones.

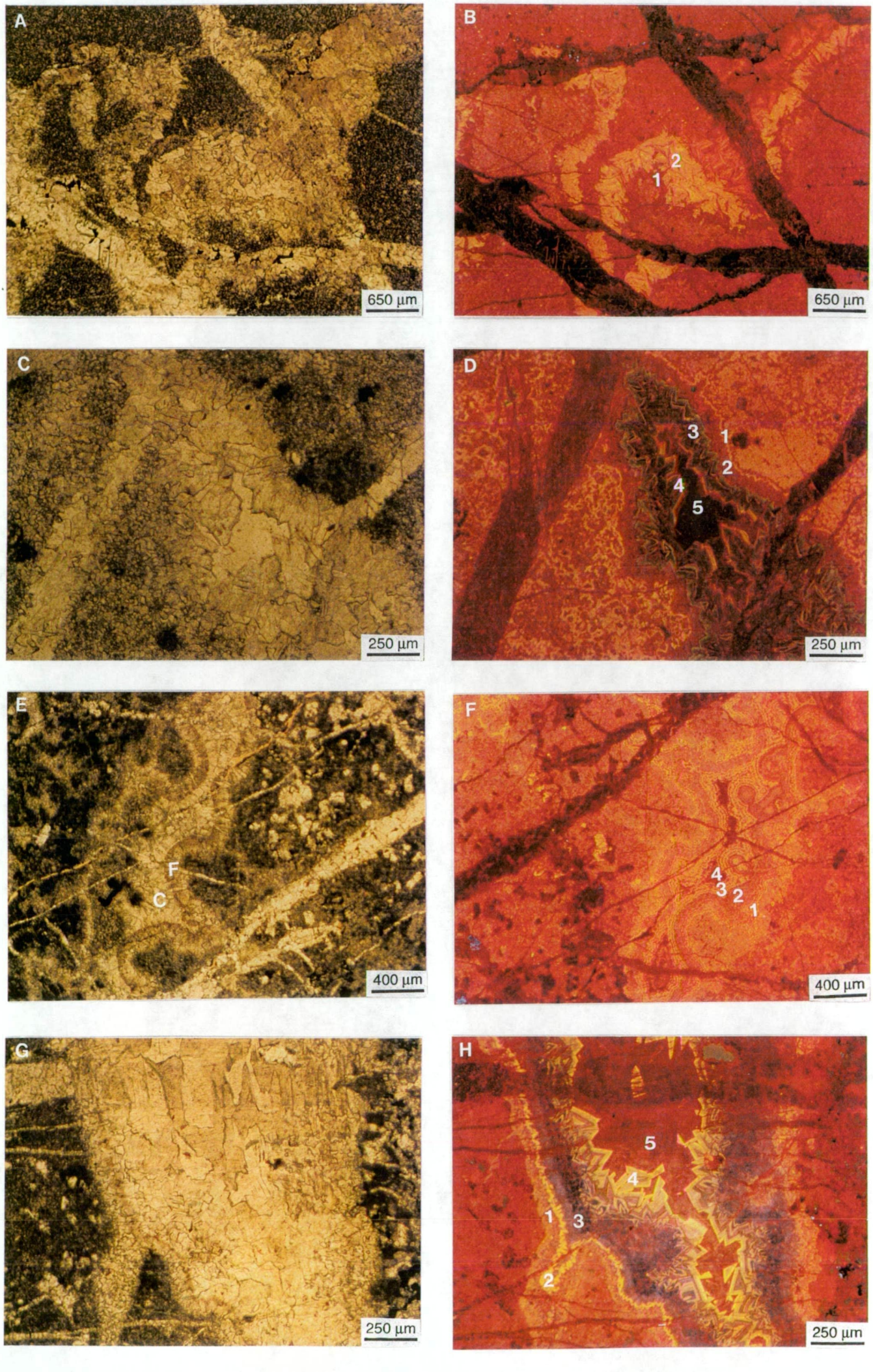
A
650 µm
B
1
2
650 µm
C
250 µm
D
1
2
3
4
5
250 µm
E
F
C
400 µm
F
1
2
3
4
400 µm
G
250 µm
H
1
2
3
4
5
250 µm

10.9 Statistical Analysis

Correlation analysis of values of elements and $\delta^{18}O$ and $\delta^{13}C$ in Renison dolomites (Table 10.1 A) indiate that Ca is unrelated to other variables, whereas Mg values are positively correlated with $\delta^{18}O$ (0.6) and inversely with Fe (-0.85) and Mn (-0.61). Fe and Mn values are positively correlated (0.74) and inversely correlated with $\delta^{18}O$ (-0.73 with Mn; -0.71 with Fe) values, because of the influence of fluids low in $\delta^{18}O$ and high in Fe and Mn concentrations in Renison dolomites. $\delta^{18}O$ and $\delta^{13}C$ are positively correlated (0.53) due to covariation of these isotope values in the diagenetic fluids.

Factor analysis of Renison chemical data (Table 10.1 B) recovered three significant factors. Factor 1 is positively related with Fe (0.94) and Mn (0.82) values and inversely with $\delta^{18}O$ (-0.87), Mg (-0.84) and $\delta^{13}C$ (-0.58) values, due to increasing Fe and Mn values with decreasing dolomite and $\delta^{18}O$, Mg and $\delta^{13}C$ values. Factor 2 is mainly associated with Na (0.80) and Ca (0.49), whereas factor 3 is mainly associated with Sr (0.56) and Ca (0.56), due to the occurrence of Sr and Na, mainly in $CaCO_3$ lattice in dolomite.

Table 10.1. Correlation matrix (A) and unrotated factor matrix (B) of elemental and isotopic data of Renison dolomites away from the mineralized area.

	Ca %	Mg %	Mn ppm	Fe ppm	Sr ppm	Na ppm	∂18O PDB	∂13C PDB
Ca %	1							
Mg %	0.263	1						
Mn ppm	-0.197	**-0.614**	1					
Fe ppm	-0.247	**-0.853**	**0.739**	1				
Sr ppm	0.032	-0.229	0.103	0.435	1			
Na ppm	0.02	-0.146	0.285	0.175	0.14	1		
∂18O PDB	0.169	**0.611**	**-0.726**	**-0.707**	-0.379	-0.214	1	
∂13C PDB	0.084	0.338	-0.33	-0.465	-0.211	0.103	**0.533**	1

Table 10.1B

	Factor 1	Factor 2	Factor 3
Ca %	-0.294	**0.491**	**0.56**
Mg %	**-0.836**	0.084	0.145
Mn ppm	**0.821**	0.061	-0.262
Fe ppm	**0.936**	-0.017	0.014
Sr ppm	0.433	0.34	**0.562**
Na ppm	0.262	**0.795**	-0.38
∂18O PDB	**-0.873**	-0.037	-0.099
∂13C PDB	**-0.575**	0.362	-0.449

10.10 Comparison with Modern Dolomites

The Sr concentrations in Renison dolomite (57 to 196 ppm; mean 102 ppm), are lower than most modern dolomites (Fig. 10.10 A), and overlap with dolomite from Eniwetak (Saller, 1984) and the Bahamas (Whitaker et al., 1994). The origin of the latter is ascribed to normal marine formation. The relatively high Sr concentrations in some dolomite reported in the literature are probably due to dolomitization of aragonite-rich sediments in partly closed diagenetic systems (Humphrey, 1988). This is not the case in Renison dolomite. Na concentrations in Renison dolomite range from 76 to 358 ppm, with a mean of 162 ppm. These values are compared with various other reported dolomites in Figure 10.10 B. Renison dolomites fall within the range of Eniwetak and Bahamas subsurface (marine origin) and Jamaica (mixed marine origin). Marine (Baffin Bay) and hypersaline (Persian Gulf) dolomites contain high Na concentrations due to a higher salinity of precipitating solutions.

Although the Fe and Mn concentrations in modern dolomites are not available, their concentrations are very low in seawater (Veizer, 1983). Fe and Mn concentrations in Renison dolomite range from 1524 to 33 195 ppm, with a mean of 8531 ppm; and 120 to 4655 ppm, with a mean of 822 ppm respectively. These apparently low Sr and Na, and high Mn and Fe values, particularly in coarsely crystalline Renison dolomites, might be due to non-marine (meteoric, mixing zone or burial) diagenesis and/or marine diagenesis conditions different from modern ones. These aspects will be discussed in the following sections.

The $\delta^{18}O$ values (-8.9 to 0.3‰ PDB; mean -4‰ PDB) of Renison dolomites are much lower than modern warm tropical and cool temperate dolomites (Fig. 10.11), due to a strong reaction with non-marine fluids and/or the late Proterozoic seawater ^{18}O value was much lighter than the modern seawater value of 0‰. In contrast to $\delta^{18}O$ values, the $\delta^{13}C$ values (-1.6 to 7.5‰ PDB; mean 3.9‰ PDB) of some Renison dolomites are heavier than modern dolomites (Fig. 10.11), either due to atmospheric conditions different from modern ones, or other causes. The $\delta^{18}O$ and $\delta^{13}C$ values of modern dolomites (Fig. 10.11) are heavier than those in modern shallow seawater $\delta^{18}O$ (0‰) and $\delta^{13}C$ (2.5‰) values, due to fractionation of these isotopes in dolomite, water temperatures and salinity. The $\delta^{18}O$ values become increasingly positive due to cooler temperatures in modern dolomites and similar relationships possibly existed in the past.

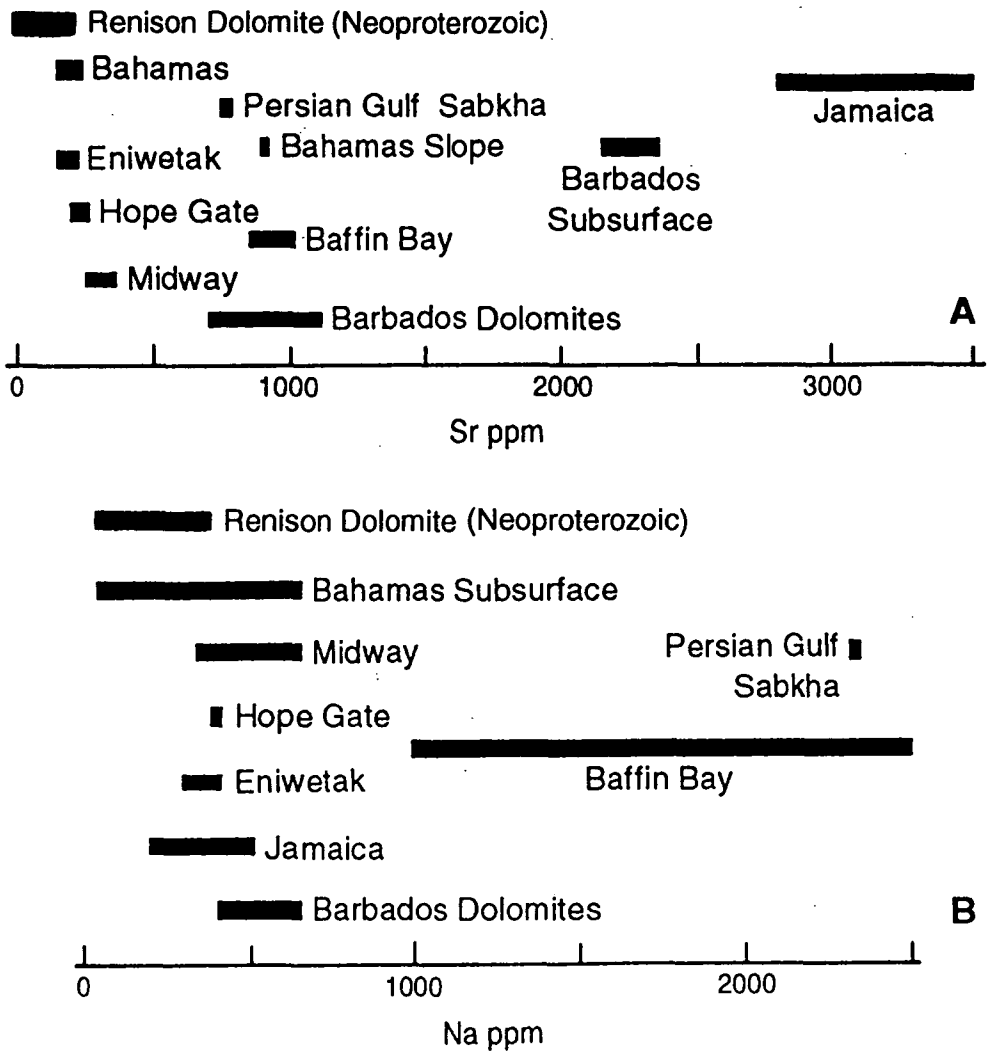

Figure 10.10. Comparison of Sr and Na concentrations of Renison dolomites with those of Holocene and Pleistocene dolomites. Sources are from Major, 1984 (Midway); Land, 1973a (Hope Gate); Land, 1973b (Jamaica); Saller, 1984 (Eniwetak); Mullins et al., 1985 (Bahamas slope); Land and Hoops, 1973 (Persian Gulf sabkha); Behrens and Land, 1972 (Baffin Bay); Videtich, 1982 (Barbados subsurface); Supko, 1977 (Bahamas subsurface); Humphrey, 1988 (Barbados surface); and Whitaker et al., 1994 (Bahamas).

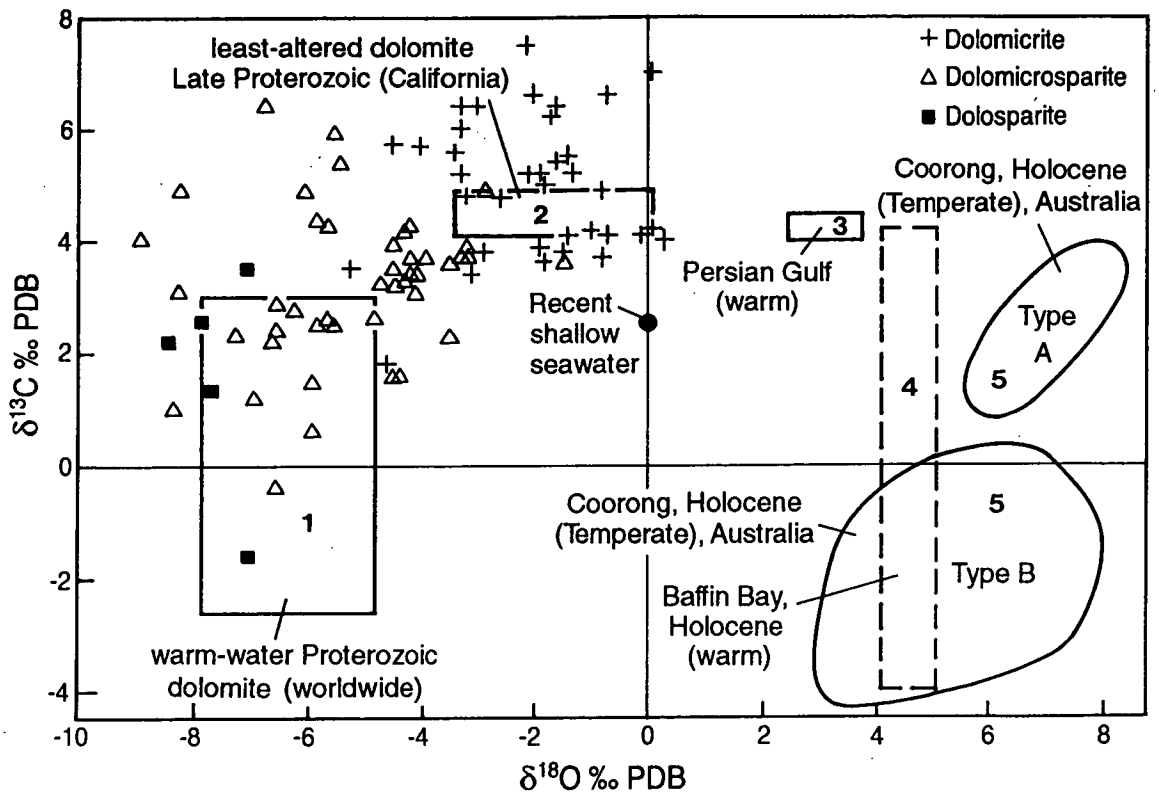

Figure 10.11. Variation of $\delta^{18}O$ and $\delta^{13}C$ values in Renison dolomites and their comparison with modern and Proterozoic dolomites. Note most of the dolomicrites are enriched in both oxygen and carbon relative to dolomicrosparite and dolosparite, because dolomicrites are the least-altered dolomite. Recent dolomites are enriched from about 3 to 8‰ relative to the Renison dolomicrites and present shallow seawater δW. Renison dolomicrites are also enriched to about 6‰ relative to Proterozoic warm-water dolomite. Souces of data for fields: 1- Williams, 1979; Veizer and Hoefs, 1976; Schidlowsky et al., 1975; 2- Zempolich et al., 1988; 3- McKenzie, 1981; 4- Behrens and Land, 1972; 5- Warren, 1988.

10.11 Alteration of Dolomites

The alteration of dolomites can be deduced from petrographic evidence, variations in concentrations of Ca, Mg, Sr, Na, Mn and Fe, and $\delta^{18}O$ and $\delta^{13}C$ values.

The change in dolomite fabric from dolomicrite to dolomicrosparite in Renison dolomites (see Figs. 10.6 A, B) indicates an increasing degree of alteration of dolomite. Dolosparite is either void or cavity-filling cement.

10.11.1 Major elements

The amount of Ca in Renison dolomite ranges from 20.7% to 22.1% (Table 10.2). The relationship between Ca and the Mg/Ca ratio is random. In contrast to Ca, the amount of Mg in Renison dolomite is inversely related to the Mg/Ca ratio (Fig. 10. 12) with a significant r^2 value of 0.7. Since the Mg/Ca ratio in pure dolomite is 0.6, the decrease of Mg values from 13.2% to 10.3% with decreasing Mg/Ca ratios is due to alteration of dolomite. Mg values are lower in coarsely crystalline dolomites than in dolomicrites.

10.11.2 Trace elements

The amount of Fe increases from 1 524 ppm to 33 195 ppm with decreasing Mg values (Fig. 10. 13), due to substitution of Fe for Mg in Renison dolomites. The amount of Mn, like Fe, increases from 120 ppm to 4 655 ppm with decreasing Mg values (Fig. 10. 13), due to substitution of Mn for Mg during alteration of dolomite. In contrast to Fe and Mn values, the relationship of Sr (Fig. 10. 14) values (and also Na) with Mg (and also Ca) is random.

Table 10.2. Minimum, maximum, mean and standard deviation values of the major and minor elements and isotopic compositions of Renison dolomites away from the mineralized area.

Variables	Minimum	Maximum	Mean	Standard deviation
Ca%	20.7	22.1	21.7	0.33
Mg%	10.3	13.2	12.2	0.69
Fe ppm	1524	33195	8531	7135
Mn ppm	120	4655	822.1	962
Sr ppm	57	196	102.3	26
Na ppm	76	358	162	59.8
$\delta^{18}O$	-8.7	0.3	-4.1	2.3
$\delta^{13}C$	-1.6	7.5	3.9	1.6

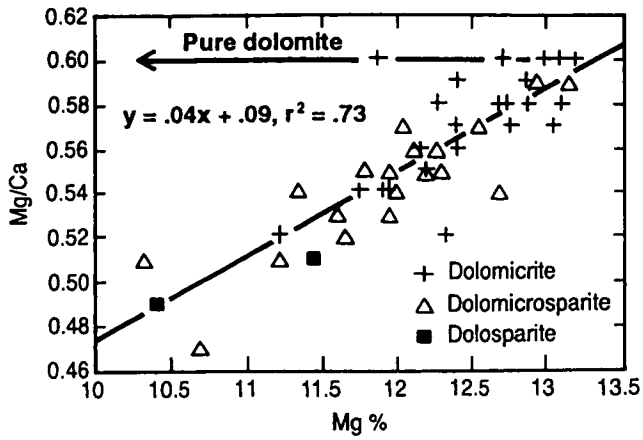

Figure 10.12. Variation of Mg/Ca versus Mg%. Note most of the dolomicrites have high Mg (>12) %.

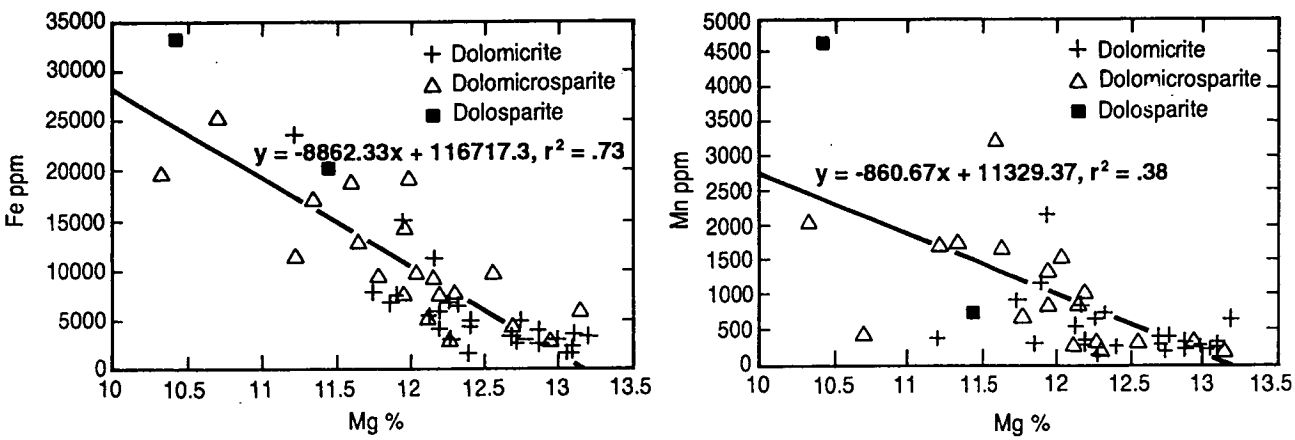

Figure 10.13. Variation of Fe and Mn versus Mg%. Note there is an inverse relationship between Fe and Mn with Mg% due to alteration by non-marine fluids.

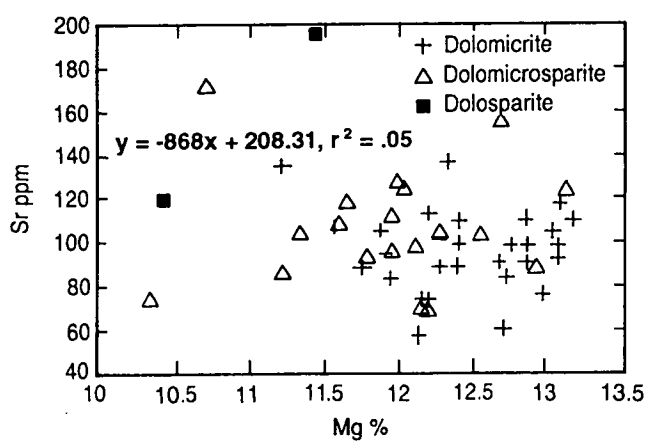

Figure 10.14. Plot of Sr versus Mg%. Similar Sr values between relatively pure and altered dolomites are due to the lack of significant change of Sr values from unaltered to altered dolomites.

10.11.2.1 Discussion

The concentration of trace elements in carbonates varies with carbonate mineralogy, partition coefficients, fluid composition and oxidising and reducing conditions. The amount of Fe and Mn in aragonite is small (< 20 ppm). In marine calcite the amounts of Mn (1 to 125 ppm) and Fe (82 to 5198 ppm) are higher than in aragonite (Rao, 1996), due to a higher partition coefficient of ≥ 15 of Fe and Mn in calcite. In dolomite, the concentrations of Fe and Mn are greater than those in coexisting calcite (Rao, 1993 c), due to the dolomite crystal structure and higher partition coefficients (greater than unity) of Fe and Mn in dolomite than in calcite. The concentrations of Mn (120 to 4655 ppm) and Fe (1524 ppm to 33 195 ppm) in Renison dolomites are much higher than those in marine calcite. The increase of Fe and Mn concentrations from least-altered dolomite to altered dolomite is due to the composition of fluids altering the dolomite (Fig. 10.15). As the Fe and Mn concentrations are low in marine fluids, the increase of Fe and Mn values from least-altered to altered dolomite is probably due to reaction with non-marine fluids. Since the incorporation of Fe and Mn in carbonate increases from oxidizing to reducing conditions, the high concentrations of Fe and Mn in Renison dolomites may be due to reducing conditions during alteration and formation of diagenetic dolomite.

Determination of Fe and Mn concentrations in dolomites is important to understand the timing of dolomitization. Early near-surface dolomites tend to have low Fe and Mn concentrations, possibly due to oxidizing conditions, relative to later diagenetic dolomites. In the case of Renison dolomite, very finely crystalline primary to very early diagenetic dolomicrites contain less Fe (range from 1524-23 473; average 5308 ppm) and Mn (range from 120-2122 ppm; average 449 ppm) than later diagenetic medium to coarsely crystalline dolomicrosparites and dolosparites (Fe range from 2980-33 195; average 12 623 and Mn range from 186-4655; average 1300 ppm). The relatively high iron enriched dolomicrites, compared to the modern ones, are probably due to availability of iron in the basin during dolomicrite formation, as evidenced by the relatively thick sequence of banded iron formation in the Red Rock Member (25-35 m) above and below of the No. 2 and No. 1 dolomite horizons in the Renison sequence. The very high iron contents in the coarsely crystalline dolomites can be attributed to mud rock dewatering, which released Fe during clay diagenesis at elevated temperature during burial. Mud rocks are abundant in lower and upper parts of all three dolomite horizons in the Renison succession (Fig. 9.5). Morrison (1982) suggested that the presence of a banded iron formation in the Red Rock Member may

explain the anomalous iron enrichment in some late diagenetic dolomites.

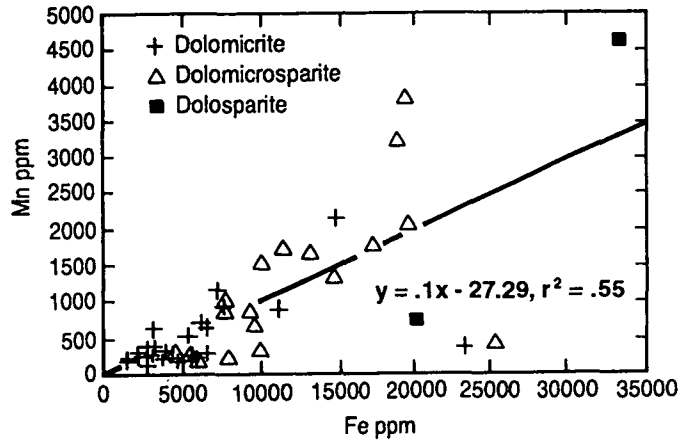

Figure 10.15. Plot of Fe versus Mn. The positive correlation between these two elements is due to alteration by diagenetic fluids.

The amount of Sr in aragonite ranges between 8000 to 10 000 ppm, whereas in biotic marine calcite, Sr ranges from 1333 ppm to 3324 ppm (Rao, 1996), and abiotic marine calcite ranges from about 200 to 1400 ppm (Carpenter and Lohmann, 1992). The amount of Sr in marine dolomite is about half that in marine abiotic calcite, when in equilibrium with ~ 25° C seawater (Land 1980). Thus Sr in marine dolomite ranges between 100 to 700 ppm. The low Sr concentrations in Renison dolomites (57 to 196 ppm; mean 102 ppm) are most likely due to the formation of dolomite in a marine environment. Sr values have not been appreciably decreased by non-marine fluids. It has been suggested that the Sr values in Tertiary marine dolomite decrease with increasing dolomite stoichiometry (Vahrenkamp and Swart, 1990). Since Sr in dolomite substitutes mainly for Ca, the Sr value decreases with increasing stoichiometry or increasing Mg CO_3 values of dolomite. The stoichiometric dolomite has about 50 ppm Sr, which increases by about 20 ppm Sr for every additional mol % Ca CO_3 (Vahrenkamp and Swart, 1990). Thus, the variation in Sr concentration (57-196 ppm) in Renison dolomites can be related to the nearly stoichiometric to nonstoichiometric composition of these dolomites (see, Fig. 10.4). Sr values between least-altered and altered dolomites are similar, indicating a lack of significant change of Sr (Fig. 10. 14) from least-altered to altered Renison dolomites.

The amount of Na in abiotic aragonite is about 2700 ppm, whereas in abiotic calcite it is about 270 ppm (Veizer, 1983). As with Sr, Na in marine dolomite is probably about half of that in marine abiotic calcite. Na values in dolomite increase with increasing salinity of seawater (Land and Hoops, 1973).

The low Na concentration in Renison dolomite (76 to 358 ppm; mean 162 ppm) is similar to marine and mixing zone dolomites of the late Pleistocene (Humphrey, 1988) and Ordovician (Rao, 1990 c). The Na values in primary to very early diagenetic dolomicrites are relatively higher (range from 105-358 ppm; mean 167) than the later diagenetic dolomicrosparite and dolosparite (range from 76-307 ppm; mean 155).

10.11.3 Oxygen and carbon isotopes and major and trace elements

In general, the correlation between $\delta^{18}O$ and $\delta^{13}C$, and major and minor element values (Table 10.1 A), indicates $\delta^{13}C$ values are unrelated to elemental composition, whereas $\delta^{18}O$ values are positively correlated with Mg content, inversely correlated with Fe and Mn contents, and mostly unrelated to Sr and Na values. The variation of $\delta^{18}O$ and Mg values is related to dolomite types (Fig. 10.16). High values of $\delta^{18}O$ and Mg are in dolomicrite, moderate values in dolomicrosparite and low in dolosparite, due to recrystallization and late dolomite cementation. The inverse relationship between Fe (and also Mn) with $\delta^{18}O$ values is also related to dolomite types (Fig. 10.17). The heaviest $\delta^{18}O$ values and lowest Fe contents are in dolomicrite, whilst light $\delta^{18}O$ values and high Fe values are in dolomicrosparite and dolosparite. This inverse relationship between $\delta^{18}O$ values and Fe (and also Mn) values might be due to alteration by non-marine fluids. Lack of correlation between Sr (and also Na) and $\delta^{18}O$ values is possibly due to least alteration of marine dolomite Sr (and also Na) values.

When the analyses are considered in terms of dolomite type, the heavier $\delta^{13}C$ values correspond to lower Mn and Fe concentrations in dolomicrites (Fig. 10.18). The lighter $\delta^{13}C$ values and higher Mn and Fe values are in dolomicrosparite and dolosparite (Fig. 10.18). There is a lack of correlation between Sr and also Na with $\delta^{13}C$ values.

10.12 Recognition of Least-Altered Dolomites

Petrographically, the Renison dolomicrites are interpreted as least-altered. They preserve primary fabrics and show little evidence of recrystallization and diagenetic reorganization. Dolomicrite $\delta^{18}O$ values range from -5.2 to +0.3‰ (Fig. 10.11), with an average value of -2‰. In contrast, dolomicrosparite $\delta^{18}O$ values range from -8.9‰ to -1.5‰, with an average value of -5.2‰. Dolosparite $\delta^{18}O$ values range from -8.4 to -6.9‰, with an average value of -7.5‰. There is a marked decrease in mean $\delta^{18}O$ values from dolomicrite (-2‰) through dolomicrosparite (-5.2‰) to dolosparite (-7.5‰) due to an increased amount of

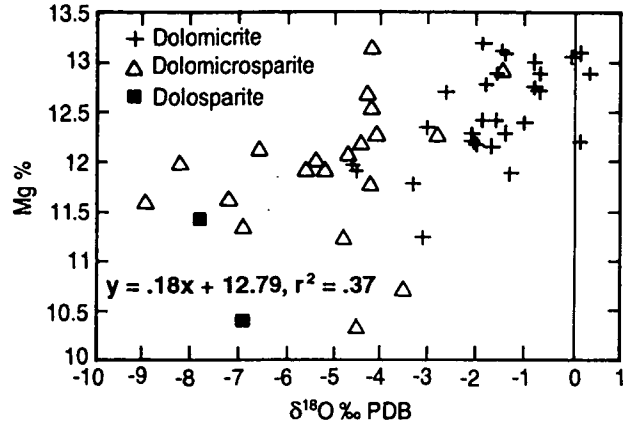

Figure 10.16. Plot of $\delta^{18}O$ versus Mg%. Note Mg content shows a positive relationship with $\delta^{18}O$. High values of $\delta^{18}O$ and Mg are in dolomicrites, as they are least affected by diagenetic alteration.

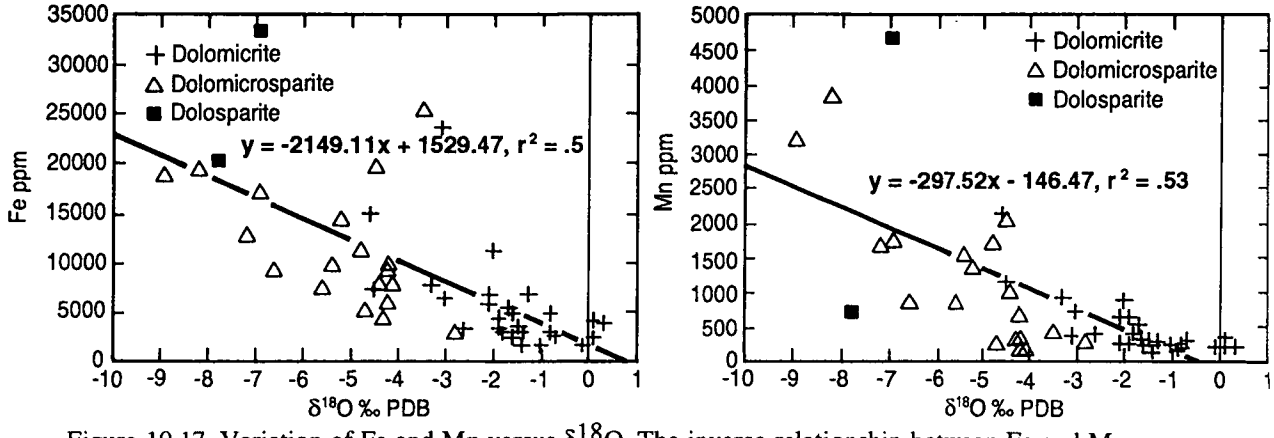

Figure 10.17. Variation of Fe and Mn versus $\delta^{18}O$. The inverse relationship between Fe and Mn with $\delta^{18}O$ is related to dolomite types. Most positive $\delta^{18}O$ and low Fe and Mn concentrations are in dolomicrites due to least alteration.

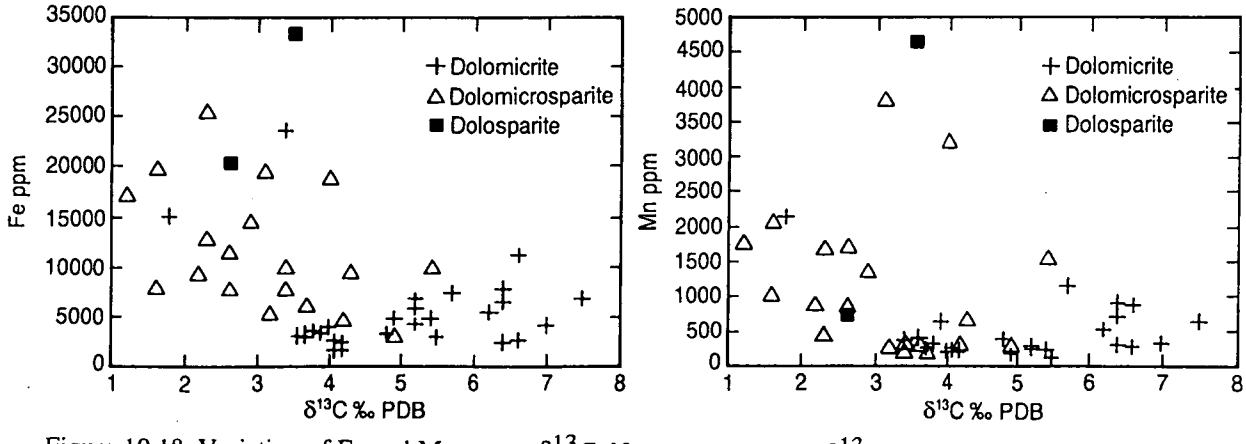

Figure 10.18. Variation of Fe and Mn versus $\delta^{13}C$. Note most positive $\delta^{13}C$ and low Fe and Mn concentrations are in dolomicrites due to least alteration.

alteration. The most likely explanation for $\delta^{18}O$ depletion in dolomicrosparite and dolosparite appears to be temperature-related fractionation. There has been much discussion about $\delta^{18}O$ depletion in the Proterozoic, with suggestions that seawater was either depleted in $\delta^{18}O$, or temperatures were hotter in these earlier times (e.g., Karhu and Epstein, 1986). This study indicates that very negative $\delta^{18}O$ signatures can be due to diagenetic alteration, and seawater was more negative than -5‰ SMOW, as suggested by other workers (e.g., Fairchild and Spiro, 1987).

Dolomicrite $\delta^{13}C$ values range from 1.8 to 7.5‰ (Fig. 10.11), with an average of 5‰. In contrast, dolomicrosparite $\delta^{13}C$ values range from -0.4 to 6.4‰, with an average value of 3.2‰. Dolosparite $\delta^{13}C$ values range from -1.6 to 3.5‰ with an average value of 1.6‰. There is a marked decrease in mean $\delta^{13}C$ values from dolomicrite (5‰) through dolomicrosparite (3.2‰) to dolosparite (1.6‰), due to an increasing amount of alteration. Thus, the heaviest $\delta^{18}O$ and $\delta^{13}C$ values are in dolomicrite because dolomicrites are the least-altered samples from Renison.

Chemically least-altered dolomites from Renison can also be deduced from a combination of high values of Mg and Mg/Ca, heavy $\delta^{18}O$ and $\delta^{13}C$ values, and low values of Fe and Mn. Heavy $\delta^{18}O$ values correspond to high Mg values of about 12 to 13.2%. These values are from least-altered dolomicrites (Fig. 10. 16). Heavy $\delta^{18}O$ values correspond to relatively high Fe (< 5000 ppm) and also Mn (< 500 ppm). These values are from dolomicrites. Thus, petrographic and geochemical evidence confirm that dolomicrites are the least-altered dolomites. Therefore, the least-altered dolomicrites have heavy $\delta^{18}O$ values of -1± 1‰ and $\delta^{13}C$ values of 5.5 ± 2‰.

10.13 Temperatures of Formation

Petrographic criteria for recognition of temperature of carbonate formation has only recently been developed for limestones (e.g., Rao, 1981a; Nelson, 1988 and references therein). Neoproterozoic limestones are rare and highly recrystallized in the Renison mine sequence. Therefore, the temperature of formation of Renison dolomites should be calculated from least-altered finely crystalline dolomites. At present there is no petrographic evidence for recognising sedimentary dolomite temperatures. However, finely crystalline dolomites (<1μ) are abundant in temperate dolomite from Coorong, South Australia (von der Borch, 1976). Renison dolomicrites are finely crystalline and thus resemble Coorong dolomites. Non-skeletal dolomite grains are rare in Renison dolomites,

similar to temperate dolomites from Coorong.

Temperature fractionation of elements exists in limestones (Rao, 1991, 1996). Temperature fractionation of elements in dolomites is not clear. Nevertheless, Renison least-altered dolomites contain relatively high Fe (< 5000 ppm) and Mn (< 500 ppm) concentrations perhaps due to higher fractionation of Fe and Mn in dolomite.

Temperature fractionation of $\delta^{18}O$ is well established in limestones, but it is poorly documented in dolomites. Thus, there are no well-established $\delta^{18}O$ paleotemperate equations for dolomites. For this reason, three estimates are made. The first estimate is from comparison between Proterozoic dolomites interpreted to be warm-water dolomites that are not associated with glacial sediments (Fig. 10.11). This illustrates that Renison dolomites are enriched in $\delta^{18}O$ by about 5‰. If we assume a temperature of about 25° C for warm-water dolomites, the Renison dolomites probably formed at about 3° C, by considering a decrease of 4.4° C/1‰ $\delta^{18}O$.

The second temperature estimate is made from the dolomite temperature equation developed by Irwin (1980):

$$\mathbf{T=31.9 - 5.55\ (\delta_d - d_w) + 0.17\ (\delta_d - d_w)^2}$$

The least-altered $\delta^{18}O$ value of -1 ± 1‰ in Renison dolomite, substituted in the Irwin dolomite paleotemperature equation, corresponds to a temperature of about 13° ± 4° C, assuming δ_w = -4.9‰. Irwin demonstrated that early diagenetic dolomites form below the sulphate reduction zone in waters composed of a light $\delta^{18}O$ value of -4.9‰.

Determination of seawater temperatures, during the Proterozoic and into the Paleozoic, based on $\delta^{18}O$ in cherts and chert-phosphate pairs (Knauth and Epsten, 1976; Karhu and Epstein, 1986) yielded very high ocean temperatures ranging from 60° to 120° C. This might be due to diagenetic alteration of $\delta^{18}O$, or that the Proterozoic seawater $\delta^{18}O$ values were lighter than the present value of 0‰.

Lighter $\delta^{18}O$ values of the Neoproterozoic seawater have been postulated by many workers: -3 ± 1‰ at 0.6 Ma from carbonates of Spitsbergen (Fairchild and Spiro, 1987); -4 ± 2‰ at 0.8 Ma from carbonates of Death Valley, California (Tucker, 1986 b); and -0.5 ± 2‰ at 1.0 Ma from Beck Spring Dolomite (Zempolich et al, 1988). As the age of Renison dolomite ranges within 800 to 570 Ma (Adabi, in press, see Chapter 11), the Neoproterozoic $\delta^{18}O$ seawater values should be within the range of -6‰ to -2‰ (Fairchild and Spiro, 1987; Tucker,

1986 b). Using these Neoproterozoic ^{18}O seawater values (lowest -6‰ and highest -2‰) substituted in the Irwin dolomite-temperature equation, Renison dolomite $\delta^{18}O$ values of -1 ± 1‰ PDB give temperatures ranging from 8 ± 4° C (δ_W = -6‰) to 26 ± 5° C (δ_W = -2‰). Using the same method and $\delta^{18}O$ dolomite values of -6 ± 1‰ PDB for worldwide dolomites not associated with glacial sediments (Fig. 10. 11), gives temperatures ranging from 32 ± 6° C (δ_W = -6‰) to 57 ± 7° C (δ_W = -2‰). These temperatures indicate that the Renison dolomites formed at a temperatures cooler than 24° C (32-8° C) or 31° C (57-26 °C) relative to dolomites not associated with glacial sediments.

Land (1985) published an equation for calculating the temperature of dolomite formation, based on $\delta^{18}O$ values (see Chapter 8, p. 227). By using the above postulated Neoproterozoic seawater values in the Land equation, the temperature of the least-altered Renison dolomites (-1± 1‰) ranges between 12° ± 4° C (δ_W = -6‰) and 30 ± 5° C (δ_W = -2‰). However, taking the heaviest $\delta^{18}O$ value of +0.3‰, gives a temperature ranging from 6.5° C (δ_W = -6‰) to about 23° C (δ_W = -2‰). The temperature for dolomite (values -6 ± 1‰) not associated with glacial sediments ranges between 35 ± 5° C (δ_W = -6‰) to 58 ± 6° C (δ_W = -2‰). In all the above studies, the seawater $\delta^{18}O$ value was assumed to be the same as heavy $\delta^{18}O$ values of dolomite. For example, Fairchild and Spiro (1987) suggested that since the $\delta^{18}O$ is depleted by the diagenetic processes, the isotopically-heaviest values provide the best estimate of the isotopic composition of the seawater or original depositional fluid. However, in modern environments, dolomites are enriched from about 4 (Land, 1985) to 8‰ relative to a seawater value of 0‰ (Fig. 10.11), due to $\delta^{18}O$ fractionation in dolomite relative to calcite and the temperature and salinity of dolomite forming fluids. As evaporite minerals indicative of higher salinities are rare in Renison dolomite, $\delta^{18}O$ values in Renison dolomites vary mainly with temperature. Since $\delta^{18}O$ values of Renison dolomites range within -1 ± 1‰, a δ_W = -6‰ for Neoproterozoic seawater has been assumed to account for fractionation of ~4‰, as advocated by other workers.

The climate during the Neoproterozoic was intensely cold, based on the occurrence of glacial sediments at low latitudes in all continents (Frakes, 1979), low luminosity, low output of the sun (Gough, 1981) and declining atmospheric CO_2 levels (Kasting, 1992). There are no tools to check the levels of luminosity from carbonates. However, $\delta^{13}C$ values in carbonates can be used to check the atmospheric CO_2 levels (Rao and Wang, 1990; Rao, 1993 b). Very heavy $\delta^{13}C$ values in Renison least-altered dolomites (5.5 ± 2‰) and other worldwide

Neoproterozoic dolomites (e.g., Wickham and Peters, 1993; Iyer et al., 1995; Kaufman and Knoll, 1995) may indicate that atmospheric CO_2 was very low. Such heavy $\delta^{13}C$ values occur in Permian carbonates (~ +6‰; Rao, 1991) that formed during a major glacial period. Although the diamictites of Renison have not been studied in detail, available evidence from diamictite studies of Smithton Basin, equivalent to Renison diamictites, indicates that they are glaciomarine in origin, with deposition taking place from ice rafting (Calver, 1995). The cold water dolomites formed at Renison and many parts of the world during the Neoproterozoic, as indicated by heavy $\delta^{18}O$ values of dolomite from many regions, relative to a Neoproterozoic seawater value of about -6‰. Synsedimentary or very early diagenetic marine origin for the Neoproterozoic glacial-associated Cap Dolomite with $\delta^{18}O$ values ranging from -4 to -11‰ have been suggested by Wallace et al. (1995). They believed that the primary marine $\delta^{18}O$ signature in some of these dolomites is at least partially preserved at most localities.

Cold water marine dolomite from other geologic periods such as in Barremian-age sediments have been reported recently from ODP Leg 143, in Mid-Pacific Mountains (Flood and Chivas, 1995). They have calculated temperatures as low as 15° C for fluid responsible for dolomitization. Fontes and Desforges (1975) have reported dolomite in pelagic carbonates from the Mediterranean, which they interpret to have formed in "cold marine conditions". Dolomite formation by "cold deep ocean water" has also been documented from Enewetak Atoll by Saller (1984). Seawater temperature at the depth of the dolomite formation is 10-20°C. Mullins et al. (1988) also reported authigenic dolomites (10-20μ) from pore marine water as cold as 1.8-9.8° C from the Neogene Bahamian samples. Oxygen isotope data from the west Florida Neogen deep-water marine dolomite also suggests paleotemperatures of 4.5 to 11.7° C (Mullin et al., 1988).

10.14 Origin of the Renison Dolomite

The recognition of primary or penecontemporaneous dolomite is difficult in the interpretation of ancient dolomites. Several petrographic and geochemical features of the dolomite studied, however, suggest a synsedimentary or very early diagenetic marine origin, rather than a secondary or replacement origin, particularly in dolomicrite samples. These include:

- the micritic nature of the most least-altered dolomite
- well preserved original structure of some grains such as intraclasts and

cryptalgal fragments (Fig. 10.19 A)

- finely laminated dolomite (1-3 mm thick, Fig. 10.19 B)
- low Fe and Mn concentrations in dolomicrites relative to coarser diagenetic dolomites
- Positive relation between Mg and $\delta^{18}O$ values and inverse relationship between Mn, Fe and $\delta^{18}O$ values in dolomicrites
- very heavy oxygen (<-2‰) and heavy carbon values (> +3.5 ‰ up to 7.5‰) in most finely crystalline dolomicrites
- the preservation of consistent stratigraphic trends in carbon and oxygen isotopic compositions of most dolomicrite samples

All the above evidence is possibly indicative of syndepositional or early diagenetic dolomitization in most of the dolomicrite samples (e.g., Folk, 1974 a; von der Borch, 1976; Williams, 1979; Tucker, 1983; Zempolich et al., 1988; Wallace et al, 1995). Many other researchers have also suggested the possibility of precipitation of penecontemporaneous dolomite from sea water or pore water, in equilibrium with sea water, from Recent supratidal-subtidal to deep marine settings (e.g., Illing et al., 1965; Atwood and Bubb, 1970; Saller, 1984; Mullins et al., 1985; Carballo et al., 1987; Mitchell et al., 1987; Mazzullo et al., 1987; Lumsden, 1988). Microbially laminated texture in the Renison dolomicrite has been described as a product of alternating algal bloom and seawater flooding, wherein the dark layers are products of algal growth and the crystalline dolomite is a direct precipitate from seawater during flood in a supratidal to intertidal environment (Morrison, 1982). Penecontemporaneous dolomitization has been recognized from the Middle Proterozoic McArthur Group, Australia (Muir et al., 1980) and recently from a deep-marine Middle-Upper Proterozoic setting in India (Mukhopadhyay et al., 1996).

The well preserved fabric and low Sr and Na values in the least-altered dolomicrites in Renison samples argue against original aragonite mineralogy, as has been suggested for Neoproterozoic successions of Death Valley, California, by Tucker (1986 b) and Spitsbergen by Fairchild and Spiro (1987). The pronounced oxygen and carbon enrichment in almost all dolomicrite samples, also supports the lack of dissolution or alteration of a preexisting metastable carbonate phase such as aragonite. However, Tucker (1983) suggested that good fabric preservation and very low Sr values in dolomites may indicate a primary Mg-calcite or poorly-ordered and soluble dolomite precursor. The very shallow water conditions that prevailed in this basin (Morrison, 1982) may have allowed early dolomitization. Syndepositional dolomitization by seawater, as suggested in

this study, has been proposed by many researchers (e.g., Ruppel and Chander, 1988; Amthor and Friedman, 1992; Wallace et al., 1995).

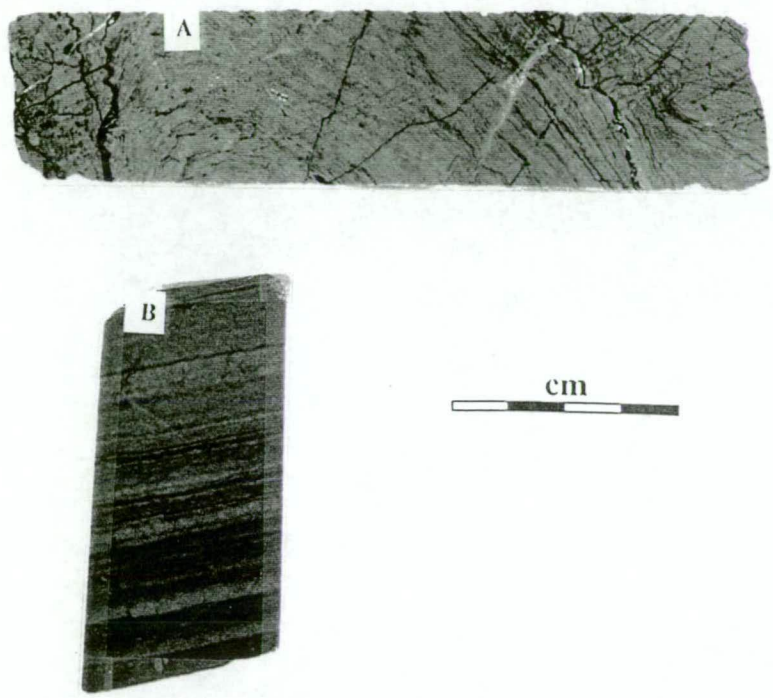

Figure 10.19. Etched slabs showing sedimentary features of the least-altered dolomites. A) wavey type stromatolite with rhombic shape microbial laminae (S705, 183 m), B) finely laminated dolomite (S705, 246.8 m).

I am fully aware of the kinetic problems of direct precipitation of dolomite at present earth surface conditions, but the distinctive physical and cathodoluminescence features, as well as the elemental and isotopic compositions of the Renison dolomicrites, suggest the possibility this may have occurred back in the Proterozoic. This conclusion is supported by Tucker (1982) who suggested that the chemistry of the Proterozoic oceans was different to that of the Phanerozoic. One might argue that it is difficult to prove or disprove whether well preserved sedimentary fabrics are primary or replacement in origin, particularly when all depositional grains are micritic, as they are in Renison. The interpretation of primary origin of dolomicrite in Renison is consistent with the data, but I freely acknowledge that from what we know of dolomite formation, a replacement origin is more likely and easily acceptable by many researchers. For example, Zenger (1982) suggested that well-preserved fabric in dolomite resulting from very early replacement and retention of actual or relative stable isotope compositions is possible. Bose (1979) and Fairchild (1980) interpreted

Proterozoic dolomites in India and Scotland, to be of a penecontemporaneous replacement origin.

However, the elemental and isotopic composition of sea water, from which primary dolomite is precipitated, and the interstitial water (close to the sediment-water interface), from which the very early diagenetic replacement dolomite is formed, are very similar. Furthermore, there is little temporal difference between primary and very early diagenetic replacement dolomite. These critical factors combine to highlight the difficulty in distinguishing between primary and very early diagenetic replacement dolomite.

The crystallized form of the dolomite (i.e. dolomicrosparite) suggests subsequent recrystallization during post depositional diagenesis. Some further evidence of diagenetic reorganization is present in these recrystallized dolomites, such as clots of structureless dolomicrite set in a dolomicrosparite matrix (grumeleuse texture), fracturing, rehealing, microstylolites and other related phenomena. Moderate increases in crystal size of dolomite (i.e. dolosparite), which correspond to high $\delta^{18}O$ depletion, also confirm post depositional diagenetic modification, possibly by non-marine fluids.

The common diagenetic alteration processes, leading to oxygen isotope depletion, are either meteoric waters and/or fluids at elevated temperatures (during burial). $\delta^{18}O$ and $\delta^{13}C$ bivariate plots show decreases of both $\delta^{18}O$ and $\delta^{13}C$ values, a characteristic feature of burial diagenetic trend (Choquette and James, 1987; Nelson and Smith, 1996). Major and trace element distributions in the Renison dolomites do not usually reveal any conspicuous patterns (in particular, plots of Sr and Na against Mg). A noteworthy exception is Fe and Mn which progressively increase with increasing Mg% (Fig. 10.13). The large-scale incorporation of bivalent (ferrous) Fe and Mn into the dolomite lattice indicates the prevalence of reducing conditions during the process of dolomite formation. The high Fe and Mn concentrations and positive correlation between these two elements have been related to burial diagenesis (Winefield et al., 1996). Thus, the oxygen and carbon isotopic trend and trace element bivariate plots, along with physical evidences (e.g., grain size and abundant stylolites), favor burial diagenesis in most recrystallized and coarsely crystalline dolomites.

10.15 Source of Magnesium

Very large volumes of Mg-rich fluids are required for thick dolomitization in the Renison mine area, and seawater is an obvious possibility, particularly in very fine grained least-altered dolomites (e.g., Land, 1985). Dolomitiziation in the

presence of seawater or by geothermal seawater convection (known as the Kohout model) is an increasingly popular mechanism, and dolomites formed in this way have heavy $\delta^{18}O$ and $\delta^{13}C$ values. In the early stages of diagenesis, soon after deposition, seawater would be a major constituent of the sediment (Taylor and Sibley, 1986). However, dolomites formed in mixing-zones may show quite negative $\delta^{18}O$ and $\delta^{13}C$ values, reflecting the depleted meteoric water and influence of soil gases, which is not the case in Renison dolomites. Thus, it is suggested that dolomicrites which are unaltered to least-altered dolomites in the study area, possibly formed close to the sea floor under conditions of a slow rate of sedimentation, with Mg^{2+} being supplied by seawater. The low (< 100 ppm) Sr and also Na concentrations in Renison dolomites do not support evaporitic conditions during the formation of dolomicrites (Veizer, 1983; Machel and Anderson, 1989), leaving Neoproterozoic seawater as the most likely source.

In contrast, magnesium for coarsely crystalline dolomites (e.g., dolomicrosparite and dolosparite), which have been formed during late diagenesis might be supplied from:

- connate waters (trapped seawater)
- pressure solution (stylolitization)
- basinal brines
- compaction of underlying shales

Although it is difficult to put weight on these possibilities, compaction of underlying shales is the most likely magnesium source for burial dolomitization in the Renison coarsely crystalline dolomites. These aspects will be discussed below.

Connate water can provide only a limited amount of magnesium to sediments. It is possible that connate water composition changes or is modified as diagenesis of sediments proceeds (Lee and Friedman, 1987).

Pressure solution is another possible source of magnesium for dolomitiztion (Wanless, 1979). Although remobilization of magnesium for pressure solution of dolomite is possible, it is volumetrically unimportant, but can be important locally. In the study area, coarsely crystalline dolomite associated with stylolites is common laterally and vertically.

Basinal brines are an important source of magnesium for dolomitization at burial depth (Gregg, 1985; Lee and Friedman, 1987). A possible source for hot brine is the Pine Hill Granite intrusion, but the lack of saddle dolomite in this study rules out basinal brines as a major possible magnesium source for burial dolomitization. This mechanism is important for dolomitization of dolomite horizons within the mine area, which has a relatively large amount of saddle

dolomite.

Shale compaction is another possible magnesium source for dolomitization under burial conditions (Mattes and Mountjoy, 1980). Clay-mineral transformation during shale diagenesis can release magnesium to the pore fluids which are migrating upward to dolomitize the the overlying carbonates (Sternbach and Friedman, 1984). As all three dolomite horizons in the Renison mine area are overlain and underlain by black and gray shale and siltstone, which can contain large volumes of seawater, Mg^{2+} could have been transferred to the upper dolomite horizon during dewatering caused by compaction and diagenesis of the shale. The presence of iron rich dolomite throughout most of the dolomite horizons suggests that shale is also the source of iron, on a basin-wide scale, because iron can be released during shale dewatering and clay mineral transformation. The Red Rock Member and Renison Bell Member, which are overlain by No.1 and No.2 dolomite horizons respectively, contain iron rich shale sequences. However, Land (1985) suggested that during shale diagenesis more calcium is released than magnesium, and magnesium is consumed locally in the formation of chlorite. The absence of cholorite in all three dolomite horizons studied here indicates that Mg^{2+} has not been consumed by cholorite. The Mg^{+2} ions were probably moved through the Renison sequence via high porosities and many fractures available in the area. In addition to Mg^{2+}, Fe^{2+} and Ca^{2+} ions, Si^{4+} is also released during clay diagenesis (Mattes and Mountjoy, 1980; McHargue and Price, 1982). The silica rich dolomite veins in some of the dolomite samples studied here indicate that silica was provided during late stage clay mineral diagenesis. Basinal shales are commonly organic rich, and diagenesis of organic matter would contribute CO_3^{2-}. Dolomite apparently forms from carbonate anion (CO_3^{2-}) rather than the bicarbonate anion (HCO_3^-) because the carbonate anion can dislodge water dipoles from Mg^{2+} ions on the growing crystal surface (Lippmann, 1973). This suggests that dolomitization is promoted from solution with high alkalinity, where the CO_3^{2-} ion dominates over the HCO_3^- (Tucker and Wright, 1990).

10.16 Environmental Significance of the Least-Altered Dolomite

Diagenetically altered recrystallized dolomite does not preserve sedimentary structures that can be used to infer the environment of deposition. Inferences based on the least-altered dolomite found nothing to contradict Morrison's (1982) interpretation, which indicated that the Renison sequence was deposited mainly in a shallow marine environment. The typical Mine Sequence

shows cyclic sedimentation as two major regressive and a partial transgressive cycle of subtidal-intertidal-supratidal and fluvial units (Morrison, 1982, Fig. 10. 20). The lower regressive cycle is ~110 m thick and includes the Dalcoath Member and No.3 dolomite. It records progressive shallowing upward from the intertidal to subtidal channel margin (dalcoath contorted and lower Dalcoath carbonaceous and non-carbonaceous), through the intertidal mixed flat and mud flat environment (Upper Dalcoath carbonaceous and non-carbonaceous) to the intertidal to supratidal saltmarsh (Dalcoath Member Upper) and algal flat (No.3 dolomite) environment (Fig. 10.20). The upper regressive cycle is ~90 m thick and includes the Renison Bell Member, No.2 dolomite and lower part of the Red Rock Member. It records an intertidal sand bar (Renison Bell Lower), followed by progressive shallowing upward from intertidal mixed flat and mudflat (Renison Bell Middle), through the intertidal to supratidal saltmarsh (Renison Bell 2.2 dolomite and Renison Bell Upper), the algal flat environment (No.2 dolomite) and into the fluvial environment (Red Rock Member). The partial transgressive cycle is ~30 m thick and includes the Upper Red Rock Member, No.1 dolomite, and Upper Contorted Units. It records overbank fluvial channel fill (Red Rock Member), followed by supratidal (No.1 dolomite), and then intertidal (Upper Contorted Units) sequences (Fig. 10.20).

Features of Renison dolomites that may have environmental significance include:

- the presence of microbial fabrics and intraclastic grains
- the micritic nature of most dolomites which are associated with silt-sized detrital quartz grains
- the rare oolitic textures
- the general lack of evaporites or their pseudomorphs
- the presence of fenestral fabrics
- the preservation of isotopic composition of dolomicrites throughout the stratigraphic section (Wallace et al, 1995, P.81)

The first two features are similar with modern dolomitic mud flats of supratidal Sabkhas in the Persian Gulf (e.g., Illing et al, 1965), and of coastal lagoons such as those in the Coorong area, South Australia (von der Borch, 1976; von der Borch and Lock, 1979). The presence of fenestral fabrics may suggest a subaerial to very shallow environment. The lack of evaporites may indicate that arid climates did not prevail, or may suggest a seasonally evaporitic/humid climate, under which evaporite minerals were not preserved (Muir et al., 1980). The characteristic lamination of some dolomites may support such seasonality.

Overall, the sedimentological features of the Renison dolomites favors deposition mainly in a marine shallow intertidal to supratidal environment, possibly under seasonal climates.

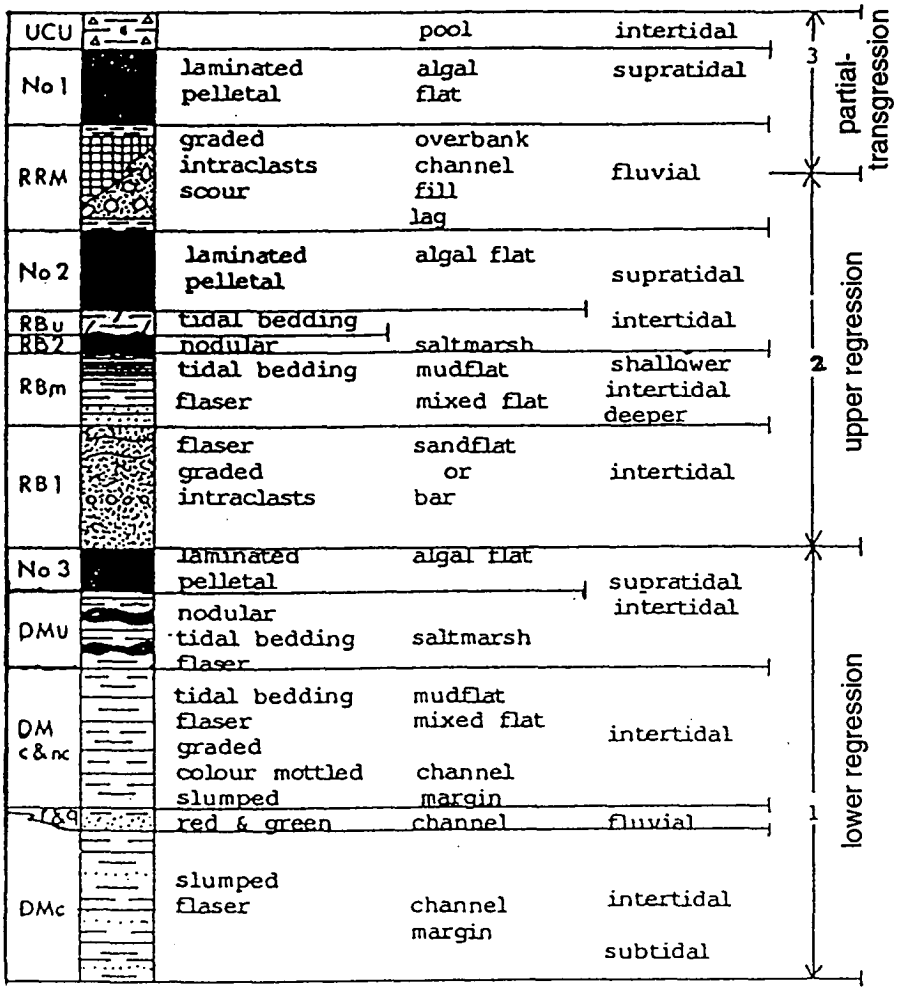

Figure 10.20. Sedimentary cycles in the Renison mine sequence. The lower two cycles are regressive, and the third cycle is transgressive (modified from Morrison, 1982). Abbreviations are explained in Figure 9.5.

10.17 Conclusions

Four major types of dolomite occur in the Neoproterozoic sequence studied outside of the Renison mine area. These dolomite types can be separated and recognised mainly on the basis of grain size, Mg%, Mn and Fe content and $\delta^{18}O$ values. Variations in dolomite types may indicate differences in formation time or formation mode. The petrographic and geochemical differences within the dolomite types clearly show that the dolomicrites are genetically unrelated to other dolomite types and thus, represent a different dolomitization event. The

dolomicrites probably formed at or near the surface by either direct precipitation or during very early diagenesis, with Mg^{2+} being supplied by seawater. This is best accomplished during early diagenesis when sediment permeability and flow rates are high. The calculated paleotemperature of seawater during the Neoproterozoic, considering δ_W = -6.‰ and the least-altered dolomite $\delta^{18}O$ value of -1 ± 1‰, indicates that the seawater temperature was around 8° ± 4° C (Irwin equation) or 12° ± 4° C (Land equation). Taking the heaviest $\delta^{18}O$ dolomite value of +0.3‰, substituted in the Land equation, gives a temperature of about 6.5° C (δ_W = -6.‰). Even if the highest δ_W = -2.‰ is used, the paleotemperature for the heaviest $\delta^{18}O$ dolomite value of +0.3‰ is only 23° C. Similarly, determination of paleotemperature of warm water dolomite ($\delta^{18}O$ value of -6 ± 1‰), not associated with glacial sediments, using δ_W = -6.‰, yielded a valid temperature result corresponding to 32 ± 6° C (Irwin equation) and 35 ± 5° C (Land equation).

The cold water marine origin can be supported by occurrences of diamictites of probable glacial origin in the Renison sequence and by the presence of till clasts within the laminated dolomite in the Smithton Basin, which has been correlated with the Renison sequence.

In contrast, the coarsely crystalline dolomites are most likely epigenetic in origin and probably began to form at shallow levels of burial, and continued to form over a range of depth and temperature. This is supported by their textures, high Mn and Fe concentrations, very depleted $\delta^{18}O$, and positive correlation between $\delta^{18}O$ and $\delta^{13}C$ values. The Mg is supplied mainly by compaction of underlying shales. Some of the coarsely crystalline dolomites occurred along large and small-scale fractures or veins, and have the most depleted $\delta^{18}O$ values. Sedimentological features of least-altered dolomicrites support deposition mainly in a marine shallow intertidal to supratidal environment, possibly under a seasonal climate.

CHAPTER 11

CARBON ISOTOPE CHEMOSTRATIGRAPHY

CHAPTER 11

CARBON ISOTOPE CHEMOSTRATIGRAPHY

11.1 Introduction

Correlation of Proterozoic sedimentary successions has proven difficult due to a lack of fossils and limited material suitable for radiometric age dating. Recent advances in sedimentary geochemistry and compilation of secular variations in the C and Sr isotopic compositions of the Neoproterozoic (1000-540 Ma, Fig.11.1) carbonates in many basins, improved correlation in these successions (e.g., Knoll et al., 1986; Lambert et al., 1987; Aharon et al., 1987; Asmerom et al., 1991; Kaufman, et al., 1991; 1992; 1993; Kaufman and Knoll, 1995). Carbon isotope chemostratigraphy is possible in the Neoproterozoic despite geographic variation of 1-2‰ in the C-isotopic composition of seawater because of the magnitude of variation and fidelity of preservation of $\delta^{13}C_{carb}$ which appears to record global events (Kaufman and Knoll, 1995).

The Proterozoic/Cambrian boundary is very important on the geological timescale, because it coincides with the major biological diversification and change from soft-bodied (non-skeletal) organisms to skeletonized fauna. This corresponds to a negative displacement in $\delta^{13}C$ values close to the Proterozoic/Cambrian boundary as determined from a number of localities by many workers (e.g., Schidlowski et al., 1975; Veizer and Hoefs, 1976; Kaufman and Knoll, 1995). The $\delta^{13}C$ chemostratigraphy played an important role in correlating Proterozoic/Cambrian boundary sections around the world in the recent search for the best Global Stratotype Section and Point (GSSP, Brasier et al., 1992).

It is generally accepted that the original marine carbon-isotope signature is less prone to alteration than the oxygen isotope, because the reservoir of carbon is much smaller than oxygen in diagenetic fluids (Anderson and Arthur, 1983). During recrystallization and dolomitization of carbonates, the carbon-isotope ratio

in most cases is not significantly altered because the carbon atoms are mostly derived from the precursor carbonate. However, incorporation of organic-derived CO_2, meteoric waters with soil-derived CO_2, deep burial and metamorphism can also alter the original carbon isotope ratio.

The $\delta^{13}C$ values of +5‰ and greater characterise Neoproterozoic marine carbonate sequences (less than ~850 Ma, corresponding to younger than Tonian period) in Svalbard and East Greenland (Knoll et al., 1986), Arctic Canada (Asmerom et al., 1991), Namibia (Kaufman et al., 1991), in carbonates of the Lesser Himalayas (Aharon et al., 1987) and India (Schidlowski et al., 1975). Significant enrichment in $\delta^{13}C$ with values as high as +7‰ has been reported in the Vendian (less than ~650 Ma) age of Yangtze Gorge of South China (Lambert et al., 1987), in the Anti Atlas Mountains of Morocco (Tucker, 1986a) and in the Mackenzie Mountains of Canada (Narbonne et al., 1994). Fairchild and Spiro (1987) and Zempolich et al. (1988) inferred that the heaviest carbon-isotope values in late Proterozoic carbonates studied by them are 5‰-7‰ PDB. High $\delta^{13}C$ values up to +12‰ for marbles from the Neoproterozoic McCoy Creek Group in the western U.S.A. have been recorded by Wickham and Peters (1993). Recently, $\delta^{13}C$ values ranging from +10‰ to +16‰ have been reported from carbonate rocks of the Neoproterozoic Bambuí Group in central Brazil (Iyer et al., 1995). In contrast, the highly enriched $\delta^{13}C$ values are not consistent with either a Cambrian or older Proterozoic age (Kaufman et al., 1992). High $\delta^{13}C$ values in these localities support the interpretation of Knoll et al. (1986) that the Neoproterozoic $\delta^{13}C$ anomaly was a global event.

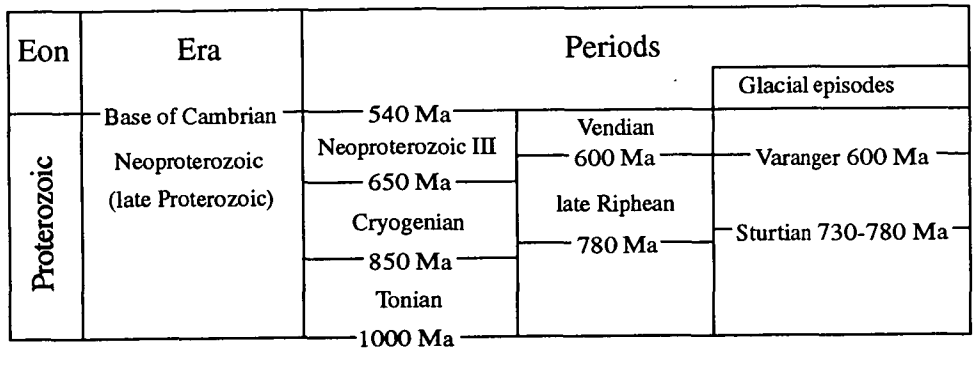

Figure 11.1. Proterozoic subdivisions used in this study (modified after Plumb, 1991; Kaufman et al., 1992; Derry et al., 1992; Kaufman and Knoll, 1995). Note the Proterozoic/ Cambrian boundary is at 540 Ma, revised from ~ 570 Ma.

11.2 Aim and Scope of Study

As there is no direct evidence of age, such as radiometric dates, paleomagnetic or reliable paleontological data within the sequence studied, carbon isotope geochemistry has been used to resolve a controversy about the age of the Renison host sediments, particularly the Crimson Creek Formation.

11.3 Methods of Study

The dolomite samples from this study were collected from two surface diamond drill holes (S705, S835, Fig. 10.1). Seventy seven uncovered polished thin sections were stained using the method of Dickson (1965) to differentiate carbonate types. Dolomite was sampled for chemical analysis using a dental drill under a binocular microscope, avoiding coarsely crystalline phases such as veins and cavity filling cements. Those samples which appeared to be strongly oxidized were removed from the sample population. Iron and manganese in dolomite samples with more than 10% insoluble residue have not been plotted on Figs. 11.3, 4 and 5. Dolomite samples in No.1 and No.2 dolomite horizons from drill hole S835 are very impure and highly altered, thus have not been used. The No.2 and No.3 dolomite data in drill hole S705 have not been plotted on the global carbon isotope curves due to low $\delta^{18}O$ and $\delta^{13}C$, high Fe and Mn values and a high Mn/Sr ratio, indicative of recrystallization or alteration during diagenesis (e.g., Brand and Veizer, 1980). Some of the altered dolomite units just mentioned may have been affected by hydrothermal alteration and contact metamorphism. Four limestone samples from the Crimson Creek Formation (drill holes No. S1450, 505m, two samples; S1454, 362m, two samples) were also selected for oxygen and carbon analyses. The two drill holes S1450 and S1454 are situated half a kilometer and one kilometer north of the Renison mine complex respectively. Geochemical techniques are described in Chapter 1. The analytical results are listed in Table A6.3 (Appendix 6).

11.4 Carbon Isotopic Compositions

11.4.1 Global compilation curves

Recently, Kaufman and Knoll (1995) and Derry et al. (1992) plotted $\delta^{13}C$ curves for 850-500 Ma old unaltered marine limestones and dolomites from different parts of the world (Figs. 11.2 B, D respectively). They show that the $\delta^{13}C$ values were high (about +4‰ to +8‰) during 850-600 Ma with brief negative excursions of about -4‰ around 600 and about -2‰ around 730 and 780

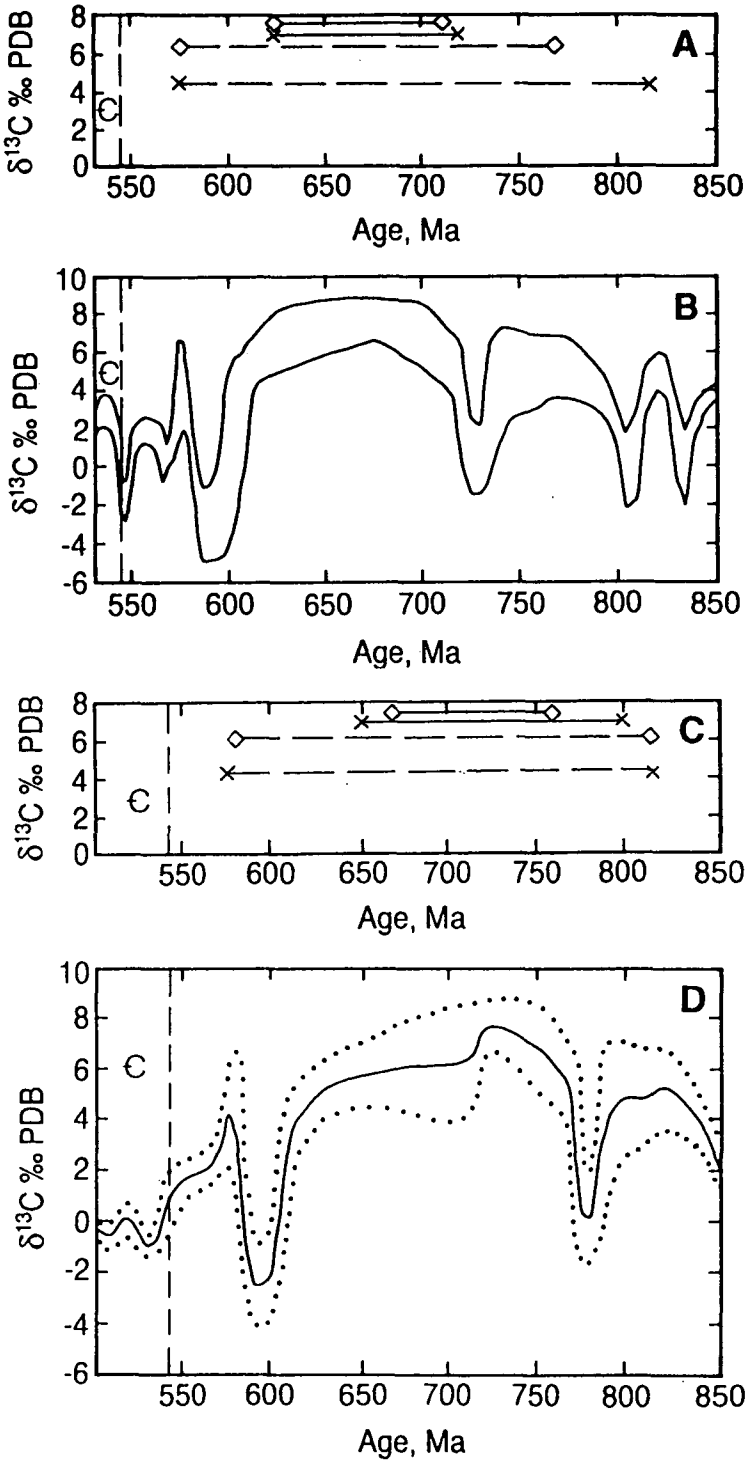

Figure 11.2. Estimated age range in dolomite horizons (No.1-No.3) in the Renison mine (A,C), corresponding to the Neoproterozoic age on the current global compilation carbon isotope curves of Kaufman and Knoll, 1995 (B) and Derry et al., 1992 (D) respectively. Note negative excursions in the $\delta^{13}C$ curves coincide with the Varangian (~600 Ma) and Sturtian (~730-780 Ma, Kaufman and Knoll, 1995; Derry et al., 1992 respectively) glacial episodes and negative shift in $\delta^{13}C$ values in the Proterozoic/Cambrian boundary. Maximum (◊) and average (x) $\delta^{13}C$ values are shown. Dashed lines represent No.1 dolomite; solid lines represent No.3 dolomite.

Ma (Kaufman and Knoll, 1995; Derry et al., 1992 respectively), corresponding to the Varanger and Sturtian glaciations respectively. After the post-Varanger glaciation, the $\delta^{13}C$ values returned to the positive values up to about +7‰, then the curve drops to a plateau of about +2‰ well before the Proterozoic/Cambrian boundary. Finally, close to Proterozoic/Cambrian boundary, the curve shows a negative excursion of about -3‰ (Kaufman and Knoll, 1995) and to about -1 ‰ (Derry et al., 1992) in global compilation curves (Figs. 11.2 B, D respectively). The global $\delta^{13}C$ curves have been compiled from carbonate $\delta^{13}C$ records from several basins around the world, each recording a relatively short part of the Neoproterozoic. Points are plotted on these diagrams by using basin subsidence modelling to interpolate ages between horizons for which numerical age data are available. The curves are lines drawn freehand to extrapolate between gaps and encompass most of the range of variation (e.g., see the original of Derry et al.'s curve 1992). Therefore, the curves give approximate chronometric determination, particularly prior to ~650 Ma.

11.4.2 Renison data

Although the isotopic composition of some dolomite samples in the study area has altered during diagenesis, the $\delta^{13}C$ values of the least-altered dark to non-luminescent dolomicrites, corresponding to heavy $\delta^{18}O$ values of > -2‰ and relatively lower Mn/Sr ratio and lower Fe and Mn concentrations, are thought to indicate the primary marine signature (Figs. 11.3, 4, Adabi, in press). It has been suggested that carbonates (both limestones and dolomites) with Mn/Sr < 10 commonly retain near primary $\delta^{13}C$ abundances (Kaufman and Knoll, 1995). The Mn/Sr ratio in all dolomicrite samples in drill hole S705 are <6 (Fig. 11.5 A). The $\delta^{13}C$ and Mn/Sr trends suggest that the least-altered dolomites are those with the most enriched carbon isotopic compositions and the lowest Mn/Sr ratio. The lower $\delta^{13}C$ value and the higher Mn/Sr ratios are in medium to coarsely crystalline dolomites due to recrystallization and late stage cementation. In the Renison mine area, the $\delta^{13}C$ values of least-altered finely crystalline dolomites fall within the Neoproterozoic age on the current global compilation carbon isotope curves (Derry et al., 1992; Kaufman and Knoll, 1995). The $\delta^{13}C$ values in the least-altered samples (with $\delta^{18}O$ > -2‰) from the No.1 dolomite horizon within the Crimson Creek Formation range from +3.6‰ to +6.4‰ with an average of +4.6‰. This average value is typical of Neoproterozoic carbonates, but not Cambrian (Kaufman et al., 1992), and falls within the age range of about 570 to 820 Ma on the Kaufman and Knoll (1995) and Derry et al. (1992) global

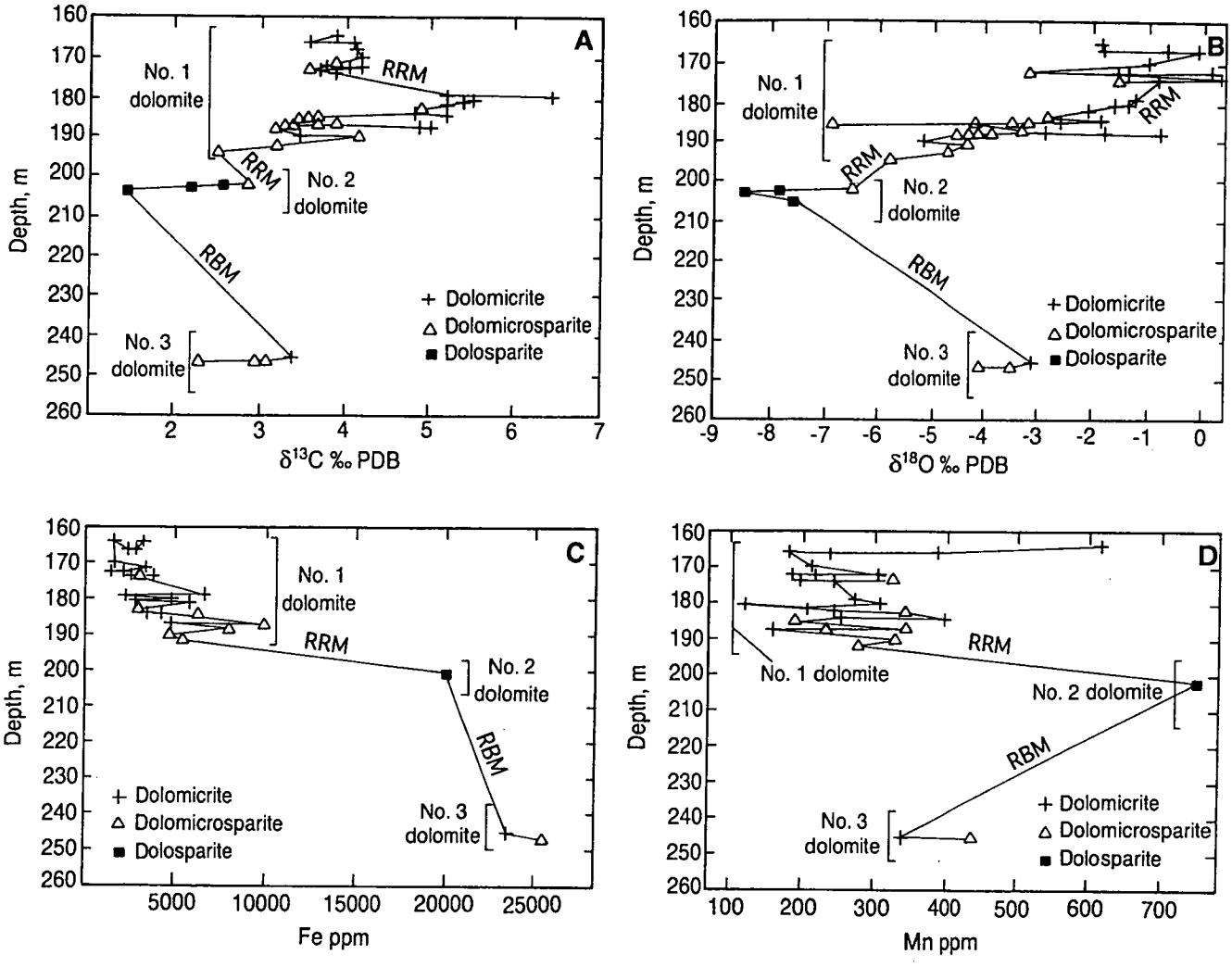

Figure 11.3. Variation of carbon (A), oxygen (B), iron (C) and manganese (D) versus depth in three dolomite horizons in drill hole S705. Note that the isotopic and elemental composition of the No.1 dolomite indicates that dolomicrites are the least-altered dolomite and the rapid shift to negative carbon values, indicates the Proterozoic/Cambrian boundary has not been observed. The apparent shift in $\delta^{13}C$, $\delta^{18}O$, Fe and Mn values in No.1 and No.2 dolomites are due to recrystallization (dolomicrosparite) and late stage cementation (dolosparite). Thus, these values are not valid for chemostratigraphy. Those dolomite samples for which no Fe and Mn data are presented were rejected because of the high percentage of insoluble residues. RRM = Red Rock Member; RBM = Renison Bell Member.

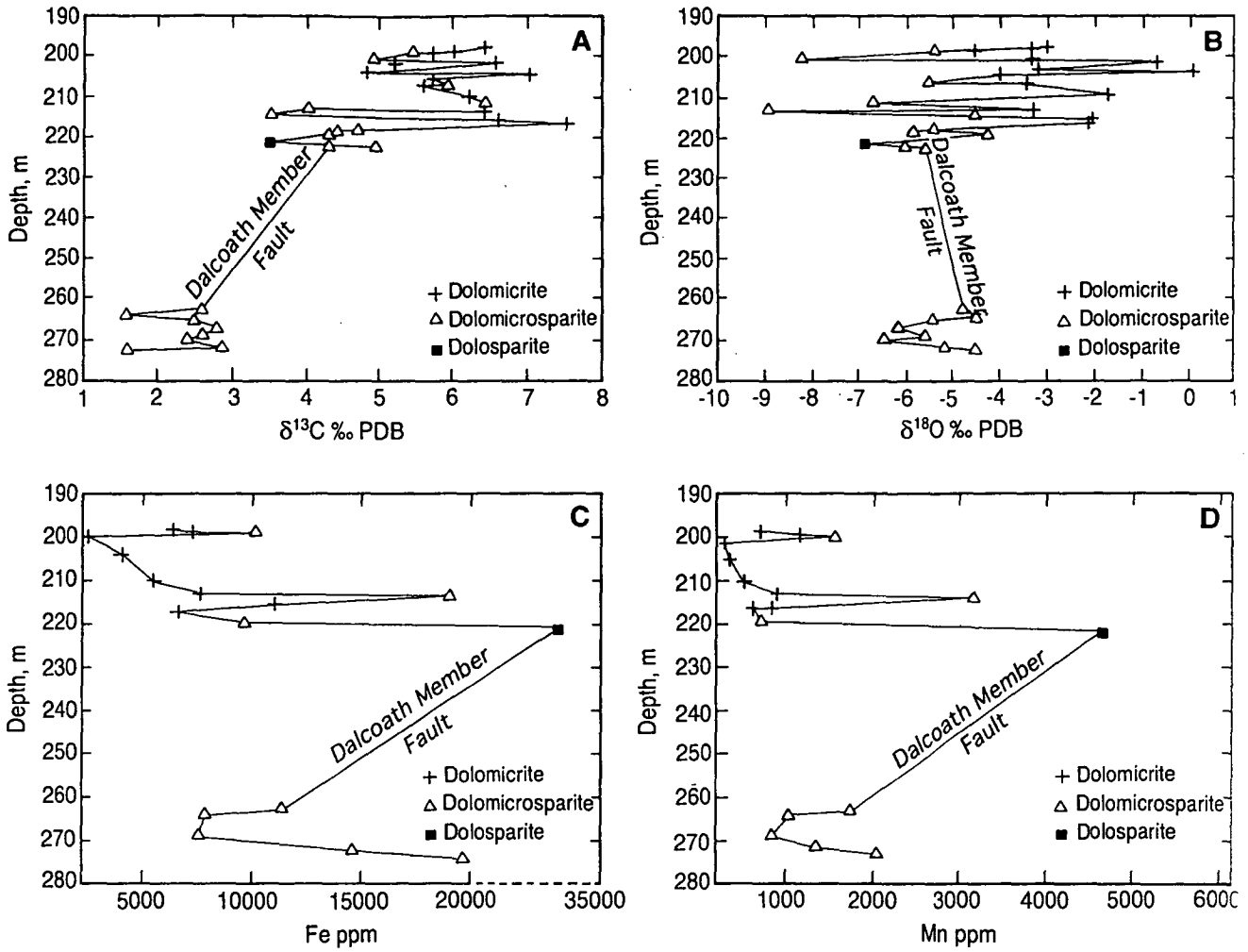

Figure 11.4. Variation of carbon (A), oxygen (B), iron (C) and manganese (D) versus depth of the No.3 dolomite in drill hole S835. Note dolomicrites are the least-altered dolomite corresponding to heavy $\delta^{13}C$ and $\delta^{18}O$, and relatively lower Fe and Mn values. The lighter $\delta^{13}C$ and $\delta^{18}O$ values and higher Fe and Mn concentrations are in coarse grained dolomites.

carbon isotope curves (Figs. 11.2 A, C respectively). The $\delta^{13}C$ values in four limestone samples from the Crimson Creek Formation, range from +2.2‰ to +6.3‰ with an average of +4.5‰. This average $\delta^{13}C$ value also falls exactly within the same age range as No.1 dolomite on the global curves.

The $\delta^{13}C$ values in the least-altered dolomicrites of the No.3 dolomite in drill hole S835 (Fig. 11.4 A), corresponding to heavy $\delta^{18}O$ values of > -2‰ (Fig. 11.4 B), lower Fe and Mn concentrations (Figs. 11.4 C, D) and relatively lower Mn/Sr ratio (Fig. 11.5 B), range from +6.2‰ to +7.5‰, with an average of +6.8 ‰. The plot of the average $\delta^{13}C$ value of +6.8‰ of the No.3 dolomite on the global carbon isotope curve of Kaufman & Knoll (1995) gives a maximum age of about 720 Ma (Fig. 11.2 A). Plotting the same average on the Derry et al. (1992) curve gives a maximum age of about 800 Ma (Fig. 11.2 C). The younger date is close to the K-Ar dating of the Oonah Formation (708 ± 6 Ma, Turner, 1993) below the Success Creek Group. Thus, by plotting the average $\delta^{13}C$ values of No.3 dolomite of the Success Creek Group, and average $\delta^{13}C$ values of the No.1 dolomites and limestones of the Crimson Creek Formation on global carbon isotope curves, the ages of the Success Creek Group and Crimson Creek Formation range within about 820 to 570 Ma respectively (Adabi, in press). In terms of correlation with the successions that formed the basis for compilation of the global curves, the high $\delta^{13}C$ values suggest that the mine sequence is probably younger than correlatives of the Sturtian glaciation in Namibia, and older than late Vendian or Ediacaran successions that are characterized by moderate $\delta^{13}C$ enrichment such as the Schwartzrand Subgroup of Namibia (Kaufman et al., 1991). The chemostratigraphic age constraint of about 570 Ma is consistent with the Neoproterozoic age based on acritarch (acid resistant, organic walled algal cysts) studies (G. Vidal, unpublished) and K-Ar date of the lithostratigraphic correlative of the Crimson Creek Formation in the Smithton Basin (588 ± 8 and 600 ± 8 Ma). Thus, all the above evidence supports the Neoproterozoic and not Cambrian age for the Success Creek Group and the Crimson Creek Formation (Adabi, in press).

In the Renison mine area, the $\delta^{13}C$ values in all three dolomite horizons studied are significantly positive (up to +7.5‰) and the negative excursion in $\delta^{13}C$ values, characteristic of the Proterozoic/Cambrian boundary, is not observed (Fig. 11.3 A). The apparent shift in $\delta^{13}C$ values of No.2 dolomites (Fig. 11.3 A) are due to recrystallization (dolomicrosparite) and late stage cementation (dolosparite), which correspond to the very light $\delta^{18}O$ values (Fig. 11.3 B) and high Fe and Mn concentrations (Figs. 11.3 C, D). In the Renison mine area, the

boundary between the Crimson Creek Formation and Success Creek Group is interpreted as a local alluvial erosional channel, but elsewhere especially near Argent Dam, the boundary could be conformable, thus, no major breaks in sedimentation have occurred. The lack of negative $\delta^{13}C$ values suggests no correlatives of the glacials are present within the dolomites. Carbon isotopic chemostratigraphy, therefore, does not support the interpretation of earlier workers (e.g., Patterson et al., 1981; Morrison, 1982; Moreland, 1988) of the No.1 dolomite (youngest dolomite horizon) and consequently the Crimson Creek Formation as Cambrian. It is predicted that if the Proterozoic/Cambrian boundary is present in the Renison mine area it should be at least above the limestone sequence studied in the Crimson Creek Formation. On the basis of isotope chemostratigraphy of the Togari Group in the Smithton Basin, Calver (1995) suggested that the entire Crimson Creek Formation is Neoproterozoic.

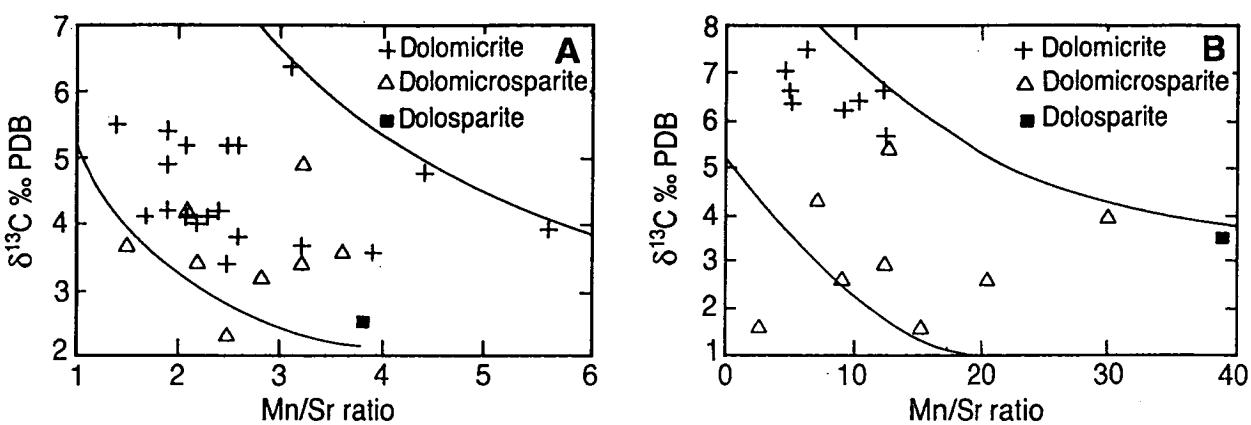

Figure 11.5. Crossplots of $\delta^{13}C$ versus Mn/Sr ratio in dolomite No.1 from drill hole S705 (A) and in dolomite No.3 from drill hole S835 (B). Note dolomicrites have the heaviest $\delta^{13}C$ values and relatively lower Mn/Sr ratio.

11.5 Proposed Mechanism for Highly Positive Carbon Values in the Neoproterozoic

Previous studies have documented that variation in $\delta^{13}C$ values in most Phanerozoic limestones worldwide is moderate (-2‰ < $\delta^{13}C$ <+2‰, Veizer and Hoefs, 1976; Veizer et al., 1980). In contrast, Proterozoic carbonates, particularly Neoperoterozoic sequences, have much higher $\delta^{13}C$ values than Phanerozoic carbonates and mostly range between +4.5‰ and +7.5‰ (e.g., Knoll et al., 1986; Derry et al., 1992; Knoll and Walter, 1992). There are several mechanisms

proposed to explain highly positive carbon values in the Neoproterozoic:

• low atmospheric CO2 level (see Fig. 9.1)

• photosynthesis, during which the isotopically light ^{12}C preferental uptake by organic matter leaves the dissolved inorganic carbon of the surface ocean relatively enriched in ^{13}C (Kaufman and Knoll, 1995)

• high burial rate of ^{12}C-enriched organic matter which would result in ^{13}C-enriched seawater and therefore ^{13}C-enriched carbonates (Scholle and Arthur, 1980; Magaritz et al., 1986; Kaufman et al., 1991; Knoll and Walter, 1992). This was probably associated with an increase in atmospheric oxygen levels, perhaps favoring biological processes (Knoll et al., 1986; Knoll, 1991)

• prolonged period of marine anoxia (Kaufman et al., 1993), in concert with low erosion rates (Derry et al., 1992)

• bacterial methanogenesis (Irwin et al., 1977), as proposed for the Miocene Monterey Formation in California (Murata et al., 1967) or the Permian Irati Formation in Brazil (DeGiovani et al., 1974). In these Phanerozoic limestones the $\delta^{13}C$ values show wide variations (-18.2‰to +19‰)

• persistent evaporitic conditions on a basin-wide scale (Knoll et al., 1986). Isotopically heavy carbon up to +5.6‰ is forming today by this mechanism in Shark Bay Australia (Ferguson, J., Plumb, L.a and Walter, M.R., unpublished data). Extremly high $\delta^{13}C$ values up to +16.5 ‰ have been reported in shallow water saline environments due to the loss of CO_2 from the brines (Stiller et al., 1985)

• increase in organic productivity due to high nutrient supply (Froelich et al., 1982)

• an increase in the preservation potential of the organic carbon (Tucker, 1986 a) which is attributed to high sedimentation rates (Berner and Canfield, 1989), and absence of bioturbation.

Derry et al. (1992) suggested that the enhanced rate of burial will depend mainly on the rate of erosion. However, low Sr-isotopic ratios during the Cryogenian or late Riphean interval (600-850 Ma) suggest rather low erosion rates, and hence a low sedimentation rate or less erosional flux to the ocean

(Asmerom et al., 1991; Iyer et al., 1995). Thus, positive $\delta^{13}C$ values in the late Riphean interval were not due to high global sedimentation rates. According to Derry et al. (1992) there was a rapid rise of organic carbon burial, coeval with a rapid rise in marine Sr isotopes, corresponding to an increase in the erosion rate, only during Vendian time (~600 Ma). Wickham and Peters (1993) and Iyer et al. (1995) supported the interpretations of Derry et al. (1992) but suggested an even greater rate of organic burial and a higher flux of O_2 to the Neoproterozoic hydrosphere and atmosphere, perhaps long prior to 600 Ma.

11.5.1 Renison data

In the Renison mine area, the uniformity of $\delta^{13}C$ in any single bed or hand specimen in the Success Creek Group and Crimson Creek Formation, the lack of negative $\delta^{13}C$ values and a relatively narrow positive $\delta^{13}C$ range (+3.4‰ to +7.5‰ in dolomicrites, Figs. 11.3 A, 11.4 A) suggest that the values are mostly homogeneous and primary and were not caused by diagenetic processes such as bacterial methanogenesis (Adabi, in press). Within the sequence of three dolomite horizons, no actual evaporitic deposits have been reported and no positive correlation between $\delta^{13}C$ values and Na/Ca ratio (an indicator of salinity) has been observed. Thus, persistent evaporitic conditions are not the cause of $\delta^{13}C$ enrichment. The high $\delta^{13}C$ values in the Renison dolomite samples are most probably due to a lower atmospheric CO2 level during the Neoproterozoic, compared to the higher CO_2 level in the Mesoproterozoic and Paleoproterozoic (see Fig. 9.1). The possibility of the global enrichment of $\delta^{13}C$ can be examined by comparison of carbon isotope values of this work with the curve representative of worldwide $\delta^{13}C$ isotopic data (Derry et al., 1992; Kaufman and Knoll, 1995). There is a significant enrichment of $\delta^{13}C$ (+4‰ to +8‰) during most of the late Riphean (~900-600 Ma) with brief negative excursion corresponding to periods of more limited organic C burial, which correlates with glacial events (Knoll et al., 1986; Kaufman et al., 1991) in these curves. Existing data are consistent with the idea that the $\delta^{13}C$ values of this study (ranging from +3.6‰ to +7.5‰) reflect global trends (Adabi, in press).

11.6 Conclusions

This study has attempted to use carbon isotopes along with oxygen and trace elements to test chemostratigraphy in the Renison mine area. Although diagenesis has altered the isotopic composition of some dolomite samples, the least-altered, mostly dark to non-luminescent finely crystalline dolomites,

corresponding to $\delta^{18}O$ values of > -2‰, low Mn/Sr ratios and low Fe and Mn concentrations have $\delta^{13}C$ values similar to numerous Neoproterozoic examples world-wide. The average $\delta^{13}C$ value of the least-altered dolomicrites in the youngest No.1 dolomite horizon was +4.6‰, typical of Neoproterozoic but not Cambrian carbonates. Plotting the average least-altered $\delta^{13}C$ data from the three Renison dolomite horizons on the global compilation carbon isotope curves, gives an age range between about 570-820 Ma (Cryogenian to Neoproterozoic III). This is consistent with paleontological evidence (*Baicalia cf. B. burra*), K-Ar dating of the two dikes in the Smithton Basin, similar to the basalt flows in a correlative of the Crimson Creek Formation (588 ± 8 and 600 ± 8 Ma), and with the K-Ar dating of detrital muscovite from the Oonah Formation below the Success Creek Group (708 ± 6 Ma). The $\delta^{13}C$ values are strongly enriched in all dolomite studied and the negative excursion characteristic of the Proterozoic/Cambrian boundary, and/or presence of correlatives of Sturtian and Varanger glacigene units in the dolomite succession has not been observed. Thus, chemostratigraphy along with paleontological evidence and radiometric dating support the Neoproterozoic and not Cambrian age for the Success Creek Group and Crimson Creek Formation. It is predicted that the Precambrian-Cambrian boundary is above the limestone samples studied.

CHAPTER 12

HYDROTHERMAL ALTERATION: SOURCE OF THE FLUIDS

CHAPTER 12

HYDROTHERMAL ALTERATION: SOURCE OF THE FLUIDS

12.1 Introduction

Extensive Proterozoic carbonates occur in Tasmania (Calver, 1989). The replacement tin deposits are associated with carbonate rocks at Renison, Cleveland and Mount Bischoff. However, little is known about dolomite types, elemental compositions, and isotope values ($\delta^{18}O$ and $\delta^{13}C$) which can aid the understanding of both dolomite origins and their relationships to mineralization.

Petrographic studies of carbonate grain sizes, textural relationships, and overprinting mineralization can assist differentiation of sedimentary (early diagenetic) dolomite from altered varieties. Depletion in Ca and Mg concentrations, and Mg/Ca ratios in carbonates, may also assist differentiation of sedimentary dolomites from altered carbonates (Rao, 1990 b). High Sr and Na contents of unaltered dolomites may reflect original carbonate compositions and salinities of diagenetic fluids, whereas Mn and Fe concentrations can typically increase during alteration of sedimentary dolomites (Veizer, 1983; Rao, 1990 b and references therein). $\delta^{18}O$ and $\delta^{13}C$ values of carbonates can provide useful criteria to determine the extent of alteration, together with possible temperature and isotopic compositions of infiltrating fluids.

12.2 Aim and Scope of Study

This Chapter aims to present:

- petrographic, elemental and isotopic compositions for the Renison carbonates which are indicative of hydrothermal activity
- the source(s) of hydrothermal fluids responsible for carbonate alteration
- the temperature range for carbonate replacement mineralization, which may have implications for exploration for new mineral deposits.
- the extent of fluid/rock interaction

12.3 Methods of Study

Carbonate samples from five diamond drill holes and underground workings (S574, S562, S302, S301, S300, Murchison and South Stebbins orebodies) were selected for analysis in this investigation, following preliminary investigations by Collins (1972) and Morrison (1982; Fig. 10.1). Underground samples from the Murchison and South Stebbins orebodies were collected by Collins (1972) and housed in the Geology Department at the University of Tasmania. The drill holes occur within the immediate mine area, except for S574. Eighty two thin sections were stained to differentiate various carbonate types (Dickson, 1965). Powders of 45 and 50 different dolomite types were selected for elemental and isotopic analyses respectively. Representative powdered samples of 10 relatively pure dolomites were analyzed by XRD to identify dolomite mineralogy and determine the mol.% Mg substitution in the dolomite lattice as a measure of the dolomite stoichiometry. Quartz was used as an internal standard and the 104 peak position measured as accurately as possible. The mol. % Mg was determined from the Goldsmith et al. (1961) method. Powders of 10 siderite samples were selected for oxygen and carbon analyses. Siderite powders were allowed to react with phosphoric acid in reaction tubes under a vacuum at 50° C for 96 hours. For oxygen and carbon analyses, dolomite powders were also allowed to react with phosphoric acid at 50° C for 24 hours. $\delta^{18}O$ value in siderite and dolomite samples heated at 50° C were corrected by subtracting 1‰ from each measured $\delta^{18}O$ value to standardize the value. In this Chapter because hydrothermal fluids are responsible for alteration of Renison dolomites, the $\delta^{18}O$ values are reported in both PDB and SMOW.

Major and minor element analyses were performed on 9 powder samples of different dolomite components of unmineralized and unaltered Proterozoic sedimentary dolomites (PSD), from the late Proterozoic Weld River Group, South-West Tasmania. Weld River Group dolomites were donated to the Geology Department teaching collection at the University of Tasmania by C. Calver. The unaltered and unmineralized Weld River Group dolomites are thought to be the same age as the Renison dolomites. To be sure that there was no possibility of hydrothermal alteration in any of the samples used as an unalterd bench mark, I have used unaltered late Proterozoic sedimentary dolomites of the Weld River Group of Tasmania and unaltered dolomicrite data from the late Proterozoic of California (Zempolich et al., 1988). These data provide a useful standard by which to assist the interpretation of alteration in the Renison carbonates. Details of geochemical techniques were described in Chapter 1.

12.4 Analytical Results

The data on major and minor elements and oxygen and carbon isotope values of different dolomite types from surface diamond drill holes and underground workings, oxygen and carbon values of siderites from the Renison mine area and major and minor elements of unmineralized and unaltered late Proterozoic sedimentary dolomites from the Weld River Group, southern Tasmania are listed in Table A6.4 (Appendix 6). The XRD results of dolomite samples are listed in Table A6.1 (Appendix 6). The oxygen and carbon isotope values of Renison dolomites and siderites (Jones and Evans, 1985; Patterson et al., 1981; Holyland, 1987) are listed in Tables A6.5 and A6.6 (Appendix 6).

12.5 Dolomite Stoichiometry

X-ray studies of seven dolomite samples in the 28-32 degree 2θ range reveal d_{104} values of 2.889 or nearly so. The mol.% Mg ranges from 45 to 49% with an average of 48%. These values clearly indicate calcian to near-stoichiometric composition.

12.6 Mineralization at Renison

Tin deposition at Renison Bell was associated with stratabound carbonate-replacement mineralization and vein deposits resulting from the passage of hydrothermal fluids through major fault structures (Fig. 9.10; Patterson et al., 1981; Holyland, 1987; Kitto, 1992, 1994). The regional fault structures at Renison are attributed to a tensional regime associated with emplacement of the Devonian Pine Hill Granite (Fig. 9.10; Kitto, 1992, 1994). Renison ore is dominated by massive pyrrhotite with minor cassiterite (~1%), which partially replaced three dolomite horizons in the mine sequence. The No. 2 and No. 3 dolomite horizons were heavily mineralized, particularly at the intersections of major fault structures in close proximity to hydrothermal feeders, whereas the No.1 dolomite was extensively altered but contains only minor mineralization of economic grade (Patterson, et al., 1981; Holyland, 1987; Moreland, 1988; Cannard, 1991; Kitto, 1994).

The Federal-Bassett Fault (FBF) was the primary structural control on distribution of ascending magmatic hydrothermal fluids at Renison. Other significant fault structures which controlled the distribution of fluid were the Blow Fault Complex (BFC), subparallel to the Federal-Bassett Fault, and a series of east-west transverse faults that interconnect the Federal-Bassett Fault and Blow Fault Complex (Kitto, 1992, Fig. 9.10).

Patterson et al. (1981) determined temperatures for mineralizing fluids in the Federal-Bassett Fault at Renison from fluid inclusions in fluorite (140 to 280° C; mean 190° C), quartz (150 to 310° C; mean 210° C) and in pyrrhotite-rich veins (150 to 270° C; mean 170° C). Similar temperatures were also obtained from other studies on fluid inclusions in fluorite (Collins, 1972; 120 to 280° C; mean 165° C; Davies, 1985; 130 to 220° C) and in quartz (Davies, 1985; mainly 140 to 260° C). More recently, detailed fluid inclusion investigations of the various paragenetic stages from the Federal-Bassett Fault have been documented by Kitto (1994). These studies have shown that the homogenization temperatures for the earliest oxide-silicate stage of mineralization (quartz-arsenopyrite-cassiterite) ranged from >400° C at the base of the Federal-Bassett Fault (3000 m beneath the Devonian paleo-surface) to nearly 300° C at the top of the mine workings. These early NaCl-KCl-H_2O brines had average salinities between ~8 and 12 eq. wt.% NaCl, and fluid pressures of 250 bars (hydrostatic). $\delta^{18}O_{fluid}$ values of 9‰ SMOW were determined from quartz associated with this stage of mineralization. These magmatic $\delta^{18}O_{fluid}$ values are consistent with a fluid which ascended and cooled within the Federal-Bassett Fault before interacting with the carbonate wallrocks in the higher mine levels. Wallrock interaction and dolomite dissolution in the upper mine levels resulted in the ore fluids becoming $CaCl_2$-$MgCl_2$-NaCl-H_2O-rich brines (Davies, 1985; Kitto, 1994).

A near linear trend exists between $\delta^{18}O$ and $\delta^{13}C$ values in diagenetic dolomites at Renison (Jones and Evans, 1985), however, such trends are absent from hydrothermal carbonates (siderite). $\delta^{18}O$ values in sedimentary and hydrothermal dolomites (-2.5 to -21‰ PDB; 28.3 to 9.2‰ SMOW) are thought to correspond to decreasing temperatures from above 350° C at feeder faults to less than 150° C at a distance of 200 - 1000 m from these regions (Holyland, 1987). The major controls on cassiterite deposition were probably an increase in pH, due to dolomite dissolution, and changes in redox conditions associated with arsenopyrite deposition (Patterson et al., 1981; Kitto, 1994).

12.7 Carbonate Mineralogy

Chemical analyses and stained thin sections of Renison sedimentary carbonates, within the mineralized area, indicate a predominance of ferroan dolomite with minor calcite (Adabi et al., 1996 a, b). Studies of the relative percentages of Ca, Mg and Fe+Mn in individual minerals reveal that Renison sedimentary carbonates range from ferroan dolomites to ankerites (Fig. 12.1). These samples do not contain pure end-member dolomite, siderite or calcite.

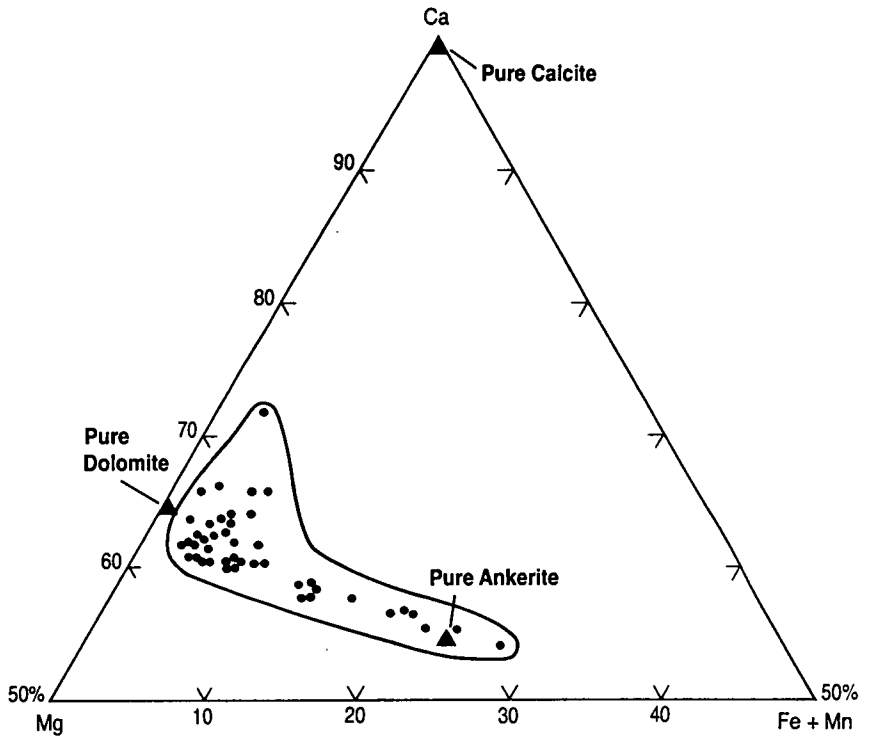

Figure 12.1. Relative percentages of Ca, Mg and Fe+Mn in Renison carbonates. Compositions of end-member dolomite, calcite and ankerite are shown. Renison carbonates range from ferroan dolomite (>1000 ppm Fe) to ankerite and do not contain pure dolomite or calcite (siderite compositions not shown).

12.8 Petrographic Study

12.8.1 Normal petrographic microscopy

12.8.1.1 Dolomite

In the mineralized area the original depositional textures in most dolomite samples have largely been destroyed by diagenetic, hydrothermal and to some extent, contact metamorphic alteration in shallow to deep burial environments. The intensity of the alteration is mainly related to the proximity to fractures, faults or mineralization. Dolomite within the mineralized area is divided into five different types, based on crystal size and mode of origin. These include: dolomicrites (<5μm to ~16μm), dolomicrosparites (~16μm to ~62μm), dolosparites (~16μm to ~250μm), coarsely crystalline dolomite (~250μm to 1 mm), and vein dolomite (>250μm). Dolomites occur as both cements and recrystallized carbonates. Multiple cross-cutting veins, brecciation, crack-seal texture, recrystallization, silicification, deformation and oblitration of original texture is more pronounced in these dolomite samples than in the dolomites from the unmineralized area. The unmineralized area refers to those drill holes (such as,

S594, S705, S835) located far away from the mineralized Renison mine area (see Chapter 11). These variations can be related to the presence of many fracture and fault structures within the mineralized area, which have been attributed to the tensional regime associated with emplacement of the Pine Hill Granite (Lea, 1991; Kitto, 1994). Five different dolomite types are characterized as follows:

Type 1 Very finely crystalline dolomite (dolomicrite)

Dolomicrites are the most abundant dolomite type in this study. They are very similar in size and color to dolomicrites observed in the unmineralized area. However, the original depositional textures are less well preserved in these dolomicrites, compared to dolomicrite samples away from the mineralized area. The finely laminated nature of these dolomicrites is often disrupted or deformed due to the presence of many fractures, cross-cutting veins and faults (Fig. 12.2 A). For example, ductile deformation in finely laminated dolomicrites (or dolosiltite) in contact with rigid coarse grained dolomite veins is a common feature in the dolomicrite studied (Fig. 12.2 B). The laminae are generally less than a few millimeters thick. Microbial fabric is rare, but intraclasts are present in a few dolomite samples. Intraclastic dolomite with different grain size and texture with rounded and irregular margins in some dolomicrites are rip up clasts (Fig. 12.2 C). Rounded dolomite clasts indicate some transport, while clasts with irregular margins indicate minimal transport. Silicate minerals such as talc and chlorite are present in some samples. In a few samples, dolomicrites are cut by late stage medium crystalline dolomite veins or extensively replaced by silica (Fig. 12.2 D). Inclusion of dolomicrites within the silica supports a replacement origin. The presence of coss-cutting veins through many of the dolomicrite samples produces a pseudo clastic texture. The veins include floating remnants of angular dolomicrite clasts. Jig-saw fit breccia is also common in dolomicrite samples due to different cross cutting veins (Fig. 12.2 E). Dolomite rock texture includes unimodal planar-s type boundaries.

Type 2 Finely crystalline dolomite (dolomicrosparite)

Dolomicrosparites are very common in this study. They are generally similar in size and texture to dolomicrosparite samples observed in the unmineralized area. Recrystallization of dolomicrites occurs throughout most samples from a number of closely spaced centers (Fig. 12.3 A), which eventually resulted in total recrystallization to dolomicrosparite (Adabi et al., 1996 a, b). Scattered flakes of silicate minerals such as talc and chlorite are characteristic

Figure 12.2. Sedimentary and diagenetic texture in dolomicrite.

A. Photomicrograph illustrating that sedimentary laminations in dolomicrites are deformed due to cross-cutting silica and dolomite veins. Silica vein appears to be offset along the margin of dolosparite vein, which caused displacement. There is some vertical flattening in this photograph. Thin section S574, 76 m.

B. Ductile deformation in finely laminated dolomicrite, in contact with coarsely crystalline dolomite. These rocks are able to sustain under a given set of conditions before fracturing. Thin section S574, 75.5 m.

C. Rip up dolomite clasts. The rounded intraclastic dolomite shows some transport while the other clasts with irregular margins (white arrow) show minimal transport. Fibrous silicate minerals such as talc and cholorite are distributed within the dolomicrite matrix. Thin section S562, 129 m.

D. Pervasive replacement of dolomicrite by silica. Note dolomite inclusion within the silica. Thin section S562, 62 m.

E. Jig-saw fit breccia texture in dolomicrite. Thin section S574, 27 m.


A
500 µm


B
500 µm

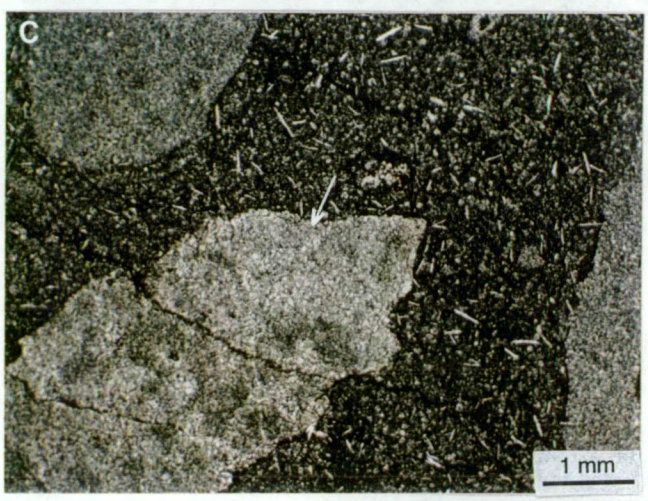
C
1 mm

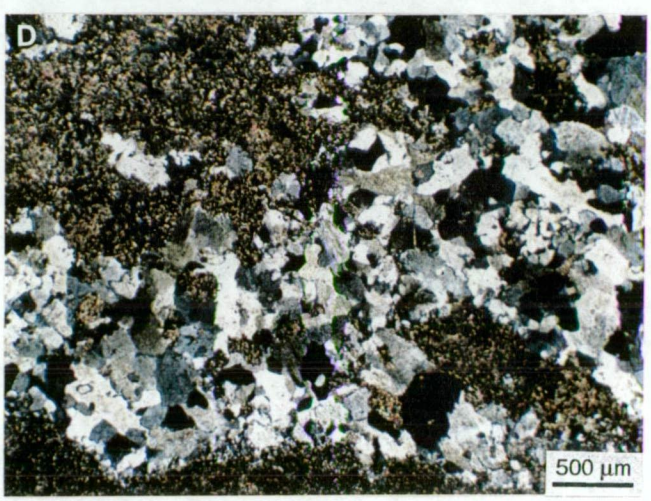
D
500 µm

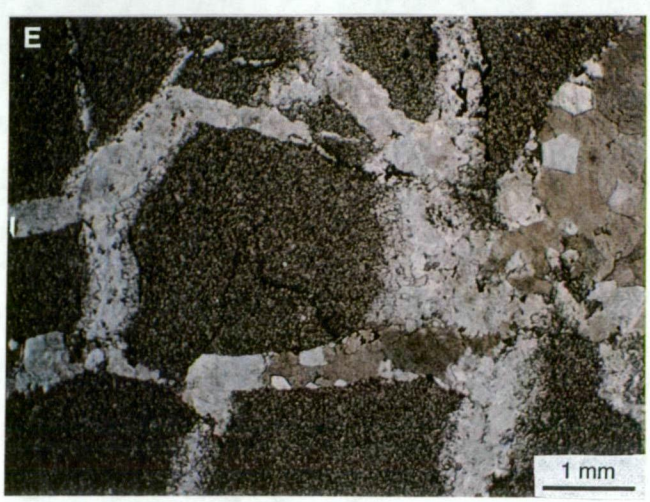
E
1 mm

features of some dolomicrosparite in this study (Fig. 12.3 B).

In terms of dolomite rock texture, dolomicrosparites are mostly unimodal and crystals are suhhedral to anhedral with planar-s type boundaries.

Type 3 Medium crystalline dolomite (dolosparite)

Dolosparites occur mostly in cavities and vugs, with a crystal size similar to the dolosparite cements observed in the unmineralized area. However, in some cavities, dolosparite cements have a larger crystal size (>250μm) and often display undulose extiction (Fig. 12.3 C). Dolosparite cements are cut by talc and chlorite minerals, indicating that silicate minerals post-date dolomite precipitation. Cavities are generally patchy and irregular in shape.

In terms of dolomite rock texture, dolosparites consist of polymodal, dense, closely packed mosaics of coarse subhedral to anhedral nonplanar crystals, with mostly curved, or irregular intercrystalline boundaries.

Type 4 Coarsely crystalline dolomite

Coarsely crystalline dolomites, which are volumetrically unimportant compared to other dolomite types, are present only in dolomite samples from the mineralized area. They range in size from about 250μm to one millimeter. This type of dolomite forms due to subsequent recrystallization of dolomicrosparite, as evidenced by inclusions of earlier dolomite crystals (Fig. 12.3 D, Adabi et al., 1996 a, b). These dolomites have been replaced locally by coarsely crystalline silica which contains inclusions of dolomite rhombs, exhibiting poikilotopic texture (Fig. 12.3 E). The dolomite rock texture includes, closely packed subhedral planar-s crystals with largely straight compromise boundaries.

Type 5 Vein dolomite

Dolomite veins with a larger crystal size (normally >250μm) are more common in the mineralized than the unmineralized area, particularly where they are associated with faulting. Individual veins rarely exceed 3.5 cm thick. Most are displacive and in sharp contact with the host wall rock. Multiple cross-cutting veins (Fig. 12.4 A) are characteristic features of dolomite samples from the mineralized area. In a few samples, inclusions of undigested dolomicrite are present within the multiple cross-cutting dolomite veins, forming a pseudo clastic texture (Fig. 12.3 B). Many dolomite veins display undulose extinction (Fig. 12.4 C). Original dolomite, early diagenetic (dolomicrosparite) and late diagenetic dolomites (medium to coarsely crystalline dolomites) are cut by vein dolomite. In

Figure 12.3. Sedimentary and diagenetic texture in dolomicrosparite, dolosparite and medium to coarsely crystalline dolomite.

A. Dolomicrosparite with clots of original dolomicrite. Note recrystallization of dolomicrites occur from a number of closely spaced centers. Thin section 40071.

B. Photomicrograph of disseminated silicate minerals such as talc and chlorite throughout the dolomicrosparite. Thin section S562, 111.1 m.

C. Cavity filled by coarsely crystalline dolosparite cement. Note the dolomite cement shows undulose extinction. Silicate minerals cut dolomite crystals.

D. Photomicrograph of medium to coarsely crystalline dolomite. Note the presence of undigested crystals of earlier dolomicrosparite (arrow). Thin section S574, 30 m.

E. Coarse crystalline dolomite has been partially replaced by silica. Inclusion of dolomite rhombs in coarse grained silica supports replacement origin. Thin section S574, 82.3 m.


A
250 µm


B
250 µm

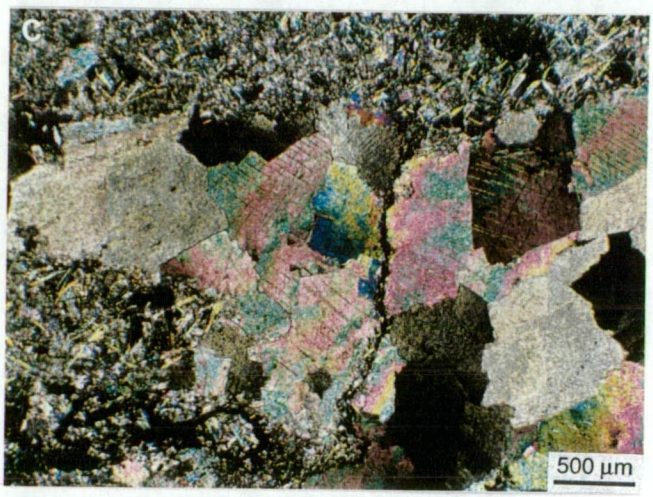
C
500 µm


D
500 µm

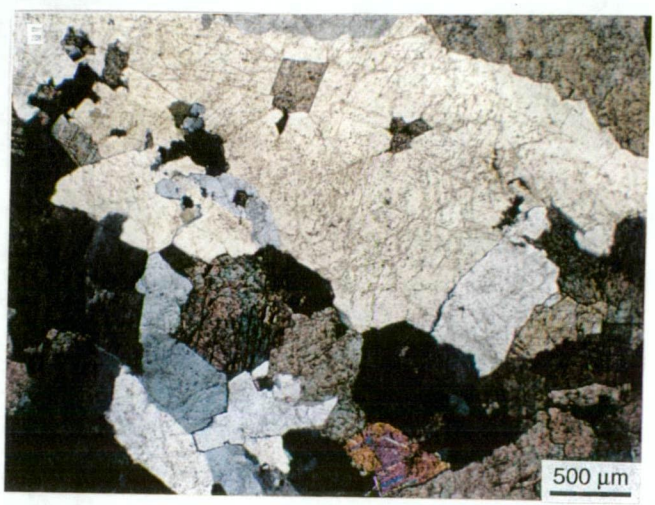
E
500 µm

Figure 12.4 Sedimentary and diagenetic texture in vein dolomite.

A. Photomicrograph illustrating multiple generations of dolosparite veins. In this example No.1 dolomite vein is cut by No.2 dolomite vein which in turn is cut by No.3 dolomite vein. Thin section S574, 82.3 m.

B. Pseudo clastic texture. Note multiple fractures cutting dolomicrites. These veins are now filled by coarse crystalline dolosparite cements. Thin section S574, 30 m.

C. Photomicrograph of a coarsely crystalline dolomite vein. Note the dolomite crystals are very large, have curved cleavage and undulose extinction. This is similar to saddle dolomites formed at higher temperatures. These dolomite veins are associated with sulphide mineralization and hydrothermal activity. Thin section S562, 121 m.

D. Photomicrograph of coarsely crystalline dolomite veins, showing undulose extinction, and disseminated silicate minerals. Thin section S562, 80 m.

E. Crack-seal vein. Repeated crack-seal increments build up a fibrous to columnar microstructure. Fine laminations in dolomite crystals correspond to successive crack-seal increments (arrow). Thin section S 574, 27 m.

F. Crack-seal texture. Quartz fibres developed against dolomite crystals with lattic preferred orientation. Thin section S574, 27 m.

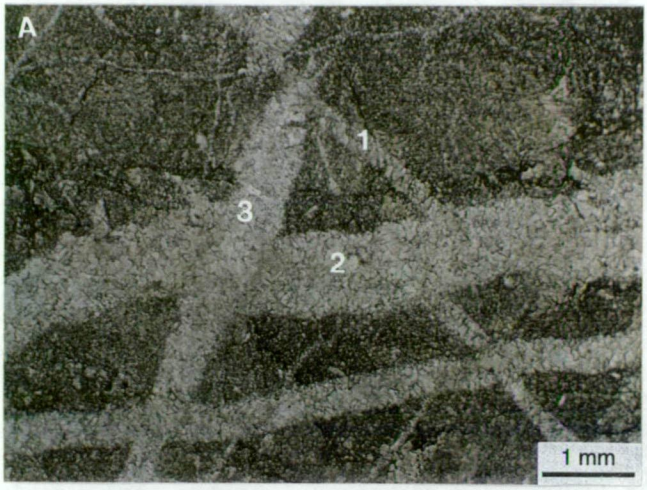
A
1
3
2
1 mm

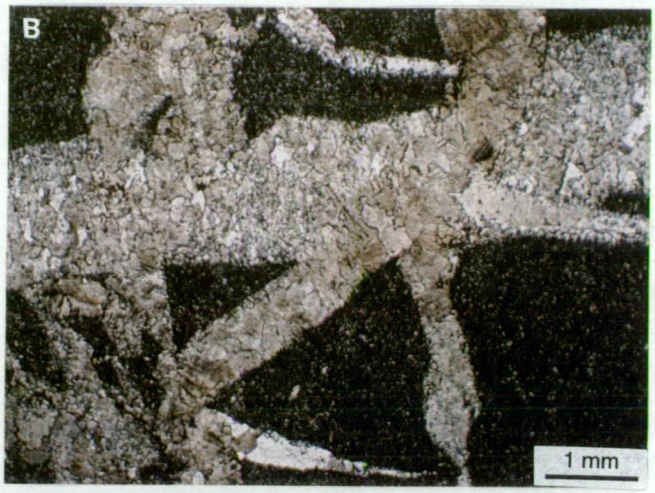
B
1 mm


C
500 µm

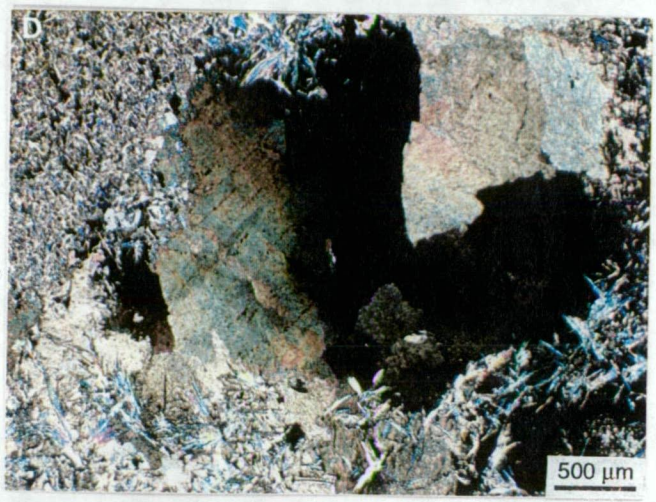
D
500 µm


E
500 µm

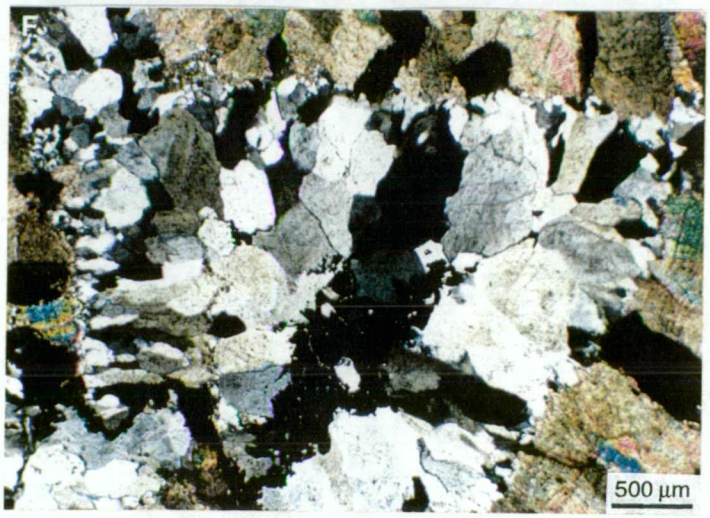
F
500 µm

a few examples, talc and chlorite minerals grow out of the wallrock into the coarsely crystalline dolomite veins (Fig. 12.4 D).

Crack-seal texture (syntectonic veins) occur in some dolomite samples (Fig. 12.4 E). As is shown in Fig. 12.4 E, fibrous to elongated dolomite crystals develop crystallographic preferred orientations perpendicular to the vein. In this example the late stage silica with preferred growth orientation has also developed on the dolomite crystal substrate (Fig. 12.4 F).

In terms of dolomite rock texture, the vein fill typically consists of a nonplanar, coarse mosaic of dolomite crystals with irregular to serrated intercrystalline boundaries. Preserved crystal-face junctions are absent and crystals often have undulatory extinction.

12.8.1.2 Siderite

Siderites are very abundant in samples very close to the orebody. They consist of massive coarse grained crystals, generally in the range of 250μm to >1mm (Fig. 12.5 A). Siderites form a narrow zone that separates the pyrrhotite-cassiterite ore from dolomite. The siderite zone varies in width from about 10 cm in parts of the No.3 dolomite to more than 100 m in parts of the No.1 dolomite. Contacts between the siderite zone and unreplaced dolomite, and between the siderite zone and massive sulfides, are commonly knife-sharp in hand specimens and underground exposures (Patterson et al., 1981).

12.8.1.3 Silicification

Silicification is a common feature in the Renison dolomites (Figs. 12.2 D, 12.5 B-D). Silica occurs as a cement, filling voids, cavities and veins and as a replacement of dolomite. Silica cement is in the form of microquartz and megaquartz, with crystal sizes reaching to about 850μm. Megaquartz commonly occurs as pore-filling cement and often has a good crystal shape, with crystals displaying unit exinction. Multiple cross cutting silica veins and veinlets are present in a few dolomite samples. Dolomicrite, coarsely crystalline dolomite and vein dolomite are partially replaced by coarse silica (Figs. 12.2 D, 12.3 E). Inclusion of dolomite crystals within the silica supports replacement origin. Authigenic quartz replacement has been observed within the dolomitized horizons (Fig. 12.5 B). Authigenic quartz crystals in dolomite often show perfect euhedral terminations but have central cores of undigested carbonate (Scholle, 1978, Fig. 12.5 B). Vertical stylolites are occasionally silicified (Fig. 12.5 C). In a few examples, fibrous quartz developed under pressure, is shadowed around rigid

Figure 12.5 Siderite replacement and silicification.

A. Photomicrograph of very coarse grained crystals of siderite. Rhombic dolomite crystal inclusions in the siderite, along with dirty inclusions present in all siderite grains, support siderite replacement origin. Thin section S594, 243 m.

B. Photomicrograph of abundant authigenic quartz replacement. Note that some of the authigenic quartz crystals show excellent crystal terminations, but they have some undigested fine grained dolomite in central cores. Thin section S835, 204.5 m.

C. Silicification along sutured stylolite. Dark lines are solution interfaces with concentrations of insoluble minerals. Thin section S835, 215.8 m.

D. Photomicrograph showing development of fibrous quartz crystals in pressure shadow around rigid sulphid grains. Thin section S574, 76 m.

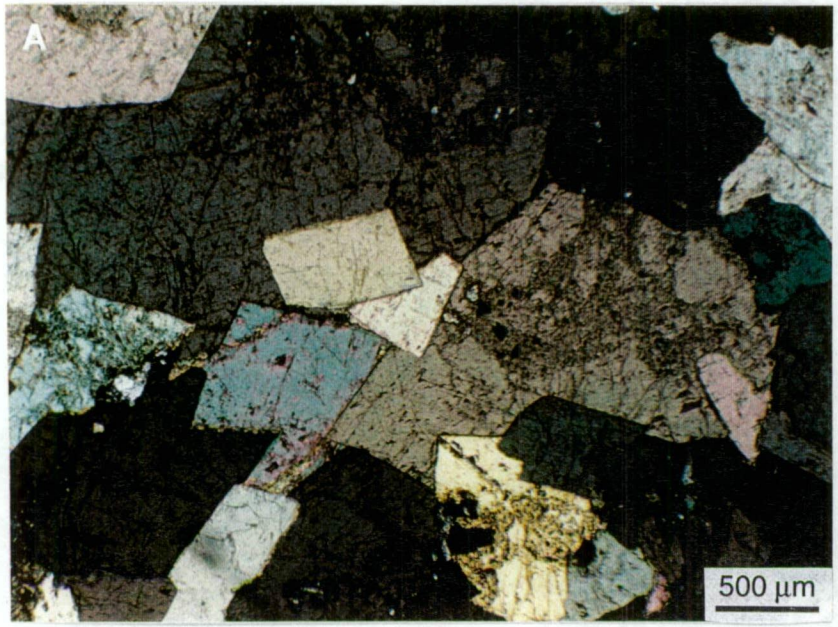
A
500 µm

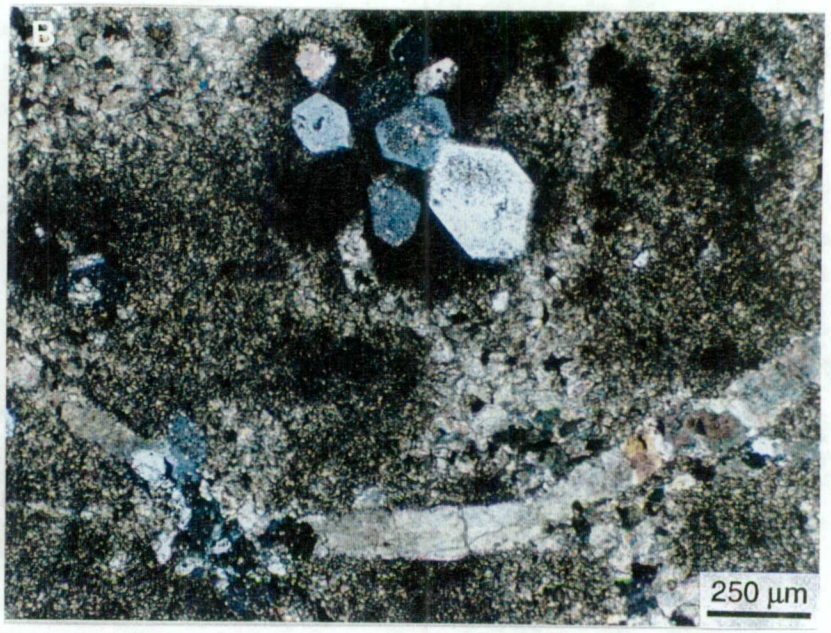
B
250 µm

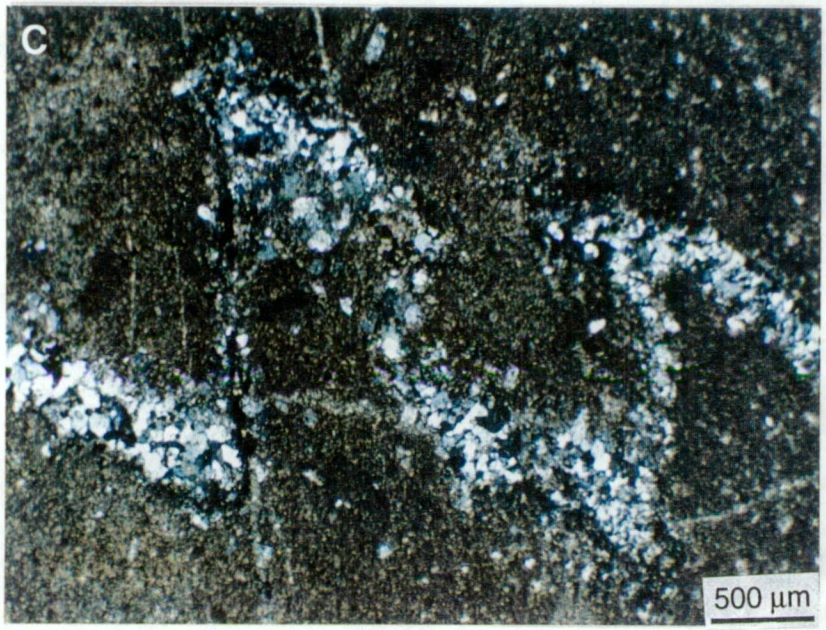
C
500 µm

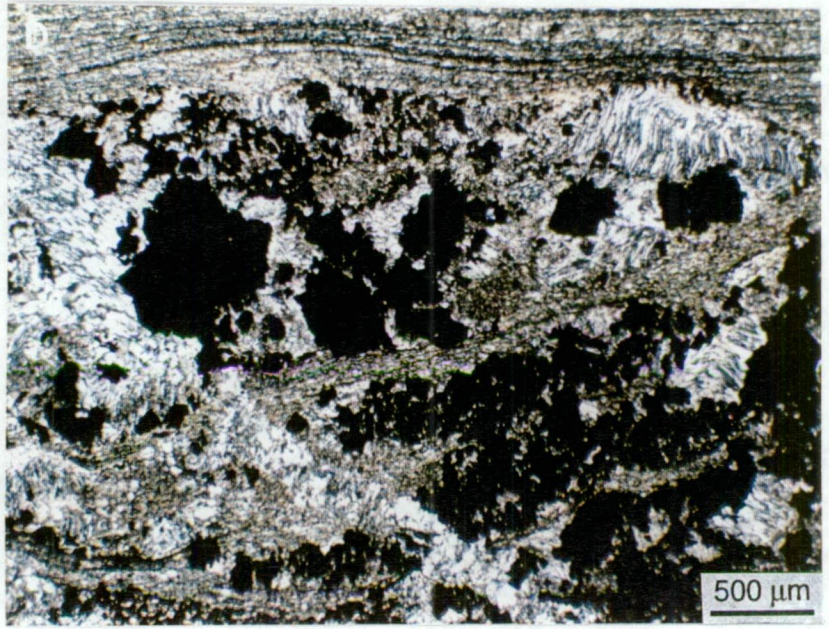
D
500 µm

sulphide grains (Fig. 12.5 D).

12.8.2 Cathodoluminescence microscopy

This study has concentrated on the relatively rare luminescent samples selected from a total of over 80 samples. The remaining dolomite samples were typically dull to non-luminescent. The cathodoluminescence features of different dolomite types are discussed below:

Type 1 Very finely crystalline dolomite (dolomicrite)

The very finely crystalline massive dolomicrites display only dark red-brown luminescence similar to the dolomicrites observed in the unmineralized area (Fig. 10.9 B).

Type 2 Finely crystalline dolomite (dolomicrosparite)

Dolomicrosparites show dark red-brown with scattered bright-yellow luminescence, similar to the dolomicrosparites observed in the unmineralized area (Fig. 10.9 D).

Type 3 Medium crystalline dolomite (dolosparite)

Dolosparite cements showing many generations of delicate zonation under cathodoluminescence (Fig. 12.6 B). Most of the cavities filled by alternating finely banded moderately bright zone 1, dark brown zone 2, orange zone 3, very fine dark red- brown zone 4, very brightly banded zone 5 and dark brown (dull) zone 6. There are also a few thin subzones between zones 5 and 6. Dull cement is generally the final void fill in most cavities and therefore post-dates other luminescent cement generations. Delicate luminescent zonations are absent from very fine to finely crystalline dolomicrite and dolomicrosparite respectively.

Type 4 Coarsely crystalline dolomite

Under cathodoluminescence the coarsely crystalline dolomite displays many alternating sequences of finely laminated bright and dull luminescent zones (Fig. 12.6 D). A few dolomite rhombs have red-brown (dull) luminescent centres and bright-yellow luminescent rims.

Type 5 Vein dolomite

Renison dolomites, particularly within the mineralized area, have been subjected to several episodes of fracturing. In most cases these fractures are filled by very coarse non-luminescent dolomite crystals, similar to the vein dolomite

Figure 12.6. Sequence of paired plain light and cathodoluminescence photomicrographs in dolomite types 3 and 4.

A. Thin section photomicrograph illustrating cavities filled by coarsely crystalline dolosparite (plain light). Thin section S562, 116 m.

B. Same area as in A under cathodoluminescence. Cavity filled by alternating sequences of finely banded moderately bright zone 1, dark brown zone 2, orange zone 3, very fine dark red- brown zone 4, very brightly banded zone 5 and dark brown (dull) zone 6. Note dull cement is the last void filling cement.

C. Thin section photomicrograph illustrating coarsely crystalline dolomite. Note inclusion of original dolomicrites within coarsely crystalline dolomite. Thin section S574, 30 m.

D. Same area as in C under cathodoluminescence. Multistage recrystallization is evident by alternating sequences of finely laminated bright and dull luminescent zones. Note a few dolomite rhombs show dull luminescent centres and bright-yellow luminescent rims.

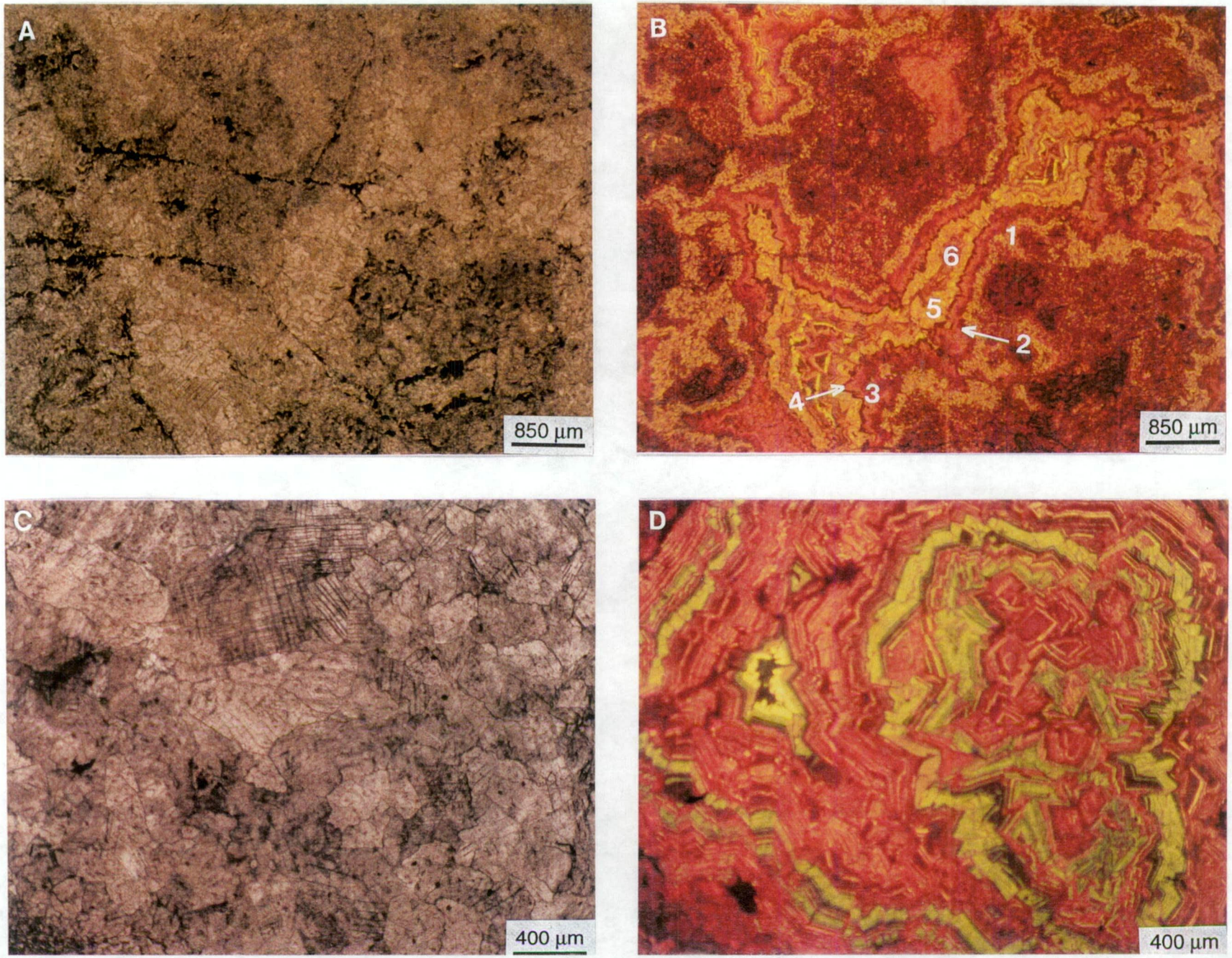
A
850 µm
B
1
6
5
2
4
3
850 µm
C
400 µm
D
400 µm

observed in Fig. 10.10 B). However, in crack-seal or syntectonic veins, multiple generations of delicate bands in dolomites are present (Figs. 12.7 a, b). The very bright luminescent dolomites generally form thin zones, in contrast to the thicker dull luminescent dolomites. The vein (Fig. 12.7 a) is filled, from oldest to youngest by: a very fine band of moderately yellow luminescent dolomite growing on the very finely crystalline dolomicrite (zone 1); dull luminescent coarsely crystalline dolomite (zone 2); first generation non-luminescent silica (zone 3); alternating bands of bright and red-brown luminescence (zone 4); two very bright-yellow luminescent zones (zone 5); relatively thick alternating bands of red-brown luminescence (zone 6); late band of very bright-yellow luminescent zone (zone 7); and very late non-luminescent silica cements (zone 8). The post-silica carbonate cement stratigraphy in a and b are quite different, in spite of the fact that these CL photographs are of the same thin sections. In a few vein dolomites, the offsetting between luminescent bands can be easily recognized using CL (Fig. 12.7 D).

12.9. Major Elements

12.9.1 Calcium, Magnesium and Mg/Ca ratio

Ca contents in the Renison dolomites range from 16.9 to 25.9 wt.%, whereas Mg values range from 6.5 to 13.0 wt.% (Figs. 12.8 A, B). Dolomites from less recrystallized sections (Fig. 12.8 A) have relatively more Ca and Mg than strongly recrystallized samples (Fig. 12.8 B). In both instances, when compared to unaltered Proterozoic sedimentary dolomites (PSD), there is a loss of Ca and Mg in Renison dolomites, as pure dolomite should plot on the line shown in figures 12.8 A and 12.8 B. Dolomicrite exhibits the highest Ca and Mg values in both the less recrystallized and strongly recrystallized dolomites. Dolomicrosparites are recrystallized dolomicrites and have depleted Ca and Mg values relative to dolomicrites and unaltered Proterozoic sedimentary dolomites (Figs. 12.8 A, B). In strongly recrystallized samples (Fig. 12.8 B) dolomicrosparites may be very depleted in both Ca and Mg. Dolosparites and vein dolomites are precipitates and typically exhibit depleted Ca and Mg values relative to unaltered Proterozoic sedimentary dolomites. A significant positive correlation between Mg/Ca ratios and Mg contents, with r^2 values between 0.8 to 0.9 (Figs. 12.8 C, D), indicates a systematic loss of both Ca and Mg. If variations in Mg content of the samples were due mainly to the percentage dolomite present in the samples studied, the Renison dolomites would have Mg/Ca ratios of ~0.58 and fall on a horizontal pure dolomite line (Figs. 13.8 C and D). Instead, the

Figure 12.7. Sequence of paired plain light and cathodoluminescence photomicrographs in dolomite type 5.

A.B. Thin section photomicrograph illustrating syntectonic (crack-seal) veins (plain light). Thin section S574, 27 m.
a.b. The same area as in A and B under cathodoluminescence. Delicate compositional banding is apparent in the coarse grained dolomite, whereas the massive dolomicrites are dull to dark red-brown luminescent. The sequence of zonations (a), oldest to youngest is: moderately bright zone 1 (yellow); dull zone 2 (dark-brown); non-luminescent (silica) zone 3; alternating band of bright and dull zone 4 (yellow and red-brown); very bright zone 5 (bright-yellow); thick alternating band of dull zone 6 (red-brown); very bright zone 7 (bright-yellow); and non-luminescent (silica) zone 8. Note post-silica carbonate cement stratigraphy in a and b are quite different. Compared to the unmineralized area, dolomite samples from the mineralized area generally contain more generations of variable luminescence.

C. Thin section photomicrograph illustrating coarsely crystalline dolomite and silica vein (plain light). Thin section S574, 30 m.

D. Same area in C under cathodoluminescence. Note compositional banding in coarse dolomite-silica vein. Microfracture is clearly visible under cathodoluminescence, but not under plain light. For the Renison deposits, the cathodoluminescence technique has been able to provide detailed information about dolomite texture and paragenesis, which is not possible to document using any other technique.

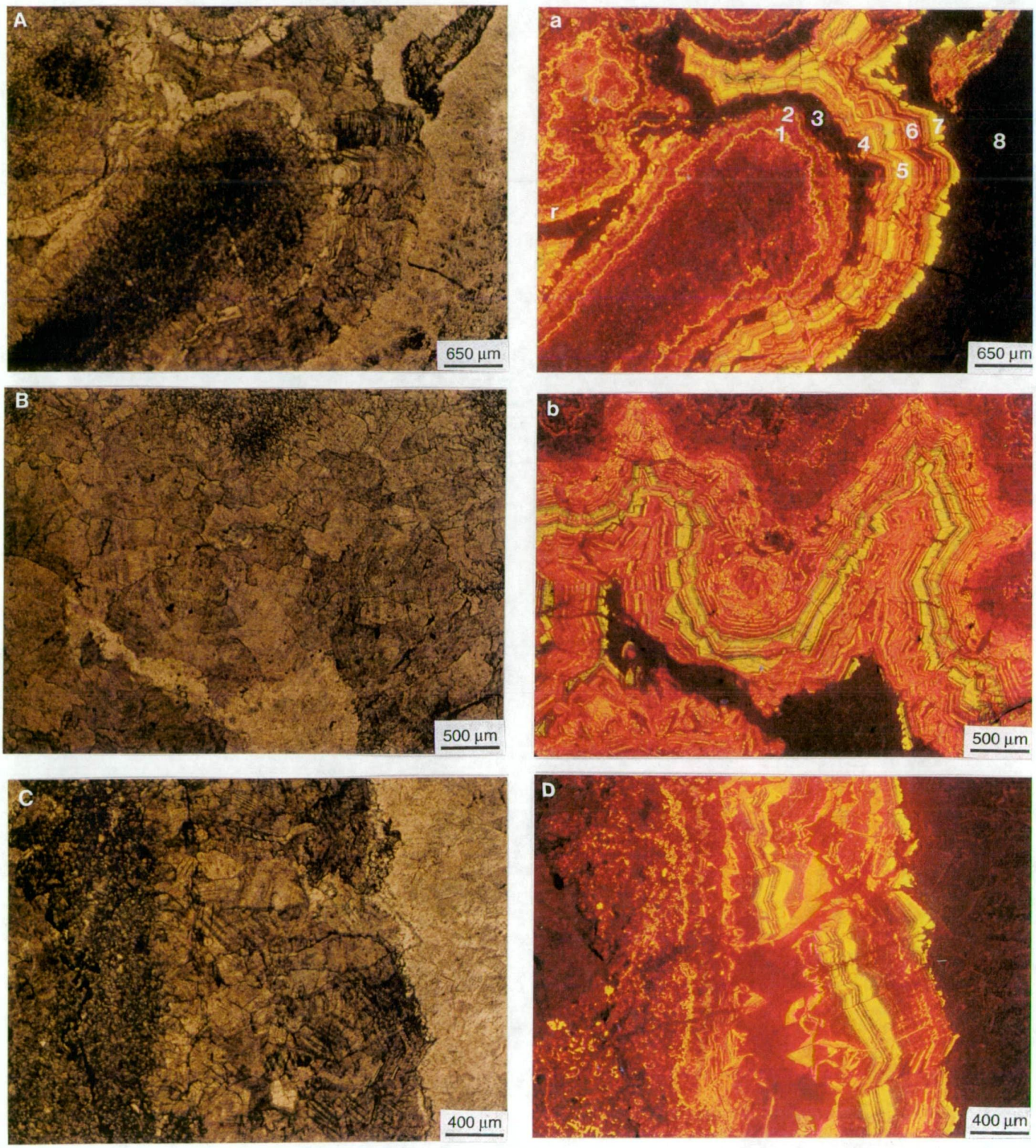
A
650 µm
a
1
2
3
4
5
6
7
8
r
650 µm
B
500 µm
b
500 µm
C
400 µm
D
400 µm

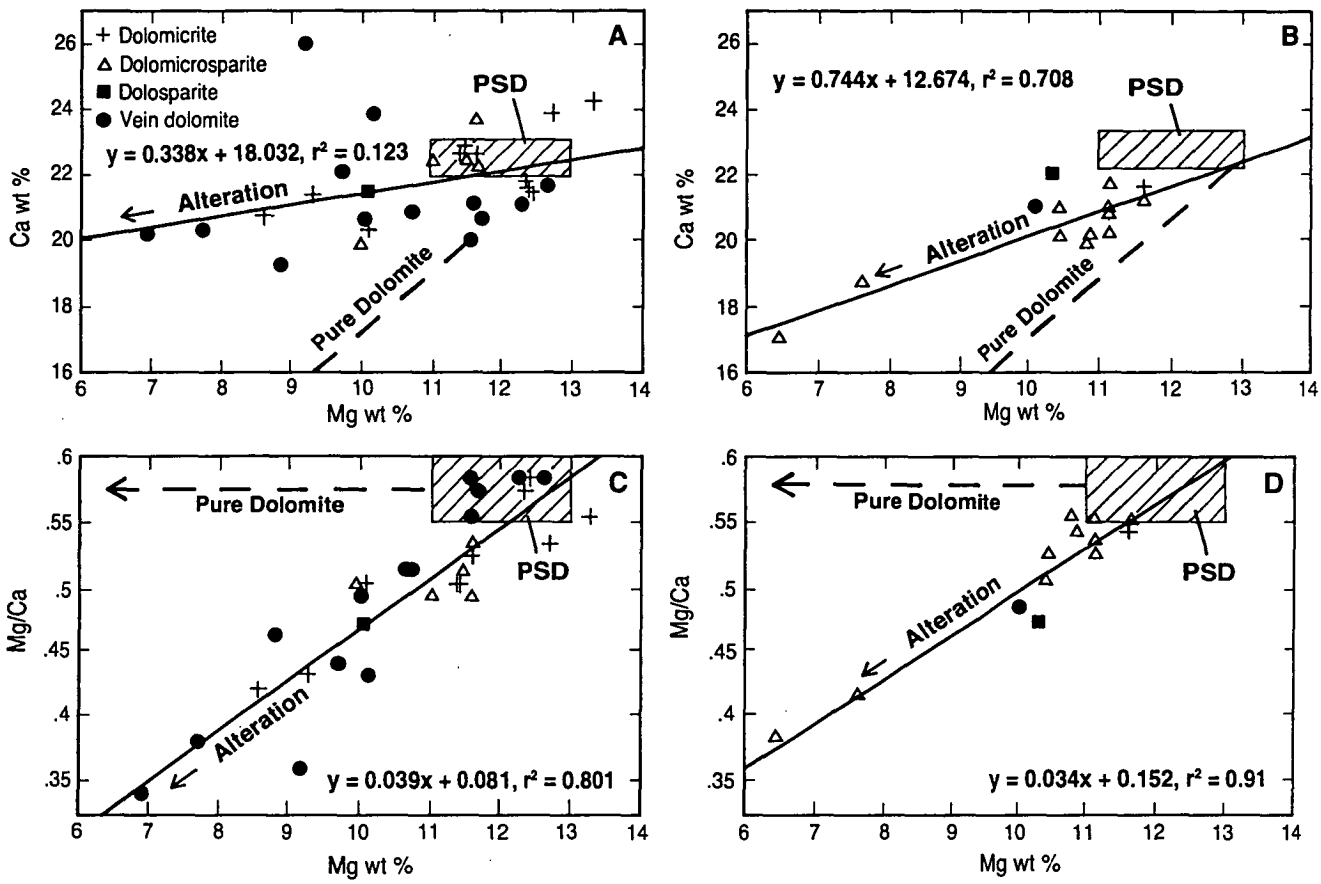

Figure 12.8 Calcium and magnesium geochemistry of the Renison carbonates. (A-B), Ca versus Mg values in less recrystallized and strongly recrystallized Renison carbonates, respectively. Ca and Mg variations, relative to unaltered Proterozoic sedimentary dolomites (PSD) and pure dolomite, are the result of alteration. (C-D), Mg/Ca versus Mg in less recrystallized and strongly recrystallized Renison carbonates, relative to unaltered PSD and pure dolomite compositions, respectively. The following symbols have been used in figures 6-10: crosses-dolomicrite, open triangles-dolomicrosparite, filled squares-dolosparite, filled circles-vein dolomite, filled triangles-coarsely crystalline dolomite.

Mg/Ca ratios range from 0.58 to 0.33 due to the loss of Mg relative to Ca.

12.10 Trace Elements

12.10.1 Strontium

Sr values in Renison dolomites range from 67 to 299 ppm and are higher than unaltered Proterozoic sedimentary dolomite values (PSD; Figs. 12.9 A, B). In less recrystallized samples (Fig. 12.9 A) Sr contents (other than in vein dolomite) are relatively constant throughout the range of Mg contents, whereas in strongly recrystallized samples (Fig. 12.9 B) Sr contents increase with decreasing Mg values. Dolomicrites exhibit the lowest average Sr values relative to Mg in both less recrystallized and strongly recrystallized dolomites (Figs. 12.9 A, B). Dolomicrosparites (recrystallized dolomicrites) have enriched Sr values relative to dolomicrites and unaltered Proterozoic sedimentary dolomites (PSD). Strongly recrystallized dolomicrosparites are most enriched in Sr values. Dolosparites and vein dolomites, both precipitates, are enriched in Sr relative to PSD, but the largest Sr variations occur in the less recrystallized dolomites.

12.10.2 Sodium

The range from 22 to 474 ppm Na in the Renison dolomites is larger than that observed in unaltered Proterozoic sedimentary dolomites (PSD) of Tasmania (325 ppm Na; Figs. 12.9 C and D). Dolomicrites show the lowest average Na contents relative to Mg in both less recrystallized Renison dolomites and unaltered Proterozoic sedimentary dolomites (PSD). Sodium contents for dolomicrosparites (recrystallized dolomicrites) are uniformly low in both less recrystallized and strongly recrystallized dolomites (Figs. 13.9 C, D). Most vein dolomites are enriched in Na relative to the remainder of the Renison dolomites (Figs. 12.9 C, D).

Since the Na contents in dolomites can be related to the salinity of formational waters (Land and Hoops, 1973; Rao, 1990 b), the wide variation in Na values in less recrystallized samples (Fig. 12.9 C) may be due to wide variations in salinity of diagenetic fluids responsible for dolomite precipitation. The uniformly low Na values in strongly recrystallized samples (Fig. 12.9 D) may result, therefore, from hydrothermal alteration of dolomite by lesser saline fluids than the original diagenetic fluids.

12.10.3 Manganese and Iron

The Mn (726 to 22 931 ppm; Figs. 12.10 A, B) and Fe (5 246 to 80 368

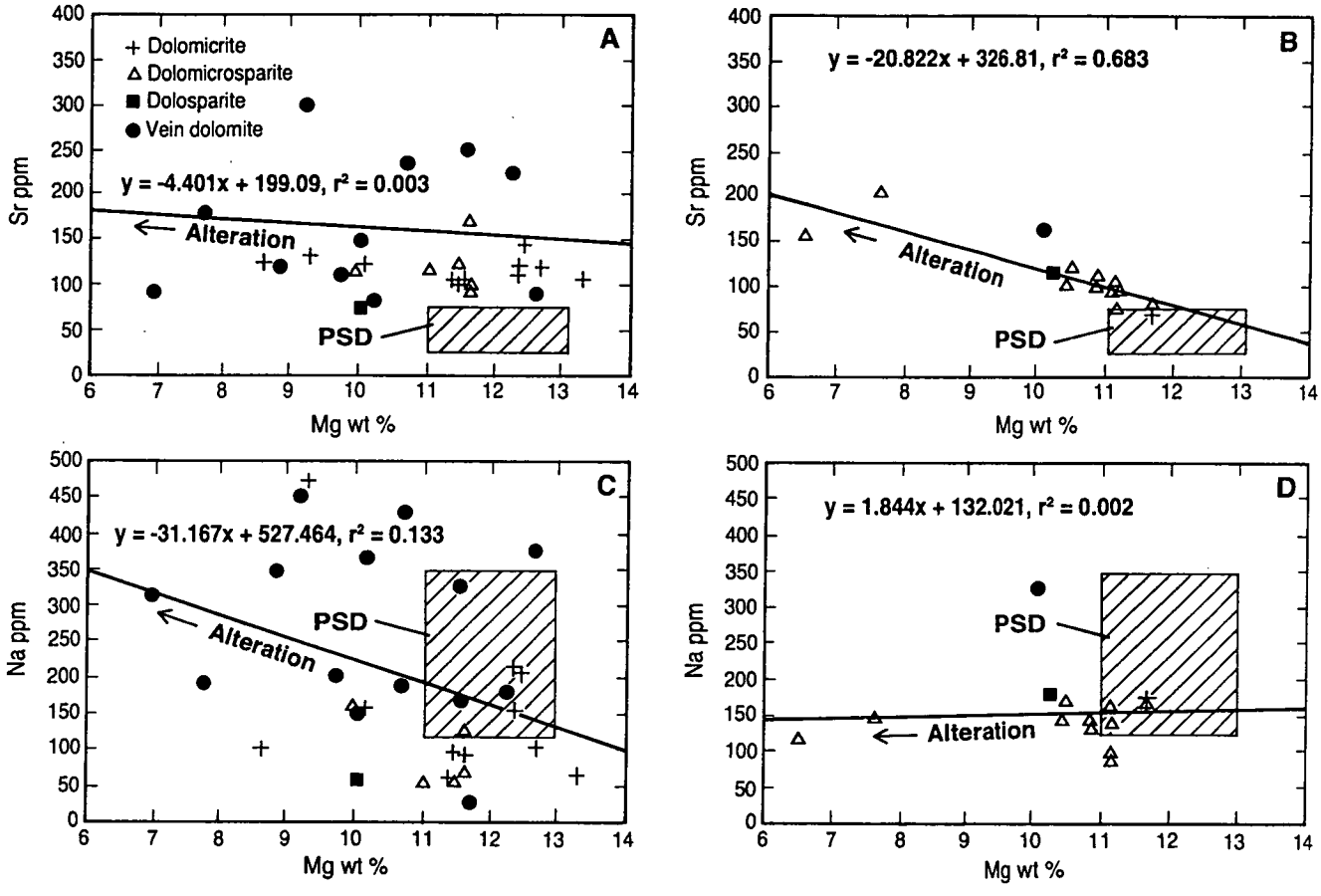

Figure 12.9. Strontium and sodium values, relative to magnesium, for the Renison carbonates. (A-B), Sr versus Mg values in less recrystallized and strongly recrystallized Renison carbonates, respectively. Increases in Sr values, relative to unaltered Proterozoic sedimentary dolomites (PSD), are the result of alteration. (C-D), Na versus Mg values in less recrystallized and strongly recrystallized Renison carbonates, relative to unaltered Proterozoic sedimentary dolomite compositions, respectively.

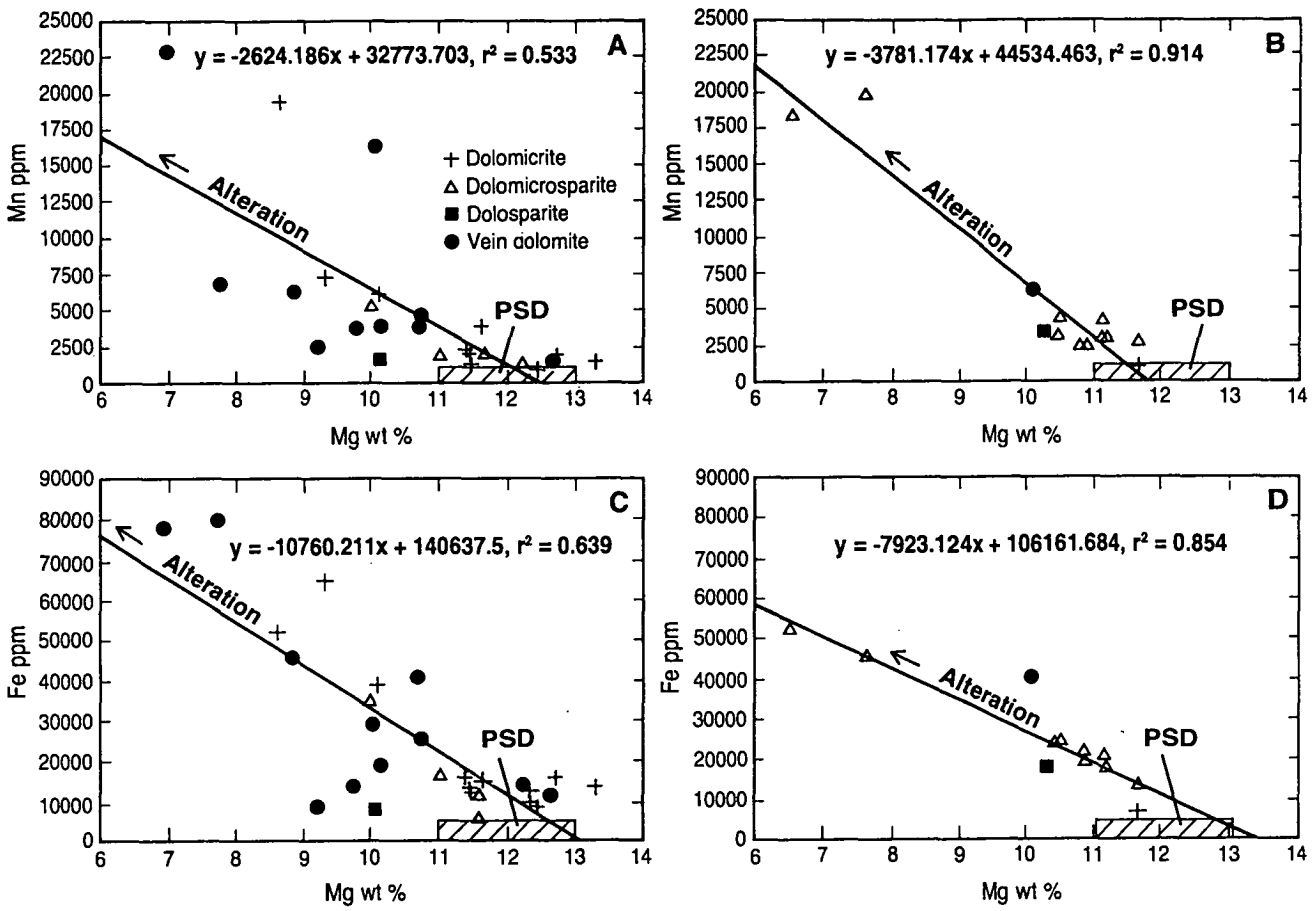

Figure 12.10. Manganese and iron values, relative to magnesium, for the Renison carbonates. (A-B), Mn versus Mg in less recrystallized and strongly recrystallized Renison carbonates, relative to unaltered Proterozoic sedimentary dolomites (PSD), respectively. (C-D), Fe versus Mg values in less recrystallized and strongly recrystallized Renison carbonates, relative to the PSD, respectively. The inverse relationship between Mn-Mg, and Fe-Mg values, relative to the PSD, is the result of alteration.

ppm; Figs. 12.10 C, D) concentrations in Renison carbonates are much higher than those of unaltered Proterozoic sedimentary dolomites (PSD), and inversely related to Mg wt.%. Dolomicrites and vein dolomites exhibit a systematic increase in both Mn and Fe in the less recrystallized dolomites (Fig. 12.10 A), with similar trends observed for dolomicrosparites in the strongly recrystallized dolomites (Fig. 12.10 B), relative to the Mg contents of the unaltered Proterozoic sedimentary dolomites (PSD).

Mn and Fe concentrations are low in seawater, whereas they are high in non-marine fluids (Pingitore, 1978). Since the distribution coefficients for both Mn and Fe in dolomite are greater than unity (Pingitore, 1978; Veizer, 1983), high Mn and Fe concentrations can occur in dolomite. The incorporation of Mn and Fe into dolomite is related to prevailing aerobic-anaerobic conditions during alteration. Aerobic conditions prevent the substitution of Mn and Fe for Mg in dolomite, whereas anaerobic conditions favor large concentrations of these elements (Pingitore, 1978; Shanmugam and Benedict III, 1983). Therefore, high concentrations of both Mn and Fe in dolomite may be due to carbonate alteration under anaerobic conditions.

12.11 Oxygen and Carbon Isotopes

12.11.1 Dolomite

Carbon and oxygen isotope values for both less recrystallized and strongly recrystallized Renison dolomites show a positive correlation (Figs. 12.11 A, B). The heaviest $\delta^{18}O$ and $\delta^{13}C$ values are -2.5‰ PDB (28.3‰ SMOW) and 4.1‰ PDB, respectively. The $\delta^{13}C$ values, in both less recrystallized and strongly recrystallized sections, decrease from 4.1 to -5.1‰ PDB with increasingly lighter $\delta^{18}O$ values. $\delta^{18}O$ values in carbonates from strongly recrystallized sections (-2.5 to -21‰ PDB, 28.3 to 9.2‰ SMOW) are lighter on average than less recrystallized carbonates (-2.7 to -15‰ PDB, 28.1 to 15‰ SMOW; Figs. 12.11 A, B). Dolomicrites have the heaviest $\delta^{13}C$ and $\delta^{18}O$ values, whereas dolomicrosparites (recrystallized dolomicrites) are more depleted in both $\delta^{13}C$ and $\delta^{18}O$ (Fig. 12.11 B). In strongly recrystallized sections, dolomicrosparites and coarsely crystalline dolomites can be markedly depleted in both $\delta^{13}C$ and $\delta^{18}O$ (Fig. 12.11 B). Dolosparites and vein dolomites, both precipitates, have light $\delta^{13}C$ and $\delta^{18}O$ values in less recrystallized dolomites (Fig. 12.11 A) and moderate to lightest $\delta^{13}C$ and $\delta^{18}O$ values in strongly recrystallized dolomites (Fig. 12.11 B).

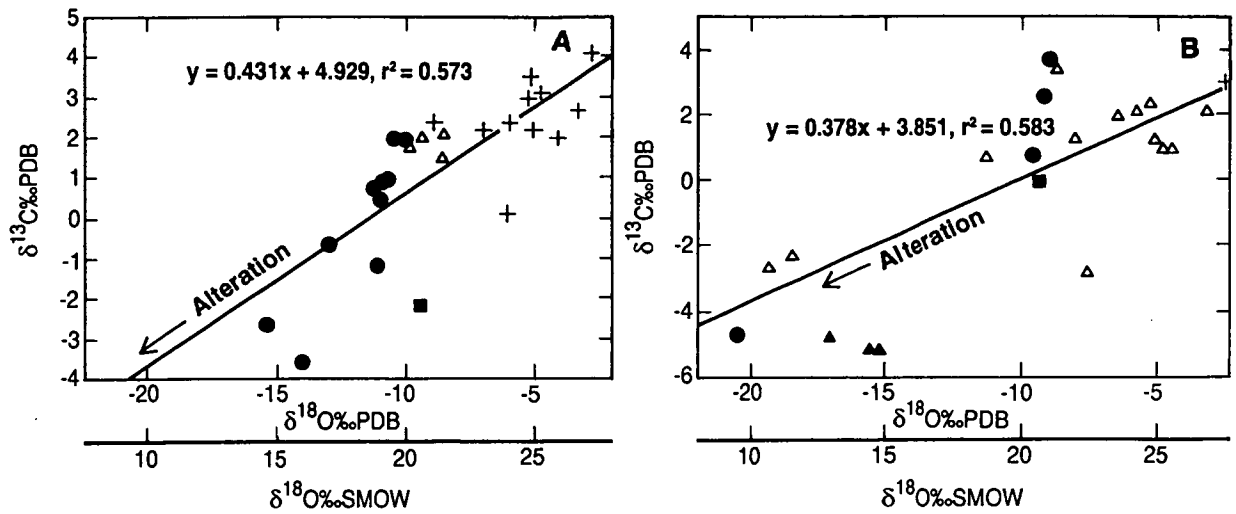

Figure 12.11. $\delta^{13}C$ (PDB) versus $\delta^{18}O$ (SMOW and PDB) values in less recrystallized (A) and strongly recrystallized (B) Renison carbonates. Strongly recrystallized carbonates exhibit the lightest $\delta^{18}O$ (PDB and SMOW) and $\delta^{13}C$ (PDB) values, whereas dolomicrites exhibit the heaviest $\delta^{18}O$ (PDB and SMOW) and $\delta^{13}C$ (PDB) values.

12.11.2 Siderite

Siderite $\delta^{18}O$ and $\delta^{13}C$ values from this study and from previous investigations (Jones and Evans, 1985; Holyland, 1987) exhibit some of the lightest carbonate isotopic values at Renison. $\delta^{13}C$ values range from -7.9 to +1.6 ‰ PDB, while $\delta^{18}O$ values range from -21 to -5‰ PDB (9.4 to 25.0 ‰ SMOW, Fig. 12.12).

The lightest isotopic data for Renison carbonates is associated with hydrothermal siderite, which includes the Devonian magmatic hydrothermal carbonate field of Collins (1981; Fig. 12.12). However, the most strongly recrystallized Renison dolomites completely overlap the Cambrian seawater derived hydrothermal carbonate field of Khin Zaw and Large (1992) and the Devonian magmatic hydrothermal carbonate field.

12.12 Oxygen Isotopes and Elemental Compositions

Isotopic analyses of the late Proterozoic Tasmanian sedimentary dolomites (PSD) from the Weld River area are not available, and therefore can not be compared with the Renison dolomites.

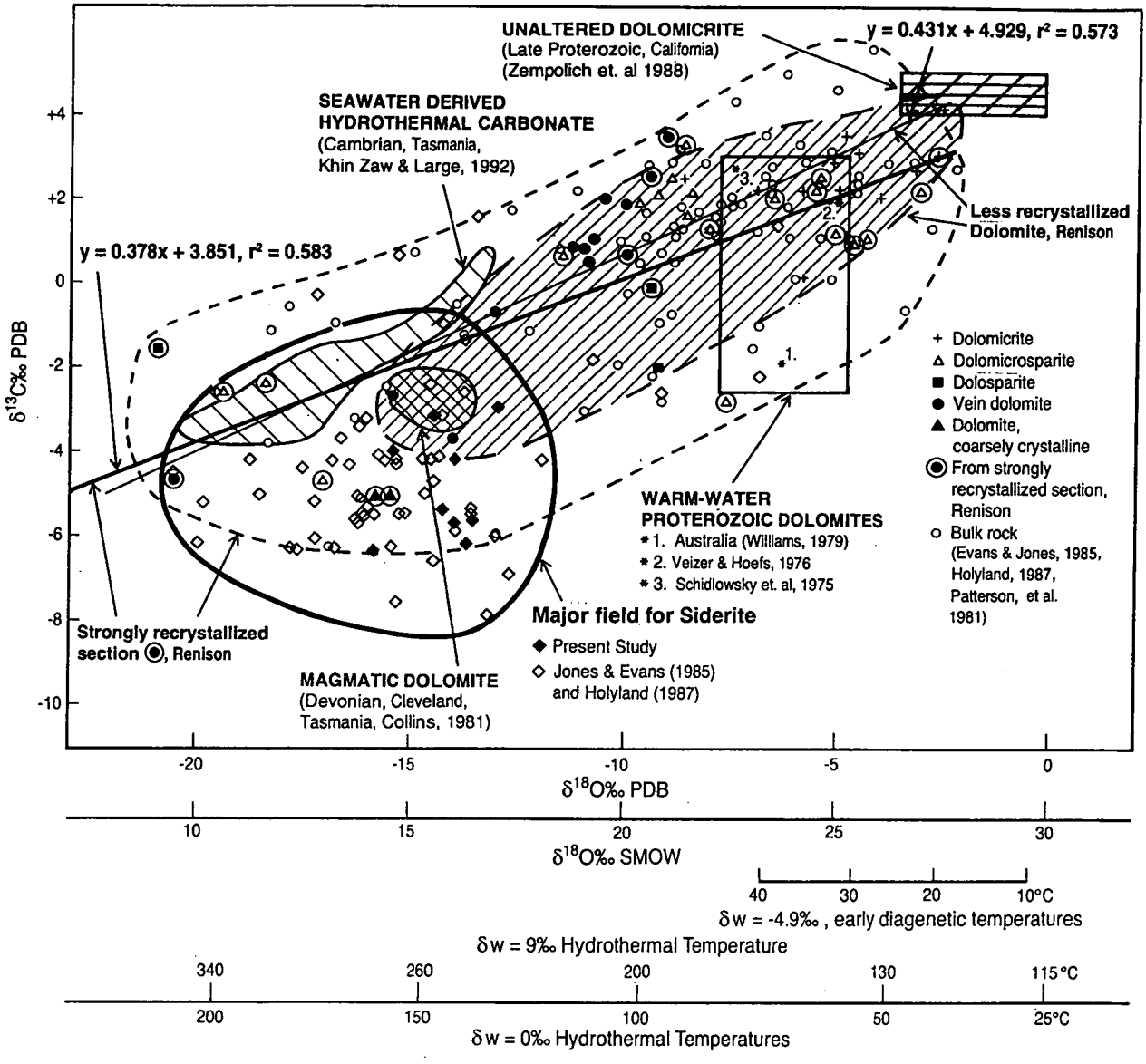

Figure 12.12. Carbon isotope versus oxygen isotope covariance diagram for the Renison carbonates. Comparisons are made between Renison carbonate types (this study) and bulk carbonates (Patterson et al, 1981; Jones and Evans, 1985; Holyland, 1987) with unaltered dolomites from the late Proterozoic of California (Zempolich et al., 1988), average warm-water Proterozoic dolomite values for Australia (Williams, 1979), worldwide (Veizer and Hoefs, 1976; Schidlowsky et al., 1975), Devonian hydrothermal dolomites from the Cleveland Mine, Tasmania (Collins, 1981) and Cambrian hydrothermal dolomites of Tasmania (Khin Zaw and Large, 1992). The regression lines through both the less and strongly recrystallized Renison dolomite data range from approximately -5‰ to 4‰ in $\delta^{13}C$ (PDB) and 10 to 28‰ in $\delta^{18}O$ (SMOW). Temperature calculations are discussed in the text.

12.12.1 Magnesium

Mg contents of the Renison carbonates decrease with increasingly lighter $\delta^{18}O$ values (Figs. 12.13 A, B). An apparent correlation between Mg and $\delta^{18}O$ (PDB and SMOW) values in the various dolomite types exists in the less recrystallized carbonates; from dolomicrite, to dolomicrosparite, to dolosparite, to vein dolomite (Fig. 12.13 A). Dolomicrosparites dominate the strongly recrystallized Renison dolomite analyses, and show a trend similar to the less recrystallized dolomites (Fig. 12.13 B).

12.12.2 Strontium and Iron

In strongly recrystallized Renison carbonates, dominated by dolomicrosparite, Sr and Fe concentrations increase with lighter $\delta^{18}O$ (PDB and SMOW) values (Figs. 12.13 C, D). A negative correlation between both Sr and Fe contents and $\delta^{18}O$ values, with r^2 values of 0.75 and 0.78 respectively reflect the systematic increase in both Sr and Fe.

12.12.3 Sodium

Na contents of the less recrystallized Renison dolomites increase with lighter $\delta^{18}O$ values (Fig. 12.14 A), but remain unchanged in strongly recrystallized dolomites (Fig. 12.14 B). Correlations exist in the less recrystallized carbonates between Na and $\delta^{18}O$ values from dolomicrite, to dolomicrosparite, to dolosparite, to vein dolomite (Fig. 12.14 A).

12.13 Carbon Isotopes and Elemental Compositions

12.13.1 Magnesium

Mg contents of the Renison dolomites decrease with increasingly lighter $\delta^{13}C$ values (Figs. 12.15 A, B). The decrease in both Mg and $\delta^{13}C$ values in medium to coarsely crystalline dolomites are due to alteration. These trends are similar to Mg-$\delta^{18}O$ bivariate plots.

12.13.2 Strontium and Sodium

There is no correlation between Na and Sr contents versus $\delta^{13}C$ values in less recrystallized and strongly recrystallized dolomites. The r^2 values are 0.0003, 0.068, 0.4 and 0.001 respectively.

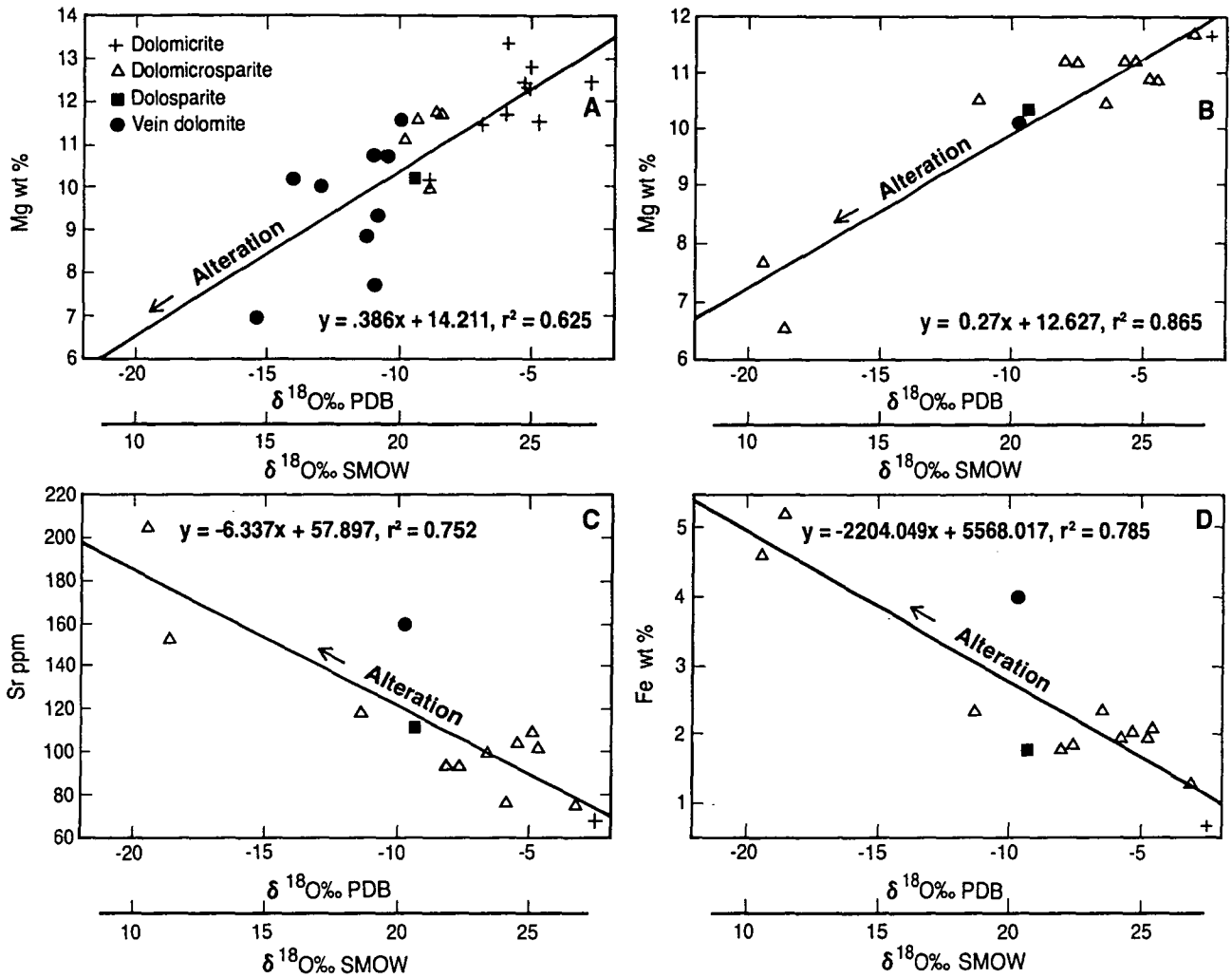

Figure 12.13. Magnesium, strontium and iron values, relative to oxygen isotope compositions, for the Renison carbonates. (A-B), Mg versus $\delta^{18}O$ (SMOW and PDB) in less recrystallized and strongly recrystallized Renison carbonates, respectively. Decreases in both Mg and $\delta^{18}O$ values are the result of alteration effects. (C), Sr versus $\delta^{18}O$ (SMOW and PDB) for strongly recrystallized Renison carbonates. (D), Fe versus $\delta^{18}O$ for strongly recrystallized Renison carbonates. Increases in Sr and Fe concentrations with lighter $\delta^{18}O$ values are the result of alteration. Note that isotopic analyses on unaltered Tasmanian Proterozoic sedimentary dolomites (PSD) are not available.

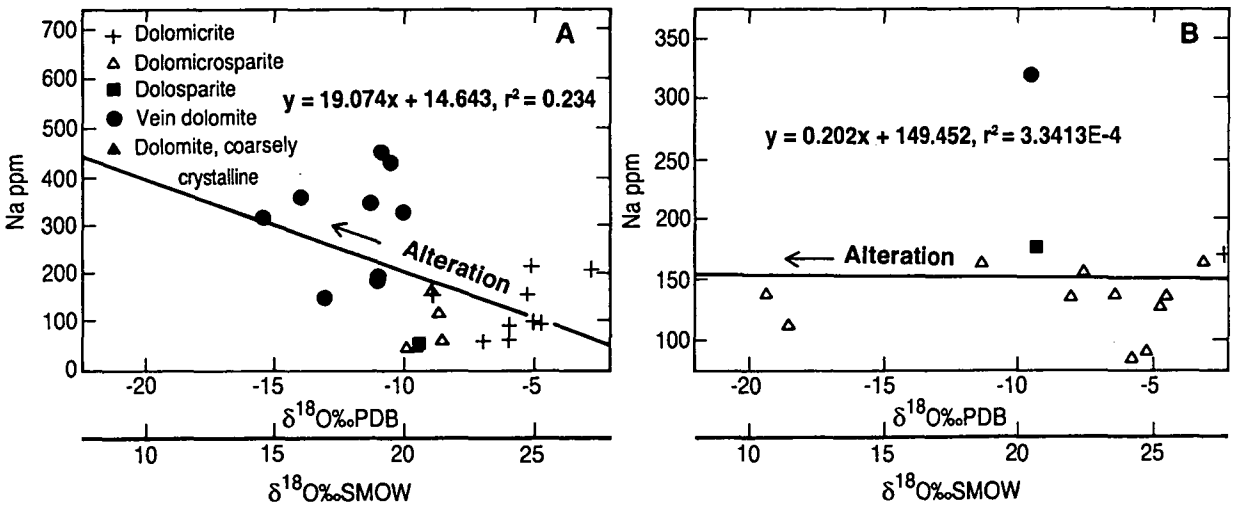

Figure 12.14. Na versus $\delta^{18}O$ (SMOW and PDB) in less recrystallized (A) and strongly recrystallized (B) Renison carbonates, respectively. Largest Na variations are more apparent in the less recrystallized Renison carbonates.

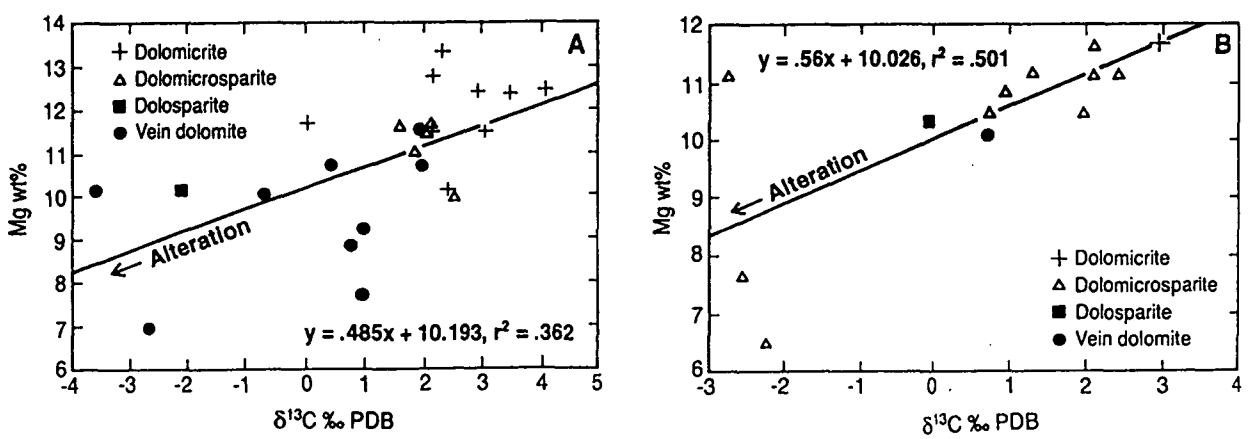

Figure 12.15. Magnesium versus $\delta^{13}C$ (PDB) values in less recrystallized (A) and strongly recrystallized (B) Renison dolomites. Note decrease in both Mg and $\delta^{13}C$ (PDB) values are the result of alteration effects.

12.13.3 Manganese and Iron

In strongly recrystallized Renison dolomites, dominated by dolomicrosparites, Mn and Fe concentrations increase with lighter $\delta^{13}C$ values (Figs. 12.16 B, D). However, in less recrystallized dolomites, dominated by dolomicrites, the inverse relationship between Mn and Fe with increasingly lighter $\delta^{13}C$ values is less pronounced (Figs. 12.16 A, C). A more positive correlation between both Mn and Fe contents and $\delta^{13}C$ values in strongly recrystallized dolomites indicates that these dolomites are more effected by alteration.

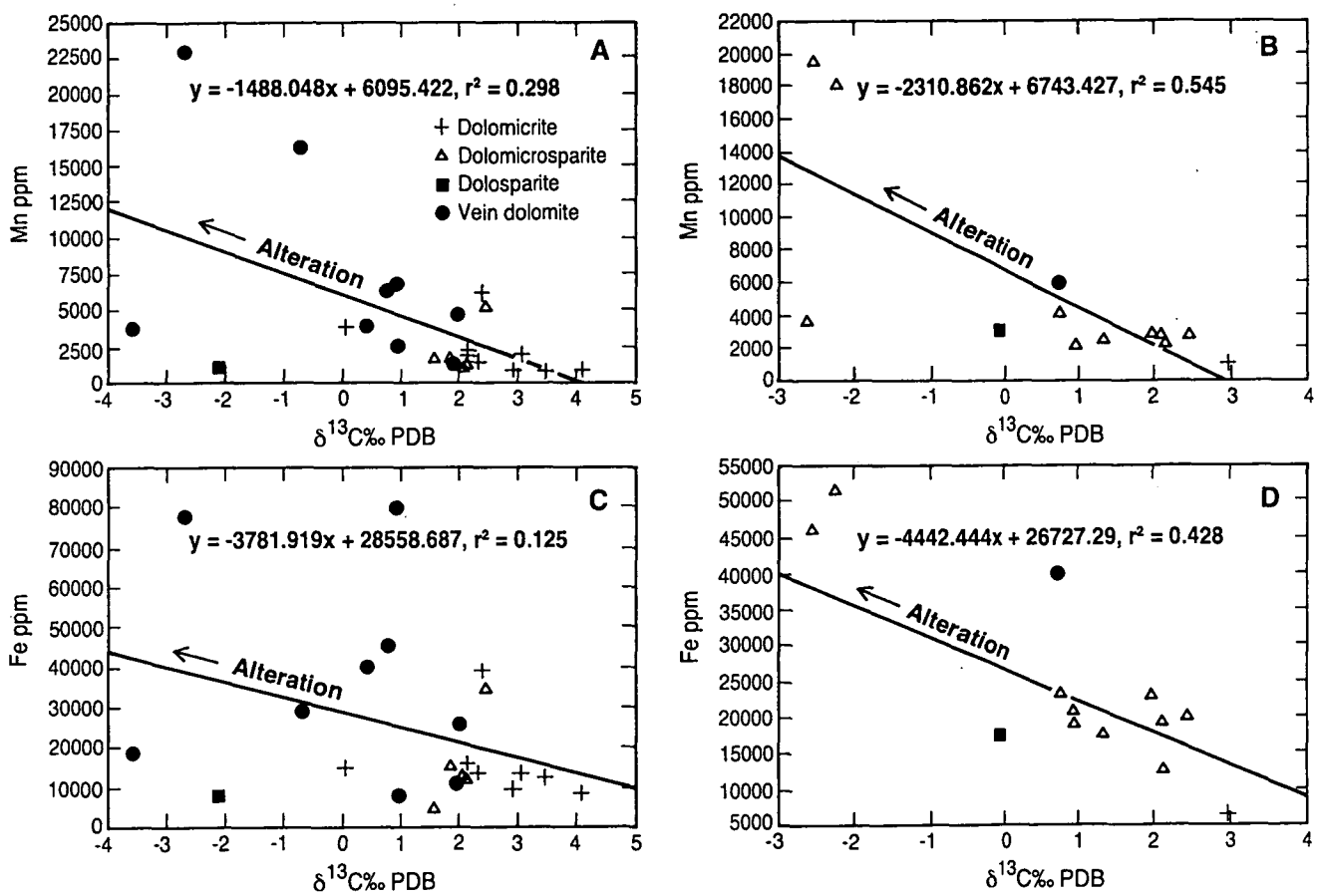

Figure 12.16. Manganese and Iron values, relative to carbon isotopic compositions in less recrystallized (A-C) and strongly recrystallized (B-D) Renison dolomites. The inverse relationship between Mn-Fe and $\delta^{13}C$ (PDB) values is the result of alteration.

12.14 Discussion

The elemental and isotopic composition of the Renison carbonates can potentially be interpreted by one or more of the following explanations:

- unaltered dolomite and early diagenetic fluid compositions
- altered carbonate compositions
- various source(s) of infiltrating fluids responsible for carbonate alteration
- equilibrium temperatures during carbonate alteration
- carbonate alteration by mixed infiltrating fluids
- models for water/rock interaction.

The following discussion critically evaluates the importance of each of the above factors in explaining the observed elemental and isotopic compositions of the Renison carbonates.

12.14.1 Unaltered dolomite and early diagenetic fluid compositions

The Ca, Mg, Mg/Ca, Sr, Na, Fe, and Mn values in least-altered dolomite samples are closest in composition to unaltered Proterozoic sedimentary dolomite (PSD; Figs. 12.8, 9, 10; Table 12.1). $\delta^{18}O$ and $\delta^{13}C$ values of Renison samples also provide an indication of unaltered carbonate compositions. The Ca (22.2 wt.%), Mg (13 wt.%) and Mg/Ca ratios (0.58) in these least-altered dolomites correspond to a pure dolomite end member. Low Sr (67 ppm) and Na (325 ppm) values are indicative of normal marine fluids and high concentrations of Mn (726 ppm) and Fe (5246 ppm), are due to the formation of dolomite in an anaerobic environment. Heavy $\delta^{18}O$ values (> -8‰ PDB, >22.6‰ SMOW; Fig. 12.12) of Renison dolomite overlap the isotopic fields of warm-water Proterozoic dolomites from both Australia (Williams, 1979), and worldwide (Schidlowski et al., 1975; Veizer and Hoefs, 1976); extending into the isotopic field of unaltered dolomicrite of late Proterozoic age from California (Zempolich et al., 1988).

12.14.2 Altered carbonate compositions

Minimum Ca, Mg and Mg/Ca; maximum Fe and Mn; and lightest $\delta^{18}O$ and $\delta^{13}C$ in the Renison dolomites (Table 12.1) correspond to the maximum extent of alteration in the original dolomites and provide support for the potential composition of the infiltrating fluid(s). Final values of Ca (16.9 wt.%), Mg (6.5 wt.%) and Mg/Ca ratio (0.35) indicate that the altered dolomites contain higher concentrations of Sr (299 ppm), Na (474 ppm), Mn (22 931 ppm) and Fe (80 368 ppm) relative to least-altered Renison and unaltered Proterozoic sedimentary

Table 12.1. Maximum loss and gain of major, trace element and initial and final isotope values ($\delta^{18}O$ and $\delta^{13}C$) for Renison dolomites.

Variables	Initial value	Final value	Difference	Max. loss%	Max. gain%
Mg wt %	13	6.5	6.5	50	-
Ca wt %	25.9	16.9	9.0	35	-
Mg/Ca	0.58	0.35	0.23	40	-
Sr ppm	67	299	232	-	346
Na ppm	325	474	149	-	46
Fe ppm	5246	80,368	75,122	-	1431
Mn ppm	726	22,931	22,205	-	3059
$\delta^{18}O$‰	28.3‰ SMOW (-2.5‰ PDB)	9.2‰ SMOW (-21‰ PDB)	19.1(18.5)		
$\delta^{13}C$‰	4.1‰ PDB	-5.1‰ PDB	9.0		

dolomites (PSD) of Tasmania. The maximum calculated percentage loss and gain between each variable relative to the initial value of the least-altered Renison dolomite (Table 12.1) indicate losses in Ca (35%), Mg (50%), Mg/Ca (40%), $\delta^{13}C$ and $\delta^{18}O$; and gains in Na (46%), Sr (346%), Fe (1431%) and Mn (3059 %). The final values of the most altered Renison dolomite reflect the composition of fluid(s) reacted with the original dolomite. The wide ranges of both $\delta^{13}C$ and $\delta^{18}O$ relative to major elemental compositions in the Renison carbonates result from the isotopic values being more sensitive to hydrothermal alteration than Ca, Mg and Mg/Ca ratio. Appreciable gains in Fe (1431%) and Mn (3059%) reflect hydrothermal alteration of the original dolomite which incorporated these elements into the carbonate lattice in an anaerobic environment. Elemental compositions for siderite are unavailable but isotopically siderite has the lightest average $\delta^{13}C$ and $\delta^{18}O$ values of all Renison carbonates (Table A6.4 in Appendix 6).

12.14.3 Source(s) of infiltration fluids responsible for carbonate alteration

The potential source(s) for fluids responsible for carbonate alteration at Renison may range from connate (burial), meteoric, marine or magmatic derivations. Concentrations of trace elements in seawater, meteoric water and magmatic water vary markedly (Table 12.2). Seawater has low concentrations of Mn (0.2 ppb) and Fe (2 ppb), moderate concentrations of Sr (8 ppb), and high concentrations of Na (10 760 ppm); whereas meteoric water has the lowest concentrations of Na (5 ppm), moderate concentrations of Mn (8 ppb), and highest concentrations of Sr (60 ppb) and Fe (40 ppb, Veizer, 1983). Preliminary PIXE probe analyses of fluid inclusions at Renison, corresponding to main stage cassiterite deposition (Kitto, 1994) indicate that potential magmatic fluids had the highest concentrations of Sr (3400 ppm), Na (23 000 ppm), Mn (180-7400 ppm) and Fe (10 000 to 20 000 ppm) relative to seawater and meteoric water.

Table 12.2. Concentrations of the trace elements Sr, Na, Mn, and Fe in average seawater and meteoric water (Veizer, 1983). Preliminary PIXE probe data from fluid inclusions associated with cassiterite deposition (magmatic fluids) at Renison (Kitto, 1994).

	Seawater	Meteoric water (stream)	Magmatic fluid (fluid inclusion, Renison main stage cassiterite)
Sr ppb	8	60	3 400 x 10^3
Na ppm	10 760	5.1	23 000
Mn ppb	0.2	8	180-7400 x 10^3
Fe ppb	2	40	10 000- 20 000 x 10^3

12.14.3.1 Burial (connate) fluids

Since burial (connate) fluids occur in anaerobic environments, the altered Renison dolomites can have high Mn and Fe concentrations, low Ca, Mg and Na concentrations, and lighter $\delta^{18}O$ values relative to the unaltered Renison dolomite. Burial diagenesis of carbonates, however, without organic matter is characterized by uniform $\delta^{13}C$ values and decreasingly lighter $\delta^{18}O$ values resulting in a horizontal shift of the $\delta^{18}O$ and $\delta^{13}C$ field (Fig. 12.17; Al-Aasm and Veizer, 1986; Choquette and James, 1987; Hurley and Lohmann, 1989; Rao, 1993 c). This is not observed in the Renison carbonates and therefore connate (burial) fluids are not thought to have been responsible for the observed changes in elemental and isotopic values of the Renison carbonates.

12.14.3.2 Meteoric fluids

The high Mn and Fe, low Ca, Mg and Na concentrations, and lighter $\delta^{18}O$ values in the Renison carbonates may be due to meteoric fluids which were involved in increased water/rock interaction in an open system. However, with increasingly higher temperatures, there is an expected upward shift on a covariance diagram to heavier $\delta^{13}C$ values (Fig. 12.17), and lighter $\delta^{18}O$ values (Rao, 1993 c). This trend is not observed in the Renison carbonates, and pure meteoric fluids are not thought to have been solely responsible for the observed changes in elemental and isotopic values of the Renison carbonates.

12.14.3.3 Marine fluids

Appreciable gains in Sr (346%) and lighter $\delta^{18}O$ and $\delta^{13}C$ values in the Renison carbonates might be due to increased temperatures and water/rock interaction by marine hydrothermal fluids. These hot marine waters can pick up high concentrations of Mn and Fe from rocks through which they pass and subsequently alter Renison dolomites. However, the lack of appreciable change in Na values of the Renison dolomites (Figs. 12.9 C, D) may not be indicative of hypersaline conditions. This contradicts typical increases in Na values in carbonates altered by heated seawater.

12.14.3.4 Magmatic fluids

High Mn and Fe concentrations, low Ca, Mg and Na concentrations, and lighter $\delta^{18}O$ and $\delta^{13}C$ values observed in the Renison carbonates may be due to magmatic fluids. Granite derived magmatic fluids may have high concentrations of Sr, Na, Mn and Fe (Table 12.2) and distinct $\delta^{13}C$ values ($-5 \pm 2‰$; Deines and

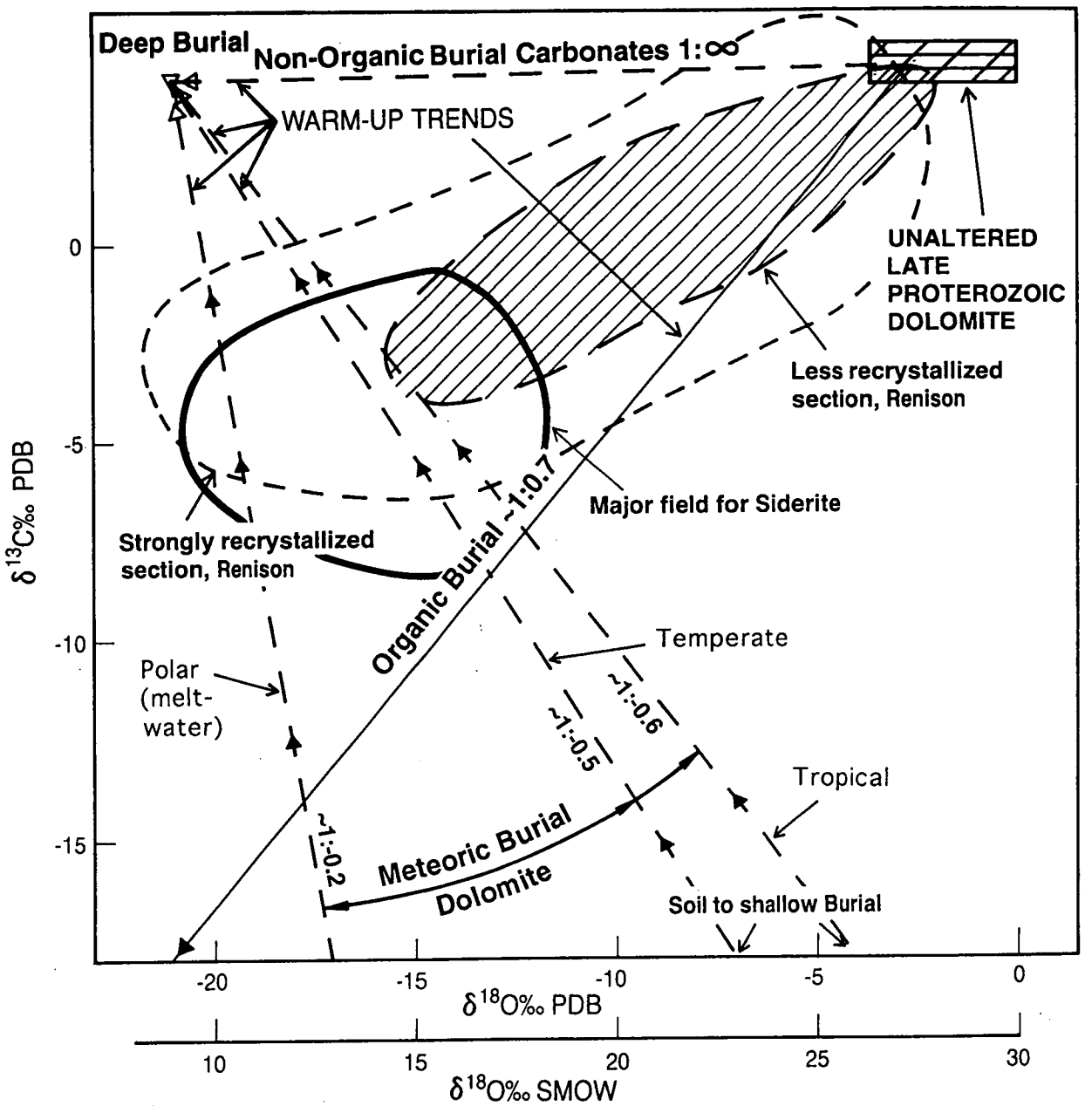

Figure 12.17. Carbon isotope versus oxygen isotope covariance diagram for the Renison carbonates together with isotope models for non-organic, organic and meteoric burial trends. $\delta^{18}O$ values for carbonates from tropical (-4‰ PDB, 26‰ SMOW), temperate (-7‰ PDB, 23‰ SMOW) and polar (-17‰ PDB, 13‰ SMOW) regions are after Rao (1993 c). Organic diagenesis may have partly influenced $\delta^{13}C$ values in the Renison carbonates. Warm-up trends refer to temperature increases during burial. The arrows indicate the $\delta^{13}C$ values enriched with increasing depth of burial.

Gold, 1973; Pineau et al., 1976; Ohmoto and Rye, 1979; Golding and Wilson, 1983). The $\delta^{13}C$ values for hydrothermal fluids responsible for alteration of the Renison dolomite must have an isotopic value between the unaltered Renison dolomite value of ~4‰ PDB and lightest siderite value of -7.9‰ (Figs. 12.12 and 12.17). This is demonstrated by the linear trend between $\delta^{18}O$ and $\delta^{13}C$ in the less altered Renison dolomites (Fig. 12.11 A), strongly altered Renison dolomites (Fig. 12.11 B) and the altered bulk carbonates analyses (Fig. 12.12). However, a linear trend in carbonates involving the depletion of $\delta^{13}C$ (downward shift) with increasingly lighter $\delta^{18}O$ values, can also occur in the presence of organic matter during burial diagenesis with increasing temperature (Fig. 12.17). This is common in some ancient carbonates (Al-Aasm and Veizer, 1986; Rao, 1993 c). At Renison, carbonate $\delta^{13}C$ values of -5‰ PDB correspond to $\delta^{18}O$ values between -15 to -21‰ PDB (15 and 9.2‰ SMOW, Fig. 12.12), which imply temperatures between 260 and 350° C. As the normal geothermal gradient is 25° C/km, burial depths between 10 to 14 km are required to account for the estimated high temperatures associated with alteration. Renison carbonates were never buried to such pre-Devonian paleo-depths, as indicated by the current overburden of approximately 1.2 km near the mine area, and an estimated 4.5 km of sediments (including the Dundas Group) away from the mine (Patterson et al., 1981). Moreover, the area under investigation was uplifted during the late Devonian Tabberabberan orogeny and subsequently intruded by the Devonian Pine Hill granite (Kitto, 1992). Estimates of the depth to mineralization, based on fluid inclusion studies, range from 2 to 4 km (Kitto, 1994). In conclusion, both elemental and isotopic variations in the Renison carbonates could have resulted from a shallow granite-derived magmatic hydrothermal fluid.

12.14.4 Alteration equilibrium temperatures

$\delta^{18}O$ and $\delta^{13}C$ values of carbonates can be used to determine the equilibrium temperatures responsible for carbonate alteration. Calculation of depositional temperatures from early diagenetic dolomite values (-2.5 to -8‰ PDB, 28.3 to 22‰ SMOW) using seawater $\delta^{18}O$= 0‰ SMOW in the paleotemperature equation of Irwin (1980; see Chapter 10), indicates a range of temperatures from +40 to +80° C, which are considerably warmer than the -2 to +40° C range for modern carbonates (Rao, 1988 a, 1991). Modern dolomite precipitates in equilibrium with temperate pore waters having $\delta^{18}O$ values of -4.9‰ SMOW (Irwin, 1980). Therefore, a calculation of hypothetical temperatures for early diagenetic dolomites using a $\delta^{18}O$ water value of -4.9‰

SMOW gives temperatures around 20° C for heavy $\delta^{18}O$ values of Renison dolomites, and between 30 to 45° C for warm-water Proterozoic carbonates worldwide (Fig. 12.12). The calculated $\delta^{18}O$ temperatures are consistent with expected values and suggest Renison dolomites formed in temperate waters.

Calculation of $\delta^{18}O$ temperatures for hydrothermal solutions, using $\delta^{18}O_{fluid}$ (magmatic) values of 9‰ SMOW (Kitto, 1994), indicate a range of depositional temperatures up to 350° C (Fig. 12.12). These temperatures are similar to those obtained for mineralizing fluids at Renison based on studies of fluid inclusions and $\delta^{18}O$ values of quartz and carbonate (Patterson et al., 1981; Davies, 1985; Holyland, 1987; Kitto, 1994).

12.14.5 Alteration by infiltrating fluids

Theoretical dolomite-fluid $\delta^{18}O$ and $\delta^{13}C$ equilibrium fractionation curves of Rye and Williams (1981) can be used to assist the interpretation of dolomite alteration from various types of fluid. Dolomite-seawater $\delta^{18}O$ and $\delta^{13}C$ fractionation curves corresponding to Recent or Proterozoic seawater with $\delta^{18}O$ and $\delta^{13}C$ values of 0‰, and a Devonian seawater $\delta^{18}O$ value of -4.5‰ (Hurley and Lohmann, 1989), and $\delta^{13}C$ value of 0‰, lie above the Renison dolomite field (Fig. 12.18). This suggests that the Renison dolomites were unaffected by either pure Proterozoic or pure Devonian seawater derived hydrothermal fluids. Average $\delta^{18}O$ and $\delta^{13}C$ values of magmatic fluids derived from the Pine Hill Granite at Renison are +9‰ SMOW and -5‰ PDB, respectively (Kitto, 1994). The hydrothermal carbonate $\delta^{18}O$ and $\delta^{13}C$ equilibrium fractionation curve for such a fluid falls below the Renison dolomite and only partially overlaps the siderite fields for Renison (Fig. 12.18). This curve represents isotopic compositions for hydrothermal carbonates precipitated in equilibrium from a proposed magmatic hydrothermal fluid responsible for main stage tin-rich carbonate replacement mineralization (Adabi et al., 1996 a, b).

Based on homogenization temperatures from fluid inclusions and $\delta^{18}O$ values of quartz at Renison (Patterson et al., 1981; Kitto, 1994), a $\delta^{18}O_{fluid}$ value of -3‰ SMOW could correspond to mixed magmatic and meteoric water with temperatures between 150 and 200° C; equivalent to fluids responsible for late stage base metal mineralization. The hydrothermal carbonate equilibrium fractionation curve corresponding to a $\delta^{18}O$ value of -3‰ SMOW and $\delta^{13}C$ value of -5.5‰ for such a fluid bisects the isotope field for Renison dolomites (Fig. 12.19).

$\delta^{18}O$ values of recent meteoric water vary with latitude and are lighter

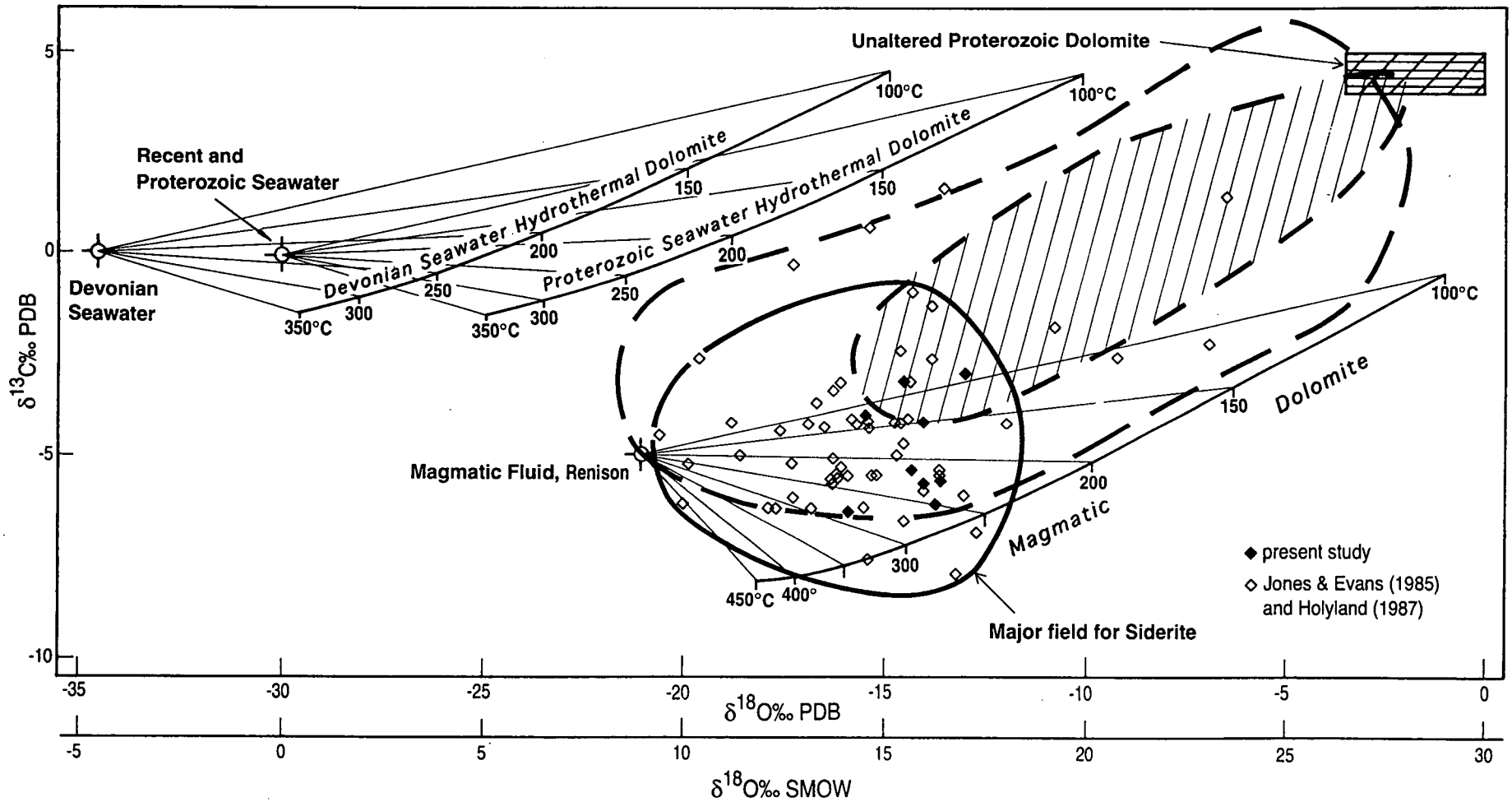

Figure 12.18. Carbon isotope versus oxygen isotope covariance diagram for the Renison carbonates with dolomite-water $\delta^{18}O$ (SMOW) and $\delta^{13}C$ (PDB) fractionation curves (after Rye and Williams, 1981) corresponding to Recent and Proterozoic seawater ($\delta^{18}O$=0‰, $\delta^{13}C$=0‰), Devonian seawater ($\delta^{18}O$=-4.5‰, $\delta^{13}C$=0‰), and a Devonian magmatic fluid ($\delta^{18}O$=9‰, $\delta^{13}C$=-5‰).

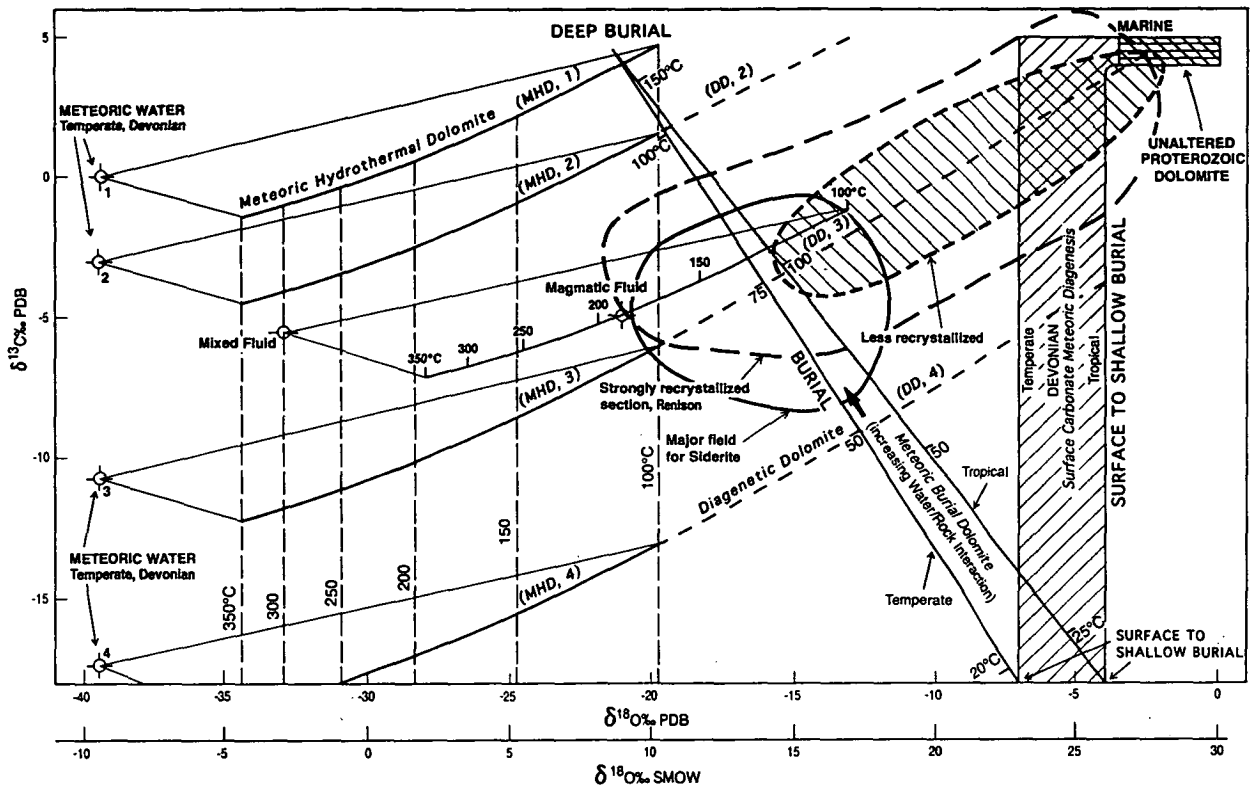

Figure 12.19. Carbon isotope versus oxygen isotope covariance diagram for the Renison carbonates with dolomite-water $\delta^{18}O$ (SMOW) and $\delta^{13}C$ (PDB) fractionation curves (after Rye and Williams, 1981) corresponding to temperate Devonian meteoric water ($\delta^{18}O$=-9.5‰) with variable $\delta^{13}C$ values ($\delta^{13}C$=0‰; -3‰; -11‰; -17.5‰) and a mixed fluid ($\delta^{18}O$=-3‰, $\delta^{13}C$= -5.5‰). Note the location of the inverted 'J' diagenetic trend for temperate normal surface sedimentary meteoric carbonate diagenesis (after Meyers and Lohmann, 1985; Lohmann, 1988; Rao, 1991) and meteoric burial dolomite diagenetic trends with increasing water temperatures (Rao, 1993 c). The Temperate Devonian Meteoric Hydrothermal Dolomite #2 fractionation curve (MHD 2) was used relative to the Devonian Surface Carbonate Meteoric Diagenesis Trend (Tropical Devonian meteoric water $\delta^{18}O$=-6.5‰; and temperate Devonian meteoric water $\delta^{18}O$ =-9.5‰). The lightest $\delta^{13}C$ value for surface to shallow burial calcite is considered to be -18‰ PDB, which is close to -14‰ for Pleistocene speleotherm deposits of Tasmania (Goede et al., 1986). Diagenetic dolomites are informally considered as those formed at <100° C.

than seawater by 2‰ SMOW in the tropics, 5‰ SMOW in temperate regions and >17‰ SMOW in polar regions (Dansgaard, 1964; Craig and Gordon, 1965). Similar relationships are thought to occur in ancient carbonates (Meyers and Lohmann, 1985; Rao, 1988 b, 1991; Rao and Green, 1983; Rao and Wang, 1990). During the lower Devonian, Tasmania was thought to be at latitude 40° S (Lee, 1993), in a temperate region with temperatures <20° C (Fig. 12.19). Sedimentary carbonate diagenesis between surface conditions and shallow burial is characterized by an inverted J-trend (Meyers and Lohmann, 1985; Lohmann, 1988; Rao, 1988 b, 1991) due to uniform $\delta^{18}O$ values of meteoric water, and variable $\delta^{13}C$ due to enrichment of ^{12}C by diagenesis of organic matter (Fig. 12.19). Dolomite-meteoric water $\delta^{18}O$ and $\delta^{13}C$ equilibrium fractionation curves (after Rye and Williams, 1981) for variable $\delta^{13}C$ and uniform $\delta^{18}O$ values of temperate Devonian meteoric water (-9.5‰ SMOW) indicate that Renison dolomites were in equilibrium with meteoric water having $\delta^{13}C$ values near -10‰ PDB. Such light $\delta^{13}C$ bearing meteoric waters occur in exposed to very shallow depths (<1 km), as observed presently in Tasmania, in the formation of shallow speleothems (Goede et al., 1986). The temperate meteoric burial dolomite line indicates that $\delta^{13}C$ values increase, due to increased water/rock interaction, which coincides with decreasing $\delta^{18}O$ values associated with increased temperatures during burial.

The mixed fluid $\delta^{18}O$ value of -3‰ SMOW could be due to mixing of magmatic fluid with Devonian temperate meteoric water (65%), tropical meteoric water (77%), Devonian seawater (89%), or Cambrian seawater (75%, Fig. 12.20). Since a mixed fluid $\delta^{13}C$ value of -5.5‰ PDB coincides with Devonian temperate meteoric water (Fig. 12.19) and not with seawaters of Proterozoic or Devonian periods (Fig. 12.18), a portion of the hydrothermal alteration may have resulted from a mixed fluid consisting of Devonian magmatic and temperate meteoric waters.

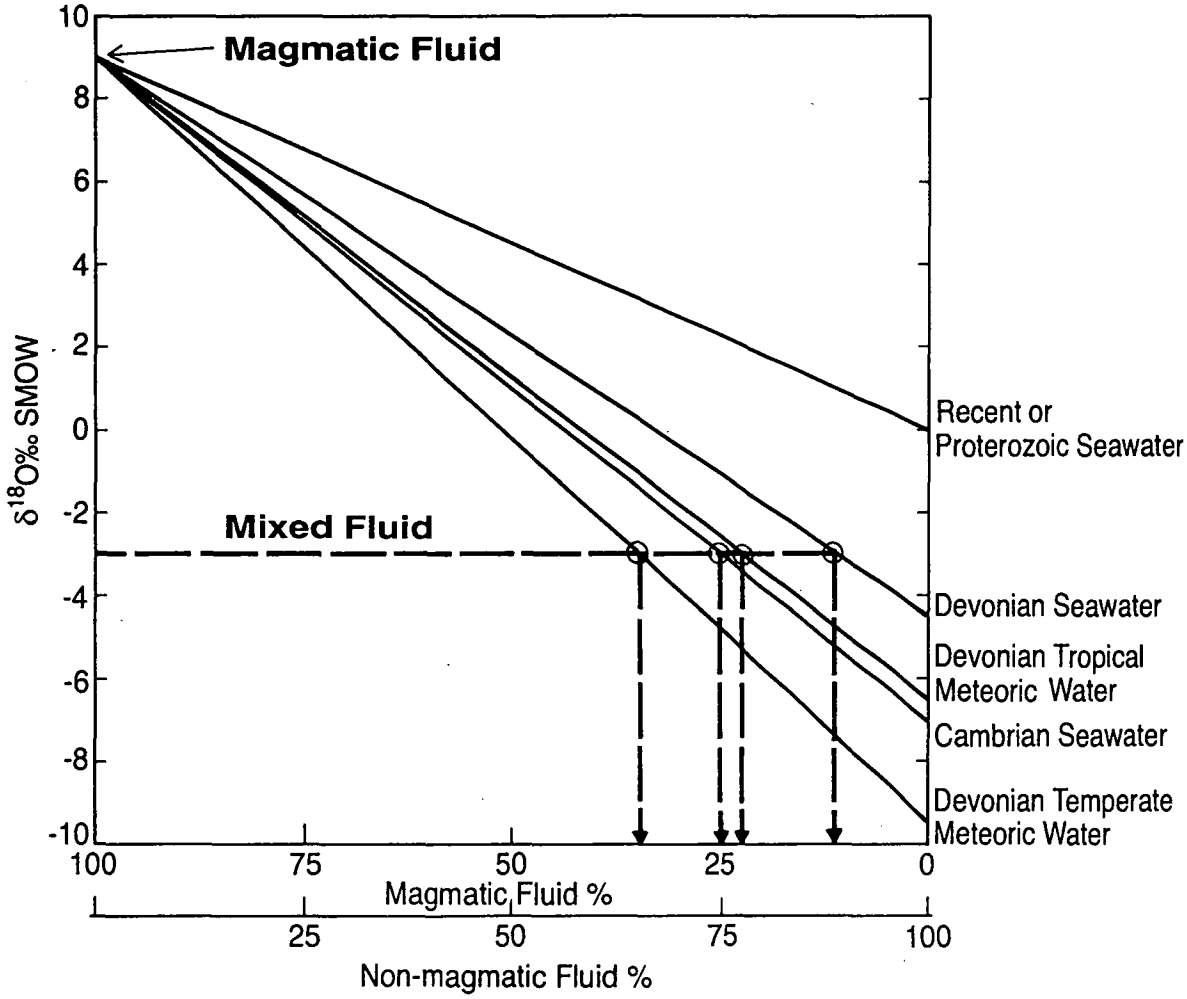

Figure 12.20. Potential alteration fluids resulting from combinations of Devonian magmatic fluid with Recent, Proterozoic, Devonian and Cambrian seawater, and alternatively, Devonian temperate and tropical meteoric waters. Late stage carbonate alteration may have resulted from a mixed magmatic fluid with up to 65% Devonian temperate meteoric water. See text for details.

12.14.6 Water/Rock interaction model

Appreciable loss and gain of elemental and isotopic compositions in samples studied at Renison may be due to water/rock interaction. As potential hydrothermal fluids were low in Ca and Mg concentrations and light in $\delta^{18}O$ and $\delta^{13}C$ values, increased water/rock interaction will progressively reduce the concentrations of these elements and isotopes in the altered carbonates (Figs. 12.8 A-D and Figs. 12.13 A, B). Elements like Sr, Fe and Mn, were thought to be high in the infiltrating fluids and thus any increased water/rock interaction would progressively increase the concentration of these elements in the altered carbonates (Figs. 12.9 A, B and Figs. 12.10 A-D).

In the carbonate horizons at Renison, a complex array of fault structures

has been recognized by many workers down to the millimeter scale (Patterson et al., 1981; Davies, 1985; Holyland, 1987; Kitto, 1992). These structures have been crucial for fluid infiltration, advection and dispersion/diffusion mechanisms associated with carbonate replacement. Traditional studies in fluid-rock interaction have relied on mixing models developed for either open or closed systems (e.g., Taylor, 1974, 1977), and this section evaluates the extent of fluid-rock interaction in the Renison carbonates using this approach. On a C/O covariance plot, the shape of the mixing curves associated with fluid-rock interaction can be used to interpret: the initial isotopic compositions of the infiltrating hydrothermal fluid and the host carbonates; the extent of mixing in a closed versus open system; the temperature of isotopic exchange; and the CO_2 concentration in the mineralizing fluid.

All carbon and oxygen isotopic data for carbonates from Renison are shown on a $\delta^{18}O_{(SMOW)}$ versus $\delta^{13}C_{(PDB)}$ covariance diagram in Figure 12.21. The data of Zempolich et al. (1988) have been used in this diagram to represent unaltered late Proterozoic dolomite. This negates the possibility of hydrothermal alteration in any of the Renison samples biasing the choice of an unaltered bench mark. The composition of the "Magmatic Fluid" in this diagram represents the isotopic composition of the hydrothermal fluid in equilibrium with the Pine Hill Granite. The $\delta^{18}O$ value of +9‰ SMOW for this fluid was estimated using the fractionation factors from Matsuhisa et al. (1979) on $\delta^{18}O_{qz}$ from main sulfide stage mineralization (Patterson et al., 1981; Kitto, 1994), together with temperature estimates from fluid inclusions (Kitto, 1994). The $\delta^{13}C$ value of -5.0‰ PDB for the magmatic fluid is an approximate average igneous carbon value based on Faure (1977), Hoefs (1980), Ohmoto (1986), and Taylor (1987). The "Magmatic Hydrothermal Carbonate" curve is the theoretical dolomite-fluid $\delta^{18}O_{SMOW}$-$\delta^{13}C_{PDB}$ fractionation curve for dolomites formed from, or in equilibrium with the hydrothermal magmatic fluid, of constant composition, and at a range of temperatures from 450 to 100° C (Rye and Williams, 1981). The $\delta^{18}O_{SMOW}$ values for this line were calculated from the fractionation factors (Equ. 1) of Land (1983), after Sheppard and Schwarcz (1970).

$$\Delta^{18}O_{(Dolomite\text{-}H_2O)} = 3.23(10^6T^{-2}) - 3.29 \qquad \text{Equation 1}$$

The $\delta^{13}C_{PDB}$ values were calculated using the fractionation factors (Equ. 2) of Deines et al. (1974), together with Ohmoto and Rye (1979).

$$\Delta^{13}C_{(Dolomite\text{-}H2CO3)} = (-8.914T^{-3})\ 10^8 + (8.737T^{-2})\ 10^6 - (18.11T^{-1})10^3 + 7.53 \qquad \text{Equation 2}$$

Hydrothermal carbonates with compositions that plot on the "Magmatic Hydrothermal Carbonate" line would have potentially precipitated in the Federal-Bassett Fault from a magmatic fluid without significant isotopic exchange due to water-rock interaction.

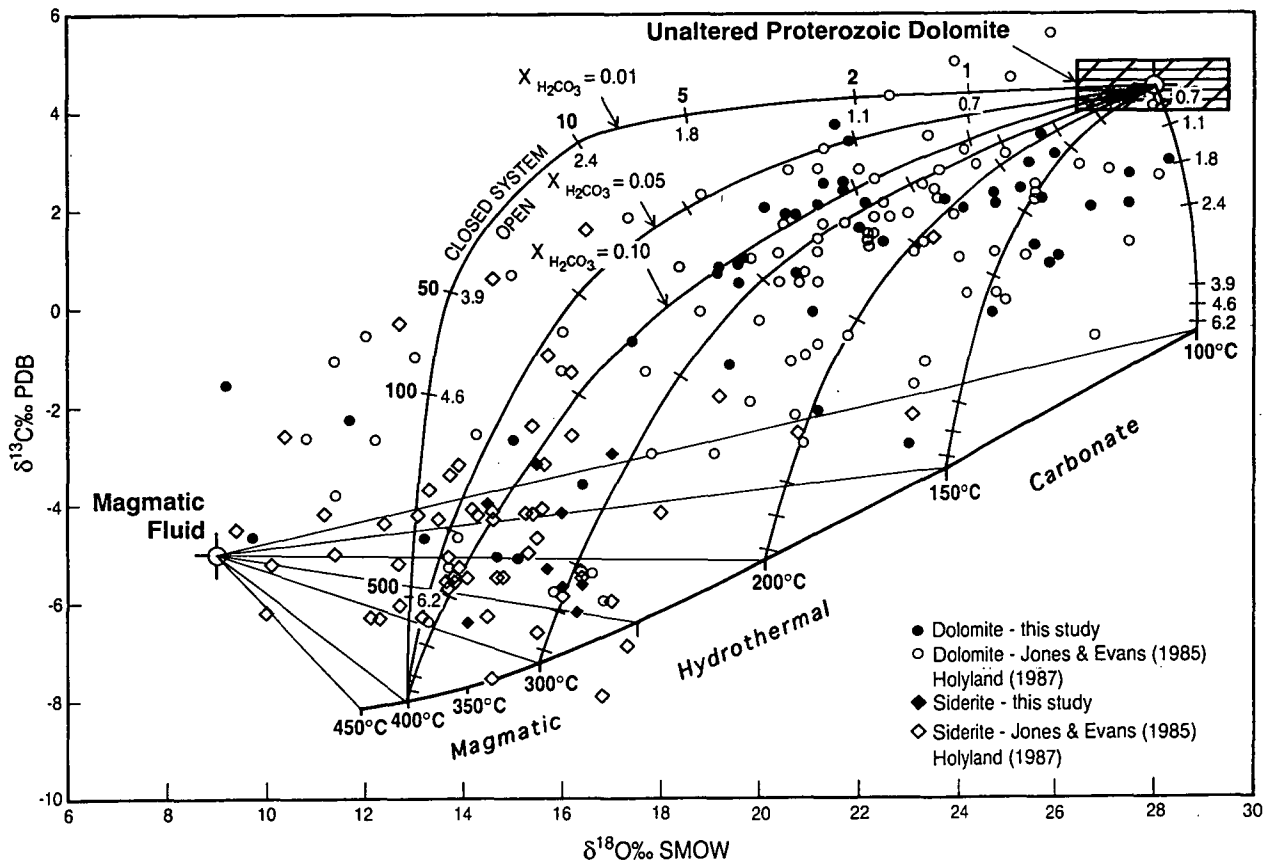

Figure 12.21. $\delta^{18}O_{(SMOW)}$ - $\delta^{13}C_{(PDB)}$ covariance plot of isotope analyses for the Renison carbonates. Superimposed upon the data are the Renison magmatic fluid ($\delta^{18}O$=9‰, $\delta^{13}C$=-5‰), the field for unaltered late Proterozoic dolomites (Zampolich et al., 1988), the dolomite-fluid equilibrium fractionation curve (after Rye and Williams, 1981), and isothermal mixing curves for specified X_{H2CO3} values (after Shelton, 1983) associated with fluid-rock interaction in open and closed systems.

To use the theoretical dolomite-fluid fractionation curve shown in Figure 12.21, it must be assumed that all carbon is present in the +4 oxidation state, and that CH_4 is absent. Bulk extraction analyses of fluid inclusions by Patterson and Ohmoto (1976) revealed the presence of methane, with CO_2/CH_4 ratios between

1.0 and 0.5 in late stage fluids (?) associated with vein calcites at 200° C. Patterson and Ohmoto (1976) incorrectly reported that $\delta^{13}C_{PDB}$ values ranged from +5‰ to -14‰. These values were used by Ohmoto and Rye (1979) as the best example of variations in $\delta^{13}C_{PDB}$ values due to changing CO_2/CH_4 ratios of fluids near the CO_2/CH_4 boundary. However, the carbonate $\delta^{13}C_{PDB}$ values at Renison range from +5‰ to -8‰ (Fig. 12.21), negating the interpretation of Ohmoto and Rye (1979). The presence of CH_4 in the late stage (?) 200° C hydrothermal fluid at Renison is therefore not considered the major cause of variations in the $\delta^{13}C_{PDB}$ values of the carbonates associated with cassiterite mineralization at Renison. Instead, the systematic variation in carbon and oxygen isotopes is thought to be due to water-rock interaction during the formation of the carbonate replacement orebodies.

Data in Figure 12.21 demonstrates the progressive interaction of Proterozoic dolomites with a magmatic fluid derived from the Devonian granite. The fluids responsible for carbonate replacement mineralization were apparently in equilibrium with an igneous rock prior to entering the Federal-Bassett Fault. Decarbonation is not considered an important process in the distal skarn environment, as the development of talc and tremolite assemblages are restricted to an irregular zone less than 0.5 m thick, which formed at the interface between massive pyrrhotite and the siderite reaction front in the host dolomite horizons. Decarbonation would cause large shifts in $\delta^{13}C_{PDB}$ values compared to $\delta^{18}O_{SMOW}$ values (Brown et al., 1985; Bowman et al., 1985; Taylor and Bucher-Nurminen, 1986), which are not observed.

Sverjensky (1981) calculated theoretical isotopic compositions of host-rock calcites during hydrothermal isotopic alteration as a function of increasing water-rock ratios at constant temperature, and applied this technique to the Upper Mississippi Valley Pb-Zn district. The same technique was applied by Shelton (1983; Table 12.3) to the Mines Gaspe porphyry copper and skarn deposit to explain the isotopic alteration observed in calcites as a function of water-rock ratios. Isotopic alteration in the Renison carbonates as a function of increasing water-rock ratios is discussed below.

Isotopic alteration paths for carbonate host-rocks are shown in Figure 12.21 as a function of water-rock ratios. The equations shown in Table 12.3 have been used to calculate the changing isotopic composition of the host-rock dolomites with increasing water to rock ratios. The following parameters were specified: initial $\delta^{13}C_{PDB}$ and $\delta^{18}O_{SMOW}$ values of the host dolomites were 4.1‰ and 28.3‰ respectively; H_2CO_3 was the dominant carbon bearing species

in solution; H_2CO_3 = 0.01 to 0.10 molal; $\delta^{13}C_{fluid}$ = -5.0‰ PDB; $\delta^{18}O_{fluid}$ = 9.0‰ SMOW. $\Delta^{13}C_{(Dolomite\text{-}H2CO3)}$ and $\Delta^{18}O_{(Dolomite\text{-}H2O)}$ values were calculated for the temperatures of mineralization. The fractionation factors in equations 2 and 3 were used to calculate the $\delta^{18}O_{SMOW}$ and $\delta^{13}C_{PDB}$ values of the final dolomites, respectively. The mixing lines in Figure 12.21 are drawn assuming fluid-rock interaction with dolomite; the equivalent lines for siderite are almost identical (33 C to 197° C; Carothers et al.; 1988). As a consequence, all fluid-rock calculations have been made for dolomite and applied to the siderite data from Renison.

Table 12.3. Equations used to calculate the isotopic alteration of Renison dolomites as a function of progressively increasing water to rock ratios (modified from Shelton, 1983; after Sverjensky, 1981).

$$\left(\frac{W}{R}\right)X_{H_2CO_3} = \frac{\delta^{13}C^{f}_{Dol} - \delta^{13}C^{i}_{Dol}}{\Delta^{13}C_{Dol-H_2CO_3} + \delta^{13}C^{i}_{H_2CO_3} - \delta^{13}C^{f}_{Dol}}$$

W/R = mole ratio of water to host dolomite, $\delta^{13}C^{i}_{Dol}$ and $\delta^{13}C^{f}_{Dol}$ are the initial and final carbon isotopic compositions of host dolomites, $\delta^{13}C^{i}_{H_2CO_3}$ is the initial carbon isotopic composition of $H_2CO_{3(aq)}$, and $\Delta^{13}C_{Dol-H_2CO_3}$ is the carbon isotopic fractionation between dolomite and aqueous H_2CO_3.

$$\frac{\left(W/R\right)}{3} = \frac{\delta^{18}O^{f}_{Dol} - \delta^{18}O^{i}_{Dol}}{\Delta^{18}O_{Dol-H_2O} + \delta^{18}O^{i}_{H_2O} - \delta^{18}O^{f}_{Dol}}$$

W/R = mole ratio of water to host dolomite, $\delta^{18}O^{i}_{Dol}$ and $\delta^{18}O^{f}_{Dol}$ are the initial and final oxygen isotopic compositions of the host dolomites, $\delta^{18}O^{i}_{H_2O}$ is the initial oxygen isotopic composition of the fluid, and $\Delta^{18}O_{Dol-H_2O}$ is the oxygen isotopic fractionation between dolomite and water.

$$\left(\frac{W}{R}\right)_{open} = ln\left[\left(\frac{W}{R}\right)_{closed} + 1\right]$$

Three mixing lines showing fluid-rock ratios as a function of X_{H2CO3} at 400° C are shown in Figure 12.21. The curvature of the lines primarily depends on the concentration of CO_2 in the hydrothermal fluid.Values of 0.01, 0.05 and 0.10 molal were chosen for the major carbon-bearing species, representing successive increases or gradients in CO_2 concentrations in the hydrothermal fluid during carbonate replacement-style mineralization (Patterson et al., 1981; Davies, 1985; Holyland, 1987; Kitto, 1994). Isothermal fluid-rock curves at X_{H2CO3} (apparent) = 0.10 molal are also shown for 300 , 200 , 150 and 100° C.

The calculated curves for fluid-rock interaction shown in Figure 12.21

encompass the field of isotopic data for Renison carbonates and explain the shift to lighter isotopic values with increased fluid-rock interaction. The mixing curves suggest that for an open system, an initial water-rock ratio of ~6, in association with decreasing temperatures (≤ 400° C), can explain the extent of isotopic exchange in the carbonate-bearing host rocks (Adabi et al., 1996 a, b). Fluid inclusion data from the major fluid conduits, the Federal-Bassett Fault and the Transverse Faults, support this temperature (Davies, 1985; Kitto, 1994). The concentration of CO_2 in the hydrothermal fluid during carbonate replacement is predicted to increase from 0.01 to 0.10 molal, consistent with fluid inclusion studies for the stratabound carbonate replacement mineralization (Davies, 1985).

This simple model of fluid-rock interaction is consistent with the geology at Renison and adequately explains chemical and isotopic systematics associated with carbonate replacement orebodies. The fluid-rock interaction model supports the hypothesis that Devonian granite-derived magmatic-hydrothermal fluid (main sulfide stage) had initial $\delta^{18}O_{SMOW}$ and $\delta^{13}C_{PDB}$ values of +9‰ and -5‰, respectively. These values remained unmodified during ascent of the Federal-Bassett Fault, while temperatures decreased to ~300° C (Kitto, 1994). Isotopic evolution occurred during reactions with the dolomite horizons, which had initial $\delta^{18}O$ and $\delta^{13}C$ values of +28.3‰ and +4.1‰ respectively. Fluid-rock ratios were around 6 (open system) close to the replacement orebodies, and decreased in conjunction with decreasing temperatures away from mineralization along the carbonate horizons (Holyland, 1987). X_{H2CO3} values in solution may have increased from around 0.01 to 0.10 molal during dolomite dissolution.

12.15 Geologic Implications

The occurrence of shallow marine sediments ranging in age from Proterozoic to Early Devonian in the Renison area (Fig. 9.2), confirm the presence of a prehistoric sea from Proterozoic to Early Devonian times in this region. The Middle Devonian Tabberabberan Orogeny resulted in regional north-northwest trending open folds intruded by post-orogenic tin-bearing granitoids between 332 and 367 Ma (McDougall and Leggo, 1965; Brooks and Compston, 1965; Brooks, 1966; Williams, 1989; Sawka et al., 1990). Lack of marine sediments during the mid? to late Devonian in western Tasmania indicate potential periods for sea regression, and circulation of meteoric fluids, whereby mixing between magmatic and meteoric waters would be possible. Since the age of the Pine Hill Granite at Renison is late Devonian (355 ± 4 Ma; Brooks, 1966), extensive alteration of Renison dolomites by pure magmatic fluids and alteration

by mixed magmatic and meteoric water was possible at this time. Sulfur and oxygen isotope values, and fluid inclusion studies (Patterson et al., 1981; Holyland, 1987; Kitto, 1994) from the Renison orebody indicate the importance of magmatic hydrothermal fluids during carbonate replacement tin mineralization, together with mixed magmatic-meteoric solutions during the base metal stages of mineralization. Renison siderites were in equilibrium with fluid temperatures from about 350 to 150° C ($\delta^{18}O_{fluid}$ = 9‰ SMOW), whereas Renison dolomites are in equilibrium with fluid temperatures from 190 to 20° C ($\delta^{18}O_{fluid}$ = 0‰ SMOW; Fig. 12.22).

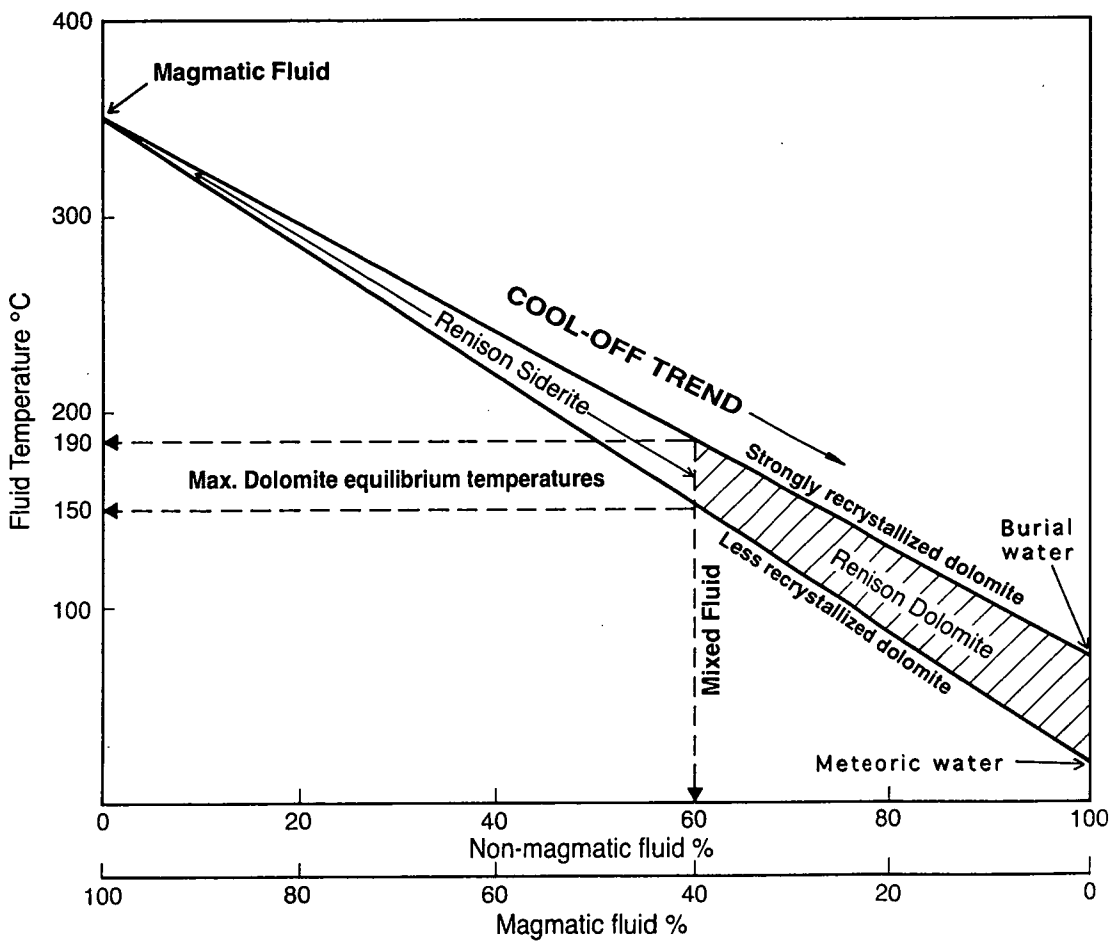

Figure 12.22. Variation in fluid temperatures and the percentage of non-magmatic and magmatic fluids. Temperatures of siderite and dolomite samples from Renison were calculated from $\delta^{18}O$ and $\delta^{13}C$, using Irwin (1980; equation 1). Renison siderites may have formed at temperatures between 150 and 350° C, and the Renison dolomites from 20 to 190° C. Late stage carbonate alteration may have resulted from the mixing of 65% non-magmatic fluid with 35% magmatic fluid.

The maximum dolomite temperatures of 190° C correspond to the lighter $\delta^{18}O$ values for strongly recrystallized Renison dolomites, and 150° C coincides with the lightest $\delta^{18}O$ values for less recrystallized Renison dolomites (Fig. 12.12). The amount of Devonian temperate meteoric water in the mixed fluids was potentially as high as 65% (Fig. 12.20, Adabi et al., 1996 a, b).

12.16 Conclusions

Renison carbonates range mainly from ferroan dolomite to ankerite with minor siderite and calcite. Petrographic features together with elemental and isotopic compositions ($\delta^{18}O$ and $\delta^{13}C$) indicate Renison carbonates have been altered mainly by diagenetic and hydrothermal alteration which has progressively oblitrated original depositional texture. The variations in the intensity of the alteration is mainly dependent on proximity to fractures, faults or mineralization. Magmatic and later meteoric fluids were responsible for alterations. These conclusions are based on the following evidence:

- Initial unaltered Renison dolomite Ca, Mg, Mg/Ca, Sr, Na, Fe and Mn values are similar to those of other unaltered Proterozoic sedimentary dolomite of Tasmania.

- Fluid infiltration resulted in diagenetic dolomite being recrystallized to dolomicrosparite and coarsely crystalline dolomite. Less recrystallized dolomite generally contains relatively more Ca and Mg; less Mn and Fe; and heavier $\delta^{18}O$ and $\delta^{13}C$ values than strongly recrystallized samples.

- The range of Ca, Mg, Mg/Ca, Sr, Fe and Mn values in the Renison carbonates from least to most altered indicate that fluid infiltration has occurred. This fluid infiltration resulted in a maximum loss of Ca (35%), Mg (50%), Mg/Ca (40%), and a gain in Sr (346%), Fe (1431%) and Mn (3059%). The wide ranges in $\delta^{18}O$ and $\delta^{13}C$ values result from the isotopic values being more sensitive to alteration than the loss in major and minor elements. The gain of Na is smaller than Sr due to the low to moderate salinity of the mineralizing fluids. Appreciable gains in Fe and Mn in the altered carbonates are due to their reaction with hydrothermal fluids in an anaerobic environment.

- Variation in carbonate $\delta^{13}C_{PDB}$ values from -5.1 to 4.1‰ and the linear trend between $\delta^{18}O_{SMOW}$ and $\delta^{13}C_{PDB}$ values are due to alteration by magmatically derived hydrothermal fluids and later mixed magmatic-meteoric fluids.

Overlapping $\delta^{18}O$ and $\delta^{13}C$ fields for Renison carbonates with the Devonian magmatic dolomite field support a magmatic source for the hydrothermal fluids.

- $\delta^{18}O$ and $\delta^{13}C$ values of unaltered Renison sedimentary dolomite correspond to formational temperatures of ~20° C in a temperate paleoclimate.

- The $\delta^{18}O$ and $\delta^{13}C$ values of altered Renison carbonates indicate that they were magmatically derived Devonian hydrothermal fluids of approximately 350° C. These temperatures are similar to those obtained from fluid inclusion studies and from calculations based on $\delta^{18}O$ variations in vein quartz.

- Dolomite-water $\delta^{18}O$ and $\delta^{13}C$ equilibrium fractionation curves for the Renison carbonates are significant in assisting to understand hydrothermal alteration by magmatic fluids and mixed magmatic-meteoric waters. The Renison siderites formed from magmatic fluids.

- Water/rock ratios may have been as high as 6 (open system) in the carbonate horizons close to the replacement orebodies, and decreased with declining temperatures away from mineralization. X_{H2CO3} values in solution may have increased from 0.01 to 0.1 molal during dolomite dissolution.

- Renison siderites were potentially in equilibrium with a magmatic hydrothermal fluid with temperatures from 150 to 350° C, and having initial $\delta^{18}O_{SMOW}$ and $\delta^{13}C_{PDB}$ values of +9‰ and -5‰ respectively. Similarly, the dolomites were potentially in equilibrium with fluid temperatures from 20 to 190° C and formed from either magmatic or mixed magmatic-meteoric fluids.

- Carbonate replacement mineralization at Renison resulted from magmatic hydrothermal fluids derived from the underlying Devonian Pine Hill Granite. Mixing of magmatic fluids with meteoric water was possible during the Devonian Tabberabberan Orogeny. The proportion of meteoric water that infiltrated late into the Renison hydrothermal system may have been 65% of the fluid.

CHAPTER 13

DIAGENETIC INTERPRETATION AND PARAGENETIC SEQUENCE

CHAPTER 13

DIAGENETIC INTERPRETATION AND PARAGENETIC SEQUENCE

13.1 Introduction

The crystal size of dolomite has been used to differentiate between early and late diagenetic dolomitization. The modern penecontemporaneous dolomites have crystal sizes of the order of a few microns (e.g., von der Borch, 1976, Mullins et al., 1985; Carballo et al., 1987; Mitchell et al., 1987; Mazzullo et al., 1987). If the rock consists completely of dolomite, the coarser the grain size, the later the dolomitization.

The shallow water Renison dolomites have undergone a complex and varied diagenetic history. The paragenetic sequence includes nine distinct processes. This sequence (Fig. 13.1) is based on petrographic observation, cross-cutting relationships, cathodoluminescence and elemental and isotopic compositions. Although there are a range of elemental and isotopic data in different dolomite types, the paragenetic interpretation is based on the majority of the data. These paragenetic sequences will be discussed below:

13.2 Dolomicrite

Dolomicrite is the most abundant dolomite type in the Renison mine area. Dolomicrites are considered marine cements, as the original depositional and early diagenetic textures are well preserved and there is no evidence of a replacement origin. The presence of a microbially laminated texture, scattered detrital quartz silt and a fenestral fabric (possibly indicative of subaerial exposure) in dolomicrites may support a shallow water origin (see Fig. 10.6). In terms of geochemistry, different dolomite types show a distinct trend of elemental and isotope compositions. Dolomicrites contain lower iron and manganese and low positive to very low negative oxygen isotopes, and have high positive carbon isotope values (up to ~7.5‰), compared to other coarser grained dolomite types in the Renison mine area (see Tables A6.3 and A6.4 in Appendix 6). These

Major Diagenetic Processes and Products	Relative Time =======>
Primary precipitation	
Dolomicrite	
Recrystallization	
Dolomicrosparite	
Coarsely crystalline dolomite	
Cementation	
Dolosparite	
Fibrous	
Clear (coarse)	
Vein emplacement	
Dolomite (including saddle dolomite)	
Silica (quartz)	
Crack-seal	
Replacement	
Siderite	
Silica	
Pressure dissolution	
Stylolite	
Dissolution seam	
Mineralization	
Metamorphism	
Talc/chlorite	
Fracturing	

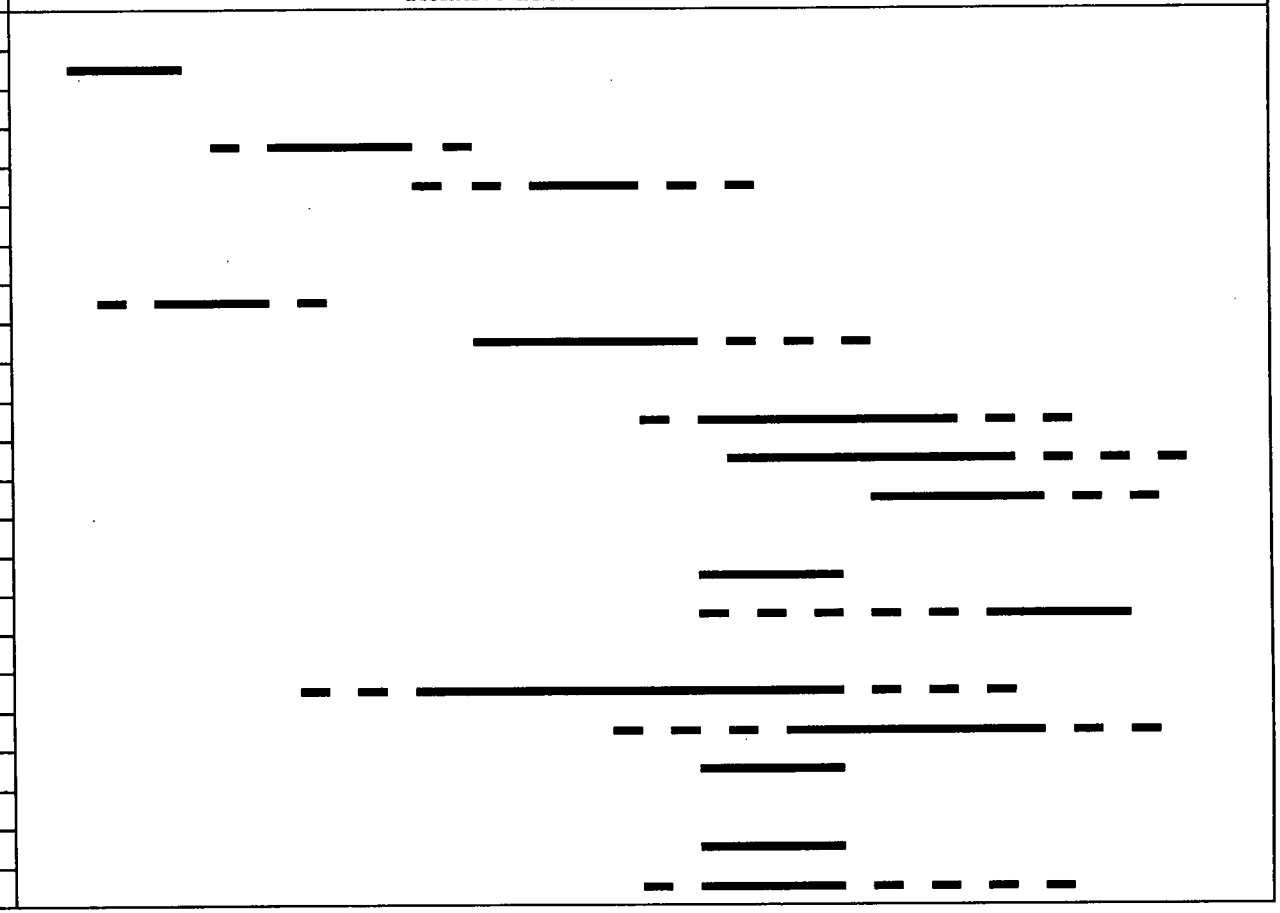

Figure 13.1. Summary diagram illustrating the overall paragenetic sequence in the Renison dolomite. Dashed line represents inferred ranges of diagenetic sequences. Solid lines represent ranges interpreted from petrographic and geochemical relationships and previous works by other researchers.

features provide independent evidence for a primary origin of dolomicrite. Under CL, the volumetrically dominant dolomicrite displays a dull to dark-brown luminescence, which may further support precipitation in an oxic (possibly marine) environment. The conclusion of primary origin is thus not based solely on fabric relations, but also on the pattern of elemental and isotopic compositions and cathodoluminescence petrography. In this study, a low surface temperature, low PCO_2, low SO_4^{2-} and higher Mg/Ca ratio are proposed for Proterozoic seawater (see Chapter 10). These features, together with certain organic matter, could influence precipitation of dolomicrites (probably a disordered calcian dolomite which in time goes stoichiometric) in the shallow subtidal to intertidal zones.

13.3 Dolomicrosparite

The distribution, texture and association with stylolites, suggests that dolomicrosparites formed during early diagenetic recrystallization of dolomicrites (see Fig. 10.7), possibly in shallow burial. In a few samples, the clots of original dolomicrite within dolomicrosparite support diagenetic recrystallization. In the mineralized area, dolomicrosparites are associated with scattered flakes of talc and cholorite minerals, which have been related to contact metamorphism (Morrison, 1982). Dolomicrosparites contain relatively higher iron and manganese, and lighter oxygen and carbon isotope values than those of dolomicrites (see Figs. 12.10 A-D, 12.11 A, B). Under CL, the dolomicrosparites display dark red-brown with scattered bright-yellow luminescence. The scattered bright-yellow luminescence possibly indicates the beginnings of a reducing condition (probably early shallow burial) which is conducive for Mn^{2+} ions, other trace elements or rare-earth elements, to substitute readily for Ca or Mg in the dolomite crystal lattice.

13.4 Dolosparite

Dolosparites, which fill pore spaces, cavities and vugs, are referred to as late diagenetic cements. One of the most distinctive features of the late diagenetic stage is the cavities rimmed with red-lined finely banded Fe-bearing dolomite. This suggests the cavities are related to dissolution and reprecipitation prior to emplacement of the Red-Rock Member (Morrison, 1982). Dolosparites are characterised by clear, coarser crystal size, higher iron and manganese concentrations and lighter carbon and oxygen isotope values than those of the least-altered dolomicrites and dolomicrosparites (see Figs. 12.10 A-D, 12.11 A,

B). However, very early diagenetic fibrous dolomite cements filling rims of a few cavities are also present. The high iron content of up to ~3% in some late diagenetic cements, may be explained by the presence of a banded iron formation in the Red Rock Member. Morrison (1982) suggested that this was caused by the supersaturation of ground water with respect to iron during late diagenesis. The wide variation in CL intensities in these dolomite cements reflects the complex chemical evolution of subsurface pore waters. The cathodoluminescence zonation in the dolosparite cements are not always identical. This may indicate that dolomite cements were precipitated from different pore fluids. The paragenetic sequences of CL zonation in dolosparite cements are shown in Figs.10.10 B, F and 12.6 B).

Two scenarios can be visualized concerning the variation in CL intensities of dolomite cements. First, it can be argued that these variations may reflect progressive cementation during early diagenesis (dull luminescent fibrous cements), to shallow (bright luminescence) and then deep burial (dull to nonluminescent) diagenesis. In the second case, it can be argued that variation in CL intensity in dolomite cement is due to the variation in trace element composition of pore fluids, possibly Mn and Fe contents, which caused the color zonation. Adabi et al. (1996 b) suggested that the proportion of meteoric water that infiltrated late into the Renison hydrothermal system was potentially as high as 65% by volume. However, Savard et al. (1995) has suggested that variation in CL intensity does not necessarily reflect different diagenetic environments.

As the number of zones and CL patterns are not consistent within samples from individual horizons, the dolomite cement zones can not be used for cement stratigraphy in this study.

13.5 Coarsely Crystalline Dolomite

Coarsely crystalline dolomites are a product of subsequent recrystallization of dolomicrosparite during late diagenesis. Coarsely crystalline dolomite is characterized by very coarse crystal size, very light oxygen and carbon isotope values, and many alternating sequences of finely laminated bright and dull luminescent zones (see Fig. 12.12). The wide variation in CL intensities may indicate multistage recrystallization as a result of evolving fluid chemistry.

13.6 Vein Dolomite

Vein dolomites are volumetrically more important in the mineralized than unmineralized area. Tectonic stress in the Renison mine area caused several

episodes of fracturing. Resulted fractures are filled by late to very late coarse grained dolomites. Vein dolomites generally cut original (dolomicrite), early diagenetic (dolomicrosparite) and late diagenetic dolomites (dolosparite), indicating formation in a very late diagenetic stage. However, irregular cross-cutting networks between late stage veins, which are present in a few dolomite samples, suggest a complex tectonic regime. Vein dolomites, particularly in the mineralized area, often show undulose extinction, similar to saddle dolomites of Radke and Mathis (1980), indicating formation at a higher temperature. These vein dolomites, which in many cases, are associated with sulphide mineralization, are possibly formed by hydrothermal fluids. In a few examples, the presence of talc and chlorite minerals growing out of the wall rock into vein dolomites, may indicate that the silicate minerals and vein dolomites crystallized synchronously.

Crack-seal texture, evidence of syntectonic vein formation, occurs in some dolomite samples from the mineralized area (see Figs. 12.4 E, F). It has been suggested that this type of syntectonic fibrous vein infilling develops by repeated increments of microcrack opening, followed by sealing of the microcrack through deposition of material from solution (Ramsay, 1980). This process, called "crack-seal " deformation, occurs where accumulation of elastic strain is followed by brittle failure, release of elastic strain, solution transfer of material to the microfracture site, and deposition therein (Ramsay, 1980). Once sealing of the microfracture is accomplished, stresses can once again be transmitted across the region of the initial microcrack, and elastic strains again build up until there is renewed microfracture (Cox and Etheridge, 1983). Each fine lamination in the crack-seal vein (see Fig. 12.4 E) indicates growth during successive crack-seal increments (Cox and Etheridge, 1983). As has been suggested by Bathurst (1975), oriented or syntaxial overgrowth of phases in the microcrack wall, may occur if the depositing species is the same as the substrate. During successive crack-seal increments, preferred orientation may develop due to competition between neighbouring grains having anisotropic growth kinetics (Cox and Etheridge, 1983, see Fig.2A, p.149 for more detail). The preferred orientation of the dolomite crystals in Fig. 12.4 E is due to growth of dolomite crystals in the microcrack wall, in response to anisotropic growth kinetics and competitive growth between neighbours (Cox and Etheridge, 1983). The growth orientation of non-syntaxial phases (silica over dolomite crystals, see Fig. 12.4 F) in a microcrack is possibly controlled by substrate orientation. The crack-seal processes are important in developing and enhancing foliation during deformation

involving microfracture and solution transfer processes (Cox and Etheridge, 1983).

Under CL, most cross-cutting veins, paticularly saddle dolomites, are non-luminescent, possibly due to their higher iron contents (ranging up to ~8%, e.g., S574, 76.3m). In contrast, crack-seal veins exhibit sequences of many delicate luminescent zones. These variations in luminescence intensity reflect compositional variations of pulsing fluids, responsible for crack-seal development during successive crack-seal increments after the main mineralization. The paragenetic sequence of CL zonation in crack-seal veins are shown in Figs. 12.7 a, b, c. The chevron shape of laminated bands are the result of euhedral dolomite crystal growth. In a few vein dolomite samples, microfracture is clearly visible under CL (see Fig. 12.7 D). These breaks can be due to either competitive dolomite crystal growth between neighbouring grains or tectonic stress.

Vein dolomites contain higher iron and manganese, and much lighter oxygen and carbon isotope values than the other dolomite types studied. The very coarse crystal size, undulatory extinction, cross-cutting of other dolomite types, along with very high iron and manganese and very light oxygen and carbon isotope values (see Figs. 12.10 A, C, 12.11 A, B), may indicate dolomite veins are formed by hydrothermal (possibly magmatic) fluids in a very late stage of diagenesis.

13.7 Siderite

Siderites are characterized by very coarse grained crystals and very light oxygen and much lighter carbon isotope values (-7.9‰) compared with the dolomites (see Fig. 12.12). Textures observed in hand specimens and evidence of rhombic dolomite crystal inclusion in the siderite, indicates that dolomites have been replaced by siderite. Renison ore, which is dominated by massive pyrrhotite, is followed by siderite and dolomite respectively. Therefore, temporal and spatial relationships with host rocks, mineralization and textural and isotopic compositions indicate that siderites are formed by replacement of host rock dolomites during the passage of magmatic hydrothermal fluids through major fault structures during mineralization (Adabi et al., 1996 b). The relatively high Mg content of the siderite (~19 mol% $MgCO_3$, Morrison 1982) supports the above interpretation that the siderite zone formed by replacement of the dolomite, while retaining much of the dolomite Mg.

13.8 Silicification

Silicification is a common process in Renison dolomites. Silica occurs as cement, veins or replaces dolomite grains. Inclusion of dolomite crystals within the silica, present in many samples, and authigenic quartz crystals with inclusions of undigested carbonates support a replacement origin. In a few examples, fibrous quartz is developed in a pressure shadow around rigid sulphide grains, indicating deformation postdates sulphide precipitation (Fig. 12.5 D). Some coarse quartz crystals that cut or replaced dolomite veins (S705, 169.8m) indicate formation in a very late diagenetic stage.

Silica can originate from different sources (e.g., dissolution of diatomes, radiolaria, sponge spicules, silicate minerals such as feldspars and amphiboles and hydrothermal fluids). The possible sources for silica in Renison dolomites are ground water, the mineral transformation of montmorillonite to illite and magmatic hydrothermal fluids. Ground water can be super-saturated with respect to silica, if it is moved through silica-rich sediments. The extent of silica-rich sediments in the Renison mine area supports this interpretation. The silica cement in the form of microquartz and megaquartz and also authigenic quartz crystals possibly originated from ground water rich in silica. Percolating of temperate meteoric water through Renison sequences, after main mineralization, has been suggested by Adabi et al. (1996 b). The presence of silica along stylolites (S705, 179.1m) can be related to the mineral transformation of montmorillonite to illite, which releases silica. Many silica veins and cavities also originated from magmatic hydrothermal fluids. This is supported by the presence of quartz crystals through whole mineral paragenesis in the Renison mine area (Patterson et al., 1981; Kitto, 1994).

13.9 Pressure Dissolution

Pressure dissolution textures have been widely recognized in many carbonate sequences (e.g., Wanless, 1979; Buxton and Sibley, 1981; Finkel and Wilkinson, 1990; Railsback, 1993 a, b). The products and process of pressure dissolution textures are still debated in the literature and will discussed briefly in the following paragraphs.

Two types of pressure dissolution textures, including sutured stylolites and dissolution seams are the most common diagenetic solution features in the Renison dolomites. The majority of stylolites in the Renison dolomites are at a low angle to bedding, although well developed vertical columnar stylolites occur sporadically (e.g., S705, 179.1 m). The largest and commonly the thickest

stylolites are high amplitude columnar forms in dolomicrites (e.g., S705, 172 m). However, the irregular low amplitude stylolites are generally associated with the dolosparite cements (e.g., S562, 121.5 m; S835, 227.3 m). Sharp bedding-parallel stylolite boundaries between dolomicrite and dolosparite in a few dolomite samples (see Fig. 10.7 D) may indicate that stylolite acts as effective permeability barriers to vertical flow. Thus, it can be interpreted that fluid migration and hence dolomite recrystallization post-dates stylolite formation. However, juxtaposition of different dolomite crystal sizes across a stylolite may result from the dissolution of intervening material, meaning that stylolitization could have been post-recrystallization.

Dissolution seams are the second most common diagenetic dissolution feature in the Renison dolomites. Association of dissolution seams with dolomite has been suggested by Wanless (1979), but amongst the carbonates examined by Railsback (1993 b), dissolution seams are present only in dolomitic limestones and dolostones of fine crystal size. Railsback (1993 b) noted that dolomitic rocks contain enough pressure-resistant elements to inhibit the interpenetration characteristic of stylolites and may instead allow only development of dissolution seams. Glover (1968) also noted this inhibition in Ordovician carbonates from western Australia, where stylolites were found in limestones and dolomitic limestones but not in dolostones. Railsback (1993 b) suggested that rocks that contain only one component (e.g., dolomite), generally have lower amplitude dissolution surfaces than rocks containing mixtures of grains and mud. Railsback (1993 a) noted that dissolution seams do not occur where dolomite abundances are 80 to 100%. However, the concurrence of many stylolites and dissolution seams in Renison dolomites with different crystal size and texture is a potential rebuttal of this hypothesis. Dissolution seams are assumed to be late to very late diagenetic features, because they cut wispy stylolites (S705, 201.5 m), late quartz and silica veins (see Fig. 12.2 A), and talc/chlorite silicate minerals (S574, 76 m).

Pressure dissolution is believed to be related to burial depth. Estimates of burial depths are 1500 m in northen Michigan (Buxton and Sibley, 1981); 700-1500 m in Kentucky (Shaver et al, 1984); 700 m in southern Indiana (Finkel and Wilkinson, 1990); and 800-1500 m in the mid continent region of U.S.A (Railsback, 1993b). However, Bathurst (1975) reported that microstylolites developed in a clay-rich limestone under as little as 90 m of overburden and James and Bone (1989) documented sutured grain contacts in Tertiary limestones buried no more than 100 m. A minimum estimate of burial depth of the Renison dolomites comes from the present thickness of overlying strata, which is 1200 m

in the mine area. In some dolomite samples, stylolites both cut or are cut by veins, indicating formation during early to late burial diagenesis. The cross-cutting relationship between stylolites and different dolomite fabrics indicates that the stylolites were formed during late burial diagenesis (Bathurst, 1987). However, the presence of stylolites in the siderite and massive sulphide zone, which contain talc-chlorite-tourmaline-sulphide minerals, have been related to a hydrothermal origin (Morrison, 1982).

It has been suggested that pressure dissolution features are developed preferentially at a lithological transition, probably due to competency contrasts between adjacent units (Buxton and Sibley, 1981). The data presented here show only one example of a pressure dissolution feature developed at a lithologic contact (see Fig. 10.7 D), and so do not support Buxton and Sibley's (1981) claim. It has been stressed that the style of pressure dissolution is different in various lithologies (Buxton and Sibley, 1981; Railsback, 1993 b). The difference is interpreted to be the result of either preferential cementation or grain size. For example, well cemented and/or grain-supported rocks typically have stylolites, whereas dissolution seams are more common in poorly cemented and/or mud-supported rocks (Buxton and Sibley, 1981; Railsback, 1993 b). The occurrence of stylolites in Renison dolomites suggest that stylolitization was not limited to a specific dolomite type. Stylolites are present in original, early and late diagenetic dolomites regardless of crystal size and textures. However, the presence of stylolites in dolosparite cements may suggest that stylolite development in cement-rich dolosparite does not necessarily result from a stable lithologic framework, but may also be caused by abundance of pressure-soluble cement (possibly Ca-rich dolomite). The development of dissolution seams in Renison dolomite, particularly in dolomicrite, can be attributed to the difference in relative solubility of dolomite crystals, possibly due to the poor ordered nature of some crystals. The higher solubility of the poorly ordered, Ca-rich dolomites has been documented by James et al. (1993).

It has been recorded that increased temperature promotes pressure dissolution (Wetzel, 1989, Railsback, 1993 a). Thus, pressure dissolution in the Renison dolomites may have been enhanced by increasing temperature even at shallow burial during emplacement of the Pine Hill Granite.

13.10 Mineralization

The Neoproterozoic Renison sequence hosts significant stratabound carbonate replacement and vein styles of tin deposits. Mineralization resulted from

the passage of hydrothermal fluids, sourced from Devonian Pine Hill Granite, through major fault structures, partially replacing three dolomite horizons and forming a cassiterite-rich pyrrhotite orebody (Holyland, 1987; Kitto, 1994; Adabi et al., 1996 a, b). The regional fault structures are also attributed to a tensional regime associated with emplacement of the Devonian Pine Hill Granite (Kitto, 1994).

13.11 Metamorphism

Scattered flakes of silicate minerals such as talc and chlorite within different dolomite types have been related to contact metamorphism of original clay minerals, presumably formed during emplacement of the Pine Hill Granite (Morrison, 1982). Such metamorphism has not significantly affected the texture and composition of the original dolomites. However, Morrison (1982) suggested that there is evidence that contact metamorphism has modified local carbonate composition. The silicate minerals of the contact metamorphism are readily distinguished from their hydrothermal counterparts on the basis of composition. For example, contact metamorphic talc and chlorite are characterized by much lower iron content than their hydrothermal counterparts (Morrison, 1982).

13.12 Fracturing

Fracturing in the Renison dolomites can be related mainly to the tectonic activity during emplacement of the Pine Hill granite. However, few fractures are associated with pressure dissolution textures (S574, 76 m). The most intense fracturing occurred in the dolomite samples close to the faults and mineralized area (e.g., S574, 30 m). Fracturing and mineralization occurred synchronously and also after mineralization (Kitto, 1994).

CHAPTER 14

CONCLUSIONS

CHAPTER 14

CONCLUSIONS

Upper Jurassic Mozduran Formation

The Upper Jurrasic Mozduran Formation is a thick sequence (~1100 m) of limestones, dolomitic limestones, dolomites, mudrocks, and locally thick gypsiferous beds. Nine microfacies have been recognized in the Mozduran Formation: lime mud facies; biofacies; pelmicrite facies; intraclastic facies; oolite and oncolite facies; sandstone facies; mudrock facies; evaporite facies; and dolomite facies. Facies analysis of the Mozduran Formation indicates that sedimentation occurred in a wide range of environments, ranging from supratidal to intertidal, and shallow to relatively deeper subtidal zones. The depositional setting of the Mozduran Formation is interpreted to be a carbonate ramp with a very gentle slope, deepening to the west. The gradual facies transitions, the presence of oolite facies on the most landward margin of the basin and the lack of reefal structures, are evidence of a carbonate ramp setting. During deposition of the Upper Jurassic Mozduran carbonates, a combination of differential sediment loading subsidence and eustatic sea level changes, caused facies and thickness changes across the ramp. Although sedimentological studies suggest a gradual transgression of the Mesozoic sea over the Kopet-Dagh Basin, there are a few periods of minor regression marked by thin siliciclastic beds sporadically throughout the sequence. The formation thickness decreases considerably, from west to east of the study area, grading into near-shore, very shallow water, mostly terrigenous facies. To the west, the Mozduran Formation becomes thicker and changes into off-shore and relatively deeper marine facies. The Mozduran Formation is characterized by continuous bedding, planar lamination, cross lamination, large to small-scale cross bedding, algal structures and abundant well preserved fossils.

Markov chain analysis combined with microfacies techniques confirmed non-random sedimentation, with more than a 90% confidence level. Fischer plots indicate that observed thickness variations in beds are also non-random. The

variation in bed thickness in the Mozduran carbonates is attributed to the total amount of accommodation space provided by subsidence and eustatic sea-level changes.

Brachiopods indicate an early Tithonian-Volgian age for the Mozduran Formation. The brachiopod assemblage show affinities with European forms, especially with those of the Boreal type from Russia. This indicates Iran was part of the European plate during the Upper Jurassic, as has been previously suggested for Turkey (Ager, 1988), on the basis of similar evidence from Mesozoic brachiopods.

Petrographic, elemental and isotopic studies of the Mozduran limestones have been undertaken to determine the original carbonate mineralogy. These studies indicate that aragonite was the dominant primary mineral in the shallowest part of the basin, whilst a mixture of calcite-aragonite minerals were dominant in the relatively deeper part of the basin.

Algal-rich biota, diverse skeletal and non-skeletal grains (mainly ooids and intraclasts), evaporites, and early diagenetic dolomites, are present in the shallowest part of the basin. These are similar to those of modern subtropical shallow marine carbonates. Other petrographic features, such as acicular to fibrous isopachous cements, diffuse laminae within ooids, the presence of aragonite relics within micrites, abundant deformed and spalled ooids, and shattered micritic envelopes, are all evidence for an original aragonite mineralogy in the shallowest part of the basin. In contrast, carbonate samples from the relatively deeper part of the basin contain predominantly calcitic skeletons (mainly crinoids, brachiopods, bryozoa, and forams), radial calcite ooids, bladed and radial fibrous marine calcite cements. The most important features of these carbonates are the abundance of chert and carbonate muds, the absence of bedded evaporites, stromatolites, and gastropods, and decreasing detrital quartz content.

Trace element plots have been used to discriminate between carbonate mineralogy. Sr and Na covariance plots with respect to Mn and particularly Sr/Na ratios in the Mozduran carbonates indicate aragonite and mixture of aragonite-calcite mineralogy in the shallowest and relatively parts of the basin respectively. Sr/Na ratios of >1 indicate original aragonite, whilst Sr/Na ratios of <1 suggest calcite mineralogy. A comparison of the Sr, Na, Sr/Na and Mn fields of limestone samples from the shallowest part of the basin, with those of the subtropical aragonitic Ordovician Gordon Limestones, show that the Mozduran data fall within the aragonitic Ordovician Gordon Limestone field. In contrast, Sr, Na, and Sr/Na plots versus Mn, in the limestone samples from the relatively deeper part of

the basin, show that most of the data fall outside of the aragonitic Mozduran limestone field. These limestone data have a trend similar to that of the Recent marine calcitic temperate carbonate field, possibly due to similar mineralogy.

This study also used $\delta^{18}O$ and $\delta^{13}C$ isotopic criteria to differentiate original carbonate mineralogy. This involved the determination of lines of equilibrium between aragonite and calcite and mixtures of aragonite and calcite, as a function of temperatures, by considering present day average values of $\delta^{18}O$ of seawater (0‰) and $\delta^{13}C$ of atmospheric CO_2 (-7.2‰). The micrite, non-skeletal grains and bulk carbonate data of the Mozduran limestones mostly fall above the $\delta^{18}O$ and $\delta^{13}C$ equilibrium lines, with respect to present day atmospheric CO_2 levels of -7.2‰. The Upper Jurassic PCO_2 levels calculated from the heaviest $\delta^{13}C$ value, corresponding to the heaviest $\delta^{18}O$ value, give an atmospheric $\delta^{13}C$ value of -6.7‰. The $\delta^{18}O$ and $\delta^{13}C$ equilibrium lines of aragonite and aragonite-calcite mixtures, using CO_2 levels of -6.7‰, bisect the Mozduran limestone data. The heavy $\delta^{18}O$ brachiopod values of the Mozduran Formation fall on the shifted temperature equilibrium calcite line, as they are in equilibrium with an atmospheric PCO_2 level of -6.7‰. In contrast, the late mid Jurassic low-Mg calcite belemnites of Scotland and the mid Jurassic calcitic bulk carbonates of England, fall on the calcite equilibrium line, corresponding to an atmospheric PCO_2 level of -7.2‰. The observed $\delta^{18}O$ and $\delta^{13}C$ isotopic trend in the Mozduran limestones results from burial overprinting of earlier meteoric diagenesis. This interpretation is supported by trace element and petrographic studies.

The heaviest $\delta^{18}O$ value of micrite gives a seawater temperature of 16° C, whereas the heaviest and least-altered value of brachiopods corresponds to a warm seawater temperature of ~26° C. The temperature fluctuations in the Mozduran Formation are similar to those in the subtropical Persian Gulf, where temperatures fluctuate in the coastal areas from 40° C in summer to 15° C in winter.

The Mozduran limestones contain a variety of early to late carbonate cements, precipitated in marine, meteoric and burial diagenetic environments. The early cements exhibit variable morphology. These include: acicular to fibrous isopachous crystals; bladed and equant isopachous crystals; radial fibrous crystals; micritic cement; and turbid syntaxial rims, on echinoderm debris. Acicular to fibrous cements, which indicate original aragonite mineralogy, are only present in the shallowest part of the basin, whilst calcite cements are dominant in the relatively deeper part of the basin. These variations in cement carbonate mineralogy are related mainly to seawater temperature. Almost all early

isopachous marine cements are dull to non-luminescent. The marine cement is enriched in $\delta^{18}O$ (–2.4‰ PDB) and $\delta^{13}C$ (+ 3.6‰ PDB) values, compared with meteoric and burial calcite cements. These isotopic values of marine cement are within the range of those of modern warm water carbonate sediments.

Evidence of meteoric cementation in the Mozduran limestones includes the calcite crystal morphology (mainly drusy mosaic and play), very bright yellow luminescence, and lighter average oxygen ($\delta^{18}O$= –6.2‰ PDB) and carbon ($\delta^{13}C$= -1.6‰ PDB) values, compared to marine calcite cement. The meteoric calcite cements are most abundant in samples from the shallowst part of the basin.

Burial cementation is inferred from the calcite crystal morphology, paucity of cement (particularly prior to compaction), more positive carbon (up to ~+3.8‰ PDB), and very depleted oxygen (~-8‰ PDB) values, and the presence of dull luminescent cement, compared to marine and meteoric cements. The burial calcite cement, was mostly present in samples from the relatively deeper part of the basin.

Cathodoluminescence petrography and carbon and oxygen analysis indicate that calcite veins were precipitated in both meteoric and burial diagenetic environments.

Petrographic and geochemical studies reveal that five different varieties of dolomite have resulted from multistage dolomitization. Dolomitization in the Mozduran Formation has occurred either by penecontemporaneous or early replacement of carbonate mud (dolomite type 1) or replacement of precursor calcium carbonate (dolomite types 2, 3, and 4), and by direct precipitation in voids, vugs and fractures (dolomite type 5). In completely dolomitized parts of the sequence, the dolomite crystal size and crystal boundary shape varies from unimodal to polymodal, and from nonplanar to planar-s texture. In contrast, dolomite crystals floating within a calcitic matrix and those lining voids and vugs, show a planar-e (euhedral) texture.

On the basis of crystal size and fabric, preserved traces of depositional textures, and the most enriched $\delta^{18}O$ value (–1.1‰ PDB), dolomite type 1 is considered to have been formed in a supratidal to upper intertidal setting, under near surface, low temperature (~34° C) conditions, with Mg possibly derived from seawater.

Other dolomite types exhibit many of the characteristics associated with shallow to deep burial dolomitization. Dolomite type 2 probably formed during early shallow burial. This interpretation is based on crystal size and fabric, dolomite formation in pre-and post-stylolitization, and relatively heavier $\delta^{18}O$ values compared to dolomite types 3, 4, and 5. The most probable source of Mg in

dolomite type 2 may be from the dissolution of high-Mg calcite. Dolomite type 3 is considered to have formed in shallow to intermediate burial depths. The planar crystal boundaries, relatively lower range and average $\delta^{18}O$ values (compared to dolomite types 4 and 5), and intermediate temperature of formation, support the proposed shallow to intermediate burial origin. Dolomite type 4 is recognized as a product of late (deeper) burial diagenesis. This interpretation is based on several lines of evidence including, crystal size and fabric (nonplanar texture), very depleted $\delta^{18}O$ values, and an inferred elevated temperature, ranging from 84 to 113° C. Dolomite type 5, which consists of coarsely crystalline planar-C (cement) dolomite, comprises the last dolomitizing event. The occurence as void-filling cement in late stage fractures and vugs, cross-cutting of other dolomite types, very depleted $\delta^{18}O$ values, and the elevated temperature of formation, support a late burial diagenetic origin. Dolomite types 4 and 5, with the highest temperatures of formation, compared to other dolomite types, probably formed during the period of maximum burial (at depths of ~3.5 to -4.5 km), between Paleocene and Eocene time. Compaction of shales combined with basinal brines are two possible sources of magnesium for shallow to deep burial dolomitization (dolomite types 3, 4) and for burial dolomite cementation (dolomite type 5).

The presence of higher concentrations of organic carbon in dolomites than limestones may indicate that dolomitization is favored in limestones that originally had higher concentrations of organic matter.

Renison Mine Carbonates

Dolomites and associated clastic sediments of the late Proterozoic, at Renison in western Tasmania, host significant stratabound replacement tin deposits. These deposits occur within the central region of the Dundas Trough which consists of Proterozoic to early Paleozoic sedimentary rocks.

The petrographic, elemental and isotopic compositions of Renison dolomite outside and within the mineralized area are summarized below.

Four major types of dolomite (dolomicrite, dolomicrosparite, dolosparite and coarsely crystalline dolomite) occur in the Neoproterozoic sequence studied outside of the Renison mine area. These dolomite types can be separated and recognised mainly on the basis of grain size, Mg%, Mn and Fe content and $\delta^{18}O$ values. The petrographic and geochemical differences within the dolomite types clearly show that the dolomicrites are genetically unrelated to other dolomite types and thus, represent a different dolomitization event. The dolomicrites probably formed at near surface by either direct precipitation or during very early

diagenesis, with Mg^{2+} being supplied by seawater. This conclusion is based on several petrographic and geochemical features of the dolomicrites, which include:

- the micritic nature of the most least-altered dolomite
- well preserved original structure of some grains such as intraclasts and cryptalgal fragments
- finely laminated dolomite (1-3 mm thick)
- low Fe and Mn concentrations in dolomicrites relative to coarser diagenetic dolomites
- positive relation between Mg and $\delta^{18}O$ values and an inverse relationship between Mn, Fe and $\delta^{18}O$ values in dolomicrites
- very heavy oxygen (<-2‰) and heavy carbon values (>+3.5‰ up to 7.5‰) in the most finely crystalline dolomicrites

The well preserved fabric and low Sr and Na values in the least-altered dolomicrites in Renison samples argue against original aragonite mineralogy. The pronounced oxygen and carbon enrichment in almost all dolomicrite samples, also supports the lack of dissolution or alteration of a pre-existing metastable carbonate phase such as aragonite.

The calculated paleotemperature of seawater during the Neoproterozoic (considering δ_w = -6‰ and the least-altered dolomite $\delta^{18}O$ value of -1 ± 1‰), was around 8 ± 4° C (Irwin equation) or 12 ± 4° C (Land equation). This cool to cold water marine origin is further supported by the presence of diamictites in the Renison sequences and glacial erratics in the Smithton Dolomite, which correlate with the Renison dolomites.

Features of Renison least-altered dolomites that may have environmental significance include:

- the presence of microbial fabrics and intraclastic grains
- the micritic nature of most dolomites which are associated with silt-sized detrital quartz grains
- the rare oolitic textures
- the general lack of evaporites or their pseudomorphs
- the presence of fenestral fabrics

Sedimentological features of the least-altered dolomicrites support deposition mainly in a marine shallow intertidal to supratidal environment, possibly under a climate with considerable seasonal variation.

Other dolomite types are mostly epigenetic in origin and probably began to form at shallow levels of burial, and continued to form over a range of depths and temperatures. This is supported by their textures, relatively high Mn and Fe

concentrations, very depleted $\delta^{18}O$, and positive correlation between $\delta^{18}O$ and $\delta^{13}C$ values. The Mg is probably supplied mainly by compaction of underlying shales. Some of the coarsely crystalline dolomites occurred along large and small-scale fractures or veins, and have the most depleted $\delta^{18}O$ values.

The carbon isotope chemostratigraphy of the least-altered Renison dolomites, gives an age range of between 570-820 Ma (Cryogenian to Neoproterozoic III). This is older than that previously suggested by other researchers.

Petrographic features, major and minor elements, together with $\delta^{18}O$ and $\delta^{13}C$ studies, indicate that the Renison dolomites, within the mineralized area, have been altered mainly by diagenetic and hydrothermal processes that have progressively oblitrated original depositional textures. The variations in intensity of alteration are mainly dependent on proximity to fractures, faults or mineralization.

Dolomite within the mineralized area is divided into five different types, based on crystal size and mode of origin. These include: dolomite cements (dolomicrite, dolosparite), recrystallized dolomites (dolomicrosparite and coarsely crystalline dolomite) and vein dolomite. Renison carbonates range mainly from ferroan dolomite to ankerite with minor siderite and calcite. Dolomite samples from the mineralized area contain more generations of variable luminescence, than those samples from the unmineralized area. This reflects a more complex fluid history in the vicinity of the Renison mine area. Multiple cross-cutting veins, brecciation, crack-seal textures, recrystallization, silicification, deformation and oblitration of original texture, is more pronounced in these dolomite samples than in the dolomites from the unmineralized area. Less recystallized dolomites generally have more Ca and Mg, less Mn and Fe, and heavier $\delta^{18}O$ and $\delta^{13}C$ values than strongly recrystallized samples. The range of Ca, Mg, Mg/Ca, Sr, Fe, Mn and $\delta^{18}O$ and $\delta^{13}C$ values from the least to most altered dolomites, suggest that magmatic-meteoric hydrothermal fluid infiltration has occurred.

The $\delta^{18}O$ and $\delta^{13}C$ values of the most altered dolomites indicate that temperatures were up to 350° C for magmatically derived hydrothermal fluids. These temperatures are similar to those obtained from fluid inclusion studies and from calculations based on $\delta^{18}O$ variations in vein quartz.

Dolomite-fluid $\delta^{18}O$ and $\delta^{13}C$ fractionation curves that best fit the Renison $\delta^{18}O$ and $\delta^{13}C$ carbonate data and fluid inclusion temperatures are for an early stage Devonian magmatic fluid ($\delta^{18}O_{SMOW}$ = +9‰, $\delta^{13}C_{PD}$ = -5‰), followed by late-stage mixtures of temperate Devonian meteoric water and

magmatic fluids.

Isotherms on a $\delta^{18}O$ and $\delta^{13}C$ covariance plot illustrate that isotopic variation in the Renison carbonates is a result of changing temperatures and water/rock interactions. Water/rock ratios may have been as high as 6 (open system) in the carbonate horizons close to the replacement orebodies, and decreased with declining temperatures away from mineralization. X_{H2CO3} values in solution may have increased from 0.01 to 0.1 molal during dolomite dissolution.

Renison siderites were potentially in equilibrium with a magmatic hydrothermal fluid with temperatures from 150 to 350° C, and having initial $\delta^{18}O_{SMOW}$ and $\delta^{13}C_{PDB}$ values of +9‰ and -5‰ respectively. Similarly, the dolomites were potentially in equilibrium with fluid temperatures from 20 to 190° C and formed from either magmatic or mixed magmatic-meteoric fluids.

Mineralization resulted from the passage of hydrothermal fluids, sourced from the underlying Devonian Pine Hill Granite, through major faults and fractures, partially to completly replacing three dolomite horizons, and forming a cassiterite-rich pyrrhotite orebody. Mixing of magmatic fluids with meteoric water was possible during the Devonian Tabberabberan Orogeny. The proportion of meteoric water that infiltrated late into the Renison hydrothermal system was potentially as high as 65% by volume.

REFERENCES

REFERENCES

ADABI, M.H., 1991. Trace elements and stable isotope variations in Mozduran carbonates (Upper Jurassic), eastern Kopet-Dagh Basin: 9th Geol. Symp. Iran, Geol. Survey of Iran, (abst), p. 34-40.

ADABI, M.H., 1992. Diagenetic trend of Upper Jurassic carbonates (Oxfordian-Titonian) in Sarakhs area: 10th Geol. Symp. Iran, Geol. Survey of Iran, (abst), p. 109-112.

ADABI, M.H., 1997 (in press). Application of carbon isotope chemostratigraphy to the Renison dolomites (Tasmania, Australia): a Neoproterozoic age: Australian. Jour. Earth Sci., v. 44, No. 3.

ADABI, M.H., and AGER, D.V., 1997 (in press). Upper Jurassic brachiopods from North-East of Iran: Palaeontology, v. 40, part 1.

ADABI, M.H., and MOUSSAVI-HARAMI, R., 1986. Geomorphology of Eastern Kopet-Dagh Basin: in Papoli, M.H., (ed.): Inter. Geog. Seminar Mashhad, Iran, v.1, p. 87-104.

ADABI, M.H., and RAO, C.P., 1991. Petrographic and geochemical evidence for original aragonitic mineralogy of Upper Jurassic carbonates (Mozduran Formation), Sarakhs area, Iran: Sed. Geology, v.72, p. 253-267.

ADABI, M.H., and RAO, C.P., 1996. Petrographic, elemental and isotopic criteria for the recognition of carbonate mineralogy and climates during the Jurassic (examples from Iran and England): 13th Geol. Conv. Australia, (abst), p. 6.

ADABI, M.H., RAO, C.P., and KITTO, P.A., 1996a. The source of hydrothermal fluids responsible for carbonate alteration, Renison, Tasmania, Australia: 13th Geol. Conv. Australia, (abst), p. 7.

ADABI, M.H., RAO, C.P., and KITTO, P.A., 1996b. Elemental and isotopic composition of Late Proterozoic dolomites indicative of hydrothermal alteration, Renison, Tasmania, Australia: Econ. Geology (submitted).

ADAMS, A.E., MACKENZIE, W.S., and GUILFORD, C., 1984. Atlas of Sedimentary Rocks Under the Microscope: Longman, Harlow, 104 p.

ADAMS, A.E., and SCHOFIELD, K., 1983. Recent submarine aragonite, magnesian calcite, and hematite cements in a gravel from Islay, Scotland: Jour. Sed. Petrology, v.53, p.417-421.

AFSHAR-HARB, A., 1970. Geology of Sarakhs area and Khangiran gas field: Geol. Division, Expl. and Prod. Group, N.I.O.C., p. 1-17.

AFSHAR-HARB, A., 1979. The stratigraphy, tectonics and petroleum geology of the Kopet-Dagh region, northern Iran: Unpub. Ph.D.thesis, Imperial College London, 316p.

AFSHAR-HARB, A., 1982. Geological map of Sarakas area: Ministry of Petrol. N.I.O.C. Expl. and Prod. Tehran, 1 sheet.

AGER, D.V., 1975. The Jurassic world ocean: in Finstad, K., and Selley, R.C., (eds.), Proc. Jurassic Northern North Sea Symp: Norw. Pet. Soc. Oslo, p. 1-29.

AGER, D.V., 1988. Mesozoic Turkey as part of Europe: in Audley-Charles, M.G. and Hallam,

A., (eds.), Gondwana and Tethys: Geol. Soc. London, Spec. Pub. No. 37, p. 241-245.

AHARON, P., SCHIDLOWSKI, M., and SINGH, I.B., 1987. Chronostratigraphic markers in the end-Precambrian carbon isotope record of the Lesser Himalaya: Nature, v. 327, p.699-702.

AISSAOUI, D.M., 1988. Magnesian calcite cements and their diagenesis: dissolution and dolomitization, Mururoa Atoll: Sedimentology, v. 35, p. 821-841.

AL-AASM, I.S., and VEIZER, J., 1986. Diagenetic stabilization of aragonite and low-Mg calcite, II. Stable isotopes in rudists: Jour. Sed. Petrology, v. 56, p. 763-770.

ALLAN, J.R., and MATTHEWS, R.K., 1982. Isotope signatures associated with early meteoric diagenesis: Sedimentology, v. 29, p. 797-817.

AMTHOR, J.E., and FRIEDMAN, G.M., 1991. Dolomite-rock textures and secondary porosity development in Ellenburger Group carbonates (Lower Ordovician), west Texas and southern New Mexico: Sedimentology, v. 38, p. 343-362.

AMTHOR, J.E., and FRIEDMAN, G.M., 1992. Early-to late-diagenetic dolomitization of platform carbonates: Lower Ordovician Ellenburger Group, Permian Basin, West Texas: Jour. Sed. Petrology, v. 62, p. 131-144.

ANDERSON, T.F., and ARTHUR, M.A., 1983. Stable isotopes of oxygen and carbon and their application to sedimentologic and paleoenvironmental problems: in Stable Isotopes in Sedimentary Geology: Soc. Econ. Paleontol. Mineral., Short Course, v. 10, Section 1.1-1.151.

ANDERTON, R., BRIDGES, P.H., LEEDER, M.R., and SELLWOOD, B.W., 1979. A Dynamic Stratigraphy of the British Isles; A Study in Crustal Evolution: George Allen and Unwin, London, 301p.

ASMEROM, Y., JACOBSEN, S.B., KNOLL, A.H., BUTTERFIELD, N.J., and SWETT, K., 1991. Strontium isotopic variations of Neoproterozoic seawater: implications for crustal evolution: Geochim. Cosmochim. Acta, v. 55, p. 2883-2894.

ATWOOD, D.K., and BUBB, J.N., 1970. Distribution of dolomite in a tidal flat environment, Sugarloaf Key, Florida: Jour. Geology, v. 78, p.499-505.

AURELL, M., and MELENDEZ, A., 1993. Sedimentary evolution and sequence stratigraphy of the Upper Jurassic in the Central Iberian Chain, northeast Spain: in Posamentier, H.W., Summerhayes, C.P., Haq, B.U., and Allen, G.P., (eds.), Sequence Stratigraphy and Facies Associations: Inter. Assoc. Sed. Spec. Pub. v. 18, p. 343-368.

BANKS, M.R., 1962. Cambrian system, in the geology of Tasmania: Jour. Geol. Soc. Aust., v. 9 (2), p. 127-145.

BARBIN, V., RAMSEYER, K., DEBENAY, J.P., SCHEIN, E., ROUX, M., and DECROUEZ, D., 1991. Cathodoluminescence of Recent biogenic carbonates: an environmental and ontogenetic fingerprint: Geol. Mag., v. 128, p. 19-26.

BARNABY, R.J., and READ, J.F., 1992. Dolomitization of a carbonate platform during late burial: Lower to Middle Cambrian Shady Dolomite, Virginia Appalachian: Jour. Sed. Petrology, v. 62, p.1023-1043.

BARNOLA, J.M., RAYNAULD, D., KOROTKEVICH, Y.S., and LORIUS, C., 1987. Vostok ice core provides 160,000 years record of atmospheric CO_2: Nature, v. 329, p. 408-414.

BATHURST, R.G.C., 1975. Carbonate sediments and their diagenesis: Elsevier, North Holland, 658 p.

BATHURST, R.G.C., 1987. Diagenetically enhanced bedding in argillaceous platform limestones: stratified cementation and selective compaction: Sedimentology, v. 34, p. 749-778.

BEHRENS, E.W., and LAND, L.S., 1972. Subtidal Holocene dolomite, Baffin Bay, Texas: Jour. Sed. Petrology, v. 42, p. 155-161.

BERBERIAN, M., and KING, G.C.P., 1981. Towards a paleogeography and tectonic evolution of Iran: Canadian Jour. Earth Sci., v. 18, p. 210-265.

BERNER, R.A., and CANFIELD, D.E., 1989. A new model for atmospheric oxygen over Phanerozoic time: Am. Jour. Sci., v. 289, p. 333-361.

BERNER, R.A., 1990. Atmospheric carbon dioxide levels over Phanerozoic time: Science, v. 249, p. 1382-1386.

BERRY, R.F., 1989. The history of movement on the Henty Fault Zone, western Tasmania: an analysis of fault striation: Aust. Jour. Earth Sci., v. 36, p. 189-206.

BERRY, R.F., and CRAWFORD, A.J., 1988. The tectonic significance of the Cambrian allochthonous mafic-ultramafic complexes in Tasmania: Aust. Jour. Earth Sci., v. 35, p. 161-171.

BEZNOSOV, N.V., GORBATCHIK, T.N., MIKHAILOVA, I.A., and PERGAMENT, M.A., 1978. Soviet Union: in Moullade, M., and Nairn, A.E.M., (eds.), The Phanerozoic geology of the World II, The Mesozoic: Amsterdam, Elsevier, 529p.

BHATTACHARYYA, A., and FRIEDMAN, G.M., 1979. Exprimental compaction of ooids and lime mud and its implication for lithification during burial: Jour. Sed. Petrology, v. 49, p. 1279-1286.

BHATTACHARYYA, A., and FRIEDMAN, G.M., 1984. Exprimental compaction of ooids under deep-burial diagenetic temperatures and pressures: Jour. Sed. Petrology, v. 54, p. 362-372.

BLISSETT, A.H., 1962. Zeehan: Hobart, Tasmania Geol. Survey, Expl. Rept., 272 p.

BOGGS, S.Jr., 1987. Principles of sedimentology and stratigraphy: Merrill, Pub., Company, USA, 784 p.

BONE, Y., and JAMES, N.P., 1993. Bryozoans as carbonate sediment producers on the cool-water Lacepede Shelf, southern Australia: Sed. Geology, v. 85, p. 247-271.

BOSE, P.K., 1979. Penecontemporaneous dolomitization in the Precambrian Bhander limestone, Rajasthan, India - a petrographic attestation: Geologische Rundschau, v. 68, p. 680-695.

BOSS, S.K., and RASMUSSEN, K.A., 1995. Misuse of Fischer plots as sea-level curves: Geology, v. 23, p. 221-224.

BOWMAN, J. R., COVERT, J. J., CLARK, A. H., and MATHIESON, G. A., 1985. The CanTung E Zone scheelite skarn orebody, Tungsten, Northwest Territories: oxygen, hydrogen, and carbon isotope studies: Econ. Geology, v. 80, p.1872-1895.

BRAND, U., and MORRISON, J.O., 1987. Biogeochemistry of fossil marine invertebrates: Geosci. Canada, v. 14, p. 85-107.

BRAND, U., and VEIZER, J., 1980. Chemical diagenesis of multicomponent carbonate system, II: stable isotopes: Jour. Sed. Petrology, v. 51, p. 987-997.

BRASIER, M.D., ANDERSON, M.M., and CORFIELD, R.M., 1992. Oxygen and carbon isotope

stratigraphy of early Cambrian carbonates in southeastern Newfounland and England: Geol. Mag., v. 129, p.265-279.

BRICKER, O.P., 1971. Carbonate Cements: Johns Hopkins Press, Baltimore, 376p.

BROOKFIELD, M.E., 1988. A mid-Ordovician temperate carbonate shelf - the Blac River and Trenton Limestone Groups of southern Ontario, Canada: Sed. Geology, v. 60, p. 137-153.

BROOKFIELD, M.E., 1994. Problems in applying preservation, facies and sequence models to Sinian (Neoproterozoic) glacial sequences in Australia and Asia: Precambrian Res., v. 70, p. 113-143.

BROOKS, C., 1966. The Rb/Sr ages of some Tasmanian igneous rocks: Jour. Geol. Soc. Aust., v. 13, p. 457-469.

BROOKS, C., and COMPSTON, W., 1965. The age and initial 87Sr/86Sr of the Heemskirk Granite, western Tasmania: Jour. Geophys. Res., v. 70, p. 6249- 6262.

BROWN, A.V., 1986. Geology of the Dundas-Mt Lindsay-Mt Ramsay area: Tasmania Geol. Survey Bull., v. 62, 221 p.

BROWN, A.V., 1989. Eo-Cambrian-Cambrian: in Burrett, C.F., and Martin, E.L., (eds.), Geology and mineral resources of Tasmania: Geol. Soc. Aust. Spec. Pub., No. 15, p. 47-83.

BROWN, P. E., BOWMAN, J. R., and KELLY, W. C., 1985. Petrologic and stable isotope constraints on the source and evolution of skarn-forming fluids at Pine Creek, California: Econ. Geology, v. 80, p. 72-95.

BUCHBINDER, B., and FRIEDMAN, G.M., 1970. Selective dolomitization of micritic envelopes: a possible clue to original mineralogy: Jour. Sed. Petrology, v. 40, p. 514-517.

BUDD, D.A., 1983. Fresh-water diagenesis of 700-year old ooid sands, Schooner Cays, Bahamas (abst): Geol. Soc. Amer. Ann. Mtg., v. 15, 535p.

BUDD, D.A., 1992. Dissolution of high-Mg calcite fossils and the formation of biomolds during mineralogical stabilization: Carbonates and Evaporites, v. 7, p. 74-81.

BUDYKO, M.I., and RONOV, A.B., 1979. Chemical evolution of the atmosphere in the Phanerozoic: Geochim. International, v. 16, p. 1-9.

BUDYKO, M.I., RONOV, A.B., and YANSHIN, A.L., 1985. Changes in the chemical composition of the atmosphere during the Phanerozoic: Int. Geology, v. 27, p. 423-433.

BURDETT, J.W., GROTZINGER, J.P., and ARTHUR, M.A., 1990. Did major changes in the stable-isotope composition of Proterozoic seawater occur?: Geology, v.18, p. 227-230.

BURTON, E.A., 1988. Laboratory investigation of the effects of seawater chemistry on carbonate mineralogy: Unpub. Ph.D. thesis, Washington University, St.Louis, MO.

BURTON, E.A., and WALTER, L.M., 1987. Relative precipitation rates of aragonite and Mg calcite from seawater: temperature or carbonate ion control?: Geology, v. 15, p. 111-114

BURTON, E.A., and WALTER, L.M., 1991. The effects of PCO_2 and temperature on magnesium incorporation in calcite in seawater and Mg Cl_2-$CaCl_2$ solutions: Geochim. Cosmochim. Acta, v. 55, p. 777-785.

BUXTON, T.M., and SIBLEY, D.F., 1981. Pressure solution features in a shallow buried limestone: Jour. Sed. Petrology, v. 51, p. 19-26.

CALVER, C.R., 1989. The Weld River Group: a major Upper Precambrian dolomite sequence in southern Tasmania: Papers and Proc. Roy. Soc. Tasmania, v. 123, p. 43-53.

CALVER, C.R., 1995. Ediacarian isotope stratigraphy of Australia: Unpub. Ph.D. thesis, Macquarie Univ., 328 p.

CAMPANA, B., and KING, D., 1963. Palaeozoic tectonic, sedimentation and mineralisation in West Tasmania: Geol. Soc. Australia Jour., v. 10, p. 1-54.

CANDER, H.S., KAUFMAN, J., DANIELS, L.D., and MEYERS, W.J., 1988. Regional dolomitization of shelf carbonates in the Burlington-Keokuk Formation (Mississippian), Illinois and Missouri: constraints from cathodoluminiscent zonal stratigraphy: in Shukla, V.J., and Baker, P.A., (eds.), Sedimentology and Geochemistry of Dolostones: SEPM., Spec. Pub., v.43, p. 129-144.

CANNARD, C., 1991. Renison Bell Tin Mine ore reserves report: Unpub. Rept., Renison, Ltd., 143 p.

CANT, D.J., and WALKER, R.G., 1976. Development of a braided fluvial facies model for Devonian Battery Point sandstone, Quebec, Canada: Jour. Earth Sci., v. 13, p. 102-119.

CARBALLO, J.D., LAND, L.S., and MISER, D.E., 1987. Holocene dolomitization of supratidal sediments by active tidal pumping, Sugarloaf Key, Florida: Jour. Sed. Petrology, v. 57, p. 153-165.

CAROTHERS, W. W., ADAMI, L. H., and ROSENBAUER, R. J., 1988. Experimental oxygen isotope fractionation between siderite-water and phosphoric acid liberated CO_2-siderite: Geochim. Cosmochim. Acta, v. 52, p. 2445-2450.

CAROZZI, A.V., 1960. Microscopic Sedimentary Petrography: New York-London, John Wiley, 485 p.

CARPENTER, S.J., and LOHMANN, K.C., 1992. Sr/Mg ratios of modern marine calcite: empirical indicators of ocean chemistry and precipitation rate: Geochim. Cosmochim. Acta, v. 56, p. 1817-1849.

CARR, T.R., 1982. Log-linear models, Markov chain and cyclic sedimentation: Jour. Sed. Petrology, v. 52, p. 905-912.

CATALOV, G.A., 1983. Triassic oncoids from Central Balkanides (bulgaria): in Peryt, T.M., (ed.), Coated Grains: Springer-Verlag, Berlin, p. 398-408.

CHOQUETTE, P.W., and JAMES, N.P., 1987. Diagenesis in Limestones-3. The Deep Burial Environment: Geosci. Canada, v. 14, p. 3-35.

CHRISTIE-BLICK, N., 1982. Pre-Pleistocene glaciation on Earth; implications for climatic history of Mars: Icarus, v. 50, p. 423-443.

COLLINS, L.B., 1988. Sediments and history of the Rottnest Shelf, southwest Australia: a swell-dominated, non-tropical carbonate margin: in Nelson, C.S., (ed.), Non-tropical Shelf Carbonates–Modern and Ancient: Sed. Geology, v. 60, p. 15-49.

COLLINS, P.L.F., 1972. The geology and mineralization of the Renison tin mine, Renison Bell: Unpub. B.Sc. Honours thesis, Univ. Tasmania, 151 p.

COLLINS, P.L.F., 1981. The Geology and genesis of the Cleveland tin deposit, western Tasmania: fluid inclusion and stable isotopes studies: Econ. Geology, v. 76, p. 365-392.

CONDOR, H., 1918. The tin field of North Dundas: Geol. Surv. Tas. Bull. No. 26.

CONIGLIO, M., JAMES, N.P., and AISSAOUI, D.M., 1988. Dolomitization of Miocene carbonates, Gulf of Suez, Egypt: Jour. Sed. Petrology, v. 58, p. 100-119.

CONNOLLY, J.R., and VON der BORCH, C.C., 1967. Sedimentation and physiography of the sea floor south of Australia: Sed. Geology, v. 1 p. 181-220.

CORBETT, K.D., 1981. Stratigraphy and mineralisation in the Mt. Read Volcanics, Western Tasmania: Econ. Geology, v. 76, p. 209-230.

CORBETT, K.D., 1992. Stratigraphic-volcanic setting of massive sulfide deposits in the Cambrian Mount Read Volcanics, Tasmania: Econ. Geology, v. 87, p. 564-586.

CORBETT, K.D., and TURNER, N.J., 1989. Early Palaeozoic deformation and tectonics: in Burrett, C.F., and Martin, E.L., (eds.), Geology and Mineral Resources of Tasmania: Geol. Soc. Aust. Spec. Pub., No. 15, p. 154-181.

COWIE, J.W., and BASSETT, M.G., 1989. Global Stratigraphic Chart: Inter. Union Geol. Sci., 1p.

COX, S.F., and ETHERIDGE, M.A., 1983. Crack-seal fibre growth mechanisms and their significance in the development of oriented layer silicate microstructures: Tectonophysics, v. 92, p. 147-170.

CRAIG, H., 1965. The measurment of oxygen isotope palaeotemperatures: in Tongiorgi, E., (ed.), Stable Isotopes in Oceanographic Studies and Palaeotemperatures: Consiglio Nazionale delle Richerche, Labortorio d Geologia Nucleare, Pisa, p. 161-182.

CRAIG, H., and GORDON, L.I., 1965. Deuterium and oxygen-18 variations in the ocean and the marine atmosphere: in Stable Isotopes in Oceanographic Studies and Paleotemperatures: Consiglio Nazionale delle Ricerche, Lab. di Geol. Nucleare, Pisa, p. 1-22.

CRAWFORD, A.J., CORBETT, K.D., and EVERARD, J.L., 1992. Geochemistry of the Cambrian volcanic-hosted massive sulfide-rich Mount Read Volcanics, Tasmania, and some tectonic implications: Econ. Geology, v. 87, p. 597-619.

CROWLEY, T.J., and NORTH, G.R., 1991. Paleoclimatology: Oxford Univ. Press, 339p.

DALZIEL, I.W.D., 1992. Antarctica; a tale of two supercontinents: Ann. Rev. Earth Planet Sci., v. 20, p. 501-526.

DANSGAARD, W., 1964. Stable isotopes in precipitation: Tellus, v. 16, p. 436-468.

DAVIES, B.M., 1985. The nature and mechanism of stratabound mineralisation in the Renison Mine: Unpub. Ph.D. thesis, James Cook Univ. Queensland.

DeGIOVANI, W.F., SALATI, E., MARINI, O.J., and FRIEDMAN, I., 1974. Unusual isotopic composition of carbonates from the Irati Formation, Brazil: Geological Soc. Am. Bull., v. 85, p. 41-44.

DEINES, P., and GOLD, D.P., 1973. The isotopic composition of carbonatite and kimberlite carbonates and their bearing on the isotopic composition of deep-seated carbon: Geochim. Cosmochim. Acta, v. 37, p. 1709-1733.

DEINES, P., LANGMUIR, D., and HARMON, R.S., 1974. Stable carbon isotope ratios and the existence of a gas phase in the evolution of carbonate ground water. Geochim. Cosmochim. Acta, v. 38, p. 1147-1164.

DEMICCO, R.V., and HARDIE, L.A., 1994. Sedimentary Structures and Early Diagenetic Features of Shallow Marine Carbonate Deposits: SEPM Atlas Series No.1. Tulsa, Oklahoma, U.S.A., 265p.

DERRY, L.A., KAUFMAN, A. J., and JACOBSEN, S.B., 1992. Sedimentary cycling and environmental change in the Late Proterozoic: evidence from stable and radiogenic isotopes: Geochim. Cosmochim. Acta, v. 56, p. 1317-1329.

DICKSON, J.A.D., 1965. A modified staining technique for carbonates in thin section: Nature, v. 205, p. 587.

DJAKIC, A.W., 1981. Geology and formation of the Red Rock (Lower Cambrian chert-bearing horizon) West Tasmania: Unpub. B.Sc. Honours thesis, Univ. Tasmania, 151 p.

DOMACK, E.W., 1988. Biogenic facies in the Antarctic glacimarine environment: basis for a polar galcimarine summary: Palaeogeogr. Palaeoclimatol. Palaeoecol., v. 63, p. 357-372.

DOYLE, P., 1987. Lower Jurassic-Lower Cretaceous belemnite biogeography and the development of the Mesozoic boreal realm: Palaeogeogr. Palaeoclimatol. Palaeoecol., v. 61, p. 237-254.

DOYLE, P., 1992. A review of the biogeography of Cretaceous belemnites: Palaeogeogr. Palaeoclimatol. Palaeoecol., v. 92, p. 207-216.

EDWARDS, R.J., 1979. Tasman and Coral sea ten year mean temperature and salinity fields, 1967-1976: CSIRO Div. Fish. Oceanogr. Rep. v. 88, p. 1-4.

EFTEKHARNEZHAD, J., and BEHROZI, A., 1989. New evidence to consider Kopet-Dagh as northern extension of Afro-Arabian Palaeozoic platform (abst): 28th Inter. Geol. Congress, Washington, D.C., V. 1, p. 436-437.

ELLIS, P.M., WILSON, R.C.L., and LEINFELDER, R.R., 1990. Controls on Upper Jurassic carbonate buildup development in the Lusitanian Basin, Portugal: in Tucker, M.E., Wilson, J.L., Crevello, P.D., Sarg. J.R., and Read, J.F., (eds.), Carbonate Platforms, facies, sequences and evolution: Inter. Assoc. Sed. Spec. Pub., v. 9, p. 169-202.

ELLISTON, J., 1954. The geology of the Dundas district, Tasmania: Roy. Soc. Tasmania Paper Proc., v. 88, p. 161-183.

ELMI, S., 1990. Stages in the evolution of late Triassic and Jurassic carbonate platforms: the western margin of the Subalpine Basin (Ardèche, France): in Tucker, M.E., Wilson, J.L., Crevello, P.D., Sarg. J.R., and Read, J.F., (eds.), Carbonate Platforms, facies, sequences and evolution: Inter. Assoc. Sed. Spec. Pub., v. 9, p. 109-144.

EMBLETONE, B.J.J., and WILLIAMS, G.E., 1986. Low palaeolatitude of deposition for late Precambrian periglacial varvites in South Australia: implications for palaeoecology: Earth Planet. Sci.Lett., v. 79, p. 410-430.

EMILIANI, C., 1954. Depth habitats of some species of pelagic foraminifera as indicated by oxygen isotope ratio: Am. Jour. Sci., v. 252, p. 149-158.

EPSTEIN, S., BUCHSBAUM, R., LOWENSTAM, H.A., and UREY, H.C., 1953. Revised carbonate water isotopic temperature scale: Geol. Soc. Am. Bull., v. 64, p. 1315-1326.

EREZ, J., 1978. Vital effect on stable isotope composition seen in foraminifera and coral skeletons: Nature, v. 273, p. 199-202.

ETHIER, V.G., 1975. Application of Markov analysis to the Banff Formation (Mississippian), Alberta: Math. Geol., v. 7, p. 47-61.

FAIRCHILD, I.J., 1980. Sedimentation of a late Precambrian dolomite from Scotland: Jour. Sed. Petrology, v. 50, p. 423-446.

FAIRCHILD, I.J., and SPIRO, B., 1987. Petrological and isotopic implications of some contrasting Late Precambrian carbonates, NE Spitsbergen: Sedimentology, v. 34, p. 973-989.

FAURE, G., 1977. Principles of Isotope Geology: New York, John Wiley and Sons, 456p.

FINKEL, E.A., and WILKINSON, B.H., 1990. Stylolitization as a source of cement in mississippian Salem Limestone, west central Indiana: Am. Assoc. Petrol. Geol. Bull., v. 74, p. 174-186.

FISCHER, A.G., 1964. The Lofer cyclothems of the Alpine Triassic: in Merriam, D.F., (ed.) Symposium on cyclic Sedimentation: Kansas Geol. Survey Bull., v. 169, p. 107-150.

FLOOD, P.G., and CHIVAS, A.R., 1995. Origin of massive dolomite, Leg 143, Hole 866A, Resolution Guyot, Mid-Pacific Mountains: in Winterer, E.L., Sager, W.W., Firth, J.V., and Sinton, J.M. (eds.), Proc. ODP, Sci. Result, v. 143, p. 161-170.

FLüGEL, E., 1982. Microfacies Analysis of Limestone: Berlin, Springer-Verlag, 633 p.

FOLK, R.L., 1959. Practical petrographic classification of limestones: Am. Assoc. Petrol.Geol. Bull., v. 43, p. 1-38.

FOLK, R.L., 1962. Spectral subdivision of limestone type: Am. Assoc. Petrol. Geol. Mem., v.1, p. 62-84.

FOLK, R.L., 1965. Some aspects of recrystalization in ancient limestone: in Pray, L.C., (ed.), Dolomitization and Limestone Diagenesis: Soc. Econ. Paleont. Mineral. Spec. Pub. No. 13, p. 14-48.

FOLK, R.L., 1974a. Petrology of Sedimentary Rocks: Hemphill pub., Co., Austin, Texas, 182 p.

FOLK, R.L., 1974b. The natural history of crystalline calcium carbonate: effect of magnesium content and salinity: Jour. Sed. Petrology, v. 44, p. 40-53.

FONTES, J.C., and DESFORGES, G., 1975. Oxygen 18, carbon 13 and radiocarbon as indicators of Wurmian cold and deep diagenesis in western Mediterranean carbonate sediments: Inter. Sed. Congress, 9th, Nice, Proceedings, v.8, p. 29-35.

FONTES, J.-Ch., and POUCHAN, P., 1975. Les cheminees due Lai Abhe (TFAI): stations hydroclimatiques de l'Holocene: C.R. Academy Sci. Paris, v. 280D, p. 383-386.

FOSTER, M.W., 1974. Recent Antarctic and Subantarctic brachiopods: Antarctic Res. Series, v. 21, 189 p.

FRAKES, L.A., 1979. Climates Through Geologic Time: Amsterdam, Elsevier, 310 p.

FRAKES, L.A., and FRANCIS, J.E., 1988. A guide to Phanerozoic cold polar climates from high-latitude ice rafting in the Cretaceous: Nature, v.333, p. 547-549.

FRAKES, L.A., FRANCIS, J.E., and SYKTUS, J.I., 1992. Climate modes of the Phanerozoic: Cambridge University Press.

FRIEDMAN, G.M., 1965. Terminology of crystallization textures and fabrics in sedimentary rocks: Jour. Sed. Petrology, v. 35, p. 643-655.

FRIEDMAN, G.M., 1969. Trace elements as possible environmental indicators in carbonate sediments: in Friedman, G.M., (ed.), Depositional environments in carbonate rocks: Soc. Econ. Paleont. Mineral. Spec. Pub., v. 14, p. 193-198.

FRIEDMAN, G.M., and SANDERS, J.E., 1967. Origin and occurrences of dolostones: in Chilingar, G.V., Bissell, H.J., and Fairbridge, R.E., (eds.), Carbonate Rocks:

Amsterdam, Elsevier, p. 267-348.

FRIEDMAN, I., and O'NEIL, J.R., 1977. Compilation of stable isotope fractionation factors of geochemical interest: in Fleischer, M., (ed.), Data of Geochemistry, 6th ed: U.S. Geol. Survey Prof. Paper, 440-KK, p. 1-12.

FROELICH, P.N., BENDER, M.L., LUEDTKE, N.A., HEATH, G.R., and DEVRIES, T., 1982. The marine phosphorous cycle: Am. Jour. Sci., v. 282, p. 474-511.

FRYKMAN, P. 1986. Diagenesis of Silurian bioherms in the Klinteberg Formation, Gotland, Sweden: in Schroeder, J.H., and Purser, B.H., (eds.), Reef Diagenesis: Springer-Verlag, Berlin, p. 399-23.

FUCHTBAUER, H., and HARDIE, L.A., 1976. Experimentally determined homogeneous distribution coefficients for precipitated magnesian calcites: Geol. Soc. Am. Abst. Ann. Progr. Meet., 877p.

GAINES, A., 1980. Dolomitization kinetics; recent experimental studies: in Zenger, D.H. Dunham, J.B., and Ethington, R.L., (eds.), Concepts and Models of Dolomitization: Soc. Econ. Paleont. Mineral. Spec. Pub., v. 28, p.139-161.

GAO, G., and LAND, L.S., 1991. Early Ordovician Cool Creek Dolomite, Middle Arbuckle Group, Slick Hills, SW Oklahoma, USA: origin and modification: Jour. Sed. Petrology, v. 61, p. 161-173.

GILFILLAN, J., 1965. Tin ore deposits of Renison Bell: in McAndrew, J., (ed.), Geology of Australian ore deposits: Melbourne, Australasian Inst. Mining Metallurgy, v. 1, p. 495-496.

GINGERICH, P.D., 1969. Markov analysis of cyclic alluvial sediments: Jour. Sed. Petrology, v. 39, p. 330-332.

GIVEN, R.K., and LOHMANN, K.C., 1986. Isotopic evidence for the early meteoric diagenesis of the reef facies, Permian Reef Complex of West Texas and New Mexico: Jour. Sed. Petrology, v. 56, p. 183-193.

GIVEN, R.K., and WILKINSON, B.H., 1985. Kinetic control of morphology, composition and mineralogy of abiotic sedimentary carbonates: Jour. Sed. Petrology, v. 55, p. 109-119.

GIVEN, R.K., and WILKINSON, B.H., 1987. Dolomite abundance and stratigraphic age: constraints on rates and mechanisms of Phanerozoic dolostone formation: Jour. Sed. Petrology, v. 57, p. 1068-1078.

GLOVER, J.E., 1968. Significance of stylolites in dolomitic limestones: Nature, v. 217, p. 835-836.

GLUMAC, B., and WALKER, K.R., 1994. Differing styles of stromatolite diagenesis: implication for stromatolite origin and diagenesis of upper Cambrian peritidal carbonates: Geol. Soc. Am. southwestern sec., 43rd Annual Metting, Abst., v. 26 (4), p. 16.

GOEDE, A., GREEN, D.C., and HARMON, R.S., 1986. Late Pleistocene paleotemperature record from a Tasmanian speleothem: Aust. Jour. Earth Sci., v. 33, p. 333-342.

GOLDHAMMER, R.K., DUNN, P.A., and HARDIE, L.A., 1990. Depositional cycles, composit sea-level changes, cycle stacking pattern, and the hierarchy of stratigraphic forcing: examples from Alpine Triassic platform carbonates: Geological Soc. Am. Bull., v. 102, p. 535-562.

GOLDING, S.D., and WILSON, A.F., 1983. Geochemical and stable isotope studies of the No. 4 Lode, Kalgoorlie, Western Australia: Econ. Geology, v. 78, p. 438 450.

GOLDSMITH, J. R., GRAF, D. L., and HEARD, H. C., 1961. Lattice costants of the calcium-magnesium carbonates: Am. Mineralogist, v. 46, p. 453-45.

GONZALEZ, L.A., and LOHMANN, K.C., 1985. Carbon and oxygen isotopic composition of Holocene reefal carbonates: Geology, v. 13, p. 811-814.

GOODMAN, L.A., 1968. The analysis of cross-classified data: independence, quasi-independence, and interactions in contingency tables with or without missing entries: Jour. Am. Statist. Assoc., v. 63, p. 1091-1131.

GOSTIN, V.A., BELPERIO, A.P., and CANN, J.H., 1988. The Holocene non-tropical coastal and shelf carbonate province of southern Australia: in Nelson, C.S., (ed.), Non-tropical Shelf Carbonates–Modern and Ancient: Sed. Geology, v. 60, p. 51-70.

GOUGH, D.O., 1981. Solar interior structure and luminosity variations: Solar Physics, v. 74, p. 21-34.

GREGG, J.M., 1985. Regional epigenetic dolomitization in the Bonneterre Dolomite (Cambrian), southeastern Missouri: Geology, v. 13, p. 503-506.

GREGG, J.M., 1988. Origins of dolomite in the offshore facies of the Bonneterre Formation (cambrian), southeast Missouri: in Shukla, V., and Baker, P.A., (eds.), Sedimentology and Geochemistry of Dolostones: Soc. Econ. Paleont. Mineral. Spec. Pub., No. 43, p. 67-83.

GREGG, J.M., and SHELTON, K.L., 1990. Dolomitization and dolomite neomorphism in the back reef facies of the Bonneterre and Davies formations (Cambrian), southeastern Missouri: Jour. Sed. Petrology, v. 60, p. 549-562.

GREGG, J.M., and SIBLEY, D.F., 1984. Epigenetic dolomitization and the origin of xenotopic dolomite texture: Jour. Sed. Petrology, v. 54, p. 908-931.

GRIFFIN, B.J., and PREISS, W. V., 1976. The significance and provenance of stromatolitic clasts in a probable late Precambrian diamictite in northwestern Tasmania: Pap. Proc. Roy. Soc. Tasmania, v. 110, p.111-127.

GROSSMAN, E.L., and KU, T.L., 1981. Aragonite-water isotopic paleotemperature scale based on the benthic foraminifera Hoeglundina elegans: Geol. Soc. Am. Abst. with Progr., v. 13, 464 p.

GROSSMAN, E.L., and KU, T.L., 1986. Carbon and Oxygen isotopic fractionation in biogenic aragonite: temperature effects: Chem. Geology, v. 59, p. 59-74.

GROTZINGER, J.P., 1990. Geochemical model for Proterozoic stromatolite decline: Am. Jour. Sci., v. 290A, p. 80-103.

GROTZINGER, J.P., and READ, J.F., 1983. Evidence of primary aragonite precipitation, lower Proterozoic (1.9 Ga) Rocknest Dolomite, Wopmay orogen, northwest Canada: Geology, v. 11, p. 710-713.

GROVER, G., and READ, J.F., 1983. Paleoaquifer and deep burial related cement defined by regional cathodoluminescent patterns, Middle ordovician carbonates, Virginia: Bull. Am. Assoc. Petrol. Geol., v. 67, p. 1275-1303.

GROVES, D.I., 1968. The cassiterite-sulphide deposits of western Tasmania: Unpub. Ph.D. thesis, Univ. Tasmania, 294 p.

GROVES, D.I., MARTIN, E.L., MURCHIE, H., and WELLINGTON, H.K., 1972. A century of tin mining at Mount Bischoff, 1871-1971: Tasmanian Geol. Survey Bull., v. 54, 310p.

HAINES, J.B., 1991. The stratigraphy and sedimentology of the lower Crimson Creek Formation

and related mafic igneous rocks, Renison Bell Mine: Unpub. B.Sc. Honours thesis, Univ. Tasmania, 84 p.

HALL, G., and SOLOMON, M., 1962. Metallic mineral deposits: Geol. Soc. Australia Jour., v. 9, part 2, p. 285-309.

HALLAM, A., 1975. Jurassic environments: Cambridge University Press, Cambridge, 269p.

HALLAM, A., 1978. Eustatic cycles in the Jurassic: Palaeogeogr. Palaeoclimatol. Palaeoecol., v. 23, p. 1-32.

HALLAM, A., 1985. A review of Mesozoic climates: Jour. Geol. Soc. London, v.142, p. 433-445.

HALLAM, A., 1986. Evidence of displaced terranes from Permian to Jurassic faunas around the Pacific margins: Jour. Geol. Soc. London, v. 143, p. 209-216.

HALLAM, A., 1988. A re-evaluation of Jurassic eustasy in the light of new data and revised Exxon curve: in Wilgus, C.K., Hastings, B.S., Kendall, C.G. St.C., Posamentier, H.W., Ross, C.A., and vanWagoner, J., (eds.), Sea-Level Changes – an Integrated Approach: Soc. Econ. Paleont. Mineral. Spec. Pub., v. 42, p. 261-273.

HALLAM, A., 1993. Jurassic climates as inferred from the sedimentary and fossil record: Philos. Trans. Roy. Soc. London, Ser. B., v. 341, p. 287-326.

HALLEY, S.W., 1987. Genesis of the Mount Bischoff tin deposit: Unpub. Ph.D. thesis, A.N.U., Canberra, 392 p.

HAMBREY, M.J., 1992. Secrets of a tropical ice age: New Scientists, p. 34-41.

HAMBREY, M.J., and HARLAND, W.B., 1981. Earth' s Pre-Pleistocene Glacial Record: Cambridge Univ. Press, Cambridge, 102p.

HAQ, B.U., HARDENBOL, J., and VAIL, P.R., 1987. Chronology of fluctuating sea levels since the Triassic: Science, v. 235, p. 1156-1167.

HARDIE, L.A., 1987. Dolomitization: a critical view of some current views: Jour. Sed. Petrology, v. 57, p. 166-183.

HARLAND, W.B., 1981. Chronology of Earth's glacial and tectonic record: Jour. Geol. Soc. London, v. 138, p. 197-203.

HARLAND, W.B., 1983. The Proterozoic glacial record: Geological Soc. Am. Mem., v. 161, p. 279-288.

HEMMING, N.G., MEYERS, W.J., and GRAMS, J.C., 1989. Cathodoluminescence in diagenetic calcites: the roles of Fe and Mn as deduced from electron probe and spectrophotometric measurments: Jour. Sed. Petrology, v. 59, p. 404-411.

HERMAN, H., 1914. Australian tin lodes and tin mills: Proc. Aust. Inst. Min. Eng., v. 12, p. 288.

HEYDARI, E., 1990. Burial diagenesis of the Smackover Formation, southeast Mississippi salt basin: Unpub. Ph.D. thesis, Louisiana State University, 268 p.

HEYDARI, E., and MOORE, C.H., 1993. Zonation and geochemical patterns of burial calcite cements: Upper Smackover Formation, Clarke County, Mississippi: Jour. Sed. Petrology, v. 63, p. 44-60.

HIRD, K., and TUCKER, M.E., 1988. Contrasting diagenesis of two Carboniferous oolites from South Wales: a tale of climatic influence: Sedimentology, v. 35, p. 587-602.

HOEFS, J., 1980. Stable Isotope Geochemistry: New York, Heidelberg, Berlin. Springer-Verlag,

208p.

HOFFMAN, P., 1976. Stromatolite morphogenesis in Shark Bay, Western Australia: in Walter, M.R., (ed.), Stromatolites: Elsevier, Amsterdam, p. 261-272.

HOLLAND, H.D., 1992. Chemistry and evolution of the Proterozoic ocean: in Schopf, J.W., and Klein, C., (eds.), The Proterozoic Biosphere, A Multidisciplinary Study: Cambridge Univ., Press, p. 169-172.

HOLYLAND, P., 1987. Structure and hydrodynamics of the Renison Tin Mine: Unpub. Ph.D. thesis, Univ. Queensland, 258 p.

HOROWITZ, A.S., and POTTER, P.E., 1971. Introductory Petrography of Fossils: Berline, Springer-Verlag, 302p.

HUBER, H., 1978. Geological Map of Iran, 1:1000000, with explanatory note. North-east Iran: NIOC, Expl. and Prod. Affairs, Tehran, 1 sheet.

HUDSON, J.D., and ANDERSON, T.F., 1989. Ocean temperatures and isotopic compositions through time: Trans. Roy. Soc. Edinberg, Earth Sci., v. 80, p. 183-192.

HUMPHREY, J.D., 1988. Late Pleistocene mixing-zone dolomitization, southeastern Barbadose, West Indies: Sedimentology, v. 35, p. 327-348.

HURLEY, N.F., and LOHMANN, K.C., 1989. Diagenesis of Devonian reefal carbonates in the Oscar Range, Canning Basin, Western Australia: Jour. Sed. Petrology, v. 59, p. 127-146.

ILLING, L.V., WELLS, A.J., and TAYLOR, J.C.M., 1965. Penecontemporary dolomite in the Persian Gulf: in Pray, L.V., and Murray, R.C., (eds.), Dolomitization and limestone diagenesis: Soc. Econ. Paleont. Mineral. Spec. Pub., No. 13, p. 89-111.

IRWIN, H., 1980. Early diagenetic carbonate precipitation and pore fluid migration in the Kimmeridge Clay of Dorset, England: Sedimentology, v. 27, p. 577-591.

IRWIN, H., CURTIS, C.D., and COLEMAN, M., 1977. Isotopic evidence for source of diagenetic carbonates formed during burial of organic-rich sediments: Nature, v. 269, p. 209-213.

IYER, S.S., BABINSKI, M., KROUSE, H.R., and CHEMALE, Jr.F., 1995. Highly ^{13}C-enriched carbonate and organic matter in the Neoproterozoic sediments of the Bambuí Group, Brazil: Precambrian Res., v. 73, p. 271-282.

JACKSON, K.A., 1958. Mechanism of Growth, in Liquid Metals and Solidification: Am. Soc. Metals, Cleveland, Ohio, p. 174-186.

JACKSON, K.A., and GILMER, G.H., 1976. Critical surface roughening: Farady Discussions of the Chemical Society, No.61, The Farady Division, Chemical Society, London, p. 53-62.

JAGO, J. B., 1981. Possible Late Precambrian (Adelaidean) tillites of Tasmania: in Hambrey, M.J., and Harland, W.B., (eds.), Earth's pre-Pleistocene glacial record: Cambridge Univ. Press, p. 549-554.

JAMES, N.P., 1991. Diagenesis of carbonate sediments, a Short Course: Geol. Soc. Australia. Sedimentologists Specialist Group, p. 194.

JAMES, N.P., and BONE, Y., 1989. Petrogenesis of Cenozoic temperate water calcarenites, South Australia: Jour. Sed. Petrology, v. 59, p. 191-203.

JAMES, N.P., and BONE, Y., 1992. Synsedimentary cemented calcarenite layers in Oligo-Miocene cool-water shelf limestones, Eucla Platform, South Australia: Jour. Sed. Petrology, v. 62, p. 860-872.

JAMES, N.P., BONE, Y., and KYSER, T.K., 1993. Shallow burial dolomitization and dedolomitization of mid-Cenozoic, cool-water, calcitic, deep-shelf limestones, southern Australia: Jour. Sed. Petrology, v. 63, p. 528-538.

JAMES, N.P., BONE, Y., VON der BORCH, C.C., and GOSTIN, V. A., 1992. Modern carbonate and terrigenous clastic sediments on a cool-water, high-energy, mid-latitude shelf: Lacepede southern Australia: Sedimentology, v. 39, p. 877-904.

JAMES, N. P., BOREEN, T. D., BONE, Y., and FEARY, D.A., 1994. Holocene carbonate sedimentation on the west Eucla Shelf, Great Australian Bight: a shaved shelf: Sed. Geology, v. 90, p. 161-177.

JAMES, N.P., and CHOQUETTE, P.W., 1983. Diagenesis 6. Limestones-the sea floor diagenetic environment: Geosci. Canada, v. 10, p. 162-179.

JAMES, N.P., and CHOQUETTE, P.W., 1984. Diagenesis 9. Limestones- the seafloor diagenetic environment: Geosci. Canada, v. 11, p. 161-194.

JAMES, N.P., and GINSBURG, R.N., 1979. The seaward margine of Blize barrier and atoll reefs: Inter. Assoc. Sediment. Spec. Pub. v. 3, 191p.

JAMES, N.P., GINSBURG, R.N., MARSZALEK, D.S., and CHOQUETTE, P., 1976. Facies and fabric specificity of early sub-sea cements in shallow Belize (British Honduras) reefs: Jour. Sed. Petrology, v. 46, p. 523-544.

JENKYNS, H.C., 1980. Cretaceous anoxic events: from continents to ocean: Jour. Geol. Soc. London, v. 137, p. 171-188.

JENKYNS, H.C., and CLAYTON, C.J., 1986. Black shales and carbon isotopes in plagic sediments from the Tethyan Lower Jurassic: Sedimentology, v. 33, p. 87-106.

JONES, M., and EVANS, D., 1985. Trace elements and stable isotope variations in rocks of the Renison Mine Sequence: Unpub. Rept. Renison Ltd., 34 p.

KAHLE, C.F., 1965. Possible roles of clay minerals in the formation of dolomite: Jour. Sed. Petrology, v. 35, p. 448-453.

KAHLE, C.F., 1974. Ooids from Great Salt Lake, Utah, as an analogue for the genesis and diagenesis of ooids in marine limestones: Jour. Sed. Petrology, v. 44, p. 30-49.

KALANTARI, A., 1969. Foraminifera from the Middle Jurassic-Cretaceous successions of Kopet-Dagh region (NE Iran): N.I.O.C. Geol. Lab. Pub. No. 3, 298p.

KALANTARI, A., 1987. Biofacies map of Kopet-Dagh region: Unpub. map, N.I.O.C. Expl. and Prod., Teheran, 1 sheet.

KALDI, J., and GIDMAN, J., 1982. Early diagenetic dolomite cements: examples from the Permian Lower Magnesian Limestone of England and the Pleistocene carbonates of the Bahamas: Jour. Sed. Petrology, v. 52, p. 1073-1085.

KARHU, J., and EPSTEIN S., 1986. The implications of the oxygen isotope records in coexisting cherts and phosphates: Geochim. Cosmochim. Acta, v. 50, p. 1745-1756.

KASTING, J.F., 1992. Proterozoic climates: the effect of changing atmospheric carbon dioxide concentrations: in Schopf, J.W., and Klein, C., (eds.), The Proterozoic Biosphere, A Multidisciplinary Study: Cambridge Univ., Press, p. 165-168.

KASTING, J.F., HOLLAND, H.D., and KUMP, L.R., 1992. Atmospheric evolution: the rise of oxygen: in Schopf, J.W., and Klein, C., (eds.), The Proterozoic Biosphere, A Multidisciplinary Study: Cambridge Univ., Press, p. 159-163.

KAUFMAN , A.J., HAYES, J.M., KNOLL, A.H., and GERMS, G.J.B., 1991. Isotopic compositions of carbonates and organic carbon from Upper Proterozoic succession in Namibia: stratigraphic variation and the effects of diagenesis and metamorphism: Precambrian Res., v. 49, p. 301-327.

KAUFMAN , A.J., JACOBSEN, S.B., and KNOLL, A.H., 1993. The Vendian record of Sr- and C- isotopic variations in seawater: implications for tectonics and paleoclimate: Earth Planet. Sci. Lett., v. 120, p. 409-430.

KAUFMAN, A.J., and KNOLL, A.H., 1995. Neoproterozoic variations in the C-isotopic composition of seawater: stratigraphic and biogeochemical implications: Precambrian Res., v. 73, p. 27-49.

KAUFMAN, A.J., KNOLL, A.H., and AWRAMIK, S.M., 1992. Biostratigraphic and chemostratigraphic correlation of Neoproterozoic sedimentary successions: upper Tindir Group, northwestern Canada, as a test case: Geology, v. 20, p. 181-185.

KAUFMAN, J., CANDER, H.S., DANIELS, L.D., and MEYERS, W.J., 1988. Calcite cement stratigraphy and cementation history of the Burlington-Keokuk Formation (Mississippian), Illinois and Missouri: Jour. Sed. Petrology, v. 58, p. 312-326.

KEMPE, S. and DEGENS, E.T., 1985. An early soda ocean ?: Chem. geology, v. 53, p. 95-108.

KENDALL, A.C., 1977. Origin of dolomitic mottling in Ordovician limestones from Saskatchewan and Monitoba: Bll. Canadian Petrol. Geology, v. 25, p. 480-504.

KENDALL, A.C., 1985. Radiaxial fibrous calcite: a reappraisal: in Schneidermann, N., and Harris, P.M., (eds.), Carbonate Cements: Soc. Econ. Paleont. Mineral. Spec. Pub. No. 36, p. 59-77.

KENDALL, C.G. ST C., and WARREN, J.K., 1988. Peritidal evaporites and their sedimentary assemblages: in Schreiber B.C., (ed.), Evaporites and Hydrocarbons: Columbia Uni. Press, New York, p. 66-138.

KHIN, Zaw., and LARGE, R.R., 1992. The precious metal-rich South Hercules Mineralization, western Tasmania: a possible subsea-floor replacement volcanic-hosted massive sulfide deposit: Econ. Geology, v. 87, p. 931-952.

KINSMAN, D.J.J., and HOLLAND, H.D., 1969. The co-precipitation of cations with $CaCO_3$. The co-precipitation of Sr^{2+} with aragonite between 16^{o} and $96^{o}C$: Geochim. Cosmochim. Acta, v. 33, p. 1-17.

KIRSCHVINK, J.L., 1992a. Late Proterozoic low-latitude global glaciation: the snowball earth: in Schopf, J.W., and Klein, C., (eds.), The Proterozoic Biosphere, A Multidisciplinary Study: Cambridge Univ., Press, p. 51-52

KIRSCHVINK, J.L., 1992b. A palaeogeographic model for Vendian and Cambrian time: in Schopf, J.W., and Klein, C., (eds.), The Proterozoic Biosphere, A Multidisciplinary Study: Cambridge Univ., Press, p. 569-581.

KITTO, P.A., 1992. The geological and structural controls on mineralisation at the Renison tin mine: Bull. Geol. Survey, Tasmania, v. 70, p. 97-117.

KITTO, P.A., 1994. Structural and geochemical controls on mineralization at Renison, Tasmania: Unpub. Ph.D. thesis, Univ. Tasmania, 484 p.

KLEIN, C., 1992. Introduction: in Schopf, J.W., and Klein, C., (eds.), The Proterozoic Biosphere, A Multidisciplinary Study: Cambridge Univ., Press, p. 137-138.

KNAUTH, L.P., and EPSTEIN, S., 1976. Hydrogen and oxygen isotope ratios in nodular and bedded cherts: Geochim. Cosmochim. Acta, v. 40, p. 1095-1108.

KNOLL, A.H., 1991. End of the Proterozoic Eon: Sci. Am., v. 265, p. 64-73.

KNOLL, A.H., HAYES, J.M., KAUFMAN, A.J., SWETT, K., and LAMBERT, I.B., 1986. Secular variation in carbon isotope ratios from upper Proterozoic successions of Svalbard and East Greenland: Nature, v. 321, p. 832-838.

KNOLL, A.H., and WALTER, M.R., 1992. Late Proterozoic stratigraphy and Earth history: Nature, v. 356, p. 673-678.

KROM, M.D., and BERNER, R.A., 1983. A rapid method for the determination of organic and carbonate carbon in geological samples: Jour. Sed. Petrology, v. 53, p. 660-663.

KUEHL, S.A., NITTROUER, C.A., and DeMASTER, D.J., 1988. Microfabric study of fine-grained sediments: observations from the Amazon subaqueous delta: Jour. Sed. Petrology, v. 58, p. 12-23.

KUO, C., LINDBERG, C., and THOMPSON, D.J., 1990. Coherence established between atmospheric carbon dioxide and global temperature: Nature, v. 343, p. 709-714.

KUPECZ, J.A., and LAND, L.S., 1991. Late-stage dolomitization of the Lower Ordovician Ellenburger Group, West Texas: Jour. Sed. Petrology, v. 61, p. 551-574.

LAMBERT, I.B., WALTER, M.R., ZANG WENLONG, LU SONGNIAN and Ma GUOGAN, 1987. Paleoenvironment and carbon isotope stratigraphy of upper Proterozoic carbonates of the Yangtze Platform: Nature, v. 325, p. 140-142.

LAND, L.S., 1967. Diagenesis of skeletal carbonates: Jour. Sed. Petrology, v. 37, p. 914-930.

LAND, L.S., 1973a. Contemporaneous dolomitization of Middle Pleistocene reefs by meteoric water, North Jamaica: Bull. Mar. Sci., v. 23, p. 64-92.

LAND, L.S., 1973b. Holocene meteoric dolomitization of Pleistocene limestones, North Jamaica: Sedimentology, v. 20, p. 411-424.

LAND, L.S., 1980. The isotope and trace element geochemistry of dolomite: the state of the art: in Zenger, D.H., Dunham, J.B., and Ethington, R.L., (eds.), Concepts and Models of Dolomitization: Soc. Econ. Paleont. Mineral. Spec. Pub., v. 28, p. 87-110.

LAND, L. S., 1983. The application of stable isotopes to studies of the origin of dolomite and to problems of diagenesis of clastic sediments: in Stable Isotopes in Sedimentary Geology: Soc. Econ. Paleo. Mineral., Short Course, v. 10, p. 4.1-4.22.

LAND, L.S., 1985. The origin of massive dolomite: Jour. Geol. Education, v. 33, p. 112-125.

LAND, L.S., 1986. Environments of limestone and dolomite diagenesis: some geochemical considerations: in Bathurst, R.G.C., and Land, L.S., (eds.), Carbonate Depositional Environments, Modern and Ancient, part 5, Diagenesis: Quart. Colorado School Mines, v. 81, p. 26-41.

LAND, L.S., BEHRENS, S.W., and FRISHMAN, S.A., 1979. The ooids of Baffin Bay, Texas: Jour. Sed. Petrology, v. 49, p. 1269-1278.

LAND, L.S., and HOOPS, G.K., 1973. Sodium in carbonate sediments and rocks: a possible index to the salinity of diagenetic solutions: Jour. Sed. Petrology, v. 43, p. 614-617.

LASEMI, Y., 1992. Regressive cycles and sea level fluctuation in carbonate rocks of Mozduran Formation (abst): The first Geol. Symp. Eastern Iran, p. 56-57.

LASEMI, Y., 1996. Platform carbonates of the Upper Jurassic Mozduran Formation in the Kopet Dagh Basin, NE Iran- facies, palaeoenvironments and sequences: Sed. Geology, v.99, p. 151-164.

LASEMI, Z., BOARDMAN, M.R., and SANDBERG, P.A., 1989. Cement origin of suprital dolomite, Andros Island, Bahamas: Jour. Sed. Petrology, v. 59. p. 249-257.

LASEMI, Z., and SANDBERG, P.A., 1984. Transformation of aragonite-dominated lime muds to microcrystalline limestone: Geology, v. 12, p. 420-423.

LEA, J.R., 1991. Renison mine lease exploration: Models, concept, interpretation and future directions: Unpub. Rept. Renison Ltd., 60 p.

LEAMAN, D.E., 1990. Renison mine lease gravity survey: Unpub. report, Renison Mine. 211 p.

LEE, T.F., 1993. The determination of the positions of the Gondwana continents back to the Ordovician using a method of plate path plotting: Gondwana Eight, p. 523-529.

LEE, Y.I., and FRIEDMAN, G.M., 1987. Deep-burial dolomitization in the Lower Ordovician Ellenburger Group carbonates in west Texas and southeastern New Mexico: Jour. Sed. Petrology, v. 57, p. 544-557.

LEES, A., 1975. Possible influence of salinity and temperature on modern shelf carbonate sedimentation: Mar. Geology, v. 19, p. 159-198.

LEPZELTER, C.G., ANDERSON, T.F., and SANDBERG, P.A., 1983. Stable isotope variation in modern articulate brachiopods (abst.): Am. Assoc. Petrol. Geol. Bull., v. 67, p. 500-501.

LINDHOLM, R.C., and FINKLEMAN, 1972. Calcite staining: semiquantitive determination of ferrous iron: Jour. Sed. Petrology, v. 42, p. 239-242.

LIPPMANN, F., 1973. Sedimentary Carbonate Minerals: Springer-Verlag, Berlin, 228p.

LOGAN, B.W., REZAK, R., and GINSBURG, R.N., 1964. Classification and environmental significance of algal stromatolites: Jour. Geology, v. 72, p. 62-83.

LOHMANN, K.C., 1988. Geochemical patterns of meteoric diagenetic systems and their application to studies of paleokarst: in James, N.P., and Choquette, P.W., (eds.), Paleokarst: New York, Springer-Verlag, p. 58-80.

LOHMANN, K.C., and WALKER, J.C.G., 1989. The $\delta^{18}O$ record of Phanerozoic abiotic marine calcite cements: Geophysical Res. Letters, v. 16, p. 319-322.

LONGMAN, M.W., 1980. Carbonate diagenetic textures from near surface diagenetic environments: Am. Assoc. Petrol. Geol. Bull., v. 64, p. 461-487.

LOREAU, J.P., 1982. Sediments Aragonitiques et Leur Genese: Memoirs du Museum d'Histoire Naturelle, Serie C, 47, 312p.

LOREAU, J.P., and PURSER, B.H., 1973. Distribution and ultrastructure of Holocene ooids in the Persian Gulf: in Purser, B.H., (ed.), The Persian Gulf: Berlin, Springer-Verlag, p. 279-328.

LOWE, D.R., 1992. Other geological indicators: in Schopf, J.W., and Klein, C., (eds.), The Proterozoic Biosphere, A Multidisciplinary Study: Cambridge Univ., Press, p. 157-158.

LUCIA, F.J., 1972. Recognition of evaporite-carbonate shoreline sedimentation: in Rigby, K.J., and Hamblin, K., (eds.), Recognition of Ancient Sedimentary Environments: Soc. Econ. Paleont. Mineral. Spec. Pub., No. 16, p. 160-192.

LUMSDEN, D.N., 1988. Characteristics of deep marine dolomite: Jour. Sed. Petrology, v. 58, p. 1023-1031.

LUMSDEN, D.N., and CHIMAHUSKY, J.S., 1980. Relationship between dolomite nonstoichiometry and carbonate facies parameters: in Zenger, D.H., Dunham, J.B., and Ethington, R.L., (eds.), Concepts and Models of Dolomitization: Soc. Econ. Paleont. mineral. Spec. Pub., v. 28, p. 123-127.

MACHEL, H.G., 1985. Cathodoluminescence in calcite and dolomite and its chemical interpretation: Geosci. Canada, v. 12, p. 139-147.

MACHEL, H.G., and ANDERSON, J.H., 1989. Pervasive subsurface dolomitization of the Nisku Formation in central Alberta: Jour. Sed. Petrology, v. 59, p. 891-911.

MACHEL, H.G., and BURTON, E.A., 1991. Factors governing cathodoluminescence in calcite and dolomite, and their implications for studies of carbonate diagenesis: in Barker, C.E., and Kopp, O.C., (eds.), Luminescence Microscopy and Spectroscopy: Qualitative and Quantitative Applications: Short Course, Soc. Econ. Paleont. Mineral. Spec. Pub. No. 25, p. 37-57.

MACHEL, H.G., MASON, R.A., MARIANO, A.N., and MUCCI, A., 1991. Causes and emisson of luminescence in calcite and dolomite: in Barker, C.E., and Kopp, O.C., (eds.), Luminescence Microscopy and Spectroscopy: Qualitative and Quantitative Applications: Short Course, Soc. Econ. Paleont. Mineral. Spec. Pub. No. 25, p. 9-25.

MACHEL, H.G., and MOUNTJOY, E.W., 1986. Chemistry and environments of dolomitization: Earth Sci. Rev., v. 23, p. 175-222.

MACKENZIE, F.T., and PIGOTT, J.D., 1981. Tectonic controls of Phanerozoic rock cycling: Jour. Geol. Soc., v. 138, p. 183-196.

MADANI, M., 1977. A study of the sedimentology, stratigraphy and regional geology of the Jurassic rocks of eastern Kopet-Dagh, NE Iran: Unpub. Ph.D. thesis, Imperial College, London.

MAGARA, K., 1976. Water expulsion from clastic sediments during compaction- directions and volumes: Am. Assoc. Petrol. Geol. Bull., v. 60, p. 543-553.

MAGARITZ, M., HOLSER, W.T., and KIRSCHVINK, J.L., 1986. Carbon isotope events across the Precambrian/Cambrian boundary on the Siberian Platform: Nature, v. 320, p. 258-259.

MAHBOBI, A., and LASEMI, Y., 1992. Study of the sedimentary environments of limestone facies in Kalat Formation, eastern Kopet-Dagh Basin (abst): The first Geol. Symp. of Eastern Iran, p. 61-62.

MAJOR, R.P., 1984. The Midway Atoll Coral Cap: meteoric diagenesis, amplitude of sea-level fluctuation and dolomitization: Unpub. Ph.D. thesis, Brown University, 133p.

MAJOR, R.P., HALLEY, R.B., and LUKAS, K.J., 1988. Cathodoluminescent bimineralic ooids from the Pleistocene of the Florida continental shelf: Sedimentology, v. 35, p. 843-855.

MAJOR, R.P., WILBER, R.J., and HALLEY, R.B., 1987. Cathodoluminescent magnesian calcite marine cements, western slope, Little Bahama Bank: Geol. Soc. Am. Abstr. with Progs., v. 19, p. 757.

MALIVA, R.G., 1989. Displacive calcite syntaxial overgrowths in open marine limestones: Jour. Sed. Petrology, v. 59, p. 397-403.

MALIVA, R.G., and SIEVER, R., 1988. Diagenetic replacement controlled by force of crystallization: Geology, v. 16, p. 688-691.

MALIVA, R.G., and SIEVER, R., 1990. Influence of dolomite precipitation on quartz surface textures: Jour. Sed. Petrology, v. 60, p. 820-826.

MARJORIBANKS, R.W., 1990. Structural observations of the Renison Mine area with some exploration implications: Mine report (unpubl.).

MARSHALL, J.D., 1988. Cathodoluminescence of Geological Materials: Unwin-Hyman, Boston, Mass., 146 p.

MARSHALL, J.D., 1992. Climatic and oceanographic isotopic signals from the carbonate rock record and their preservation: Geol. Magazine, v. 129, p. 143-160.

MARSHALL, J.D., and ASHTON, M., 1980. Isotopic and trace element evidence for submarine lithification of hardgrounds in the Jurassic of England: Sedimentology, v. 27, p. 271-289.

MARTIN, G.D., WILKINSON, B.D., and LOHMANN, K.C., 1986. The role of skeletal porosity in aragonite neomorphism - *Strombus* and *Monstastrea* from the Pleistocene Key Largo Limestone, Florida: Jour. Sed. Petrology, v. 56, p. 194-203.

MASON, R.A., and MARIANO, A.N., 1990. Cathodoluminescence activation in manganese bearing and rare-earth bearing synthetic calcites: Chem. Geology, v. 88, p. 191-206.

MASSARI, F., 1983. Oncoids and Stromatolites in the Rosso Ammonitico Sequences (Middle-Upper Jurassic) of the Venetian Alps, Italy: in Peryt, T.M., (ed.), Coated Grains: Springer-Verlag, Berlin, p. 358-366.

MATSUHISHA, Y., GOLDSMITH, J. R., and CLAYTON, R. N., 1979. Oxygen isotope fractionation in the system quartz-albite-anorthite-water: Geochim. Cosmochim. Acta, v. 42, p. 1131-1140.

MATTES, B.W., and MOUNTJOY, E.W., 1980. Burial dolomitization of the Upper Devonian Miette buildup, Jasper National Park, Alberta: in Zenger, D.H., Dunham, J. B., and Ethington, R.L., (eds.), Concepts and Models of Dolomitization: Soc. Econ. Paleont. Mineral. Spec. Pub., v. 28, p. 259-297.

MAZZULLO, S.J., 1992. Geochemical and neomorphic alteration of dolomite: a review: Carbonates and Evaporites, v. 7, p. 21-37.

MAZZULLO, S.J., REID, A.M., and GREGG, J.M., 1987. Dolomitization of Holocene Mg-calcite supratidal deposits, Ambergris Cay, Belize: Geol. Soc. Am. bull., v. 98, p. 224-231.

McCONNAUGHEY, T., 1989. ^{13}C and ^{18}O isotopic disequilibrium in biological carbonates, I. Patterns: Geochim. Cosmochim. Acta, v. 53, p. 151-162.

McCREA, J.M., 1950. On the isotopic chemistry of carbonates and paleotemperature scale: Jour. Chem. Physics, v. 18, p. 849-875.

McDOUGALL, I., and LEGGO, P. J., 1965. Isotopic age determinations on granitic rocks from Tasmania: Jour. Geol. Soc. Aust., v. 12, p. 295-332.

McHARGUE, T.R., and PRICE, R.C., 1982. Dolmite from clay in argillaceous or shale associated

marine carbonates: Jour. Sed. Petrology, v. 48, p. 799-814.

McKENZIE, J.A., 1981. Holocene dolomitization of calcium carbonate sediments from the coastal sabkhas of Abu Dhabi, U.A.E: a stable isotope study: Jour. Geology, v. 89, p. 185-198.

MEYERS, W.J., 1974. Carbonate cement stratigraphy of the Lake Valley formation (Mississippian), Sacramento Mountains, New Mexico: Jour. Sed. Petrology, v. 44, p. 837-861.

MEYERS, W.J., 1978. Carbonate cements: their regional distribution and interpretation in Mississippian limestones of southwestern New Mexico: Sedimentology, v.25, p. 371-400.

MEYERS, W.J., 1989. Trace element and isotope geochemistry of zoned calcite cements, Lake Valley Formation (Mississippian, New Mexico): insights from water-rock interaction modeling: Sed. Geology, v. 65, p. 355-370.

MEYERS, W.J., and LOHMANN, K.C., 1985. Isotope geochemistry of regionally extensive calcite cement zones and marine components in Mississippian limestone, New Mexico: in Schneiderman, N., and Harris, P.M., (eds.), Carbonate Cements: Soc. Econ. Paleont. Mineral. Spec. Pub., v. 36, p. 223-240.

MIALL, D.A., 1973. Markov chain analysis applied to an ancient alluvial plain succession: Sedimentology, v. 20, p. 347-364.

MILLIKEN, K.L., and PIGOTT, J.D., 1977. Variation of oceanic Mg/Ca ratio through time–implications for the calcite sea (abst): Geol. Soc. America, South-Cent. Mtg., p. 64-65.

MILLIMAN, J.D., 1974. Marine Carbonates: New York, Springer-Verlag, 375 p.

MILLIMAN, J.D., and MULLER, J., 1977. Characteristics and genesis of shallow-water and deep-sea limestones: in Anderson, N.R., and Malahoff, A., (eds.), the fate of fossil fuel CO_2 in the oceans: New York, Plenum press, p. 655-672.

MITCHELL, J.T., LAND, L.S., and MISER, D.E., 1987. Modern marine dolomite cement in a north Jamaica fringing reef: Geology, v. 15, p. 557-560.

MOORE, C.H., 1984. The Upper Smackover of the Gulf Rim: depositional systems, diagenesis, porosity evolution and hydrocarbon production: in Ventress, W.P.S., Bebout, D.G., Perkins, R.F., and Moore, C.H., (eds.): Soc. Econ. Paleont. Mineral. Gulf. Coast sections Pub, p. 283-308.

MOORE, C.H., 1989. Carbonate Diagenesis and Porosity: Elsevier, Amsterdam, 338 p.

MOORE, C.H., and DRUCKMAN, Y., 1981. Burial diagenesis and porosity evolution, Upper Jurassic Smackover, Arkansas and Louisiana: Am. Assoc. Petrol. Geol. Bull., v. 65, p. 597-628.

MOORE, G.T., HAYASHIDA, D.N., ROSS, C.A., and JACOBSON, S.R., 1992a. Paleoclimate of the Kimmeridgian/Tithonian (Late Jurassic) world: I Results using a general circulation model: Palaeogeogr. Palaeoclimatol. Palaeoecol., v. 93, p. 113-150.

MOORE, G.T., SLOAN, L.C., HAYASHIDA, D.N., and UMRIGAR, N.P. 1992b. Paleoclimate of the Kimmeridgian/Tithonian (Late Jurassic) world: II Sensitivity tests comparing three different paleotopographic settings: Palaeogeogr. Palaeoclimatol. Palaeoecol., v. 95, p. 229-252.

MORELAND, R., 1988. The Renison Bell Tin mine, technical review: Unpub. Rept. Renison Ltd., 44 p.

MORRISON, G.W., 1982. Stratigraphy and sedimentology of the Renison mine sequence: Unpub. Rept. Renison Ltd, 102p.

MORRISON, G.W., 1993. Stratigraphy of the Crimson Creek Formation: Unpub. Rept. Renison Ltd.

MORRISON, J.O., and BRAND, U., 1986. Geochemistry of Recent marine invertebrates: Geosci. Canada, v. 13, p. 237-254.

MORROW, D.W., 1982. Diagenesis II. Dolomite-part II: dolomitization models and ancient dolostones: Geosci. Canada, v. 9, p. 95-107.

MORSE, J.W., 1985. Kinetic control of morphology, composition and mineralogy of abiotic sedimentary carbonates. Discussion: Jour. Sed. Petrology, v. 55, p. 919- 921.

MORSE, J.W., and MACKENZIE, F.T., 1990. Geochemistry of Sedimentary Carbonates: New York, Elsevier, 707 p.

MOUSSAVI- HARAMI, R., 1989. Depositional history of the Upper Jurassic (Oxfordian-Kimmeridgian) carbonate and evaporite in norheastern Iran: 28th Inter. Geol. Congress Abst., v. 2, 471 p.

MOUSSAVI- HARAMI, R., and BRENNER, R.L., 1990. Lower Cretaceous (Neocomian) fluvial deposits in eastern Kopet-Dagh Basin, north-eastern Iran: Cretaceous Res., v. 11, p. 163-174.

MOUSSAVI-HARAMI, R., and BRENNER, R.L., 1992. Geohistory analysis and petroleum reservoir characteristics of Lower Cretaceous (Neocomian) sandstones, Eastern Kopet-Dagh Basin, northeastern Iran: Am. Assoc. Petrol. Geol. Bull., v. 76, p. 1200-1208.

MOUSSAVI-HARAMI, R., and BRENNER, R.L., 1993. Diagenesis of Non-marine petroleum reservoirs: the Neocomian (Lower Cretaceous) Shurijeh Formation, Kopet-Dagh Basin, NE Iran: Jour. Pet. Geology, v. 16, p. 55-72.

MUCCI, A., 1987. Influence of temperature on the composition of magnesian calcite overgrowths precipitated from seawater: Geochim. Cosmochim. Acta, v. 51, p. 1977-1984.

MUCCI, A., 1988. Manganese uptake during calcite precipitation from seawater: conditions leading to the formation of a pseudokutnahorite: Geochim. Cosmochim. Acta, v. 52, p. 1859-1868.

MUCCI, A., and MORSE, J.W., 1983. The incorporation of Mg^{2+} and Sr^{2+} into calcite overgrowths: influences of growth rate and solution composition: Geochim. Cosmochim. Acta, v. 47, p. 217-233.

MUIR, M., LOCK, D., and VON DER BORCH, C.C., 1980. The Coorong model for penecontemporaneous dolomite formation in the Middle Proterozoic McArthur Group, Northern Territory, Australia: in Zenger, D.H., Dunham, J.B., and Ethington, R.L., (eds.), Concepts and Models of Dolomitization: Soc. Econ. Paleont. Mineral. Spec. Pub., No. 28, p. 51-67.

MUKHOPADHYAY, J., CHANDA, S.K., FUKUOKA, M., and CHAUDHURI, A.K., 1996. Deep-water dolomites from the Proterozoic Penganga Group in the Pranhita-Godavari Valley, Andhra Pradesh, India: Jour. Sed. Research, v. 66, p. 223-230.

MÜLLER, G., IRION, G., and FÖRSTNER, U., 1972. Formation and diagenesis of inorganic Ca-Mg carbonates in the lacustrine environment: Naturwissenschaften, v. 59, p. 158-164.

MULLINS, H.T., DIX, G.R., GARDULSKI, A.F., and LAND, L.S., 1988. Neogene deep-water

dolomite from the Florida-Bahamas Platform: in Shukla, V.J., and Baker, P.A., (eds.), Sedimentology and Geochemistry of Dolostones: Soc. Econ. Paleont. Mineral. Spec. Pub., No. 43, p. 235-243.

MULLINS, H.T., WISE, S.W., JR., LAND, L.S., SIEGEL, D.I., MASTERS, P.M., HINCHEY, E.J., and PRICE, K.R., 1985. Authigeneic dolomite in Bahamian peri-platform slope sediment: Geology, v. 13, p. 292-295.

MURATA, K.J., FRIEDMAN, I.I., and MADSEN, B.M., 1967. Carbon-13-rich diagenetic carbnates in Miocene formations of California and Oregon: Science, v. 156, p. 1484-1486.

MUSSMAN, W.J., MONTANEZ, I.P., and READ, J.F., 1988. Ordovician Knox paleokarst unconformity, Appalachians: in James, N.P., and Choquette, P.W., (eds.), Paleokarst: Springer-Verlag, New York, p. 211-228.

NARBONNE, G.M., KAUFMAN, A.J., and KNOLL, A.H., 1994. Integrated chemostratigraphy and biostratigraphy of the upper Windermere Supergroup (Neoproterozoic), Mackenzie Mountains, northwestern Canada: Geol. Soc. Am. Bull., v. 106, p. 1281-1291.

NELSON, C.S., 1978. Temperate shelf carbonate sediments in the Cenozoic of New Zealand: Sedimentology, v. 25, p. 737-771.

NELSON, C.S., 1988. An introductory perspective on non-tropical shelf carbonates: Sed. Geology, v. 60, p. 3-12.

NELSON, C.S., and SMITH, A.M., 1996. Stable oxygen and carbon isotope compositional fields for skeletal and diagenetic components in New Zealand Cenozoic nontropical carbonate sediments and limestones: a synthesis and review: New Zealand Jour. Geology, Geophysics, v. 39, p. 93-107.

NEUMANN, A.C., and LAND, L.S., 1975. Lime mud deposition and calcareous algae in the Bight of Abaco, Bahamas: a budget: Jour. Sed. Petrology, v. 45, p. 763-786.

NIEMANN, J.C., and READ, J.F., 1988. Regional cementation from unconformity-recharged aquifer and burial fluids. Mississippian Newman Limestone, Kentucky: Jour. sed. Petrology, v. 58, p. 688-705.

NOVAK, G.A., and COLVILLE, A.A., 1989. A practical interactive least squares cell parameter program using an electronic spreadsheet and a personal computer: Am. Mineralogist, v. 46, p. 453-457.

OHMOTO, H., 1986. Stable Isotope Geochemistry of Ore Deposits: in Valley, J.W., Taylor, H.P., and O'Neil, J. R., (eds.), Stable Isotopes in High Temperature Geological Processes: Min. Soc. Am., v. 16, p. 491-560.

OHMOTO, H., and RYE, R.O., 1979. Isotopes of sulfur and carbon: in Barnes, H.L., (ed.), Geochemistry of hydrothermal ore deposits: New York, John Wiley and Sons, p. 509-567.

OKHRAVI, R., and ALIZADEH KETEK LAHIJANI, H., 1994. Depositional environments and diagenesis of the Dorud Formation, Alborz Mountain, Iran: Sed. Geology, v. 93, p. 261-277.

O'NEIL, J.R., CLAYTON, R.N., and MAYEDA, T.K., 1969. Oxygen isotope fractionation in divalent metal carbonates: Jour. Chem. Physics, v. 51, p. 5547-5558.

OOMORI, T., KANESHIMA, H., and MAEZATO, Y., 1987. Distribution coefficient of Mg^{2+} ions between calcite and solution at 10-50^{o}C: Mar. Chemistry, v. 20, p. 327-336.

OPDYKE, B.N., and WILKINSON, B.H., 1990. Paleolatitude distribution of Phanerozoic marine ooids and cements: Palaeogeogr. Palaeoclimatol. Palaeoecol., v. 78, p. 135-148.

OSLEGER, D.A., and READ, J.F., 1991. Relation of eustasy to stacking patterns of meter-scale carbonate cycles, Late Cambrisan, U.S.A: Jour. Sed. Petrology, v. 61, p. 1225-1252.

PARK, R., 1976. A note on the significance of lamination in stromatolites: Sedimentology, v. 23, p. 379-393.

PARRISH, J.T., ZIEGLER, A.M., and SCOTESE, C.R., 1982. Rainfall patterns and the distribution of coals and evaporites in the Mesozoic and Cenozoic: Palaeogeogr. Palaeoclimatol. Palaeoecol., v. 40, p. 67-101.

PATTERSON, D.J., 1979. Geology and mineralisation at Renison Bell, western Tasmania: Unpub. Ph. D.thesis, Univ. Tasmania, 241 p.

PATTERSON, D., and OHMOTO, H., 1976. Stable isotope and fluid inclusion studies at the Renison Bell cassiterite-sulphide deposit, western Tasmania: in International Conference on Stable Isotopes: New Zealand, (abst.), p. 52.

PATTERSON, D.J., OHMOTO, H.H., and SOLOMON, M., 1981. Geologic setting and genesis of cassiterite-sulfide mineralisation at Renison Bell, western Tasmania: Econ. Geology, v. 76, p. 393-438.

PEDERSEN, T.F., and CALVERT, S.E., 1990. Anoxia vs. productivity: what controls the formation of organic-carbon rich sediments and sedimentary rocks?: Bull. Am. Assoc. petrol. Geol., v. 74, p. 454-466.

PERYT, T.M., 1983. Oncoids: Comment to Recent Developments: in Peryt, T.M., (ed.), Coated Grains: Springer-Verlag, Berlin, p. 273-275.

PETTIJOHN, F.J., 1975. Sedimentary Rocks: Harper and Row. New York, 628p.

PIERSON, B.J., and SHINN, E.A., 1985. Cement distribution and carbonate mineral stabilization in Pleistocene limestones of Hogsty Reef, Bahamas: in Schneidermann, N., and Harris, P.M., (eds.), Carbonate Cements: Soc. Econ. Paleont. Mineral. Spec. Pub., v. 36, p. 153-168.

PINEAU, F., JAVOY, M., HAWKINS, J.W., and CRAIG H., 1976. Oxygen isotope variations in marginal basin and ocean-ridge basalts: Earth Planetary Sci. Letters, v. 28, p. 299-307.

PINGITORE, N.R. Jr. 1978. The behaviour of Zn and Mn during carbonate diagenesis: theory and applications: Jour. Sed. Petrology, v. 48, p. 799-814.

PINGITORE, N.E., EASTMAN, M.P., SANDIDGE, M., ODEN, K., and FREIHA, B., 1988. The coprecipitation of manganese (II) with calcite, an experimental study: Mar. Chemistry, v. 25, p. 107-120.

PITMAN, W.C., 1978. Relationship between eustasy and stratigraphic sequences of passive margins: Geol. Soc. Am. Bull., v. 89, p. 1389-1403.

PLUMB, K.A., 1991. New Precambrian time scale: Episodes, v. 14, p. 139-140.

POMONI-PAPAIOANNOU, F., and CAROTSIERIS, Z.A., 1993. Dolomitization patterns in Jurassic-Cretaceous dissolution-collapse breccias of Mainalon Mountain (Tripolis Unit, central Peloponnesus-Greece): Carbonates and Evaporites, v. 8, p. 9-22.

POPP, B.N., ANDERSON, T.F., and SANDBERG, P.A., 1986. Brachiopods as indicators of original composition in some Paleozoic limestones: Geological Soc. Am. Bull., v. 97, p. 1262-1269.

POWELL, C. McA., PREISS, W.V., GATEHOUSE, C.G., KRAPEZ, B., and LI, Z.X., 1994. South Australian record of a Rodinian epicontinental basin and its mid-Neoproterozoic breakup (~700 Ma) to form the Palaeo-Pacific Ocean: Tectonophysics, v. 237, p. 113-140.

POWERS, D.W., and EASTERLING, R.G., 1982. Improved metodology for using embedded Markov chains to describe cyclical sediments: Jour. Sed. Petrology, v. 52, p. 913-924.

PREISS, W.V. (compiler), 1987. The Adelaide Geosyncline: Late Proterozoic stratigraphy, sedimentation, palaeontology and tectonics: Geol. Surv. South Aust. Bull., v. 53, 438p.

PREZBINDOWSKI, D.R., 1985. Burial cementation- is it important? a case study, Stuart City Trend, south-central Texas: in Schneidermann, N., and Harris, P.M., (eds.), Carbonate Cements: Soc. Econ. Paleont. Mineral. Spec. Pub. No. 36, p. 241-264.

PRICE, G.D., and SELLWOOD, B.W., 1994. Palaeotemperatures indicated by Upper Jurassic (Kimmeridgian-Tithonian) fossils from Mallorca determined by oxygen isotope composition: Palaeogeogr. Palaeoclimatol. Palaeoecol., v. 110, p. 1-10.

PRICE, G.D., and SELLWOOD, B.W., and Valdes, P.J., 1995. Sedimentological evaluation of general circulation model simulations for the "greenhouse" Earth: Cretaceous and Jurassic case studies: Sed. Geology, v. 100, p. 159-180.

PURSER, B.H., and SEIBOLD, E., 1973. The principal environmental factors influencing Holocene sedimentation and diagenesis in the Persian Gulf: in Purser, B.H., (ed.), The Persian Gulf: New York, Springer-Verlag, p. 1-9.

PYE, K., 1983. Red beds: in Goudie, A.S., Pye, K., (eds.), Chemical Sediments and Geomorphology: Academic Press, London, p. 227-263.

QING, H., and MOUNTJOY, E.W., 1989. Multistage dolomitization in Rainbow buildups, Middle Devonian Keg River Formation, Alberta, Canada: Jour. Sed. Petrology, v. 59, p. 114-126.

RADKE, B.M., and MATHIS, R.L., 1980. On the formation and occurrence of saddle dolomite: Jour. Sed. Petrology, v. 56, p. 1149-1168.

RAILSBACK, L.B., 1993a. Contrasting styles of chemical compaction in the Upper Pennsylvanian Dennis Limestone in the Midcontinent region, U.S.A: Jour. Sed. Petrology, v. 63, p. 61-72.

RAILSBACK, L.B., 1993b. Lithologic controls on morphology of pressure-dissolution surfaces (stylolites and dissolution seams) in Paleozoic carbonate rocks from the mideastern United States: Jour. Sed. Petrology, v. 63, p. 513-522.

RAILSBACK, L.B., ANDERSON, T.F., 1987. Control of Triassic seawater chemistry and temperature on the evolution of post-Paleozoic aragonite-secreting faunas: Geology, v. 15, p. 1002-1005.

RAMSAY, J.G., 1980. The crack-seal mechanism of rock deformation: Nature, v. 284, p. 135-139.

RANDAZZO, A.F., and ZACHOS, L.G., 1984. Classification and description of dolomite fabrics of rocks from the Floridan aquifer, USA: Sed. Geology, v. 37, p. 151-162.

RAO, C.P., 1981a. Criteria for recognition of cold-water carbonate sedimentation: Berriedale Limestone (Lower Permian), Tasmania, Australia: Jour. Sed. Petrology, v. 51, p. 491-506.

RAO, C.P., 1981b. Cementation in cold-water bryozoan sand, Tasmania, Australia: Mar. Geology, v. 40, p. M23-M33.

RAO, C.P., 1981c. Geochemical differences between tropical (Ordovician) and subpolar (Permian) carbonates, Tasmania, Australia: Geology, v. 9, p. 205-209.

RAO, C.P., 1986. Geochemistry of temperate-water carbonates, Tasmania, Australia: Mar. Geology, v. 71, p. 363-370.

RAO, C.P., 1988a. Paleoclimate of some Permo-Triassic carbonates of Malaysia: in Nelson, C.S., (ed.), Non-tropical Shelf Carbonates - Modern and Ancient: Sed. Geology, v. 60, p. 163-171.

RAO, C.P., 1988b. Oxygen and carbon isotope composition of cold-water Berriedale Limestone (Lower Permian), Tasmania, Australia: Sed. Geology, v. 60, p. 221-231.

RAO, C.P., 1989. Geochemistry of Gordon Limestone (Ordovician), Mole Creek, Tasmania, Australia: Aust. Jour. Earth Sci., v. 36, p. 65-71.

RAO, C.P., 1990a. Geochemical characteristics of cool-temperate carbonates, Tasmania, Australia: Carbonates and Evaporites, v. 5, p. 209-221.

RAO, C.P., 1990b. Petrography, trace elements and oxygen and carbon isotopes of Gordon Group carbonates (Ordovician), Florentine Valley, Tasmania, Australia: Sed. Geology, v. 66, p. 83-97.

RAO, C.P., 1990c. Marine to mixing zone dolomitization in peritidal carbonates: The Gordon Group (Ordovician), Mole Creek, Tasmania, Australia: Carbonates and Evaporites, v. 5, p. 153-178.

RAO, C.P., 1991. Geochemical differences between subtropical (Ordovician), temperate (Recent and Pleistocene) and subpolar (Permian) carbonates, Tasmania, Australia: Carbonates and Evaporites, v. 6, p. 83-106.

RAO, C.P., 1993a. Mixing water masses: the key in understanding the origin of temperate carbonates: Aust. Mar. Geosci. Workshop Abst., p.50.

RAO, C.P., 1993b. Carbonate minerals, oxygen and carbon isotopes in modern temperate bryozoa, eastern Tasmania, Australia: Sed. Geology, v. 88, p. 123-135.

RAO, C.P., 1993c. Oxygen and carbon isotope variation between dolomite and co-existing micrite pairs, Gordon Group (Ordovician), Mole Creek, Tasmania, Australia: Aust. Jour. Earth Sci., v. 40, p. 131-139.

RAO, C.P., 1994. Implications of isotopic fractionation and temperature on rate of formation of temperate shelf carbonates, eastern Tasmania, Australia: Carbonates and Evaporites, v. 9, p. 33-41.

RAO, C.P., 1996. Elemental composition of marine calcite from modern temperate shelf brachiopods, bryozoans and bulk carbonates, eastern Tasmania, Australia: Carbonates and Evaporites, v. 11, p. 1-18.

RAO, C.P., and ADABI, M.H., 1992. Carbonate minerals, major and minor elements and oxygen and carbon isotopes and their variation with water depth in cool, temperate carbonates, western Tasmania, Australia: Mar. Geology, v. 103, p. 249-272.

RAO, C.P., and AMINI, Z.Z., 1995. Faunal relationship to grain-size, mineralogy and geochemistry in Recent temperate shelf carbonates, western Tasmania, Australia: Carbonates and Evaporites, v. 10, p. 114-123.

RAO, C.P., and GREEN, D.C., 1983. Oxygen- and carbon-isotope composition of cold shallow-

marine carbonates of Tasmania, Australia: Mar. Geology, v. 9, p. 117-129.

RAO, C.P. and HUSTON, D., 1995. Mixing of water masses in modern temperate carbonate shelf environment, eastern Tasmania, Australia: the key in understanding the origin of temperate carbonates: Carbonates and Evaporites, v. 10, p. 105-113.

RAO, C.P., and JAYAWARDANE, M.P.J., 1994. Major minerals, elemental and isotopic composition in modern temperate shelf carbonates, eastern Tasmania, Australia: implications for the occurrence of extensive ancient non-tropical carbonates: Palaeogeogr. Palaeoclimatol. Palaeoecol., v. 107, p. 49-63.

RAO, C.P., and NELSON, C.S., 1992. Oxygen and carbon isotope fields for temperate shelf carbonates from Tasmania and New Zealand: Mar. Geology, v. 103, p. 273-286.

RAO, C.P., and WANG, B., 1990. Oxygen and carbon isotope composition of Gordon Group carbonates (Ordovician), Florentine Valley, Tasmania, Australia: Aust. Jour. Earth Sci., v. 37, p. 305-316.

READ, W.A., 1969. Analysis and simulation of Namurian sediments in central Scotland using Markov-process model: Jour. Inter. Assoc. Math. Geol., v.1, p. 199-219.

READ, J.F., and GOLDHAMMER, R.K., 1988. Use of Fischer plots to define third-order sea-level curves in Ordovician peritidal cyclic carbonates, Appalachians: Geology, v. 16, p. 895-899.

REECKMAN, S.A., 1988. Diagenetic alterations in temperate shelf carbonates from southern Australia: Sed. Geology, v. 60, p. 209-219.

REIMER, T.P., 1972. The evolution of rubidium and strontium content of shales: Neues Jahrbuch für Mineralogie Abhandlungen, v. 2, p. 167-195.

RIDING, R., 1983. Cyanoliths (Cyanoids): oncoids formed by calcified Cyanophytes: in Peryt, T.M., (ed.), Coated Grains: Springer-Verlag, Berlin, p.276-283.

ROBINSON, P., 1980. Determination of calcium, magnesium, manganese, strontium, sodium and iron in the carbonate fraction of limestones and dolomites: Chem. Geology, v. 28, p. 135-146.

ROMANEK, C.S., GROSSMAN, E.T. , and MORSE, J.W., 1992. Carbon isotope fractionation in synthetic aragonite and calcite: effects of temperature and precipitation rate: Geochim. Cosmochim. Acta , v. 56, p. 419-430.

ROSS, C.A., MOORE, G.T., and HAYASHIDA, D.N., 1992. Late Jurassic paleoclimate simulation-paleoecological implications for ammonoid provinciality: Palaios, v. 7, p. 487-506.

ROWLEY, D.B., 1992. Preliminary Jurassic reconstructions of the Circum-Pacific region: in Westermann, G.E.G., (ed.), The Jurassic of the Circum-Pacific, IGCT Project: Cambridge University Press, p. 15-27.

RUBIN, D.M., and FRIEDMAN, G.M., 1977. Intermittently emergent shelf carbonates: an example from the Cambro-Ordovician of eastern New York State: Sed. Geology, v. 19, p. 81-106.

RUBINSON, H., and CLAYTON, R.N., 1969. Carbon-13 fractionation between aragonite and calcite: Geochim. Cosmochim. Acta, v. 33, p. 997-1004.

RUPPEL, S.C., and CANDER, H.S., 1988. Dolomitization of shallow water platform carbonates by seawater and seawater-derived brines: San Andres Formation (Guadalupian), west Texas: in Shukla, V., and Baker, P.A., (eds.), Sedimentology and Geochemistry of Dolostones: Soc. Econ. Paleont. Mineral. Spec. Pub., No. 43, p. 245-262.

RUSH, P.F., and CHAFETZ, H.S., 1990. Fabric-rententive, non-luminescent brachiopods as indicators of original $d^{18}O$ and $d^{13}C$ composition: a test: Jour. Sed. Petrology, v. 60, p. 968-981.

RUTTNER, A.W., 1983. The Pre-Liassic Basement of Aghdarband Area (eastern Kopet-Dagh range): Geol. Survey of Iran Rept., v. 51, p. 451-462.

RUTTNER, A.W., 1988. The coal deposits of Aghdarband, NE Iran and its geological frame: 2nd Mining symp., Iran, p. 183-203.

RYE, D.M., and WILLIAMS, N., 1981. Studies of the base metal sulfide deposits at Mc Arthur River, Northern Territory, Australia: III the stable isotope geochemistry of the H.Y.C., Ridge, and Cooley Deposits: Econ. Geology, v. 76, p. 1-26.

SADLER, P.M., OSLEGER, D.A, and MONTANEZ, I.P., 1993. On the labelling, length, and objective basis of Fischer plots: Jour. Sed. Petrology, v. 63, p. 360-368.

SALLER, A.H., 1984. Petrologic and geochemical constrains on the origin of subsurface dolomite, Eniwetak Atoll: an example of dolomitization by normal seawater: Geology, v. 12, p. 217-220.

SAMI, T.T., and JAMES, N.P., 1993. Evolution of an early Proterozoic foreland basin carbonate platform, lower Pethei Group, Great Slave Lake, north-west Canada: Sedimentology, v. 40, p. 403-430.

SANDBERG, P.A., 1975. New interpretations of Great Salt Lake ooids and nonskeletal carbonate mineralogy: Sedimentology, v. 22, p. 497-537.

SANDBERG, P.A., 1983. An oscillating trend in Phanerozoic nonskeletal carbonate mineralogy: Nature, v. 305, p. 19-22.

SANDBERG, P.A., 1985. Aragonite cements and their occurrence in ancient limestones: in Schneidermann, N., and Harris, P.M., (eds.), Carbonate Cements: Soc. Econ. Paleont. Mineral. Spec. Pub. No. 36, p. 33-57.

SANDBERG, P.A., and HUDSON, J.D., 1983. Aragonite relic preservation in Jurassic calcite-replaced bivalves: Sedimentology, v. 30, p. 879-892.

SARKAR, S., CHANDA, S.K., and BHATTACHARRYA, A., 1982. Soft-sediment deformation fabric in the Precambrian Bhander oolite, central India: Jour. Sed. Petrology, v. 52, p. 95-107.

SARTHEIM, M., and WALGER, E., 1973. Classification of modern marl sediments in the Persian gulf by factor analysis: in Purser, B.H., (ed.), The Persian Gulf: New York, Spring-Verlag, p. 81-97.

SASS, E., and BEIN, A., 1988. Dolomites and salinity: a comparative geochemical study: in Shukla, v., and Baker, P.A., (eds.), Sedimentology and Geochemistry of Dolostones: Soc. Econ. Paleont. Mineral. Spec. Pub., v. 43, p. 223-233.

SAVARD, M.M., VEIZER, J., and HINTON, R., 1995. Cathodoluminescence at low Fe and Mn concenytrations: a SIMS study of zones in natural calcites: Jour. Sed. Petrology, v. 65, p. 208-213.

SAWKA, W.N., HEIZLER, M.T., KISTLER, R.W., and CHAPPELL, B.W., 1990. Geochemistry of highly fractionated I-and S-type granites from the tin-tungsten province of western Tasmania: in Stein, H.J., and Hannah, J.L., (eds.), Ore-bearing Granite Systems; Petrogenesis and Mineralizing Processes: Geol. Soc. Am. Spec. Pap. v 246, p. 161-179.

SCHERMERHORN, L.J.G., 1983. Late Proterozoic glaciation in the light of CO_2 depletion in the atmosphere: Geol. Soc. America Mem., v. 161, p. 309-315.

SCHIDLOWSKI, M., EICHMANN, R., and JUNGE, C.E., 1975. Precambrian sedimentary carbonates: carbon and oxygen isotope geochemistry and implications for the terrestrial oxygen budget: Precambrian Res., v. 2, p. 1-69.

SCHLAGER, W., and JAMES, N.P., 1978. Low-magnesian calcite limestones forming at the deep-sea floor, Tongue of the Ocean, Bahamas: Sedimentology, v. 25, p. 675-702.

SCHNEIDER, 1977. Diagenesis devonishcer Karbonatkomplexe Mitteleuropas: Geol. Jahrbuch, D 21, 108p.

SCHOLLE, P.A., 1978. A Colour Illustrated Guide to Carbonate Rock Constituents, Textures, Cements and Porosities: Am. Assoc. Petrol. Geol. Mem., 27, 241p.

SCHOLLE, P.A., and ARTHUR, M.A., 1980. Carbon isotope fluctuations in Cretaceous pelagic limestones: potential stratigraphic and petroleum exploration tool: Am. Assoc. Petrol. Geol. Bull., v. 64, p. 67-87.

SCHOLLE, P.A., and HALLEY, R.B., 1985. Burial diagenesis: out of mind!: in Schneidermann, N., and Harris, P.M., (eds.): Carbonate Cements: Soc. Econ. Paleont. Mineral. Spec. Pub., v. 36, p. 309-334.

SCHOPF, W.J., 1992. Times of origin and earliest evidence of major biologic groups: in Schopf, J.W., and Klein, C., (eds.), The Proterozoic Biosphere, A Multidisciplinary Study: Cambridge Univ., Press, p. 587-593.

SCHROEDER, J.H., 1972. Fabrics and sequences of submarine carbonate cements in Holocene Bermuda cup reefs: Geol. Rdsch., v. 61, p. 708-730.

SCHROEDER, J.H., 1973. Submarine and vadose cements in Pleistocene Bermuda reef rock: Sed. Geology, v. 10, p. 179-204.

SCHROEDER, J.H., 1979. Carbonate diagenesis in Quaternary beachrock of Uyombo, Kenya: sequences of processes and coexistence of heterogenic products: Geol. Rundschau, v. 68, p. 894-919.

SCOFFIN, T.P., 1987. An Introduction to Carbonate Sediments and Rocks: Blackie and Son Ltd., 274p.

SEARL, A., 1988. The limitations of "cement stratigraphy", as revealed in some Lower Carboniferous oolites from South Wales: Sed. Geology, v.57, p. 171-183.

SENGÖR, A.M.C., ALTINER, D.CIN.A., USTAÖMER, T., and HSÜ, K.J., 1988. Origin and assembly of the Tethyside orogenic collage at the expense of Gondwanaland: in Audley-Charles, M.G. and Hallam, A., (eds.), Gondwana and Tethys, p. 119-181. Oxford University Press.

SELLEY, R.C., 1970. Studies of sequence in sediments using a simple mathematical device: Quaternary. Jour. Geol. Soc. London, v. 125, p. 557-581.

SHACKLETON, N.J., and KENNETT, J.P., 1975. Paleotemperature history of the Cenozoic and the initiation of Antarctic glaciation: oxygen and carbon isotope analyses in DSDP site 277, 279 and 281: in Kennett, J.P., and Houtz, R.E., (eds.), Initial Reports of the Deep-Sea Drilling Project, XXIX: U.S. Govt. Printing Office, Washington D.C., p. 743-755.

SHANMUGAM, G., and BENEDICT III, G.L., 1983. Manganese distribution in the carbonate fraction of shallow to deep marine lithofacies, Middle Ordovician, eastern Tennessee: Sed. Gology, v. 35, p. 159-175.

SHAVER, R.H., et al., 1984. Midwestern basin and arches region correlation chart: Am. Assoc. Petrol. Geologist COSUNA Correlation Chart Series.

SHAW, A.B., 1964. Time in stratigraphy: McGraw-Hill, New York, N.Y., 365p.

SHELTON, K.L., 1983. Composition and origin of ore-forming fluids in a carbonate-hosted porphyry copper and skarn deposit: a fluid inclusion and stable isotope study of mine Gaspe, Quebec: Econ. Geology, v. 78, p. 387-420.

SHEPPARD, S.M.F., and SCHWARCZ, H.P., 1970. Fractionation of carbon and oxygen isotopes and magnesium between coexisting metamorphic calcite and dolomite: Contri. Mineral. and Petrology, v. 26, p. 161-198.

SHINN, C.A., STEINEN, R.P., LIDZ, B.H., and SWART, P.K., 1989. Whitings, a sedimentologic dilemma: Jour. Sed. Petrology, v. 59, p. 147-161.

SHINN, E.A., 1971. Aspects of diagenesis of algal cup reefs in Bermuda: Trans. Gulf Coast Assoc. of Geological Soc., v.21, p. 387-394.

SHINN, E.A., 1983. Tidal flat environment: in Scholle, P.A., Bebout, D.G., and Moore, C.H., (eds.), Carbonate Depositional Environments: Am. Assoc. Petrol. Geol. Mem., v. 33, p. 173-210.

SHINN, E.A., and ROBBIN, D. M., 1983. Compaction, pressure solution, and lithification in fine-grained shallow-water limestones: Jour. Sed. Petrology, v. 53, p. 595-618.

SHUKLA, V., and BAKER, P.A., 1988. Sedimentology and geochemistry of dolostones: Soc. Econ. Paleont. Mineral. Spec. Pub. No. 43, 266p.

SHUKLA, V., and FRIEDMAN, G.M., 1983. Dolomitization and diagenesis in a shallowing-upward sequence: the Lockport Formation (Middle Silurian), New York State: Jour. Sed. Petrology, v. 53, p. 703-717.

SIBLEY, D.F., 1980. Climatic control of dolomitization, Seroe Domi Formation (Pliocene), Bonaire, N.A: in Zenger, D.H., Dunham, J.B., and Ethington, R.L., (eds.), Concepts and Models of Dolomitization: Soc. Econ. Paleont. Mineral. Spec. Pub. No. 28, p. 247-258.

SIBLEY, D.F., DEDOES, R.E., and BARTLETT, T.R., 1987. Kinetics of dolomitization: Geology, v. 15, p. 1112-1114.

SIBLEY, D.F., and GREGG, J.M., 1987. Classificatin of dolomite rock texture: Jour. Sed. Petrology, v. 57, p. 967-975.

SLOAN, L.C. and BARRON, E.J., 1990. "Equable" climates in Earth history?: Geology, v. 18, p. 489-492.

SMITH, A.G., HURLEY, A.M., and BRIDEN, J.C., 1981. Phanerozoic Paleocontinental World Maps: Cambridge Univ. Press, Cambridge, 102pp.

SOLOMON, M., 1981. An introduction to the geology and metallic ore deposits of Tasmania: Econ. Geology, v. 76, p. 194-208.

SOLOMON, M., and GRIFFITHS, J.R., 1974. Aspects of the early history of the southern part of the Tasman Orogenic zone: in Denmead, A.K., Tweedale, G.W., and Wilson, A.F., (eds.), The Tasman geosyncline- A Symposium: Geol. Soc. Aust. Queensland Division, p. 19-44.

SPENCER, R.J., and LOWENSTEIN, T.K., 1990. Evaporites: in McIlreath, I.A., and Morrow, D.W., (eds.), Diagenesis: St. Johns, Newfounland: Geosci. Canada Reprint Series 4, Geol. Assoc. Canada, p. 141-163.

SPERBER, C.M., WILKINSON, B.H., and PEACOR, D.R., 1984. Rock composition, dolomite stoichiometry and rock/water reactions in dolomitic carbonate rocks: Jour. Geology, v.92, p. 609-622.

SPICER, R.A., and CORFIELD, R.M., 1992. A review of terrestrial and marine climates in the Cretaceous with implications for modelling the Greenhouse Earth: Geol. Mag., v. 129, p. 169-180.

SPRY, A., 1969. Metamorphic Textures: Oxford, Pergamon press, 350p.

SRINIVASAN, K., WALKER, K.R., and GOLDBERG, S.A., 1994. Determining fluid source and possible pathwayes during burial dolomitization of Maryville Limestone (Cambrian), Southern Appalachians, USA: Sedimentology, v. 41, p. 293-308.

STEINHAUFF, D.M., 1989. Marine cements: in Walkere, K.R., (ed.), The Fabric of Cements in Paleozoic Limestones: Univ. Tennessee, Studies in Geology, v. 20, p. 37-53.

STERNBACH, C.A., and FRIEDMAN, G.M., 1984. Ferroan carbonates formed at depth require porosity well-log correction: Hunton Group, deep Anadarko Basin (Upper Ordovician to Lower Devonian) of Oklahoma and Texas: Transactions of Southwest Section: Am. Assoc. Petrol. Geologist, p. 167-173.

STEWART, W.N., and TAYLOR, T.N., 1965. The peel technique: in Kummel, B., and Raup, D., (eds.), Handbook of Palaeontological Techniques: San Francisco, Freeman, p. 224-232.

STEVENS, G.R., 1971. Relationship of isotopic temperatures and faunal realms to Jurassic-Cretaceous paleogeography, particularly of the South-west Pacific: Jour. Roy. Soc. New Zealand, v. 1, p. 145-158.

STEVENS, G.R., and CLAYTON, R.N., 1971. Oxygen isotope studies on Jurassic and Cretaceous belemnites and their biogeographic significance: New Zealand, Jour. Geol. Geophys., v. 14, p. 829-897.

STILLER, M., ROUNICK, J.S., and SHASHA, S., 1985. Extreme carbon-isotope enrichments in evaporating brines: Nature, v. 316, p. 434-435.

STILLWELL, F.L., and EDWARDS, A.B., 1943. Mineral composition of the tin ores at Renison Bell, Tasmania: Proc. Aust. Inst. Min. Metall., p. 131-132, 173-186.

STRASSER, A., 1986. Ooids in Purbneck limestones (Lower most Cretaceous) of the Swiss and Ferench Jura: Sedimentology, v. 33, p. 711-727.

SUPKO, P.R., 1977. Subsurface dolomites, San Salvador, Bahamas: Jour. Sed. Petrology, v. 47, p. 1063-1077.

SVERJENSKY, D.A., 1981. Isotopic alteration of carbonate host rocks as a function of water to rock ratio - an example from the Upper Mississippi Valley zinc-lead district: Econ. Geology, v. 76, p. 154-157.

SWIRYDCZUK, K., 1988. Mineralogical control on porosity type in Jurassic Smackover ooid grainstones, southern Arkansas and Northern Louisiana Jour. Sed. Petrology, v. 58, p. 339-347.

TAN, F.C., HUDSON, J.D., and KEITH, M.L., 1970. Jurassic (Callovian) paleotemperatures from Scotland. Earth and Planetary Sci. Letters, v. 9, p. 421-426.

TARUTANI, T., CLAYTON, R.N., and MAYEDA, T.K., 1969. The effect of polymorphism and magnesium substitution on oxygen isotope fractionation between calcium carbonate and water: Geochim. Cosmochim. Acta, v. 33, p. 987-996.

TAVIANI, M., REID, D.E., and ANDERSON, J.B., 1993. Skeletal and isotopic composition and paleoclimatic significance of Late Pleistocene Carbonates, Ross Sea, Antarctica: Jour. Sed. Petrology, v. 63, p. 84-90.

TAYLOR, B. E., 1987. Stable isotope geochemistry of ore-forming fluids: in Kyser, T.K., (ed.), Short Course in Stable Isotope Geochemistry of Low Temperature Fluids, Saskatoon: Min. Assoc. Canada., v. 13, p. 337-445.

TAYLOR, B.E., and BUCHER-NURMINEN, K., 1986. Oxygen and carbon isotope and cation geochemistry of metasomatic carbonates and fluids - Bergell aureole, Northern Italy: Geochim. Cosmochim. Acta, v. 50, p. 1267-1279.

TAYLOR, B.L., 1954. Progress report on the North Pieman mineral area: Unpub. Rept. Tasmania Dept. Mines, p. 159-199.

TAYLOR, H.P., 1974. The application of hydrogen and oxygen isotope studies to problems of hydrothermal alteration and ore deposition: Econ. Geology, v. 69, p. 843-883.

TAYLOR, H.P. (Jr.), 1977. Water-rock interaction and the origin of H_2O in granitic batholiths: Jour. Geol. Soc. London, v. 133, p. 509-558.

TAYLOR, T.R., and SIBLEY, D.F., 1986. Petrographic and geochemical characteristics of dolomite types and the origin of ferroan dolomite in the Trenton Formation, Ordovician, Michigan Basin: Sedimentology, v. 33, p. 61-85.

TEN HAVE, T., and HEIJNEN, W., 1985. Cathodoluminescence activation and zonation in carbonate rocks: an experimental approach: Geologie en Mijnbouw, v. 64, p. 297-310.

TUCKER, M.E., 1982. Precambrian dolomites: petrographic and isotopic evidence that they differ from Phanerozoic dolomites: Geology, v. 10, p. 7-12.

TUCKER, M.E., 1983. Diagenesis, geochemistry, and origin of a Precambrian Dolomite: the Beck Spring Dolomite of eastern California: Jour. Sed. Petrology, v. 53, p. 1097-1119.

TUCKER, M.E., 1984. Calcitic, aragonitic and mixed calcitic-aragonitic ooids from mid-Proterozoic Belt Supergroup, Montana: Sedimentology, v. 31, p. 627-644.

TUCKER, M.E., 1985. Calcitized aragonite ooids and cements from the late Precambrian Biri Formation of southern Norway: Sed. Geology, v. 43, p. 67-84.

TUCKER, M.E., 1986a. Carbon isotope excursions in Precambrian/Cambrian boundary beds, Morocco: Nature, v. 319, p. 48-50.

TUCKER, M.E., 1986b. Formely aragonitic limestones associated with tillites in the Late Precambrian of Death Valley, California: Jour. Sed. Petrology, v. 56, p. 818-830.

TUCKER, M.E., 1989. Carbon isotopes and Precambrian-Cambrian boundary Geology, Australia: ocean basin formation, seawater chemistry and organic evolution: Terra Nova, v. 1, p. 573-582.

TUCKER, M.E., 1991. Sedimentary Petrology: an introduction to the origin of sedimentary rocks: Blackwell, Sci. Pub., London, 260 p.

TUCKER, M.E., CALVET, F., and HUNT, D., 1993. Sequence stratigraphy and carbonate ramps: system tracts, models and application to the Muschelkalk carbonate platforms of eastern Spain: in Posamentier, H.W., Summerhayes, C.P., Haq, B.U., and Allen, G.P., (eds.), Sequence Stratigraphy and Facies Associations: Inter. Assoc. Sed. Spec. Pub., v. 18, p. 397-415.

TUCKER, M.E., and WRIGHT, P.V., 1990. Carbonate Sedimentology: Blackwell, Sci. Pub.,

London, 482 p.

TURNER, J.V., 1982. Kinetic fractionation of carbon-13 during calcium carbonate precipitation: Geochim. Cosmochim. Acta, v. 46, p. 1183-1191.

TURNER, J.V., ANDERSON, T.F., SANDBERG, P.A., and GOLDSTEIN, S.J., 1986. Isotopic, chemical and textural relations during the experimental alteration of biogenic high-magnesium calcite: Geochim. Cosmochim. Acta, v. 50, p. 495-506.

TURNER, N.J., 1993. K-Ar geochronology in the Arthur Metamorphic Complex, Ahrberg Group and Oonah Formation, Corinna district: Mineral Resources Tasmania Rept., No. 27.

UREY, H.C, 1947. The thermodynamic properties of isotopic substance: Jour. Chem. Soc., p. 562-581.

USDOWSKI, E., 1989. Synthesis of dolomite and magnesite at 60°C in the system Ca^{2+}-Mg^{2+}-CO^{2-}-Cl_2^{2-}-H_2O: Naturwissenschaften, v. 76, p. 343-375.

VAHRENKAMP, V.C., and SWART, P.K., 1990. New distribution coefficient for the incorporation of strontium into dolomites and its implication for the formation of ancient dolomites: Geology, v. 18, p. 387-391.

VAIL, P.R., 1987. Seismic stratigraphy interpretation procedure: in Bally, A.W., (ed.), Seismic stratigraphy folio series: Tulsa, Oklahoma, Am. Assoc. Petrol. Geol., p. 1-11.

VALDES, P.J., 1993. Atmospheric general circulation models of Jurassic: Philos. Trans. Roy. Soc. London. Ser. B., v. 341, p. 317-326.

VALDES, P.J., and SELLWOOD, B.W., 1992. A palaeoclimate model for the Kimmeridgian: Palaeogeogr. Palaeoclimatol. Palaeoecol., v.95, p. 47-72.

VALDES, P.J., SELLWOOD, B.W., and PRICE, G.D., 1995. Modelling Late Jurassic Milankovitch climate variations: in House, M.R., and Gale, A.S., (eds.), Orbital Forcing Timescales and Cyclostratigraphy: Geol. Soc. London, Spec. Publ., No. 85, p. 115-132.

VEIZER, J., 1983. Chemical diagenesis of carbonates: theory and application of trace element technique: Stable Isotopes in Sedimentary Geology: Soc. Econ. Palaeont. Mineral. short course No.10, p. 3-1 to 3-100.

VEIZER, J., 1989. Strontium isotopes in seawater through time: Ann. Rev. Earth Planet. Sci., v. 17, p. 141-167.

VEIZER, J., and DEMOVIC, R., 1973. Environmental and climatic controlled fractionation of elements in the Mesozoic carbonate sequences of the Western Carpathians: Jour. Sed. Petrology, v. 43, p. 258-271.

VEIZER, J., FRITZ, P., and JONES, B., 1986. Geochemistry of brachiopods: oxygen and carbon isotopic records of the Paleozoic oceans: Geochim. Cosmochim. Acta, v. 50, p. 1679-1696.

VEIZER, J., and HOEFS, J., 1976. The nature of $^{18}O/^{16}O$ and $^{13}C/^{12}C$ secular trends in sedimentary carbonates: Geochim. Cosmochim. Acta, v. 40, p. 1387-1395.

VEIZER, J., HOLSER, W.T., and WILGUS, C.K., 1980. Correlation of $^{13}C/^{12}C$ and $^{34}S/^{32}S$ secular variations: Geochim. Cosmochim. Acta, v. 44, p. 579-587.

VEIZER, J., LEMIEUX, J., JONES, B., GIBLING, M.R., and SAVELLE, J., 1978. Paleosalinity and dolomitization of a Lower Paleozoic carbonate sequence, Somerset and Prince of Wales Islands, Arctic Canada: Canadian Jour. Earth Sci., v. 15, p. 1448-1461.

VIDETICH, P.E., 1982. Origin, marine diagenesis, and early freshwater diagenesis of limestones

and dolomite (Tertiary and Recent): stable isotopic, electron microprobe and petrographic studies: Unpub. Ph.D. thesis, Brown University , 298p.

VON DER BORCH, C.C., 1976. Stratigraphy and formation of Holocene dolomitic carbonate deposits of the Coorong area, South Australia: Jour. Sed. Petrology, v. 46, p. 952-966.

VON DER BORCH, C.C., and LOCK, D.E., 1979. Geological significance of Coorong dolomites: Sedimentology, v. 26, p. 813-824.

WADLEIGH, M.A., and VEIZER J., 1992. $^{18}O/^{16}O$ and $^{13}C/^{12}C$ in lower Paleozoic articulate brachiopods: implications for isotopic composition of seawater: Geochim. Cosmochim. Acta, v. 56. p. 431-443.

WALKER, G., 1985. Mineralogical applications of luminescence techniques: in Berry, F.J., and Vaughan, D.J., (eds.), Chemical Bonding and Spectroscopy in Mineral Chemistry: Chapman and Hall, London, p. 103-140.

WALLACE, M.W., KENNEDY, M., and LAVIN, C., 1995. Sedimentology and geochemistry of Late Proterozoic glacial-associated Cap Dolomite in Australia: Cool Climatic Carbonate Conference, Abst, p. 80-82.

WALLER, G.A., 1902. Rerport on the tin ore deposits of North Dundas: Report to Secr. Mines, Tasmania.

WALTER, L.M., 1986. Relative efficiency of carbonate dissolution and precipitation during diagenesis: a progress report on the role of solution chemistry: in Gautier, D.L., (ed.), Roles of Organic Matter in Mineral Diagenesis: Soc. Econ. Paleont. Mineral. Spec. Pub., v. 38. p. 1-12.

WALTER, L.M., and MORSE, J.W., 1984. Magnesium calcite stabilities- a reevaluation: Geochim. Cosmochim. Acta, v. 48, p. 1059-1069.

WALTER, M.R., and BAULD, J., 1983. The association of sulphate evaporites, stromatolitic carbonates and glacial sediments: examples from the Proterozoic of Australia and the Cainozoic of Antarctica: Precambrian Res., v. 21, p. 129-148.

WALTER, M.R., GROTZINGER, J.P., and SCHOPF, J.W., 1992. Proterozoic stromatolites: in Schopf, J.W., and Klein, C., (eds.), The Proterozoic Biosphere, A Multidisciplinary Study: Cambridge Univ., Press, p. 253-260.

WANLESS, H.R., 1979. Limestone response to stress: pressure solution and dolomitization: Jour. Sed. Petrology, v. 49, p. 437-462.

WARD, L.K., 1909. The tin field of North Dundas: Geol. Surv. Tas. Bull. No. 6.

WARD, M.A., 1981. The geology of the granites at Renison Bell-Pine Hill: Unpub. B.Sc. Honours thesis, Univ. Tasmania, 156 p.

WARREN, J.K., 1988. Sedimentology of Coorong dolomite in the Salt Creek region, South Australia: Carbonates and Evaporites, v. 3, p. 175-199.

WARREN, J.K., 1996. Evaporites, brines and base metals: what is an evaporite? defining the rock matrix: Australian Jour. Earth Sci., v. 43, p. 115-132.

WARREN, J.K., and KENDALL, C.G. ST C. 1985. Comparison of sequences formed in marine sabkha (subaerial) and salina (subaqueous) settings: modern and ancient: Am. Assoc. Petrol. Geol. Bull., v. 69, p. 1013-1023.

WASS, R.E., CONNOLLY, R.J., and MACINTYRE, R.J., 1970. Bryozoan carbonate sand continuous along southern Australia: Mar. Geology, v. 9, p. 63-73.

WEBER, J.N., and WOODHEAD, P.M. J., 1970. Carbon and oxygen isotope fractionation in the skeletal carbonate of reef building corals: Chem. Geology, v. 6, p. 93-117.

WELLS, N.A., 1989. A program in BASIC for facies-by-facies Markov chain analysis: Computer and Geoscience, v. 15, p. 143-155.

WETZEL, A., 1989. Influence of heat flow on ooze/chalk cementation: quantification from consolidated parameters in DSDP sites 504 and 505 sediments: Jour. Sed. Petrology, v. 32, p. 776-780.

WHITAKER, F.F., SMART, P.L., VAHRENKAMP, V.C., NICHOLSON, H. and WOGELIUS, R.A., 1994. Dolomitization by near-normal seawater ? Field evidence from the Bahamas: in Purser, B., Tucker, M., and Zenger, D., (eds.), Dolomites: Inter. Assoc. Sediment. Spec. Pub., v. 21, p. 111-132.

WICKHAM, S.M., and PETERS, M.T., 1993. High $\delta^{13}C$ Neoproterozoic carbonate rocks in western North America: Geology, v. 21, p. 165-168.

WILKINSON, B.H., 1982. Cyclic cratonic carbonates and Phanerozoic calcite seas: Jour. Geol. Education, v. 30, p. 189-203.

WILKINSON, B.H., BUCZYNSKI, C., and OWEN, R.M., 1984. Chemical control of carbonate phases: implication from upper Pennsylvanian calcite-aragonite ooids of southeastern Kansas: Jour. Sed. Petrology, v. 54, p. 932-947.

WILKINSON, B.H., and LANDING, ED., 1978: Eggshell diagenesis and primary radial fabric in calcite ooids: Jour. Sed. Petrology, v. 48, p. 1129-1138.

WILKINSON, B.H., OWEN, R.M., and CARROLL, A.R., 1985. Submarine hydrothermal weathering, global eustasy, and carbonate polymorphism in Phanerozoic marine oolites: Jour. Sed. Petrology, v.55, p. 171-183.

WILLIAMS, E., 1976. Tasman Fold Belt in Tasmania. Explanatory Notes for the 1:500,000 structural map of Pre-Carboniferous rocks of Tasmania: Tasmania Dept. Mines.

WILLIAMS, E., 1978. Tasman Fold Belt in Tasmania: Tectonophysics, v. 48, p. 159-205.

WILLIAMS, E., 1979. Tasman fold belt system in Tasmania. Explanatory notes for the 1:500,000 structural map of Pre-Carboniferous rocks of Tasmania. Revised ed: Tasmania Dept. Mines., 29 p.

WILLIAMS, E., 1989. Summary and Synthesis: in Burrett, C.F., and Martin, E.L., (eds.), Geology and Mineral Resources of Tasmania: Geol. Soc. Australia Spec. Pub., v. 15, P. 468-499.

WILLIAMS, G.E., 1975. Late Precambrian glacial climate and the Earth's obliquity: Geol. Mag., v. 112, p. 441-465.

WILLIAMS, G.E., 1979. Sedimentology, stable-isotope geochemistry and paleoenvironment of dolostones capping late Precambrian glacial sequences in Australia: Jour. Geol. Soc. Australia, v. 26, p. 377-386

WILLIAMS, G.E., 1993. History of the Earth's obliquity: Earth Sci. Rev., v. 34, p. 1-45.

WILSON, J.L., 1975. Carbonate Facies in Geologic History: Springer-Verlag, New York, 471 p.

WINEFIELD, P.R., NELSON, C.S., and HODDER, A.P.W., 1996. Discriminating temperate carbonates and their diagenetic environments using bulk elemental geochemistry: a reconnaissance study based on New Zealand Cenozoic limestones: Carbonates and

Evaporites, v. 11, p. 19-31.

WINLAND, H.D., and MATTHEWS, R.K., 1974. Origin and significance of grapestone, Bahama Island: Jour. Sed. Petrology, v. 44, p. 921-927.

WONG, P.K., and OLDERSHAW, A., 1981. Burial cementation in the Devonian Kaybob Reef Complex, Alberta, Canada: Jour. Sed. Petrology, v. 51, p. 507-520.

WRAY, J.L., 1977. Calcareous algae: Elsevier, Amsterdam, 186p.

WRIGHT, V.P., 1983. Morphogenesis of oncoids in the Lower Carboniferous Llanelly Formation of South Wales: in Peryt, T.M., (ed.), Coated Grains: Springer-Verlag, Berlin, p. 424-434.

WRIGHT, V.P., 1986. Facies sequences on a carbonate ramp: the carboniferous limestone of South Wales: Sedimentalogy, v. 33, p. 221-241.

YASSINI, I., and JONES, B.G., 1995. Recent foraminifera and ostracoda from estuarine and shelf environments on the southeastern coast of Australia: The University of Wollongong Press, 484p.

YE, Q., and MAZZULLO, S.J., 1993. Dolomitization of Lower Permian platform facies, Wichita Formation, north platform, Midland Basin, Texas: Carbonates and Evaporites, v. 8, p. 55-70.

YEO, G.M., 1986. Iron-formation in the late Proterozoic Rapitan Group, Yukon and Northwest Territories: in Morin, J.A., (ed.), Mineral deposits of the Northern Cordillera: Canadian Institute of Mining and Metallurgy, Spec., v. 37, p. 142-153.

ZEMPOLICH, W.G., WILKINSON, B.H., and LOHMANN, K.C., 1988. Diagenesis of Late Proterozoic carbonates: the Beck Spring Dolomite of eastern California: Jour. Sed. Petrology, v. 58, p. 656-672.

ZENGER, D.H., 1982. Precambrian dolomites: petrographic and isotopic evidence that they differ from Phanerozoic dolomites: Comments, Geology, December, 662p.

ZENGER, D.H., 1983. Burial dolomite in the Lost Burro Formation (Devonian), east-central California, and the significance of late diagenetic dolomitization: Geology, v. 11, p. 519-522.

ZENGER, D.H., and DUNHAM, J.B., 1980. Concepts and Models of Dolomitization: an introduction: in Zenger, D.H., Dunham, J.B., and Ethington, R.L., (eds.), Concepts and Models of Dolomitization: Soc. Econ. Paleont. Mineral. Spec. Pub., v. 28, p. 1-9.

ZENGER, D.H., and DUNHAM, J.B., 1988. Dolomitization of Siluro-Devonian limestones in a deep core (5350 meters), southeastern New Mexico: in Shukla, V., and Baker, P.A., (eds.), Sedimentology and Geochemistry of Dolostones: Soc. Econ. Paleont. Mineral. Spec. Pub., v. 43, p. 161-173.

ZENGER, D.H., DUNHAM, J.B., and ETHINGTON, R.L., 1980. Concepts and Models of Dolomitization: Soc. Econ. Paleont. Mineral. Spec. Pub., v. 28, 320p.

ZIEGLER, A.M., SCOTESE, C.R., and BARRETT, S.F., 1983. Mesozoic and Cenozoic paleogeographic maps: in Brosche, P., and Sündermann, J., (eds.), Tidal Friction and the Earth's Rotation II: Springer, Berlin, p. 240-252.

ZIEGLER, P.A., 1988. Evolution of the Arctic-North Atlantic and the western Tethys: Am. Assoc. Petrol. Geol. Mem., v. 43, 198p.

APPENDICES

APPENDIX 1

STRATIGRAPHIC SECTIONS OF THE MOZDURAN FORMATION

In the Shurijeh, Bagak, Padeha, Mozduran, Gorgoreh and Bazangan sections

The following stratigraphic sections were computer drafted using modified Auslog software.

LEGEND

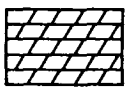 dolomite

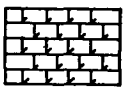 dolomitic limestone

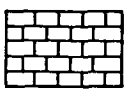 limestone

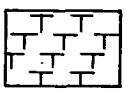 marl

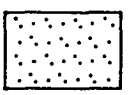 sandstone

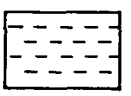 shale

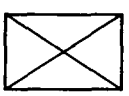 cover

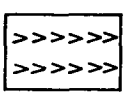 weathered gypsiferous layers

 stylolite

 subaerial exposure (fenestrae)

 algae

 anhydrite - gypsum

 cross strata

 boring

 geopetal structure

 chert

 veins

 shattered micritic envelope

 spalled ooids

 flat pebble conglomerate

 calcite pseudomorph after gypsum

 fracture

 voids andvugs

 digitate column

 oncoids

Drawn 27-May-95

STRATIGRAPHIC SECTION OF MOZDURAN FORMATION – SHURIJEH

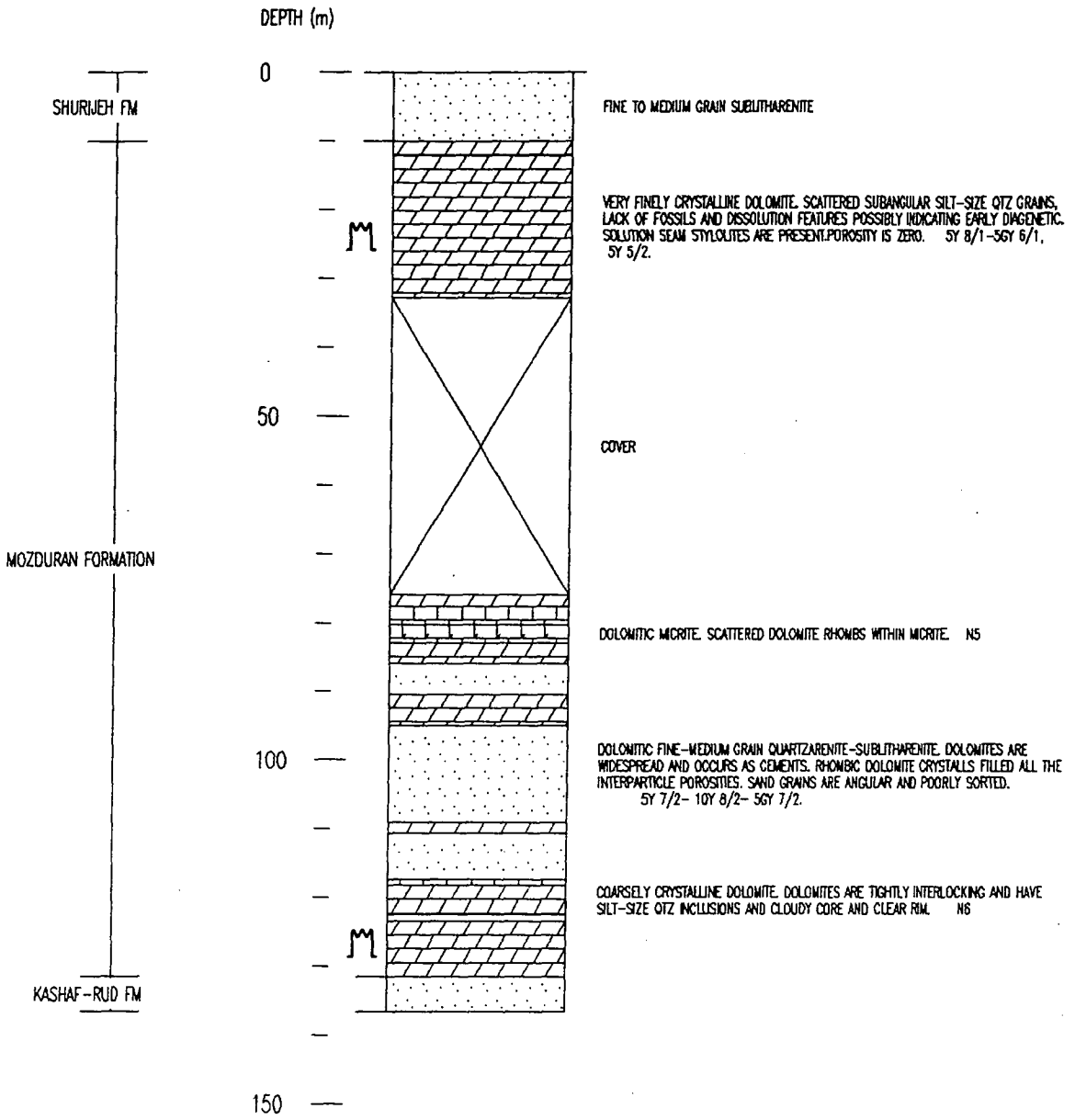

Drawn 27-May-95

STRATIGRAPHIC SECTION OF MOZDURAN FORMATION – BAGAK

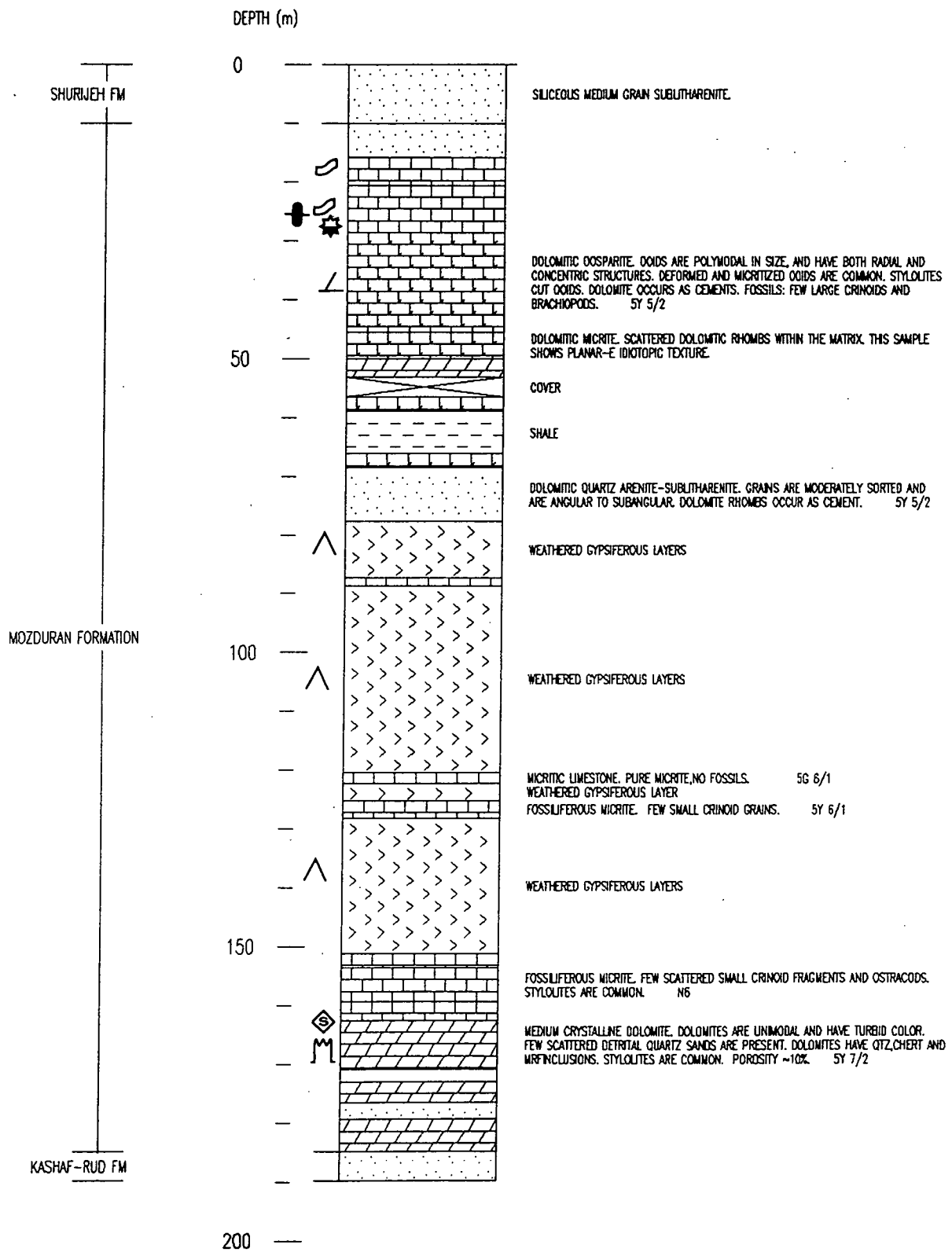

Drawn 27-May-95

STRATIGRAPHIC SECTION OF MOZDURAN FORMATION – PADEHA

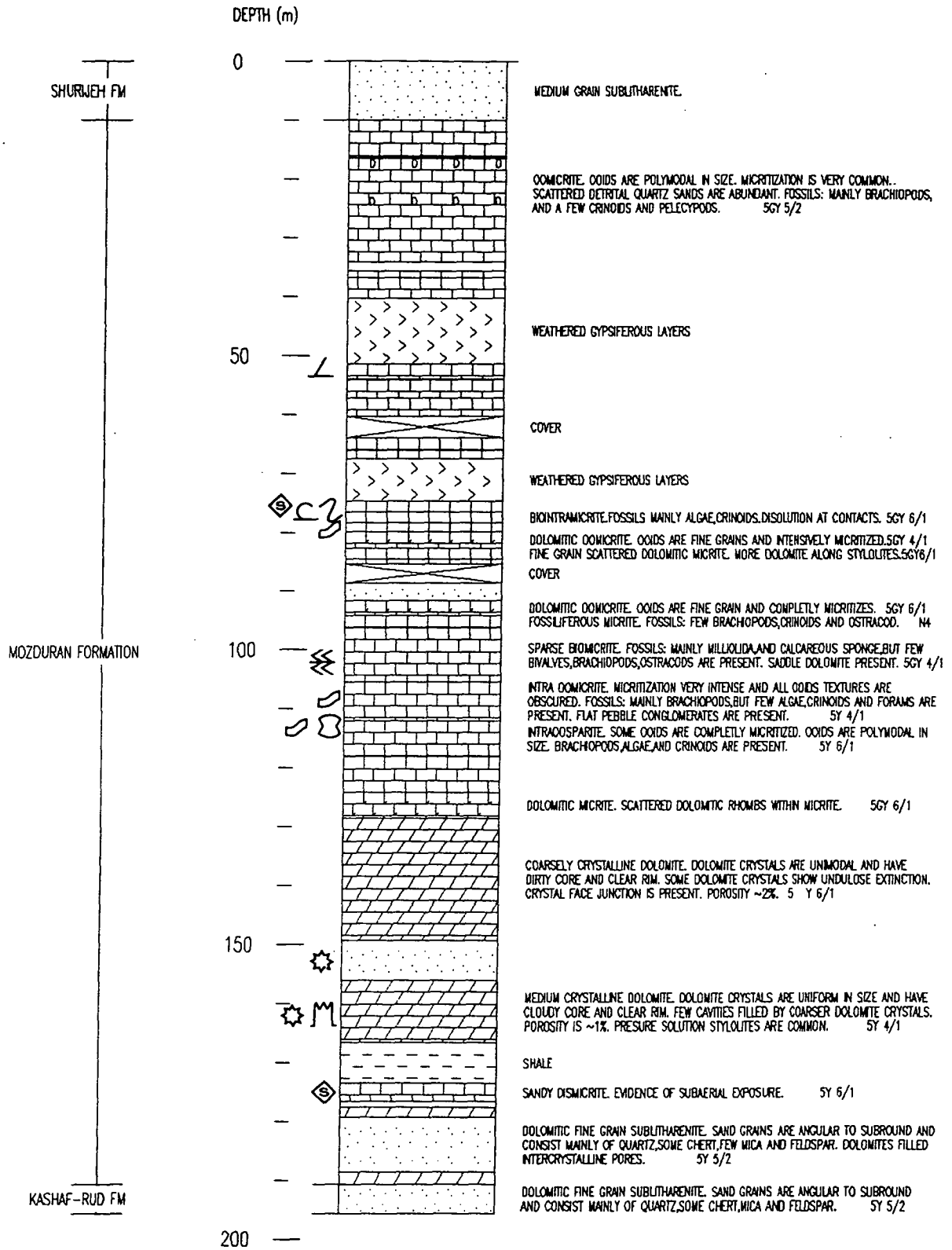

STRATIGRAPHIC SECTION OF MOZDURAN FORMATION – MOZDURAN TYPE LOCALITY

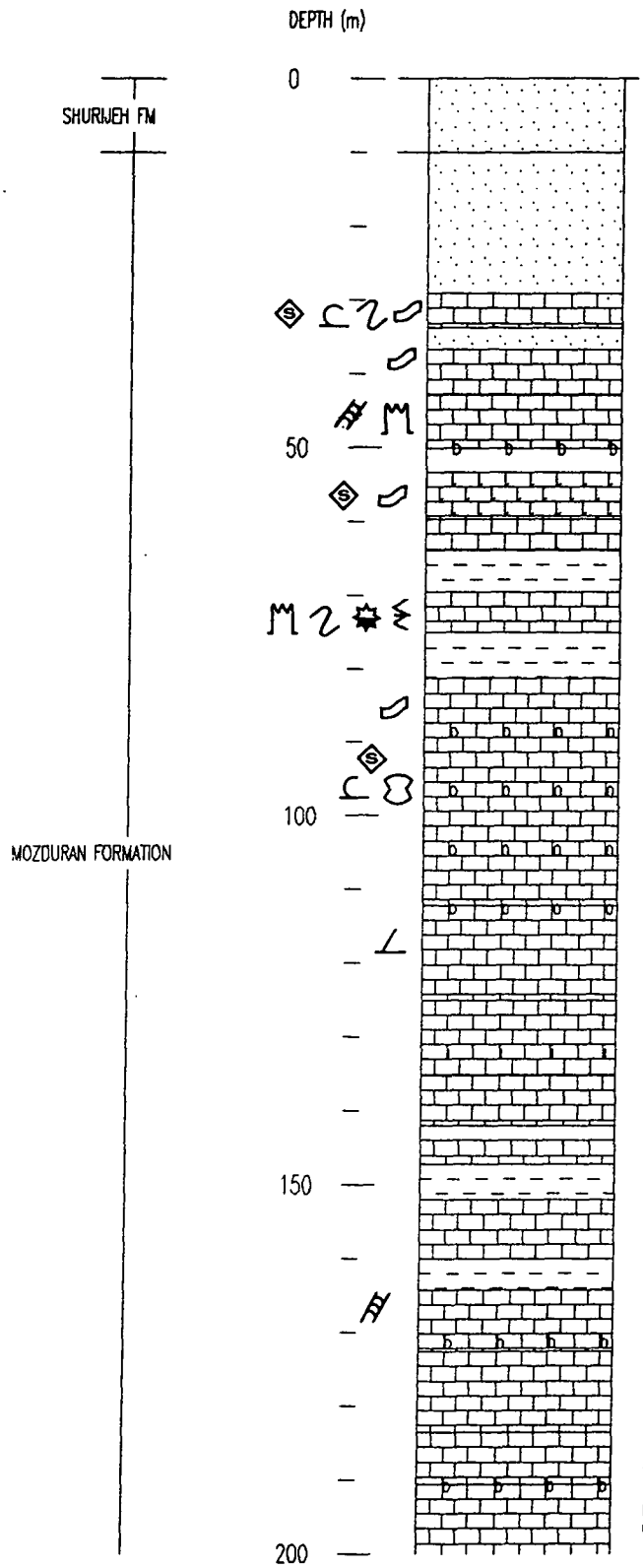

MEDIUM GRAIN CALCITIC SUBLITHARENITE. SAND GRAINS CONSIST MAINLY OF QTZ,SOME CHERT,METAQUARTZITE AND FEW PERCENT FELDSPAR. QTZ GRAINS ARE ANGULAR TO SUBROUND AND HAVE UNDULOSE EXTINCTION. 5YR 5/2

FOSSILIFEROUS FINE GRAIN CALCITIC SUBLITHARENITE. QTZ SANDS ARE VERY ABUNDANT. CHERT,MICA AND METAQUARTZITE ARE ALSO COMMON. SAND GRAINS ARE ANGULAR.5YR 6/4

ALGAL UNSORTED BIOSPARITE. FOSSILS: ALGAE ~44%, CRINOIDS~31%, PELECYPODS~20% AND BRACHIOPODS ~5%. STYLOLITES CUT ALL THE GRAINS AND CEMENTS. COMPACTION AND GRAIN TO GRAIN INTERPENETRATION IS VERY COMMON. 10R 6/2

SHALE

SHALE

SHALE

SANDY BIOOOSPARITE. OOIDS ARE MODERATELY DEFORMED,AND HAVE CLOSE PACKING FABRIC. SPALLED,COMPOUND AND SUPERFICIAL OOIDS ARE COMMON. MICRITIC COATING, MICRITIC ENVELOPE AND BREAKAGE OF SHELLS ARE COMMON. MOST OF OOIDS HAVE MICRITIC CARBONATE NUCLEI. FLAT PEBBLE CONGLOMERATES ARE PRESENT. FOSSILS: CRINOIDS,PELECYPODS AND BRACHIOPODS ARE VERY ABUNDANT. PELECYPODS % DECREASE AND BRACHIOPODS % INCREASE BY DEPTH. CRINOIDS % INCREASE AT THE MIDDLE OF THE SECTION. 5Y 5/1–5Y 6/1

OOINTRA SPARSE BIOMICRITE. SOME OOIDS STRUCTURES DESTROYED BY MICRITIZATION. COMPOUND OR AGGREGATE GRAINS ARE COMMON. FOSSILS: PELECYPODS ARE THE MOST ABUNDANT (~60%) BIOGENIC FRAGMENTS. CRINOIDS ARE SECOND(~35%),AND BRACHIOPODS AN AND GASTROPODS ARE THE THIRD (~5%) FOSSIL FRAGMENTS. 10YR 5/2

SILTY OOBIO INTRAMICRITE. MOST INTRACLASTS ARE COMPOUND OOIDS.OOIDS STRUCTURES PARTLY LOST BY MICRITIZATION. FOSSILS: PELECYPODS, CRINOIDS AND BRACHIOPODS ARE THE MOST ABUNDANT FOSSILS RESPECTIVELY. 10YR 5/2

BIOMICRITE. FOSSILS: MAINLY CRINOIDS, AND FEW % FORAMS (MILLIOLIDA). 5Y 6/1

FINE GRAIN SILICEOUS SUBLITHARENITE.SAND GRAINS ARE MODERATELY SORTED.10YR7/2
SANDY BIOOOSPARITE. MOST OOIDS ARE ROUNDED AND MODERATELY SORTED. 5Y 5/1

SHALE

FOSSILIFEROUS MICRITE. SMALL FRAGMENTS OF CRINOIDS AND A FEW BRACHIOPOD SHELLS.

SHALE

INTRA PACKED ALGAL BIOMICRITE. LARGE BRANCHING CORALLINE RED ALGE CONSTITUDE OF ~95% OF THE SAMPLE. CRINOIDS AND GASTROPODS~5%. 5Y 4/1

INTRAMICRITE.INTRACLASTS ARE POLYMODAL IN SIZE AND SHAPE,AND HAVE NO INTERNAL STRUCTURE. FOSSILS: ONLY FEW SMALL CRINOIDS AND FORAMS. 5Y 6/1

SPARSE BIOMICRITE. FOSSILS: MANY SMALL FRAGMENTS OF CRINOIDS,SOME FORAMS (MILLIOLIDA) AND A FEW BROKEN BRACHIOPODS SHELLS. 5Y 4/1

INTRAMICRITE. FEW LARGE INTRACLASTS WITH NO INTERNAL STRUCTURE. FOSSILS: ONLY FEW FORAMS AND SMALL FRAGMENTS OF BRACHIOPODS.

Drawn 29-May-95

STRATIGRAPHIC SECTION OF MOZDURAN FORMATION – MOZDURAN TYPE LOCALITY

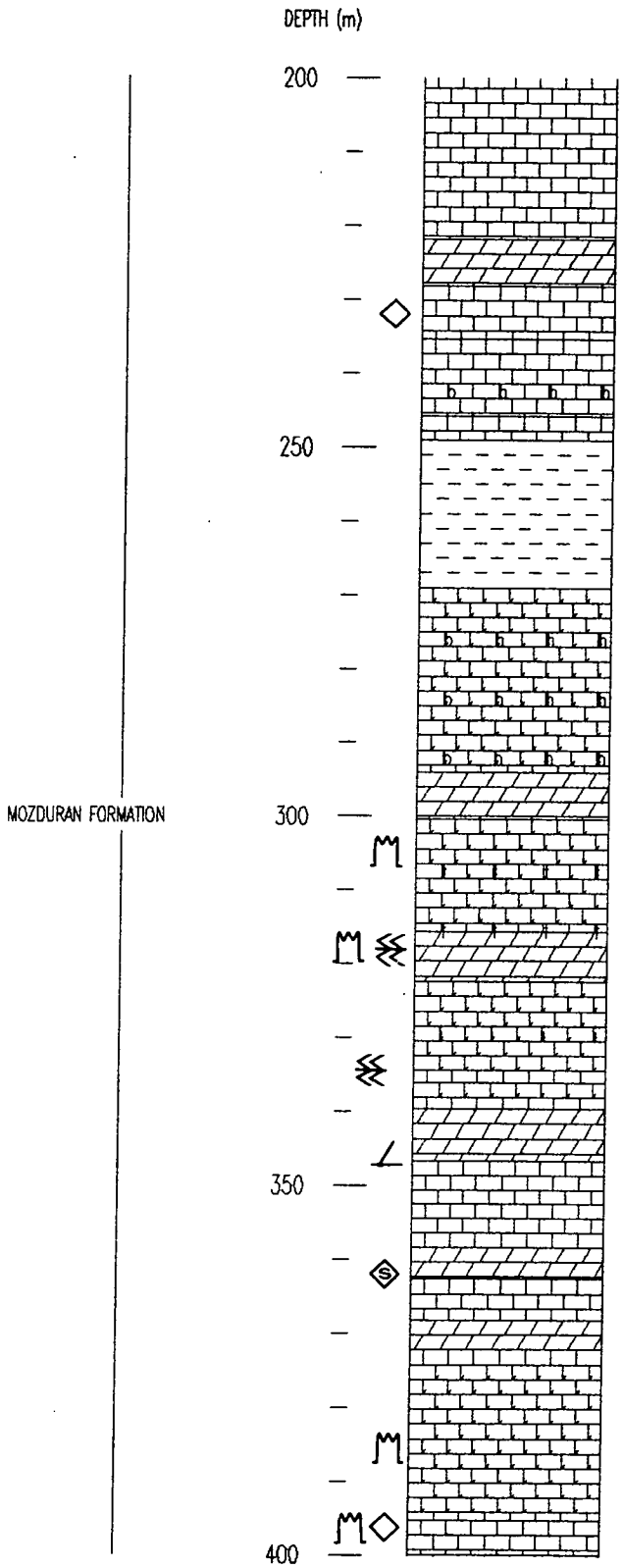

SPARSE BIOMICRITE. SCATTERED CRINOID ARM PLATES AND SOME FORAMS ARE TWO MAJOR FOSSIL TYPES IN THIS SAMPLE. FEW FINE GRAIN QTZ SANDS ARE SCATTERED WITHIN THE MATRIX. 5Y 6/1

VERY FINELY CRYSTALLINE DOLOMITE. DOLOMITES ARE UNIMODAL AND HAVE NO POROSITY. FEW VOIDS FILLED BY SPARRY CALCITE CEMENTS. 10YR 7/4

EVAPORITE BEARING MICRITE. CALCITE PESUDOMORPH AFTER EVAPORITE IS COMMON. BRECCIATION IS PRESENT. TWO GENERATION OF VEINS, PRE AND POST EVAPORITE FORMATION. SPECKELD 5Y 4/1

SANDY DOBIOSPARITE FOSSILS: FINE SAND-SIZE DETRITAL QTZ GRAINS ARE PRESENT. FOSSILS:PELECYPODS ARE VERY ABUNDANT~ 80%. CRINOIDS ~12%, AND BRACHIOPODS ARE ~8%. CEMENTS: ISOPACHOUS,EQUANT,BLOCKY AND SYNTAXIAL CALCITE CEMENTS. SPECKELD 5YR 7/2

SHALE

DOLOMITIC BIOMICRITE. MANY CIRCULAR GRAINS WHICH CAN PROBABLY BE SPONGES FILLED BY FINE TO COARSE DOLOMITE CRYSTALS (POSSIBLY CAN BE CALLED DOLOSPHER). 5Y 6/1 _

POLYMODAL MEDIUM CRYSTALLINE DOLOMITE. THERE ARE EVIDENCE OF LAMINATIONS. GRANULARDOLOMITE GRAINS OCCURS ALONG THESE LAMINATIONS. POROSITY ~3%.10YR 6/2

DOLOMITIC FOSSILIFEROUS MICRITE. SCATTERED DOLOMITE RHOMBS WIYHIN MATRIX AND ALONG STYLOLITES. FOSSILS: MAINLY SMALL FRAGMENTS OF CRINOIDS. 10YR 6/2

MEDIUM CRYSTALLINE DOLOMITE. DOLOMITES HAVE EUHEDRAL TO SUBHEDRAL CRYSTALS, AND ARE VERY BRIGHT AND CLEAR. NO EVIDENCE OF DARK INCLUSION. POROSITY ~2%. PRESSURE SOLUTION SEAMS ARE PRESENT. VEINS CUTTING THE SOLUTION SEAMS.10YR6/2

DOLOMITIC INTRAMICRITE. INTRACLASTS ARE FEW AND HAVE NO INTERNAL STRUCTURES. DOLOMITIZATION IS MORE IN THE AREA OF PRESSURE SOLUTION STYLOLITES. FERROAN AND NON-FERROAN SPARRY CALCITE VEINS ARE PRESENT.

MEDIUM CRYSTALLINE DOLOMITE. DOLOMITES HAVE EUHEDRAL TO SUBHEDRAL CRYSTALS. DOLOMITES HAVE CLOUDY SURFACE. SOME CAVITIES FILLED BY LATE COARSE DOLOMITE CRYSTALS,SHOWING UNDULOSE EXTINCTION. POROSITY ~2%. 10YR 8/2-10YR 6/2

FINELY CRYSTALLINE DOLOMITE. FEW SCATTERED SILT-SIZE QTZ GRAINS. PRESSURE SOLUTION FEATURES ARE COMMON. DOLOMITES HAVE CLOUDY APPEARENCE. SANDY MICRITE. VERY FINE LAMINATION. SCATTERED SILT-SIZE QTZ GRAINS. NO FOSSILS PRESENT. 5Y 6/1

DOLOMITIC MICRITE. DOLOMITE RHOMBS ARE DISTINCTLY ZONED AND SCATTERED WITHIN MICRITE. SOME DOLOMITE RHOMBS ARE CONCENTRATED ALONG STYLOLITES. 5Y 5/1

Drawn 29-May-95

STRATIGRAPHIC SECTION OF MOZDURAN FORMATION – MOZDURAN TYPE LOCALITY

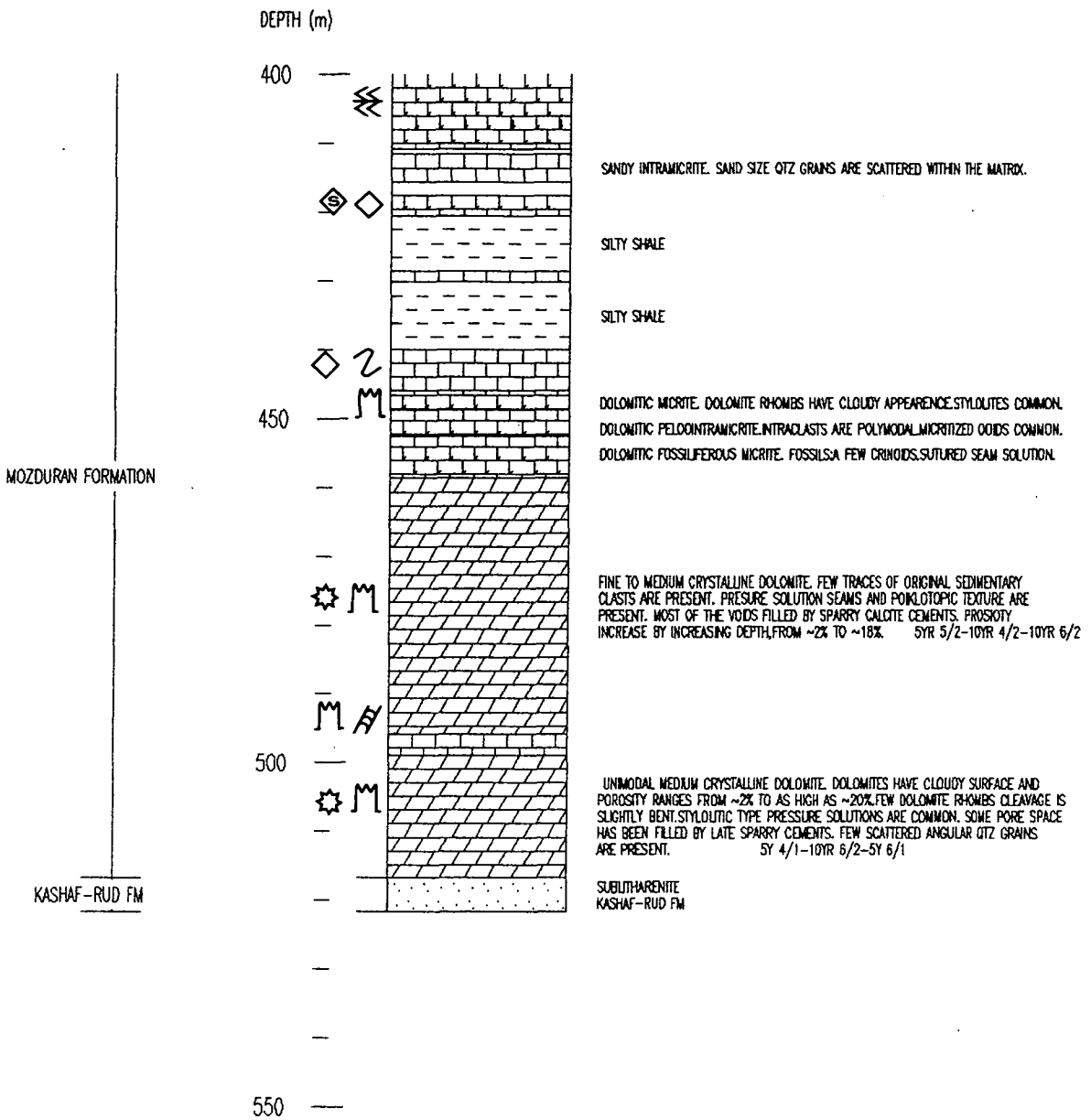

Drawn 25-May-95

STRATIGRAPHIC SECTION OF MOZDURAN FORMATION - GORGOREH

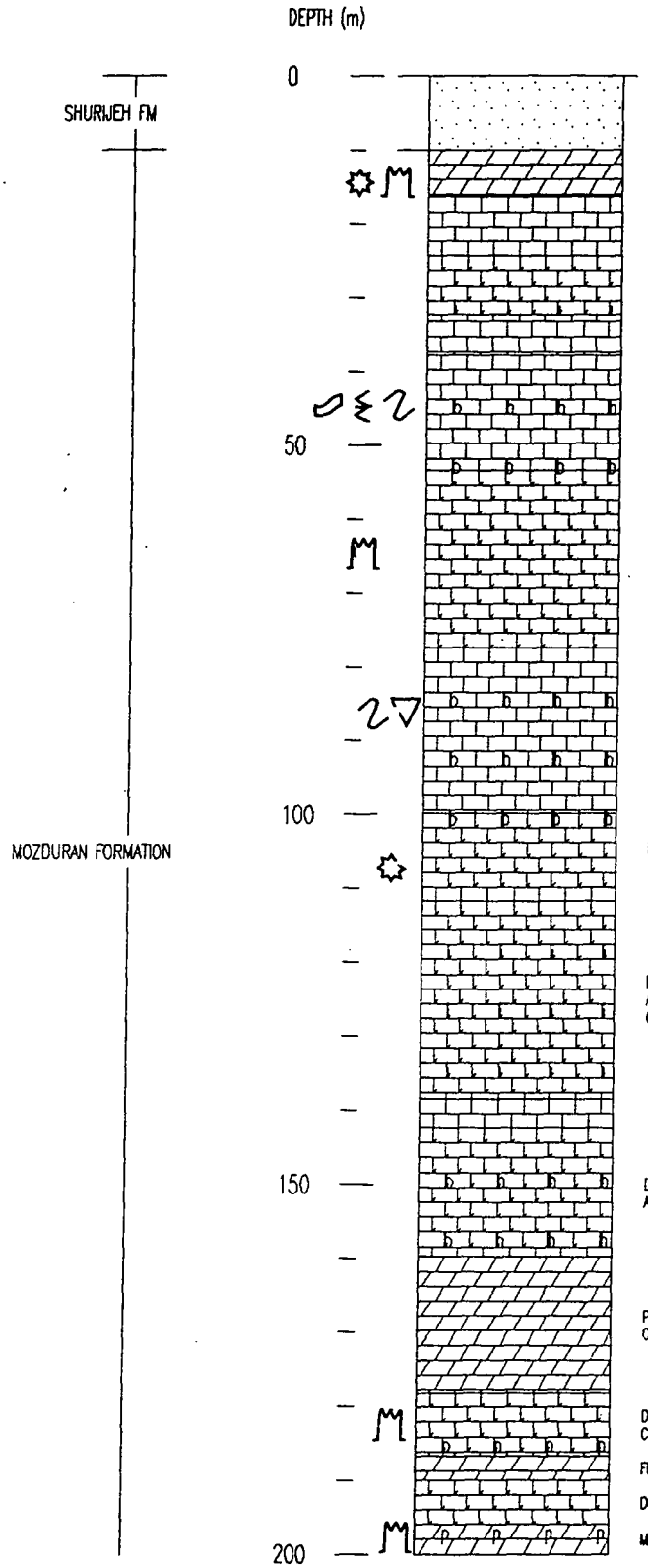

SANDSTONE. 5YR 5/2

POLYMODAL(RELATIVELY FINE) CRYSTALLINE DOLOMITE. CRINOIDS ARE MIMICALLY REPLACED BY DOLOMITE. POROSITY ~5%. 5YR 6/4

INTRAMICRITE.INTRACLASTS ARE ROUND AND RELATIVELY SORTED.FOSSILS: FEW MILLIOLIDA AND PELECYPODS. 10YR 6/2

DOLOMITIC OOBIOINTRAMICRITE.CRINOIDS~55%,BRACHIOPODS~40%,FORAMS AND PELECYPODS ~5%. SPECKELD 10YR 6/2

FINE GRAIN OOSPARITE. OOIDS ARE WELL SORTED AND HAVE MAINLY RADIAL STRUCTURE 10YR 6/2

SANDY INTRA PACKED BIOSARITE.INTRACLASTS ARE RELATIVELY LARGE AND HAVE NO INTERNAL STRUCTURE.GRAIN BREAKAGE AND SHATTERED MICRITIC ENVELOPES ARE PRESENT.FOSSILS:MAINLY BRACHIOPODS~55%,PELECYPODS~30%, CRINOIDS AND BRYOZOA ~10% AND ALGAE~ 5%. 5YR 6/2

DOLOMITIC INTRA PACKED BIOMICRITE.FOSSILS MAINLY CRINOIDS~45%,PELCYPODS ~40%,BRACHIOPODS~10%,AND BRYOZOA AND GASTROPODS ~5%. 5YR 5/2

INTRA SPARSE BIOMICRITE.FOSSILS:MAINLY BRACHIOPODS~50%,BRYOZOA~30% AND CRINOIDS~20%.FEW SILICIFICATION. SHATTERED MICRITIC ENVELOPE. DOLOMITE ZONATION. 10YR 6/2

DOLOMITIC INTRA SPARSE BIOMICRITE.FOSSILS:MAINLY CORALS~40%,BRYOZOA~30%, BRACHIOPODS~20% AND CRINOIDS,FORAMS AND OSTRACODS ~5%. 5Y 5/1.

DOLOMITIC BIOINTRAMICRITE.FOSSILS:ABUNDANT CRINOIDS AND FEW FORAMS,BRYOZOA AND OSTRACODS. INTENSIVE DOLOMITIZATION. DOLOMITE OCCURS AS CAVITY FILLING CEMENT. SPECKLED N4

DOLOMITIC INTRABIOMICRITE. FOSSILS: MAINLY CRINOIDS~75%,BRACHIOPODS,BRYOZOA AND CALCAREOUS SPONGE ~25%. 5Y 4/1

POLYMODAL MEDIUM CRYSTALLINE DOLOMITE. FEW ALTERNATION OF FINE TO RELATIVELY COARSE LAMINATIONS. N4

DOLOMITIC PELMICRITE. FAVREINA(PELLETS WITH INTERNAL PATTERN OF TUBULES)VERY COMMON.DOLOMITE PSUEDOMORPH AFTER GYPSUM. FEW OSTRACODS,FORAMS. 10YR 6/2

FINELY CRYSTALLINE DOLOMITE. POROSITY ~7%. 5Y 7/2

DOLOMITIC INTRAPELMICRITE. FAVREINA VERY COMMON. FINE LAMINATION. 5YR 6/4

MEDIUM CRYSTALLINE DOLOMITE. POROSIYT ~5%. 10YR 6/2

Drawn 25-May-95

STRATIGRAPHIC SECTION OF MOZDURAN FORMATION – GORGOREH

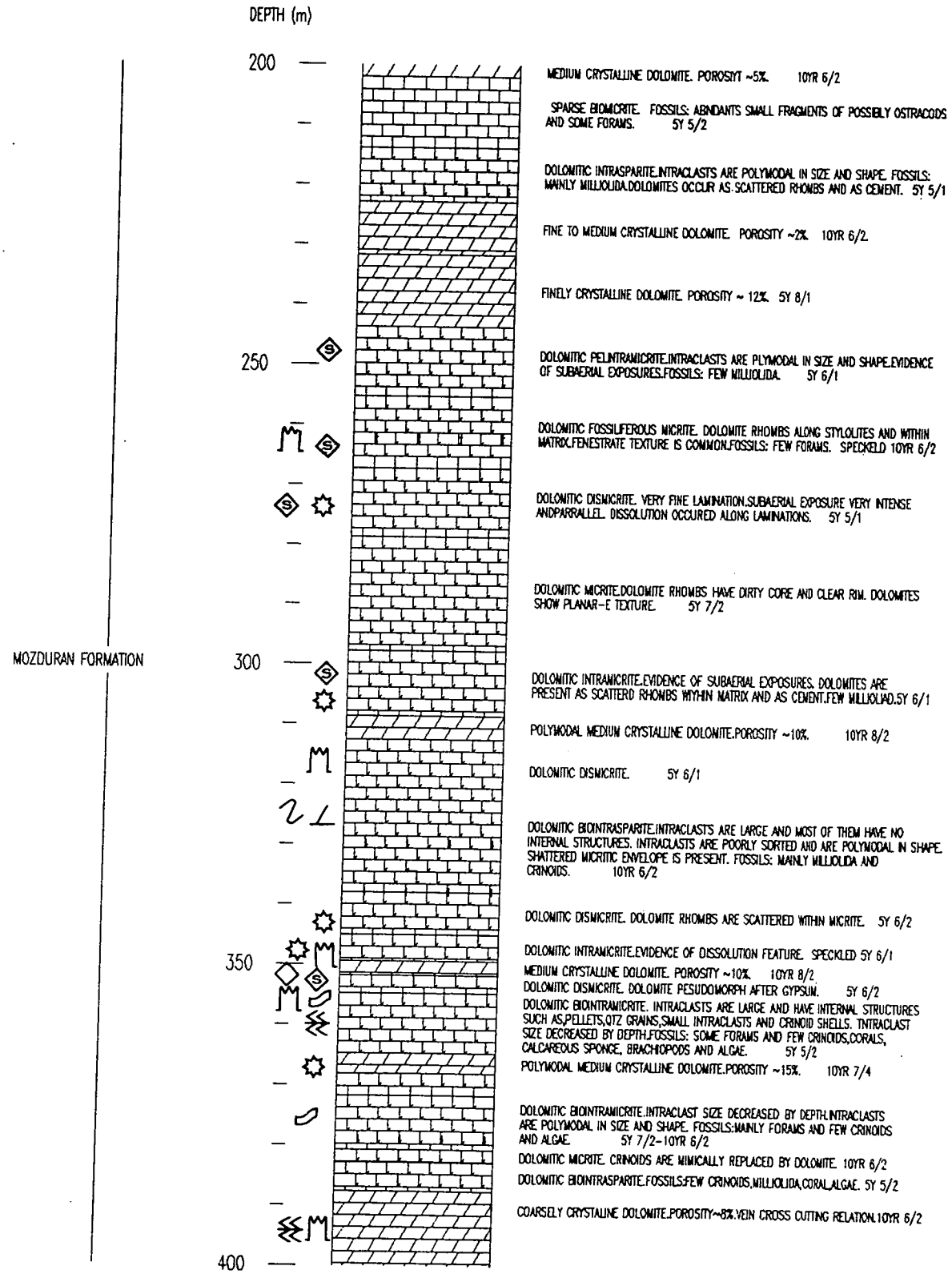

Drawn 25-May-95

STRATIGRAPHIC SECTION OF MOZDURAN FORMATION – GORGOREH

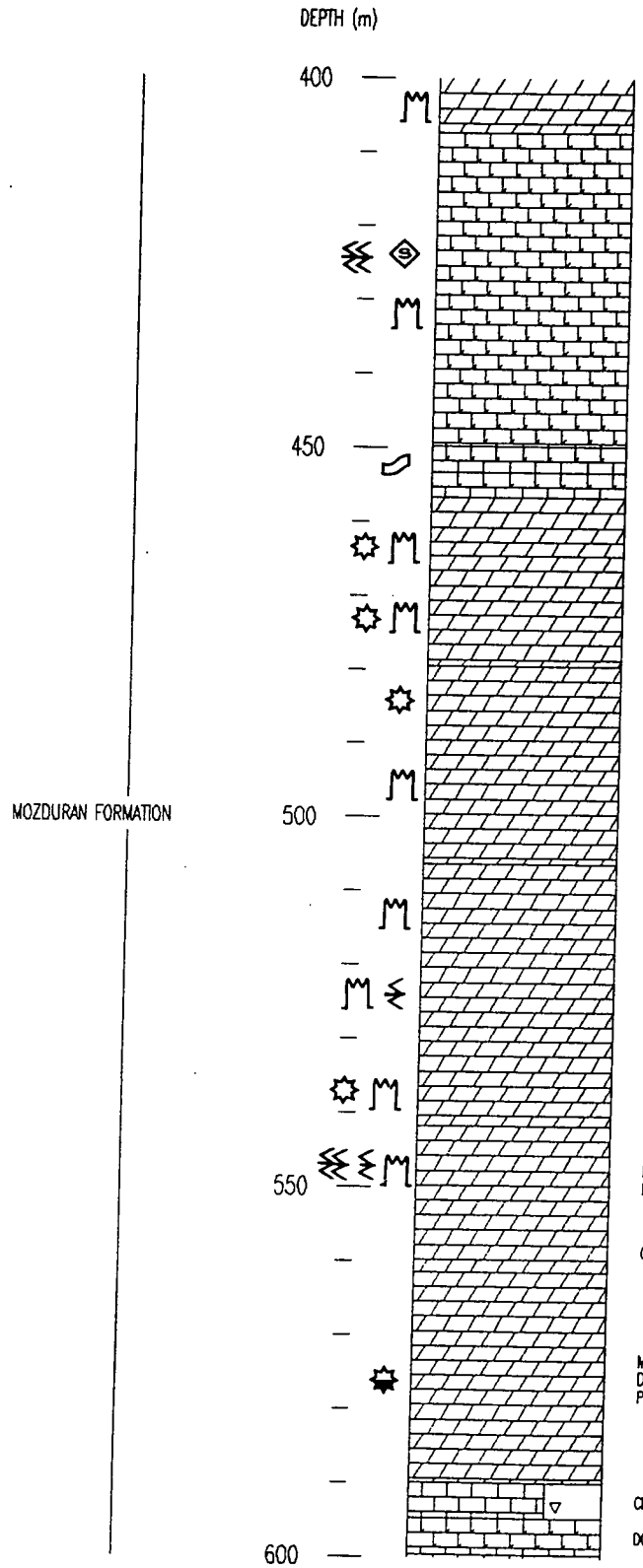

COARSELY CRYSTALLINE DOLOMITE.CRINOIDS ARE MIMICALLY REPLACED BY DOLOMITE. POROSITY ~7%. 10YR 6/2

DOLOMITIC INTRAMICRITE.INTRACLASTS ARE POLYMODAL IN SIZE AND HAVE NO INTERNAL STRUCTURES. FOSSILS: MAINLY FORAMS (MILLIOLIDA) AND FEW CRINOIDS. DOLOMITE RHOMBS ARE MAINLY CONCENTRATED AROUND INTRACLASTS AND ALONG SOLUTION SEAM STYLOLITES.FEW DOLOMITE RHOMBS CUT STYLOLITES.FEW EVIDENCE OF SUBAERIAL EXPOSURES. 5Y 6/4, 5Y 7/2, 10YR 6/2, 5Y 6/1 5Y 7/2 AND N5.

DOLOMITIC INTRASPARITE. FOSSILS:SOME CRINOIDS AND FEW ALGAE. SPECKLED 5Y 6/1

DOLOMITIC FOSSILIFEROUS MICRITE. FEW CRINOIDS ARE PRESENT.POROSITY~12%. N8

COARSELY CRYSTALLINE DOLOMITE.CAVITY FILLED BY LATE COARSE DOLOMITE. 10YR 6/2

POLYMODAL MEDIUM CRYSTALLINE DOLOMITE.LATE COARSE CRYSTALLINE PLANAR-E DOLOMITE FILLED CAVITIES. 5YR 5/2-10YR 6/2

POLYMODAL MEDIUM CRYSTALLINE DOLOMITE. CRINOIDS AND INTRACLASTS ARE MIMICALLY REPLACED BY DOLOMITE,THUS SHOWS ORIGINAL SEDIMENTARY TEXTURE.SOME DOLOMITE RHOMBS FORMED ALONG STYLOLITES. 10YR 6/2-5Y 7/2

COARSELY CRYSTALLINE DOLOMITE.SOME LATE COARSE DOLOMITES ARE CLEAR. DOLOMITE CRYSTALS SHOW UNDULOSE EXTINCTION. 10YR 6/2-5YR 6/1

MEDIUM CRYSTALLINE DOLOMITE. CRINOIDS ARE MIMICALLY REPLACED BY DOLOMITE. LATE CLEAR DOLOMITES FORMED ALONG VEINS AND FRACTURES. SOME DOLOMITE GRAINS HAVE BEEN BROKEN DUE TO INTENSE STYLOLITIZATION. 10YR 6/2-5Y 6/1-10YR 7/2

COARSELY CRYSTALLINE DOLOMITE. DOLOMITES SHOW UNDULOSE EXTINCTION. 5YR 6/1

POLYMODAL MEDIUM CRYSTALLINE DOLOMITE.LATE DOLOMITE CEMENTS ARE CLEAR. RECRYSTALLIZATION CAUSED VARIATION IN GRAIN SIZE. 5YR 5/2-10YR 6/2

COARSELY CRYSTALLINE DOLOMITE. 10YR 6/2

MEDIUM CRYSTALLINE DOLOMITE. UNIMODAL TO POLYMODAL SIZE DISTRIBUTION.MOST DOLOMITES HAVE CLOUDY CORE.SOME CAVITIES FILLED BY LATER DOLOMITE CEMENT. POROSITY ~4%. 10YR 6/2-5YR 6/1

CHERTY SPARSE BIOMICRITE.FOSSILS:MAINLY SILICEOUS SPONGE SPICULES. N6

DOLOMITIC SPARSE BIOMICRITE. FOSSILS:LARGE BRYOZOAN SHELL,SOME SPONGES.5Y 6/1

Drawn 25-May-95

STRATIGRAPHIC SECTION OF MOZDURAN FORMATION – GORGOREH

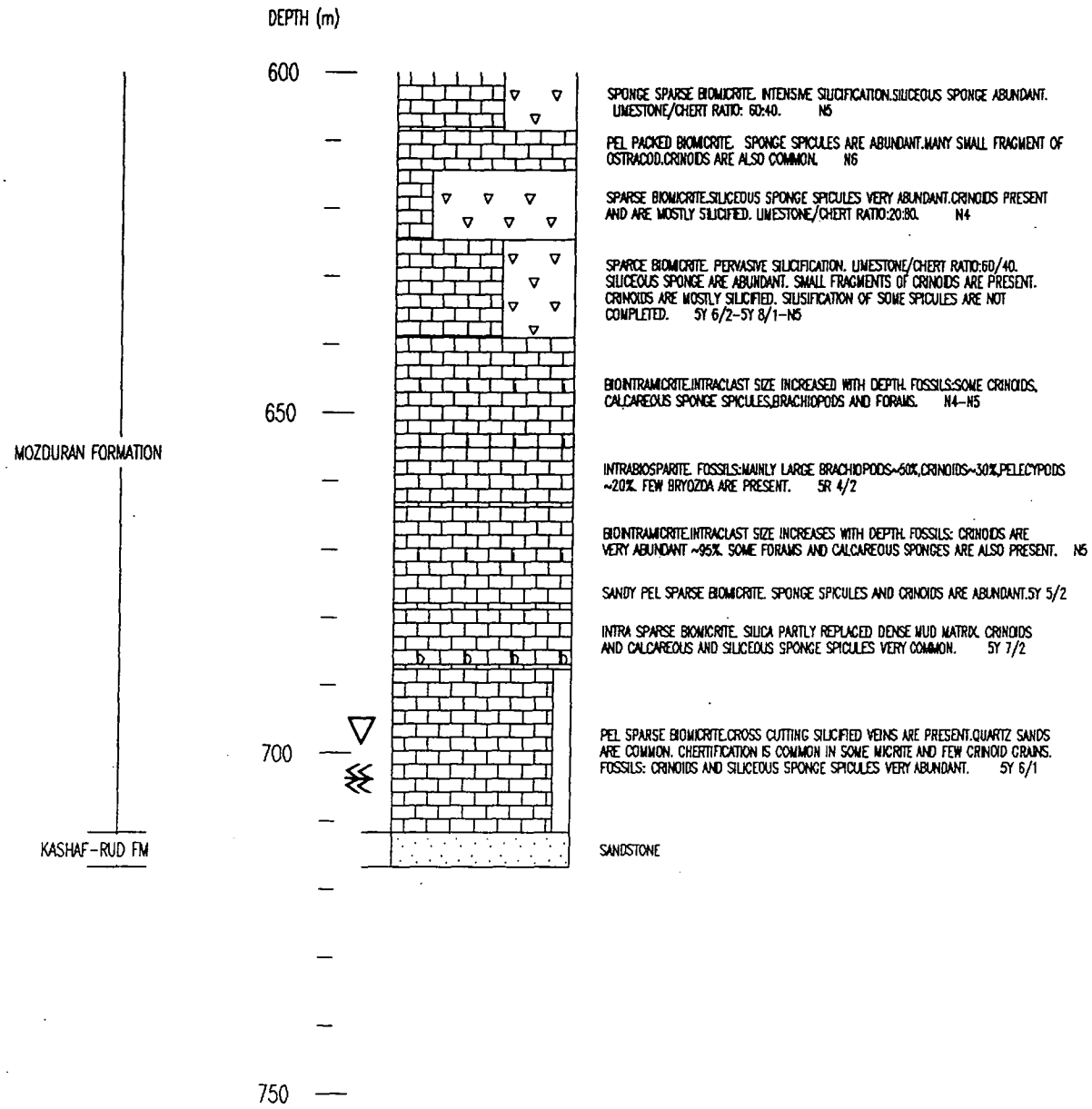

Drawn 25-May-95

STRATIGRAPHIC SECTION OF THE MOZDURAN FORMATION – BAZANGAN

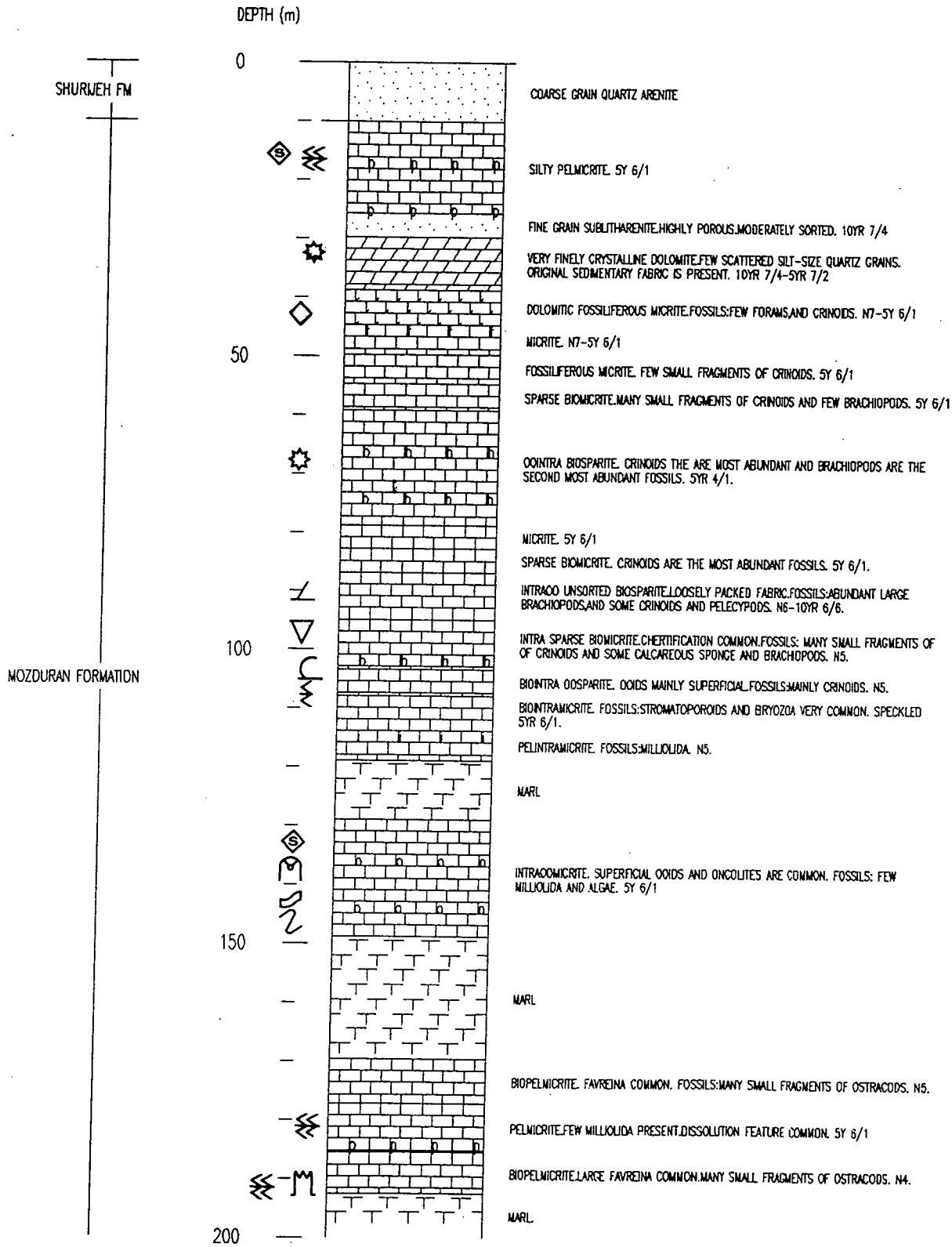

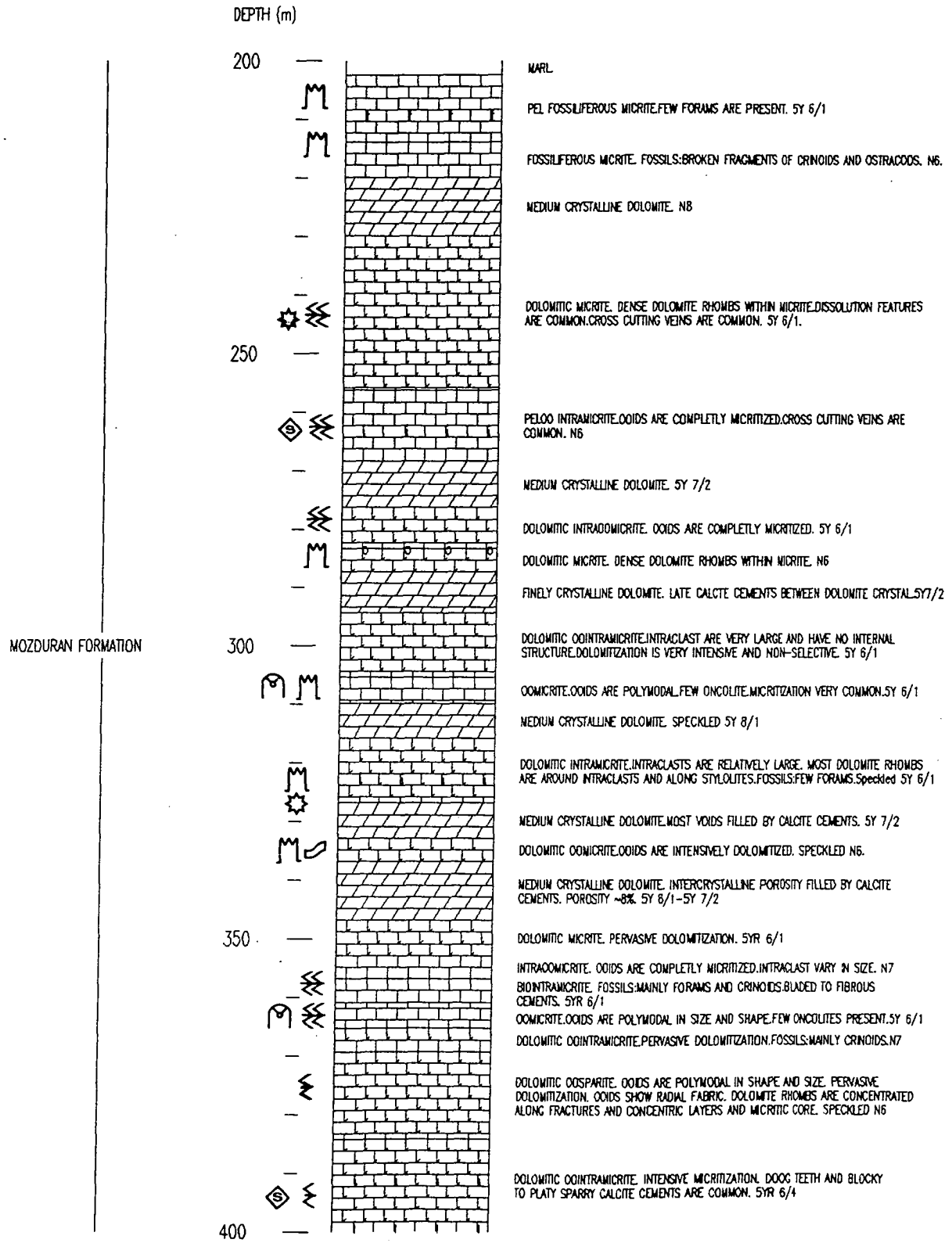
DEPTH (m)
200
250
300
350
400
MOZDURAN FORMATION
MARL
PEL FOSSILIFEROUS MICRITE.FEW FORAMS ARE PRESENT. 5Y 6/1
FOSSILIFEROUS MICRITE. FOSSILS:BROKEN FRAGMENTS OF CRINOIDS AND OSTRACODS. N6.
MEDIUM CRYSTALLINE DOLOMITE. N8
DOLOMITIC MICRITE. DENSE DOLOMITE RHOMBS WITHIN MICRITE.DISSOLUTION FEATURES ARE COMMON.CROSS CUTTING VEINS ARE COMMON. 5Y 6/1.
PELOO INTRAMICRITE.OOIDS ARE COMPLETLY MICRITIZED.CROSS CUTTING VEINS ARE COMMON. N6
MEDIUM CRYSTALLINE DOLOMITE. 5Y 7/2
DOLOMITIC INTRAOOMICRITE. OOIDS ARE COMPLETLY MICRITIZED. 5Y 6/1
DOLOMITIC MICRITE. DENSE DOLOMITE RHOMBS WITHIN MICRITE. N6
FINELY CRYSTALLINE DOLOMITE. LATE CALCITE CEMENTS BETWEEN DOLOMITE CRYSTAL.5Y7/2
DOLOMITIC OOINTRAMICRITE.INTRACLAST ARE VERY LARGE AND HAVE NO INTERNAL STRUCTURE.DOLOMITIZATION IS VERY INTENSIVE AND NON-SELECTIVE. 5Y 6/1
OOMICRITE.OOIDS ARE POLYMODAL.FEW ONCOLITE.MICRITIZATION VERY COMMON.5Y 6/1
MEDIUM CRYSTALLINE DOLOMITE. SPECKLED 5Y 8/1
DOLOMITIC INTRAMICRITE.INTRACLASTS ARE RELATIVELY LARGE. MOST DOLOMITE RHOMBS ARE AROUND INTRACLASTS AND ALONG STYLOLITES.FOSSILS:FEW FORAMS.Speckled 5Y 6/1
MEDIUM CRYSTALLINE DOLOMITE.MOST VOIDS FILLED BY CALCITE CEMENTS. 5Y 7/2
DOLOMITIC OOMICRITE.OOIDS ARE INTENSIVELY DOLOMITIZED. SPECKLED N6.
MEDIUM CRYSTALLINE DOLOMITE. INTERCRYSTALLINE POROSITY FILLED BY CALCITE CEMENTS. POROSITY ~8%. 5Y 8/1-5Y 7/2
DOLOMITIC MICRITE. PERVASIVE DOLOMITIZATION. 5YR 6/1
INTRAOOMICRITE. OOIDS ARE COMPLETLY MICRITIZED.INTRACLAST VARY IN SIZE. N7
BIOINTRAMICRITE. FOSSILS:MAINLY FORAMS AND CRINOIDS.BLADED TO FIBROUS CEMENTS. 5YR 6/1
OOMICRITE.OOIDS ARE POLYMODAL IN SIZE AND SHAPE.FEW ONCOLITES PRESENT.5Y 6/1
DOLOMITIC OOINTRAMICRITE.PERVASIVE DOLOMITIZATION.FOSSILS:MAINLY CRINOIDS.N7
DOLOMITIC OOSPARITE. OOIDS ARE POLYMODAL IN SHAPE AND SIZE. PERVASIVE DOLOMITIZATION. OOIDS SHOW RADIAL FABRIC. DOLOMITE RHOMBS ARE CONCENTRATED ALONG FRACTURES AND CONCENTRIC LAYERS AND MICRITIC CORE. SPECKLED N6
DOLOMITIC OOINTRAMICRITE. INTENSIVE MICRITIZATION. DOOG TEETH AND BLOCKY TO PLATY SPARRY CALCITE CEMENTS ARE COMMON. 5YR 6/4

Drawn 24-May-95

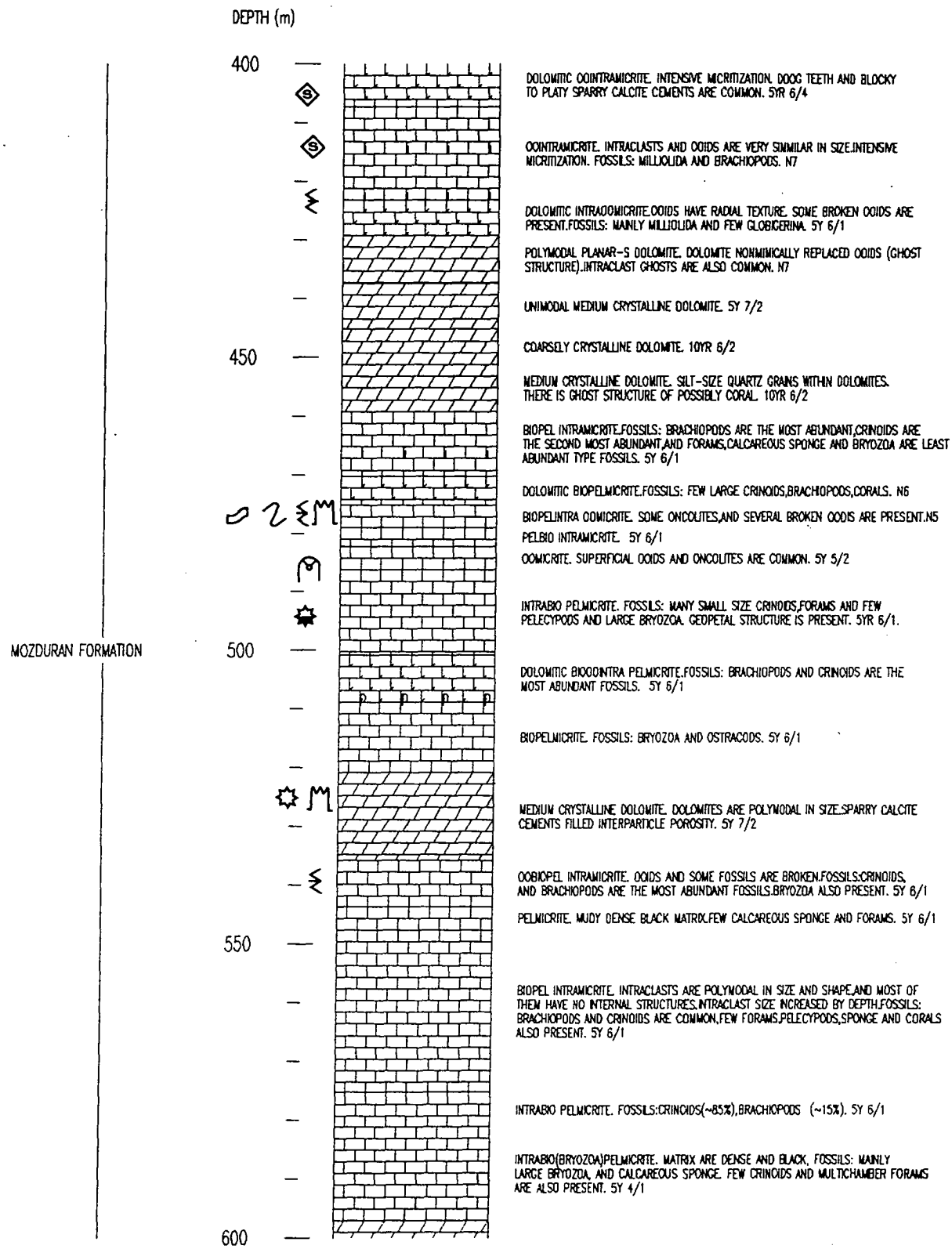

Drawn 24-May-95

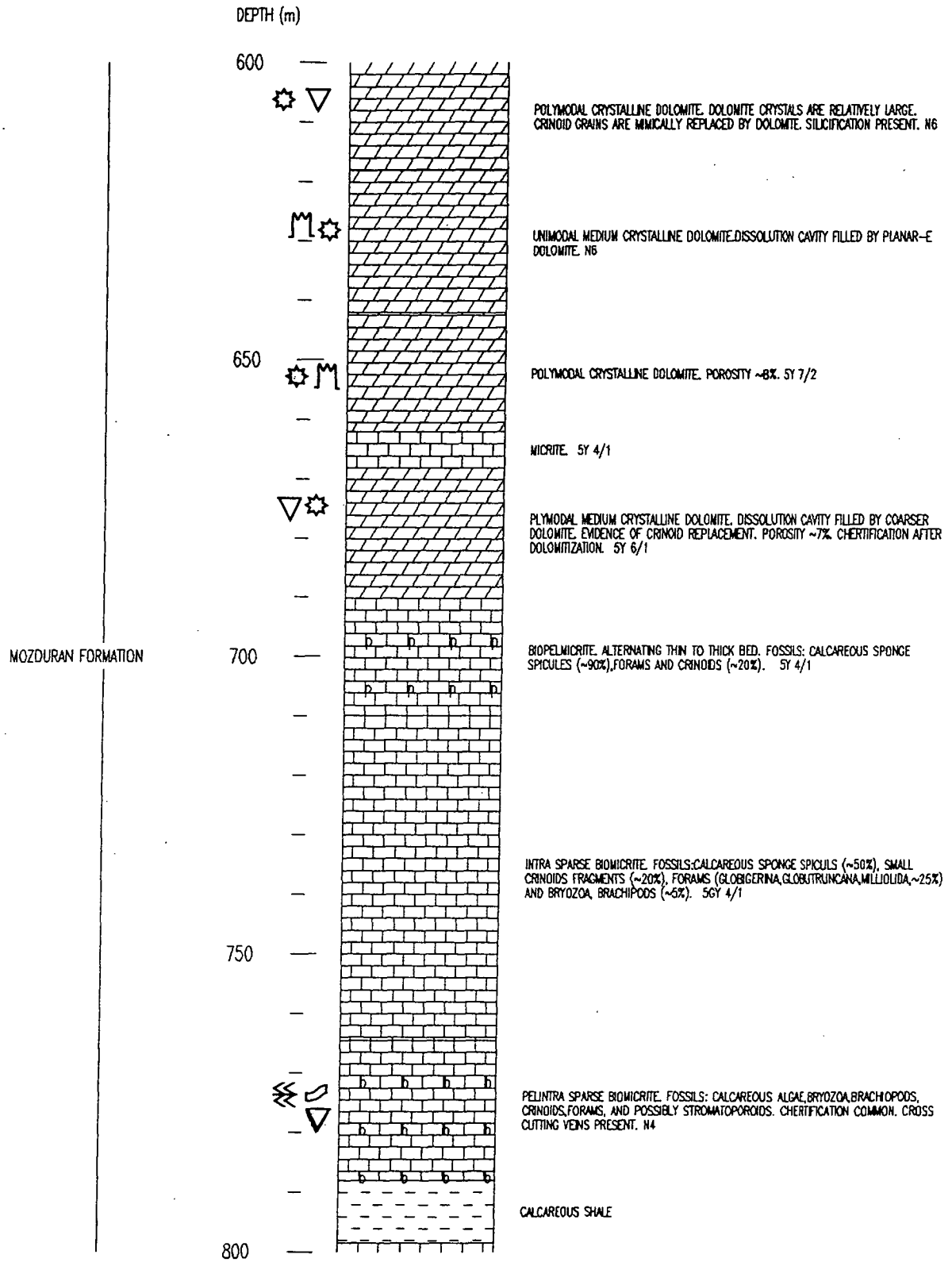

Drawn 24-May-95

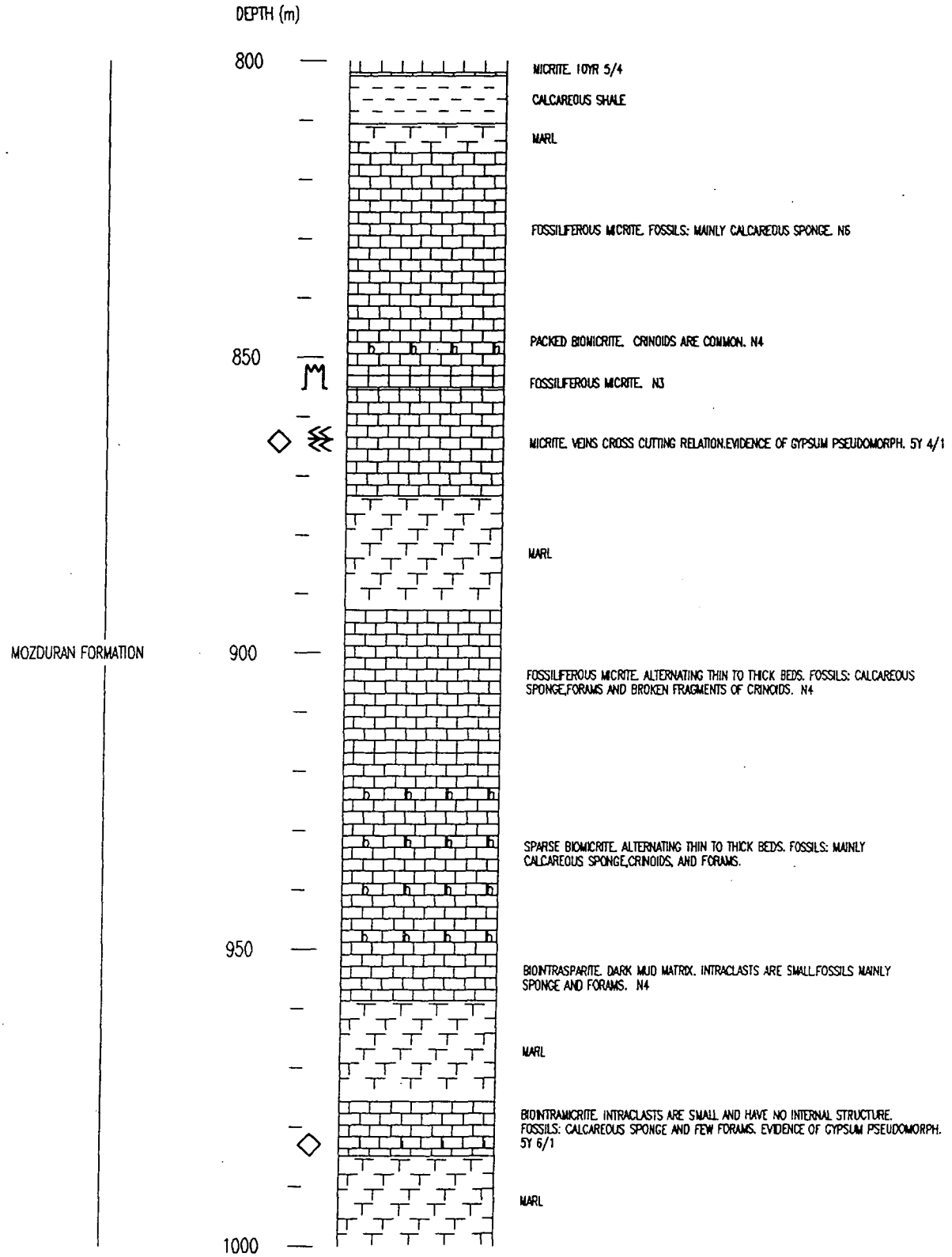

Drawn 24-May-95

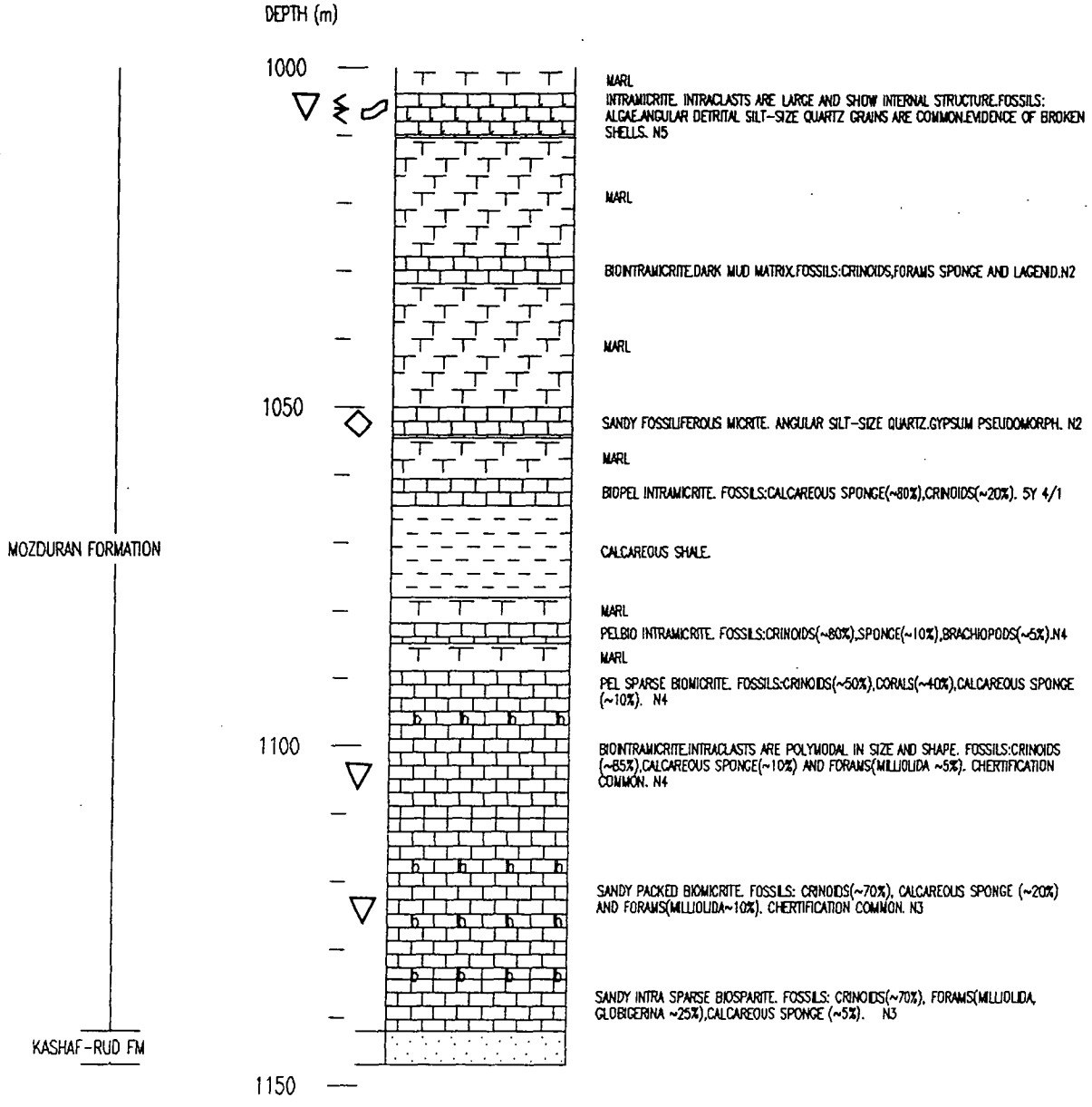

APPENDIX 2

MARKOV CHAIN DATA OF THE MOZDURAN CARBONATES

The following Markov chain analysis, utilised two custom-written BASIC programs based on Powers and Easterling (1982) and Wells (1989).

MARKOV ANALYSIS OF THE MOZDURAN FORMATION IN PADEHA SECTION. WELLS (1989) METHOD.

Number of facies: 9

Facies:

1 Micrite-biomicrite (variably fossiliferrous)
2 Biosparite
3 Intramicrite
4 Weathered gypsiferous layers
5 Oomicrite
6 Oosparite
7 Dolomite
8 Shale
9 Sublitharenite

Raw-data matrix

No	#1	#2	#3	#4	#5	#6	#7	#8	#9	Total
1	0	0	1	0	2	1	0	1	0	5
2	0	0	0	0	0	1	0	0	0	1
3	0	0	0	0	0	1	0	0	0	1
4	0	0	0	0	0	2	0	0	0	2
5	3	0	0	0	0	1	0	0	1	5
6	0	1	0	2	3	0	0	0	0	6
7	1	0	0	0	0	0	0	0	3	4
8	0	0	0	0	0	0	1	0	0	1
9	2	0	0	0	0	0	2	0	0	4
	6	1	1	2	5	6	3	1	4	29

Expected values for quasi-independence

No	1	2	3	4	5	6	7	8	9
1	-	0.19	0.19	0.39	1.12	1.43	0.64	0.19	0.85
2	0.22	-	0.03	0.06	0.18	0.23	0.1	0.03	0.14
3	0.22	0.03	-	0.06	0.18	0.23	0.1	0.03	0.14
4	0.46	0.06	0.06	-	0.38	0.48	0.21	0.06	0.29
5	1.3	0.18	0.18	0.38	-	1.36	0.61	0.18	0.81
6	1.65	0.23	0.23	0.48	1.36	-	0.77	0.23	1.04
7	0.95	0.13	0.13	0.28	0.78	1	-	0.13	0.6
8	0.22	0.03	0.03	0.06	0.18	0.23	0.1	-	0.14
9	0.99	0.14	0.14	0.29	0.81	1.04	0.46	0.14	-

Difference matrix

No	1	2	3	4	5	6	7	8	9
1	-	-0.19	0.81	-0.39	0.88	-0.43	-0.64	0.81	-0.85
2	-0.22	-	-0.03	-0.06	-0.18	0.77	-0.1	-0.03	-0.14
3	-0.22	-0.03	-	-0.06	-0.18	0.77	-0.1	-0.03	-0.14
4	-0.46	-0.06	-0.06	-	-0.38	1.52	-0.21	-0.06	-0.29
5	1.7	-0.18	-0.18	-0.38	-	-0.36	-0.61	-0.18	0.19
6	-1.65	0.77	-0.23	1.52	1.64	-	-0.77	-0.23	1.04
7	0.05	-0.13	-0.13	-0.28	-0.78	-1	-	-0.13	2.4
8	-0.22	-0.03	-0.03	-0.06	-0.18	-0.23	0.9	-	-0.14
9	1.01	-0.14	-0.14	-0.29	-0.81	-1.04	1.54	-0.14	-

Sequence chi-squared matrix

No	1	2	3	4	5	6	7	8	9
1	-	0.19	3.45	0.39	0.69	0.13	0.64	3.45	0.85
2	0.22	-	0.03	0.06	0.18	2.55	0.1	0.03	0.14
3	0.22	0.03	-	0.06	0.18	2.55	0.1	0.03	0.14
4	0.46	0.06	0.06	-	0.38	4.84	0.21	0.06	0.29
5	2.24	0.18	0.18	0.38	-	0.1	0.61	0.18	0.04
6	1.65	2.55	0.23	4.83	1.96	-	0.77	0.23	1.04

7	0	0.13	0.13	0.28	0.78	1	-	0.13	9.69	
8	0.22	0.03	0.03	0.06	0.18	0.23	7.8	-	0.14	
9	1.04	0.14	0.14	0.29	0.81	1.04	5.12	0.14	-	

Asymmetry chi-square matrix

No	1	2	3	4	5	6	7	8	9	
1	-	-	-	-	-	-	-	-	-	
2	0	-	-	-	-	-	-	-	-	
3	1	0	-	-	-	-	-	-	-	
4	0	0	0	-	-	-	-	-	-	
5	0.2	0	0	0	-	-	-	-	-	
6	1	0	1	0	1	-	-	-	-	
7	1	0	0	0	0	0	-	-	-	
8	1	0	0	0		0 0	1	-	-	
9	2	0	0	0	1	0	0.2	0	-	

Sequence chi-squared sum= 69.5301 55 degrees of freedom
Asymmetry chi-squared = 10.3999 13 degrees of freedom

Principal succession for facies
(binomial probabilities listed)

Micrite-biomicrite (variably fossiliferrous) to Oomictric	(conf.<0.95;	BP=0.3126)
Biosparite to Oosparite	(conf.<0.95;	BP=0.2313)
Intramicrite to Oosparite	(conf.<0.95;	BP=0.2313)
Weathered gypsiferous layers to Oosparite	(conf. 0.95-0.99;	Bp=0.0572)
Oomictric to Micrite-biomicrite (variably fossiliferrous)	(conf.<0.95;	Bp=0.1135)
Oosparite to Oomictric	(conf.<0.95;	Bp=0.1351)
Dolomite to Sublitharenite	(conf. >0.99;	BP=0.0118)
Shale to Dolomite	(conf.>0.99;	BP=0.1031)
Sublitharenite to Dolomite	(conf.0.95-0.99;	BP=0.0683)

Other significant preferred transitions

(NB: binomial probabilities between 0.1 and 0.2 don't mean much)

Micrite-biomicrite (variably fossiliferrous) to Intramicrite.	BP=0.176
Micrite-biomicrite (variably fossiliferrous) to Shale	BP=0.176
Oosparite to weathered gypsiferous layers	BP=0.077

MARKOV ANALYSIS OF THE MOZDURAN FORMATION IN MOZDURAN SECTION. WELLS (1989) METHOD.

Number of facies: 9

Facies:

1 Micrite-biomicrite (variably fossiliferrous)
2 Biosparite
3 Intramicrite
4 Pelmicrite
5 Oomicrite
6 Oosparite
7 Dolomite
8 Shale
9 Sublitharenite

Raw-data matrix

No	#1	#2	#3	#4	#5	#6	#7	#8	#9	Total
1	0	0	6	1	0	1	4	5	0	17
2	2	0	0	0	0	1	0	1	0	4
3	4	1	0	0	1	0	2	1	1	10
4	0	0	1	0	0	0	0	0	0	1
5	1	0	0	0	0	1	0	0	0	2
6	1	0	0	0	0	0	1	1	3	6
7	6	0	0	0	1	1	0	0	0	8
8	2	3	1	0	0	2	0	0	0	8
9	1	0	2	0	0	1	0	0	0	4
	17	4	10	1	2	7	7	8	4	60

Expected values for quasi-independence

No	1	2	3	4	5	6	7	8	9
1	-	1.5	4.2	0.36	0.73	2.71	2.81	3.21	1.5
2	1.49	-	0.68	0.06	0.12	0.44	0.45	0.52	0.24
3	4.2	0.68	-	0.16	0.33	1.23	1.27	1.46	0.68
4	0.36	0.06	0.16	-	0.03	0.1	0.11	0.12	0.06
5	0.72	0.12	0.33	0.03	-	0.21	0.22	0.25	0.12
6	2.36	0.38	1.07	0.09	0.18	-	0.71	0.82	0.38
7	3.16	0.51	1.43	0.12	0.25	0.93	-	1.1	0.51
8	3.21	0.52	1.46	0.12	0.25	0.94	0.97	-	0.52
9	1.49	0.24	0.68	0.06	0.12	0.44	0.45	0.52	-

Difference matrix

No	1	2	3	4	5	6	7	8	9
1	-	-1.5	1.8	0.64	-0.73	-1.71	1.19	1.79	-1.5
2	0.51	-	-0.68	-0.06	-0.12	0.56	-0.45	0.48	-0.24
3	-0.2	0.32	-	-0.16	0.67	-1.23	0.73	-0.46	0.32
4	-0.36	-0.06	0.84	-	-0.03	-0.1	-0.11	-0.12	-0.06
5	0.28	-0.12	-0.33	-0.03	-	0.79	-0.22	-0.25	-0.12
6	-1.36	-0.38	-1.07	-0.09	-0.18	-	0.29	0.18	2.62
7	2.84	-0.51	-1.43	-0.12	0.75	0.07	-	-1.1	-0.51
8	-1.21	2.48	-0.46	-0.12	-0.25	1.06	-0.97	-	-0.52
9	-0.49	-0.24	1.32	-0.06	-0.12	0.56	-0.45	-0.52	-

Sequence chi-squared matrix

No	1	2	3	4	5	6	7	8	9
1	-	1.5	0.78	1.16	0.73	1.08	0.51	0.99	1.5
2	0.17	-	0.68	0.06	0.12	0.72	0.45	0.45	0.24
3	0.01	0.15	-	0.16	1.37	1.23	0.42	0.14	0.15
4	0.36	0.06	4.33	-	0.03	0.1	0.11	0.12	0.06
5	0.1	0.12	0.33	0.03	-	2.92	0.22	0.25	0.12
6	0.78	0.38	1.07	0.09	0.18	-	0.11	0.04	18

7	2.56	0.51	1.43	0.12	2.29	0.01	-	1.1	0.51
8	0.46	11.85	0.14	0.12	0.25	1.19	0.97	-	0.52
9	0.16	0.24	2.58	0.06	0.12	0.72	0.45	0.52	-

Asymmetry chi-square matrix

No	1	2	3	4	5	6	7	8	9
1	-	-	-	-	-	-	-	-	-
2	2	-	-	-	-	-	-	-	-
3	0.4	1	-	-	-	-	-	-	-
4	1	0	1	-	-	-	-	-	-
5	1	0	1	0	-	-	-	-	-
6	0	1	0	0	1	-	-	-	-
7	0.4	0	2	0	1	0	-	-	-
8	1.29	1	0	0	0	0.33	0	-	-
9	1	0	0.33	0	0	1	0	0	-

Sequence chi-squared sum=73.5573 55 degrees of freedom
Asymmetry chi-squared =17.7523 21 degrees of freedom

Principal succession for facies
Binomial probabilities listed

Micrite-biomicrite (variably fossiliferrou) to Intramicrite	(conf. <0.95;	BP=0.2251)
Biospartie to Oosparite	(conf. <0.95;	BP=0.3712)
Intramicrite to Dolomite	(conf. <0.95;	BP=0.3695)
Pelmicrite to Intramicrite	(conf. 0.95-0.99	BP=0.1620)
Oomicrite to Oosparite	(conf. <0.95;	BP=0.2011)
Oosparite to Sublitharenite	(conf. >0.99;	BP=0.0044)
Dolomite to Micrite-biomicrite (variably fossiliferrous)	(conf. <0.95;	BP=0.0466)
Shale to Biosparite	(conf. >0.99;	BP=0.0120)
Sublitharenite to Intramicrite	(conf. <0.950	BP=0.1359)

Other significant preferrd transitions

(NB: binomial probabilities between 0.1 and 0.2 don't mean much)

Binomial probability for cell 1 , 3 = 0.225092425942421
Binomial probability for cell 1 , 5 = 0.476625919342041
Binomial probability for cell 7 , 1 = 4.655976966023445E-002

MARKOV ANALYSIS OF THE MOZDURAN FORMATION IN GORGOREH SECTION. POWERS AND EASTERLING (1982) METHOD.

OBSERVED TRANSITIONS							TOTAL
0	1	4	2	0	0	4	11
0	0	1	0	0	1	0	2
5	1	0	0	0	0	4	10
3	0	1	0	0	0	0	4
0	0	0	0	0	0	2	2
0	0	1	0	0	0	0	1
2	0	3	2	2	0	0	9
TRANSITION PROBABILITY MATRIX							
0	0.9	0.36	0.18	0	0	0.36	
0	0	0.5	0	0	0.5	0	
0.5	0.1	0	0	0	0	0.4	
0.75	0	0.25	0	0	0	0	
0	0	0	0	0	0	1	
0	0	1	0	0	0	0	
0.22	0	0.33	0.22	0.22	0	0	
EXPECTED TRANSITIONS FOR QUASI-INDEPENDENCE							
0	0.657	4.306	1.379	0.657	0.322	3.679	11
0.657	0	0.559	0.179	0.085	0.042	0.478	2.0000002
4.306	0.559	0	1.173	0.559	0.274	3.13	10
1.379	0.179	1.173	0	0.179	0.088	1.002	4
0.657	0.085	0.559	0.179	0	0.042	0.478	2.0000002
0.322	0.042	0.274	0.088	0.042	0	0.234	1
3.679	0.478	3.13	1.002	0.478	0.234	0	9.0000009
PROBABILITIES OF EXPECTED TRANSITIONS							
0	0.06	0.39	0.13	0.06	0.03	0.33	
0.33	0	0.28	0.09	0.04	0.02	0.24	
0.43	0.06	0	0.12	0.06	0.03	0.31	
0.34	0.04	0.29	0	0.04	0.02	0.25	
0.33	0.04	0.28	0.09	0	0.02	0.24	
0.32	0.04	0.27	0.09	0.04	0	0.23	
0.41	0.05	0.35	0.11	0.05	0.03	0	
PROBABILITY DIFFERENCES							
0	0.03	-0.03	0.06	-0.06	-0.03	0.03	
-0.33	0	0.22	-0.09	-0.04	0.48	-0.24	
0.07	0.04	0	-0.12	-0.06	-0.03	0.09	
0.41	-0.04	-0.04	0	-0.04	-0.02	-0.25	
-0.33	-0.04	-0.28	-0.09	0	-0.02	0.76	
-0.32	-0.04	0.73	-0.09	-0.04	0	-0.23	
-0.19	-0.05	-0.01	0.11	0.17	-0.03	0	
NORMALISED PROBABILITY DIFFERENCES							
0	0.42	-0.15	0.53	-0.81	-0.57	0.17	
-0.81	0	0.59	-0.42	-0.29	4.69	-0.69	
0.33	0.59	0	-1.08	-0.75	-0.52	0.49	
1.38	-0.42	-0.16	0	-0.42	-0.3	-1	
-0.81	-0.29	-0.75	-0.42	0	-0.2	2.2	
-0.57	-0.2	1.39	-0.3	-0.2	0	-0.48	
-0.88	-0.69	-0.07	1	2.2	-0.48	0	

CHI-SQUARED TEST OF SIGNIFICANCE
CHI- SQUARED= 47.7
DEGREES OF FREEDOM = 29

MARKOV ANALISIS OF THE MOZDURAN FORMATION IN GORGOREH SECTION. WELLS (1989) METHOD.

Number of facies: 7

Facies:

1 Micrite-biomicrite (variably fossiliferrous)
2 Biosparite
3 Intramicrite
4 Intrasparite
5 Pelmicrite
6 Oosparite
7 Dolomite

Raw-data matrix

No	#1	#2	#3	#4	#5	#6	#7	Total
1	0	1	4	2	0	0	4	11
2	0	0	1	0	0	1	0	2
3	5	1	0	0	0	0	4	10
4	3	0	1	0	0	0	0	4
5	0	0	0	0	0	0	2	2
6	0	0	1	0	0	0	0	1
7	2	0	3	2	2	0	0	9
	10	2	10	4	2	1	10	39

Expected values for quasi- independence

No	1	2	3	4	5	6	7
1	-	0.63	4.14	1.32	0.63	0.31	3.97
2	0.59	-	0.56	0.18	0.09	0.04	0.54
3	3.86	0.56	-	1.18	0.56	0.28	3.55
4	1.23	0.18	1.18	-	0.18	0.09	1.14
5	0.59	0.09	0.56	0.18	-	0.04	0.54
6	0.29	0.04	0.28	0.09	0.04	-	0.26
7	3.43	0.5	3.28	1.05	0.5	0.24	-

Difference matrix

No	1	2	3	4	5	6	7
1	-	0.37	-0.14	0.68	-0.63	-0.31	0.03
2	-0.59	-	0.44	-0.18	-0.09	0.96	-0.54
3	1.14	0.44	-	-1.18	-0.56	-0.28	0.45
4	1.77	-0.18	-0.18	-	-0.18	-0.09	-1.14
5	-0.59	-0.9	-0.56	-0.18	-	-0.04	1.46
6	-0.29	-0.04	0.72	-0.09	-0.04	-	-0.26
7	-1.43	-0.5	-0.28	0.95	1.5	-0.24	-

Sequence chi- squared matrix

No	1	2	3	4	5	6	7
1	-	0.22	0	0.35	0.63	0.31	0
2	0.59	-	0.34	0.18	0.09	21.87	0.54
3	0.34	0.34	-	1.18	0.56	0.28	0.06
4	2.53	0.18	0.03	-	0.18	0.09	1.14
5	0.59	0.09	0.56	0.18	-	0.04	3.93
6	0.29	0.04	1.9	0.09	0.04	-	0.26
7	0.59	0.5	0.02	0.86	4.5	0.24	-

Asymmetry chi- square matrix

No	1	2	3	4	5	6	7
1	-	-	-	-	-	-	-
2	1	-	-	-	-	-	-
3	0.11	0	-	-	-	-	-
4	0.2	0	1	-	-	-	-

5	0	0	0	0	-	-	-
6	0	1	1	0	0	-	-
7	0.67	0	0.14	2	0	0	-

Sequence chi-squared sum= 46.7550 29 degrees of freedom
Asymmetry chi-squared = 7.1206 11degrees of freedom

Principal succession for facies
binomial probabilities listed

Micrite -biomicrite (variably fossiliferrous) to Intrasparite	(conf. < 0.95:	BP=0.3883)
Biosparite to Oosparite	(conf. >0.99;	BP=0.0415)
Intramicrite to Micrite-biomicrite (variably fossiliferrous)	(conf. <0.95;	BP=0.3328)
Intrasparite to Micrite- biomicrite (variably fossiliferrorus)	(conf. <0.95:	BP=0.0903)
Pelmicrite to Dolomite	(conf. 0.95-0.99;	BP=0.0732)
Oosparite to Intramicrite	(conf. <0.95;	BP=0.2755)
Dolomite to Pelmicrite	(conf. 0.95-0.99;	BP=0.0856)

Other significant preferred transitions:

(NB: binomial probabilities between 0.1 and 0.2 don't mean much)
Binomial probability for cell 3 , 1 = .3327803015708923
Binomial probability for cell 1 , 3 = .5986893177032471
Binomial probability for cell 3 , 7 = .5005292296409607

MARKOV ANALYSIS OF THE MOZDURAN FORMATION IN BAZANGAN SECTION. POWERS AND ESTERLING (1982).

OBSERVED TRANSITIONS										TOTAL
0	2	1	0	1	1	0	4	6	0	15
3	0	0	0	0	0	0	0	0	0	3
2	0	0	0	1	3	2	4	5	0	17
1	0	0	0	0	0	0	0	0	0	1
0	0	3	0	0	1	0	1	1	0	6
1	0	4	0	1	0	0	2	1	0	9
1	0	1	0	0	0	0	0	0	0	2
3	0	2	0	2	3	0	0	0	1	11
4	0	6	1	1	1	0	0	0	0	13
0	0	0	0	1	0	0	0	0	0	1

TRANSITION PROBABILITY MATRIX

0	0.13	0.07	0	0.07	0.07	0	0.27	0.4	0	
1	0	0	0	0	0	0	0	0	0	
0.12	0	0	0	0.06	0.18	0.12	0.24	0.29	0	
1	0	0	0	0	0	0	0	0	0	
0	0	0.5	0	0	0.17	0	0.17	0.17	0	
0.11	0	0.44	0	0.11	0	0	0.22	0.11	0	
0.5	0	0.5	0	0	0	0	0	0	0	
0.27	0	0.18	0	0.18	0.27	0	0	0	0.09	
0.31	0	0.46	0.08	0.08	0.08	0	0	0	0	
0	0	0	0	1	0	0	0	0	0	

EXPECTED TRANSITION FOR QUASI-INDEPENDENCE

0	0.625	4.507	0.204	1.299	2.034	0.412	2.568	3.147	0.204	15
0.625	0	0.745	0.034	0.215	0.336	0.068	0.424	0.52	0.034	3
4.507	0.745	0	0.243	1.547	2.422	0.491	3.057	3.747	0.243	17
0.204	0.034	0.243	0	0.07	0.109	0.022	0.138	0.169	0.011	1
1.299	0.215	1.547	0.07	0	0.698	0.141	0.881	1.08	0.07	5.999
2.034	0.336	2.422	0.109	0.698	0	0.221	1.38	1.691	0.109	9
0.412	0.068	0.491	0.022	0.141	0.221	0	0.28	0.343	0.022	2
2.568	0.424	3.057	0.138	0.881	1.38	0.28	0	2.135	0.138	11
3.147	0.52	3.747	0.169	1.08	1.691	0.343	2.135	0	0.169	13
0.204	0.034	0.243	0.011	0.07	0.109	0.022	0.138	0.169	0	1

PROBABILITIES OF EXPECTED TRANSITIONS

0	0.04	0.3	0.01	0.09	0.14	0.03	0.17	0.21	0.01	
0.21	0	0.25	0.01	0.07	0.11	0.02	0.14	0.17	0.01	
0.27	0.04	0	0.01	0.09	0.14	0.03	0.18	0.22	0.01	
0.2	0.03	0.24	0	0.07	0.11	0.02	0.14	0.17	0.01	
0.22	0.04	0.26	0.01	0	0.12	0.02	0.15	0.18	0.01	
0.23	0.04	0.27	0.01	0.08	0	0.02	0.15	0.19	0.01	
0.21	0.03	0.25	0.01	0.07	0.11	0	0.14	0.17	0.01	
0.23	0.04	0.28	0.01	0.08	0.13	0.03	0	0.19	0.01	
0.24	0.04	0.29	0.01	0.08	0.13	0.03	0.16	0	0.01	
0.2	0.03	0.24	0.01	0.07	0.11	0.02	0.14	0.17	0	

PROBABILITY DIFFERENCES

0	0.09	-0.23	-0.01	-0.02	-0.07	-0.03	0.1	0.19	-0.01	
0.79	0	-0.25	-0.01	-0.07	-0.11	-0.02	-0.14	-0.17	-0.01	
-0.15	-0.04	0	-0.01	-0.03	0.03	0.09	0.06	0.07	-0.01	
0.8	-0.03	-0.24	0	-0.07	-0.11	-0.02	-0.14	-0.17	-0.01	
-0.22	-0.04	0.24	-0.01	0	0.05	-0.02	0.02	-0.01	-0.01	
-0.11	-0.04	0.18	-0.01	0.03	0	-0.02	0.07	-0.08	-0.01	

0.29	-0.03	0.25	-0.01	-0.07	-0.11	0	-0.14	-0.17	-0.01	
0.04	-0.04	-0.1	-0.01	0.1	0.15	-0.03	0	-0.19	0.08	
0.07	-0.04	0.17	0.06	-0.01	-0.05	-0.03	-0.16	0	-0.01	
-0.2	-0.03	-0.24	-0.01	0.93	-0.11	-0.02	-0.14	-0.17	0	

NORMALISED PROBABILITY DIFFERENCES

0	1.74	-1.65	-0.45	-0.26	-0.72	-0.64	0.89	1.61	-0.45	
3	0	-0.86	-0.18	-0.46	-0.58	-0.26	-0.65	-0.72	-0.18	
-1.18	-0.86	0	-0.49	-0.44	0.37	2.15	0.54	0.65	-0.49	
1.76	-0.18	-0.49	0	-0.26	-0.33	-0.15	-0.37	-0.41	-0.1	
-1.14	-0.46	1.17	-0.26	0	0.36	-0.38	0.13	-0.08	-0.26	
-0.72	-0.58	1.01	-0.33	0.36	0	-0.47	0.53	-0.53	-0.33	
0.92	-0.26	0.73	-0.15	-0.38	-0.47	0	-0.53	-0.59	-0.15	
0.27	-0.65	-0.6	-0.37	1.19	1.38	-0.53	0	-1.46	2.32	
0.48	-0.72	1.16	2.02	-0.08	-0.53	-0.59	-1.46	0	-0.41	
-0.45	-0.18	-0.49	-0.1	3.52	-0.33	-0.15	-0.37	-0.41	0	

CHI- SQUARED TEST OF SIGNIFICANCE
CHI-SQUARED = 77.5
DEGREES OF FREEDOM = 71

MARKOV ANALYSIS OF THE MOZDURAN FORMATION IN BAZANGAN SECTION. WELLS (1989) METHOD.

Number of facies: 10

Facies:

1 Micrite-biomicrite (variably fossiliferrous)
2 Biosparite
3 Intramicrite
4 Intraspari te
5 Pelmicrite
6 Oomicrite
7 Oosparite
8 Dolomite
9 Marl-shale(fine clastic sediment)
10 Sublitharenite

Raw-data matrix

No	#1	#2	#3	#4	#5	#6	#7	#8	#9	#10	Total
1	0	2	1	0	1	1	0	4	6	0	15
2	3	0	0	0	0	0	0	0	0	0	3
3	2	0	0	0	1	3	2	4	5	0	17
4	1	0	0	0	0	0	0	0	0	0	1
5	0	0	3	0	0	1	0	1	1	0	6
6	1	0	4	0	1	0	0	2	1	0	9
7	1	0	1	0	0	0	0	0	0	0	2
8	3	0	2	0	2	3	0	0	0	1	11
9	4	0	6	1	1	1	0	0	0	0	13
10	0	0	0	0	1	0	0	0	0	0	1
	15	2	17	1	7	9	2	11	13	1	78

Expected values for quasi-independence

No	1	2	3	4	5	6	7	8	9	10	
1	-	0.42	4.5	0.2	1.52	2.03	0.41	2.57	3.15	0.2	
2	0.62	-	0.74	0.03	0.25	0.33	0.07	0.42	0.51	0.03	
3	4.5	0.5	-	0.24	1.8	2.42	0.49	3.06	3.74	0.24	
4	0.2	0.02	0.24	-	0.08	0.11	0.02	0.14	0.17	0.01	
5	1.31	0.14	1.56	0.07	-	0.71	0.14	0.89	1.09	0.07	
6	2.03	0.22	2.42	0.11	0.81	-	0.22	1.38	1.69	0.11	
7	0.41	0.05	0.49	0.02	0.17	0.22	-	0.28	0.34	0.02	
8	2.57	0.28	3.05	0.14	1.03	1.38	0.28	-	2.13	0.14	
9	3.15	0.35	3.74	0.17	1.26	1.69	0.34	2.13	-	0.17	
10	0.2	0.02	0.24	0.01	0.08	0.11	0.02	0.14	0.17	-	

Difference matrix

No	1	2	3	4	5	6	7	8	9	10	
1	-	1.58	-3.5	-0.2	-0.52	-1.03	-0.41	1.43	2.85	-0.2	
2	2.38	-	-0.74	-0.03	-0.25	-0.33	-0.07	-0.42	-0.51	-0.03	
3	-2.5	-0.5	-	-0.24	-0.8	0.58	1.51	0.94	1.26	-0.24	
4	0.8	-0.02	-0.24	-	-0.08	-0.11	-0.02	-0.14	-0.17	-0.01	
5	-1.31	-0.14	1.44	-0.07	-	0.29	-0.14	0.11	-0.09	-0.07	
6	-1.03	-0.22	1.58	-0.11	0.19	-	-0.22	0.62	-0.69	-0.11	
7	0.59	-0.05	0.51	-0.02	-0.17	-0.22	-	-0.28	-0.34	-0.02	
8	0.43	-0.28	-1.05	-0.14	0.97	1.62	-0.28	-	-2.13	0.86	
9	0.85	-0.35	2.26	0.83	-0.26	-0.69	-0.34	-2.13	-	-0.17	
10	-0.2	-0.02	-0.24	-0.01	0.92	-0.11	-0.02	-0.14	-0.17	-	

Sequence chi-squared matrix

No	1	2	3	4	5	6	7	8	9	10	

1	-	6.02	2.73	0.2	0.18	0.52	0.41	0.8	2.59	0.2	
2	9.18	-	0.74	0.03	0.25	0.33	0.07	0.42	0.51	0.03	
3	1.39	0.5	-	0.24	0.36	0.14	4.65	0.29	0.42	0.24	
4	3.11	0.02	0.24	-	0.08	0.11	0.02	0.14	0.17	0.01	
5	1.31	0.14	1.32	0.07	-	0.12	0.14	0.01	0.01	0.07	
6	0.52	0.22	1.03	0.11	0.04	-	0.22	0.28	0.28	0.11	
7	0.84	0.05	0.53	0.02	0.17	0.22	-	0.28	0.34	0.02	
8	0.07	0.28	0.36	0.14	0.92	1.91	0.28	-	2.13	5.38	
9	0.23	0.35	1.36	4.08	0.05	0.28	0.34	2.13	-	0.17	
10	0.2	0.02	0.24	0.01	10.34	0.11	0.02	0.14	0.17	-	

Asymmetry chi-square matrix

No	1	2	3	4	5	6	7	8	9	10	
1	-	-	-	-	-	-	-	-	-	-	
2	0.2	-	-	-	-	-	-	-	-	-	
3	0.33	0	-	-	-	-	-	-	-	-	
4	1	0	0	-	-	-	-	-	-	-	
5	1	0	1	0	-	-	-	-	-	-	
6	0	0	0.14	0	0	-	-	-	-	-	
7	1	0	0.33	0	0	0	-	-	-	-	
8	0.14	0	0.67	0	0.33	0.2	0	-	-	-	
9	0.4	0	0.09	1	0	0	0	0	-	-	
10	0	0	0	0	1	0	0	1	0	-	

Sequence chi-square Sum= 77.5809 71 degrees of freedom
Asymmetry chi-squared= 9.8432 21 degrees of freedom
Principal succession for facies
Binomial probabilities listed
Micrite-biomicrite (variably fossiliferrous)

Marl-shale (fine clastic sediment)	(conf.<0.95;	BP=0.0744)
Biosparite to Micrite-biomicrite (variably fossiliferrous)	(conf.>0.99;	BP=0.0087)
Intramicrite to Oosparite	(conf.0.95-0.99;	BP=0.0850)
Intrasparite to Micrite-biomicrite (variably fossiliferrous)	(conf.<0.95-0.99;	BP= 0.2036)
Pelmicrite to Intramicrite	(conf.<0.95;	BP=0.1869)
Oomicrite to Intramicrite	(conf.<0.95;	BP=0.2027)
Oosparite to Micrite-biomicrite (variably fossiliferrous)	(conf.<0.95;	BP=0.3695)
Dolomite to Oomicrite	(conf.<0.95;	BP=0.1506)
Marl-shale (fine clastic sediment) to intramicrite	(conf.<0.95;	BP=0.1417)
Sublitharenite to Pelmicrite	(conf. >0.99;	BP=0.0816)

Other significant preferred transitions
(NB: binomial probabilities between 0.1 and 0.2 don't mean much)

Micrite-biomicrite (variably fossiliferrous) to Biosparite	BP=0.064
Micrite-biomicrite (variably fossiliferrous) to Intramicrite	BP=0.035
Dolomite to Sublitharenite	BP=0.130
Marl-shale (fine clastic sediment) to Intrasparite	BP=0.157

APPENDIX 3

FISCHER PLOTS OF THE MOZDURAN CARBONATES

In the Padeha, Mozduran, Gorgoreh and Bazangan sections

The following Fischer plots were generated using a custom-written spread sheet.

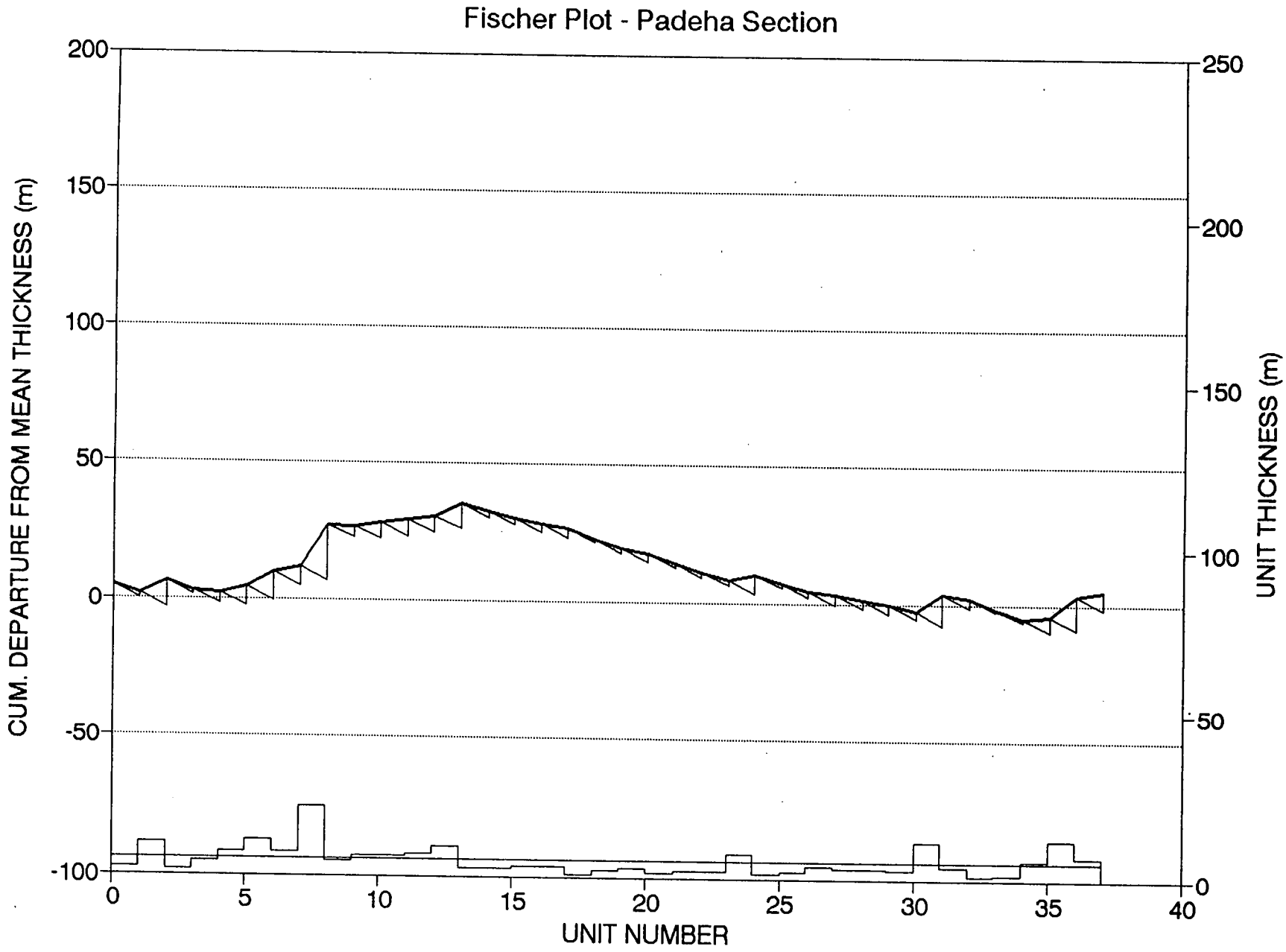
Fischer Plot - Padeha Section
CUM. DEPARTURE FROM MEAN THICKNESS (m)
UNIT THICKNESS (m)
UNIT NUMBER
200
150
100
50
0
-50
-100
250
200
150
100
50
0
0
5
10
15
20
25
30
35
40

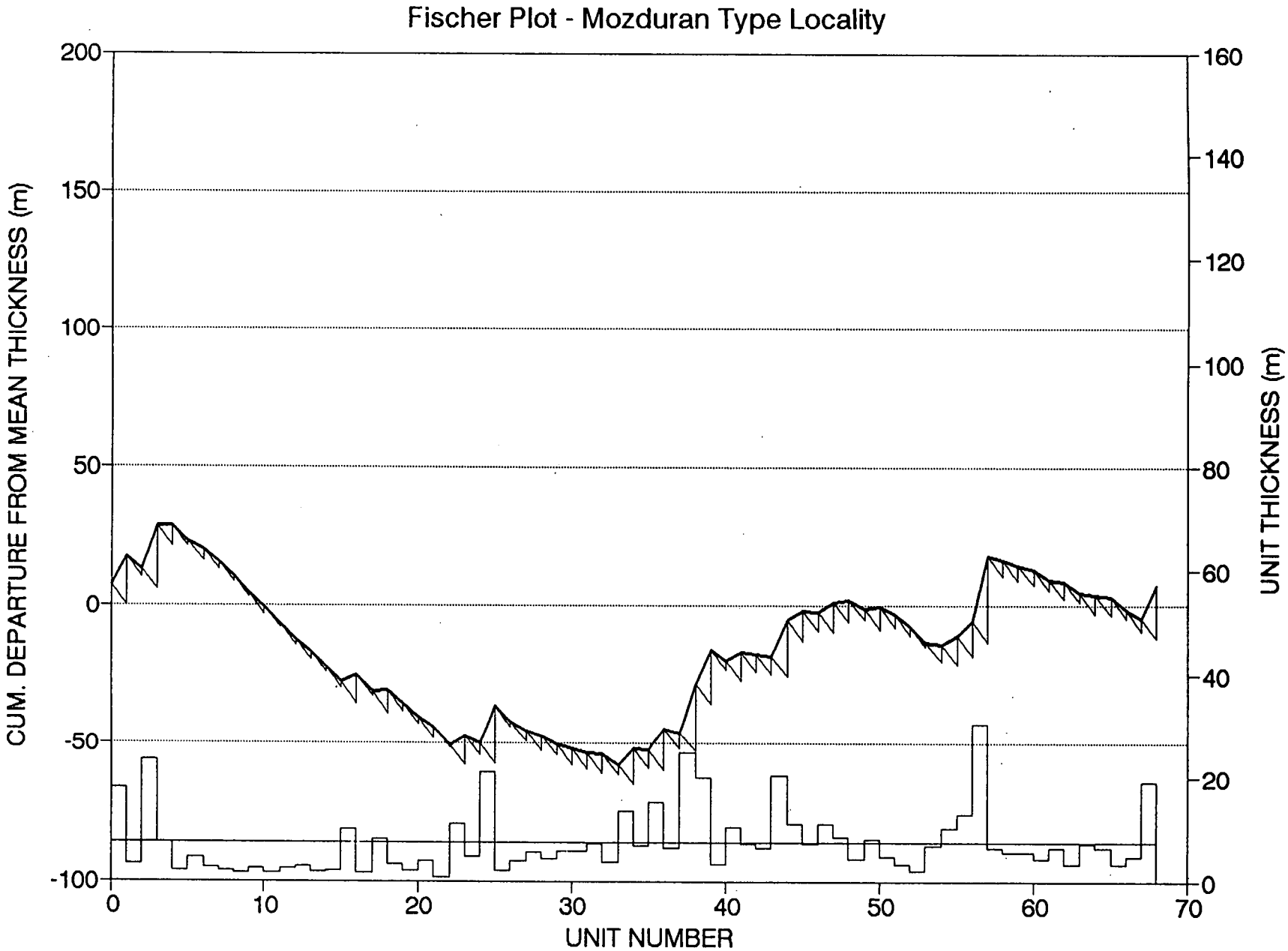
Fischer Plot - Mozduran Type Locality
CUM. DEPARTURE FROM MEAN THICKNESS (m)
UNIT THICKNESS (m)
UNIT NUMBER
200
150
100
50
0
-50
-100
160
140
120
100
80
60
40
20
0
0
10
20
30
40
50
60
70

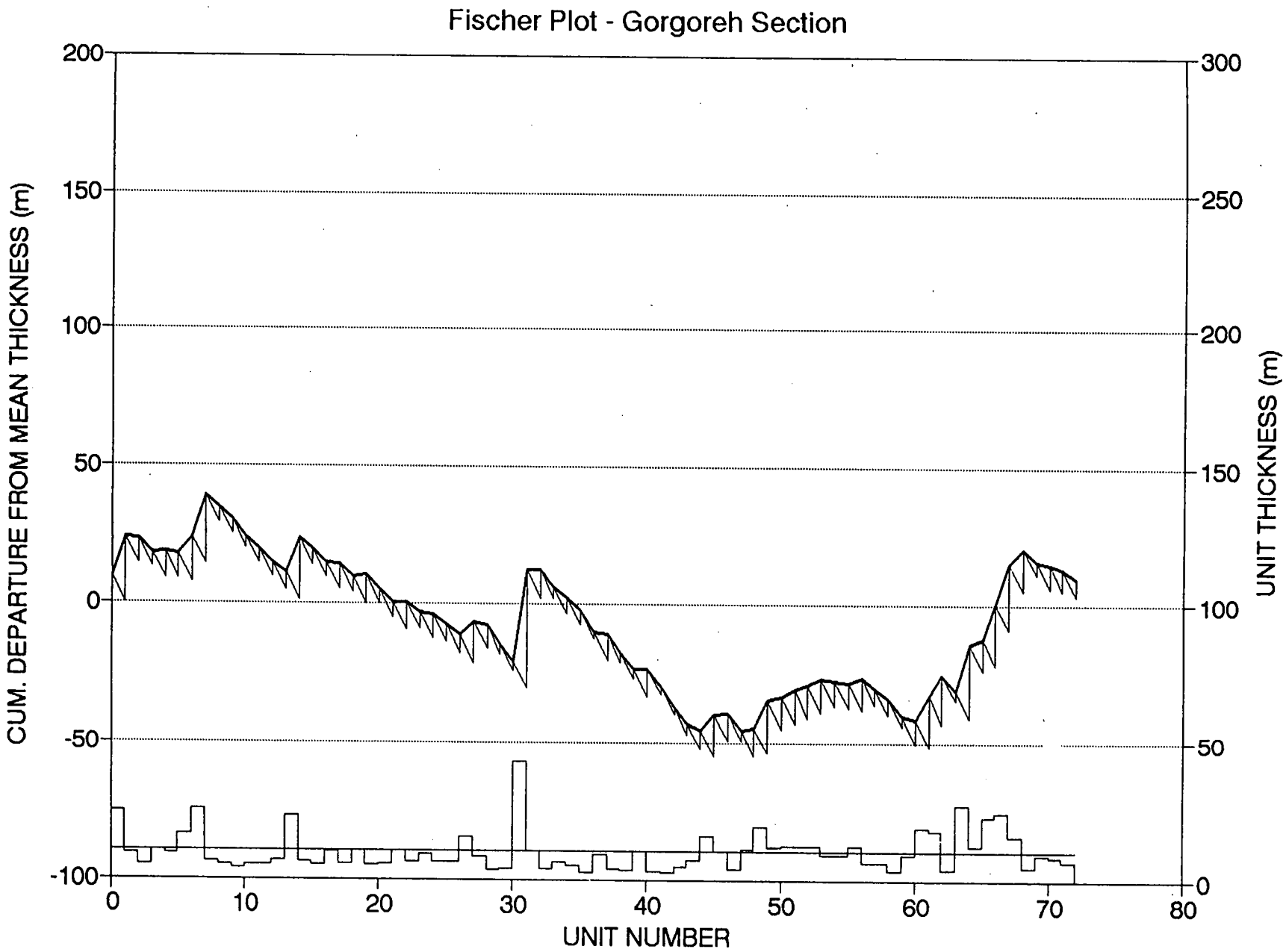
Fischer Plot - Gorgoreh Section
CUM. DEPARTURE FROM MEAN THICKNESS (m)
UNIT THICKNESS (m)
UNIT NUMBER
200
150
100
50
0
-50
-100
300
250
200
150
100
50
0
0
10
20
30
40
50
60
70
80

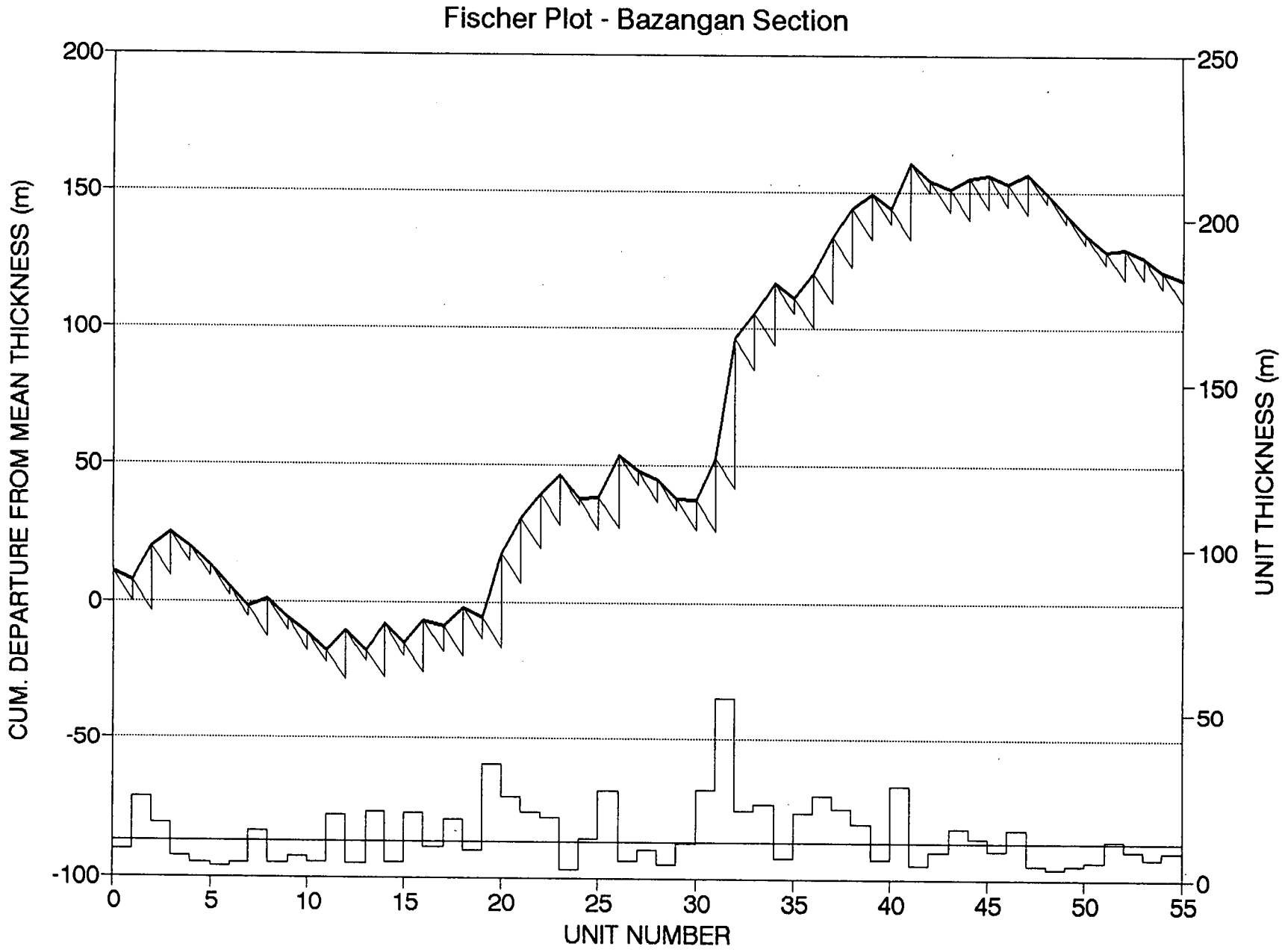
Fischer Plot - Bazangan Section
CUM. DEPARTURE FROM MEAN THICKNESS (m)
UNIT THICKNESS (m)
UNIT NUMBER
200
150
100
50
0
-50
-100
250
200
150
100
50
0
0
5
10
15
20
25
30
35
40
45
50
55

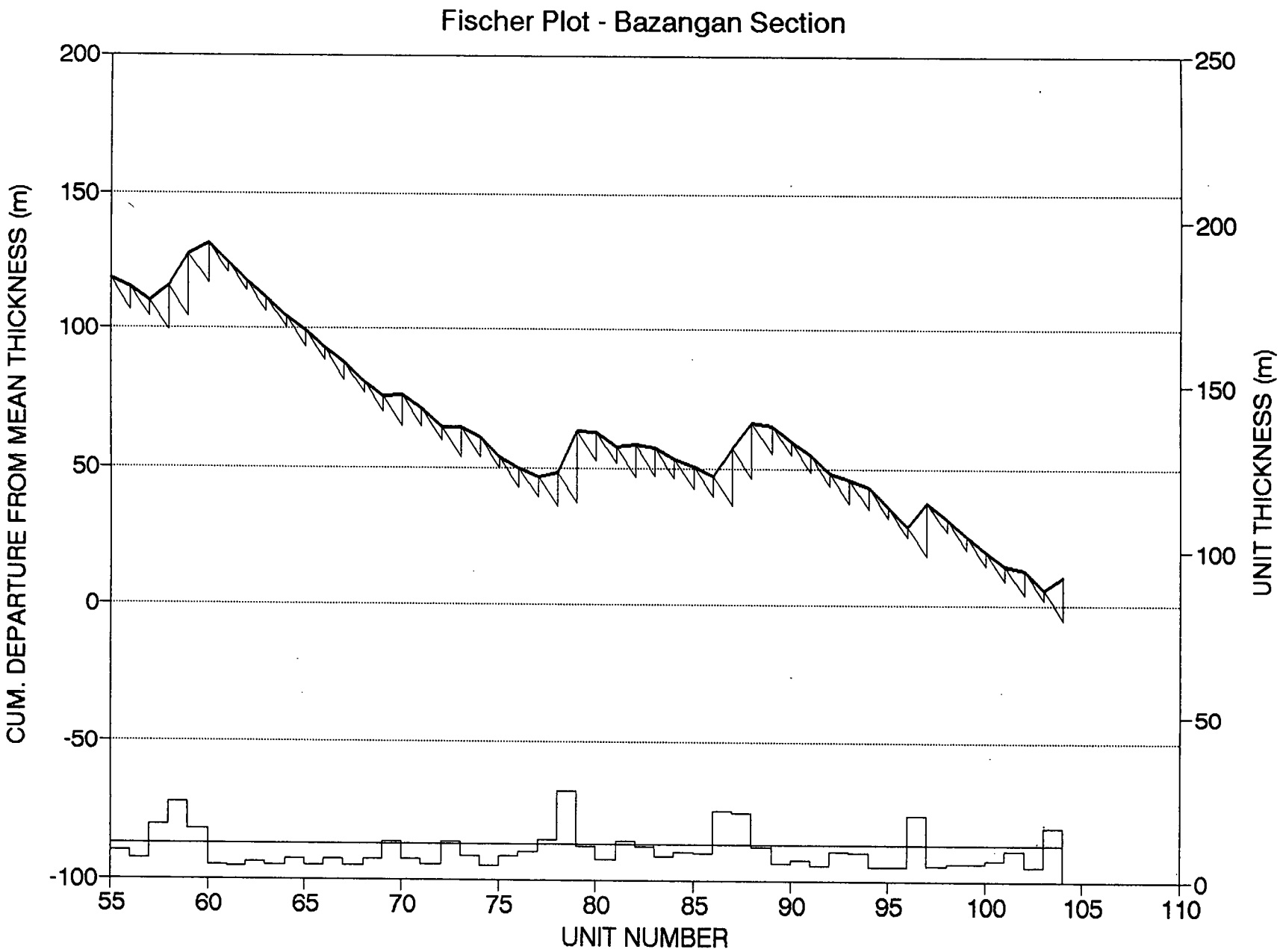
Fischer Plot - Bazangan Section
CUM. DEPARTURE FROM MEAN THICKNESS (m)
UNIT THICKNESS (m)
UNIT NUMBER
200
150
100
50
0
-50
-100
250
200
150
100
50
0
55
60
65
70
75
80
85
90
95
100
105
110

APPENDIX 4

ELEMENTAL AND ISOTOPIC COMPOSITION OF RECENT TEMPERATE BULK CARBONATES OF TASMANIA

The following chemical data is base on 86 (from a total of 120) bulk carbonate samples with <10% insoluble residue published by Rao and Adabi (1992), Rao and Jayawardane (1994) from western and eastern temperate shelf carbonate of Tasmania respectively and by Rao and Amini (1995) from King Island (north of Tasmania).

TAS BULK COMPOSITION <10% Ins. Residue

X_1: Rev Calcite%

Mean:	Std. Dev.:	Std. Error:	Variance:	Coef. Var.:	Count:
87.7	9.31	1.004	86.67	10.615	86
Minimum:	**Maximum:**	**Range:**	**Sum:**	**Sum of Sqr.:**	**# Missing:**
52.77	97.28	44.51	7542.2	668817.919	1

X_2: Rev Aragonite%

Mean:	Std. Dev.:	Std. Error:	Variance:	Coef. Var.:	Count:
12.3	9.31	1.004	86.668	75.687	86
Minimum:	**Maximum:**	**Range:**	**Sum:**	**Sum of Sqr.:**	**# Missing:**
2.72	47.23	44.51	1057.81	20377.981	1

X_3: ∂18 O

Mean:	Std. Dev.:	Std. Error:	Variance:	Coef. Var.:	Count:
1.134	.448	.048	.2	39.482	86
Minimum:	**Maximum:**	**Range:**	**Sum:**	**Sum of Sqr.:**	**# Missing:**
-.2	3.2	3.4	97.53	127.647	1

X_4: ∂13 C

Mean:	Std. Dev.:	Std. Error:	Variance:	Coef. Var.:	Count:
1.884	.32	.034	.102	16.977	86
Minimum:	**Maximum:**	**Range:**	**Sum:**	**Sum of Sqr.:**	**# Missing:**
1.1	2.6	1.5	162.01	313.894	1

X_5: Rev Ca%

Mean:	Std. Dev.:	Std. Error:	Variance:	Coef. Var.:	Count:
36.357	1.807	.194	3.267	4.971	87
Minimum:	**Maximum:**	**Range:**	**Sum:**	**Sum of Sqr.:**	**# Missing:**
31.47	42.32	10.85	3163.03	115278.159	0

TAS BULK COMPOSITION <10% Ins. Residue

X_6: Rev Mg%

Mean:	Std. Dev.:	Std. Error:	Variance:	Coef. Var.:	Count:
1.304	.327	.035	.107	25.096	87
Minimum:	**Maximum:**	**Range:**	**Sum:**	**Sum of Sqr.:**	**# Missing:**
.03	2.17	2.14	113.43	157.097	0

X_7: Rev Sr ppm

Mean:	Std. Dev.:	Std. Error:	Variance:	Coef. Var.:	Count:
3270.954	692.509	74.245	479568.696	21.171	87
Minimum:	**Maximum:**	**Range:**	**Sum:**	**Sum of Sqr.:**	**# Missing:**
1642	5007	3365	284573	972068107	0

X_8: Rev Mn ppm

Mean:	Std. Dev.:	Std. Error:	Variance:	Coef. Var.:	Count:
69.316	50.301	5.393	2530.204	72.568	87
Minimum:	**Maximum:**	**Range:**	**Sum:**	**Sum of Sqr.:**	**# Missing:**
1	311	310	6030.5	635608.25	0

X_9: Rev Na ppm

Mean:	Std. Dev.:	Std. Error:	Variance:	Coef. Var.:	Count:
3993.862	713.718	76.519	509394.074	17.87	87
Minimum:	**Maximum:**	**Range:**	**Sum:**	**Sum of Sqr.:**	**# Missing:**
1844	5482	3638	347466	1431539168	0

X_{10}: Rev Fe ppm

Mean:	Std. Dev.:	Std. Error:	Variance:	Coef. Var.:	Count:
1577.506	1166.901	125.105	1361658.927	73.971	87
Minimum:	**Maximum:**	**Range:**	**Sum:**	**Sum of Sqr.:**	**# Missing:**
202	6932	6730	137243	333604289	0

TAS BULK COMPOSITION <10% Ins. Residue

X_{11}: Residue%

Mean:	Std. Dev.:	Std. Error:	Variance:	Coef. Var.:	Count:
4.373	2.256	.242	5.088	51.578	87
Minimum:	**Maximum:**	**Range:**	**Sum:**	**Sum of Sqr.:**	**# Missing:**
1.06	9.75	8.69	380.48	2101.54	0

X_{12}: Depth/m

Mean:	Std. Dev.:	Std. Error:	Variance:	Coef. Var.:	Count:
111.908	55.242	5.923	3051.643	49.363	87
Minimum:	**Maximum:**	**Range:**	**Sum:**	**Sum of Sqr.:**	**# Missing:**
18	399	381	9736	1351978	0

APPENDIX 5

ANALYTICAL RESULTS OF THE MOZDURAN CARBONATES

Tables A5.1 and A5.2 list limestone analyses of those samples with less than 1% Mg and less than 10% insoluble residue.

Tables A5.3, A5.4, A5.5, A5.6 show all inclusive limestone elemental analysis in the Shurijeh, Bagak, Padeha and Mozduran sections.

Table A5.7 lists weight percent inorganic and organic carbon in the Mozduran limestones.

Table A5.8 lists elemental and isotopic analysis of the Mozduran limestone cements and calcite veins.

Table A5.9 lists dolomite type, insoluble residue, elemental and isotopic composition of dolomites from Mozduran Formation.

Table A5.10 shows XRD results of representative dolomite samples from the Mozduran Formation.

Table A5.11 lists weight percent inorganic and organic carbon in the Mozduran dolomites.

Table A5.1. Major and minor element, insoluble residue and stable isotope composition of the Mozduran limestones in the Shurijeh, Bagak, Padeha and Mozduran sections.

Sample No	Description	Ca %	Mg %	Mn ppm	Fe ppm	Sr ppm	Na ppm	Sr/Na ratio	Sr/Mn ratio	I.R %	∂13C‰ PDB	∂18O‰PDB
Sh-33	Bulk sediment	39.25	0.74	252	1190	114	85	1.34	0.45	3.47	-0.3	-4.2
Sh-34	" "	39.47	0.4	212	1001	150	83	1.81	0.71	2.62	0.8	-4.6
Ba-11	" "	39.74	0.15	483	1018	154	92	1.67	0.32	4.57	2.1	-6.4
Ba-13	" "	39.75	0.17	393	1006	167	79	2.11	0.42	10	1.7	-4.9
Ba-15	" "	39.37	0.28	278	1632		123			6.87	3	-6.8
Ba-16	" "	39.76	0.33	270	1362	278	137	2.02	1.03	4.32	2.5	-7.2
Ba-27c	" "	39.5	0.51	338	1438	259	130	2	0.77	9.8		
Pa-10	" "	39.4	0.31	378	2650	261	114	2.29	0.69	7.32	1.6	-7.8
Pa-12	" "	39.5	0.38	184	872	342	196	1.74	1.86	7.17	3.9	-4.1
Pa-19	" "	39.7	0.37	257	1908	278	152	1.83	1.08	4.57		
Pa-27	" "	39.37	0.4	240	1665	323	193	1.67	1.34	8.77	1.3	-6.5
Pa-28	" "	39.4	0.34	369	2772	266	131	2.03	0.72	9.77	1.5	-7.4
Pa-36	" "	39.7	0.34	275	1835	319	152	2.1	1.16	7.22	1.8	-7.2
Mz-17	Micrite	39.48	0.42	193	781	187	116	1.6	0.97	1.35	3.3	-5.6
Mz-21	Bulk sediment	39.51	0.38	174	621	293	136	2.15	1.68	2.9	2.4	-7.9
Mz-22	Micrite	39.49	0.36	164	578	240	280	0.86	1.46	3.8	3.7	-2.8
Mz-24	" "	39.7	0.27	180	458	175	206	0.85	0.97	2.9	4.3	-2.6
Mz-26	Bulk sediment	39.77	0.21	413	682	151	148	1.02	0.36	5.6	2	-4.4
Mz-36	" "	39.76	0.24	55	554	173	140	1.23	3.14	9.2		
Mz-41	Micrite	39.08	0.38	56	489	299	154	1.94	5.33	2.05	4.3	-3.4
Mz-66	Bulk sediment										1.8	-7.2
Mz-71	" "	39.69	0.35	53	420	315	145	2.17	5.94	1.9	1.5	-6.4
Mz-87	" "	39.41	0.33	289	3745	408	123	3.31	1.41	8.9	0.8	-7.3
Mz-90	" "	39.7	0.34	205	1041	358	180	1.99	1.75	5.55	2	-7.4
Mz-95	" "	39.59	0.32	215	933	325	148	2.2	1.51	5.25	2	-7.8
Mz-96	" "	39.61	0.29	185	947	339	209	1.62	1.83	3.65		
Mz-102	" "	39.5	0.4	101	436	261	100	2.61	2.58	2.8	1	-7.5
Mz-105	" "	39.9	0.34	150	494	317	166	1.9	2.11	3.2	1.7	-7.8
Mz-107	" "	39.82	0.28	322	901	307	99	3.1	0.95	3.55	1.9	-7.7
Mz-109	" "	39.33	0.42	529	1960	281	111	2.53	0.53	6.55	1.3	-7.7
Mz-110	Micrite	39.48	0.52	63	328	313	194	1.61	4.97	0	4.3	-1.2
Br-O	Terebratula	39.43	0.46	114	721	497	171	2.9		8.25	1.7	-3.5
Br-1	Rhynchonellid	39.5	0.49	121	535	447	159	2.81		9.1	1.2	-6.5
Br-2	" "	39.6	0.38	113	680	368	181	2.03		8.8	2	-4.4
Br-3	" "										1.3	-4.3
Br-4	" "										1.8	-5.1
Cr-1	Crinoid	39.22	0.58	164	1400	333	401	0.83		2.95	1.8	-4.5

Table A5.2. Major and minor element, insoluble residue and stable isotope composition of the Mozduran limestones in the Gorgoreh and Bazangan sections.

Sample No	Description	Ca %	Mg %	Mn ppm	Fe ppm	Sr ppm	Na ppm	Sr/Na ratio	Sr/Mn ratio	I.R %	∂13C‰PDB	∂18O‰PDB
Go-54	Intraclast	39.64	0.25	51	233	166	178	0.93	3.25	1.12	3	-2.4
Go-54	Micrite	39.41	0.24	56	339	151	144	1.04	2.69	3.28	2.9	-3.2
Go-56	" "	39.22	0.35	47	126	100	88	1.14	2.12	3.36	3.3	-4.5
Go-56	Intraclast	39.44	0.54	43	156	92	93	0.99	2.14	1.12	3.1	-4.4
Go-58	" "	39.59	0.28	76	397	155	186	0.83	2.03	2	3.3	-3.4
Go-60	Micrite	38.69	0.3	34	263	112	108	1.04	3.29	2.48	3.6	-2.6
Go-70	Intraclast	39.81	0.19	61	200	99	105	0.94	1.62	1.6	3.1	-4.2
Go-73	Micrite	39.74	0.14	37	212	74	81	0.91	2	1.92	2.9	-4.7
Go-76	" "	39.33	0.61	58	276	118	139	0.85	2.03	2.88	3.2	-3.6
Go-76	Intraclast	39.68	0.3	40	241	171	206	0.83	4.27	3.68	3.3	-2.7
Go-81	" "	39.04	0.89	50	285	103	117	0.88	2.06	1.2	3.1	-3.8
Go-82	" "										3.4	-3.2
Go-83	Micrite	39.81	0.29	48	301	117	116	1	2.43	2.72	3.2	-3.9
Go-84	" "	39.62	0.26	33	368	134	172	0.78	4.06	2.24	2.5	-3.3
Go-84	Oncoid	39.66	0.26	28	327	204	188	1.08	7.28	1.76	2.9	-2.1
Go-84	Oncoid core										2.5	-2.8
Go-86	Intraclast	39.68	0.44	49	424	179	186	0.96	3.56	4.4	2.9	-3.1
Go-87	Micrite	39.45	0.46	43	343	99	112	0.88	2.3	1.2	3.8	-1.9
Go-99	" "	39.3	0.75	21	239	140	164	0.85	6.66	2.72	4.2	-1.7
Go-100	" "	39.71	0.25	17	116	145	128	1.13	8.52	0	4.1	-1.9
Go-100	Bulk sediment										4.1	-6.1
Go-104	" "	39.79	0.21	65	301	194	113	1.72	2.98	1.68	2.9	-6.1
Go-113	" "	39.12	0.41	155	1507	254	223	1.14	1.64	6.72	2.1	-6.3
Go-115	" "	38.45	0.9	188	1157	273	219	1.24	1.45	2.8	1.8	-6.4
Bz-3	Micrite	39.44	0.31	328	1190	218	186	1.17	0.66	10	3.5	-4.3
Bz-4	Bulk sediment	39.16	0.28	190	1199	163	123	1.32	0.85	6.24	1.3	-4.9
Bz-6	Micrite	39.06	0.39	161	1252	249	274	0.91	1.55	3.76	4.2	-3.5
Bz-7	Bulk sediment									13.2	3.2	-5.6
Bz-8	Micrite	39.43	0.47	192	2498	372	461	0.8	1.93	4.88	4	-3.1
Bz-9	Intraclast									14.72	4	-3.5
Bz-10	Bulk sediment	39.46	0.17	245	3552	214	84	2.55	0.87	3.92	3.5	-5.7
Bz-12	Micrite	39.41	0.46	131	2278	336	469	0.71	2.56	6.8	4.2	-3.2
Bz-13	" "	38.63	0.54	99	1686	424	525	0.81	4.28	6.24	4.5	-2.5

Sample No	Description	Ca %	Mg %	Mn ppm	Fe ppm	Sr ppm	Na ppm	Sr/Na ratio	Sr/Mn ratio	I.R %	∂13 C PDB	∂18 O PDB
Bz-14	Bulk sediment									12.48	3.6	-4.9
Bz-15	" "	39.59	0.22	175	1646	326	97	3.36	1.86	7.04	4	-6.4
Bz-18	Micrite	39.28	0.16	128	939	145	111	1.3	1.13	5.92	3.7	-4.4
Bz-21	" "	38.94	0.36	152	777	242	226	1.07	1.59	6.4	3.2	-4.5
Bz-23	Bulk sediment	39.19	0.26	136	1032	183	179	1.02	1.34	4.64	3.7	-5.1
Bz-25	Micrite	39.6	0.29	97	392	179	206	0.87	1.84	6.08	3.8	-4
Bz-27	" "	39.16	0.33	88	274	240	256	0.94	2.73	6.64	3.1	-3.6
Bz-32	Bulk sediment	39.8	0.26	52	87	140	136	1.02	2.69	1.6	2.4	-4.7
Bz-33	" "	39.87	0.17	50	76	82	71	1.15	1.64	2.08	2.4	-6.2
Bz-34	" "	39.69	0.31	47	185	72	44	1.64	1.53	1.12	2	-5.8
Bz-35	" "	39.29	0.2	56	101	130	112	1.16	2.32	2	2.1	-4.4
Bz-37	" "	39.93	0.12	43	76	91	104	0.9	2.1	0.96	2.7	-4.8
Bz-40	" "	39.55	0.18	47	105	112	91	1.23	2.38	1.2	2.6	-4
Bz-42	" "	39.94	0.08	85	155	61	54	1.13	0.72	0.4	2	-5.5
Bz-43	" "	39.21	0.19	50	118	109	112	0.97	2.18	6.16	2.3	-4.7
Bz-44	" "	39.77	0.12	65	63	87	78	1.11	1.34	0.56	2.9	-4.5
Bz-45	" "	39.6	0.22	42	151	154	163	0.95	3.67	2	2.7	-3.5
Bz-46	" "	39.53	0.42	45	69	70	69	1	1.55	0	2.4	-4.9
Bz-46A	" "	39.4	0.66	47	106	75	72	1.04	1.59	0	2.2	-5.2
Bz-54	" "	39.51	0.49	33	88	113	95	1.19	3.42	1.36	2.7	-3.6
Bz-55	" "	39.6	0.19	39	127	87	72	1.21	2.23	3.52	2.6	-5.1
Bz-56	" "	39.56	0.38	58	120	97	69	1.4	1.67	5.92	2.3	-5
Bz-56	Oolite	39.75	0.26	88	250	100	91	1.09	1.13	6.8	2.1	-5.8
Bz-60	Bulk sediment	39.62	0.21	40	97	121	91	1.33	3.02	0	2.7	-4
Bz-60	Oolite	39.82	0.2	30	101	129	103	1.26	4.3	2.56		
Bz-61	Bulk sediment	39.6	0.24	47	222	123	125	0.98	2.62	7.28	2.6	-3.8
Bz-61	Micrite										2.5	-3.8
Bz-69	" "	39.83	0.18	36	103	88	67	1.31	2.4	1.04	3.2	-4.8
Bz-69	Oolite	39.8	0.15	35	84	98	75	1.31	2.8	0	2.8	-4.9
Bz-71	Bulk sediment	39.91	0.27	44	115	80	84	0.95	1.82	5.84	1.4	-6.3
Bz-78	" "	39.94	0.14	48	126	74	44	1.68	1.54	2.24	2.2	-5.8
Bz-82	" "	40.02	0.12	53	180	79	49	1.6	1.49	0	2.8	-5.9
Bz-82A	" "	40.08	0.13	50	113	70	46	1.52	1.4	0	2.5	-5.8
Bz-83	" "	40	0.15	45	133	85	59	1.45	1.89	0	3.1	-6
Bz-83A	" "	39.88	0.17	53	127	80	68	1.18	1.51	0	2.9	-6.1

Sample No	Description	Ca %	Mg %	Mn ppm	Fe ppm	Sr ppm	Na ppm	Sr/Na ratio	Sr/Mn ratio	I.R %	∂13 C PDB	∂18 O PDB
Bz-84	Bulk sediment	39.93	0.27	111	532	158	134	1.18	1.42	2.64	2.8	-4.6
Bz-85	" "	39.89	0.18	128	750	122	84	1.45	0.95	2.56	2.3	-5.3
Bz-86	" "	39.63	0.29	60	314	185	115	1.6	3.08	2.16	3.2	-5.8
Bz-87	" "	39.66	0.26	72	308	151	110	1.37	2.09	2.48	3.2	-5.2
Bz-88	" "	39.77	0.3	94	381	174	86	2.02	1.85	4	3.2	-5.4
Bz-89	Micrite	39.8	0.18	28	106	106	92	1.15	3.78	3.84	3.1	-4.1
Bz-89	Oolite	39.92	0.18	33	107	115	126	0.91	3.48	2.32		
Bz-91	Bulk sediment	39.7	0.26	37	256	189	98	1.93	5.1	0.8	3	-5.7
Bz-92	" "	39.72	0.36	50	349	245	165	1.48	4.9	2.88	2.6	-5
Bz-93	" "	39.68	0.36	113	1035	377	250	1.51	3.33	8	2	-5.4
Bz-93	Micrite	39.24	0.36	123	1394	381	295	1.29	3.09	7.28		
Bz-94	Bulk sediment	39.67	0.38	118	1010	407	198	2.04	3.45	8.16	1.7	-4.9
Bz-95	" "									13	0.9	-6.9
Bz-97	" "									16.97	1.2	-5
Bz-98	" "									13.84	1.4	-5.6
Bz-99	" "	39.22	0.47	136	1885	320	250	1.28	2.35	5.2	1.9	-6.7
Bz-100	" "	39.31	0.38	147	1634	409	252	1.62	2.78	4	1.7	-6.7
Bz-101	" "	39.34	0.5	151	1291	285	194	1.47	1.89	7.28	2	-5.9
Bz-101	Micrite	39.47	0.48	160	1830	263	224	1.17	1.64	8.56		
Bz-102	Bulk sediment	39.78	0.31	110	687	207	124	1.68	1.88	5.36	2.3	-7
Bz-104	" "	38.95	0.85	81	908	264	145	1.82	3.26	3.6	2.3	-7
Bz-105	" "									11.12	2.3	-5.8
Bz-111	" "	39.8	0.26	49	304	153	111	1.38	3.12	1.52	2.2	-5
Bz-111	Micrite	39.61	0.25	55	275	185	136	1.36	3.36	1.68	2.6	-4.9

Table A5.3. All major and minor elements and insoluble residue of the Mozduran carbonates in the Shurijeh section.

Sample No	Description	Ca%	Mg%	Mn ppm	Fe ppm	Sr ppm	Na ppm	I.R%
Sh-3	Bulk sediment	21.79	11.66	1798	18305	82	197	32.97
Sh-4	Fine grain dolomite	21.66	11.62	1928	20339	65	205	44.57
Sh-8	" "	22.11	12.05	1574	12327	62	159	22.67
Sh-9	Bulk sediment	23.11	9.33	2460	31489	309	145	83.82
Sh-13	Coarse grain dolomite	22.09	11.24	2259	21544	72	274	27.72
Sh-14	Bulk sediment	24.8	6.8	1362	19601	389	836	89.72
Sh-15	" "	20.53	10.86	1527	14168	61	186	54.42
Sh-18	" "	20.37	9.39	2126	47393	213	308	85.42
Sh-22	Fine grain dolomite	22.03	12.26	844	9336	57	172	37.07
Sh-25	Bulk sediment	21.99	12.16	443	5702	61	250	46.07
Sh-27	" "	22.39	12.38	382	4990	84	212	30.07
Sh-28	Fine grain dolomite	22.36	12.55	329	4215	45	338	3.76
Sh-29	" "	22.18	12.54	351	4486	65	381	5.68
Sh-31	Bulk sediment	21.86	12.28	373	4415	211	285	13.47
Sh-32	Coarse grain dolomite	21.93	12.45	637	7332	46	311	3.04
Sh-33	Bulk sediment	39.25	0.74	252	1190	114	85	3.47
Sh-34	" "	39.47	0.4	212	1001	150	83	2.62
Sh-36	Coarse grain dolomite	23.47	11.42	443	6171	79	300	3.12
Sh-37	Fine grain dolomite	22.65	11.46	667	10306	112	397	9.6
Sh-38	" "	22.91	11.22	738	9576	124	375	16.72
Sh-39	" "	22.91	11.44	769	7940	137	391	18.47
Sh-41	" "	22.82	11.57	1090	4606	90	330	16.77
Sh-42	Coarse grain dolomite	22.1	12.55	1179	4523	49	271	3.68
Sh-42a	" "	21.72	12.27	1171	4508	55	272	3.2
Sh-42b	" "	22.21	12.35	1163	4492	58	292	3.12

Table A5.4. All major and minor elements and insoluble residue of the Mozduran carbonates in the Bagak section.

Sample No	Description	Ca%	Mg%	Mn ppm	Fe ppm	Sr ppm	Na ppm	I.R%
Ba-2	Bulk sediment	22.31	12.19	1454	9026	67	225	22.17
Ba-5	" "	22	12.27	1016	8086	198	625	21.07
Ba-6	" "	22.62	11.76	900	9207	88	424	60.12
Ba-8	" "	22.28	12.33	963	7290	74	349	7.76
Ba-10	" "	24.85	11.06	804	5115	92	178	7.52
Ba-11	" "	39.74	0.15	483	1018	154	92	4.57
Ba-13	" "	39.75	0.17	393	1006	167	79	10
Ba-15	" "	39.37	0.28	278	1632		123	6.87
Ba-16	" "	39.76	0.33	270	1362	278	137	4.32
Ba-17	" "	21.39	9.72	424	9780	88	138	57.32
Ba-18	" "	38.37	1.15	414	3252	203	163	9.82
Ba-19	" "	33.86	4.67	330	3570	195	249	9.77
Ba-20	" "	30.94	6.61	295	5145	155	317	17.37
Ba-21	" "	27.2	9.08	302	5150	98	251	9.62
Ba-23	" "	31.67	6.28	272	3080	123	186	9.32
Ba-25	" "	37.77	1.53	463	2495	220	135	9.97
Ba-26	" "	31.62	6.14	593	6998	155	152	29.17
Ba-27a	" "	39.37	0.35	410	1962	226	124	15.92
Ba-27c	" "	39.5	0.51	338	1438	259	130	9.8

Table A5.5. All major and minor elements and insoluble residue of the Mozduran carbonates in the Padeha section.

Sample No	Description	Ca%	Mg%	Mn ppm	Fe ppm	Sr ppm	Na ppm	I.R%
Pa-5	Bulk sediment	24.2	10.08	3122	32517	382	800	85.62
Pa-8	" "	22.07	12.7	327	4550	88	187	5.92
Pa-10	" "	39.4	0.31	378	2650	261	114	7.32
Pa-12	" "	39.5	0.38	184	872	342	196	7.17
Pa-19	" "	39.7	0.37	257	1908	278	152	4.57
Pa-22	" "	39.15	0.44	534	4630	290	174	84.47
Pa-24	" "	36.08	3.5	298	5296	219	179	9.72
Pa-27	" "	39.37	0.4	240	1665	323	193	8.77
Pa-28	" "	39.4	0.34	369	2772	266	131	9.77
Pa-31	" "	39.07	1.2	361	2874	304	269	34.97
Pa-34	" "	38.15	1.87	432	3950	283	437	43.77
Pa-35	" "	39.17	0.49	377	1798	264	87	17.07
Pa-36	" "	39.7	0.34	275	1835	319	152	7.22
Pa-39	" "	39.02	1.29	439	1902	418	143	26.02

Table A5.6. All major and minor elements and insoluble residue of the Mozduran carbonates in the Mozduran section (type locality).

Sample No	Description	Ca%	Mg%	Mn ppm	Fe ppm	Sr ppm	Na ppm	I.R%
Mz-4	Bulk sediment	25.84	11.09	303	1128	68	216	2.65
Mz-6	" "	23.92	12.11	277	1006	62	297	3.85
Mz-10	" "	23.18	12.78	374	1514	61	260	1.14
Mz-13	" "	25.26	10.73	251	939	73	217	4.2
Mz-15	" "	25.64	10.48	275	1033	68	226	0.8
Mz-17	" "	34.78	3.73	180	749	143	189	1.45
Mz-17	Micrite	39.48	0.42	193	781	187	116	1.35
Mz-19	Bulk sediment	38.02	1.76	166	427	174	126	2.7
Mz-21	" "	39.51	0.38	174	621	293	136	2.9
Mz-22	Micrite	39.49	0.36	164	578	240	280	3.8
Mz-24	" "	39.7	0.27	180	458	175	206	2.9
Mz-26	Bulk sediment	39.77	0.21	413	682	151	148	5.6
Mz-29	" "	40.85	0.45	139	1009	245	275	13.25
Mz-32	" "	37.35	2.33	117	1410	200	207	9.2
Mz-36	" "	39.76	0.24	55	554	173	140	9.2
Mz-39	" "	23.31	10.94	157	2851	127	261	9.75
Mz-41	Micrite	39.08	0.38	56	489	299	154	2.05
Mz-43	Bulk sediment	24.45	11	173	5251	99	151	3.12
Mz-44	" "	22.72	12.56	135	4384	51	172	3.2
Mz-45	" "	29.46	7.72	83	1806	100	117	3.37
Mz-46	" "	37	2.06	58	653	153	157	3.7
Mz-48	" "	24.13	11.65	132	2615	93	126	3.2
Mz-49	" "	23.24	12.03	156	4582	75	244	1.55
Mz-53	" "	22.41	11.76	316	6271	76	419	1.85
Mz-55	" "	26.7	9.38	439	4346	161	175	5.25
Mz-58	" "	40.58	3.48	346	3404	269	145	36.45
Mz-71	" "	39.69	0.35	53	420	315	145	1.9
Mz-84	" "	35.45	0.58	400	6909	2927	636	94.5
Mz-87	" "	39.41	0.33	289	3745	408	123	8.9
Mz-89	" "	40.48	0.35	516	3978	493	231	11.2
Mz-90	" "	39.7	0.34	205	1041	358	180	5.55
Mz-95	" "	39.59	0.32	215	933	325	148	5.25
Mz-96	" "	39.61	0.29	185	947	339	209	3.65
Mz-102	" "	39.5	0.4	101	436	261	100	2.8
Mz-105	" "	39.9	0.34	150	494	317	166	3.2
Mz-107	" "	39.82	0.28	322	901	307	99	3.55
Mz-108	" "	40.5	0.58	803	2152	317	245	77.6
Mz-109	" "	39.33	0.42	529	1960	281	111	6.55
Mz-110	Micrite	39.48	0.52	63	328	313	194	0

Table A5.7. Weight percent inorganic and organic carbon in the Mozduran limestones.

Sample No	Wt. of Crusible	Crusible+Sample	After 24 hrs @ 450 °C	% Losses	Correction factor	%C inorganic (ashed samples)	%C inorganic in carbonate	%C total (unashed samples)	%C organic (TOC)
Sh-33	7.71598	9.71598	9.71135	0.23	0.997685	11.75	11.72	11.77	0.05
Ba-11	8.74952	10.74952	10.74236	0.36					
Ba-16	6.72392	8.72392	8.71505	0.45	0.995565	11.5	11.45	11.55	0.1
Pa-27	8.39727	10.39727	10.38479	0.62	0.99376	10.99	10.92	11.04	0.12
Pa-36	5.34426	7.34426	7.3357	0.43					
Mz-36	5.73414	7.73414	7.7258	0.42	0.99583	10.86	10.81	10.89	0.08
Go-76	6.27789	8.27799	8.27058	0.37					
Go-81	6.0401	8.04028	8.03503	0.26					
Go-84	6.99565	8.99579	8.98866	0.36	0.996435	11.76	11.71	11.92	0.21
Go-115	8.74901	10.74901	10.74239	0.33					
Bz-12	5.38192	7.38192	7.37111	0.54	0.994595	11.16	11.09	11.14	0.05
Bz-18	7.0542	9.0542	9.04889	0.26					
Bz-25	5.33741	7.33741	7.32788	0.48	0.995235	11.46	11.4	11.55	0.15
Bz-27	5.91648	7.91648	7.90611	0.52	0.994815	11.38	11.32	11.74	0.42
Bz-35	7.17716	9.17716	9.17218	0.25					
Bz-40	7.20145	9.20145	9.19728	0.21					
Bz-54	6.58813	8.58813	8.58512	0.15	0.998495	12.01	11.99	11.99	0
Bz-60	6.1204	8.1204	8.11636	0.2					
Bz-89	6.21645	8.21645	8.2124	0.2	0.997975	11.66	11.63	11.74	0.11
Bz-102	8.05437	10.05437	10.05005	0.21					

Table A5.8. Elemental and isotopic analysis of the Mozduran limestone cements and calcite veins.

Sample No	Description	Ca%	Mg%	Mn ppm	Fe ppm	Sr ppm	Na ppm	I.R%	∂13 C PDB	∂18 O PDB
Pa-12	Poikilitic sparry calcite cement								2.4	-7.6
Pa-28	Poikilitic sparry calcite cement	39.1	0.84	72	113	108	30	0	2	-7.2
Mz-31	Platy sparry calcite cement	39.09	0.75	129	73	23	29	0	-2.8	-6.2
Mz-66	Equant sparry calcite cement								1.1	-6
Mz 109	Platy sparry calcite cement	39.69	0.33	126	48	30	32	0	-0.3	-6
Mz 109	Syntaxial overgrowth cement	39.62	0.3	95	365	37	56	0	2.7	-6
Go-70	Equant sparry calcite cement	39.77	0.17	72	42	55	69	0	3.6	-5.7
Go-83	Equant sparry calcite cement	39.63	0.27	98	75	62	93	0	3.2	-6.1
Go-91	Equant sparry calcite cement								3.7	-6.1
Go-99	Equant sparry calcite cement	39.83	0.27	40	180	86	87	0	3.8	-6.5
Go-116	Turbid syntaxial overgrowth cement	39.8	0.24	85	32	321	107	0.56	3.6	-2.4
Bz-26	Equant drusy sparry calcite cement								0.4	-6.6
Bz-55	Equant sparry calcite cement								2.2	-4.4
Bz-57	Equant sparry calcite cement	39.9	0.21	73	70	61	81	0	2.3	-4.7
Go-26	Vein calcite	39.5	0.42	117	52	81	132	0	1.9	-9.8
Go-49	Vein calcite	39.8	0.28	29	147	80	11	0	-5.2	-9.4
Go-78	Vein calcite	38.94	0.95	135	145	211	39	0	-1.3	-12.6
Go-82	Vein calcite	39.87	0.09	170	49	103	207	0	-3.6	-12.4
Go-85	Vein calcite	39.63	0.33	70	64	137	50	0	3.4	-11

Table A5.9. Dolomite type, major and minor elements, insoluble residue, $\delta^{18}O$, $\delta^{13}C$ values of the Mozduran dolomites in the Shurijeh (Sh), Bagak (Ba), Padeha (Pa), Gorgoreh (Go) and Bazangan (Bz) sections.

Sample No	Description	Ca%	Mg %	Mn ppm	Fe ppm	Sr ppm	Na ppm	Mg/Ca ratio	I.R %	∂13 C PDB	∂18 O PDB
Sh-3	Very fine-to fine xtalline dolomite (laminated, unimodal, planar-s)								32.97	0.4	-4.4
Sh-8	Medium xtalline dolomite (sandy, planar-s)								22.67	0.4	-4.9
Sh-13	Medium- to coarse xtalline dolomite (nonplanar)								27.72	-0.2	-6.8
Sh-22	Very fine-to fine xtalline dolomite (sandy, unimodal, planar-s)								37.07	2.4	-4.6
Sh-28	Very fine-to fine xtalline dolomite (sandy, unimodal, planar-s)	22.36	12.55	329	4215	45	338	0.56	3.76	3.3	-3.9
Sh-29	Very fine-to fine xtalline dolomite (sandy, unimodal, planar-s)	22.18	12.54	351	4486	65	381	0.56	5.68	3.6	-3.9
Sh-32	Medium- to coarse xtalline dolomite (nonplanar)	21.93	12.45	637	7332	46	311	0.57	3.04	1.2	-7.3
Sh-36	Medium- to coarse xtalline dolomite (nonplanar)	23.47	11.42	443	6171	79	300	0.49	3.12	0.8	-7.1
Sh-37	Very fine-to fine xtalline dolomite (unimodal, planar-s)	22.65	11.46	667	6306	112	397	0.51	9.6	1.1	-1.6
Sh-38	Very fine-to fine xtalline dolomite (unimodal, planar-s)								16.72	0.6	-1.1
Sh-39	Very fine-to fine xtalline dolomite (unimodal, planar-s)								18.47	2.35	-1.45
Sh-41	Very fine-to fine xtalline dolomite (unimodal, planar-s)								16.77	-0.5	-1.5
Sh-42	Medium- to coarse xtalline dolomite (nonplanar)	22.1	12.55	1179	4523	49	271	0.57	3.68	-1.3	-7.8
Sh-42a	Medium- to coarse xtalline dolomite (nonplanar)	21.72	12.27	1171	4508	55	272	0.56	3.2		
Sh-42b	Medium- to coarse xtalline dolomite (nonplanar)	22.21	12.35	1163	4492	58	292	0.55	3.12		
Ba-5	Very fine-to fine xtalline dolomite (sandy, unimodal, planar-s)									2.6	-4.3
Ba-8	Medium- to coarse xtalline dolomite (planar-s)	22.28	12.33	963	6290	74	349	0.55	7.76	1.5	-6.4
Ba-10	Medium xtalline dolomite (unimodal, planar-s)	24.85	11.06	804	5115	92	178	0.44	7.52	2.5	-5.6
Ba-19	Fine-to medium xtalline dolomite (scattered dolomite rhombs, planar-e)	33.86	4.67	330	3570	195	249	0.13	9.77		
Ba-21	Fine-to medium xtalline dolomite (scattered dolomite rhombs, planar-e)	27.2	9.08	302	5150	98	251	0.33	9.62	1.5	-5.8
Ba-23	Fine-to medium xtalline dolomite (scattered dolomite rhombs, planar-e)	31.67	6.28	272	3080	123	186	0.2	9.32		
Pa-8	Medium- to coarse xtalline dolomite (planar-s)	22.07	12.7	327	4550	88	187	0.57	5.92	4	-7.7
Pa-24	Fine-to medium xtalline dolomite (scattered dolomite rhombs, planar-e)	36.08	3.5	298	2296	219	179	0.11	9.72		
Mz-4	Medium- to coarse xtalline dolomite (planar-s)	25.84	11.09	303	2128	68	216	0.43	2.65	0.6	-7.8
Mz-6	Medium xtalline dolomite (unimodal, planar-s)	23.92	12.11	277	2006	62	297	0.51	3.85	2	-6.3
Mz-10	Medium- to coarse xtalline dolomite (planar-s)	23.18	12.78	347	2514	61	260	0.55	1.14	2.7	-5.6
Mz-13	Very fine-to fine xtalline dolomite (unimodal, planar-s)	25.26	10.73	251	939	73	217	0.42	4.2	2.4	-6.6
Mz-15	Medium- to coarse xtalline dolomite (planar-s)	25.64	10.48	275	1033	68	226	0.41	0.8	3.2	-6.4
Mz-16	Coarse- to very coarse xtalline dolomite cement (planar-s)									2.5	-6.8
Mz-17	Fine-to medium xtalline dolomite (scattered dolomite rhombs, planar-e)	34.87	3.73	180	749	143	189	0.11	1.45	3.4	-6.6
Mz-34	Coarse- to very coarse xtalline dolomite cement (planar-e)									2.8	-7.3
Mz-34	Medium xtalline dolomite (unimodal, planar-s)									4.02	-5.35
Mz-39	Very fine-to fine xtalline dolomite (unimodal, planar-s)	23.31	10.94	157	2851	127	261	0.47	9.75	3.7	-1.2
Mz-42	Medium- to coarse xtalline dolomite (planar-s)	24.45	11	173	4384	99	151	0.45	3.12	4.4	-7
Mz-44	Medium xtalline dolomite (unimodal, planar-s)	22.72	12.56	235	5251	51	117	0.55	3.2	5	-3.3
Mz-45	Fine-to medium xtalline dolomite (scattered dolomite rhombs, planar-e)	29.46	7.72	83	1806	100	172	0.26	3.37	4.3	-4.2
Mz-48	Medium xtalline dolomite (unimodal, planar-s)	24.13	11.65	132	2615	93	126	0.48	3.2	3.4	-5.1
Mz-49	Medium- to coarse xtalline dolomite (planar-s)	23.24	12.03	156	4582	75	244	0.52	1.55	4.6	-6.4
Mz-53	Medium xtalline dolomite (unimodal, planar-s)	22.41	11.76	316	6271	76	419	0.52	1.85	4.3	-5.8
Mz-55	Fine-to medium xtalline dolomite (scattered dolomite rhombs, planar-e)	26.7	9.38	439	4346	161	175	0.35	5.25	3.3	-3.7
Mz-56	Fine-to medium xtalline dolomite (scattered dolomite rhombs, planar-e)									3.4	-5.1

Sample No	Description	Ca %	Mg %	Mn ppm	Fe ppm	Sr ppm	Na ppm	Mg/Ca ratio	I.R %	∂13 C PDB	∂18 O PDB
Go-26	Medium- to coarse xtalline dolomite (planar-s, bulk sample)	22.56	12.29	185	548	45	380	0.54	2.72	3	-7.1
Go-28	Medium- to coarse xtalline dolomite (planar-s, bulk sample)	22.52	12.31	220	429	26	389	0.55	1.44	3.3	-7.8
Go-29	Medium- to coarse xtalline dolomite (planar-s, bulk sample)	22.14	13	160	317	46	418	0.55	4.72	3.3	-7
Go-31	Medium- to coarse xtalline dolomite (planar-s, bulk sample)	22.6	12.57	156	401	49	451	0.56	3.36	3.2	-6.9
Go-32	Medium- to coarse xtalline dolomite (planar-s, bulk sample)	22.25	13.05	179	665	38	440	0.58	4.48	3.4	-6.9
Go-36	Medium- to coarse xtalline dolomite (nonplanar, bulk sample)	26.96	9.05	241	308	69	248	0.33	0	2.8	-7
Go-42	Medium- to coarse xtalline dolomite (nonplanar, bulk sample)	23.23	12.05	130	334	42	319	0.52	0	3.1	-6.5
Go-47	Medium- to coarse xtalline dolomite (planar-s, bulk sample)	28.12	9.2	307	513	82	225	0.33	2.48	2.2	-8
Go-67	Medium- to coarse xtalline dolomite (nonplanar, bulk sample)	22.6	12.48	129	452	24	314	0.54	2.24	3.3	-9
Go-79	Fine-to medium xtalline dolomite (scattered dolomite rhombs, planar-e)	35.37	3.1	75	245	69	134	0.09	0.88	2.2	-5.6
Go-101	Medium xtalline dolomite (planar-s, bulk sample)	25.35	11.63	117	670	61	235	0.46	5.28	3	-6.7
Go-102	Medium xtalline dolomite (planar-s, bulk sample)	23.06	12.2	127	675	51	238	0.53	3.28	3.9	-6.8
Go-105	Medium- to coarse xtalline dolomite (planar-s, bulk sample)	25.28	11.6	269	3264	78	302	0.46	5.92	3.7	-8.9
Go-28	Medium- to coarse xtalline dolomite (planar-s, dark matrix)	22.56	12.27	178	359	30	421	0.54	0	3.6	-7.4
Go-29	Medium- to coarse xtalline dolomite (planar-s, dark matrix)	22.4	12.5	220	328	40	452	0.56	0	3.7	-7.3
Go-30	Medium- to coarse xtalline dolomite (planar-s, dark matrix)	22.47	12.1	161	152	43	462	0.54	0.56	3.6	-6.2
Go-30	Medium- to coarse xtalline dolomite (planar-s, white matrix)	23.45	11.73	144	139	53	380	0.5	0	3.4	-6.4
Go-31	Medium- to coarse xtalline dolomite (planar-s, dark matrix)	22.44	12.64	156	464	49	471	0.56	0.72	3.7	-6.8
Go-32	Medium- to coarse xtalline dolomite (planar-s, matrix)	22.25	13	279	665	40	437	0.55	0	3.7	-6.9
Go-33	Medium- to coarse xtalline dolomite (planar-s, dark matrix)	22.12	12.63	258	823	27	353	0.57	0.8	3.2	-7.8
Go-35	Medium- to coarse xtalline dolomite (planar-s, white matrix)	23.86	11.62	175	635	64	293	0.49	1.04	3.5	-7
Go-35	Medium- to coarse xtalline dolomite (planar-s, dark matrix)	22.05	12.27	269	423	37	399	0.56	1.2	3.8	-6.7
Go-36	Medium- to coarse xtalline dolomite (nonplanar, dark matrix)	24.29	11.03	249	387	67	309	0.45	0.96	3.1	-7.3
Go-36	Medium- to coarse xtalline dolomite (nonplanar, white matrix)	26.45	9.62	260	1100	73	255	0.36	0	2	-6.9
Go-37	Medium- to coarse xtalline dolomite (planar-s, dark matrix)	22	12.26	228	340	37	522	0.56	1.6	3.8	-6.1
Go-37	Medium- to coarse xtalline dolomite (planar-s, white matrix)	30.37	6.72	201	296	58	156	0.22	0		
Go-38	Medium- to coarse xtalline dolomite (planar-s, white matrix)	31.01	6.88	191	328	76	169	0.22	0	0.6	-8.2
Go-38	Medium xtalline dolomite (planar-s, dark matrix)	21.22	9.07	216	506	53	353	0.43	0.8	3.4	-6.7
Go-39	Medium xtalline dolomite (planar-s, dark matrix)	22.2	12.27	288	631	40	416	0.55	1.44	3.8	-6.5
Go-40	Medium- to coarse xtalline dolomite (planar-s, dark matrix)	22.3	12.18	221	740	43	406	0.55	0.56	3.9	-7
Go-41	Medium- to coarse xtalline dolomite (nonplanar, dark matrix)	22.21	12.71	216	506	36	303	0.57	0.64	3.8	-6.9
Go-41	Medium- to coarse xtalline dolomite (nonplanar, white matrix)	22.95	12	157	430	42	241	0.52	0.56	2.8	-7.2
Go-42	Medium- to coarse xtalline dolomite (nonplanar, dark matrix)	22.36	12.17	129	359	46	358	0.54	0	3.7	-6.1
Go-42	Medium- to coarse xtalline dolomite (nonplanar, white matrix)	27.57	8.85	162	303	42	178	0.32	0	1.6	-7
Go-43	Medium xtalline dolomite (planar-s, dark matrix)	23.22	11.6	127	316	46	322	0.5	0	3	-5.1
Go-46	Medium- to coarse xtalline dolomite (planar-s, dark matrix)	22.22	12.38	243	330	33	378	0.56	0	3.9	-7
Go-46	Medium- to coarse xtalline dolomite (planar-s, white matrix)	27.89	8.73	214	279	69	239	0.3	0	1.9	-7.5
Go-49	Medium- to coarse xtalline dolomite (planar-s, dark matrix)	23.4	12.24	164	322	38	347	0.53	0	3.2	-7.8
Go-52	Medium- to coarse xtalline dolomite (planar-s, dark matrix)	26.68	10.63	182	341	45	289	0.39	0	3.4	-7.8
Go-56	Fine-to medium xtalline dolomite (scattered dolomite rhombs, planar-e)									3.3	-6
Go-65	Medium- to coarse xtalline dolomite (nonplanar, white matrix)	25.08	11.27	382	1302	44	304	0.45	0	3.3	-8.4
Go-65	Medium- to coarse xtalline dolomite (nonplanar, dark matrix)	22.18	12.74	329	1189	29	468	0.57	0	3.8	-8.3
Go-66	Medium- to coarse xtalline dolomite (nonplanar, dark matrix)	21.8	13.04	278	686	35	353	0.59	0	3.7	-9.3
Go-67	Medium- to coarse xtalline clear dolomite (planar-s, white matrix)	22.85	12.45	132	485	41	326	0.54	1.52	3.4	-9.1
Go-68	Medium- to coarse xtalline dolomite (nonplanar, dark matrix)	23.91	12.19	268	526	39	403	0.51	0	3.3	-9.1
Go-78	Medium- to coarse xtalline dolomite (planar-s, white matrix)	26.29	10.85	221	854	46	331	0.41	1.6	2.4	-7.4

Go-88	Medium- to coarse xtalline clear dolomite (planar-s, white matrix)	23.28	12.22	330	985	26	362	0.52	1.68	3.4	-9
Go-94	Medium- to coarse xtalline dolomite (planar-s, white matrix)	25.93	10.34	279	612	35	239	0.4	1.44	3	-7.9
Go-107	Medium xtalline dolomite (planar-s, dark matrix)	24.01	10.78	471	4073	49	254	0.45	3.52	3.8	-8.5
Go-109	Medium- to coarse xtalline dolomite (nonplanar, matrix)	22.76	11.84	611	5063	55	222	0.52	1.6	3.4	-9.3
Go-120	Fine-to medium xtalline dolomite	27.92	8.66	332	2878	96	145	0.31	5.04	1.5	-6.7

Sample No	Description	Ca %	Mg %	Mn ppm	Fe ppm	Sr ppm	Na ppm	Mg/Ca ratio	I.R %	∂13 C PDB	∂18 O PDB
Bz-26	Medium xtalline dolomite (planar-s, bulk sample)	22.66	11	157	253	44	269	0.48	4.48	2.6	-6.6
Bz-28	Medium xtalline dolomite (planar-s, bulk sample)	24.25	11.06	232	320	23	227	0.45	0.08	1.6	-4.6
Bz-29	Medium xtalline dolomite (planar-s, bulk sample)	23.57	11.8	189	227	39	255	0.5	0.56	2.2	-4.3
Bz-30	Medium- to coarse xtalline dolomite (planar-s, bulk sample)	22.58	11.83	207	164	45	283	0.52	0.88	2.3	-7.1
Bz-31	Medium- to coarse xtalline dolomite (nonplanar, bulk sample)	23.52	11.46	249	414	50	273	0.49	1.84	2.5	-8
Bz-38	Medium- to coarse xtalline dolomite (planar-s, bulk sample)	26.3	9.8	191	338	69	223	0.36	0.64	0.7	-7.2
Bz-39	Medium xtalline dolomite (planar-s, bulk sample)	25.04	9.83	224	166	49	171	0.39	2.72	1.6	-6.5
Bz-48	Medium- to coarse xtalline dolomite (planar-s, bulk sample)	20.9	12.62	233	434	28	300	0.54	0.48	2.4	-6.8
Bz-49	Medium- to coarse xtalline dolomite (planar-s, bulk sample)	21.84	12.7	215	370	25	232	0.58	0.72	3	-7
Bz-50	Medium- to coarse xtalline dolomite (planar-s, bulk sample)	21.79	12.52	195	116	22	289	0.59	0.4	2.9	-6.9
Bz-52	Medium- to coarse xtalline dolomite (nonplanar, bulk sample)	23.03	11.36	316	409	35	245	0.49	2.48	3.1	-7.3
Bz-53	Medium- to coarse xtalline dolomite (nonplanar, bulk sample)	23.62	10.7	238	323	23	247	0.45	0.8	1.3	-7.7
Bz-57	Fine-to medium xtalline dolomite (scattered dolomite rhombs, planar-e)	30.89	5.38	103	154	50	164	0.17	0	2.4	-6.4
Bz-62	Medium xtalline dolomite (planar-s, bulk sample)	31.94	5.29	166	313	38	128	0.16	2.08		
Bz-63	Coarse- to very coarse xtalline dolomite cement (planar-e)	28.05	7.43	138	164	44	172	0.26	0	1.9	-8.2
Bz-64	Coarse- to very coarse xtalline dolomite cement (planar-e)	29.05	8.52	201	233	38	210	0.29	1.28	1.4	-8.2
Bz-65	Medium- to coarse xtalline dolomite (planar-s, bulk sample)	22.72	11.71	221	213	19	267	0.51	0.8	2.3	-8.4
Bz-66	Fine-to medium xtalline dolomite (scattered dolomite rhombs, planar-e)	33.75	3.66	82	138	67	150	0.11	0	2.2	-5.7
Bz-67	Coarse- to very coarse xtalline dolomite cement (planar-s)	24.33	10.59	235	194	25	322	0.43	0.56	2.1	-8.1
Bz-72	Fine-to medium xtalline dolomite (scattered dolomite rhombs, planar-e)	32.2	4.82	64	161	66	135	0.15	1.28	3.3	-6.2
Bz-74	Coarse- to very coarse xtalline dolomite cement (planar-e)	27.05	8.35	176	217	34	214	0.31	0	2.3	-7.9
Bz-75	Fine-to medium xtalline dolomite (scattered dolomite rhombs, planar-e)	32.05	5.5	106	113	60	142	0.17	3.92	2.7	-6.9
Bz-77	Medium xtalline dolomite (planar-s, bulk sample)	31.83	5.27	278	288	57	116	0.17	0.72		
Bz-79	Coarse- to very coarse xtalline dolomite cement (planar-s)	29.05	7.57	206	301	50	228	0.26	0.72	2.7	-7.9
Bz-80	Medium xtalline dolomite (planar-s, bulk sample)	31.91	7.69	255	623	39	211	0.24	3.2	1.1	-8.4
Bz-81	Coarse- to very coarse xtalline dolomite cement (planar-s)	26.56	9.03	257	454	60	214	0.34	0	2.2	-8.8
Bz-106	Fine-to medium xtalline dolomite (scattered dolomite rhombs, planar-e)	30.69	4.96	124	1769	143	170	0.16	1.76	3.1	-4.7
Bz-107	Very fine-to fine xtalline dolomite (unimodal, planar-s)	21.36	11.73	251	4435	66	183	0.57	7.6	2.8	-6.9
Bz-108	Very fine-to fine xtalline dolomite (sandy, unimodal, planar-s)	21.56	11.58	476	5378	74	203	0.54	4.08	2.2	-6.3
Bz-109	Very fine-to fine xtalline dolomite (sandy, unimodal, planar-s)	21.02	12.06	513	5292	72	207	0.57	7.28	2.2	-3.2

Table A5.10. XRD analyses of dolomite samples from the Mozduran Formation.

Sample No	aO (A°)	cO (A°)	d-spacing (104 peak)	2θ° (104)	Mol.% Mg
Sh 28	4.807	16.008	2.887	30.97	48.7
Sh 32	4.809	16.025	2.888	30.96	48.4
Sh 37	4.812	16.084	2.896	30.88	45.7
Sh 42	4.806	16.008	2.887	30.97	48.7
Mz 44	4.809	16.026	2.888	30.96	48.4
Go 29	4.805	16.008	2.886	30.99	49.1
Go 32	4.808	16.019	2.888	30.96	48.4
Bz 30	4.806	16.008	2.886	30.99	49.1
Error (+/-)	**0.005**	**0.008**	**0.001**	**0.01**	
Sh 29				30.97	50.5
Sh 34				30.96	50
Sh 36				30.89	47.5
Ba 10				30.97	50.5
Pa 8				30.98	51
Mz 10				30.98	51
Mz 15				30.97	50.5
Mz 34				30.92	48
Mz 48				30.97	50.5
Mz 53				30.96	50
Go 39			2.887	30.97	49
Go 41			2.886	30.99	49
Go 66			2.887	30.97	49
Bz 48			2.886	30.99	49
Bz 50			2.887	30.97	49

D-spacing, (104) reflection in dolomite is 2.888 A°.

Table A5.11. Weight percent inorganic and organic carbon in the Mozduran dolomites.

Sample No	Wt. of Crusible	Crusible+Sample	After 24 hrs @ 450 °C	% Losses	Correction factor	%C inorganic (ashed samples)	%C inorganic in carbonate	%C total (unashed samples)	%C organic (TOC)
Sh-28	8.58055	10.58063	10.53962	2.05	0.979495	12.26	12	12.57	0.57
Sh-32	7.74689	9.74693	9.71727	1.48	0.98517	12.43	12.24	12.61	0.36
Ba-8	5.73252	7.73261	7.72256	0.5	0.994975	11.11	11.05	11.2	0.15
Ba-10	5.71324	7.71333	7.70476	0.43					
Mz-39	6.7909	8.79096	8.75512	1.9	0.98208	11.25	11.04	11.39	0.35
Mz-49	7.41226	9.41235	9.39228	1	0.989965	12.61	12.48	12.69	0.2
Go-28	5.3435	7.3435	7.28634	2.86	0.9714	12.51	12.15	13	0.85
Go-32	8.39482	10.39501	10.32161	3.67	0.9633	12.37	11.9	12.9	1
Go-42	6.72092	8.72093	8.66955	2.57	0.97431	12.73	12.4	13	0.6
Go-102	7.71528	9.7154	9.69173	1.18	0.988165	12.6	12.45	12.74	0.29
Bz-29	6.12948	8.12948	8.0712	2.9	0.97086	12.68	12.3	13.31	1.01
Bz-48	7.60012	9.60038	9.48922	5.5	0.94442	12.17	11.49	13.09	1.6
Bz-49	6.733	8.73329	8.63784	4.77	0.952275	12.19	11.6	13.19	1.59
Bz-65	7.43743	9.43748	9.37127	3.3	0.966895	12.44	12.02	12.98	0.96
Bz-107	6.9766	8.9766	8.95718	0.97	0.99029	11.71	11.59	11.9	0.31
Bz-109	8.64755	10.64762	10.63484	0.64					

APPENDIX 6

ANALYTICAL RESULTS OF THE RENISON CARBONATES

Table A6.1 shows XRD results of representative dolomite and siderite samples in Renison mine area.

Table A6.2 shows organic and inorganic carbon results of representative dolomite samples in Renison mine area.

Table A6.3 shows dolomite type, insoluble residue, elemental and isotopic composition of Renison dolomites and oxygen and carbon isotope values of siderites away from the mine area.

Table A6.4 lists dolomite type, insoluble residue, elemental and isotopic composition of Renison dolomites and oxygen and carbon isotope values of siderites within the mine area and elemental composition of unaltered late Proterozoic sedimentary dolomites from the Weld River Group, southern Tasmania.

Table A6.5 lists oxygen and carbon isotope values of Renison dolomites and siderites (Jones and Evans, 1985) and sedimentary dolomites (Patterson et al., 1981).

Table A6.6 shows oxygen and carbon isotope values of Renison dolomites and siderites (Holyland, 1987).

Table A6.1. XRD analyses of dolomite and siderite in Renison mine.

Sample No	aO (A°)	cO (A°)	d-spacing (104 peak) A°	2θ ° (104)	Mol.% Mg
S594, 233.5 m	4.813	16.042	2.891	30.93	47.4
S594, 281.2 m	4.815	16.028	2.889	30.95	48
S705, 166 m	4.81	16.016	2.89	30.94	47.7
S705, 171.7 m	4.817	16.002	2.889	30.95	48
S705, 172 m	4.817	16.004	2.888	30.96	48.4
S705, 172.8 m	4.816	16.006	2.887	30.97	48.7
S705, 179.8 m	4.817	16.005	2.89	30.94	47.7
S705, 181.4 m	4.815	16.011	2.885	31	49.4
S705, 185.2 m	4.809	16.027	2.889	30.95	48
S705, 187.4 m	4.815	16.027	2.89	30.94	47.7
S705, 189.4 m	4.809	16.021	2.889	30.95	48
S705, 192.1 m	4.809	16.026	2.889	30.95	48
S705, 202.3 m	4.814	16.031	2.89	30.94	47.7
S705, 202.9 m	4.809	16.009	2.89	30.94	47.7
S705, 245.6 m	4.808	16.035	2.89	30.94	47.7
S705, 246.8 m	4.817	16.065	2.895	30.89	46
S835, 201.6 m	4.817	16.001	2.887	30.97	48.7
S835, 204.5 m	4.814	16.03	2.89	30.94	47.7
S835, 213.4 m	4.812	16.041	2.891	30.93	47.4
S835, 215.8 m	4.816	16.014	2.89	30.94	47.7
S835, 221.5 m	4.812	16.036	2.891	30.93	47.4
S835, 222.7 m	4.813	16.034	2.892	30.92	47
S835, 269.2 m	4.807	16.016	2.887	30.97	48.7
S835, 272.3 m	4.808	16.021	2.889	30.95	48
Error (+/-)	**0.005**	**0.01**	**0.001**	**0.01**	**0.01**
S562, 69 m			2.887	30.97	49
S562, 121.5 m			2.889	30.95	48
S562, 129 m			2.89	30.94	48
S562, 173 m			2.889	30.95	48
S574, 27 m			2.89	30.95	48
S574, 70 m			2.899	30.84	45
S574, 76.3 m			2.895	30.89	47
S574, 82.3 m			2.889	30.95	48
40053			2.89	30.94	48
40068			2.915	30.67	40
Siderite					
S594, 238 m			2.793		
S594, 242.2 m			2.79		
S835, 221.5 m			2.787		
S835, 259 m			2.783		
S835, 260 m			2.778		
40072			2.786		
40084			2.782		
40087			2.782		
40089			2.78		
40091			2.779		

D-spacing, (104) reflection in dolomite is 2.888 Å.

D-spacing for siderite is 2.79 Å.

Table A6.2. Weight percent inorganic and organic carbon in Renison dolomites.

Sample No	Wt. of Crusible	Crusible+Sample	After 24 hrs @ 450° C	% Losses	Correction factor	%C inorganic (ashed samples)	%C inorganic in carbonate	%C total (unashed samples)	%C organic (TOC)
S705-179.1m	7.60116	9.60116	9.59273	0.42	0.995785	11.21	11.16	12.22	1.06
S705-179.8m	6.73343	8.73343	8.72214	0.56					
S705-180.4m	7.4386	9.4386	9.42598	0.63	0.99369	12.69	12.6	12.43	?
S705-181.4m	6.97856	8.97856	8.96881	0.49					
S705-184m	8.65177	10.65177	10.63522	0.83	0.991725	11.85	11.75	12.47	0.72
S705-187.1m	6.28018	8.28018	8.27141	0.44					
S705-187.4m	6.04037	8.04037	8.02585	0.73	0.99274	12.01	11.92	12.02	0.1
S705-202.3m	6.99929	8.99929	8.98888	0.52					
S835-198.4m	5.38284	7.38284	7.36427	0.93	o.990715	12.64	12.5	12.9	0.4
S835-199m	7.05669	9.05669	9.04603	0.53					
S835-201.6m	5.34156	7.34156	7.32253	0.95	0.99048	12.5	12.38	12.93	0.55
S835-204.5m	5.917	7.917	7.90918	0.4					
S835-209.9m	7.18022	9.18022	9.16407	0.81	0.99192	12.27	12.17	12.41	0.25
S835-215.8m	7.20451	9.20451	9.19311	0.57					
S835-216.8m	6.59038	8.59038	8.57935	0.55					
S835-221.5m	6.1218	8.1218	8.10339	0.92	0.990795	12.68	12.56	12.97	0.41
S835-222.7m	6.21719	8.21719	8.20758	0.48					
S835-264.1m	8.0551	10.0551	10.04389	0.56	0.994395	12.28	12.21	12.48	0.27
S835-270m	6.13099	8.13099	8.12054	0.52	0.994775	11.61	11.54	11.76	0.22
S835-273.3m	5.71407	7.71407	7.7099	0.21					

Table A6.3. Dolomite type, major and minor elements, insoluble residue, $\delta^{18}O$ and $\delta^{13}C$ values of the least altered Renison dolomites, and $\delta^{18}O$ and $\delta^{13}C$ values of siderites, away from the mine area.

Core No and depth	Dolomite type	Dolomite No	Ca %	Mg %	Mn ppm	Fe ppm	Sr ppm	Na ppm	Mg/Ca ratio	I.R %	∂18O SMOW	∂18O PDB	∂13C PDB
S705-164.3 m	Very finely xtalline dolomite (dolomicrite)	DN1	21.54	13.2	615	3243	109	112	0.6	4.56	28.8	-1.9	3.9
S705-166 m	Very finely xtalline dolomite (dolomicrite)	DN1	22.13	12.78	385	2812	98	120	0.57	3.92	28.9	-1.8	3.6
S705-166.2 m	Very finely xtalline dolomite (dolomicrite)	DN1	21.37	12.88	234	2442	109	185	0.59	0	30.1	-0.7	4.1
S705-166.4 m	Very finely xtalline dolomite (dolomicrite)	DN1	21.6	13.06	180	1524	104	185	0.57	0	30.7	-0.1	4.1
S705-169.8 m	Very finely xtalline dolomite (dolomicrite)	DN1	21.78	12.4	209	1600	88	112	0.57	0	30.8	-1	4.2
S705-171.7 m	Finely xtalline dolomite (altered dolomicrosparite)	DN1									27.6	-3.2	3.9
S705-171.7 m	Very finely xtalline dolomite (altered dolomicrite B)	DN1	22.09	13.11	306	3430	117	166	0.58	2.8	29.3	-1.5	3.8
S705-171.7 m	Very finely xtalline dolomite (pure dolomicrite C)	DN1	21.86	13.1	183	2226	98	196	0.6	4.16	31	0.1	4.2
S705-172 m	Very finely xtalline dolomite (dolomicrite)	DN1	22	13.1	214	1548	92	107	0.6	4.8	29.4	-1.4	4.1
S705-172.8 m	Very finely xtalline dolomite (pure dolomicrite)	DN1	21.8	12.88	194	3757	90	146	0.59	2	31.1	0.3	4
S705-172.8 m	Very finely xtalline dolomite (white dolomicrospar B)	DN1	21.98	12.94	317	3016	88	98	0.59	0	29.3	-1.5	3.6
S705-172.8 m	Very finely xtalline dolomite (dark patchy dolomicrite C)	DN1	21.71	13	240	2825	75	115	0.6	2.4	30	-0.8	3.7
S705-179.1 m	Very finely xtalline dolomite (dolomicrite)	DN1	20.91	11.87	268	6673	105	117	0.6	9.76	29.5	-1.3	5.2
S705-179.8 m	Very finely xtalline dolomite (laminated white dolomicrite)	DN1	22.04	12.89	304	2204	98	115	0.58	2.96	29.2	-1.6	6.4
S705-180.4 m	Very finely xtalline dolomite (dolomicrite, dolobreccia)	DN1	21.14	12.41	205	4706	109	125	0.59	8.08	29.2	-1.6	5.4
S705-180.4 m	Very finely xtalline dolomite (dolomicrite)	DN1	21.23	12.28	120	2882	88	108	0.58	3.76	29.4	-1.4	5.5
S705-181.4 m	Very finely xtalline dolomite (dolomicrite)	DN1	21.99	12.2	238	5756	113	115	0.55	2.32	28.7	-2.1	5.2
S705-183 m	Finely xtalline dolomite (stromatolitic dolomicrosparite)	DN1	22	12.27	333	2980	105	97	0.56	4.32	27.9	-2.8	4.9
S705-184 m	Very finely xtalline dolomite (dolomicrite)	DN1	21.85	12.7	395	3180	90	311	0.58	5.52	28.2	-2.6	4.8
S705-184 m	Very finely xtalline dolomite (dolomicrite, dolobreccia)	DN1	21.95	12.41	252	4118	99	179	0.56	4.08	28.9	-1.9	5.2
S705-185 m	Finely xtalline dolomite (dolomicrosparite)	DN1									27.5	-3.2	3.7
S705-185 m	Finely xtalline dolomite (silty dark laminated dolomicrosparite)	DN1									23.7	-6.9	3.5
S705-185.2 m	Finely xtalline dolomite (dolomicrosparite, dolobreccia)	DN1								**15.52**	27.2	-3.5	3.6
S705-185.2 m	Finely xtalline dolomite (dolomicrosparite, algal lamination)	DN1	21.59	13.15	186	6134	123	76	0.59	6.48	26.5	-4.2	3.7
S705-186.5 m	Finely xtalline dolomite (dolomicrosparite,with algal lamination)	DN1									27.5	-3.3	3.7
S705-186.5 m	Medium xtalline dolomite (dolomicrosparite, with intraclast)	DN1									26.9	-3.9	3.7
S705-187 m	Very finely xtalline dolomite (dolomicrite)	DN1								**19.2**	27.9	-2.9	3.8
S705-187 m	Finely xtalline dolomite (dolomicrosparite, shaley lamination)	DN1	21.61	12.55	333	10015	104	96	0.57	8.56	26.6	-4.2	3.4
S705-187.1 m	Finely xtalline dolomite (dolomicrosparite, with intraclast)	DN1									26.2	-4.5	3.9
S705-187.4 m	Very finely xtalline dolomite (dolomicrite, dolobreccia)	DN1	21.72	12.75	157	4782	83	169	0.58	6.24	29.9	-0.8	4.9
S705-187.4 m	Medium xtalline dolomite (dolomicrosparite, rounded clasts)	DN1	21.88	12.3	228	7881	103	116	0.55	8.32	26.6	-4.1	3.4
S705-187.5 m	Very finely xtalline dolomite (dolomicrite, large intraclast)	DN1								**16.08**	29	-1.8	5
S705-187.5 m	Finely xtalline dolomite (white dolomicrosparite)	DN1									26.2	-4.5	3.2
S705-187.5 m	Finely xtalline dolomite (dark dolomicrosparite)	DN1								**20.48**	26.4	-4.3	3.3
S705-189.4 m	Very finely xtalline dolomite (dolomicrite, rounded intraclast)	DN1									25.5	-5.2	3.5
S705-189.8 m	Finely xtalline dolomite (white dolomicrosparite)	DN1	22.04	12.69	329	4685	155	128	0.54	8.9	26.4	-4.3	4.2
S705-192.1 m	Finely xtalline dolomite (dolomicrosparite, intraclast,ghost ooids)	DN1	21.4	12.11	276	5444	99	131	0.56	0	26	-4.7	3.2
S705-194 m	Finely xtalline dolomite(dolomicrosparite, few intraclast)	DN1									24.9	-5.8	2.5
S705-201.8 m	Finely xtalline dolomite (dolomicrosparite)	DN2								**19.84**	24.1	-6.5	2.9
S705-202.3 m	Medium xtalline dolomite (dark dolosparite)	DN2	21.58	11.44	751	20233	196	307	0.51	7.04	22.8	-7.8	2.6
S705-202.9 m	Medium xtalline dolomite (dolosparite)	DN2									22.2	-8.4	2.2
S705-203.8 m	Medium xtalline dolomite (dolosparite)	DN2								15.44	23	-7.6	1.4

S705-245.6 m	Very finely xtalline dolomite (dolomicrite, with intraclast)	DN3	21.42	11.22	343	23473	135	105	0.52	0	27.6	-3.1	3.4
S705-246.4 m	Finely xtalline dolomite (finely laminated dolomicrosparite)	DN3	22.01	10.7	433	25426	172	120	0.47	9.44	27.3	-3.5	2.3
S705-246.8 m	Finely xtalline dolomite (white laminated dolomicrosparite)	DN3								40.8	26.6	-4.1	3
S705-246.8 m	Finely xtalline dolomite (dark laminated dolomicrosparite)	DN3									26.6	-4.1	3.1
S835-198.1 m	Very finely xtalline dolomite (dolomicrite)	DN3	22.14	12.33	699	6268	136	358	0.52	9.6	27.7	-3	6.4
S835-198.4 m	Very finely xtalline dolomite (dolomicrite, with intraclast)	DN3									27.4	-3.3	6
S835-199 m	Very finely xtalline dolomite (finely laminated dolomicrite A)	DN3	21.93	11.9	1158	7217	94	193	0.54	1.52	26.2	-4.5	5.7
S835-199 m	Finely xtalline dolomite (laminated dolomicrosparite B)	DN3	21.29	12.03	1571	9918	125	199	0.57	9.92	25.2	-5.4	5.4
S835-200.8 m	Finely xtalline dolomite (white dolomicrosparite A)	DN3									22.4	-8.2	4.9
S835-200.8 m	Very finely xtalline dolomite (dark dolomicrite B)	DN3									27.4	-3.3	5.2
S835-201.6 m	Very finely xtalline dolomite (pure dolomicrite)	DN3	21.07	12.72	282	2471	59	240	0.6	2.88	30	-0.7	6.6
S835-203.4 m	Very finely xtalline dolomite (dolomicrite, many veins)	DN3									27.5	-3.2	4.8
S835-204.5 m	Very finely xtalline dolomite (pure dolomicrite)	DN3	21.99	12.2	332	4008	73	102	0.55	8.72	30.9	0.1	7
S835-205.2 m	Very finely xtalline dolomite (dolomicrite)	DN3									26.7	-4	5.7
S835-205.2 m	Vein dolomite	DN3									19.6	-10.9	4
S835-206.9 m	Finely xtalline dolomite (white dolomicrosparite A)	DN3									25.2	-5.5	5.9
S835-206.9 m	Very finely xtalline dolomite (dark dolomicrite B)	DN3									27.4	-3.4	5.6
S835-209.9 m	Very finely xtalline dolomite (dolomicrite, with intraclast)	DN3	21.6	12.14	529	5424	57	226	0.56	0	29.1	-1.7	6.2
S835-211.4 m	Finely xtalline dolomite (white dolomicrosparite)	DN3									23.9	-6.7	6.4
S835-213.4 m	Very finely xtalline dolomite (dark dolomicrite)	DN3	21.86	11.75	906	7688	88	164	0.54	1.2	27.4	-3.3	6.4
S835-213.4 m	Finely xtalline dolomite (white highly altered dolomicrosparite)	DN3	21.72	11.6	3235	18940	109	156	0.53	10	21.6	-8.9	4
S835-214.7 m	Finely xtalline dolomite (dolomicrosparite)	DN3									26.2	-4.5	3.5
S835-215.8 m	Very finely xtalline dolomite (pure dolomicrite, with intraclast)	DN3	21.72	12.17	873	11122	73	244	0.56	8.4	28.8	-2	6.6
S835-216.8 m	Very finely xtalline dolomite (pure dolomicrite)	DN3	21.84	12.27	628	6638	101	147	0.56	8.08	28.7	-2.1	7.5
S835-218.4 m	Finely xtalline dolomite (dolomicrosparite, disseminated sulfide)	DN3									24.9	-5.8	4.4
S835-218.4 m	Dolomitic clast	DN3									25.3	-5.4	4.7
S835-219.4 m	Finely xtalline dolomite (finely laminated dolomicrosparite)	DN3	21.4	11.78	675	9605	93	139	0.55	9.76	26.5	-4.2	4.3
S835-221.1 m	Coarse to very coarse grain siderite	DN3									18.1	-12.3	-5.8
S835-221.5 m	Coarse to very coarse grain siderite	DN3									18.2	-12.3	-6.3
S835-221.5 m	Medium xtalline dolomite (dolosparite)	DN3	21.32	10.41	4655	33195	120	189	0.49	0	23.7	-6.9	3.5
S835-222.7 m	Finely xtalline dolomite (dolomicrosparite, with intraclast A)	DN3									24.7	-6	4.9
S835-222.7 m	Finely xtalline dolomite (dolomicrosparite B)	DN3									25	-5.6	4.3
S835-258.4 m	Medium grain siderite	DN3									19.7	-10.8	-4.3
S835-259 m	Medium grain siderite	DN3									17.8	-12.7	-4.2
S835-259 m	Vein siderite	DN3									17.5	-12.9	-4.1
S835-260 m	Coarse grain siderite	DN3									17.7	-12.8	-5.1
S835-260.5 m	Coarse grain siderite	DN3									16.8	-13.6	-3.9
S835-263 m	Finely xtalline dolomite (dolomicrosparite)	DN3	22.04	11.22	1748	11435	86	190	0.51	2.32	25.9	-4.8	2.6
S835-264.1 m	Finely xtalline dolomite (dolomicrosparite, with few intraclast)	DN3	21.98	12.19	1034	7789	69	158	0.55	8.08	26.3	-4.4	1.6
S835-265.3 m	Finely xtalline dolomite (dolomicrosparite)	DN3									23.1	-5.5	2.5
S835-267.5 m	Finely xtalline dolomite (dolomicrosparite)	DN3									22.4	-6.2	2.8
S835-269.2 m	Finely xtalline dolomite (dolomicrosparite, disseminated sulfide)	DN3	21.6	11.94	861	7709	96	169	0.55	2.24	23.1	-5.6	2.6
S835-270 m	Finely xtalline dolomite (dolomicrosparite)	DN3									22.1	-6.5	2.4
S835-272.3 m	Dolomite clast	DN3	21.8	11.94	1378	14620	113	172	0.53	8.24	23.4	-5.2	2.9
S835-273.3 m	Finely xtalline dolomite (dolomicrosparite, cross cutting veins)	DN3	21.26	10.32	2070	19700	75	153	0.51	9.84	24.2	-4.5	1.6
S594-231.1 m	Finely xtalline dolomite (finely laminated dolomicrosparite)	DN3								24.88	24.8	-5.9	0.6
S594-232.3 m	Finely xtalline dolomite (finely laminated dolomicrosparite)	DN3									24.1	-6.5	-0.4

S594-233.5 m	Very finely xtalline dolomite (dark dolomicrite A)	DN3	22.11	11.95	2122	14832	83	221	0.54	9.12	26.1	-4.6	1.8
S594-233.5 m	Finely xtalline dolomite (white dolomicrosparite B,birds eye text)	DN3	21.92	11.65	1690	13082	119	213	0.52	3.68	23.4	-7.2	2.3
S594-234.7 m	Coarse grain siderite, A	DN3									17.4	-13	-4.2
S594-234.7 m	Very coarse grain siderite, B	DN3									16.5	-13.9	-2.5
S594-236.8 m	Finely xtalline dolomite (dolomicrosparite)	DN3	21.31	11.98	3836	19421	127	226	0.54	5.92	22.3	-8.2	3.1
S594-238 m	Coarse grain siderite	DN3									16.4	-14	-5.1
S594-239.8 m	Coarse grain siderite	DN3									14.9	-15.4	-3.5
S594-242.2 m	Very coarse grain siderite	DN3									15.3	-15	-3.4
S594-275 m	Medium xtalline dolomite (dolosparite)	DN3									23.6	-7	-1.6
S594-279 m	Finely xtalline dolomite (dolomicrosparite, with oolite ghosts)	DN3	20.73	11.34	1765	17178	105	169	0.54	9.36	23.7	-6.9	1.2
S594-279.9 m	Finely xtalline dolomite (dolomicrosparite, with many veins)	DN3									22.3	-8.3	1
S594-281.2 m	Finely xtalline dolomite (dolomicrosparite, with many veins)	DN3	21.6	12.15	867	9308	70	107	0.56	0.5	24	-6.6	2.2
S594-282 m	Finely xtalline dolomite (dolomicrosparite)	DN3									24.7	-5.9	1.5

Table A6.4. Dolomite type, major and minor elements, $\delta^{18}O$ and $\delta^{13}C$ values of Renison dolomites, $\delta^{18}O$ and $\delta^{13}C$ values of siderites, within the mine area and major and minor elements of unmineralized and unaltered late Proterozoic sedimentary dolomites from Weld River Group, southern Tasmania.

Sample No	Dolomite type	Dolomite No	Ca %	Mg %	Mn ppm	Fe ppm	Sr ppm	Na ppm	Mg/Ca ratio	I.R %	δ18O SMOW	δ18O PDB	δ13C PDB
S300-21m	Medium xtalline dolomite (dolosparite)	DN1	22	10.3	3141	17488	110	175	0.47	7.04	21.1	-9.4	-0.1
S300-24m	Finely xtalline dolomite (dolomicrosparite)	DN1	20.8	11.1	3902	18302	92	157	0.53	5.6	23	-7.6	-2.8
S300-36m	Vein dolomite	DN2									9.7	-20.5	-4.7
S301-2m	Finely xtalline dolomite (dolomicrosparite)	DN2	21.1	11.7	2395	12762	74	164	0.55	4.56	27.5	-3.2	2.1
S301-4m	Finely xtalline dolomite (dolomicrosparite)	DN2	20	10.9	2244	19122	109	128	0.54	20.32	25.9	-4.8	0.9
S301-4m	Finely xtalline dolomite (dolomicrosparite)	DN2	19.8	10.8	2285	20967	101	137	0.55	17.6	26.1	-4.6	1
S302-56m	Coarsely xtalline dolomite	DN3									15.1	-15.3	-5.1
S300-111.5m	Finely xtalline dolomite (dolomicrosparite)	DN3	20	10.5	4256	23425	117	163	0.52	8.8	19.1	-11.4	0.7
S300-111.5m	Vein dolomite	DN3									21.3	-9.3	2.5
S300-117.5m	Finely xtalline dolomite (dolomicrosparite)	DN3									25.6	-5.2	1.2
S300-123.5m	Vein dolomite	DN3									21.5	-9.1	3.7
S300-123.5m	Finely xtalline dolomite (dolomicrosparite)	DN3									21.8	-8.8	3.4
S301-107m	Finely xtalline dolomite (dolomicrosparite)	DN3	21.7	11.2	2703	17548	92	135	0.52	7.36	22.5	-8.1	1.3
S301-107m	Vein dolomite	DN3	20.9	10.1	5955	39858	159	322	0.48	0	20.8	-9.7	0.7
USS 65300N-44100E	Finely xtalline dolomite (dolomicrosparite, with talc)	DN2	16.9	6.5	18270	51604	152	112	0.38	44.08	11.7	-18.5	-2.3
USS 65410N-44120E	Finely xtalline dolomite (dolomicrosparite)	DN2	18.6	7.6	19665	45950	204	138	0.41	37.2	10.8	-19.4	-2.6
USS 65400N-44150E	Medium xtalline dolomite (dolosparite)	DN2									9.2	-21	-1.6
USS 65450N-44155E	Finely xtalline dolomite (dolomicrosparite)	DN2	20.2	11.2	2909	19129	75	86	0.55	3.2	24.8	-5.9	2.1
USS 65455N-44160E	Coarsely xtalline dolomite	DN2									13.2	-17.1	-4.7
USS 65455N-44160E	Coarsely xtalline dolomite	DN2									14.7	-15.6	-5.1
USS 65470N-44170E	Very finely xtalline dolomite (dolomicrite)	DN2	21.6	11.7	964	6259	67	170	0.54	1.6	28.3	-2.5	3
USS 65500N-44200E	Finely xtalline dolomite (dolomicrosparite)	DN2	21	10.4	2956	23300	98	138	0.5	2.8	24.1	-6.6	2
USS 65520N-44220E	Finely xtalline dolomite (dolomicrosparite)	DN2	20.8	11.2	2811	20112	102	91	0.53	2.8	25.3	-5.4	2.4
S574 -27m	Vein dolomite	DN2	21.6	12.7	1322	11090	90	373	0.58	8.64			
S574-27m	Very finely xtalline dolomite (dolomicrite, with talc)	DN2	21.8	12.3	726	12066	110	214	0.57	6.72	25.7	-5	3.5
S574-27m	Very finely xtalline dolomite (dolomicrite)	DN2	21.4	12.4	817	8418	141	204	0.58	9.84	28.1	-2.7	4.1
S574-27.80	Vein dolomite	DN2	21.1	11.6	1023	11999	250	166	0.55	18.08			
S574-30m	Vein dolomite(coarse)	DN2	20	11.6	1379	11282	106	326	0.58	9.6	20.6	-10	1.9
S574-30m	Very finely xtalline dolomite (dolomicrite)	DN2	21.6	12.4	785	9288	121	153	0.57	6.56	25.5	-5.2	2.9
S574-30m	Vein dolomite	DN2	21.1	12.3	1012	13652	222	180	0.58	18.56			
S574-70m	Vein dolomite	DN3	20.1	7	22931	77971	94.5	317	0.34	0	15	-15.4	-2.7
S574-71.5m	Very finely xtalline dolomite (dolomicrite)	DN3	20.7	8.6	19410	52047	125	102	0.42	8.24			
S574-75.5m	Vein dolomite	DN3	19.2	8.8	6242	45967	117	348	0.46	5.2	19.2	-11.3	0.8
S574-75.5m	Very finely xtalline dolomite (dolomicrite)	DN3	21.4	9.3	7421	64480	131	474	0.43	14.56			
S574-76.30m	Vein dolomite	DN3	20.3	7.7	6765	80368	180	194	0.38	0	19.6	-10.9	0.9
S574-82.20m	Vein dolomite(coarse)	DN3	20.6	10	16439	29193	148	149	0.49	14.96	17.4	-13	-0.7
S574-82.20m	Vein dolomite	DN3	20.9	10.7	4632	25647	233	428	0.51	3.2	20.1	-10.5	2
S574-82.30	Vein dolomite	DN3	20.8	10.7	3856	40499	117	187	0.51	18.16	19.6	-10.9	0.5

S574-82.30m	Finely xtalline dolomite (dolomicrosparite)	DN3	19.9	10	5326	34816	114	160	0.5	4.8	21.7	-8.9	2.5
S574-82.30m	Very finely xtalline dolomite (dolomicrite)	DN3	20.3	10.1	6190	39031	123	156	0.5	4.4	21.7	-8.8	2.4
S562-69m	Vein dolomite	DN1	25.9	9.2	2427	8339	299	450	0.36	14.8	19.7	-10.8	1
S562-69m	Finely xtalline dolomite (dolomicrosparite)	DN1	23.6	11.6	1773	5246	168	121	0.49	8.24	22	-8.6	1.6
S562-78.5m	Vein dolomite	DN1	23.7	10.2	3822	18842	79	360	0.43	8.8	16.4	-14	-3.6
S562-78.5m	Finely xtalline dolomite (dolomicrosparite)	DN1	21.4	10.1	1108	7975	74	51	0.47	8.4	21.2	-9.4	-2.1
S562-113m	Very finely xtalline dolomite (dolomicrite)	DN2	22.6	11.7	3843	14566	100	90	0.52	8.24	24.7	-5.9	0.1
S562-113.6m	Vein dolomite	DN2									19.4	-11.1	-1.2
S562-116m	Vein dolomite	DN2	22	9.8	3792	13536	109	199	0.44	11.68			
S562-121.5m	Very finely xtalline dolomite (dolomicrite)	DN2	22.2	13	1410	13103	106	60	0.58	6.48	24.8	-5.9	2.3
S562-121.6m	Very finely xtalline dolomite (dolomicrite)	DN2									26.7	-4	2
S562-122m	Very finely xtalline dolomite (dolomicrite)	DN2	23.8	12.7	1766	15924	119	99	0.53	10.88	25.7	-5	2.2
S562-122m	Very finely xtalline dolomite (dolomicrite, dark)	DN2									27.5	-3.2	2.7
S562-122m	Vein dolomite	DN2	20.5	11.7	1286	14660	97	22	0.57	7.6			
S562-129m	Very finely xtalline dolomite (dolomicrite, with clast)	DN2	22.8	11.5	1910	13169	100	92	0.5	5.84	26	-4.7	3.1
S562-129m	Very finely xtalline dolomite (dolomicrite)	DN2	22.5	11.4	2170	15920	105	58	0.5	8	23.7	-6.9	2.2
S562-173m	Finely xtalline dolomite (dolomicrosparite)	DN3	22.1	11.7	1307	12560	89	63	0.53	3.36	22.1	-8.5	2.1
S562-175m	Finely xtalline dolomite (dolomicrosparite)	DN3	22.5	11.5	1278	13012	121	53	0.51	5.28	21.2	-9.4	2.1
S562-175.3m	Finely xtalline dolomite (dolomicrosparite)	DN3	22.3	11	1586	15799	113	48	0.49	4.24	20.7	-9.8	1.9
Proterozoic Sedimentary dolomite(PSD)													
K23	Micrite		20.83	10.2	919	5124	26	154	0.49	9.2			
K23	Intraclast		22.65	11.21	980	6284	36	148	0.5	15.04			
W60	Oolite		21.93	12.4	275	923	66	249	0.57	0.96			
W60	Micrite		21.91	12.25	287	895	63	325	0.56	0.88			
W104	Intraclast		22.18	12.63	667	3020	45	141	0.57	0			
W104	Micrite		22.61	11.89	733	3076	55	194	0.55	0			
68205	Dark micrite		22.5	12.5	25	160	42	171	0.58	0			
68205	Intraclast		22.38	12.23	32	240	38	215	0.57	0			
68205	White micrite		22.27	12.53	69	698	48	175	0.59	0			
	Siderite												
USS-40072	Very coarse grain siderite (sidero-rudite)	DN2									14.5	-15.9	-4
USS-40076	Very coarse grain siderite (sidero-rudite)	DN2									16	-14.4	-4.2
USS-40076	Medium to coarse grain siderite (sidero-arenite)	DN2									17	-13.5	-3
UM-40083	Very coarse grain siderite (sidero-rudite)	DN2									15.7	-14.7	-5.3
UM-40083	Very coarse grain vein siderite (vein sidero-rudite)	DN2									16.4	-14	-5.6
UM-40084	Medium to coarse grain siderite (sidero-arenite)	DN2									14.1	-16.2	-6.4
UM-40085	Very coarse grain siderite (sidero-rudite)	DN2									15.7	-14.7	-5.3
UM-40087	Medium to coarse grain siderite (sidero-arenite)	DN2									16.3	-14.1	-6.2
UM-40089	Very coarse grain siderite (sidero-rudite)	DN2									16	-14.4	-5.7
UM-40091	Medium to coarse grain siderite (sidero-arenite)	DN2									15.5	-14.9	-3.2

(eg S300-21m=Surface diamond drillhole 300 at 21m)
(USS=South Stebbins Orebody, underground sample, 65300N-44100E)
(UM=Underground,Murchison Ore Zone)

Table A6.5. Oxygen and carbon isotope values of dolomites and siderites (Jones and Evans, 1985) and sedimentary dolomites (Patterson et al., 1981), Renison mine area.

Sample No	Drill hole No	δ18O SMOW	δ18O PDB	δ13C PDB
52118	255	23.1	-7.5	1.2
52119	256	21.2	-9.4	-0.8
28558/2	262	22.8	-7.8	1.9
28570	329	21.2	-9.4	1.4
28585/3	344	12.0	-18.3	-0.6
52120	371	21.9	-8.7	2.8
28551	376	23.9	-6.7	5.0
52121	429	21.7	-8.9	1.7
28596	459	21.3	-9.3	1.7
28619	461	20.4	-10.1	1.1
52122	470	26.8	-3.9	-0.6
52123	471	24.4	-6.3	2.9
52124	499	22.6	-8.0	1.8
28624	504	20.5	-10.0	1.7
28600	507	22.3	-8.3	2.6
52125	512	11.4	-18.9	-3.8
28591	519	22.3	-8.3	1.5
28594	521	21.2	-9.4	0.5
52126	574	22.6	-8.0	4.3
52127	574	21.2	-9.4	2.8
52128	594	23.5	-7.1	2.4
52129	594	22.2	-8.4	1.2
28532	623	20.6	-9.9	2.8
52130	628	23.4	-7.2	3.5
52131	632	19.1	-11.4	-3.0
28540/2	664	18.8	-11.7	2.3
28544	674	21.2	-9.4	1.1
28616	681	15.0	-15.4	0.7
52132	686	18.4	-12.1	0.9
52133	693	22.5	-8.1	2.1
52134	695	13.0	-17.3	-1.0
52135	705	25.0	-5.7	3.1
52136	824	19.8	-10.7	1.0
28523	835	25.9	-4.8	5.6
28529	835	23.6	-7.0	2.8
52137	839	17.7	-12.8	-1.3
52138	935	21.3	-9.3	3.2
52139	1015	25.0	-5.7	4.7
28607	1060	20.4	-10.1	0.5
52140	1064	23.9	-6.8	1.9
52141	1109	16.0	-14.4	-0.5
52142	1143	17.3	-13.2	1.8

Siderite

Sample No	Drill hole No	∂18O SMOW	∂18O PDB	∂13C PDB
28567	255	16	-14.4	-5.9
28566	259	16.4	-14.0	-5.4
28558/1	262	15.6	-14.8	-4.1
28585/2	344	15.3	-15.1	-5.0
28597	459	15.6	-14.8	-3.2
28625	504	16.4	-14.0	-5.5
28590	519	15.4	-15.0	-4.3
28595	521	16.8	-13.6	-7.9
28537	664	14.6	-15.8	-4.3
28542	674	13.7	-16.6	-3.4
28615	681	11.4	-18.9	-5.0
28525	835	15.3	-15.1	-4.2
28527	835	18.0	-12.5	-4.2
28609	1060	17.3	-13.1	-6.9
Patterson et al., 1981 Sedimentary dolomite				
103735		20.9	-9.7	-2.8
103768		19.8	-10.7	-1.9
103772		11.4	-18.9	-1.1
104129		21.3	-9.3	1.3

Table A6.6. Oxygen and carbon isotope values of dolomites and siderites (Holyland, 1987), Renison mine area.

Sample No	Dolomite No	∂18O SMOW	∂18O PDB	∂13C PDB
45630	DN3	14.3	-16.1	-2.6
45633	DN3	12.8	-17.5	-6.3
45633	DN3	13.3	-17.0	-6.4
45643	DN3	16.2	-14.2	-1.3
45604	DN3	20.0	-10.5	-0.3
45615	DN3	24.1	-6.6	3.2
45616	DN3	20.7	-9.8	-2.2
45616	DN3	20.9	-9.7	-1.0
45601	DN3	22.2	-8.4	1.5
45600	DN3	22.3	-8.3	1.8
45644	DN3	17.0	-13.4	-6.0
45614	DN3	23.6	-7.0	2.1
45617	DN3	23.3	-7.3	2.5
45613	DN3	20.9	-9.7	0.7
45631	DN2	23.3	-7.3	-1.1
45607	DN1	17.8	-12.7	-3.0
45606	DN2	24.0	-6.6	1.0
45618	DN2	13.6	-16.7	-3.4
45627	DN2	24.8	-5.9	1.1
45626	DN2	27.5	-3.3	1.3
45625	DN2	26.5	-4.2	2.9
45623	DN2	13.7	-16.6	-5.2
45622	DN2	23.1	-7.5	-1.6
45624	DN2	24.2	-6.5	0.3
45621	DN2	25.0	-5.7	0.1
45620	DN2	22.2	-8.4	1.3
45619	DN2	25.4	-5.3	1
45660	DN3	20.8	-9.8	0.5
45660a	DN3	18.8	-11.7	-0.1
45660b	DN3	13.9	-16.4	-4.7
45660c	DN3	12.2	-18.1	-2.7
45475	RBM	15.8	-14.61	-8.5
45609	DN2	20.6	-9.9	-1.1
45609a	DN2	21.8	-8.8	-0.6
45609b	DN2	24.8	-5.9	0.3
45602	DN2	25.6	-5.1	2.3
45602	DN2	25.6	-5.1	2.5
45602	DN2	25.6	-5.1	2.2
45602	DN2	27.1	-3.6	2.8
45602	DN2	28.1	-2.7	2.7
Siderite				
45643	DN3	16.2	-14.2	-1.3
45646	DN3	14.6	-15.8	-4.1
45635	DN3	14.2	-16.2	-4.1
45644	DN3	17.0	-13.4	-6.0

45638	DN3	12.7	-17.6	-5.2
45636	DN3	13.8	-16.5	-5.5
45640	DN2	13.8	-16.5	-5.6
45647	DN2	13.9	-16.4	-5.3
45634	DN3	14.1	-16.3	-5.5
45639	DN3	13.1	-17.2	-4.2
45602	DN3	15.5	-14.9	-6.6
45637	DN3	14.6	-15.8	0.6
45645	DN1	13.9	-16.4	-3.2
45641	DN2	15.4	-15.0	-2.4
45661	DN2	14.7	-15.7	-5.5
U786 75	DN2	12.7	-17.6	-0.3
45607	DN2	11.2	-19.1	-4.2
S 436 5	DN2	13.3	-17.0	-3.7
Dr 2015		10.1	-20.1	-5.2
45624	DN3	12.1	-18.2	-6.3
45664	DN2	12.5	-17.8	-6.3
45648	DN3	25.0	-5.7	-5.1
45602	DN2	13.7	-16.7	-5.1
45606	DN2	20.8	-9.8	-2.5
45651	DN2	14.6	-15.8	-7.6
45649	DN2	16.2	-14.2	-2.6
45664	DN2	13.7	-16.7	-5.7
45661a	DN2	15.7	-14.7	-0.9
45661b	DN2	18.8	-11.7	6.1
U786 43		18.8	-11.7	7.6
45653	DN2	14.3	-16.1	-4.2
Dr 2125	DN2	14.8	-15.6	-5.5
45486	DN2	14.5	-15.9	-6.3
51264	DN2	9.4	-20.8	-4.5
U1189	DN2	10.4	-19.8	-2.6
S385 813	DN2	16.5	-13.9	1.6
45714	DN2	23.1	-7.5	-2.2
U716 107	DN2	23.5	-7.1	1.4
45662	DN3	10.0	-20.2	-6.2
45607	DN3	19.2	-11.3	-1.8
45862	DN3	13.5	-16.8	-4.3
45654	DN2	13.7	-16.6	-5.6
45650	DN2	13.2	-17.1	-6.3
45648	DN3	12.4	-17.9	-4.4
45657	DN3	15.5	-14.9	-4.7

APPENDIX 7

PUBLICATIONS

1- ADABI, M.H. and RAO, C.P., 1991. Petrographic and geochemical evidence for original aragonitic mineralogy of Upper Jurassic carbonates (Mozduran Formation), Sarakhs area, Iran: Sed. Geology, v.72, p. 253-267.

2- RAO, C.P., and ADABI, M.H., 1992. Carbonate minerals, major and minor elements and oxygen and carbon isotopes and their variation with water depth in cool, temperate carbonates, western Tasmania, Australia: Mar. Geology, v. 103, p. 249-272.

Sedimentary Geology, 72 (1991) 253–267
Elsevier Science Publishers B.V., Amsterdam

Petrographic and geochemical evidence for original aragonite mineralogy of Upper Jurassic carbonates (Mozduran Formation), Sarakhs area, Iran

Mohammad H. Adabi * and C. Prasada Rao

Department of Geology, University of Tasmania, G.P.O. Box 252C, Hobart, Tasmania 7001, Australia

Received September 12, 1990; revised version accepted June 4, 1991

ABSTRACT

Adabi, M.H. and Rao, C.P., 1991. Petrographic and geochemical evidence for original aragonite mineralogy of Upper Jurassic carbonates (Mozduran Formation), Sarakhs area, Iran. Sediment. Geol., 72: 253–267.

Diverse skeletal and non-skeletal grains with abundant red and blue-green calcareous algae, evaporites and early diagenetic dolomites in the Mozduran carbonates are similar to those of modern warm-water shallow-marine carbonates. Isopachous and fibrous intragranular sparry calcite cements resemble modern aragonite morphologies. Concentric and radial ooids are like modern aragonitic forms which are formed in turbulent and in low-energy environments, respectively. Deformed ooids, shattered micritic envelopes and spalled ooids indicate aragonite dissolution during meteoric diagenesis. Meteoric cements are equant, mosaic to drusy calcites. Burial cements only occur as vein fillings.

Sr and Na covariance with Mn supports evidence of inversion of aragonite to calcite, with subsequent open phreatic diagenesis. Fe concentrations are a magnitude higher than Mn due to a reducing phreatic environment. High Sr/Na ratios suggest original aragonite mineralogy.

The $\delta^{18}O$ and $\delta^{13}C$ field of Mozduran limestone lies at the edge of the modern shallow-marine field indicating a range from marine to meteoric cements. Differences in $\delta^{18}O$ values between marine calcites and meteoric-derived calcites is similar to that in the modern tropics. The surface marine diagenetic trend line that passes through shallow-marine modern whole carbonates cuts the Mozduran limestone isotope field due to their formation in warm, shallow-marine waters, given that atmospheric CO_2 levels were similar to those at present.

Increasing Mn and Fe values, decreasing Na and uniform Sr values with increasingly lighter values of both $\delta^{18}O$ and $\delta^{13}C$ are explained by extensive meteoric diagenesis. The least altered marine calcite $\delta^{18}O$ value of $-2.6‰$ PDB corresponds to 29 or 24°C, depending on whether $\delta w = 0‰$ (of present seawater) and $\delta w = -1.2‰$ (of ancient seawater with no ice caps) are taken as a base. An original calcite mineralogy postulated for some Jurassic limestones is related to a non-tropical origin.

Introduction

Aragonite is the predominant mineral, along with some high-Mg calcite forming in modern tropical warm waters (Milliman, 1974). In modern temperate carbonates, high-Mg calcite predominates over low-Mg calcite and minor amounts of aragonite (Rao, 1981a; Nelson, 1988 and references therein). In subpolar cold-water carbonates, the low-Mg calcite is the dominant carbonate mineral (Rao, 1981b). The amount of Mg in calcite decreases with decreasing water temperature (Fuchtbauer and Hardie, 1976), with low-Mg calcite alone precipitating from seawater in water with temperatures $< 5°C$ (Schlager and James, 1978). Experimental studies (Kinsman and Holland, 1969; Burton and Walter, 1987) also confirm that carbonate mineralogy varies with water temperature, similar to that observed in natural carbonate sediments. Therefore, in the ancient carbonates, recognition of original carbonate mineralogy along with geochemical characteristics

* Present address: Faculty of Sciences, Geology Department, University of Ferdowsi (Mashhad), Mashhad, Iran.

0037-0738/91/$03.50

can be used to differentiate tropical, temperate and subpolar carbonates (Rao, 1988, 1991).

Some workers have suggested that the ancient carbonate mineralogy may have been different from that of modern sediments (Sandberg, 1975; MacKenzie and Pigott, 1981; Wilkinson, 1982; Tucker, 1984) and calcite was considered to have been dominant during early and middle Palaeozoic and Jurassic. This assumption of change of original mineralogy needs to be re-evaluated with the concept of mineralogical change with water temperature (Nelson, 1988). Evaluation of Ordovician carbonates of Tasmania based on petrographic and geochemical criteria (Rao, 1990a) indicated that aragonite was the predominant mineral in warm tropical Ordovician carbonates.

The present study uses petrographic evidence, major (Ca, Mg) and minor (Sr, Mn, Na, Fe) elements, $\delta^{18}O$ and $\delta^{13}C$ isotopes and their variation with minor elements and compares these with modern tropical and temperate carbonates and originally aragonitic Ordovician tropical carbonates and originally calcitic Permian subpolar cold water carbonates of Tasmania to understand the original mineralogy of the Upper Jurassic Mozduran limestones of Iran.

Stratigraphy and geologic setting

The study area is a part of the Kopet-Dagh, Hezar Massjed basin, which contains a sequence (about 5000 m thick) of almost continuous shallow-marine sediments which range from Mesozoic to Tertiary in age and which exhibit no major sedimentary breaks or volcanic activity. Mozduran carbonates from the Sarakhs area provide favourable reservoirs for the accumulation of gas. The general stratigraphy of the Kopet-Dagh basin in the Sarakhs area includes 15 different formations from Dogger to Lower Oligocene (Afshar, 1970, 1982). This study deals with the Upper Jurassic Mozduran Formation that is exposed in northeast Iran (Fig. 1). A sedimentary gap occurs between the Kashafrud and Mozduran formations of the Bathonian and part of the Callovian stages. Callovian Mozduran dolomites overlie the Bajocian Kashfrud Formation (Afshar, 1982). The Mozduran Formation comprises alternating sequences of thick limestones and thin dolomites which locally contain about 40 m of gypsum. The thickness of carbonates in the Mozduran, Padeha, Bagak and Shurijeh sections (Fig. 1) varies from 500 to 181, 180 and 125 m, respectively. From Mozduran eastwards, the formation thickness decreases and grades into near-shore, relatively shallow-water, mostly terrigenous facies. To the west, the Mozduran carbonates interfinger laterally into offshore and deeper, shallow-marine facies (Chaman Bid Formation; Afshar, 1970). The Mozduran Formation conformably overlies mainly fluvial sandstones and siltstones of the Kashafrud Formation and is succeeded conformably by the Shurijah fluvial siliciclastics. It ranges in age from Callovian to Kimmeridgian (Afshar, 1982), but brachiopod studies by D. Ager (pers. commun., 1990) indicate that in places it may reach the Tithonian. During the Upper Jurassic, the Kopet

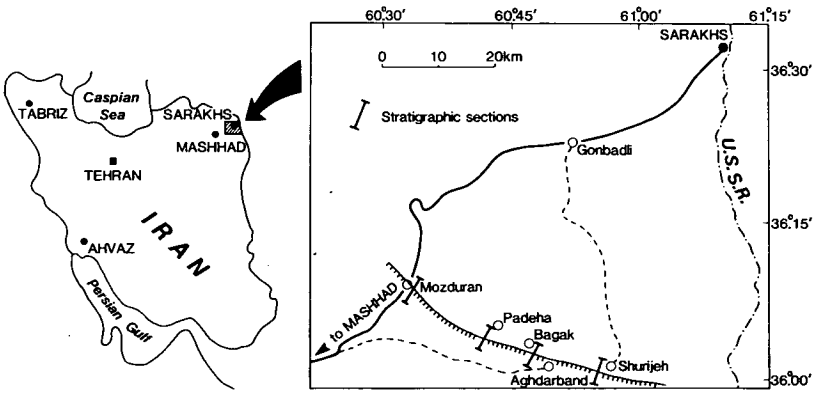

Fig. 1. Location map of the study area in Iran and the sections studied.

Dagh basin was situated at a palaeolatitude of about 10°N (Smith et al., 1981).

In the Sarakhs area, the first major transgression occurred during Middle Jurassic, from the northwest towards the southeastern part of the Kopet-Dagh basin and continued through Tithonian time, except for a minor marine regression, which is evidenced by few thin layers of fluvial clastics. Lack of deep-water sediments, predominance of shallow-water carbonates and clastics, underlain and overlain by fluvial sediments, all indicate a low sea stand during much of the Upper Jurassic in northeast Iran.

Methods of study

Samples were collected near significant lithologic changes within the stratigraphic succession of the Mozduran, Padeha, Bagak and Shurijeh formations. We studied 173 uncovered polished thin sections. These were stained with potassium ferricyanide and alizarin-red S solutions (Dickson, 1965). Whole-rock powders of the 94 samples were dissolved in 1 *N* HCl and those with less than 10% insoluble residue were analyzed by atomic absorption spectrometer for Ca, Mg, Sr, Na, Mn and Fe at the Geology Department, University of Tasmania. Precision was ±1% for Ca and Mg and ±5 ppm for Sr, Na, Mn and Fe (Robinson, 1980). Various types of calcite components were sampled for oxygen and carbon isotope analysis employing a microscope with a dental drill to extract calcite powders from polished slabs. For stable isotope analyses, about 15 mg of the whole-rock powders of 30 representative samples of limestones, which were previously analysed for major and minor elements, were allowed to react with anhydrous phosphoric acid in reaction tubes under vacuum at 25°C for 24 h. The CO_2 extracted from each sample was analysed for $\delta^{18}O$ and $\delta^{13}C$ by mass spectrometry (Micromass, 602 D). Precision of data is ±0.1‰ for both $\delta^{18}O$ and $\delta^{13}C$ and these values are reported relative to PDB. Selected samples were observed by Scanning Electron Microscopy (SEM), using a Phillips SEM 505 at the Central Science Laboratory, University of Tasmania.

Petrography

The Mozduran carbonates consist of a large diversity of skeletal and non-skeletal grains, abundant sparry calcite cement, micrite, early and late diagenetic dolomites and some evaporites.

Skeletal grains

Skeletal grains are mostly bivalves, brachiopods, crinoids, gastropods and abundant calcareous algae. Most of the skeletal grains are micritized due to algal boring (Fig. 2A). Shell structures of brachiopods and crinoids are generally well preserved, whereas those of bivalves and gastropods are not preserved due to dissolution and precipitation of sparry calcite cement (Fig. 2A). Syntaxial rim cements on crinoids are abundant. Algae (Fig. 2B) occur as crustose coralline-red algae (*Lithophyllum*) and to a lesser extent as laminated blue-green algae. Cellular structure and reproductive organs of red algae are well preserved.

Non-skeletal grains

Non-skeletal grains are abundant and consist mainly of ooids, intraclasts and minor pellets. Ooids show concentric (Fig. 2C) and radial structure and combinations of these (Figs. 2D, 2E). The development of concentric or radial fabric is probably determined by environmental factors.

Radial structure reflects a less turbulent environment than concentric ones. In modern marine aragonitic ooids, the concentric structures dominate in high-energy environments, such as platform margin oolitic shoals of the Bahamas and tidal channels and deltas of the Arabian Gulf (Loreau and Purser, 1973). Quiet-water ooids of the Trucial coast lagoons have radial cortical layers. Ooids in the limestones studied have been partially or completely micritized due to algal boring (Fig. 2C). There are some large irregular aggregate grains with botryoidal external forms (Fig. 2G), which resemble grapestones in modern environments. These composite ooids contain smaller ooids within them, probably due to very high-energy or storm deposition. The cortex thick-

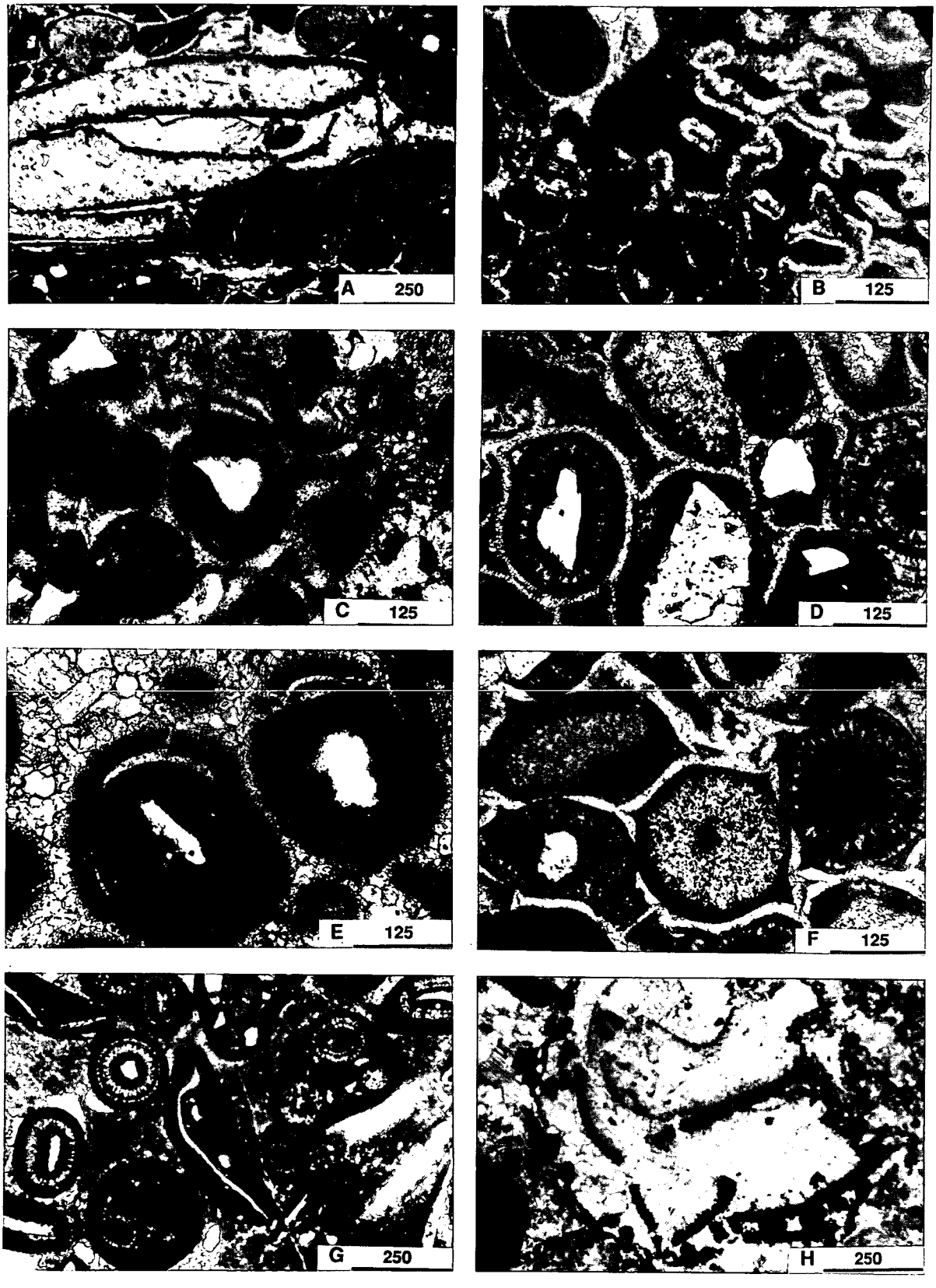
A 250
B 125
C 125
D 125
E 125
F 125
G 250
H 250

ness of ooids is inversely related to the size of the nucleus. Many ooids are deformed (Figs. 2C to 2F) after micritization.

Intraclasts are abundant and vary in internal compositions from biomicrites (Fig. 2G), oomicrites (Fig. 2H), pelmicrites to micrites. Intraclasts associated with ooids indicate penecontemporaneous reworking during oolitisation in tidal channels where forces of erosion are prevalent. Flat pebble conglomerates which formed by the impingement of tides in lower supratidal environments are present in a few samples. Large intraclasts containing bioclasts suggest that the subtidal zone was very shallow and that the intraclasts formed by reworking of lithified sediment by strong currents.

Pellets occur in some samples, are generally associated with gastropods, and are surrounded by micritic matrix. Uniformity of pellet sizes (~ 0.05 mm) indicates that these are faecal pellets, which are produced primarily in quiet saline sea waters with a muddy substrate. The presence of faecal pellets usually indicates low-energy, warm seas supersaturated with respect to $CaCO_3$ and having a restricted circulation (Scoffin, 1987).

Cementation

Different generations of sparry calcite cementation are recognised in the Mozduran limestones ranging from marine through meteoric to some burial cements. Marine cements are fibrous (Figs. 2B–2D) and occur as intra- and intergranular cements. Isopachous cements (Figs. 2C, 2D) form fringes around allochems and are interpreted as early marine cements. These are succeeded by meteoric equant to mosaic sparry calcite cement and later by drusy to platy phreatic to burial cements. Sparry calcite fills fenestrae, which typically form during early diagenesis and are indicative of subaerial exposure. Vadose cementation such as meniscus, pendant or gravitational cements are absent, probably due to a dry climate. Staining indicates that coarse phreatic meteoric sparry cements range from nonferroan followed by ferroan cements suggestive of a change from oxidising near-surface water to more reducing pore fluids. Some coarse sparry calcite cements fill veins and consist of up to three generations of cements, which are interpreted as burial cements. The first generation in these cements is nonferroan, succeeded by ferroan and then by nonferroan sparry calcite cements due to fluctuation in Fe contents.

Micritization is a common feature in the Mozduron limestones, and is considered to be an important process in modern marine phreatic environments (Longman, 1980). Most micritization occurs near the sediment–water interface (Kobluk and Risk, 1977), but it may also continue in water depths of more than a metre (May and Perkins, 1979).

Evidence for deformation is common in Mozduran limestones, such as deformation of fibrous marine cements (Figs. 2D, 2E) around ooids, shattered micritic envelopes (Fig. 2H) and deformed ooids (Fig. 2F). Meteoric equant, mosaic and drusy cements succeed deformed marine cements and deformed ooids and shattered micritic envelopes, all indicating that meteoric cementation formed after deformation.

Evaporites

Evaporite beds up to 40 m thick occur in the study area. Calcitized pseudomorphs after gypsum (Fig. 3A) are common. Intraformational collapse breccias (Fig. 3B) are also present, which apparently formed due to the dissolution of evaporites.

Fig. 2. Photomicrographs of limestones from the Mozduran Formation. Scale in microns. A. Biosparite. Note micritization of bioclasts. Bivalves are dissolved and the molds are filled with sparry calcite cement, whereas the crinoid structure is preserved due to their aragonite and high-Mg calcite mineralogy, respectively. B. Biosparite. Note fibrous cement within red algae components. C. Oosparite. Note isopachous sparry calcite cement. D. Oosparite. Note radial and concentric structure of ooids. Some of the ooids are mitritised. E. Oosparite. Spalled ooids. Note outer layers are broken, whereas the inner ones are intact. F. Oosparite. Ooids with both concentric and radial structures are deformed. G. Oointramicrite. Note large ooids have smaller ooids within them (composite ooids). These resemble grapestones. H. Shattered micritic envelopes.

Dolomitization

Two types of dolomite occur in the Mozduran Formation. The early diagenetic dolomites are equicrystalline (Fig. 3C) and are mainly confined to unfossiliferous supratidal sediments. The late diagenetic dolomites (Fig. 3D) are inequicrystalline and completely replace limestones, siliciclastics and veins formerly filled by sparry calcite cements.

Warm-water characteristics and original aragonite mineralogy

The occurrence of algal-rich biota, diverse skeletal grains, abundant ooids, intraclasts and some pellets and evaporites and early diagenetic dolomites in the Mozduran limestones is similar to that in modern tropical warm waters (Lees, 1975). The substantial accumulation of ooids in the limestones studied is similar to that developed in modern tropical channels, shoals and deltas such as those forming on the Bahama Bank and along the Trucial Coast of the Arabian Gulf (Purser and Evans, 1973; Bathurst, 1975). Modern ooids are composed of aragonite, and those that form in turbulent waters have a tangential fabric oriented parallel to the ooid surface. Aragonite ooids in quieter water, such as those in protected subtidal and lagoonal areas in the Persian Gulf, have cortical layers with a radial fabric (Loreau and Purser, 1973; Davies and Martin, 1976), and similar aragonitic ooids are forming in the Great Salt Lake, Utah (Kahle, 1974; Sandberg, 1975; Halley, 1977). Ooids, intraclasts and pellets are absent in nontropical calcitic sediments (Lees, 1975; Nelson, 1988). Marine evaporites are also most common in modern warm shallow-water areas. Early

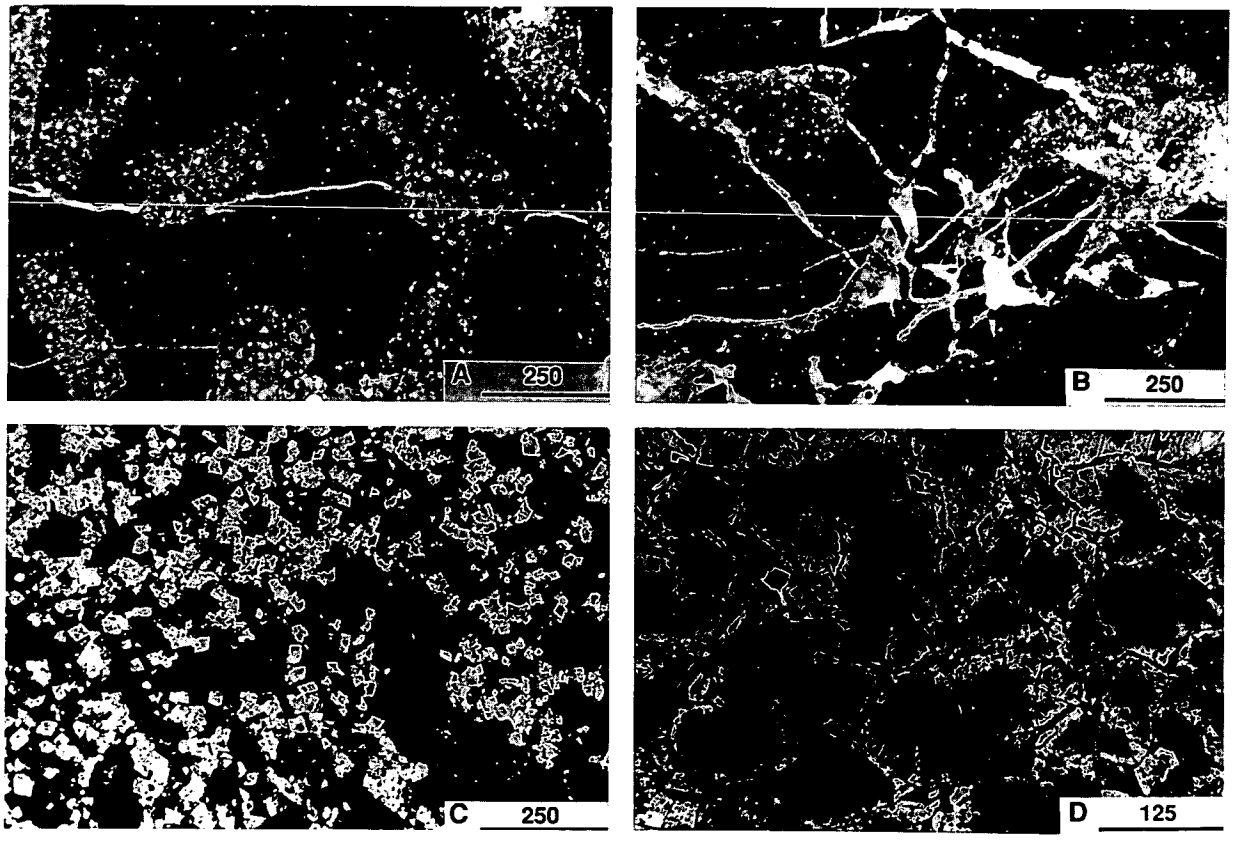

Fig. 3. Evaporites and dolomites of the Mozduran carbonates. Scale in microns. A. Calcitized pseudomorphs after gypsum. B. Collapse solution breccia formed from dissolution of evaporites. C. Dolomitic micrite. Dolomites are equicrystalline and contain inclusions of micrite because dolomite replaced micrite. D. Coarsely crystalline dolomite. Note relict ooids and abundant inclusions. Dolomite replaces oosparite.

diagenetic dolomites are found mainly today in tropical settings. All of the above features are characteristic of the Mozduran carbonates and thus strongly suggest that these limestones formed in warm tropical waters. So does the 10° palaeolatitude. In addition, originally aragonitic bivalve and gastropod shells are completely dissolved and filled with meteoric sparry calcite cements, whereas the high-Mg calcite crinoids and red algae are well preserved.

Fibrous marine cements in the Mozduran limestones were probably originally aragonites which are the dominant marine cement in modern warm waters. Deformed ooids are considered to reflect more dissolution of aragonite than compaction processes, whereas calcitic ooids are undeformed (Wilkinson et al., 1984). In the Mozduran limestones, diffused laminae within the ooids provide evidence for aragonite to calcite inversion (Fig. 4A). The tangential nature of crystals in concentric ooids (Fig. 4B) is similar to that in modern aragonite ooids in high-energy environments, in contrast to radial ooids which occur in protected environments (Loreau and Purser, 1973). Preservation of the original structure in ancient limestones is probably due to semiclosed meteoric

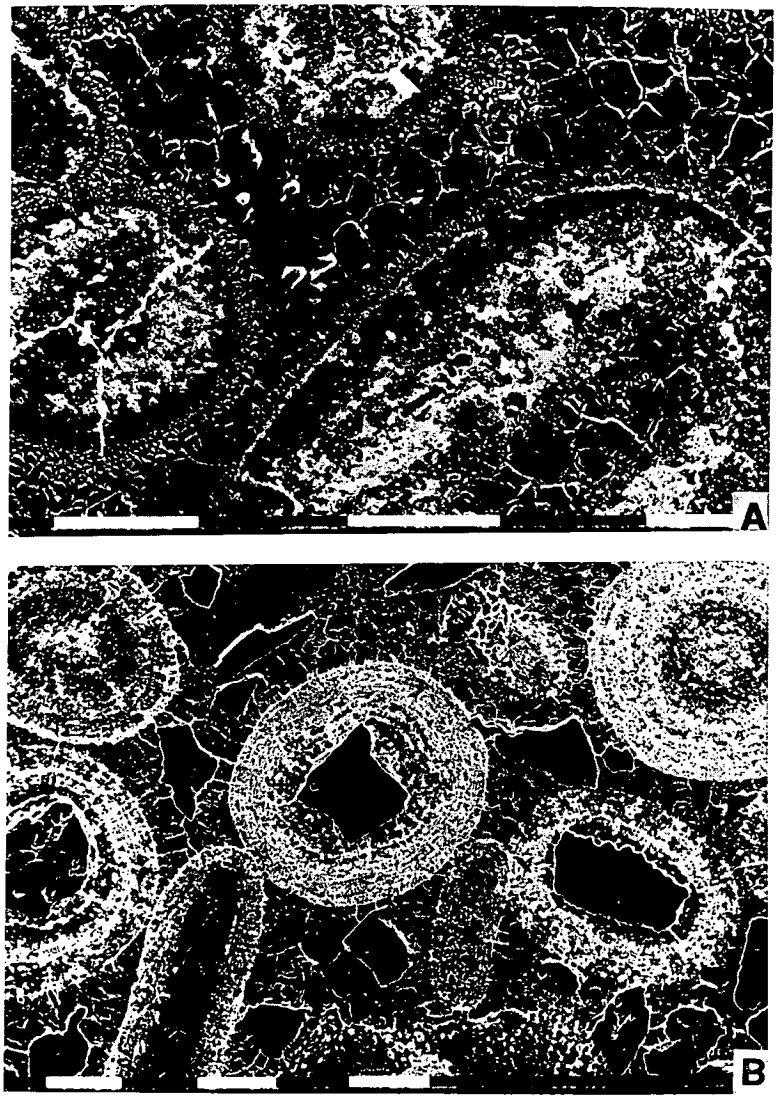

Fig. 4. Scanning Electron Microscope photomicrographs of etched polished thin sections. Scale bar is 0.1 mm. A. Tangential crystals within concentric ooids. Note diffuse laminae. B. Diffuse laminae in ooids indicate aragonite to calcite inversion.

diagenesis (Wilkinson et al., 1984). In spalled cortices (Fig. 2E), where outer laminae are detached from inner laminae, the outer laminae are broken and may result from collapse due to dissolution of aragonite. Our petrographic evidence suggests that aragonite was the original mineral during the formation of Jurassic warm-water carbonates.

Trace elements

Comparison with Recent and ancient carbonates

Modern aragonitic sediments in tropical warm shallow-marine waters have low Mn and Fe (~ 20 ppm), moderate Na (~ 2,500 ppm) and high Sr (~ 10,000 ppm) concentrations (Milliman, 1974). Modern temperate shallow-marine calcitic sediments on average have low Sr (~ 3000 ppm) and high Na (~ 5,000 ppm), Mn (~ 150 ppm) and Fe (~ 1000 ppm) concentrations (Rao, 1986, 1990b). Concentrations of Sr (114–408 ppm; mean 264 ppm), Na (83–280 ppm; mean 114 ppm), Mn (53–529 ppm; mean 250 ppm) and Fe (420–3,745 ppm; mean 1,252 ppm) in the Mozduran limestone suggest appreciable loss of Sr and Na, and gain of Mn and Fe during diagenesis when compared with modern tropical aragonitic and temperate calcitic carbonates. We still view this data as consistent with a tropical origin because Sr and Na values in the Mozduran limestones are similar to those of warm-water Ordovician limestones and much lower than those of calcitic subpolar cold-water Permian limestones of Tasmania (Figs. 5 and 6). Fe and Mn are positively correlated and iron concentrations are an order of magnitude higher than Mn concentrations (Fig. 7), probably due to higher partition coefficients for Fe than Mn.

Diagenetic trends

The concentrations of Sr and Na in diagenetic calcite depend mostly on their partition coefficients and their concentrations in diagenetic solutions. Because Sr and Na have partition coefficients < 1 and low concentrations in meteoric waters, their diagenetic imprint will show low concentrations of Sr and Na. On the other hand, Mn concentrations increase with the increasing influence of meteoric diagenesis (Brand and Veizer, 1980; Rao, 1990a) because the partition coefficient of Mn is ~ 15 and it occurs in high con-

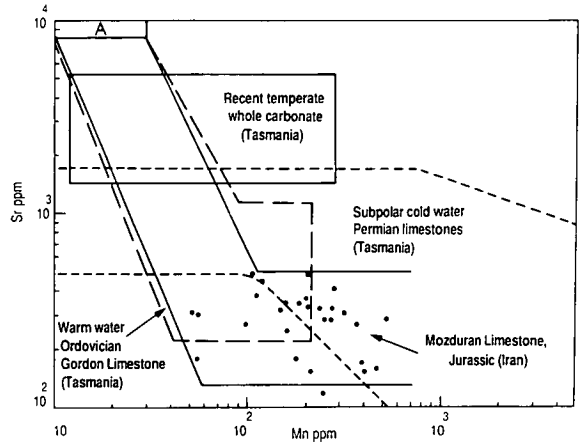

Fig. 5. Comparison of the Sr and Mn field of the Mozduran limestones with those of the tropical Ordovician Gordon limestone (Rao, 1990a), subpolar cold-water Permian limestones (Rao, 1991), Recent tropical aragonite (*A*; Milliman, 1974) and Recent temperate whole carbonate from Tasmania (Rao, 1990b). Note that the Mozduran pattern is similar to that of the tropical Ordovician Gordon limestone.

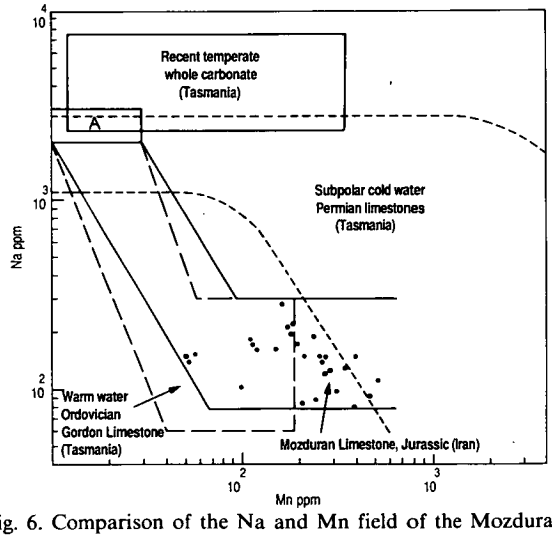

Fig. 6. Comparison of the Na and Mn field of the Mozduran limestone with those of the tropical warm-water Ordovician Gordon limestone (Rao, 1990a), subpolar cold-water Permian limestones (Rao, 1991), Recent tropical aragonite (A; Milliman, 1974) and Recent temperate whole carbonate from Tasmania (Rao, 1990b). Note that the Mozduran pattern is similar to that of the tropical Ordovician Gordon limestone.

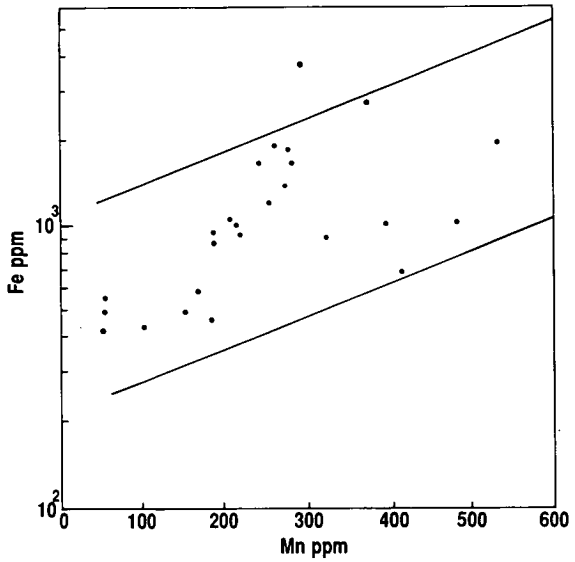

Fig. 7. Variation of Fe versus Mn in the Mozduran limestone. Note that the concentrations of Fe are a magnitude higher than those of Mn.

centrations in meteoric waters (Pingitore, 1978). The concentration of Mn in calcite decreases with increasing rates of precipitation (Pingitore et al., 1988; Mucci, 1988). Initial concentrations of Mn in Mozduran limestones were also lower because of the high rate of sedimentation which was about 30 m/m.y. Calcite under oxidizing conditions carries little Mn, but if formed in reducing conditions, it may have a few percent Mn (Pingitore, 1978; Shanmugam and Benedict, 1983). In the Mozduran limestones, Mn is interpreted to reflect an original mineralogy of predominantly aragonite with high-Mg calcite, oxidizing conditions during deposition, and the increasing influence of meteoric diagenesis. Fe values increase with increasing Mn concentrations, as evidence of redox gradients. Sr and Na variation with Mn concentrations (Figs. 5 and 6) indicate two diagenetic stages. The first stage coincides with a significant decrease of Sr and Na, with no appreciable increase of Mn, and is interpreted in terms of aragonite to calcite inversion. The second stage coincides with an appreciable increase in Mn with no significant change in Sr and Na concentrations, attributed mainly to meteoric diagenesis involving calcite recrystallisation and sparry calcite cementation.

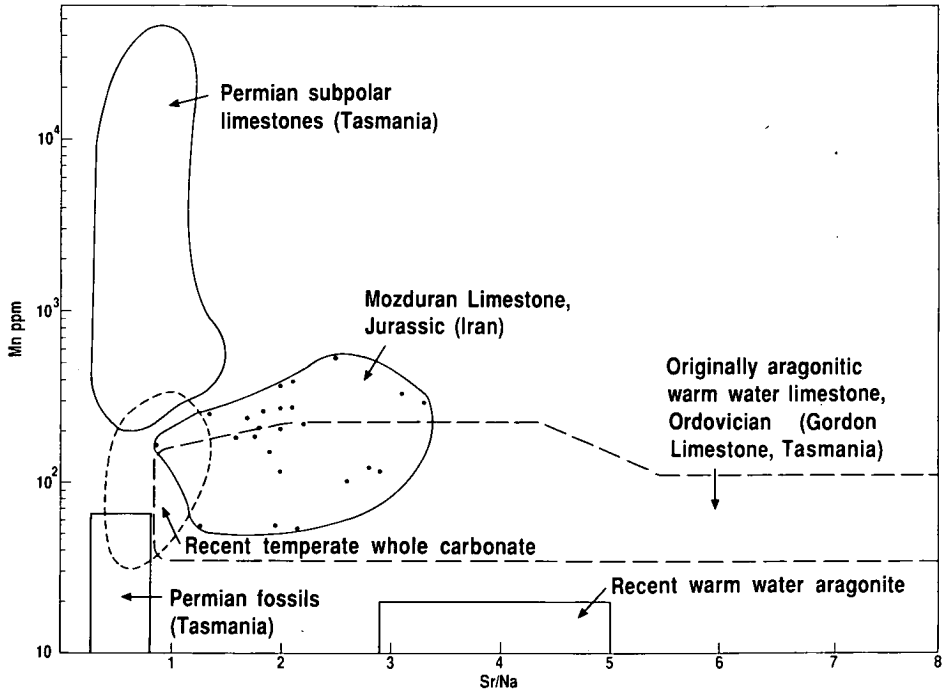

Fig. 8. Mn versus Sr/Na variation in the Mozduran limestone in comparison with the tropical Ordovician Gordon limestone and Permian subpolar limestones (Rao, 1991), Recent tropical aragonite and Recent temperate whole carbonate from Tasmania (Rao, 1990b).

Original aragonite mineralogy

Modern and ancient tropical carbonates are differentiated from non-tropical counterparts by their Sr/Na ratio and Mn content (Rao, 1981c, 1990b, 1991). Modern tropical aragonitic limestones have low Mn and high Sr/Na ratios from 3 to ~ 5 in contrast to modern temperate calcitic ones, which have high Mn and low Sr/Na ratios, ~ 1 (Fig. 8). The subpolar calcitic Permian cold-water fauna has very low Sr/Na ratios (~ 0.5) and low Mn contents, whereas the Permian carbonates have an Sr/Na ratio of ~ 1 and high Mn concentrations. The Jurassic limestones of Iran have high Sr/Na ratios (up to 3.3) and moderate to high Mn (Fig. 8), similar to the originally aragonitic warm-water Ordovician Gordon limestone of Tasmania. The similarity of the trace-element data with modern and ancient carbonates support the interpretation that the Mozduran limestones were originally aragonitic warm-water carbonates.

Oxygen and carbon isotopes

Comparison with modern carbonates

The $\delta^{18}O$ (−2.6 to −7.8‰ PDB) and $\delta^{13}C$ (+0.8 to +4.3‰ PDB) isotope data for the Mozduran limestones (Fig. 9) plot at the edge of the field for modern shallow-warm-marine limestones and it is far removed from the modern temperate calcitic shallow-marine sediment isotope field of Tasmania and New Zealand (Rao and Green, 1983; Rao, 1990b; Rao and Nelson, 1991). The Mozduran isotope field is cut by the shallow surface marine temperature equilibrium calcite line that passes through that of modern whole sediments rich in non-skeletal grains (Rao and Green, 1983), indicating that the Mozduran limestones were in equilibrium with atmospheric CO_2, similar to that of present values. The $\delta^{18}O$ values that are lighter than the marine calcite value (−2.6‰ PDB) are due to equilibration with non-marine waters.

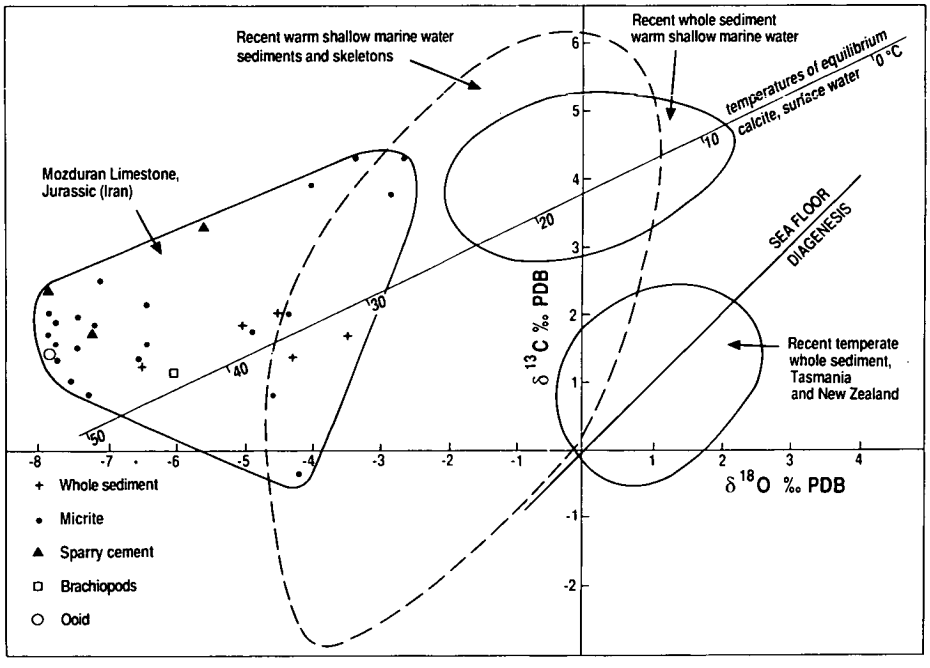

Fig. 9. Comparison of $\delta^{18}O$ and $\delta^{13}C$ values of whole sediments and components from the Mozduran limestone with the Recent warm shallow-marine whole carbonate field (Milliman and Muller, 1977), Recent warm shallow-marine sediments and skeletons field (James and Choquette, 1983) and the Recent temperate whole sediment field of Tasmania and New Zealand (Rao and Green, 1983; Rao, 1990b; Rao and Nelson, 1991). Lines of equilibrium calcite in surface waters and sea floor diagenesis. Note that the Mozduran isotope field lies at the edge of that of modern tropical sediments and skeletons and is cut by a diagenetic line for surficial samples that passes through Recent tropical shallow-marine whole sediments.

diagenetic dolomites are found mainly today in tropical settings. All of the above features are characteristic of the Mozduran carbonates and thus strongly suggest that these limestones formed in warm tropical waters. So does the 10° palaeolatitude. In addition, originally aragonitic bivalve and gastropod shells are completely dissolved and filled with meteoric sparry calcite cements, whereas the high-Mg calcite crinoids and red algae are well preserved.

Fibrous marine cements in the Mozduran limestones were probably originally aragonites which are the dominant marine cement in modern warm waters. Deformed ooids are considered to reflect more dissolution of aragonite than compaction processes, whereas calcitic ooids are undeformed (Wilkinson et al., 1984). In the Mozduran limestones, diffused laminae within the ooids provide evidence for aragonite to calcite inversion (Fig. 4A). The tangential nature of crystals in concentric ooids (Fig. 4B) is similar to that in modern aragonite ooids in high-energy environments, in contrast to radial ooids which occur in protected environments (Loreau and Purser, 1973). Preservation of the original structure in ancient limestones is probably due to semiclosed meteoric

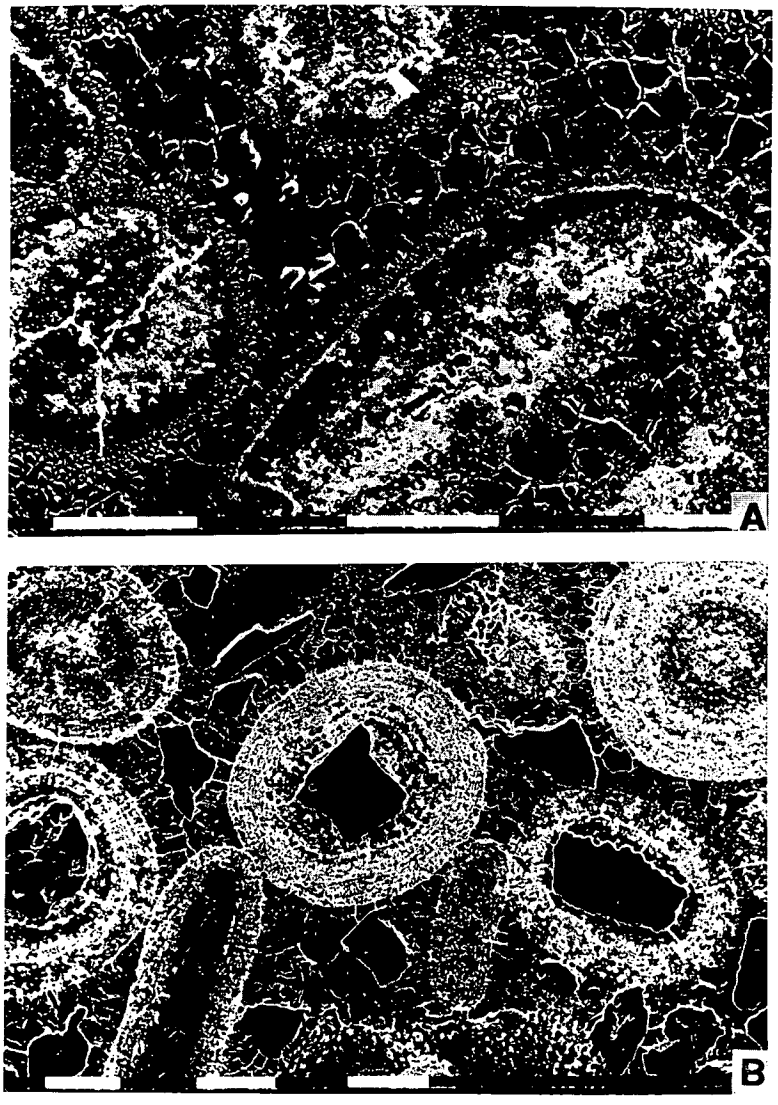

Fig. 4. Scanning Electron Microscope photomicrographs of etched polished thin sections. Scale bar is 0.1 mm. A. Tangential crystals within concentric ooids. Note diffuse laminae. B. Diffuse laminae in ooids indicate aragonite to calcite inversion.

diagenesis (Wilkinson et al., 1984). In spalled cortices (Fig. 2E), where outer laminae are detached from inner laminae, the outer laminae are broken and may result from collapse due to dissolution of aragonite. Our petrographic evidence suggests that aragonite was the original mineral during the formation of Jurassic warm-water carbonates.

Trace elements

Comparison with Recent and ancient carbonates

Modern aragonitic sediments in tropical warm shallow-marine waters have low Mn and Fe (~ 20 ppm), moderate Na (~ 2,500 ppm) and high Sr (~ 10,000 ppm) concentrations (Milliman, 1974). Modern temperate shallow-marine calcitic sediments on average have low Sr (~ 3000 ppm) and high Na (~ 5,000 ppm), Mn (~ 150 ppm) and Fe (~ 1000 ppm) concentrations (Rao, 1986, 1990b). Concentrations of Sr (114–408 ppm; mean 264 ppm), Na (83–280 ppm; mean 114 ppm), Mn (53–529 ppm; mean 250 ppm) and Fe (420–3,745 ppm; mean 1,252 ppm) in the Mozduran limestone suggest appreciable loss of Sr and Na, and gain of Mn and Fe during diagenesis when compared with modern tropical aragonitic and temperate calcitic carbonates. We still view this data as consistent with a tropical origin because Sr and Na values in the Mozduran limestones are similar to those of warm-water Ordovician limestones and much lower than those of calcitic subpolar cold-water Permian limestones of Tasmania (Figs. 5 and 6). Fe and Mn are positively correlated and iron concentrations are an order of magnitude higher than Mn concentrations (Fig. 7), probably due to higher partition coefficients for Fe than Mn.

Diagenetic trends

The concentrations of Sr and Na in diagenetic calcite depend mostly on their partition coefficients and their concentrations in diagenetic solutions. Because Sr and Na have partition coefficients < 1 and low concentrations in meteoric waters, their diagenetic imprint will show low concentrations of Sr and Na. On the other hand, Mn concentrations increase with the increasing influence of meteoric diagenesis (Brand and Veizer, 1980; Rao, 1990a) because the partition coefficient of Mn is ~ 15 and it occurs in high con-

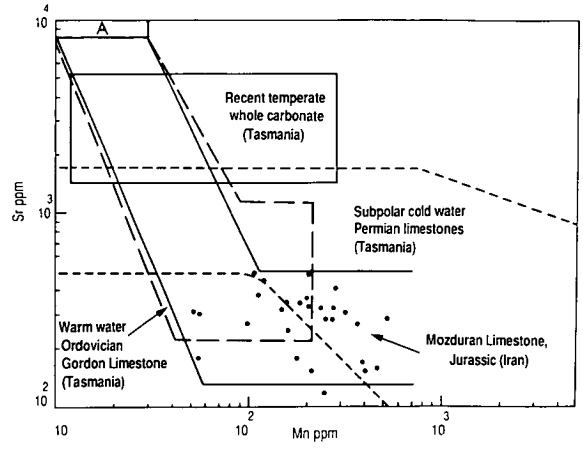

Fig. 5. Comparison of the Sr and Mn field of the Mozduran limestones with those of the tropical Ordovician Gordon limestone (Rao, 1990a), subpolar cold-water Permian limestones (Rao, 1991), Recent tropical aragonite (*A*; Milliman, 1974) and Recent temperate whole carbonate from Tasmania (Rao, 1990b). Note that the Mozduran pattern is similar to that of the tropical Ordovician Gordon limestone.

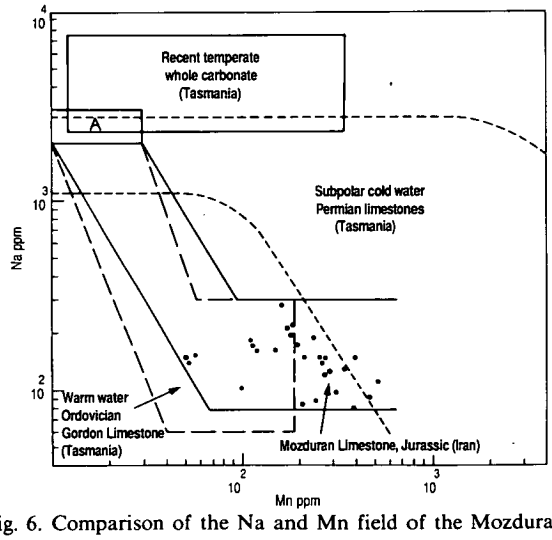

Fig. 6. Comparison of the Na and Mn field of the Mozduran limestone with those of the tropical warm-water Ordovician Gordon limestone (Rao, 1990a), subpolar cold-water Permian limestones (Rao, 1991), Recent tropical aragonite (A; Milliman, 1974) and Recent temperate whole carbonate from Tasmania (Rao, 1990b). Note that the Mozduran pattern is similar to that of the tropical Ordovician Gordon limestone.

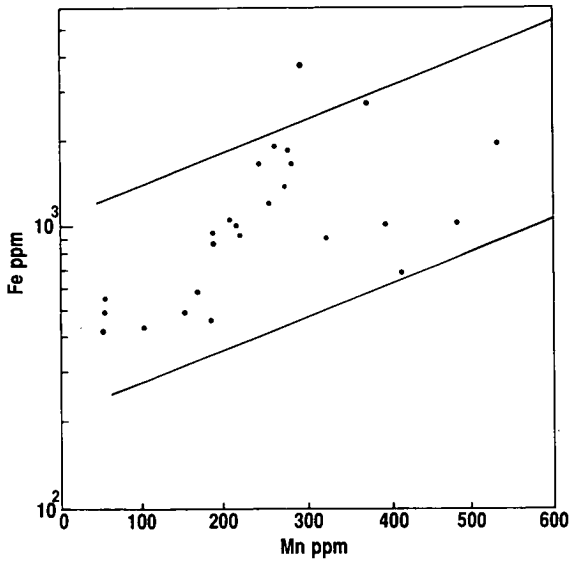

Fig. 7. Variation of Fe versus Mn in the Mozduran limestone. Note that the concentrations of Fe are a magnitude higher than those of Mn.

centrations in meteoric waters (Pingitore, 1978). The concentration of Mn in calcite decreases with increasing rates of precipitation (Pingitore et al., 1988; Mucci, 1988). Initial concentrations of Mn in Mozduran limestones were also lower because of the high rate of sedimentation which was about 30 m/m.y. Calcite under oxidizing conditions carries little Mn, but if formed in reducing conditions, it may have a few percent Mn (Pingitore, 1978; Shanmugam and Benedict, 1983). In the Mozduran limestones, Mn is interpreted to reflect an original mineralogy of predominantly aragonite with high-Mg calcite, oxidizing conditions during deposition, and the increasing influence of meteoric diagenesis. Fe values increase with increasing Mn concentrations, as evidence of redox gradients. Sr and Na variation with Mn concentrations (Figs. 5 and 6) indicate two diagenetic stages. The first stage coincides with a significant decrease of Sr and Na, with no appreciable increase of Mn, and is interpreted in terms of aragonite to calcite inversion. The second stage coincides with an appreciable increase in Mn with no significant change in Sr and Na concentrations, attributed mainly to meteoric diagenesis involving calcite recrystallisation and sparry calcite cementation.

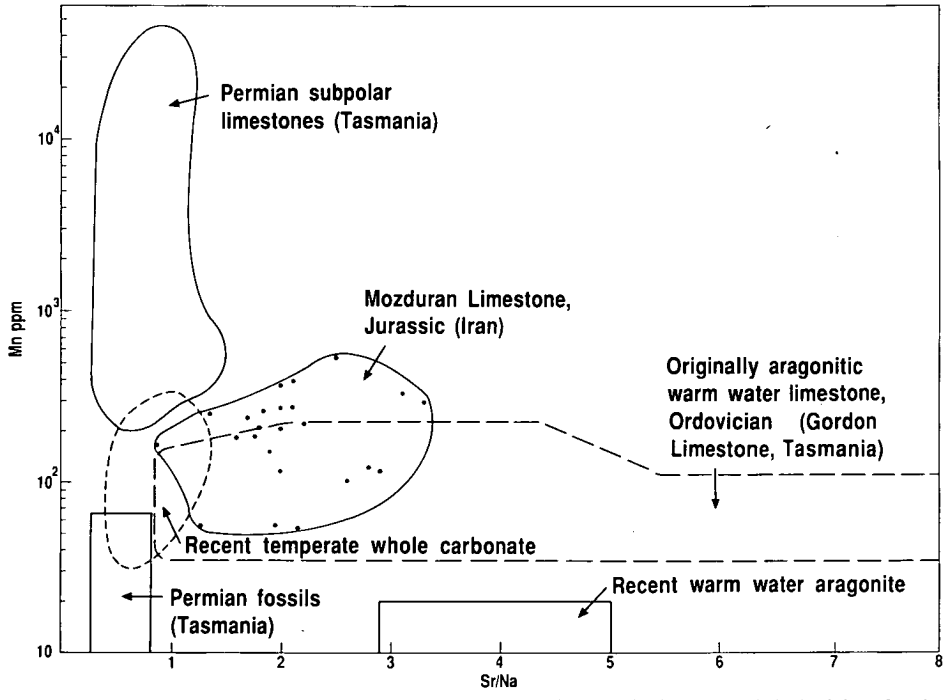

Fig. 8. Mn versus Sr/Na variation in the Mozduran limestone in comparison with the tropical Ordovician Gordon limestone and Permian subpolar limestones (Rao, 1991), Recent tropical aragonite and Recent temperate whole carbonate from Tasmania (Rao, 1990b).

Original aragonite mineralogy

Modern and ancient tropical carbonates are differentiated from non-tropical counterparts by their Sr/Na ratio and Mn content (Rao, 1981c, 1990b, 1991). Modern tropical aragonitic limestones have low Mn and high Sr/Na ratios from 3 to ~ 5 in contrast to modern temperate calcitic ones, which have high Mn and low Sr/Na ratios, ~ 1 (Fig. 8). The subpolar calcitic Permian cold-water fauna has very low Sr/Na ratios (~ 0.5) and low Mn contents, whereas the Permian carbonates have an Sr/Na ratio of ~ 1 and high Mn concentrations. The Jurassic limestones of Iran have high Sr/Na ratios (up to 3.3) and moderate to high Mn (Fig. 8), similar to the originally aragonitic warm-water Ordovician Gordon limestone of Tasmania. The similarity of the trace-element data with modern and ancient carbonates support the interpretation that the Mozduran limestones were originally aragonitic warm-water carbonates.

Oxygen and carbon isotopes

Comparison with modern carbonates

The $\delta^{18}O$ (−2.6 to −7.8‰ PDB) and $\delta^{13}C$ (+0.8 to +4.3‰ PDB) isotope data for the Mozduran limestones (Fig. 9) plot at the edge of the field for modern shallow-warm-marine limestones and it is far removed from the modern temperate calcitic shallow-marine sediment isotope field of Tasmania and New Zealand (Rao and Green, 1983; Rao, 1990b; Rao and Nelson, 1991). The Mozduran isotope field is cut by the shallow surface marine temperature equilibrium calcite line that passes through that of modern whole sediments rich in non-skeletal grains (Rao and Green, 1983), indicating that the Mozduran limestones were in equilibrium with atmospheric CO_2, similar to that of present values. The $\delta^{18}O$ values that are lighter than the marine calcite value (−2.6‰ PDB) are due to equilibration with non-marine waters.

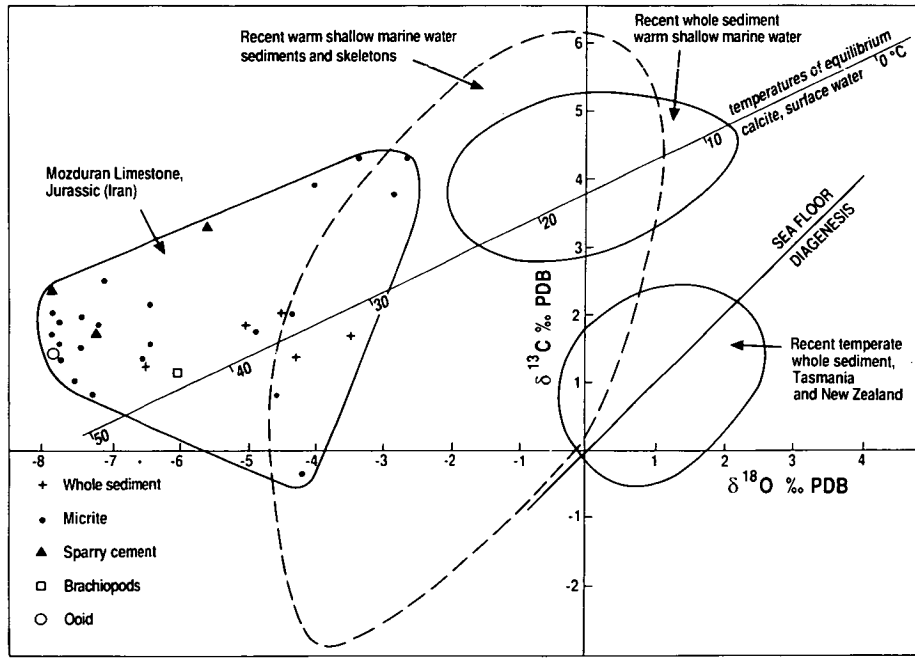

Fig. 9. Comparison of $\delta^{18}O$ and $\delta^{13}C$ values of whole sediments and components from the Mozduran limestone with the Recent warm shallow-marine whole carbonate field (Milliman and Muller, 1977), Recent warm shallow-marine sediments and skeletons field (James and Choquette, 1983) and the Recent temperate whole sediment field of Tasmania and New Zealand (Rao and Green, 1983; Rao, 1990b; Rao and Nelson, 1991). Lines of equilibrium calcite in surface waters and sea floor diagenesis. Note that the Mozduran isotope field lies at the edge of that of modern tropical sediments and skeletons and is cut by a diagenetic line for surficial samples that passes through Recent tropical shallow-marine whole sediments.

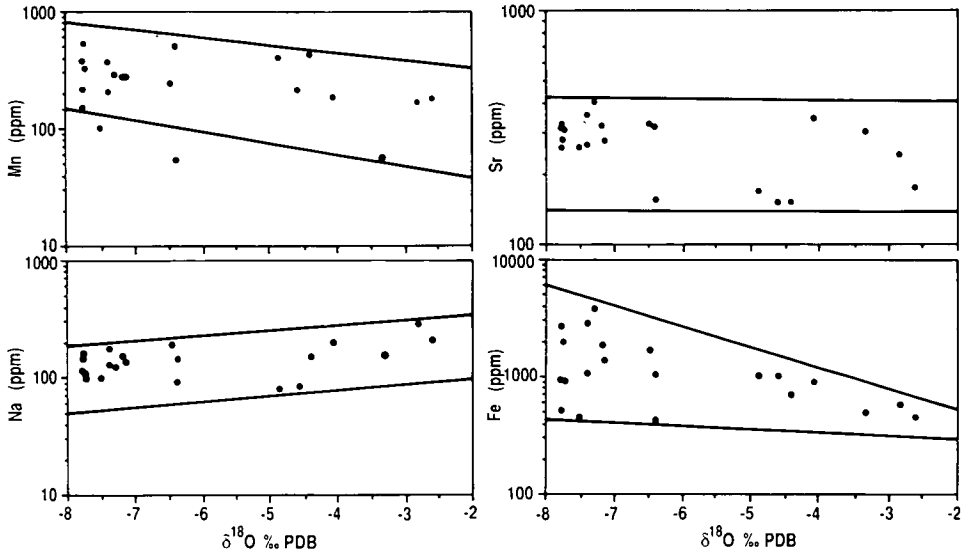

Fig. 10. Variations of Mn, Na, Sr and Fe versus $\delta^{18}O$ values in whole rocks and components from the Mozduran limestone. See text.

Diagenetic trends

Because tropical and subtropical coastal meteoric waters are 2 to 3‰ (SMOW) lighter in ^{18}O than marine waters (Anderson and Arthur, 1983), the calcites of the Mozduran limestones ranging up to −7.8‰ PDB in $\delta^{18}O$ are interpreted to be profoundly affected by meteoric diagenesis (Fig. 9). The Mozduran limestones in the Shurijeh section, consisting of thin limestones and thick terrigenous clastics, show a depletion of $\delta^{13}C$, whereas the remainder of samples have $\delta^{13}C$ values similar to those of brachiopods (Fig. 9). The depletion of $\delta^{13}C$ is characteristic of vadose diagenesis, where the soil CO_2 enrichment in ^{12}C occurs due to decomposition of organic matter. The $\delta^{13}C$ levels in phreatic meteoric calcites approach marine calcite levels due to increasing amounts of water–

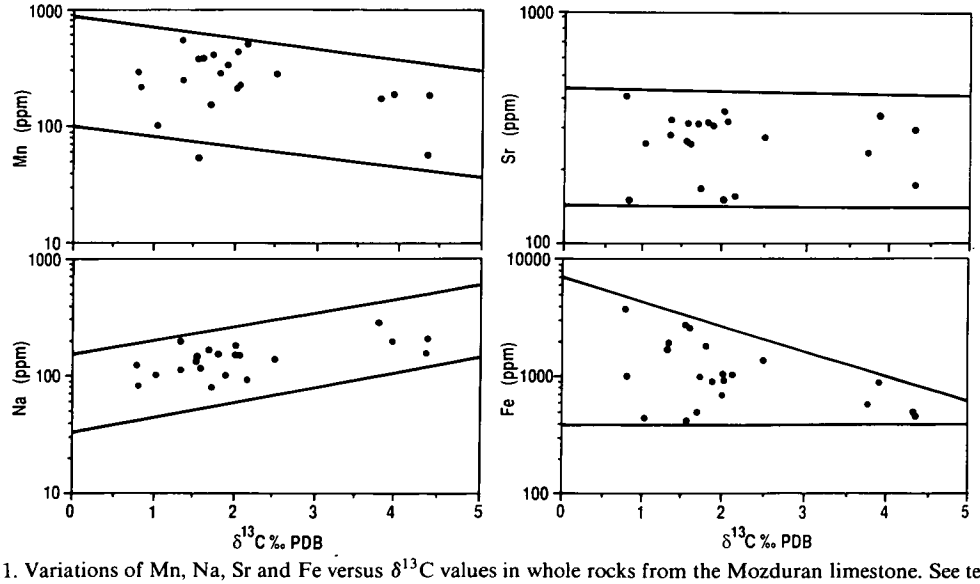

Fig. 11. Variations of Mn, Na, Sr and Fe versus $\delta^{13}C$ values in whole rocks from the Mozduran limestone. See text.

rock interaction (Meyers and Lohmann, 1985; Lohmann, 1988). Because $\delta^{13}C$ values of Mozduran samples are near marine calcite brachiopod values, we interpret these by extensive phreatic meteoric diagenesis after deposition.

The extent of meteoric diagenesis in the Mozduran limestones can be illustrated from the covariation of $\delta^{18}O$ and $\delta^{13}C$ with trace elements, illustrated in Figs. 10 and 11, respectively. Mn and Fe values increase and Na values decrease with increasingly lighter values of $\delta^{18}O$ because of dissolution of aragonite by meteoric waters and reprecipitation of calcite. These trends are similar to those of other ancient limestones affected by meteoric diagenesis (Brand and Veizer, 1980, 1981; Al-Aasm and Veizer, 1986a, b; Rao, 1990a). The Sr values are relatively constant through the entire range of $\delta^{18}O$. Sr values are much lower and Mn values much higher in the Mozduran limestones compared with those of the tropical Ordovician limestones of Tasmania (Fig. 5). These are explained by an open-system phreatic meteoric diagenesis. This conclusion is supported by the $\delta^{13}C$ variation (Fig. 11) of trace elements. Mn and Fe values increase and Na values decrease, whereas Sr values remain constant with increasingly lighter $\delta^{1}3C$ values due to extensive meteoric diagenesis. Stable-isotope studies indicate that the Mozduran limestones underwent significant changes in meteoric waters, whereas burial diagenesis had a relatively minor impact.

Water temperatures

The least altered marine calcite $\delta^{18}O$ values of -2.6‰ PDB, corresponding to the lowest Mn and Fe values and highest Na values (Fig. 11), was used to calculate ambient water temperature using the equation of Shackleton and Kennett (1975) assuming present-day seawater values of 0 (SMOW):

$$T = 16.9 - 4.38(\delta c - \delta w) + 0.10\,(\delta c - \delta w)^2$$

where T is temperature (in °C), δc is the isotopic ratio of CO_2 produced from the carbonate at 25°C, and δw the isotopic ratio of CO_2 in equilibrium with formation water.

This calculation gives an ambient temperature of 29°C for the inversion of aragonite to calcite of the Mozduran limestones. However, the δw value of 0 (SMOW) used in the above equation corresponds to the present-day seawater value with large ice caps. As glacial sediments have not been reported from the Jurassic (Frakes, 1979; Hambrey and Harland, 1981), a δw of -1.2‰ of seawater without ice caps may be more appropriate (Rao and Green, 1982; Anderson and Arthur, 1983), which lowers the temperature by about 5°C. The calculated temperatures (29 or 24°C) indicate that the Mozduran limestones formed in warm water, rich in aragonite, which agrees with the trace-element and petrographic evidence.

Geologic significance

Petrographic, trace-element and isotopic characteristics independently and collectively confirm that the Mozduran limestones were deposited in warm, shallow waters at a temperature of $\geqslant 24$ or 29°C. The original $CaCO_3$ mineralogy in Jurassic tropical shallow-water carbonates was predominantly aragonite, the same as its modern counterparts. The atmospheric CO_2 levels during the Jurassic were similar to those at present. The $\delta^{13}C$ and $\delta^{18}O$ surface water temperature equilibrium calcite line (Rao and Green, 1983) provides a means of assessing past atmospheric CO_2 levels.

Extensive carbonates are now forming in non-tropical settings (Nelson, 1988 and references therein) in which calcite is the predominant mineral. Because the present is the key to the past, we should expect to find widespread ancient non-tropical carbonates. Yet only a few of such non-tropical carbonate deposits are known (Nelson, 1988; Rao, 1988). This anomaly may exist because most ancient carbonates have not yet been studied in order to differentiate non-tropical and tropical carbonates. Nelson (1978) and Rao (1981b, 1988, 1991) studied ancient non-tropical carbonates, suggesting that the carbonate mineralogy varies with water temperature and that calcite predominates in ancient cold, shallow-marine limestones.

Conclusions

Our results strongly indicate that aragonite was the predominant primary mineral in Jurassic warm-water carbonates deposited in the Mozduran area of Iran. The criteria include the following:

(a) The limestones show warm-water characteristics, such as abundant algae, diverse skeletal and non-skeletal grains, evaporites and early diagenetic dolomites. Aragonite skeletons occur as molds filled with sparry calcite cements. Concentric and radial ooids indicate aragonite mineralogy. Isopachous and fibrous sparry calcite cements be as common as in modern aragonitic ones. Deformed ooids, shattered micritic envelopes and spalled ooids indicative of aragonite dissolution during meteoric diagenesis occur commonly.

(b) Inversion of aragonite involves an appreciable decrease in Sr and Na concentrations with no significant increase of Mn values. The Sr/Na ratios are > 1.

(c) The $\delta^{18}O$ and $\delta^{13}C$ field is at the edge of that of modern aragonitic carbonates and is cut by the surface marine diagenetic trend line that passes through modern warm-water aragonites because of atmospheric CO_2 levels similar to present-day values. The meteoric water composition approaches that the present-day tropics. Meteoric diagenesis may leave a strong isotopic signature. The $\delta^{18}O$ values indicate temperatures of $\sim 25°C$.

The model of mineralogic changes related to ambient water temperature is useful to discriminate warm tropical from cold non-tropical carbonates. The original calcitic nature of some Jurassic limestones is due to their non-tropical origin.

Acknowledgements

This research was financially supported by the University of Mashhad, Iran and the Department of Geology, University of Tasmania, Hobart. We would like to thank Simon Stephens for assistance in the preparation of thin sections, Philip Robinson for trace element analysis, Mike Power for isotope analysis, Wis Jablonski for the scanning electron microscopy, Laura Hurd for drafting illustrations, Gary Davidson and Joe Stolz and *Sedimentary Geology* reviewers J. Veizer, K. Kelts and B.W. Sellwood for critically reading the early version of the manuscript and making helpful suggestions. We are thankful to Professor Derek Ager (Swansea, England) for age determinations based on brachiopods.

References

Afshar, A., 1970. Geology of Sarakhs Area and Khangiran Gas Field. Geological Division, Exploration and Production Group, National Iranian Oil Company, pp. 1–17.

Afshar, A., 1982. Geological Map of Sarakhs Area. National Iranian Oil Company, Exploration and Production.

Al-Aasm, I.S. and Veizer, J., 1986a. Diagenetic stabilization of aragonite and low-Mg calcite, II. Stable isotopes in rudists. J. Sediment. Petrol., 56: 763–770.

Al-Aasm, I.S. and Veizer, J., 1986b. Diagenetic stabilization of aragonite and low-Mg calcite, II. Stable isotopes in rudists. J. Sediment. Petrol., 56: 763–770.

Anderson, T.F. and Arthur, M.A., 1983. Stable isotopes of oxygen and carbon and their application to sedimentologic and paleoenvironmental problems. In: Stable Isotopes in Sedimentary Geology. Soc. Econ. Paleontol. Mineral., Short Course, 10: 1–151.

Bathurst, R.G.C., 1975. Carbonate Sediments and Their Diagenesis. Elsevier, Amsterdam, 658 pp.

Brand, U. and Veizer, J., 1980. Chemical diagenesis of a multicomponent carbonate system, I. Trace elements. J. Sediment. Petrol., 50: 1219–1236.

Brand, U. and Veizer, J., 1981. Chemical diagenesis of a multicomponent carbonate system, II. Stable isotopes. J. Sediment. Petrol., 51: 987–997.

Burton, E.A. and Walter, L.K., 1987. Relative precipitation of aragonite and Mg-calcite from seawater: temperature or carbonate ion control? Geology, 15: 111–114.

Davies, P.J. and Martin, K., 1976. Radial aragonite ooids, Lizard Island, Great Barrier Reef, Queensland, Australia. Geology, 4: 120–122.

Dickson, J.A.D., 1965. A modified staining technique for carbonates in thin section. Nature, 205: 587.

Frakes, L.A., 1979. Climates through Geologic Time. Elsevier, Amsterdam, 310 pp.

Fuchtbauer, H. and Hardie, L.A., 1976. Experimentally determined homogeneous distribution coefficients for precipitated magnesian calcites. Abstr. Ann. Progr. Mtg. Geol. Soc. Am., p. 877.

Halley, R.B., 1977. Ooid fabric and fracture in the Great Salt Lake and the geologic record. J. Sediment. Petrol., 47: 1099–1120.

Hambrey, M.J. and Harland, W.B., 1981. Earth's Pre-Pleistocene Glacial Record. Cambridge University Press, Cambridge, 1021 pp.

James, N.P. and Choquette, P.W., 1983. Diagenesis, 6. Limestones—the sea floor diagenetic environment. Geosci. Can., 10: 162–179.

Kahle, C.F., 1974. Ooids from Great Salt Lake, Utah, as an analogue for the genesis and diagenesis of ooids in marine limestones. J. Sediment. Petrol., 44: 30–49.

Kinsman, D.J.J. and Holland, H.D., 1969. The co-precipitation of cations with $CaCO_3$, IV. The co-precipitation of Sr^{2+} with aragonite between 16° and 96°C. Geochim. Cosmochim. Acta, 33: 1–17.

Kobluk, D.R. and Risk, M.J., 1977. Micritization and carbonate-grain binding by endolithic algae. Am. Assoc. Pet. Geol. Bull., 61: 1069–1082.

Lees, A., 1975. Possible influence of salinity and temperature on modern shelf carbonate sedimentation. Mar. Geol., 19: 159–198.

Lohmann, K.C., 1988. Geochemical patterns of meteoric diagenetic systems and their application to studies of paleokarst. In: N.P. James and P.W. Choquette (Editors), Paleokarst. Springer-Verlag, New York, N.Y., pp. 58–80.

Longman, M.W., 1980. Carbonate diagenetic textures from near surface diagenetic environments. Am. Assoc. Pet. Geol. Bull., 64: 461–487.

Loreau, J.P. and Purser, B.H., 1973. Distribution and ultrastructure of Holocene ooids in the Persian Gulf. In: B.H. Purser (Editor), The Persian Gulf. Springer-Verlag, Berlin, pp. 279–328.

MacKenzie, F.T. and Pigott, J.D., 1981. Tectonic controls of phanerozoic rock cycling. J. Geol. Soc., 138: 183–196.

May, J.A. and Perkins, R.D., 1979. Endolithic infestation of carbonate substrates below the sediment–water interface. J. Sediment. Petrol., 49: 357–377.

Meyers, W.J. and Lohmann, K.C., 1985. Isotope geochemistry of regionally extensive calcite cement zones and marine components in Mississippian limestone, New Mexico. In: N. Schneiderman and P.M. Harris (Editors), Carbonate Cements. Soc. Econ. Paleoontol. Miner. Spec. Publ., 36: 223–240.

Milliman, J.D., 1974. Recent Sedimentary Carbonates, I. Marine Carbonates. Springer-Verlag, Berlin, 375 pp.

Mucci, A., 1988. Manganese uptake during calcite precipitation from seawater: conditions leading to the formation of a pseudokutnahorite. Geochim. Cosmochim. Acta, 52: 1859–1868.

Nelson, C.S., 1978. Temperate shelf carbonate sediments in the Cenozoic of New Zealand. Sedimentology, 25: 737–771.

Nelson, C.S., 1988, An introductory perspective on non-tropical shelf carbonates. In: C.S. Nelson (Editor), Non-Tropical Shelf Carbonates—Modern and Ancient. Sediment. Geol., 60: 3–12.

Pingitore, N.E., 1978. The behaviour of Zn^{2+} and Mn^{2+} during carbonate diagenesis: theory and applications. J. Sediment. Petrol., 48: 799–814.

Pingitore, N.E., Eastman, M.P., Sandidge, M., Oden, K. and Freiha, B., 1988. The coprecipitation of manganese(II) with calcite: an experimental study. Mar. Chem., 25: 107–120.

Purser, B.H. and Evans, G., 1973. Regional sedimentation along the Trucial coast, SE Persian Gulf. In: B.H. Purser (Editor), The Persian Gulf. Springer-Verlag, Berlin, pp. 211–231.

Rao, C.P., 1981a. Cementation in cold-water bryozoan sand, Tasmania, Australia. Mar. Geol., 40: M25–M33.

Rao, C.P., 1981b. Criteria for recognition of cold-water carbonate sedimentation: Berriedale Limestone (Lower Permian), Tasmania, Australia. J. Sediment. Petrol., 51: 491–506.

Rao, C.P., 1981c. Geochemical differences between tropical (Ordovician) and subpolar (Permian) carbonates, Tasmania, Australia. Geology, 9: 205–209.

Rao, C.P., 1986. Geochemistry of temperate-water carbonates, Tasmania, Australia. Mar. Geol., 71: 363–370.

Rao, C.P., 1988. Paleoclimate of some Permo–Triassic carbonates of Malaysia. In: C.S. Nelson (Editor), Non-Tropical Shelf Carbonates—Modern and Ancient. Sediment. Geol., 60: 221–231.

Rao, C.P., 1990a. Petrography, trace elements and oxygen and carbon isotopes, Gordon Group carbonates (Ordovician), Florentine Valley, Tasmania, Australia. Sediment. Geol., 66: 83–97.

Rao, C.P., 1990b. Geochemical characteristics of cool–temperate carbonates, Tasmania, Australia. Carbonates and Evaporites, 5: 209–221.

Rao, C.P., 1991. Geochemical differences between subpolar (Permian), temperate (Recent and Pleistocene) and tropical (Ordivician) carbonates, Tasmania, Australia. Carbonates and Evaporites, 6: 83–106.

Rao, C.P. and Green, D.C., 1982. Oxygen and carbon isotopes of Early Permian cold-water carbonates, Tasmania, Australia. J. Sediment. Petrol., 52: 1111–1125.

Rao, C.P. and Green, D.C., 1983. Oxygen–carbon-isotope composition of cold shallow-marine carbonates of Tasmania, Australia. Mar. Geol., 53: 117–129.

Rao, C.P. and Nelson, C.S., 1991. Oxygen and carbon isotope fields for temperate shelf carbonates from Tasmania and New Zealand. Mar. Geol. (submitted).

Rao, C.P. and Wang, B., 1990. Oxygen and carbon isotope composition of Gordon Group carbonates (Ordovician), Florentine Valley, Tasmania, Australia. Aust. J. Earth Sci., 37: 305–316.

Robinson, P., 1980. Determination of calcium, magnesium, manganese, strontium, sodium and iron in the carbonate fraction of limestones and dolomites. Chem. Geol., 28: 135–146.

Sandberg, P.A., 1975. New interpretations of Great Salt Lake ooids and nonskeletal carbonate mineralogy. Sedimentology, 22: 497–537.

Schlager, W. and James, N.P., 1978. Low-magnesian calcite limestones forming at the deep-sea floor, Tongue of the Ocean, Bahamas. Sedimentology, 25: 675–702.

Scoffin, T.P., 1987. An Introduction to Carbonate Sediments and Rocks. Blackie, Glasgow, 274 pp.

Shackleton, N.J. and Kennett, J.P., 1975. Paleotemperature

history of the Cenozoic and the initiation of Antarctic glaciation: oxygen and carbon isotope analyses in DSDP site 277, 279 and 281. In: J.P. Kennett and R.E. Houtz (Editors), Initial Reports of the Deep-Sea Drilling Project, XXIX.U.S. Govt. Printing Office, Washington, D.C., pp. 743–755.

Shanmugam, G. and Benedict, III, G.L., 1983. Manganese distribution in the carbonate fraction of shallow to deep marine lithofacies, Middle Ordovician, eastern Tennessee. Sediment. Geol., 35: 159–175.

Smith, A.G., Hurley, A.M. and Briden, J.C., 1981. Phanerozoic Paleocontinental World maps. Cambridge University Press, Cambridge, 102 pp.

Tucker, M.E., 1984. Calcitic, aragonitic and mixed calcititic–aragonitic ooids from the mid-Proterozoic Belt Supergroup, Montana, Sedimentology, 31: 627–644.

Wilkinson, B.H., 1982. Cyclic cratonic carbonates and phanerozoic calcite seas. J. Geol. Educ., 30: 189–203.

Wilkinson, B.H., Buczynski, C. and Owen, R.M., 1984. Chemical control of carbonate phases: implication from upper Pennsylvanian calcite–aragonite ooids of southeastern Kansas. J. Sediment. Petrol., 54: 932–947.

Marine Geology, 103 (1992) 249–272
Elsevier Science Publishers B.V., Amsterdam

Carbonate minerals, major and minor elements and oxygen and carbon isotopes and their variation with water depth in cool, temperate carbonates, western Tasmania, Australia

C. Prasada Rao and Mohammad H. Adabi*

Department of Geology, University of Tasmania, GPO Box 252 C, Hobart, Tasmania 7001, Australia

(Received September 25, 1990; revision accepted May 24, 1991)

ABSTRACT

Rao, C.P. and Adabi, M.H., 1992. Carbonate minerals, major and minor elements and oxygen and carbon isotopes and their variation with water depth in cool, temperate carbonates, western Tasmania, Australia. Mar. Geol., 103: 249–272.

Cool temperate bryomol carbonates predominate on shallow shelves around western Tasmania. Many samples are bored and encrusted due to the occurrence of submarine hardgrounds and to slow rates of sedimentation. Intragranular $CaCO_3$ cementation is common.

Tasmanian whole carbonates are mainly mixtures of high-Mg calcite (HMC) and low-Mg calcite (LMC) with minor amounts of aragonite. HMC and aragonite contents decrease while LMC content increases with increasing water depth due to a decrease in water temperature. Mg concentrations in calcite correspond to temperatures of < 10°C. Sr and Na concentrations in bryozoa decrease due to calcite cementation, whereas their concentrations increase with aragonite content. Mn and Fe concentrations are higher than in warm shallow marine counterparts and increase with increasing aragonite percentage. Sr and Na concentrations in calcite slightly increase with increasing LMC percentage due to decreasing water temperatures; Mn and Fe values in calcite are independent of water temperature. HMC percentage and HMC/LMC ratios decrease while LMC percentage increases with increasingly heavier $\delta^{18}O$ values due to decreasing temperatures. LMC is a marine mineral and not a product of meteoric diagenesis.

Unusually high concentrations of Sr, Na, Mn and Fe in aragonite are due either to the tendency of aragonite formed in cold seas to incorporate more of these elements or to aragonite formation by transformation of metastable cold water $CaCO_3$ minerals such as vaterite or hydrous calcite.

Sr contents decrease with increasing water depth due to a decrease in aragonite and increase in low-Mg calcite. Na values increase with increasing water depth due to increasing salinity. Mn and Fe concentrations decrease with increasing water depth due to decreasing continental terrigenous input. Depth related variations in Mg, Sr, Na, Mn and Fe are due to marine diagenesis and are unrelated to meteoric diagenesis.

$\delta^{18}O$ and $\delta^{13}C$ values are positively correlated and this isotopic field is bisected by the diagenesis trend line for upwelling water that passes through the point −1‰ $\delta^{18}O$, 0‰ $\delta^{13}C$. The $\delta^{18}O$ values become heavier and Mg values decrease with increasing water depth due to decreasing temperatures, from about 17 to 6°C for normal seawater and from 13 to 2°C for upwelling water. These temperatures are lower than measured summer values because of the strong seasonal effect of surface waters, influx of subantarctic water in winter, and mixing of cold upwelling waters in the bottom water. As carbonates in upwelling regions are in equilibrium with upwelling water having $\delta^{18}O$ values of −1‰, in paleotemperature determinations seawater values that are lower by 1‰ than those postulated for different geological periods should be considered for those carbonates suspected of being non-tropical in origin on the basis of geological and geochemical evidence.

Originally calcitic limestones are abundant in ancient sequences and their temperatures of formation and diagenesis can be better understood by using the data base provided by this study.

*Present address: Faculty of Sciences, Geology Department, University of Ferdowsi (Mashhad), Mashhad, Iran

0025-3227/92/$05.00

Introduction

Extensive temperate shelf carbonates are now forming in many areas (Lees, 1975; Nelson, 1988 and references therein), particularly in southern Australia (Conolly and Von der Borch, 1967; Wass et al., 1970). In Tasmania, cool temperate carbonates are predominant compared to siliciclastic sediments and are now forming at average water temperatures < 13°C. Based on uniformitarianism principles, the widespread occurrence of similar temperate carbonates is to be expected in ancient stratigraphic sequences, but only a few have been documented so far (e.g., Nelson, 1978; Brookfield, 1988; Draper, 1988; Rao, 1988; James and Bone, 1989). This apparent anomaly exists because more data are needed on modern temperate carbonates and additional studies are required of more ancient carbonates to interpret their temperatures of formation. The present study deals with carbonate minerals, major and minor elements and oxygen and carbon isotopes and their variation with water depth in modern cool temperate Tasmanian carbonate sediments.

In modern tropical shallow marine carbonates, aragonite and high-Mg calcite are the predominant minerals (Milliman, 1974). Earlier studies on individual bryozoan sands from temperate shelf carbonates indicated that calcite is the predominant mineral with some aragonite (Rao, 1981a, 1990a). The variation in high-Mg calcite and low-Mg calcite in bulk samples of temperate shelf carbonates has not been fully documented. Recent isotopic studies have indicated that whole sediments from Tasmania and New Zealand are much more in equilibrium with ambient waters than individual skeletons (Rao and Nelson, 1992). Experimental studies indicate that low-Mg calcite alone forms in water temperatures of < 5°C from normal seawater (Kinsman and Holland, 1969; Burton and Walter, 1987). Calcite was considered to be the main original mineral in many early and middle Paleozoic and Jurassic carbonates (Sandberg, 1975; MacKenzie and Pigott, 1981; Wilkinson, 1982; Tucker, 1984). This might be due to the extensive occurrence of non-tropical carbonates during these periods as coeval tropical carbonates were originally aragonitic (Rao, 1990b; Adabi and Rao, 1991). Quantitative variation in carbonate mineralogy in modern temperate carbonates and their relationship with major and minor elements and oxygen and carbon isotopes should be useful in understanding diagenesis and in the recognition of non-tropical carbonates.

At low temperatures, calcite is associated with metastable $CaCO_3$ phases, such as vaterite and hydrous calcites (Albright, 1971; Turnbull, 1973; Hull and Turnbull, 1973; Marland, 1975). These metastable $CaCO_3$ minerals change rapidly to calcite and aragonite under normal collecting conditions. As these are impure minerals, major and minor element concentrations in sediments combined with their mineralogical variation might aid in the detection of original metastable cold water carbonate minerals.

Modern temperate carbonates are commonly mixed with Last Glacial carbonates, formed when sea level was up to 130 m lower than present. Relic carbonate material may have been subaerially exposed and affected by meteoric diagenesis during low sea-level stands, which might have converted aragonite and high-Mg calcite to low Mg-calcite. O and C isotopes aid in the differentiation of meteorically derived low-Mg calcite from that forming now in seawater. Meteorically affected carbonates are characterized by depletion in $\delta^{18}O$ relative to marine sediments and in light $\delta^{13}C$ because of ^{12}C enrichment by soil CO_2 (Lohmann, 1988). The variation in carbonate minerals in both $\delta^{18}O$ and $\delta^{13}C$ is therefore important in distinguishing meteorically derived low-Mg calcite from that now forming in seawater.

The contents of Mg, Sr, Na, Mn and Fe and their variation with water depth are useful in understanding the mineralogy, composition of water masses and temperature related fractionation of elements.

Other studies on oxygen and carbon isotopes on Tasmanian (Rao and Green, 1983) and New Zealand (and Tasmanian) (Rao and Nelson, 1992) modern shelf carbonates indicated that the isotopic fields of temperate carbonates differ markedly from modern tropical shallow marine carbonates, overlap with Recent cold deep sea carbonates and follow the seafloor diagenetic trend line. The relationship between oxygen and carbon isotopes indi-

cated that these temperate carbonates are in equilibrium with upwelling deep waters. To understand the nature of upwelling water, closely spaced samples of shelf carbonates from western Tasmania (Fig. 1) were analyzed for oxygen and carbon isotopes and their variation with depth is considered.

Sedimentology

Surface sediment samples (Fig. 1) were collected several years ago on a 10 nautical mile grid off the coast of western Tasmania (Davies and Marshall, 1973). Data on grain size, carbonate content and distribution of skeletal components are given elsewhere (Davies and Marshall, 1973; Marshall and Davies, 1978). Coastal sediments are siliciclastics and carbonate occurs at depths ranging from ca. 50 m to the shelf edge (ca. 200 m) and beyond into deeper waters. Tasmanian shelf carbonates range from micrite to coarse sand-size grains and reef-like accumulations. Bryozoa dominate all samples. Mollusca, foraminifera, echinoderms, sponge spicules, algae, brachiopods and coccoliths occur in minor amounts. Many samples are cemented and contain borings, which indicate the occurrence of submarine hardgrounds and a relatively slow rate of sedimentation (Rao, 1990a). Encrustations are common (Fig. 2A), as is intragranular $CaCO_3$ cementation (Fig. 2B, C and D), which ranges up to 90% by volume in Tasmanian bryozoan sand (Rao, 1981a). These submarine cements occur as fibrous spherulitic aggregates (Fig. 2D) and well-developed rhombohedra (Rao, 1981a, 1990a). Mg, Sr, Na, Mn and Fe contents and their relationship to O and C isotope composi-

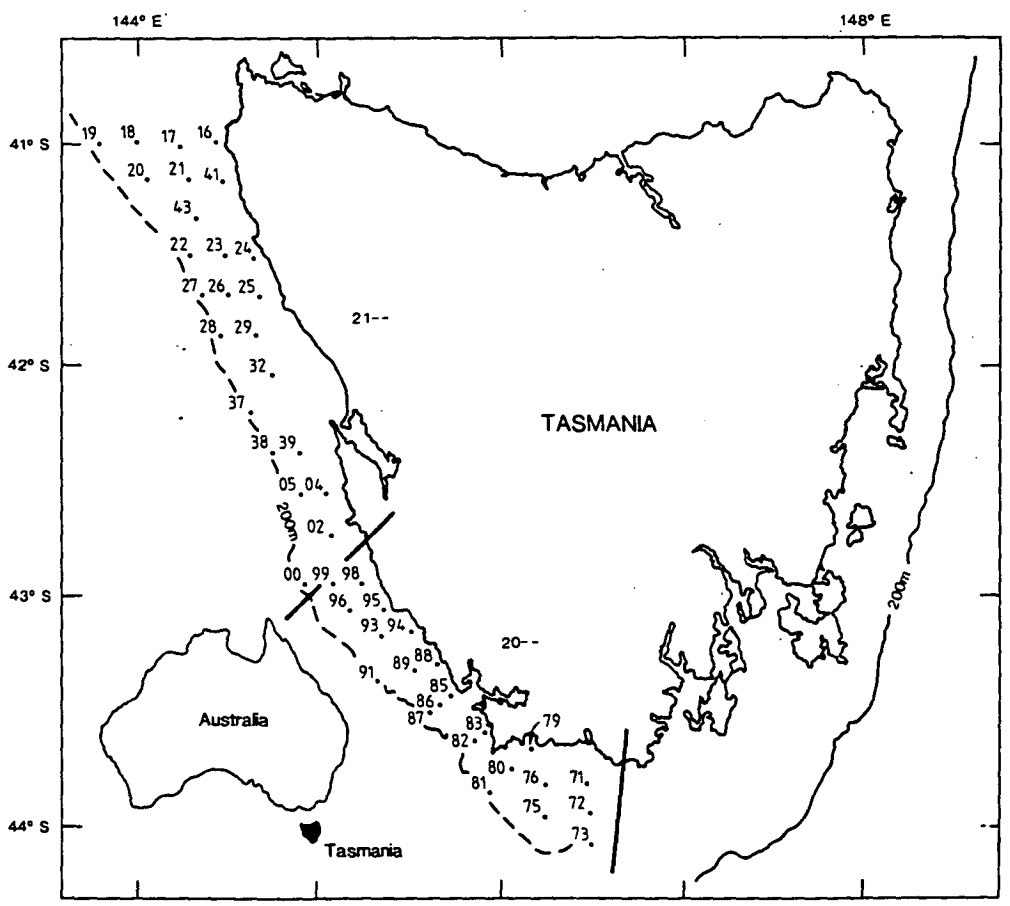

Fig. 1. Location of samples on Tasmanian shelves.

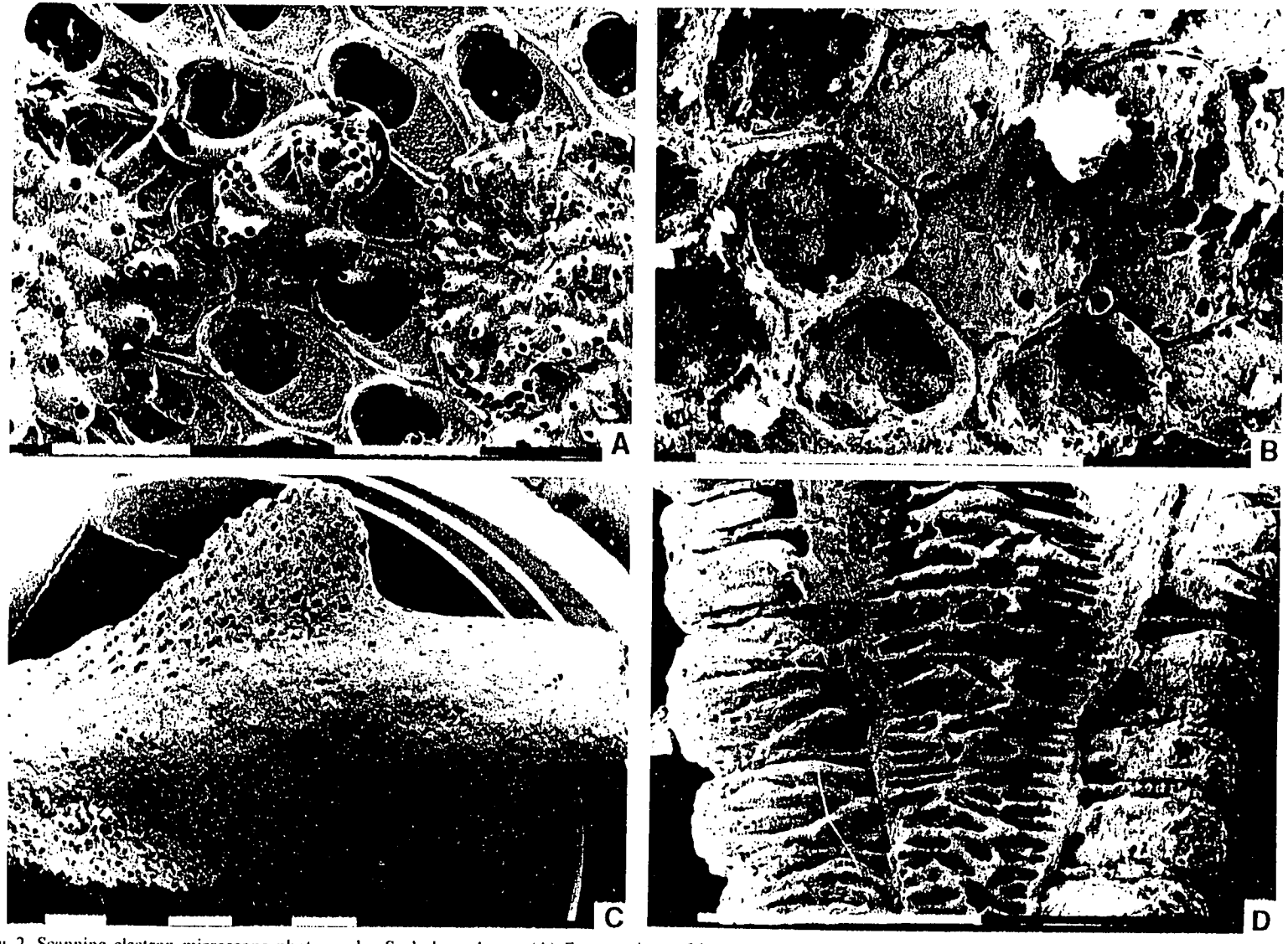

Fig. 2. Scanning electron microscope photographs. Scale bar = 1 mm. (A) Encrustations of bryozoa on old bryozoan grain. (B) $CaCO_3$ cement filling cells of a bryozoan grain. (C) Bryozoan grain with $CaCO_3$ intragranular cement. (D) Fibrous $CaCO_3$ cement fillings of a fossil (alga?).

tion (Rao, 1990a) indicate marine diagenesis in cold waters and are quite unlike meteoric diagenetic trends.

Methods of study

Whole sediment powders were analyzed for carbonate minerals, with fluorite as in internal standard, by X-ray diffraction (XRD). The peak area ratios of high-Mg calcite, low-Mg calcite and aragonite were used in the calculation of the percentages of these minerals. The portions of powders used for XRD analyses were dissolved in 1*N* HCl and analyzed for Ca, Mg, Sr, Na, Fe and Mn by atomic absorption spectrophotometry (AAS). These values were corrected to the 100% carbonate fraction using the percentage of insoluble residues, which is $<5\%$ in most samples. The precision is $\pm 1.5\%$ for Ca and Mg and $\pm 5\%$ for Sr, Na, Mn and Fe (Robinson, 1980). Portions of the same powders used for XRD and AAS were allowed to react with anhydrous phosphoric acid in reaction tubes in a vacuum at 25°C for 24 hours. The CO_2 extracted from each sample was analyzed for $\delta^{18}O$ and $\delta^{13}C$ by mass spectrometry (Micromass, 602D). The precision of the data is $\pm 0.1‰$ for both $\delta^{18}O$ and $\delta^{13}C$, and these values are reported relative to PDB.

Carbonate minerals

X-ray diffractograms (Fig. 3) of bulk sediments from Tasmania show the occurrence of calcites and some aragonite. The calcite peaks are asymmetric, with broad bases and range from 29.3° to 29.6° due to the presence of a spectrum of low-Mg calcite (LMC) ranging to high-Mg calcite (HMC). In some diffractograms the peaks of LMC and HMC are clearly separated from one another (Fig. 3A and C), whereas in others the peaks of LMC merge with the HMC peaks (Fig. 3B and D) due to the occurrence of a continuous spectrum of LMC through to HMC. The calcite peaks ranging from 29.3° to 29.6°, when compared with the chart of peak angle and mole% $MgCO_3$ (Scholle, 1978), indicate that calcite contains up to 9 mole% Mg.

The percentages of LMC, HMC and aragonite calculated from peak area ratios (Fig. 4) indicate that the Tasmanian sediments are characterized by a mixture of HMC and LMC, with minor amounts ($<28\%$) of aragonite. HMC is the dominant mineral in all samples and LMC and aragonite occur in most samples. The total amount of metastable HMC and aragonite predominates over LMC in all samples.

Aragonite and HMC contents and HMC/LMC ratios increase with decreasing water depth (Fig. 5), and the LMC content increases with increasing water depth. As water temperatures decrease with increasing water depth, the increase in LMC content with increasing water depth is due to cooler water temperatures. The increase in aragonite and HMC contents and HMC/LMC ratios with decreasing water depth is due to increasing water temperatures. There is no mineralogical change attributable to the sea-level drop of 130 m during the last glaciation.

Major and minor elements

Magnesium

The magnesium concentrations are positively correlated with HMC% (Fig. 6) as HMC contains most Mg. By extending the HMC lines to 100% HMC (Fig. 6), the Mg values of pure HMC can be obtained, which are in range 1.86 to 2.34% (i.e., 6–8 mole% $MgCO_3$). The maximum concentration of Mg in Tasmanian bryozoan sand is 2.65% (9 mole% $MgCO_3$; Rao, 1986). Magnesium values are negatively correlated with LMC% (Fig. 7). By extrapolating the LMC trend lines to 100% LMC, the Mg values of pure LMC can be obtained, and they range between 0.12 and 0.54% Mg (i.e., 0.4–1.9 mole% $MgCO_3$).

Experiments and thermodynamic considerations led Fuchtbauer and Hardie (1976) to suggest that the Mg content in calcite decreases almost linearly with decreasing water temperature. The maximum Mg concentration of 2.34% (8 mole% $MgCO_3$) in the whole samples studied corresponds to a water temperature of 10°C (experimental data). This 10°C water temperature is close to the average Tasmanian maximum surface temperature of 13°C. Experimental studies indicate that low-Mg calcite

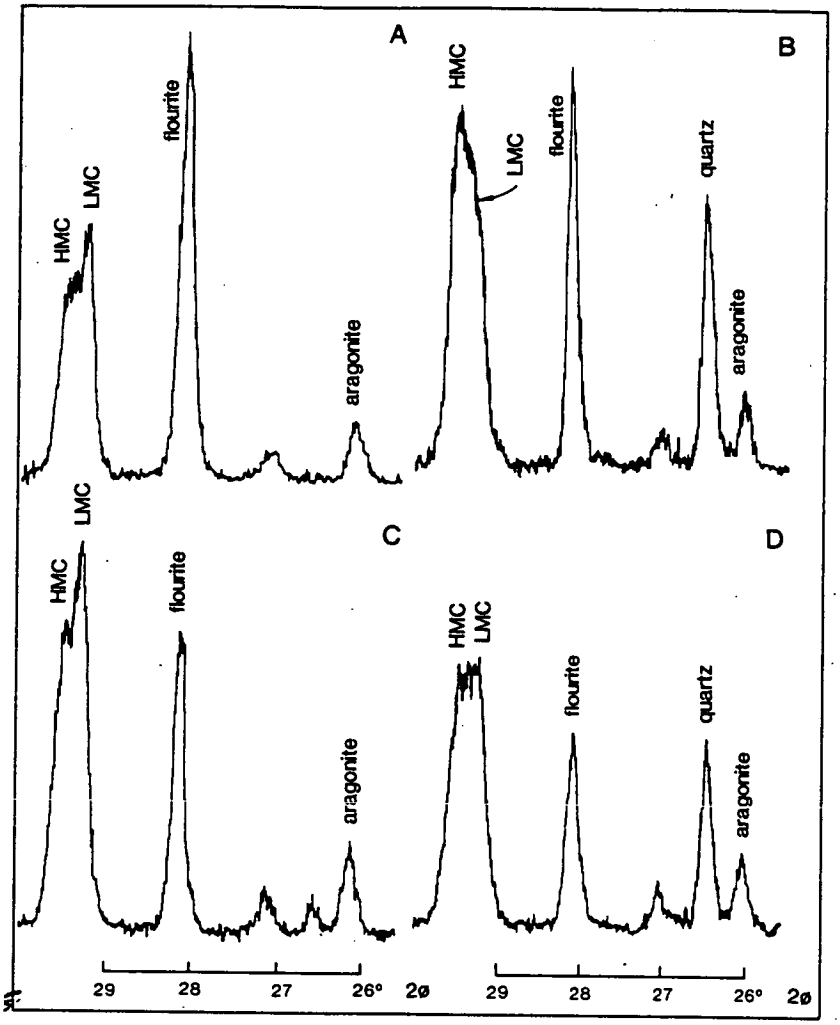

Fig. 3. Four typical X-ray diffractograms of whole sediments. Note in some (A, C and D) low-Mg calcite (LMC) and high-Mg calcite (HMC) peaks are clearly separated, whereas in others (B) LMC peaks merge with HMC.

precipitates from seawater at 3–5°C (Kinsman and Holland, 1969; Burton and Walter, 1987). Therefore, the ambient water temperatures of Tasmanian carbonates range from about 3° to 10°C. Chemically bryozoans behave like inorganic precipitates.

The Mg content decreases with increasing water depth (Fig. 8) because HMC% decreases and LMC% increases with increasing water depth. The Mg contents are inversely related to those of Sr concentrations (Fig. 9) due to changing concentrations of aragonite and calcite. Aragonite contains 8000–10,000 ppm Sr (Milliman, 1974), whereas in marine calcite Sr concentrations range from 1200 to 1400 ppm.

Strontium

The variations in Sr and in calcite and aragonite in whole Tasmanian sediments are shown in Fig. 10. The Sr concentrations increase with increasing aragonite content. By extending the aragonite-Sr lines to 0% aragonite, the Sr values of bryozoa with no aragonite can be obtained, and these are in the range 1350–2800 ppm. The 2800 ppm Sr value is close to the 3000 ppm Sr value in modern high-Mg calcite bryozoa (Milliman, 1974). The lowest Sr value of 1350 ppm at 0% aragonite is identical to the Sr value in low-Mg calcite at a water temperature of 3°C (Kins-

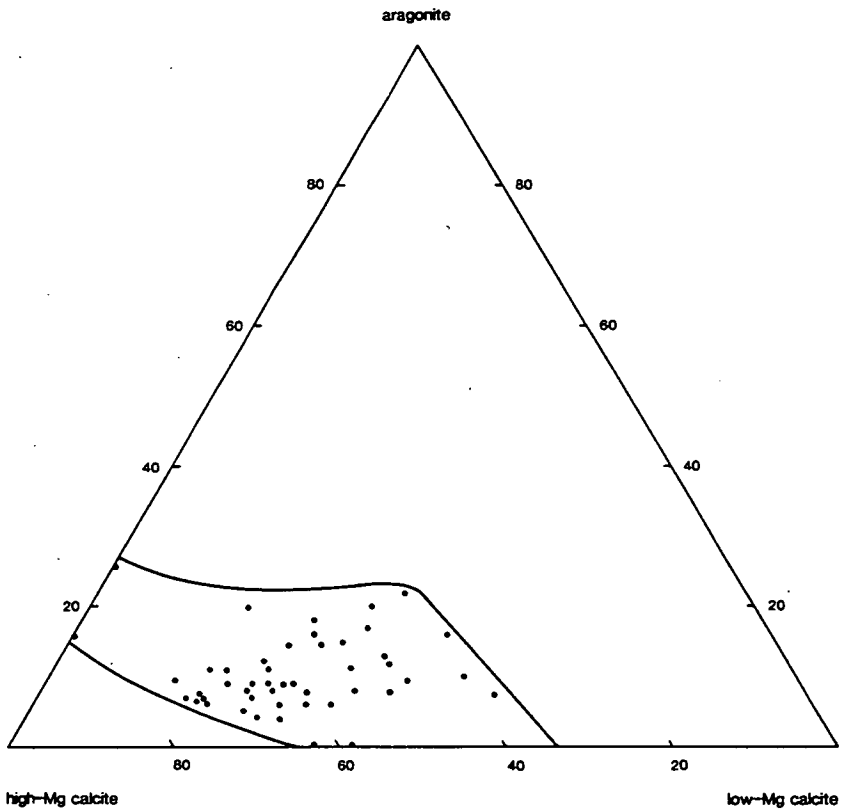

Fig. 4. Variation in HMC%, LMC% and aragonite% in whole Tasmanian sediments. Note the whole carbonates are mainly a mixture of HMC and LMC with minor amounts of aragonite.

man, 1969). The shift from 2800 to 1350 ppm Sr in pure calcite is due to increasing calcite cementation within bryozoa, as pure HMC bryozoa will have 2800 ppm Sr but calcite cement values will be lower, in the range 1250–1350 ppm depending on water temperature. Bryozoan sand previously analyzed for Sr and aragonite and calcite indicated up to 90% calcite cementation within the bryozoa (Rao, 1981a), which is consistent with petrographic observations.

The plot of Sr content versus water depth (Fig. 11) shows a general trend of decreasing Sr with increasing water depth due to a decreasing aragonite content with increasing water depth. Samples from water depths of <130 m generally have high Sr contents due to the occurrence of aragonite. Some samples at water depths of about 100 m have low Sr contents because of their greater high-Mg calcite contents (Figs. 9 and 11). Therefore, Sr concentrations in Tasmanian carbonates are dependent on the carbonate minerals present.

Sodium

Figure 12 illustrates that Na values increase with aragonite%. By extrapolating the Na-aragonite correlation to 0% aragonite, Na in pure calcite is found to range from 1900 to 4400 ppm. The maximum of 4400 ppm Na is similar to that seen in HMC bryozoa (Land and Hoops, 1973). The decrease in Na in bryozoa (from 4400 to 1900 ppm) results from intragranular calcite cementation, inorganic calcites containing smaller amounts of Na than the HMC bryozoa (Rao, 1990a). The Sr/Na ratio is about 1, much lower than the Sr/Na ratios of 3–4 in aragonite from warm, shallow marine waters (Rao, 1990a, 1991).

The Na concentrations increase with increasing water depth (Fig. 13). Na concentrations in car-

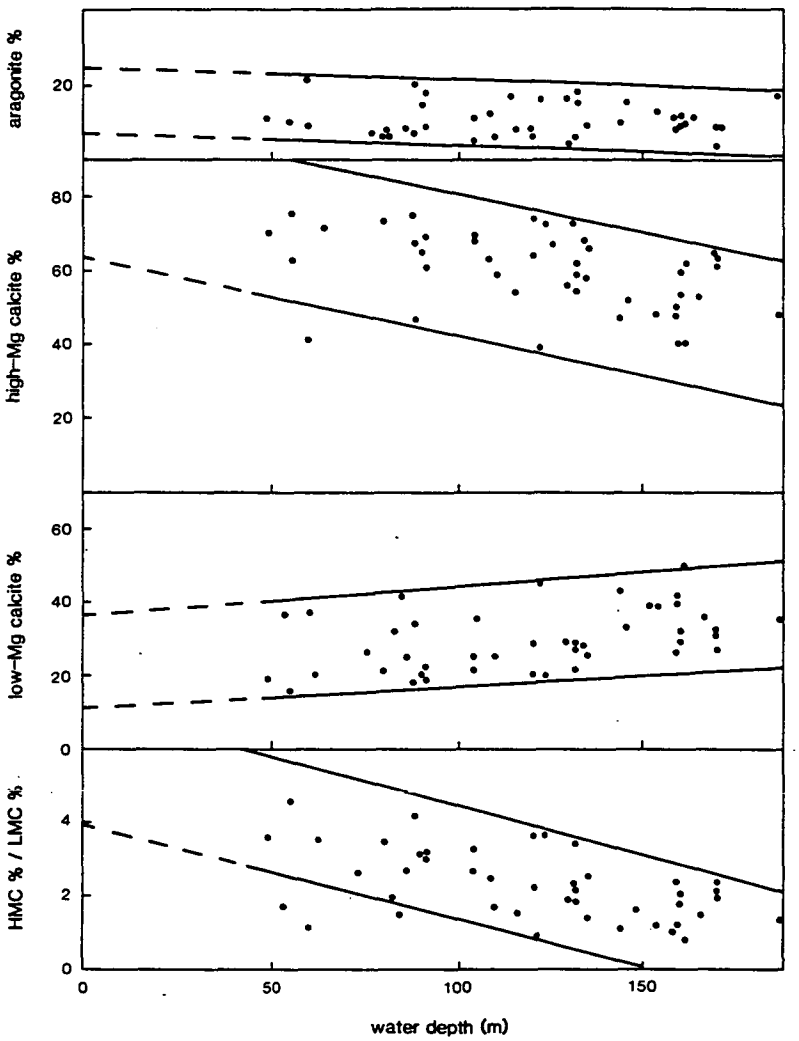

Fig. 5. Variation in HMC%, LMC%, aragonite% and HMC/LMC ratios with water depth. Note aragonite and HMC values decrease where LMC% and HMC/LMC ratios increase with increasing water depth.

bonate sediments and rocks are related to salinity, biochemical fractionation and mineralogy (Land and Hoops, 1973; Rao, 1990a). High-Mg calcite and low-Mg calcite bryozoa contain Na concentrations ranging from 3800 to 4400 ppm (Land and Hoops, 1973; Rao, 1986, 1990a) due to biochemical fractionation. As inorganic aragonite and low-Mg calcite contain lower concentrations than the bryozoa, the decrease in Na values to less than ca. 4000 ppm is probably due to appreciable amounts inorganic cementation. Samples with values of >4000 ppm Na might be the result of higher than normal salinities.

Manganese and iron

Mn concentrations increase with increasing aragonite% (Fig. 14). This aragonite is significantly enriched in Mn compared to warm water aragonite, which contains <20 ppm Mn (Milliman, 1974). Fe concentrations also increase with increasing aragonite% (Fig. 15) and again these values are much higher than those of warm water aragonite, which also contains <20 ppm Fe (Milliman, 1974). The carbonate minerals in cool temperate Tasmanian carbonates are impure phases and are unlike those in warm shallow marine waters.

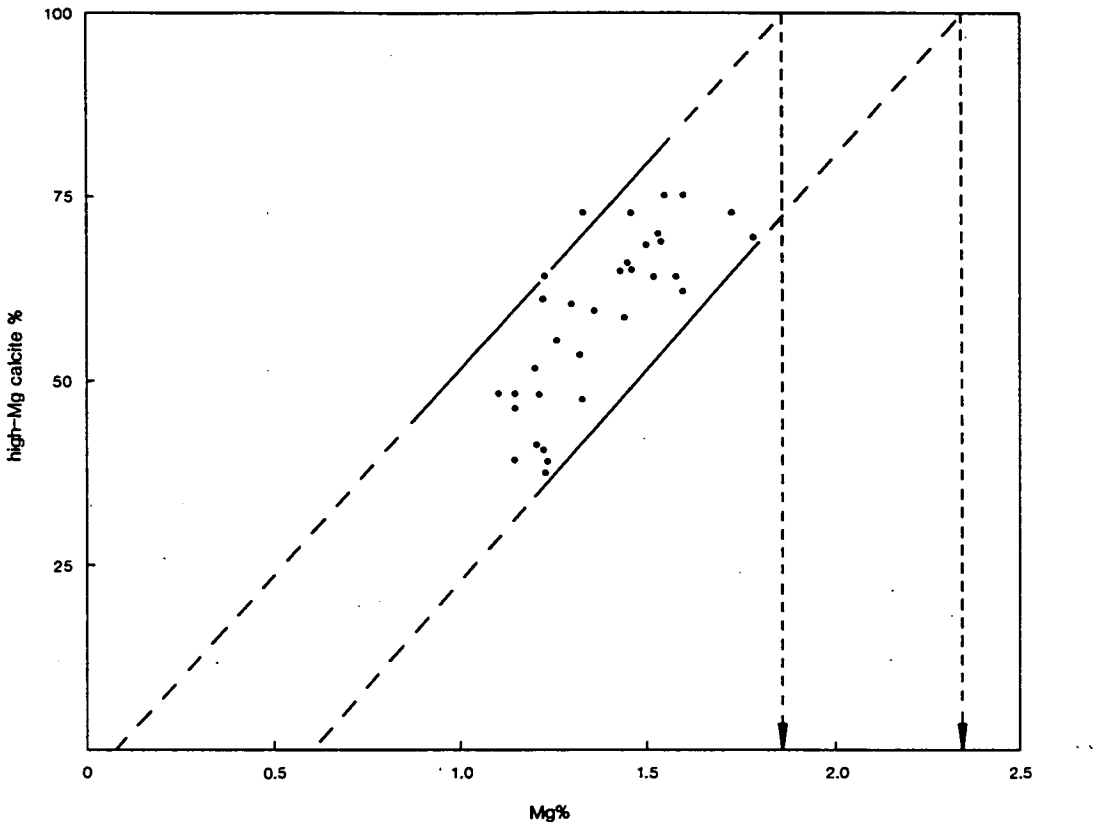

Fig. 6. Variation of HMC% and Mg values obtained by AAS analysis. Note Mg in 100% HMC contents are in the range 1.86–2.34%.

Mn and Fe concentrations decrease with increasing water depth (Fig. 16) due to the increasing distance from shore, which causes a progressive reduction in terrigenous content. The source of both these elements is continental material.

Variations in minor elements with HMC/LMC ratios

As Tasmanian sediments are mainly mixtures of HMC and LMC (Fig. 4), the HMC/LMC ratios can be used to understand the variation in trace elements compared to HMC and LMC. Sr concentrations slightly increase with decreasing HMC/LMC ratios (Fig. 17), which is consistent with a slight increase in the partitioning coefficient of Sr in calcite with decreasing temperature (Kinsman, 1969). For example, the Sr concentration in HMC at 25°C is 1200 ppm, whereas in LMC at 3°C it is 1350 ppm. A slight increase in partitioning coefficient, this time of Na, in calcite with decreasing water temperatures may also be the cause of Na values slightly increasing with decreasing HMC/LMC ratios (Fig. 17). Mn and Fe concentrations are uniform throughout the range of HMC/LMC ratios (Fig. 17), probably due to lack of temperature dependent fractionation of these elements. The partition coefficient for Mn in calcite is ca. 15 (Pingitore, 1978). Fe concentrations an order of magnitude higher than those of Mn are due to a higher partition coefficient of Fe than that of Mn in calcite.

Oxygen and carbon isotopes

The oxygen and carbon isotope data for western Tasmanian carbonates are plotted in Fig. 18. Both $\delta^{18}O$ and $\delta^{13}C$ values are mainly positive values, unlike the light $\delta^{18}O$ and variable $\delta^{13}C$ values for warm, tropical whole carbonates (Milliman, 1974).

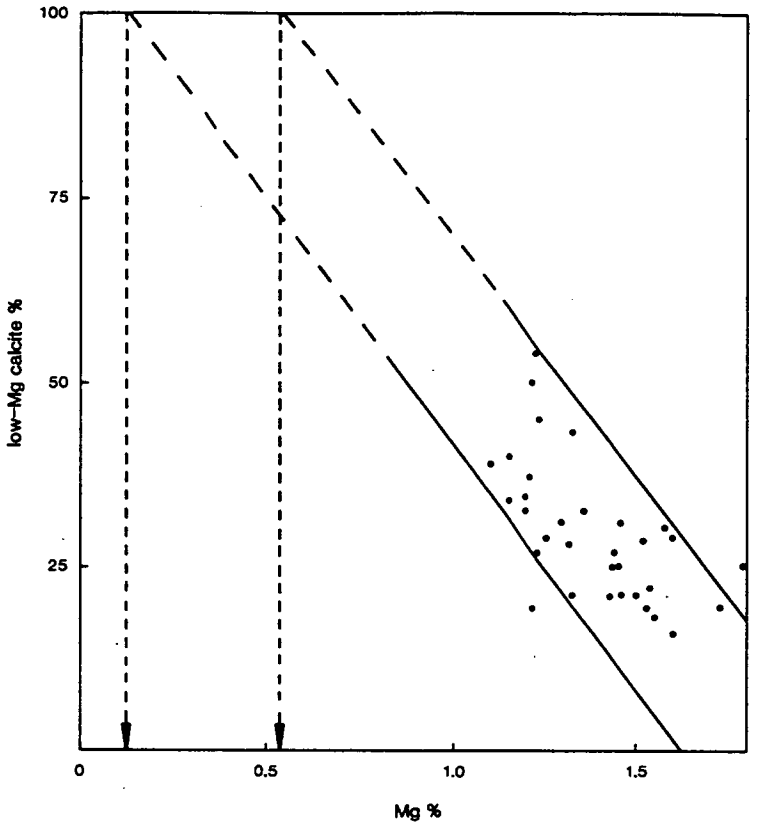

Fig. 7. Variation in low-Mg calcite% and Mg values from AAS analysis. Note Mg in 100% LMC contents range from 0.12 to 0.5% Mg.

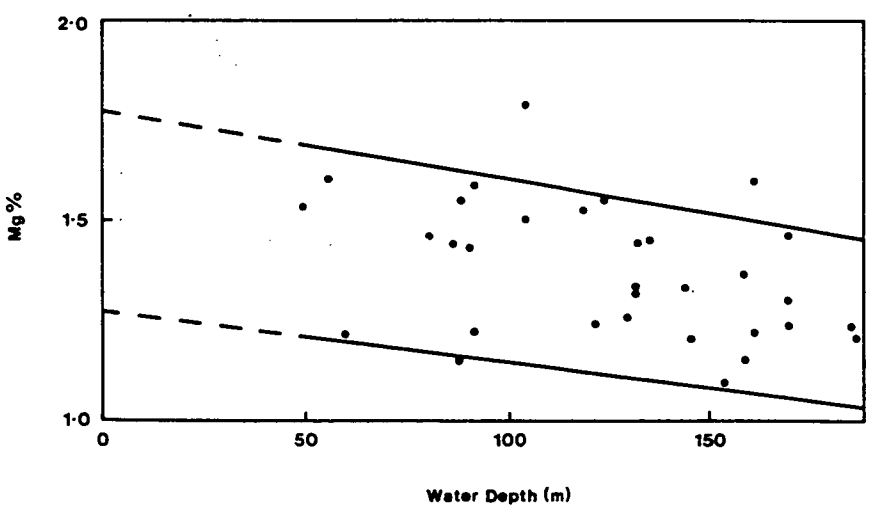

Fig. 8. Variation of Mg% with water depth.

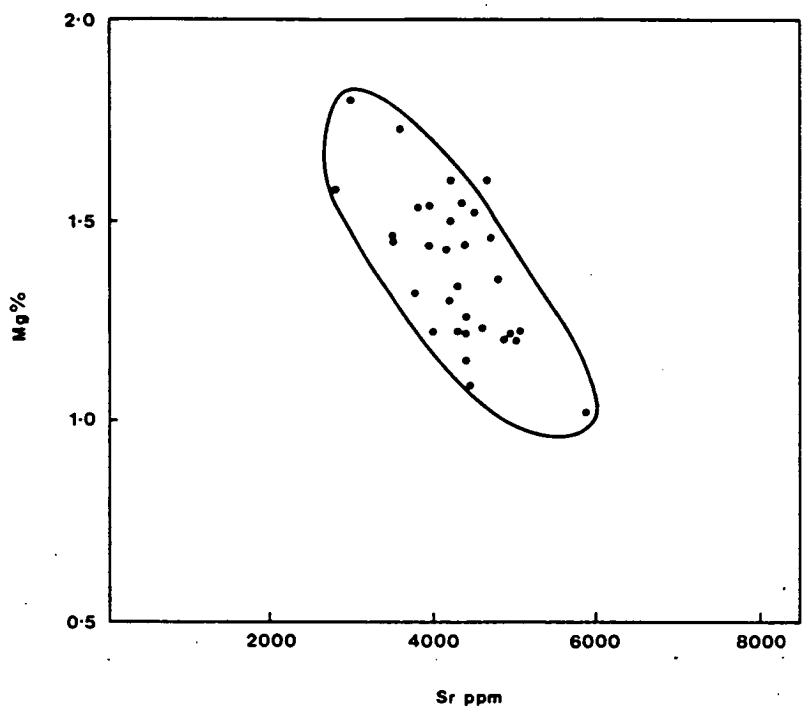

Fig. 9. Variation of Mg% with Sr.

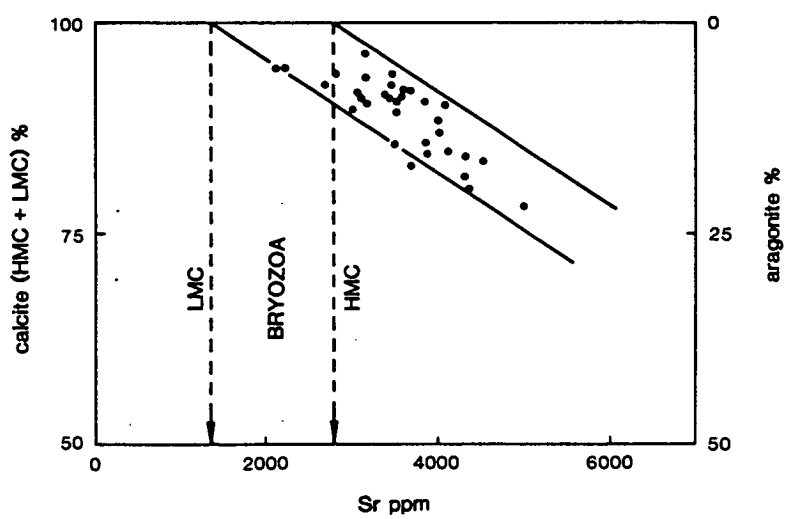

Fig. 10. Variation of Sr with total calcite% (HMC% + LMC%) and aragonite%. Note 100% calcites coinciding with 0% aragonite Sr lines range in Sr from 1350 (LMC) and from 2800 ppm (HMC). 100% aragonites have Sr concentrations ranging from 10,600 to 10,800 ppm.

The modern temperate whole carbonate isotope field is bisected by the seafloor diagenesis trend line, which passes through the origin (Rao and Nelson, 1992). The western Tasmanian isotope field falls close to the seafloor diagenesis trend line but deviates towards lighter $\delta^{18}O$ values (Fig. 18). The $\delta^{13}C$ values are similar to those of other temperate carbonates.

The variations of $\delta^{18}O$ with aragonite%, HMC%, LMC% and HMC/LMC ratios are

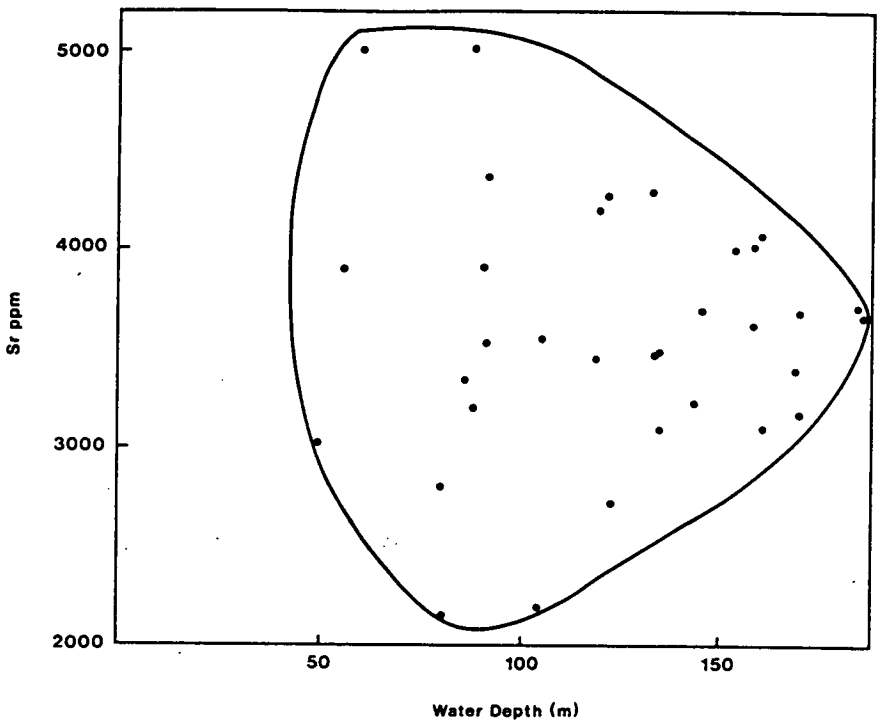

Fig. 11. Variation of Sr with water depth.

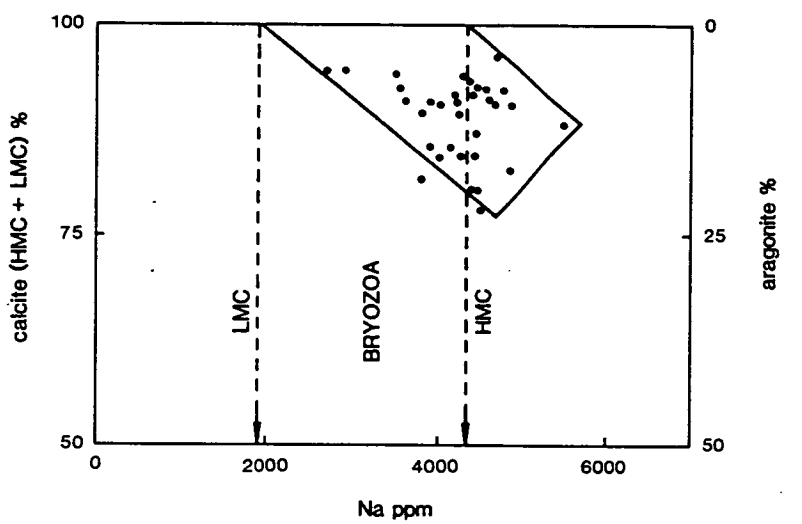

Fig. 12. Variation of Na with total calcite% (HMC% + LMC%) and aragonite. Note 100% calcite coinciding with 0% aragonite-Na lines ranging in Na from 1900 (LMC) and 4400 ppm (HMC). 100% aragonite has Na values ranging from 16,000 to 18,000 ppm.

shown in Fig. 19. Ambient water temperatures calculated, using the equation proposed by Shackleton and Kennett (1975), from $\delta^{18}O$ values with a δ_w of normal seawater of 0‰ and a δ_w of upwelling water of -1‰ are shown at the foot of Fig. 19. Aragonite% is uniform throughout the range of $\delta^{18}O$ values. The aragonite content is low, as is expected in cooler temperatures, but it is unusual that concentrations of aragonite occur throughout the range of water temperatures. The

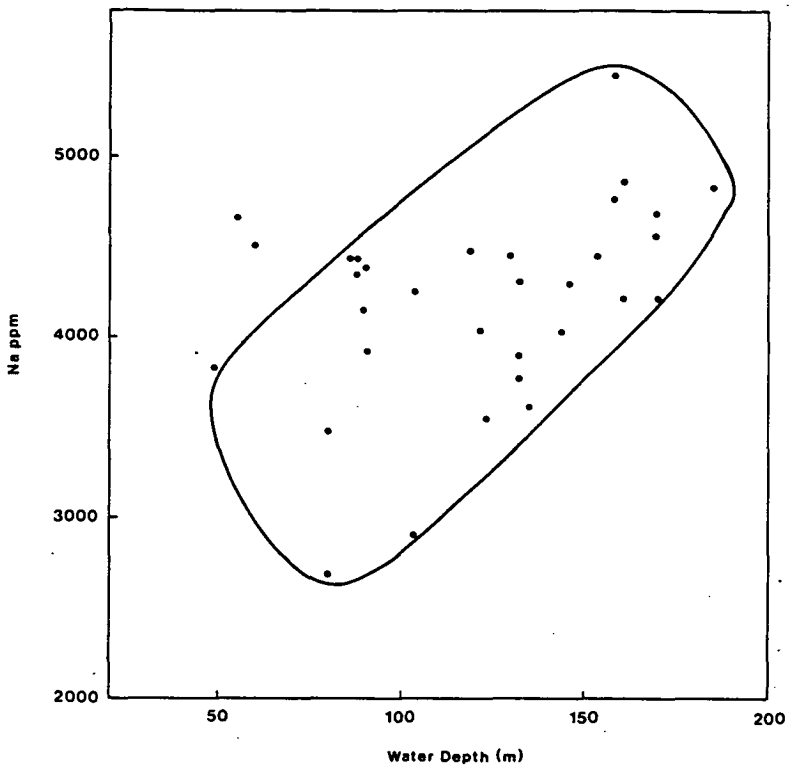

Fig. 13. Variation of Na with water depth.

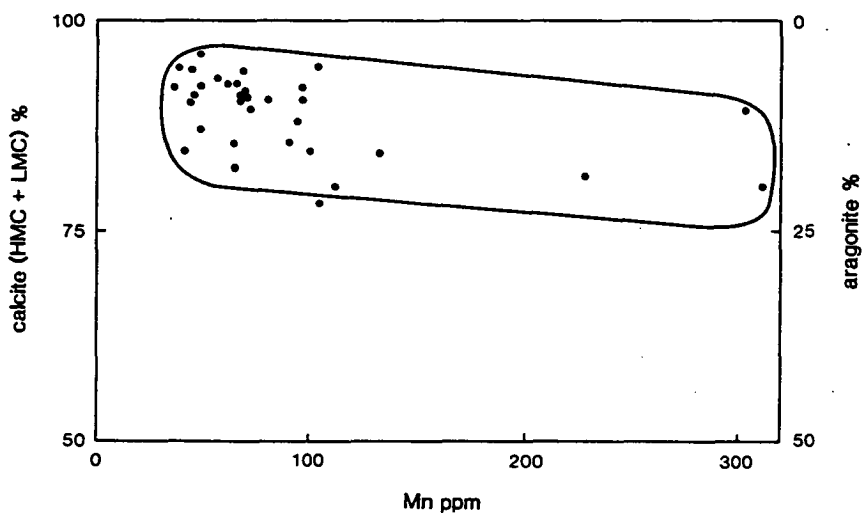

Fig. 14. Variation of Mn with total calcite% (HMC% + LMC%) and aragonite. Note Mn values increasing with increasing aragonite%.

decreases in HMC% and the HMC/LMC ratio, however, and the increasing LMC% with increasingly heavier $\delta^{18}O$ values, are consistent with expectations at decreasing water temperatures. There is an ^{18}O enrichment of 0.06‰ for each mole% $MgCO_3$ (Tarutani et al., 1969).

The variations of $\delta^{13}C$ with aragonite%, HMC%, LMC% and the the HMC/LMC ratio

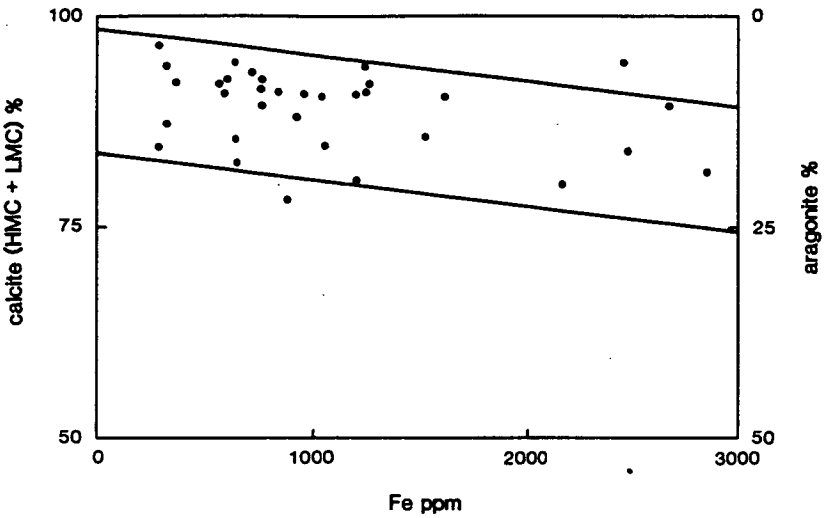

Fig. 15. Variation of Fe with total calcite% (HMC% + LMC%) and aragonite. Note Fe values increasing with increasing aragonite%.

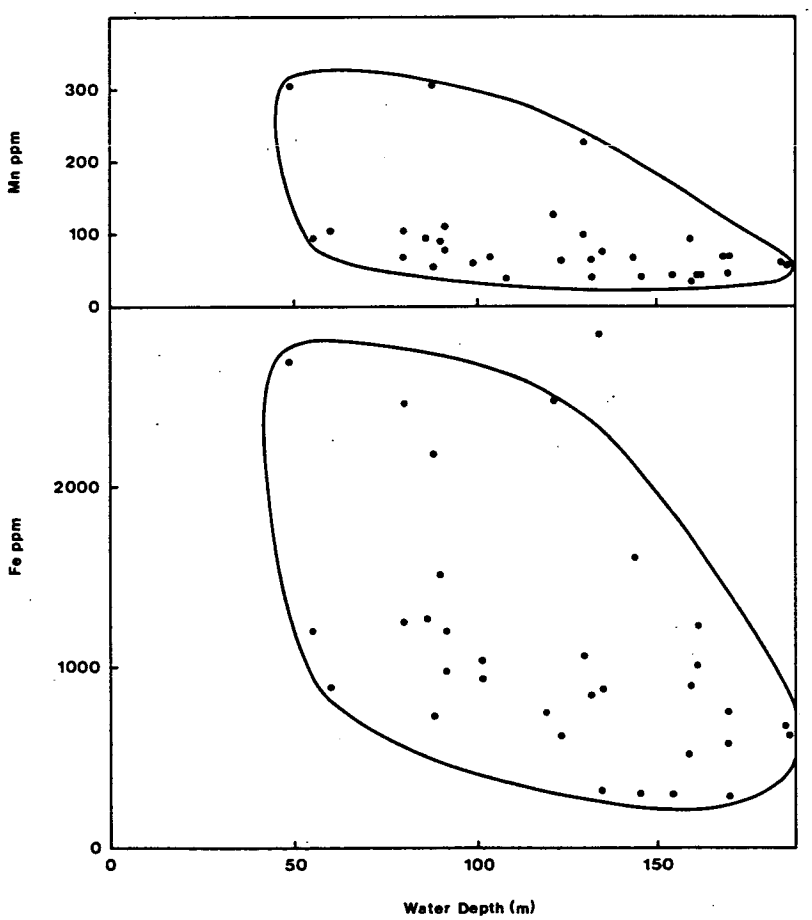

Fig. 16. Variation of Mn and Fe with water depth.

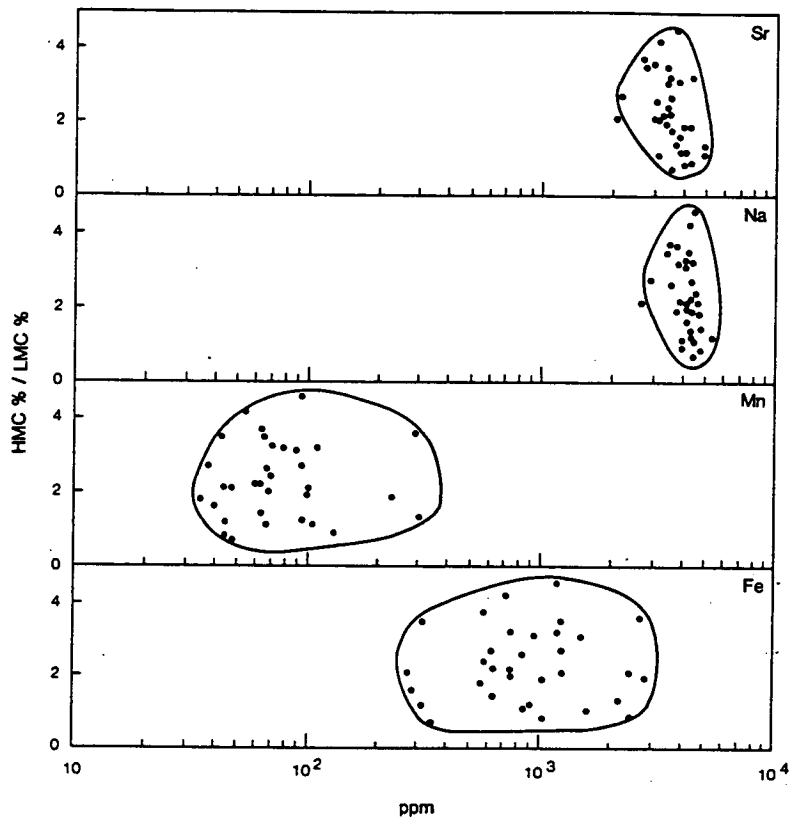

Fig. 17. Variation of Sr, Na, Mn and Fe with HMC/LMC ratios. See text for explanation.

are illustrated in Fig. 20. Aragonite% and LMC% increase with heavier $\delta^{13}C$, whereas HMC% and HMC/LMC ratios decrease slightly with heavier $\delta^{13}C$. Unlike $\delta^{18}O$, there is a strong positive correlation of $\delta^{13}C$ with aragonite%. Experimental studies (Rubinston, 1969) have indicated that the $\delta^{13}C$ is enriched in aragonite relative to calcite by 1.8‰. In modern temperate carbonates $\delta^{13}C$ and $\delta^{18}O$ are positively correlated (Rao and Green, 1983; Rao and Nelson, 1992).

The $\delta^{18}O$ values (Fig. 21) generally become heavier with increasing water depth due to a decrease in water temperatures. Comparison of calculated temperatures based on $\delta^{18}O$ values with those of measured summer values between 39° and 60°S (Fig. 21) shows that $\delta^{18}O$-based temperatures are much lower than measured summer values in the Southern Ocean.

The $\delta^{13}C$ values are positive and do not vary appreciably with water depth (Fig. 22). Comparison of $\delta^{13}C$ variation with that of the Tasmania and New Zealand field of Rao and Nelson (1992) shows that most values correspond to those at the shelf edge and are much higher than those in found in deeper waters.

Discussion

The variation in carbonate minerals, major and minor elements and oxygen and carbon isotopes and their relationship to water depth may be related to: (a) meteoric diagenesis, (b) marine diagenesis, (c) metastable cold water $CaCO_3$ minerals, (d) upwelling water, (e) water temperatures and (f) mixing of water masses.

Meteoric diagenesis

Modern temperate carbonates are mixed with Last Glacial carbonates formed when the sea level was up 130 m lower than present. Relic carbonates formed at depths of greater than 130 m would

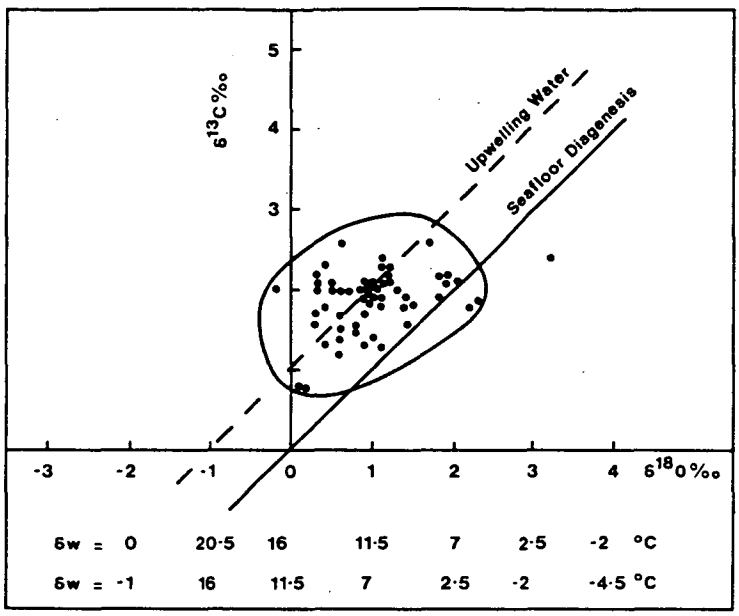

Fig. 18. Variation of $\delta^{18}O$ and $\delta^{13}C$. Water temperatures are based on $\delta^{18}O$ values of carbonate, with seawater ^{18}O values of 0‰ and −1‰. The seafloor diagenesis trend line is after Milliman and Muller (1977) and the upwelling water diagenetic trend line is constructed passing through −1‰ $\delta^{18}O$ after Craig and Gordon (1965) parallel to the seafloor diagenesis trend line. δ_w = isotopic ratio of CO_2 in equilibrium with formation water.

have been unaffected by meteoric diagenesis as they were always within marine waters, whereas those formed in depths of less than 130 m would have been subaerially exposed and affected by meteoric diagenesis, which might have converted aragonite and HMC to LMC. The lack of pure LMC and the dominance of HMC and aragonite in all samples indicates that they have not been affected by meteoric diagenesis. If LMC is derived from conversion of aragonite and HMC, the LMC concentrations should have been markedly higher at depths of less than 130 m than those at depths of greater than 130 m, which is not the case in Recent Tasmanian samples (Fig. 5). Modern Tasmanian meteoric waters have average $\delta^{18}O$ values of −5.2‰ SMOW (Goede et al., 1986), which means meteorically affected calcites would have $\delta^{18}O$ values of around −4.5‰ PDB at a temperature of 10°C, which is not the case in Tasmanian sediments (Fig. 18). Recent and Pleistocene speleothem deposits from caves in Tasmania have very light $\delta^{13}C$ values of −6.7 to −13.7‰ (Goede et al., 1986), unlike the positive values in Tasmanian sediments (Fig. 18). The inverted "J" trend characteristic of meteoric diagenesis (Lohmann, 1988) is absent. The lack of markedly lighter values of $\delta^{18}O$ and $\delta^{13}C$ at depths of less than 130 m indicates that these carbonates are modern ones. Meteoric diagenesis results in a loss of Mg, Sr and Na and a gain in Mn and Fe (Brand and Veizer, 1980; Al-Aasm and Veizer, 1986; Rao, 1990b). The decrease in Mg, Sr and increase in Na with increasing water depth (Figs. 8, 11 and 13) are unlike the trends attributed to meteoric diagenesis. Also, there is no marked change in Mn and Fe concentrations (Fig. 16) in samples from depths below and above 130 m, which should have been the case if samples from depths of less than 130 m were affected by meteoric diagenesis. Instead, Mn and Fe concentrations gradually decrease with increasing water depth (Fig. 16). All the above evidence suggests that the Tasmanian cool temperate carbonates are unaffected by meteoric diagenesis.

Marine diagenesis

The increase in LMC% with increasing water depth (Fig. 5) coupled with the evidence against

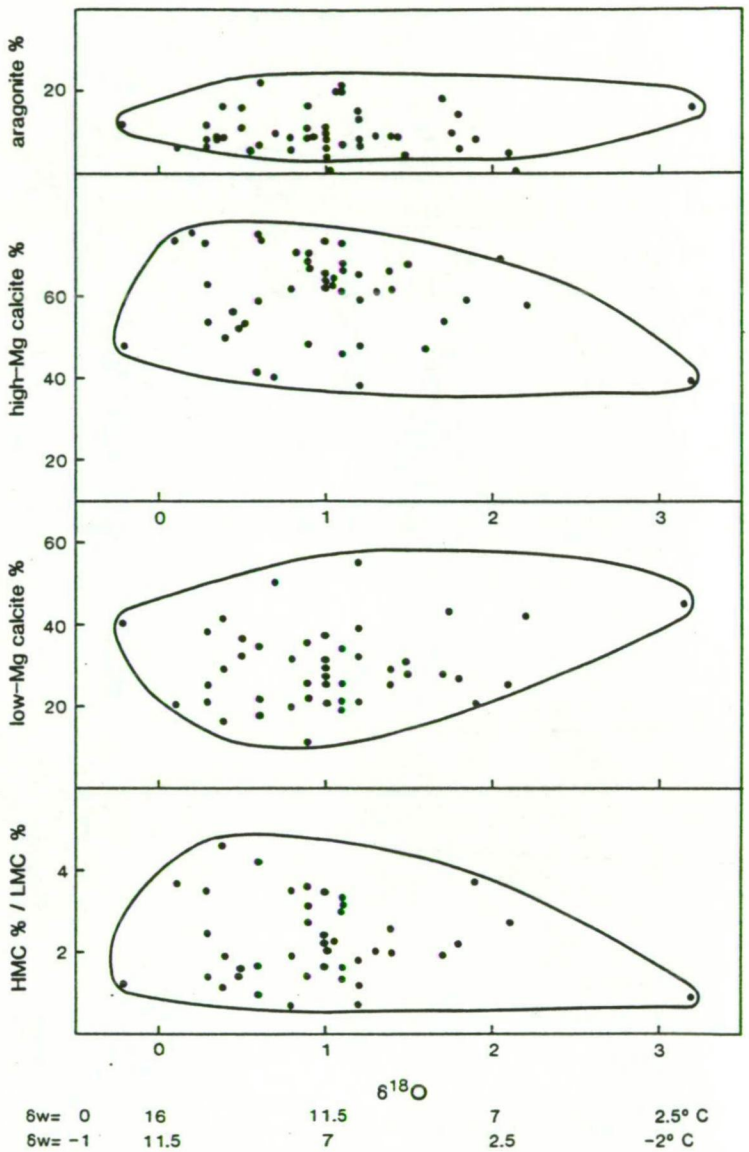

Fig. 19. Variation of aragonite%, HMC%, LMC% and HMC/LMC ratios with $\delta^{18}O$.

meteoric diagenesis presented above, confirm that LMC is an original cold shallow marine mineral. The concentrations of Mg in HMC observed chemically and by XRD peak shifts are consistent with those expected from carbonate formed within the range of temperatures below 13°C. The decreasing HMC/LMC ratios are also due to the temperature-dependent formation of these minerals. The increasing aragonite content with decreasing water depth (Fig. 5) is also in accordance with higher temperatures with decreasing water depths. All this evidence confirms that marine diagenesis and water temperatures have controlled the mineralogy of Tasmanian carbonates. Abundant calcite cements in Tasmanian carbonates (Fig. 2B, C and D; Rao, 1981a) also indicate the significant role played by marine diagenesis. Increasingly heavy $\delta^{18}O$ and decreasing concentrations of Mg, Sr, Mn and Fe with increasing water depth indicate marine diagenesis. The $\delta^{13}C$ values are within the range of marine temperate carbonates. Positive correlation of $\delta^{18}O$ and $\delta^{13}C$ is similar to that observed

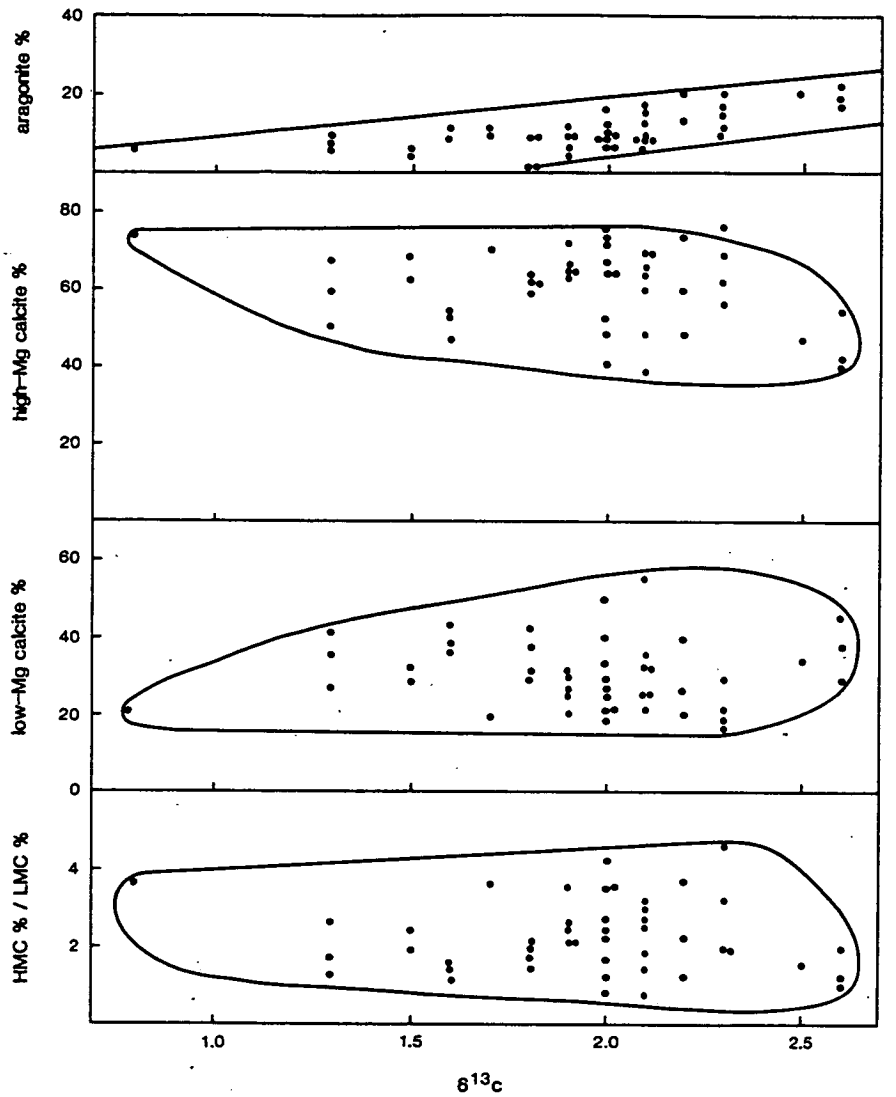

Fig. 20. Variation of aragonite%, HMC%, LMC% and HMC/LMC ratios with $\delta^{13}C$.

in other temperate carbonates (Rao and Green, 1983; Rao and Nelson, 1992). All this evidence confirms that marine diagenesis and a decrease in water temperatures with depth have controlled isotopic composition and concentrations of major and minor elements of Tasmanian carbonates.

Metastable cold water $CaCO_3$ minerals

The Mn and Fe concentrations in the Tasmanian carbonates are positively correlated with aragonite% (Figs. 14 and 15) and, unusually, are higher than those of warm shallow marine aragonitic sediments. Similarly, Sr-aragonite lines (Fig. 10) and Na-aragonite lines (Fig. 12), if extended to 100% aragonite, show values of Sr between 10,600 and 10,800 ppm and of Na between 16,000 and 18,000 ppm. Such high Na values are not reported in warm shallow marine aragonite. In experiments at $<10°C$, calcite precipitates from seawater together with metastable $CaCO_3$ phases, such as vaterite and hydrous calcites (Albright, 1971; Turnbull, 1973; Hull and Turnbull, 1973; Marland, 1975), which invert to both calcite and aragonite

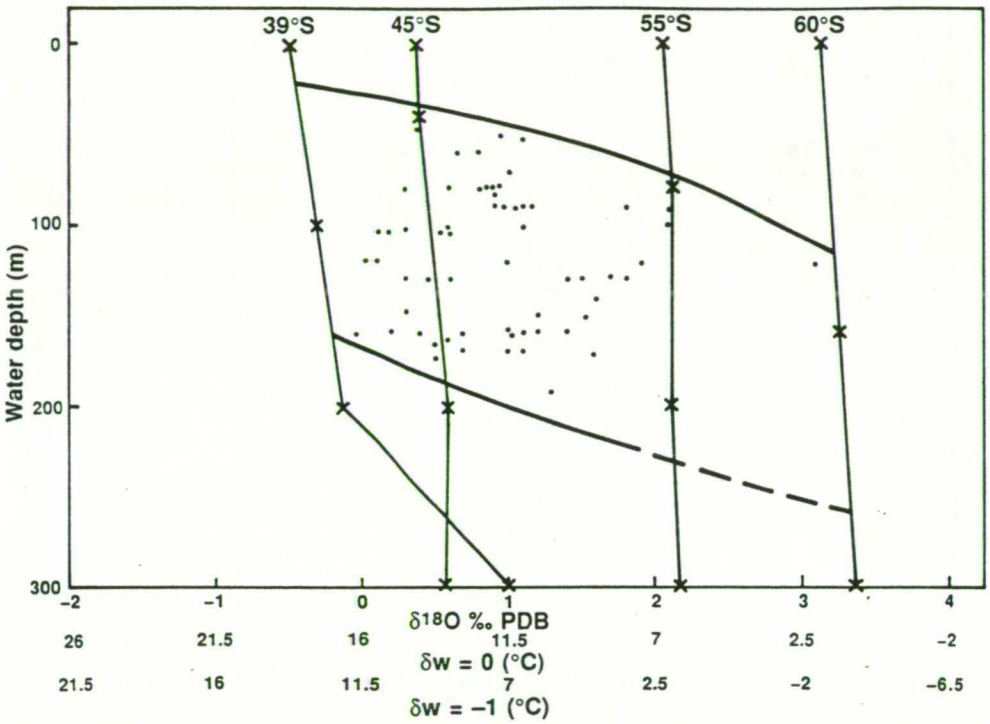

Fig. 21. Variation of $\delta^{18}O$ with water depth. Water temperatures are based on $\delta^{18}O$ values of carbonate, with seawater ^{18}O values of 0‰ and −1‰. The water temperatures measured against depth at various southern latitudes correspond to temperatures calculated with a ^{18}O value of 0‰. Note isotopic temperatures are cooler than measured values.

as soon as they are exposed to open atmospheric conditions. These minerals are impure phases. Two interpretations are possible for the unusually high concentrations of Sr, Na, Mn and Fe observed in the aragonite of the Tasmanian carbonates. Firstly, aragonite in cold shallow marine waters contains higher concentrations of Sr, Na, Mn and Fe than that of warm shallow marine conditions. Secondly, the impure aragonite, detected only by XRD analysis, might be due to inversion of vaterite or hydrous calcites, which are common in cold waters. Earlier studies on Tasmanian bryozoan sand (Rao, 1981a) also indicated the possible occurrence of vaterite, which occurs as fibrous spherulitic aggregates. "Vital effect" on carbonate mineralogy and geochemistry is minimal in the samples studied.

Upwelling water

Other studies on O and C isotopes in temperate carbonates (Rao and Green, 1983; Rao and Nelson, 1992) have indicated that these carbonates overlap in their isotopic character with deep sea carbonates. The two isotopic ratios are positively correlated as these isotopes are in equilibrium with upwelling deep waters. The western Tasmanian O and C isotope field (Fig. 18) overlaps with that of other temperate carbonates and extends to lighter $\delta^{18}O$ values due to the light $\delta^{18}O$ of seawater. The lighter than normal ^{18}O values of seawater (0‰ SMOW) occur in upwelling regions. Craig and Gordon (1965) give values of around −1‰ PDB for $\delta^{18}O$ in upwelling bottom waters. The upwelling water trend line can be constructed parallel to the seafloor diagenesis trend line, passing through −1‰ $\delta^{18}O$ and 0‰ $\delta^{13}C$ (Fig. 18). This upwelling water trend line bisects the western Tasmanian isotope field due to the samples being in strong equilibrium with upwelling water and not with deep sea water. These upwelling waters were more saline than normal seawater, as indicated by increasing Na concentrations with increasing

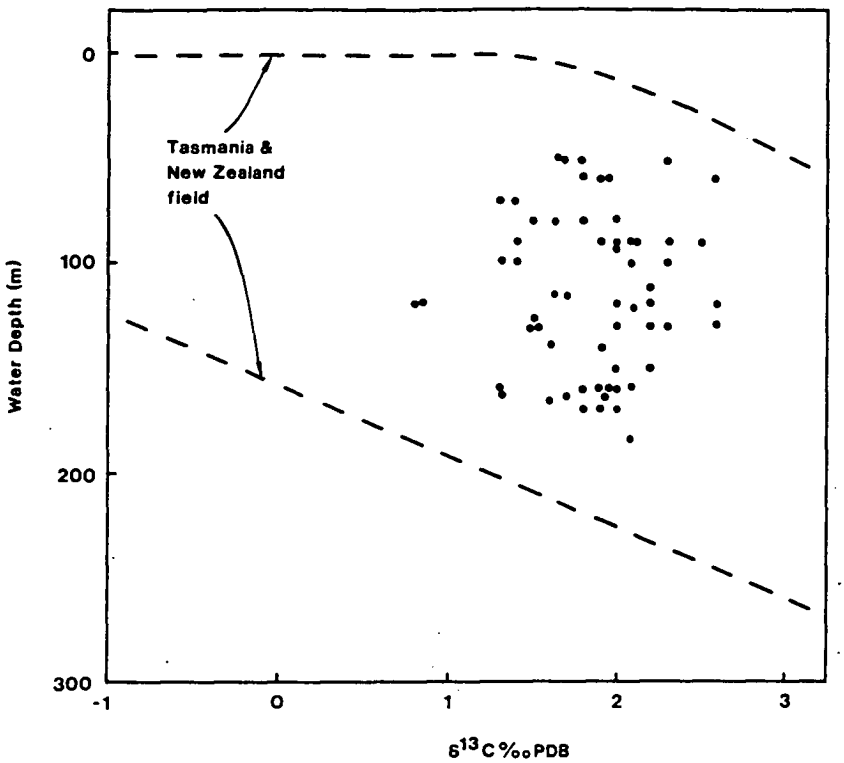

Fig. 22. Variation of $\delta^{13}C$ with water depth. The Tasmania and New Zealand field is after Rao and Nelson (1992).

depth. The greater the influence of upwelling nutrient-rich waters the higher the rate of carbonate productivity.

Water temperature

Water temperatures calculated from $\delta^{18}O$ values using 0‰ and −1‰ $\delta^{18}O$ values of normal seawater and upwelling seawater in the equation proposed by Shackleton and Kennett (1975) range from about 6° to 17°C and 2° to 13°C respectively. These temperatures are shown at the bottom of Fig. 18, 19 and 21 and are mostly within < 10°C of those values obtained from Mg values based on experimental studies of Mg fractionation over a range of water temperatures (see Fuchtbauer and Hardie, 1976).

Mixing of water masses

Water temperatures obtained from $\delta^{18}O$ values for western Tasmanian carbonates are much lower than the measured values (Fig. 21) because of the mixing of water masses. Surface seawater temperatures in temperate regions are strongly affected by seasonal changes (Rao and Nelson, 1992). A winter–summer rhythm in the circulation of surface waters exists around Tasmania (Newell, 1961). In summer, the subtropical convergence moves just south of Tasmania with the introduction of Indian Ocean water along the coast of western Tasmania. In winter, the subtropical convergence moves northwards with the westerly wind system, bringing cold, low-salinity subantarctic water from the Circumpolar West Wind Drift around Tasmania. Lower temperatures in the mixed layer are due to mixing with cold upwelling waters. The $\delta^{18}O$ water temperatures at about 900 m are around 2°C (Rao and Nelson, 1992), and upwelling waters are probably cooler than this.

Geologic significance

Carbonate mineralogy in Recent shallow marine carbonates is dependent on water temperatures. In

warm shallow marine carbonates, aragonite is the predominant mineral, with variable amounts of HMC (Milliman, 1974). LMC inorganic precipitates do not form in warm waters because of inhibition by Mg ions. In modern warm temperate carbonates, HMC predominates, with some aragonite (Collins, 1988). In cool temperate carbonates, as indicated by this study, the carbonate minerals are a mixture of HMC and LMC with minor amounts of aragonite, which might have been inverted from vaterite or hydrous calcites. In subpolar carbonates LMC predominates over HMC or pure LMC forms (Rao, 1981c, 1988, 1991). Cold water deep sea carbonates contain mainly LMC (Schlager and James, 1978). Experimental studies (Kinsman and Holland, 1969; Burton and Walter, 1987) also confirm that carbonate mineralogy varies with water temperature, similar to observations in natural carbonates. Therefore, in ancient carbonates, recognition of original carbonate mineralogy can be used to differentiate tropical, temperate and subpolar carbonates (Nelson, 1978; Rao, 1981b, c; 1988, 1991).

Some workers have suggested that ancient carbonate mineralogy may have been different from that of modern sediments (Sandberg, 1975; MacKenzie and Pigott, 1981; Wilkinson, 1982; Tucker, 1984) due to different atmospheric pCO_2 levels and resultant water chemistries. When the atmospheric pCO_2 was similar to the present levels aragonite was the dominant mineral, and when the atmospheric pCO_2 was higher than today calcite was predominant. Calcite was considered to have been dominant during early and middle Palaeozoic and Jurassic (James and Choquette, 1983; Tucker, 1984). Evaluation of Ordovician tropical carbonates of Tasmania (Rao and Wang, 1990) using values of $\delta^{13}C$ relative to $\delta^{18}O$ indicate that during the early Ordovician there were higher pCO_2 levels than at present but that during the middle and late Ordovician they became comparable with those of the present because of glacial conditions. On the basis of petrographic and geochemical criteria, aragonite was the predominant mineral in warm tropical carbonates during the Ordovician (Rao and Naqvi, 1977; Rao, 1989; Rao, 1990b). Similar observations have been made on the originally aragonitic tropical Jurassic limestones of Iran (Adabi and Rao, 1991). As ancient tropical limestones coeval with originally calcitic limestones contain aragonite, the extensive occurrence of originally calcitic carbonates in the geological record is due to their non-tropical origin.

Vast volumes of cold seawater in high latitudes are presently undersaturated in $CaCO_3$, and the carbonate sediments in contact with these waters are affected by submarine dissolution and breakdown (Alexandersson, 1978). These destructive processes, if continued without interruption, would obliterate cold water carbonates within a short period of time. Upwelling waters maintain higher saturation levels of $CaCO_3$ in the water column and provide nutrients for the luxurient growth of fauna. Earlier workers (Conolly and Von der Borch, 1967; Wass et al., 1970) have postulated that upwelling of cold Antarctic waters is the main reason for the occurrence of extensive temperate carbonates on the southern Australian shelves. Isotopic studies (Rao and Green, 1983; Rao and Nelson, 1992) have shown the validity of this upwelling model for the formation of cold water carbonates. However, these isotopic studies considered the upwelling of deep sea water as the main mechanism for providing saturation of $CaCO_3$ and nutrient supply. This study demonstrates upwelling of seawater—and not just *deep sea* water—as the main process responsible for the formation of carbonates in western Tasmania. Therefore, in paleotemperature determinations a $\delta^{18}O$ value 1‰ lower than the postulated seawater values for the different geological periods should be considered for those carbonates suspected to be of cold water origin on the basis of geological (Rao, 1981b; Nelson, 1988 and references therein) and geochemical (Rao, 1981c, 1990a, 1991) evidence.

Variation of $\delta^{18}O$ and $\delta^{13}C$ values and concentrations of Mg, Sr, Na, Mn and Fe in the Tasmanian carbonates related to water depth indicates that the carbonate sediments are modern. Marine diagenesis and temperature have controlled the fractionation of these isotopes and the concentrations of major and minor elements; the variations in these components are unrelated to meteoric diagenesis. Last Glacial sediments formed at depths of less than 130 m either occur below the modern sediments or have been totally destroyed

by meteoric diagenesis. As the sediments are modern and of marine origin, the isotopic variation and patterns of major and minor elements can be used as baselines for the marine diagenesis of ancient, orginally calcitic limestones. The depth variation in O and C isotopic ratios and major and minor elements can also be used to deduce original depths of deposition in stratigraphic sequences.

The mineralogical variation with major and minor elements and oxygen and carbon isotopes in the modern temperate calcitic carbonates of Tasmania presented here can be used as a data base for understanding the marine, meteoric and burial diagenesis of originally calcitic ancient limestones, which are abundant in the geological record.

Conclusions

The cool temperate carbonates of Tasmania contain bryomol assemblages and intragranular $CaCO_3$ cements. They are bored and encrusted due to slow rates of sedimentation. The following conclusions can be drawn from the carbonate minerals, the major and minor elements and the oxygen and carbon isotopes and their variation with water depth:

(1) Carbonate minerals detected by XRD analysis are mainly a mixture of high-Mg calcite (HMC) and low-Mg calcite (LMC), with minor amounts of aragonite.

(2) HMC% and aragonite% decrease and LMC% increases with increasing water depth as a result of decreasing water temperature.

(3) Mg concentrations obtained from XRD peak shifts and chemical analysis correspond to temperatures of $< 10°C$.

(4) Sr, Na, Mn and Fe concentrations are related to bryozoa, intragranular calcite cements and aragonite%.

(5) Carbonate mineral variation with $\delta^{18}O$ is related to ambient upwelling seawater temperatures ranging from 2° to 13°C.

(6) LMC of both fauna and cements is a marine mineral in cold seas and it is not a product of meteoric diagenesis.

(7) Unusually high concentrations of Sr, Na, Mn and Fe in aragonite are either due to aragonite being capable of incorporating these elements in the cold seas, or, more likely, to its having been inverted from vaterite or hydrous calcites, which are common in cold waters.

(8) The O and C isotope field is bisected by upwelling water seafloor diagenesis trend lines because the western Tasmanian carbonates are in equilibrium with upwelling waters.

(9) O and Mg values vary with water depth due to decreasing water temperatures.

(10) The variation in the O and C isotopic ratios and the variation in the concentrations of Mg, Sr, Na, Mn and Fe related to water depth are not related to meteoric diagenesis. Therefore, these sediments are modern and the geochemical variation within them is due to marine diagenesis.

(11) Surface water temperatures are affected by seasonal changes and by the influx of subantarctic water during the winter. Bottom water temperatures are strongly influenced by upwelling waters.

(12) Cold water carbonates form in regions of upwelling, which provides nutrients for the growth of fauna and maintains the saturation of $CaCO_3$, thus preventing dissolution and permitting the formation of precipitates in the form of cements.

(13) In paleotemperature determinations, $\delta^{18}O$ values 1‰ lower than those postulated for seawater during different geological periods should be used for originally calcitic non-tropical carbonates.

Originally calcitic ancient limestones are common in the geological record, particularly in the early and mid-Paleozoic and Jurassic, and these limestones may have formed in non-tropical waters, because coeval limestones from the tropics contain mainly original aragonite.

Acknowledgements

CSIRO and the University of Tasmania provided financial assistance. We also thank the BMR for providing samples, David Houston and Mike Worthing for reading an early version of the manuscript, Mike Power for isotope analysis, Philip Robinson for chemical analysis, and Debbie Harding and June Pongratz for drafting the illustrations.

References

Adabi, M.H. and Rao, C.P., 1991. Petrographic and geochemical evidence for original aragonite mineralogy of Upper Jurassic carbonates (Mozduran Formation), Sarakhs area, Iran. Sediment. Geol., 72: 253–267.

Al-Aasm, I.S. and Veizer, J., 1986. Diagenetic stabilization of aragonite and low-Mg calcite. I. Trace elements in rudists. J. Sediment. Petrol., 56: 138–152.

Albright, J.N., 1971. Vaterite stability. Am. Mineral., 56: 620–624.

Alexandersson, E.T., 1978. Destructive diagenesis of carbonate sediments in the eastern Skagerrak, North Sea. Geology, 6: 324–327.

Brand, U. and Veizer, J., 1980. Chemical diagenesis of a multicomponent carbonate system. I. Trace elements. J. Sediment. Petrol., 50: 1219–1236.

Brookfield, M.E., 1988. A mid-Ordovician temperate carbonate shelf—the Black River and Trenton Limestone Groups of southern Ontario, Canada. In: C.S. Nelson (Editor), Non-tropical Shelf Carbonates—Modern and Ancient. Sediment. Geol., 60: 137–153.

Burton, E.A. and Walter, L.K., 1987. Relative precipitation of aragonite and Mg-calcite from seawater: temperature or carbonate ion control? Geology, 15: 111–114.

Collins, L.B., 1988. Sediments and history of the Rottnest Shelf, southwest Australia: a swell-dominated, non-tropical carbonate margin. In: C.S. Nelson (Editor) Non-tropical Shelf Carbonates—Modern and Ancient. Sediment. Geol., 60: 15–49.

Conolly, J.R. and Von der Borch, C.C., 1967. Sedimentation and physiography of the sea floor south of Australia. Sediment. Geol., 1: 181–220.

Craig, H. and Gordon, L.I., 1965. Deuterium and oxygen-18 variations in the ocean and marine atmosphere. In: Stable Isotopes in Oceanographic Studies and Paleotemperatures, Spoleto, July 26–27. 1965. CNR, Lab. Geol. Nucl., Pisa, pp. 1–122.

Davies, P.J. and Marshall, J.F., 1973. BMR marine geology cruise in Bass Strait and Tasmanian waters—February to May, 1973. Bur. Miner. Resour., Aust., Rec. 134, 19 pp.

Draper, J.J., 1988. Permian limestone in the southeastern Bowen Basin, Queensland: an example of temperate carbonate deposition. In: C.S. Nelson (Editor), Non-tropical Shelf Carbonates—Modern and Ancient. Sediment. Geol., 60: 155–162.

Fuchtbauer, H. and Hardie, L.A., 1976. Experimentally determined homogeneous distribution co-efficients for precipitated magnesian calcites. Abstr. Annu. Progr. Meet. Geol. Soc. Am., p. 877.

Goede, A., Green, D.C. and Harmon, R.S., 1986. Late Pleistocene palaeotemperature record from a Tasmanian speleothem. Aust. J. Earth Sci., 33: 333–342.

Hull, H. and Turnbull, A.G., 1973. A thermochemical study of monohydrocalcite. Geochim. Cosmochim. Acta, 37: 685–694.

James, N.P. and Bone, Y., 1989. Petrogenesis of Cenozoic temperate water calcarenites, South Australia: a model for meteoric/shallow burial diagenesis of shallow water calcite cements. J. Sediment. Petrol., 59: 191–203.

James, N.P. and Choquette, P.W., 1983. Diagenesis, 6. Limestones—the sea floor diagenetic environment. Geosci. Can., 10: 162–179.

Kinsman, D.J.J., 1969. Interpretation of Sr^{+2} concentrations in carbonate minerals and rocks. J. Sediment. Petrol., 39: 486–508.

Kinsman, D.J.J. and Holland, H.D., 1969. The co-precipitation of cations with $CaCO_3$-IV. The co-precipitation of Sr^{+2} with aragonite between 16° and 96°C. Geochim. Cosmochim. Acta, 33: 1–17.

Land, L.S. and Hoops, G.K., 1973. Sodium in carbonate sediments and rocks: a possible index to salinity of diagenetic solutions. J. Sediment. Petrol., 43: 614–617.

Lees, A., 1975. Possible influence of salinity and temperature on modern shelf carbonate sedimentation. Mar. Geol., 19: 159–198.

Lohmann, K.C., 1988. Geochemical patterns of meteoric diagenetic systems and their application to studies of paleokarst. In: N.P. James and P.W. Choquette (Editors), Paleokarst. Springer, New York, pp. 58–80.

MacKenzie, F.T. and Pigott, J.D., 1981. Tectonic controls of Phanerozoic rock cycling. J. Geol. Soc. London, 138: 183–196.

Marland, G., 1975. The stability of $CaCO_3 \cdot H_2O$ (ikaite). Geochim. Cosmochim. Acta, 39: 83–91.

Marshall, J.F. and Davies, P.J., 1978. Skeletal carbonate variation on the continental shelf of eastern Australia. BMR J. Aust. Geol. Geophys., 3: 85–92.

Milliman, J.D., 1974. Marine Carbonates, Recent Sedimentary Carbonates, Part 1. Springer, New York, 375 pp.

Milliman, J.D. and Muller, J., 1977. Characteristics and genesis of shallow-water and deep-sea limestones. In: N.R. Anderson and A. Malahoff (Editors), The Fate of Fossil Fuel CO_2 in the Oceans. Plenum, New York, pp. 655–672.

Nelson, C.S., 1978. Temperate shelf carbonate sediments in the Cenozoic of New Zealand. Sedimentology, 25: 737–771.

Nelson, C.S., 1988. An introductory perspective on non-tropical shelf carbonates. In: C.S. Nelson (Editor), Non-tropical Shelf Carbonates—Modern and Ancient. Sediment. Geol., 60: 3–12.

Newell, B.S., 1961. Hydrology of S-E Australian waters: Bass Strait and New South Wales tuna fishing area. CSIRO Div. Fish. Oceanogr. Tech. Pap. 10, 20 pp.

Pingitore, N.E., 1978. The behavior of Zn^{+2} and Mn^{+2} during carbonate diagenesis: Theory and applications. J. Sediment. Petrol., 48: 799–814.

Rao, C.P., 1981a. Cementation in cold-water bryozoan sand, Tasmania, Australia. Mar. Geol., 40: M23–M33.

Rao, C.P., 1981b. Criteria for recognition of cold-water carbonate sedimentation: Berriedale Limestone (lower Permian), Tasmania, Australia. J. Sediment. Petrol., 51: 491–506.

Rao, C.P., 1981c. Geochemical differences between tropical (Ordovician) and subpolar (Permian) carbonates, Tasmania, Australia. Geology, 9: 205–209.

Rao, C.P., 1986. Geochemistry of temperate-water carbonates, Tasmania, Australia. Mar. Geol., 71: 363–370.

Rao, C.P., 1988. Paleoclimate of some Permo-Triassic carbonates of Malaysia. In: C.S. Nelson (Editor), Non-tropical Shelf Carbonates—Modern and Ancient. Sediment. Geol., 53: 117–129.

Rao, C.P., 1989. Geochemistry of Gordon Limestone (Ordovician), Mole Creek, Tasmania, Australia. Aust. J. Earth Sci., 36: 65–71.

Rao, C.P., 1990a. Geochemical characteristics of cool-temperate carbonates, Tasmania, Australia. Carbonates Evaporites, 5: 209–221.

Rao, C.P., 1990b. Petrography, trace elements and oxygen and carbon isotopes of Gordon Group carbonates (Ordovician), Florentine Valley, Tasmania, Australia. Sediment. Geol., 66: 83–97.

Rao, C.P., 1991. Geochemical differences between subtropical (Ordovician), temperate (Recent and Pleistocene) and subpolar (Permian) carbonates, Tasmania, Australia. Carbonates Evaporites, 6: 83–106.

Rao, C.P. and Green, D.C., 1983. Oxygen- and carbon-isotope composition of cold shallow-marine carbonates of Tasmania, Australia. Mar. Geol., 53: 117–129.

Rao, C.P. and Naqvi, I.H., 1977. Petrography, geochemistry and factor analysis of a lower Ordovician subsurface sequence, Tasmania, Australia. J. Sediment. Petrol., 47: 1036–1055.

Rao, C.P. and Nelson, C.S., 1992. Oxygen and carbon isotope fields for temperate shelf carbonates from Tasmania and New Zealand. Mar. Geol., 103: 273–286.

Rao, C.P. and Wang, B., 1990. Oxygen and carbon isotope composition of Gordon Group carbonates (Ordovician), Florentine Valley, Tasmania, Australia. Aust. J. Earth Sci., 37: 305–316.

Robinson, P., 1980. Determination of calcium, magnesium, manganese, strontium, sodium and iron in the carbonate fraction of limestones and dolomites. Chem. Geol., 28: 135–146.

Rubinston, H. and Clayton, R.N., 1969. Carbon-13 fractionation between aragonite and calcite. Geochim. Cosmochim. Acta, 33: 997–1004.

Sandberg, P.A., 1975. New interpretations of Great Salt Lake ooids and nonskeletal carbonate mineralogy. Sedimentology, 22: 497–537.

Schlager, W. and James, N.P., 1978. Low-magnesian calcite limestones forming at the deep floor, Tongue of the Ocean, Bahamas. Sedimentology, 25: 675–702.

Scholle, P.A., 1978. A Color Illustrated Guide to Carbonate Rock Constituents, Textures, Cements and Porosities. Am. Assoc. Pet. Geol. Mem., 27: 241 pp.

Shackleton, N.J. and Kennett, J.P., 1975. Paleotemperature history of the Cenozoic and the initiation of Antarctic glaciation: oxygen and carbon isotope analyses in DSDP sites 277, 279 and 281. Init. Rep. Deep-Sea Drill. Proj., XXIX: 743–755.

Tarutani, T., Clayton, R.N. and Mayeda, T.K., 1969. The effect of polymorphism and magnesium substitution on oxygen isotope fractionation between calcium carbonate and water. Geochim. Cosmochim. Acta, 33: 987–996.

Tucker, M.E., 1984. Calcitic, aragonitic and mixed calcitic–aragonitic ooids from mid-Proterozoic Belt Supergroup, Montana. Sedimentology, 31: 627–644.

Turnbull, A.G., 1973. A thermochemical study of vaterite. Geochim. Cosmochim. Acta, 37: 1593–1601.

Wass, R.E., Connolly, R.J. and MacIntyre, R.J., 1970. Bryozoan carbonate sand continuous along southern Australia. Mar. Geol., 9: 63–73.

Wilkinson, B.H., 1982. Cyclic cratonic carbonates and Phanerozoic calcite seas. J. Geol. Educ., 30: 189–203.